RUSSIAN ACADEMIC MONOGRAPHS

E. V. Romanenko

Fish and Dolphin Swimming

PENSOFT

RUSSIAN ACADEMY OF SCIENCES
A. N. Severtsov Institute of Ecology and Evolution

Fish and Dolphin Swimming

by

E. V. Romanenko

PENSOFT

Sofia – Moscow
2002

FISH AND DOLPHIN SWIMMING
First published 2002
ISBN 954-642-150-2

Russian Academic Monographs *No. 2*

Pensoft Publishers, Acad. G. Bonchev Str., Bl.6, 1113 Sofia, Bulgaria
Fax: +359-2-70-45-08, e-mail: pensoft@mbox.infotel.bg, **www.pensoft.net**

Printed in Bulgaria, August 2002

Contents

PREFACE ix

INTRODUCTION xi

CHAPTER 1. THEORETICAL MODELS OF SWIMMING 1

1.1. The planar approach to the problem. 1
1.1.1. The theory of thin profile with undulating oscillations. 1
1.1.2. Comparison with the experiment. 6
1.1.3. The profile in the time-variable flow 6
1.1.4. The thickness of the oscillating profile as affecting the hydrodynamic forces induced by this profile 10
1.1.5. The value of thrust, caused by the two-dimensional thin platelet, as affected by the free surface of liquid 14
1.1.6. The possibility of animals' intake of energy from the wave flow 17
1.1.7. The decrease of hydrodynamic drag of dolphin and fish due to propulsive wave 22
1.2. The spatial problem 24
1.2.1. The theory of the thin fish-shaped body 25
1.2.2. Theory of swimming for fishes with large amplitudes of body oscillations 41
1.3. Theory of swimming for animals with the semilunar caudal fin 46
1.3.1. Two-dimensional theory of the lunate tail 46
1.3.2. Further progress of the semilunar fin theory 49
1.3.3. Comparison with the experiment 58
1.3.4. Peculiarities of scombroid swimming 64
1.3.5. Applicability of the hypothesis on stability for estimation of the hydrodynamic forces developed by the lunate tail 70
1.3.6. Hydrodynamic forces exerting a rigid wing moving with high heaving and pitching amplitude 72
1.4. Threshold values of the thrust and efficiency of dolphin's and fishes' propulsors estimated with the phase velocity of the propulsive wave striving to the velocity of body motion 92
1.5. Evolution of fish locomotion function: whether it was influenced by the sound factor 97
Brief conclusions 107

CHAPTER 7. EVALUATION OF DOLPHIN'S HYDRODINAMIC CHARACTERISTICS ON THE BASIS OF MEASURED KINEMATICAL PARAMETERS. THEORY AND EXPERIMENT 335

7.1 Estimate of theoretical distribution of the dynamic pressure on dolphin's body surface in comparison to experimental data 335
7.1.1 The dynamic pressure caused by the body undulation 335
7.1.2 Dynamic pressure caused by the fluke oscillation 340
7.2 Thrust, hydrodynamic drag and coefficient of efficiency 346
7.2.1. The thrust 347
7.2.2 Distribution of thrust force and thrust along dolphin's body 359
7.2.3 Drag and efficiency coefficients 365
7.3. Ultimate speed of swimming 369
7.4. Body shape assessment for the dolphin and other cetaceans 373
7.5. Hydrodynamics of dolphin according to recent data 375
Brief conclusions 376

CONCLUSION 377

REFERENCES 379

PREFACE

The proposed book is the result of almost 40 years of the author's research. In the early 1960s of the 20th century there were started some studies on biohydrodynamics in the Acoustic Institute of the Academy of Sciences. It was the initiative of academician N. N. Andreev who was the head of these studies for about 10 years. Then the researches were carried on for almost 30 years in the Severtsev Institute of Ecology and Evolution of the Russian Academy of Sciences under the leadership of academician V. E. Sokolov. His wide knowledge and managerial talent helped to involve a lot of scientists from different cities of the former USSR in these studies. Consequently in our country there were obtained unique results in the field of biohydrodynamics, which beat everything that has been done in the world.

INTRODUCTION

The active studies of biohydrodynamics started in the middle 1930s when an English zoologist, James Gray, published his works (Gray, 1933; 1936). He noticed that dolphin swimming speed does not match the reserve of its muscle power. Having analyzed published data on dolphin swimming speed and their muscle power, Gray concluded that the reserve muscle power several times less than that necessary to provide the observed speed of swimming. This conclusion became known as Gray's paradox. He also proposed a hypothesis to explain this paradox. He hypothesized that dolphins could maintain laminar flow at speeds when laminar flow should become turbulent. He proposed a mechanism that postpones the transformation of laminar flow into the turbulent flow. Gray thought that actively swimming dolphin may have a favorable (negative) gradient of dynamic pressure on their body that causes a delay in the transformation of flow from laminar to turbulent flow. He thought that the negative gradient of dynamic pressure is generated by the fluke, which throws the water back while crating thrust.

Since this paradox was formulated, almost every experimental and theoretical study on biohydrodynamics has attempted to prove or disprove Gray's conclusions on these unique abilities of dolphins. It also attracted attention to fish swimming since most of fishes have the same mechanism of thrust generation. Researches expected to find the same interesting hydrodynamic peculiarities in swimming fish. Initially, theoretical studies were prevalent (e.g. Parry, 1949; Lighthill, 1960; Smith, Stone, 1961; Wu, 1961; Lavretyev, Lavretyev, 1962; Siekmann, 1962, 1963). Following these theoretical studies, experiments begin on fish (Bainbridge, 1963), dolphins (Lang, 1963, 1966a, 1966b; Lang, Daybell, 1963, Lang, Pryor, 1966, Lang, Norris, 1966) and then models were developed (Kelly, Rentz, Siekmann, 1964).

Most of the studies in that period were carried out in the UK and the USA. In the USSR, such efforts began ten years later with theoretical (Logvinovitch, 1970, 1972, 1973; Merkulov, 1970) and experimental studies (Babenko, Gnitetskyi, Kozlov, 1969; Pyatetskyi, 1970a, 1970б; Pyatetskyi, Savtchenko, 1969; Pyatetskyi, Kayan, 1971, 1972a, 1972б, 1975; Romanenko, 1972; Kozlov, Shakalo, 1973; Romanenko, Yanov, 1973; Yanov, Romanenko, 1972; Semenov, Babenko, Kayan, 1974).

In the USA, studies on dolphin hydrodynamic were almost completely ceased by 1965 – 1966 because of studies by Lang, (1963); Lang and Pryor, (1966) and Lang and Norris (1966). They measured dolphin swimming speed under the varying conditions and concluded that Gray's estimations were wrong. For the three decades passed since the publication of these works there were several articles (Webb, 1975; Yates, 1983; Fish, Hui, 1991; Fish, 1993), which revised Gray's conclusion. They proved the previous conclusion that there are not any mechanisms, which decrease hydrodynamic resistance in dolphins. However the analysis of these works showed some considerable mistakes,

which completely devaluated their conclusions. These works are analyzed in detail in chapter 7 of this book.

In the USSR the practice of the researches on biohydrodynamics differed from the one in other countries. Soviet scientists trusted Gray's studies and conclusions, so they made great efforts to find mechanisms, which reduced hydrodynamic resistance in dolphins. Not only biologists but also experts in hydromechanics took part in the researches (L. F. Kozlov; V. V. Babenko; E. V. Romanenko; V. P. Kayan; B. N. Semenov; V. M. Shakalo etc.). To study the fine structure of boundary layer on freely swimming dolphin and resilient features of dermal integument there were used direct methods of experiment. Wu (1972, 1973) there were obtained and published first proofs that dolphins have some mechanisms to control the boundary layer. Since then and till now in Russia and the former USSR states there have been carried out intensive researches, described in this book. Unfortunately for many years there has been no exchange of information between Russian and foreign scientists. The main reasons for this were the language barrier and secrecy, as well as prejudice of western scientists. As a result they knew nothing about the researches carried out in the USSR, and by now the scientists in the USA and other countries are 20-25 years behind of the scientists of the former USSR in the of studies of dolphins biohydrodynamics. We mean mainly experimental studies. As for theoretical studies, their level in the USA and UK is rather high.

In this book there is an attempt to critical analysis and systematic presentation of the results of the researches on swimming mechanisms in fish and cetacean (dolphin). Critical approach helped to unclose both strong and weak points of the theory, and to mark the questions still unexplored. The theory of slender body in three-dimensional definition made it possible to obtain relatively simply calculation formulas for estimation of energy and power characteristics of animal swimming. Small modifications make it possible to use this theory for the case of arbitrary amplitude swimming. This is persuasively shown in the work of Lighthill, 1971. The theory of recoil developed by Lighthill and his colleagues proved to be very fruitful, and helped to explain some peculiarities of the kinematics of fish, which swim like mackerel (Lighthill, 1960, 1970; Kambe, 1978).

It turned out that the theory of crescent shape tail fin did not sufficiently take into account some important peculiarities, such as the thickness and form of cross section of tail fin, location of its pitch-axis, aspect ratio, flexibility, and wide range of slopes to trajectory of movement, etc. These questions still need clarification.

On analyzing theoretical models of swimming we concluded that the law of body deformation in actively swimming fish and dolphin is the least known. Although many researchers used its variants based on qualitative observations for different numeric estimate. Moreover, practically all the empirical variants of the deformation law used by researches do not explain some peculiarities of fish and dolphin kinematics. And even lead to physical controversy in the marginal case, when phase velocity of propulsive wave approaches animal swimming velocity. In this case there appears a contradiction:

the thrust is negative and the coefficient of efficiency tends to negative infinity. But it is the knowledge of the true law of deformation, which allows the correct usage of the given theory to estimate swimming efficiency.

To overcome these difficulties it is necessary to make phase velocity of the propulsive wave of fish and cetacean dependant on coordinate in the coordinate system attached to animal body (Romanenko, 1980б). In other words we can not consider phase velocity of the propulsive wave a constant as all researchers did. The assumption that phase velocity depends on coordinate was proved during the experiments with dolphins (Romanenko, 1980a, 1986) and fish (Videler, Hess, 1984; Hess, Videler 1984).

The idea that phase velocity of propulsive wave depends on coordinate, which was proved experimentally, turned out to be very useful in theoretical analysis of distribution of dynamic pressure gradient on the body of actively swimming dolphin and in explanation of some experimental results. Such results are known from literature. They are: the data on fine structure of boundary layer on dolphin body (Romanenko, 1972), some peculiarities of cetacean body shape (for example: body elongation, convergence angle); measurements of tangential stresses in boundary layer; distribution of flow velocities in different points on animal body (Romanenko, 1986a), etc. These facts can be explained only on the basis of such dependence.

In the book there is formulated the law of deformation of the body of actively swimming dolphin, which takes into account the space alterations of phase velocity of locomotive wave. It allows obtaining calculating relations for estimation of hydrodynamic forces of propulsive system of dolphin and performing these estimations.

The similar law of body deformation is also proposed for fish. It helps to explain the experimental data obtained on three fish species (Bainbridge, 1963).

In this book considerable attention is paid to the base of statistical hydrodynamics, which is necessary to study the fine structure of boundary layer in biological objects.

There is given detailed description of methods and instruments for kinematic and biohydrodynamic researches. There is a chapter where some original results of experimental studies of kinematics and hydrodynamics of the Black Sea dolphins are represented. It is shown that on actively swimming dolphin there forms substantial negative gradient of dynamic pressure. It influences the fine structure of boundary layer, and increases critical Reynolds number, which defines the transition from laminar flow to turbulent one. For the first time the kinematics of the tail fin has been studied in detail. It is found that the near harmonic law characterizes the angle of fluke slope to horizontal axis but not angle of attack as it was supposed in the majority of mathematical models.

In the final chapter of the book there are given estimates of thrust and resistance coefficients of actively swimming dolphin, and the description of dolphin hydrodynamics in the light of modern scientific data.

There are interesting estimates of the marginal velocity of dolphin swimming, which take into account animal hydrodynamics and energy abilities. It turned out that these estimates fairly well match the measurements of the maximal swimming velocity.

The book does not claim the full representation of every theoretical model and experimental work. In particular, there is no mention of the theory of boundary layer on deformed bodies; the sliding of cetacean of waves, the estimates of hydrodynamic characteristics of aquatic animal on the basis of their bioenergetical abilities; the theory of turbulent boundary layer on damping surface, which can partially or wholly absorb pulsation energy in layer.

All these issues are discussed in detail in the books of L. F. Kozlov (1983) and S. V. Pershin (1988).

While writing the survey chapter we met some technical difficulties concerning arbitrary denotations. Each survey is inevitably implies an alternative: either to introduce a unified system of denotations or to stick to the original denotations of the discussed work. In the proposed book the second variant has been chosen. We kept the denotations of the discussed works (but rare exceptions). This variant was chosen in order to help the reader to get acquainted with the originals. It can prove to be inevitable if the reader likes to study thoroughly the theory of one issue or another. As a matter of fact the proposed book does not aim the comprehensive representation of all theoretical approaches. It only gives problem definitions and main conclusions, leaving the details for further studies of the originals. Such an approach inevitably leads to ambiguous denotations.

The book is intended for scientists and university students, who are interested in the problems of biohydrodynamics.

The author is sincerely grateful to academician of the Ukrainian Academy of Sciences G. V. Logvinovitch, S. G. Pushkov, professor K. A. Naugolnikh for the interest in the work and valuable advice; V. A. Tchikalkin, V. A. Tarchevskaya, O. V. Savinkin, V. G. Yanov for the help in carrying out the experiments with dolphins; and also T. M. Borsheva and T. N. Sidorova for the essential help in the preparation of the manuscript and illustrations for print. The author is sincerely grateful also to those who translated this book: T. E. Abrashkina, M. K. Viktorova , T. V. Kitaina, O. A. Shokhina.

The work on the book has been carried out with the financial support from Russian Foundation for Basic Research.

CHAPTER 1. THEORETICAL MODELS OF SWIMMING

Theoretical investigations of the mechanisms explaining the swimming of fishes and dolphins were addressed in a great number of publications (Shuleykin, 1968; Logvinovitch, 1969; Lighthill, 1975; Kozlov, 1983; Romanenko, 1986). It would be more accurate to say that these papers analyse the mechanism of swimming by means of wave movements irrespective of whom they relate to - fishes or dolphins, because in both the principle of thrusting is the same. A retrospective look at the history of the problem helps tracing the evolution of the ideas and methods of investigations on the swimming mechanisms in fishes and dolphins. Some of the above papers are now only of historical interest, to a certain extent. This is true of investigations advancing rather simplified suggestions which permit only very general understanding of the principles of thrusting (Smith, Stone, 1961; Lavrentyev, Lavrentyev, 1962; Shuleykin, 1968). Certain publications (Lighthill, 1975; Kozlov, 1983; Romanenko, 1986 and other) contain a more or less completed mathematical analysis of the problem, and their simplifications seem logical. These authors present design formula, providing for experimental verifications. Such papers, in their turn, can be divided into two categories. Some of them consider the problem to be planar, others - as a spatial one. The spatial approach to such studies is essentially more interesting because it can more adequately reflect the real conditions of swimming in fishes and in dolphins.

1.1. The planar approach to the problem

In this case, by the planar pattern of the problem we mean the movement of an infinitely extended profile (along the third coordinate). With that, the parameters of the movement vary only in terms of two coordinates. Planar problems are also called two-dimensional ones.

1.1.1. The theory of fine profile with undulating oscillations

We shall begin with the discussion of Siekmann's (1962) and Wu's (1961). papers. These authors were the first to strictly solve the two-dimensional problem of small oscillations of the thin wing within a stationary flow. These two publications are physically equivalent, though they do differ in details. They are both based on the previous studies of the behaviour of the thin wing within an non-steady-state flow, which were advanced by Theodorsen (1935) and Schwarz (1940).

Siekmann and Wu considered the behaviour of the flexible thin wing making small transverse oscillations and longitudinally streamlined by the stationary two-dimensional flow of an incompressible ideal liquid.

Siekmann developed Schwarz's theory (1940) of boundary and free vortexes. In that theory, thin wing is represented by the distribution of boundary vortexes and the trace - by free ones. Wu used the theory of Theodorsen (1935) but instead of the potential of velocities he employed that of accelerations.

Fig.1.1 displays the scheme from Siekmann's paper. The plate P_0 (the skeleton line is marked as P) extends from $x = -1$ to $x = +1$. In the general case, the transverse shifts of the wing are given by the function

$$y = h(x,t), \quad -1 \le x \le +1, \tag{1.1}$$

It is suggested that

$$|y| << 1, \quad \left|\frac{\partial y}{\partial x}\right| << 1, \quad \left|\frac{\partial y}{\partial t}\right| << 1. \tag{1.2}$$

In further consideration, the wing is replaced by circulation. The author believes that from the tail part of the wing there runs off a vortex sheet situated within the wing $y = 0$. With that, he thinks that Zhukovskii's postulate about the finitude of transverse velocity is effected on the back end of the wing.

There are concrete calculations for harmonic oscillations of the wing. The main hydrodynamic forces are computed by means of the following relations.

The lift

$$L = \int_{-1}^{1} \Delta p(x,t)dx. \tag{1.3}$$

The moment with respect to 0

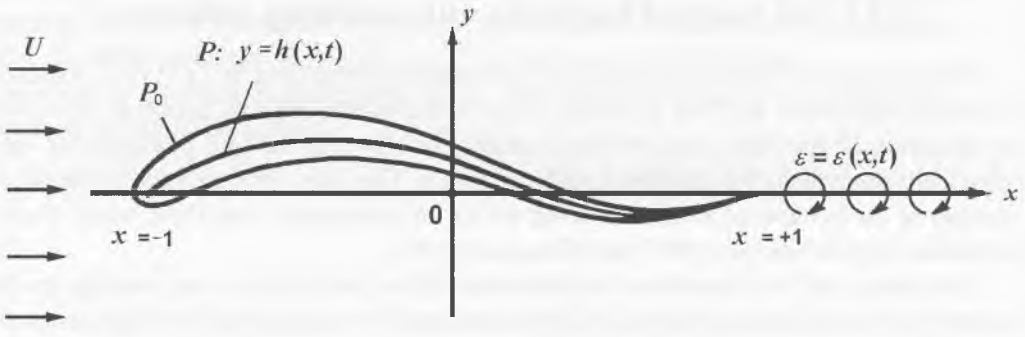

Fig. 1.1. Flexible solid plate immersed in a uniform parallel flow with velocity U from the left. (Redrawn from Siekmann, 1962).

$$M = \int_{-1}^{1} x\Delta p(x,t)dx. \tag{1.4}$$

The thrust

$$T = \int_{-1}^{1} (\Delta p)_R \left(\frac{\partial h}{\partial x}\right)_R dx + T_s. \tag{1.5}$$

The power input

$$P = -\int_{-1}^{1} (\Delta p)_R \left(\frac{\partial h}{\partial t}\right)_R dx. \tag{1.6}$$

In the relationships cited above Δp is the distribution of pressure on the wing derived by the wing theory with the help of Theodorsen's function, $(\Delta p)_R$, $\left(\frac{\partial h}{\partial x}\right)_R$ and $\left(\frac{\partial h}{\partial t}\right)_R$ mean the real part of the values, T_s is the suction force at the front edge of the wing.

The hydrodynamic efficiency was found as the relation

$$\eta = \frac{\overline{TU}}{\overline{P}}. \tag{1.7}$$

Here, the dash above means the time averaging.

The final expression for the thrust, the capacity and the efficiency are very bulky and include the special functions of Theodorsen and of Bessel.

Siekmann made his calculation for the case when the wing makes oscillations following the law

$$y = (c_0 + c_1 x + c_2 x^2)\cos(\alpha x - \beta t). \tag{1.8}$$

Here, a is the wave number equalling $\alpha = \frac{2\pi}{\lambda}$, and $\beta = \frac{2\pi}{T_0}$ is the circular frequency, λ is the length of the propulsive wave, T_0 is the oscillation period.

Figs. 1.2 - 1.4 show the calculations of the thrust coefficient (the solid lines) for three laws of the wing deformations: with a constant amplitude on the wing length, with a linearly increasing amplitude and with that increasing by the square law. The latter case

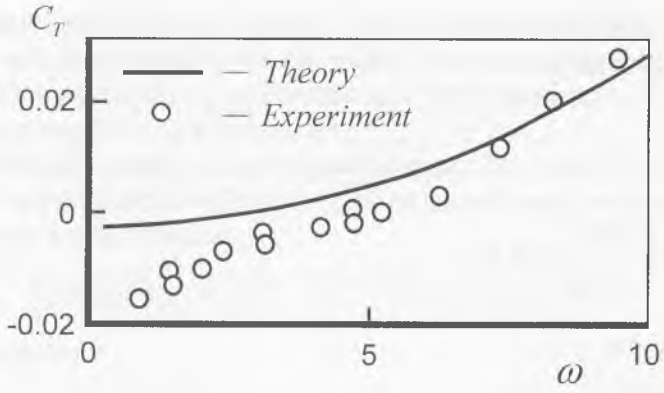

Fig. 1.2. Thrust coefficient *vs.* reduced frequency for constant amplitude. (Redrawn from Siekmann, 1962).

is regarded to be most corresponding to the real law of deformation in the fish body. The so-called reduced frequency is thought to be the argument in these graphs.

$$\omega = \frac{\beta}{U}. \tag{1.9}$$

It is noteworthy that the thrust coefficient equals zero when the reduced frequency is

$$w = a, \tag{1.10}$$

which corresponds to the case when the propulsive wave velocity equals the velocity of the flow of liquid

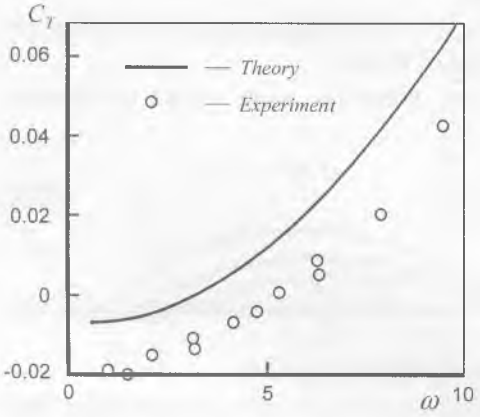

Fig. 1.3. Thrust coefficient *vs.* reduced frequency for linear amplitude function. (Redrawn from Siekmann, 1962).

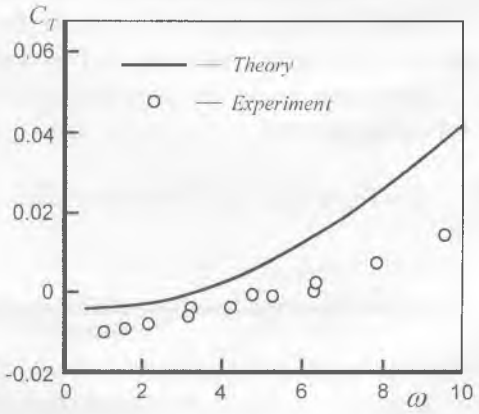

Fig. 1.4. Thrust coefficient *vs.* reduced frequency for quadratic amplitude. (Redrawn from Siekmann, 1962).

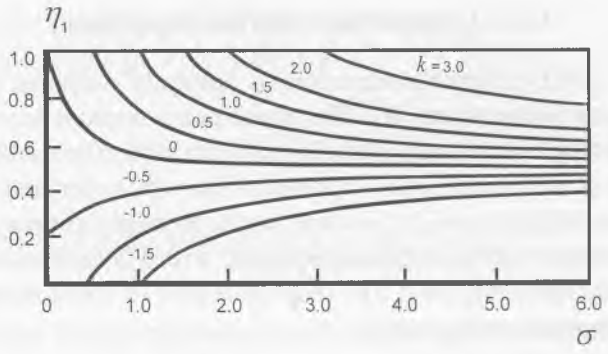

Fig. 1.5. Swimming efficiency for a uniform wave amplitude. (Redrawn from Wu, 1961).

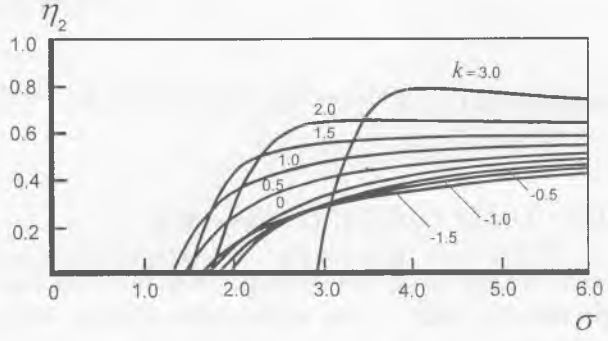

Fig. 1.6. Swimming efficiency for a linearly varying wave amplitude. (Redrawn from Wu, 1961).

$$C = U. \tag{1.11}$$

Here, it is again very useful to emphasize that the calculations were effected on the wing with its thickness striving to zero.

Figs. 1.5 and 1.6 (both are taken from the paper of Wu (1971)) demonstrate the efficiency as depending on the reduced frequency in cases of the constant and of the linearly increasing amplitudes respectively (σ in the paper of Wu is equivalent to ω in that of Siekmann, like α and k). The negative values of k correspond to the propulsive wave spreading from the tail to the head of the wing.

A similar problem was considered in paper (Smith, Stone, 1961). However, because the authors disregarded the vortex sheet, results were wrong. The authors of paper (Pao, Siekmann, 1964) pointed out these mistakes and introduced their own corrections.

1.1.2. Comparison with the experiment

Paper (Kelly, 1961) describes experiments specially designed for verifying the theoretical results of Sikmann and Wu. The experiments employed a metal and a rubber plates of the following dimensions: 30 cm long, 10 cm wide. The rubber plate was 3 mm thick. The plates were placed into a stationary flow of water and were induced to oscillations by special plungers. In this way, it was possible to provide the plate with three regimes of motion: with a constant amplitude, with a linearly increasing amplitude and with a squarely increasing one. The respective laws of transformation of the plates were regarded as some running waves

$$h_1(x,t) = \frac{1}{12}\cos(\omega t - kx), \tag{1.12}$$

$$h_2(x,t) = \frac{x}{16}\cos(\omega t - kx), \tag{1.13}$$

$$h_3(x,t) = (0.023 - 0.028x + 0.035x^2)\cos(\omega t - kx). \tag{1.14}$$

The last formula is thought to be best corresponding to the motion of the salmon.

In another experimental study of the same author (Kelly, 1961) the last law of deformation is regarded as

$$h_3(x,t) = (0.023 + 0.042x + 0.035x^2)\cos(\omega t - kx). \tag{1.15}$$

The velocity of the flow could vary from zero to 0.9 ms^{-1}.

The results of the thrust measurements are presented by circles in Figs. 1.2 - 1.4. It came out that in all three cases the measured values of thrust were smaller than the calculated ones. This can be attributed to the fact that the theory disregards the surface friction on the plate and the respective losses of expenditures.

1.1.3. The profile in the time-variable flow

Paper (Wu, 1971) considers the problem similar to that discussed in papers (Wu, 1961; Siekmann, 1962) but here for the case of the time-variable velocity of swimming (the velocity of the onrunning flow $U = U(t)$). With that, the motion begins at the moment $t = 0$. The scheme explaining the formulation of the problem is similar to that in Fig.1.1. The problem is solved by the technique based upon Prandtl's potential of accelerations.

The following expressions were derived for the thrust and the kinetic energy of liquid

$$T = \frac{1}{2}\pi\rho\left(a_0 + b_0 - \dot{\beta}_0\right)\left(a_0 - b_1 + \dot{\beta}_1\right) + \dot{\beta}_0\dot{\beta}_1 - \frac{d}{dt}\sum_{n=1}^{\infty}\beta_n\left(b_{n-1} - b_{n+1}\right) \qquad (1.16)$$

and

$$E = \frac{1}{2}\pi\rho\left[U(t)(a_0 + b_0)(b_1 - a_0) + \frac{d}{dt}\sum_{n=1}^{\infty}\frac{1}{4n}\left(b_{n-1} - b_{n+1}\right)^2\right]. \qquad (1.17)$$

The expression for the capacity can be obtained by using the law of energy conservation

$$P = TU + E. \qquad (1.18)$$

In the above expression

$$a_0(\tau) = -\int_0^{\tau}\left[b_0(\tau') + b_1(\tau')\right]H(\tau - \tau')d\tau' + b_1(\tau), \qquad (1.19)$$

$$b_n(\tau) = \frac{2}{\pi}\int_0^{\pi} v(x, t(\tau))\cos n\theta d\theta \qquad (x = \cos\theta, \quad n = 0,1,2\ldots), \qquad (1.20)$$

$$H(\tau) = \frac{1}{2\pi i}\int_{\varepsilon - i\infty}^{\varepsilon + i\infty} e^{s\tau}\tilde{H}(s)ds \quad (\varepsilon > 0), \qquad (1.21)$$

$$\tilde{H}(s) = \frac{K_1(s)}{K_0(s) + K_1(s)}.$$

K_0 and K_1 are modified Bessel's functions of the second type

$$\beta_n(t) = \frac{2}{\pi}\int_0^{\pi} h(x, t)\cos n\theta d\theta \qquad (x = \cos\theta; \quad n = 0,1,2,\ldots), \qquad (1.22)$$

$$\dot{\beta}_n = \frac{d\beta_n(t)}{dt}, \quad \tau(t) = \int_0^{t} U(t)dt \quad (t \geq 0). \qquad (1.23)$$

The obtained expressions were used to estimate the motion of the wing in two particular cases:

1. the motion begins at the moment $t = 0$ and continues at constant velocity of the onrunning flow U;

2. the motion begins at the moment $t = 0$ and continues with a constant acceleration.

Let us discuss both cases one after the other.

In the first case, the motion is described by the expression

$$h(x,t) = h_1(x)e^{i\omega t}, \quad (-1 \le x \le 1, \quad t > 0) \tag{1.24}$$

and $h = 0$ for $t < 0$. U = const, Hence, $\tau = Ut$. Then,

$$v(x,t) = v_1(x)e^{i\omega t} \quad (-1 \le x \le 1, \quad t > 0), \tag{1.25}$$

$$v_1(x) = U\left(\frac{d}{dx} + i\sigma\right)h_1(x), \tag{1.26}$$

$\sigma = \omega/U$ and $v = 0$ for $t < 0$

The estimates show that for small values of τ

$$a_0(t) = b_1 - \frac{1}{2}(b_0 + b_1), \tag{1.27}$$

and for very large ones -

$$a_0(t) = b_1 - \Theta(\sigma)(b_0 + b_1), \tag{1.28}$$

where $\Theta(\sigma) = \dfrac{K_1(i\sigma)}{K_0(i\sigma) + K_1(i\sigma)} = F(\sigma) + iG(\sigma) -$ is Theodorsen's function.

Expressions (1.16) and (1.17) may be used to compute T, E and P. These values prove to be asymptotically close to stationary ones already at $\tau > 10$, i.e. after the body moves to a distance measured only by five chords, if σ is not very small.

In the second case, the motion is described by the expressions.

$$U(t) = \alpha t (\alpha > 0, t > 0) \tag{1.29}$$

and

$$h(x,t) = \frac{1}{2}\beta_0(t) + \sum_{n=1}^{3} \beta_n(t)\cos\theta (x = \cos n\theta, 0 < \theta < \pi). \tag{1.30}$$

Here, the cubic law of deformation is accepted for the wing. Hence,

$$v(x,t) = \frac{\partial h}{\partial t} + \alpha t \frac{\partial h}{\partial x} = \frac{1}{2} b_0(t) + \sum_{n=1}^{3} b_n(t)\cos n\theta, \tag{1.31}$$

$$\tau = \int_0^t U(t)dt + \frac{1}{2}\alpha t^2 \tag{1.32}$$

and

$$b_n = \dot{\beta}_n + O(t^3) \qquad (n = 0,1,2,3),\ O(t^3) \text{ is the remainder of } b_n. \tag{1.33}$$

It is suggested that for small values of t we can write

$$\beta_n(t) = \sum_{m=2}^{\infty} \beta_{nm} t^m (n = 0,1,2,3). \tag{1.34}$$

As a result, we get

$$T = \tfrac{1}{2}\pi\rho(\beta_{02}{}^0 + \beta_{12}^0 - 4\beta_{02}\beta_{12})t^2 + \\ + 3\left[\beta_{03}(\beta_{02} - 3\beta_{12}) + \beta_{13}(\beta_{12} - \frac{5}{3}\beta_{02})\right]t^3 + O(t^4), \tag{1.35}$$

$$P = \frac{1}{2}\pi\rho\left(\frac{2}{3}\beta_{02}^2 + \frac{1}{2}\beta_{12}^2\right)t + 3\left[\beta_{02}\beta_{03} + \frac{3}{4}\beta_{12}\beta_{13}\right]t^2 + O(t^3). \tag{1.36}$$

It is noteworthy that the thrust increases like t^2, and with small value of t it is very small. The capacity is increasing like t, because the capacity expenditures after the onset of the motion are already quite obvious, while practically the thrust is still absent.

A qualification of the optimal law of deformation at the initial stage of motion shows that

$$\frac{\beta_{12}}{\beta_{02}} = -1.24. \tag{1.37}$$

With this condition, the thrust is maximum at some fixed power.

The expression of the vortex sheet intensity in the trace can be derived in the following way

$$\gamma(1,t) = \frac{1}{2}\frac{\pi}{\sqrt{\alpha}}\left[(\beta_{02} + \beta_{12}) + \frac{6}{\pi}(\beta_{03} + \beta_{13})t + O(t^2)\right]. \tag{1.38}$$

One can see that right after the start (with $t \to 0$) there begins an initial vortex from the back edge.

1.1.4. The thickness of the oscillating profile as affecting the hydrodynamic forces induced by this profile

The next group of papers (Uldrick, Siekmann, 1964; Reece, Uldrick, Siekmann, 1964; Uldrick, 1968) deals with the impact rendered by the thickness of the oscillating profile upon the hydrodynamic forces, developed by this profile, and with their efficiency. The problem is still considered as two-dimensional. Fig.1.7 displays a scheme explaining the formulation of the problem. The scheme is taken from paper (Uldrick, 1968). The system of coordinates is linked with the profile. Unlike the papers discussed above (Siekmann, 1962; Wu, 1961), these ones (Uldrick, Siekmann, 1964; Reece, Uldrick, Siekmann, 1964; Uldrick, 1968) employ the theory of the complex pattern of the flow streamlining the profile. The pattern is variable in computations. Instead of studying the pattern of streamlining over the profile, the authors examine the streamlining over a circular cylinder by using the method of conformal transformation (Fig.1.8). From complex variables $z=x+iy$ in the plane section of the profile the authors transit to complex variables $\zeta = \xi + i\eta$ in the circular plane where the profile is transformed. The expression for the complex potential of velocities, satisfying the stationary boundary conditions, is accepted as

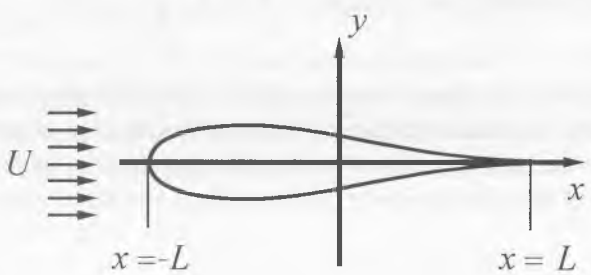

Fig. 1.7. Profile plane (z – plane). (Redrawn from Uldrick, 1968).

$$F_0(\zeta) = \frac{U}{2}\left(\zeta + \frac{b^2}{\zeta}\right), \tag{1.39}$$

where b is the radius of the circle.

As the profile, the authors take the symmetric profile of Zhukovskii situated along the axis x from -L to +L and, after the transformation, described by the following expression

$$z = f(\zeta) = \frac{1}{2}\left[\zeta - \varepsilon + \frac{(b-\varepsilon)^2}{\zeta - \varepsilon}\right] + E, \tag{1.40}$$

where ε is a small positive value characterising the profile thickness, while

$$0 \le \varepsilon \le b \tag{1.41}$$

and

$$E = L - b + e. \tag{1.42}$$

The displacements of the profile are given as

$$D(z,t) = iH^*(x)e^{i\omega t}, \tag{1.43}$$

where $i = \sqrt{-1}$ and the symbol i only shows that the displacements are perpendicular to the axis x; H*(x) is a complex value.

Within the frameworks of the theory of small perturbations the total potential of velocities can be presented as the total of three components

$$F = F_0(\zeta) + F_1(\zeta,t) + F_2(\zeta,t), \tag{1.44}$$

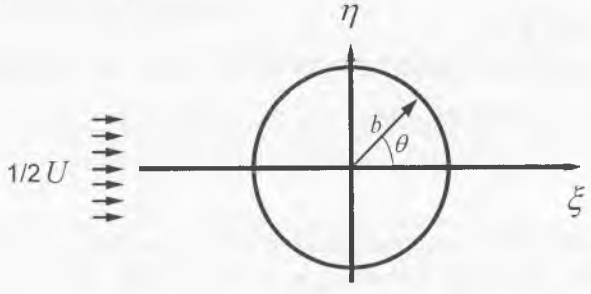

Fig. 1.8. Circle plane (ζ – plane). (Redrawn from Uldrick, 1968).

where the first component is revealed by the expression (1.39). The second component characterises the complex potential of velocities, satisfying the non-steady-state boundary conditions, and looks as

$$F_1(\zeta,t)=\frac{Ue^{i\omega t}}{2\pi}\int_0^{2\pi}G(\vartheta)\log(\zeta-be^{i\vartheta})^2 bd\vartheta, \tag{1.45}$$

where

$$G(\vartheta)=-\mathrm{Re}\frac{1}{b^2}\left\{\frac{dz}{d\vartheta}\left(i\sigma H_1^*(\vartheta)-\frac{\sin\vartheta}{\left|f'(be^{i\vartheta})\right|^2}\frac{dH_1^*(\vartheta)}{d\vartheta}\right)\right\}_{z=f(be^{i\vartheta})}. \tag{1.46}$$

Here, Re demonstrates the real part of the complex value,

$$\sigma=\omega b/U \tag{1.47}$$

and

$$H_1^*(\vartheta)=H^*(x). \tag{1.48}$$

The third component is the complex potential of velocities and is related with the vortex sheet in the trace. It is written as follows

$$F_2(\zeta,t)=\frac{i\gamma_0}{2\pi}\int_b^{\infty}\log\frac{\zeta-\xi_0}{\zeta-b^2/\xi_0}e^{i\omega(t-\tau)}f'(\xi_0)d\xi_0, \tag{1.49}$$

where

$$\gamma_0=\frac{2U\sum_{n=1}^{\infty}P_n}{\frac{1}{2\pi b}\int_b^{\infty}\frac{\xi_0+b}{\xi_0-b}e^{-i\omega\tau}f'(\xi_0)d\xi_0}, \tag{1.50}$$

$$\tau=\int_{x_\tau}^{x}\frac{dx_0}{F_0^{\circledcirc}(\zeta_0)/f'(\xi_0)}=\int_b^{\zeta_0}\frac{\left|f'(\xi_0)\right|^2}{F_0^{\circledcirc}(\xi_0)}d\zeta_0, \tag{1.51}$$

$$P_n = \frac{(b_n - c_n)}{b^2}. \tag{1.52}$$

The values b_n and c_n can be calculated from the expression (1.52) by the reverse transform of Fourier, because they may be presented as

$$G(\vartheta) = 2\sum_{n=1}^{\infty} P_n \sin n\vartheta = 2\sum_{n=1}^{\infty} \frac{1}{b^2}(b_n - c_n)\sin n\vartheta. \tag{1.53}$$

The hydrodynamic pressure affecting the profile can be found by using the non-steady-state equation of Bernoulli. As a result, the pressure distribution can be written as

$$\Pi(\vartheta, t) = -\rho \operatorname{Re}\left(\frac{\partial F}{\partial t} + \frac{1}{2|f'|^2} \frac{\overline{\partial F}}{\partial \zeta} \frac{\partial F}{\partial \zeta} \right)_{\zeta = be^{i\vartheta}}. \tag{1.54}$$

Here, Re, as before, demonstrates the real part, the dash above - the complex conjunction.

The force and the moment exercised by the profile can, as usual, be integrated from the pressure distribution along the profile length. Here, the expressions for the force, the moment, the thrust, the capacity and the kinetic energy of liquid are not cited because of their bulkiness.

The numerical estimates are made for the profile in which the law of deformation is expressed by (1.43) and the amplitude function looks as

$$H^*(x) = (d_0 + d_1 x + d_2 x^2)e^{-i\alpha x}, \quad (-L \le x \le L). \tag{1.55}$$

This law reveals a wave running along the profile from the point $x = -L$ towards the point $x = L$. The amplitude of the latter increases according to the expression (1.55). For the coefficients d_0, d_1 and d_2 the authors accept the following values

$$d_0 = 0.023,\ d_1 = 0.042,\ d_3 = 0.034. \tag{1.56}$$

Fig. 1.9 demonstrates the thrust coefficient determined by the expression

$$C_T = \frac{T}{\pi\rho U^2}, \tag{1.57}$$

where T is the thrust depending on the reduced frequency for different values of the profile thickness at $\alpha = \pi$. One can see that the thrust is slightly decreasing with the

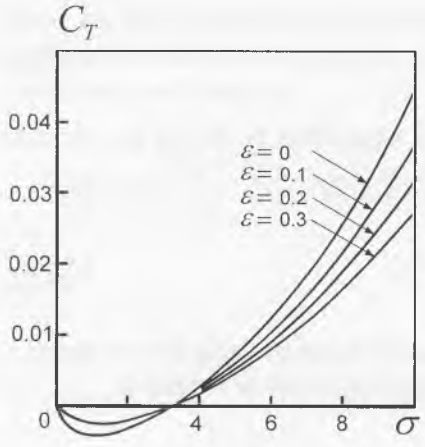

Fig. 1.9. Thrust coefficient *vs.* reduced frequency. (Redrawn from Uldrick, 1968).

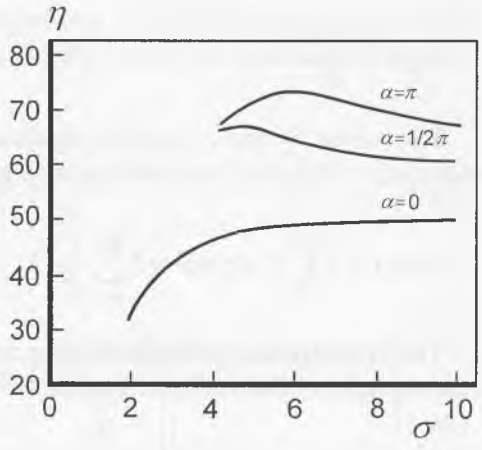

Fig. 1.10. Hydrodynamic efficiency *vs.* reduced frequency. (Redrawn from Uldrick, 1968).

increasing profile thickness. A similar picture is observed in the power coefficient found by the expression

$$c_P = \frac{P}{\pi\rho U^3}, \tag{1.58}$$

where P is the power spent on actuating the profile.

Fig.1.10 shows the dependence between the hydrodynamic efficiency and the reduced frequency for various values of the wave number α (0, $1/2\pi$ and π) at $\varepsilon = 0.2$. It is clearly seen that the efficiency increases with the increase in α.

Fig. 1.11 also presents the dependence between the efficiency and the reduced frequency at $\alpha = 0$, but here the parameter is the value ε. It comes out that the effectiveness of the oscillating profile increases when its thickness grows.

The paper compares numerical estimates with the results of special experiments. The experimental profile corresponded to the theoretical one and was made of rubber. Fig.1.12 demonstrates the experimental data as compared with the theoretical ones.

1.1.5. The value of thrust, caused by the two-dimensional thin platelet, as affected by the free surface of liquid

Paper (Reece, Uldrick, Siekmann, 1964) examines another very important problem, namely that of the impact rendered by the free surface (in the general case - disturbed surface) on the value of thrust in the thin plate oscillating under this surface. The scheme explaining the problem is presented in Fig.1.13.

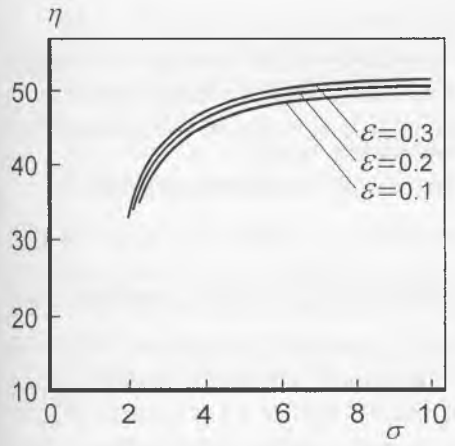

Fig. 1.11. Hydrodynamic efficiency *vs.* reduced frequency. (Redrawn from Uldrick, 1968).

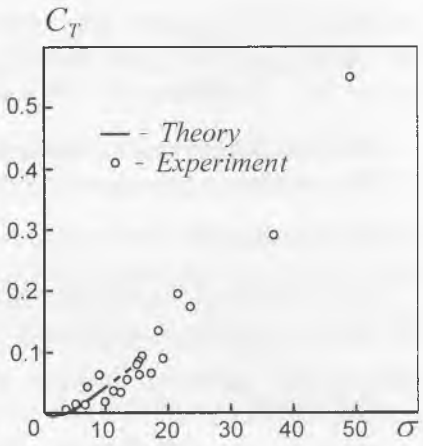

Fig. 1.12. Thrust coefficient *vs.* reduced frequency. (Redrawn from Uldrick, 1968).

The thin plate with undulating oscillations is situated along the axis x in the section from $x = -1$ to $x = +1$. The plate is deepened beneath the free surface to the value D. The flow runs on the plate towards the positive values of the axis x at the velocity U. The deformation of the plate is determined by the equation

$$y = Y(x,t), \; -1 \leq x \leq +1. \tag{1.59}$$

It is suggested that the displacements of the plate are small as compared with the semichord of the plate, i.e.

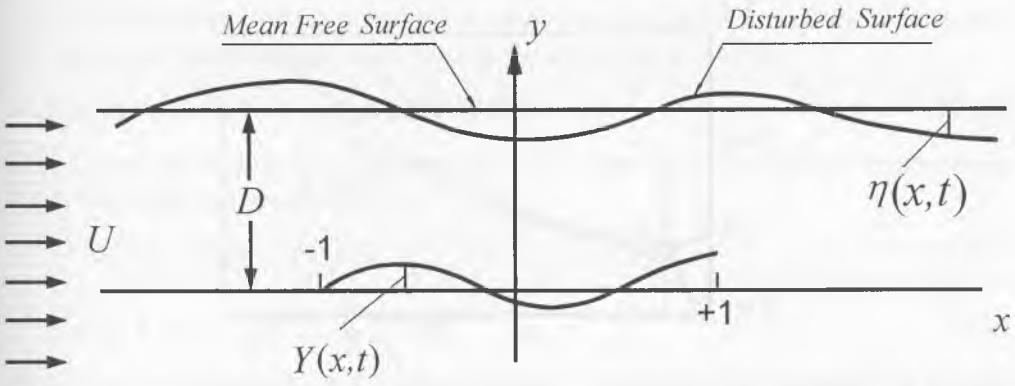

Fig. 1.13. The flexible plate. (Redrawn from Reece, Uldrick, Siekmann, 1964).

$$|Y| 7 << 1, \left|\frac{\partial Y}{\partial x}\right| << 1, \left|\frac{\partial Y}{\partial t}\right| << 1 \tag{1.60}$$

The free surface may be subjected to perturbations like $\eta(x, t)$.

The problem is formulated for the case of a periodically oscillating plate, i.e.

$$Y(x, t)=H(x)e^{i\omega t}. \tag{1.61}$$

In the course of the experiment the plate is substituted by a vortex circulation with its intensity varying in accordance with the law

$$\gamma = \bar{\gamma}(x)e^{i\omega t}, \quad -1 \le x \le 1. \tag{1.62}$$

When the plate is moving, the vortex sheet from its sharp back edge goes off into the trace and presumably remains in the plane $y = 0$. The intensity of the vortex sheet in the trace can be presented as

$$\varepsilon(x,t)= - ik\Gamma e^{i\omega t} e^{ik(x-1)}, \quad x \ge 1. \tag{1.63}$$

Here, $k = \omega/U$ is the reduced frequency and

$$\Gamma = \int_{-1}^{1} \bar{\gamma}(x)dx. \tag{1.64}$$

Further on, as usual, the potential of velocity Φ is introduced, satisfying the equation of Laplace and certain boundary conditions on the plate and the free surface. Then the pressure distribution on the plate is found, as well as the hydrodynamic forces.

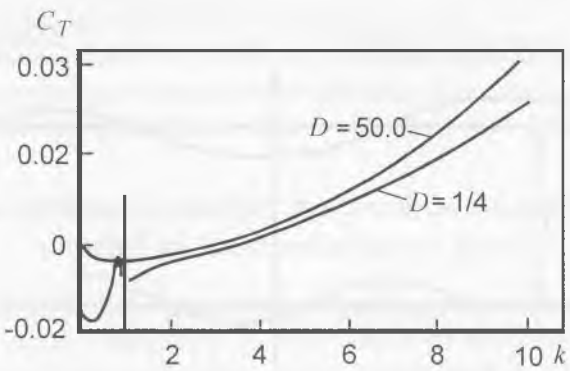

Fig. 1.14. Thrust coefficient *vs.* reduced frequency for quadratic amplitude function. (Redrawn from Reece, Uldrick, Siekmann, 1964).

Fig. 1.14 shows the calculated dependence between the thrust coefficient and the reduced frequency for two values of deepening. In one case (the upper curve) the deepening equals 50 semichords, in the second case D - 1/4 semichord. The law of deformation for the plate is accepted as

$$H(x)=(c_0+c_1x+c_2x^2)e^{-\alpha x} \tag{1.65}$$

at $c_0 = 0.023$; $c_1 = 0.042$; $c_2 = 0.034$ and $\alpha = \pi$. One can see that the impact of the free boundary of liquid is significant only when the plate is situated directly beneath this boundary. But even in this case such impact is obvious only at very small and very large values of the reduced frequency. It is characteristic that within the range of low values of the reduced frequency this impact is particularly essential, beginning with a certain critical frequency $k = 0.8935$. Within the range of zero values of the reduced frequency, one sees the wave resistance due to the impact of the free surface.

1.1.6. The possibility of animals' intake of energy from the wave flow

Some observations demonstrate that, under certain conditions, animals (fishes, birds) seem to move in such a way as if the part of the energy, necessary for their motion, is borrowed from the environment. For example, when in turbulent rivers we see salmons striving to their spawning areas, their movement does seem to depend much on the velocity of the counterflow, though the resistance to their motion should sharply increase when the flow velocity grows. Seagulls can make long flies over the turbulent surface of water and do not seem to be spending particularly great energy. These observations encouraged scientists to address the theoretical problem of the animals' possible borrowing of energy from the environment when there are optimal relationships between the animal's kinematics and the wave parameters in the onrunning flow. Paper (Wu, Chwang, 1975) examines a simplified physical problem about oscillations of the two-dimensional carrying surface (of the wing) in the wave flow. The scheme of the wing motion is displayed in Fig.1.15. The onrunning flow has a constant velocity U. Besides, a simple transverse wave is spreading in the flow towards the axis x. The velocity of this transverse wave towards the axis looks as

$$V_0(x, t) = \varepsilon U \sin(kx - \omega t) = i\varepsilon U e^{i(\omega t - kx)}. \tag{1.66}$$

Here, ε is a scale multiplier regarded to be small. Under such conditions, the movement of the thin wing can be described as

$$y = h(x,t) = y_h + y_p, \quad -1<x<1; \tag{1.67}$$

$$y_h = (\xi_1 + i\xi_2)e^{i\omega t}, \; y_p = (\xi_3 + i\xi_4)xe^{i\omega t}, \tag{1.68}$$

where y_h is the heaving motion of the wing and y_p is the pitching motion. The motion amplitudes can be presented as

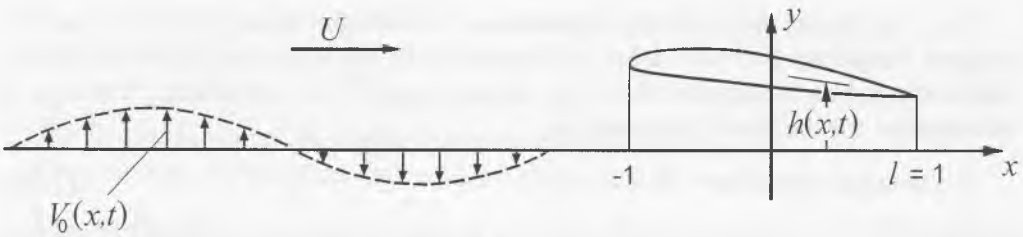

Fig. 1.15. A schematic representation of the wing in a wavy stream. (Adopted from Wu, Chwang, 1975).

$$\xi_h = (\xi_1^2 + \xi_2^2)^{1/2}, \quad \xi_p = (\xi_3^2 + \xi_4^2)^{1/2}, \tag{1.69}$$

and the respective phases as

$$\alpha_h = arctg\left(\frac{\xi_2}{\xi_1}\right), \alpha_p = arctg\left(\frac{\xi_3}{\xi_4}\right). \tag{1.70}$$

The wing is believed to be oscillating with the same frequency as the flow. The problem of the wing oscillations in stationary flows was discussed in several papers (Wu, 1971; Lighthill, 1970). Therefore, without going into too many details, the solution of the problem can be written as the expression for the density distribution of the lifting power on the wing

$$\mathcal{L}(x,t)=p^-(x,t)- p^+(x,t), \quad |x| < 1. \tag{1.71}$$

With this, the respective boundary conditions on the wing and in the trace are regarded to be accomplished.

The instantaneous values of the lifting power and of the moment in respect to the middle of the chord look as

$$L=\int_{-1}^{1} \mathcal{L}(x,t)dx=\pi\rho U^2\{a_0-b_1-b_0 i\sigma/2+2\varepsilon(1-\sigma/\chi)J_1(\chi)\}e^{i\omega t}, \tag{1.72}$$

$$M=-\int_{-1}^{1} x\mathcal{L}(x,t)dx=(\pi\rho U^2/2)\{a_0+b_1 i\sigma/4+2i\varepsilon(1-\sigma/\chi)J_2(\chi)\}e^{i\omega t}, \tag{1.73}$$

where

$$v(x) = \frac{V(x,t)}{U} e^{i\omega t} = \frac{b_0}{2} + b_1 x, \tag{1.74}$$

$$a_0 = b_1 - (b_0 + b_1)\Theta(\sigma) - 2\varepsilon[W_1(\chi, \sigma) - i\, W_2(\chi, \sigma)], \tag{1.75}$$

$$\Theta(\sigma) = K_1(i\sigma)/[K_0(i\sigma) + K_1(i\sigma)] = F(\sigma) + iG(\sigma), \tag{1.76}$$

$$W_1 - iW_2 = J_1(\chi)\,[1 - \Theta(\sigma)]. \tag{1.77}$$

Here, $\Theta(\sigma)$ is Theodorsen's function of the frequency, J_n is Bessel's function of the first type, K_n is Bessel's modified function of the second type, χ is the wave number. The distribution of forces on the wing is displayed in Fig.1.15.

Using the expressions (1.72) and (1.73), it is easy to compute the thrust

$$T = L\left(\frac{\partial h}{\partial x}\right) + S, \tag{1.78}$$

the power necessary to support the motion

$$P = -Ly_h + M\left(\frac{\partial y_p}{\partial x}\right) \tag{1.79}$$

and the kinetic energy transferred to the liquid per unit of time

$$E = P - TU. \tag{1.80}$$

Here, S is the suction force on the anterior edge of the wing.

It is more convenient for the analysis to calculate not the very expressions (1.78) - (1.80) but the respective coefficients

$$c_p = \mathrm{Re}\left\{-i\sigma\left[\langle v_1 f_1\rangle - 2\varepsilon(J_1 + iJ_0)\right]\langle g_1, \tilde{h}\rangle + 2\varepsilon\left(\frac{\sigma}{\chi}\right)\langle v_1 g_2\rangle\right\}, \tag{1.81}$$

$$c_E = \mathrm{Re}\left\{B\left|\langle v_1 f_1\rangle\right|^2 + 2\varepsilon\left[c(\chi,\sigma)\langle v_1 f_1\rangle + \left(\frac{\sigma}{\chi} - 1\right)\langle v_1 g_2\rangle\right] - 4\varepsilon^2 W^2\right\} \tag{1.82}$$

and

$$\tilde{h} = h(x,t)e^{-i\omega t}, \tag{1.83}$$

where the following symbols are introduced

$$f_1(x) = l+x, \quad g_1(x) = (1- \Theta)x + \Theta, \tag{1.84}$$

$$g_2(x) = \frac{i}{\pi}(1-x^2)\int_{-1}^{1} e^{-i\chi\xi}(1-\xi^2)^{-1/2}\frac{d\xi}{\xi - x}, \tag{1.85}$$

$$B(\sigma) = F - (F^2 + G^2), \tag{1.86}$$

$$c(\chi,\sigma) = (1 - 2\Theta)(W_1 + iW_2), \tag{1.87}$$

$$W^2 = |W_1 + iW_2|^2 = W_1^2 + W_2^2, \tag{1.88}$$

The parentheses $\langle\rangle$ denote the scalar products of the following type

$$\langle f_1 g\rangle = \frac{2}{\pi}\int_{-1}^{1} f(x)g^*(x)(1-x^2)^{-1/2}dx = \langle g_1 f\rangle^*. \tag{1.89}$$

Froude's efficiency can be written as

$$\eta = \frac{U\bar{T}}{\bar{P}} = \frac{c_T}{c_p} = 1 - \frac{c_E}{c_p}. \tag{1.90}$$

The problem under consideration may reveal the following cases:

$$0<\eta<1,\ 0<c_E<c_p, \tag{1.91}$$

$$\eta > 1,\ c_E<0<c_p, \tag{1.92}$$

$$\eta < 0,\ c_E < c_p < 0. \tag{1.93}$$

The case (1.91) has been already discussed before. It demonstrates the situation when the wing is streamlined by an undisturbed flow with the constant velocity U. Part of the energy, transferred to the wing, is consumed by the flow, the rest of the energy is realised as the thrust.

The case (1.92) reflects some partial consumption of the energy from the flow, but still certain excessive energy is necessary to actuate the wing.

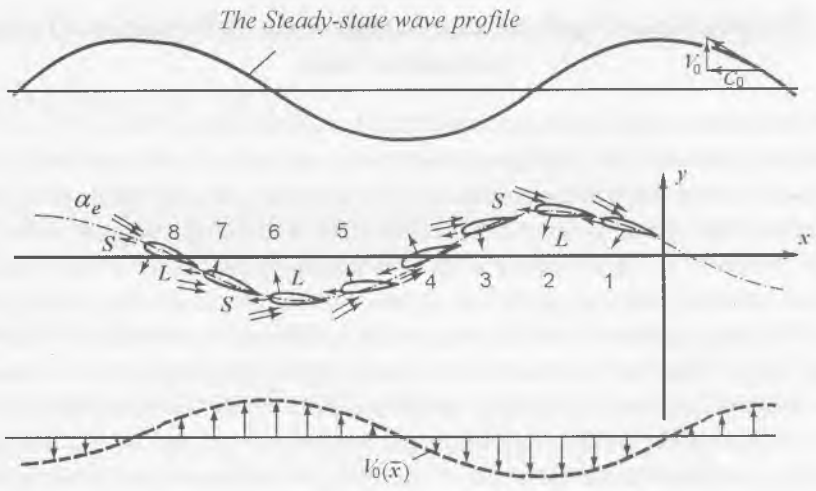

Fig. 1.16. The qualitative illustration of the extraction of flow energy by fish and birds in a wavy stream. (Adopted from Wu, Chwang, 1975).

The case (1.93) describes the situation when much energy is consumed from the flow, but the excessive energy is not spent at all.

Possibilities for realisation of the two last cases depend upon the relationships between the parameters ε, σ and χ. If we consider the problem of optimisation, it may be demonstrated that in reality there can be such relationship between the above parameters at which animals can utilise the energy of the flow so that to considerably facilitate their own motion. For example, in such cases when the wing chord must be approximately 1/ 30 of the wave length in the flow.

Fig.1.16 illustrates the mechanism explaining how the animal, for the sake of its motion, borrows the energy of the flow. The onrunning flow has components of velocity: c_0 is the velocity of the wave propagation, V_0 is the transverse amplitude of velocity. The wing is moving at the mean velocity $U + c_0$ towards the negative values of x. One oscillation period is divided into 8 moments.

Fig.1.16 also indicates the forces affecting the wing at these moments of time (the arrows). The double arrows show the direction of the local flow in respect of the wing. The scheme presents the motion of the wing as optimal and the transverse velocity of the wave $V_0(x)$ as increasing the effective angle of streamlining over the wing, which leads to the growth of the thrust at all stages of its movement.

The described scheme is strongly simplified and explains the energy - borrowing from the onrunning flow in birds flying above the stormy sea surface rather than in fishes swimming in turbulent flows. But in the second case, too, the principle of consideration remains the same, though the turbulence of the flow should be regarded as more complicated.

1.1.7. The decrease of hydrodynamic resistance of dolphin and fish due to propulsive wave

There is an interesting hypothesis in works of L. I. Korennaya (1983, 1987). It describes a possible mechanism of the friction resistance decrease on the undulated body. By simple reasoning she shows that while a propulsive wave spreads along a flexible plate moving in water, its particular elements can move in either directions: along and against the flow. The profile of velocities in the boundary layer at elements, which move streamwise, is more disturbance resistant than the profile on a plate without propulsive wave. But due to the increase of velocity gradient in the velocity profile, local friction resistance at these elements is slightly higher than the resistance at the plate without propulsive wave. However, the positive effect of increase of velocity profile stability under the supercritical Reynolds number is significantly greater than the negative effect of increase of friction resistance. The velocity profile at those elements of the plate, which move antistreamwise, is less disturbance resistant. However, due to decrease of velocity gradient in the boundary layer velocity profile, local friction resistance coefficient is a bit less than the resistance coefficient at the plate without propulsive waving. In subcritical Reynolds number conditions risk of turbulization of the boundary layer at these elements of the plate is small, and the positive effect of friction reduction is dominant. Thus, according to L. I. Korennaya, the mechanisms which control the boundary layer and friction resistance under subcritical and supercritical Reynolds numbers conditions are different. The characteristics of the forming boundary layer depend on the relation between the velocity of the plate surface movement and the flow velocity, which looks like

$$P = \frac{w_l}{w_t^*} = \frac{c}{c - v}, \tag{1.94}$$

when $Y = Y_{max}$ and like

$$P = \frac{w_l}{w_t^*} = \frac{c + v_y \dfrac{dy}{dx}}{c - v - v_y \dfrac{dy}{dx}}, \tag{1.95}$$

when $Y = 0$. Here v is the velocity of the plate movement, c is the velocity of the propulsive wave, which spreads along the plate streamwise, $v=dy/dt$, y is instantaneous value of the plate deflection caused by the propulsive wave, x is a coordinate in the direction of the plate movement. The coordinate system, direction of the plate movement and of the wave movement are shown in fig. 1.17.

The values presented in the figure are defined by the following expressions:

$$y = A(x)\sin(\omega t + \beta x + \varphi_0), \tag{1.96}$$

$$\vec{v}_y^* = -v_y = -\frac{dy}{dt} = -A(x)\omega\cos(\omega t + \beta x + \varphi_0), \tag{1.97}$$

$$\vec{w}_t^* = (\vec{c}^* + \vec{v}^*)\cos\alpha_n + \vec{v}_y^* \sin\alpha_n, \tag{1.98}$$

$$w_t^* = |\vec{w}_t^*| = (c - v)\cos\alpha_n - v_y \sin\alpha_n = \cos\alpha_n \left[(c - v) - v_y \frac{dy}{dx}\right], \tag{1.99}$$

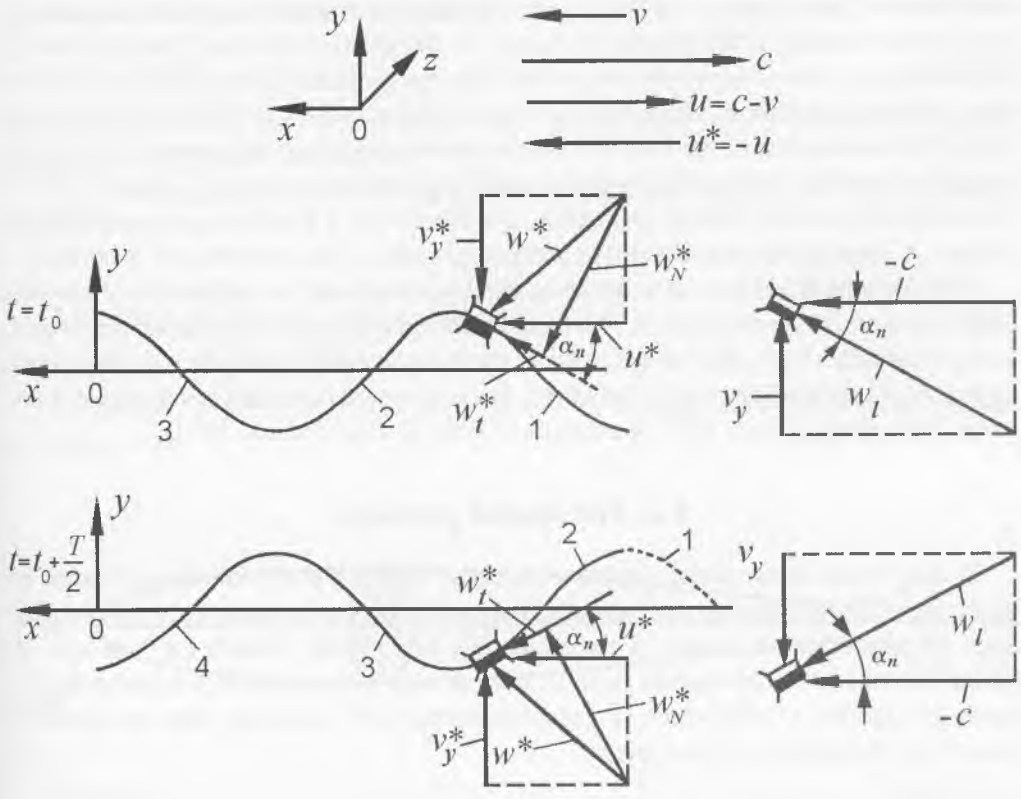

Fig. 1.17. The co-ordinate system, the plate moving direction and the velocities scheme. 1, 2, 3, 4 – is a working elements of the wave propulsor. (Redrawn from Korennaya, 1987).

$$\vec{w}_l = -\vec{c}\cos\alpha_n + \vec{v}_y \sin\alpha_n, \tag{1.100}$$

$$w_l = |\vec{w}_l| = \cos\alpha_n \left(c + v_y \frac{dy}{dx} \right). \tag{1.101}$$

The case of $P>0$ corresponds to the streamwise movement of the plate element, the case of $P<0$ corresponds to the antistreamwise movement of the plate element.

According to this hypothesis of L. I. Korennaya, decrease of swimming resistance can be explained by the fact that while a dolphin swims under supercritical Reynolds number the case of $P>0$ takes place, and while a fish swims under subcritical Reynolds number the case of $P<0$ takes place.

According to L. I. Korennaya this hypothesis is justified by the work of S. Taneda and Y. Tomonari (1974). They experimentally researched profiles of the velocity in the boundary layer of undulating flexible plate in a water stream. They discovered that undulation of plate causes velocity increase within the boundary layer. In this case if $c>v$ (c is the velocity of the propulsive wave, v is the speed of the flow) then profiles of the velocity are more convex in comparison with the profiles of the velocity on the flat plate without undulation. However it is known (Romanenko 1972b, 19860 and this work), that undulation of the flexible plate is accompanied by formation of favourable (negative) gradient of dynamic pressure, which explains the results of S. Taneda and Y. Tomonari. It is possible, that the mechanism described by L. I. Korennaya also contributes its part. A thorough theoretical and experimental study of this mechanism is needed.

Now we have to add several words about this hypothesis and the explanation of how the dolphin controls its boundary layer. This mechanism can work only on the dorsal and ventral sides of dolphin's body. But modification of the boundary layer structure was discovered experimentally on the lateral side of dolphin's body, where the described mechanism can not work (Romanenko, Yanov 1973, Romanenko 19860, Kozlov, Shakalo 1973).

1.2. The spatial problem

Spatial (three-dimensional) problems analyse the motion of volumetric bodies in which the shape, dimensions and parameters of the motion vary towards three coordinates. Such problems are dealt with in a considerably few papers, though the latter are of special interest. We shall discuss them in more details. To begin with, we shall take the paper of Lighthill (1960) which is a most important one, regarding both the author's results and the priority of the topic.

1.2.1. The theory of the thin fish-shaped body

The author considers the motion of a thin fish-shaped body in an ideal liquid (Fig.1.18). The body is situated along the axis x and is streamlined by the flow with the velocity U. The body is believed to be of cylindrical shape, its cross section does not change much in the length. The flow of liquid streamlining the body is regarded to consist of two components: the constant flow streamlining the immobile body, and the flow conditioned by the transverse movements of the body. These movements follow a certain law $h(x,t)$. In this case, the transverse velocity of the body's elements may be presented as

$$v(x) = \frac{\partial h}{\partial t} + U\frac{\partial h}{\partial x}. \tag{1.102}$$

The pattern of the flow, streamlining the fish-shaped cylindrical body during its transverse movements, is thought to be identical to the two-dimensional potential flow formed during the transverse motion of an infinitely long cylinder at the velocity $v(x,t)$. In this case, the pulse of the flow looks as

$$\rho\, v\,(x,\, t)\, A\,(x). \tag{1.103}$$

Here, the value $rA(x)$ has the pattern of the "virtual mass" of the cylinder per unit of length for such transverse motion.

The instantaneous force, affecting a unit of body length towards the body's normal, may be written as

$$L(x,t) = -\rho\left(\frac{\partial}{\partial t} + U\frac{\partial}{\partial x}\right)\{v(x,t)A(x)\} \tag{1.104}$$

The power, developed by the body during its motion, may be calculated in the following way

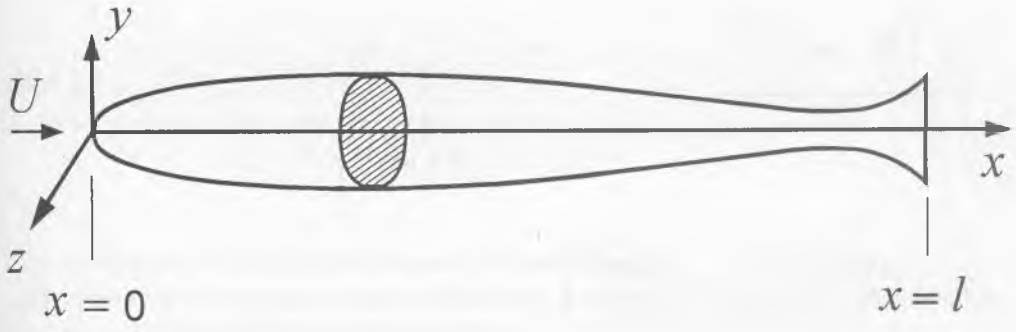

Fig. 1.18. The co-ordinate system in the body frame of reference. (Adopted from Lighthill, 1960).

$$W = -\int_0^l \left(\frac{\partial h}{\partial t}\right) L(x,t)dx = \left\{\rho \int_0^l \left(\frac{\partial h}{\partial t}\right)\left(\frac{\partial}{\partial t} + U\frac{\partial}{\partial x}\right)[v(x,t)A(x)]\right\} =$$

$$\left\{\rho \int_0^l \left(\frac{\partial}{\partial t} + U\frac{\partial}{\partial x}\right)\left[\frac{\partial h}{\partial t} v(x,t)A(x)\right]dx\right\} - \left\{\rho \int_0^l \frac{\partial v}{\partial t} v(x,t)A(x)dx\right\} = \tag{1.105}$$

$$\frac{\partial}{\partial t}\left\{\rho \int_0^l \frac{\partial h}{\partial t} v(x,t)A(x)dx - \frac{1}{2}\rho \int_0^l v^2(x,t)A(x)dx\right\} + \rho U\left[\frac{\partial h}{\partial t} v(x,t)A(x)\right]_0^l.$$

After averaging the data obtained for a long time, the first member, which is a time-product, will disappear and only the second member will remain in the equation

$$\overline{W} = \rho U A(l)\left\{\overline{\left(\frac{\partial h}{\partial t}\right)\left(\frac{\partial h}{\partial t} + U\frac{\partial h}{\partial x}\right)}\right\}_{x=l}. \tag{1.106}$$

The integration was effected along the body length from the head (its coordinate is $x = 0$) to the tail (its coordinate is $x = l$).

The time-averaged kinetic energy of the liquid, actuated by the transverse oscillations of the body, can be described as

$$\overline{E} = \frac{1}{2}\rho \overline{v^2} A \quad \text{and } x = l. \tag{1.107}$$

The value of total thrust can be derived from the difference between the power, developed by the body, and the power of the flow of liquid in the trace. This difference is divided by the forward velocity motion of the body:

$$\overline{T} = \frac{\left(\overline{W} - \rho \overline{v^2}\frac{AU}{2}\right)}{U} \tag{1.108}$$

or

$$\overline{T} = \left(\frac{\rho A(l)}{2}\right)\left\{\overline{\left(\frac{\partial h}{\partial t}\right)^2} - U^2\overline{\left(\frac{\partial h}{\partial x}\right)^2}\right\}_{x=l}. \tag{1.109}$$

The hydrodynamic efficiency can be found as the relation

$$\eta = \frac{\overline{TU}}{\overline{W}} = 1 - \frac{\overline{\left(\frac{\partial h}{\partial t} + U\frac{\partial h}{\partial x}\right)^2}_{x=l}}{2\left\{\left(\frac{\partial h}{\partial t}\right)\left(\frac{\partial h}{\partial t} + U\frac{\partial h}{\partial x}\right)\right\}_{x=l}}. \tag{1.110}$$

If we want to stick to some concrete law of body deformation, for example as

$$h(x,t) = f(x)g\left(t - \frac{x}{C}\right), \tag{1.111}$$

where the function $g(t)$ may look as

$$g(t) = \cos\omega\left(t - \frac{x}{C}\right), \tag{1.112}$$

the hydrodynamic efficiency may be presented in an expanded form

$$\eta = 1 - \frac{1}{2}\frac{\overline{\left\{\left(1 - \frac{U}{C}\right)f(l)g\left(t - \frac{l}{C}\right) + Uf'(l)g\left(t - \frac{l}{C}\right)\right\}^2}}{f(l)g\left(t - \frac{l}{C}\right)\left\{\left(1 - \frac{U}{C}\right)f(l)g\left(t - \frac{l}{C}\right) + Uf'(l)g\left(t - \frac{l}{C}\right)\right\}} \tag{1.113}$$

or

$$\eta = 1 - \frac{1}{2}\frac{\left(1 - \frac{U}{C}\right)f^2(l)\overline{(g')^2} + U^2(f')^2\overline{g^2}}{\left(1 - \frac{U}{C}\right)f^2(l)\overline{(g')^2}}. \tag{1.114}$$

Here, as before, the dash above means the time-averaging.

Searching for the optimal shape of the body oscillations, when the efficiency could be close to 1, Lighthill derives the condition

$$f'(l) \to 0 . \tag{1.115}$$

This condition is satisfied by two versions of the law of body deformation: the constant amplitude along the entire body and the constant amplitude only within the tail area. It is very hard to understand this condition physically and its modulation seems to be even more difficult.

The problem, similar to that solved by Lighthill, was formulated in similar situations by G.V. Logvinovich, Academician of the Ukrainian Academy of Sciences (1970a, 1970b). However, Logvinovich'es approach to the solution of this problem is physically more understandable, owing to the theory of the "penetrated layer" on which he bases his explanations. Besides, unlike Lighthill, Logvinovich calculates the thrust not from the law of energy conservation but directly by integrating along the body length the elementary forces projected on the motion direction. As a result, it becomes possible to calculate the suction and the thrusting forces separately.

G.V. Logvinovich analysed the motion of the thin body in an inertial system with the coordinates *x, y* and *z*. The system is moving in an unlimited liquid medium towards the axis *x*. The scheme, as well as all of the symbols, were taken by the author from paper (1970a): the abscissas of the body ends x_1 and x_2; hence, the body length $L_p = x_2 - x_1$, $R(x)$ is a big semiaxis of the elliptical transverse section of the body; the value dR/dx is small throughout the body length, s is the longitudinal curvilinear axis of the body , which does not differ much from the axis of the abscissas.

As it was mentioned before, this theory was based upon the concept of the "penetrated layer". According to this concept, the body, passing through a certain layer of liquid ("the penetrated layer"), which is immobile in respect of the stationary liquid, induces in this layer some transverse, almost plane, close to that of ideal liquid. With that, a flow of pulses $m_1 * V v_n$ is running off from the caudal fin of the body tangentially to the fin. Here, m_1* is the apparent virtual mass equalling $\rho\pi R^2(x_1)$, ρ is the density of the liquid, V is the velocity of the body, v_n is the velocity of the layer normal to the curvilinear axis of the body found by the expression

$$v_n = \frac{\partial \eta}{\partial t} - V \frac{\partial \eta}{\partial x} . \tag{1.116}$$

The specific normal force, affecting the body, develops there when the body passes through the penetrated layer and can be expressed as

$$dF_n = -\frac{d}{dt}[m^*(x)v_n(x,t)]ds =$$

$$= \left[\frac{dm^*}{dx}V\left(\frac{\partial\eta}{\partial t} - V\frac{\partial\eta}{\partial x}\right) - m^*\left(\frac{\partial^2\eta}{\partial t^2} - 2V\frac{d^2\eta}{\partial x\partial t} + V^2\frac{\partial^2\eta}{\partial x^2}\right)\right]dx. \quad (1.117)$$

Besides the normal force, the body is also affected by the so-called ("circular pressure" integrated by the counter of the body's cross section s^* of the excessive pressure due to the velocity head when the body moves transversely. In such case, the specific suction force will be determined by the expression

$$\frac{dP}{ds} = -\oint(p - p_0)\cos(n,x)ds^*. \quad (1.118)$$

The specific thrust is a total of projections on the axis of the normal (with the reverse sign) elementary force and the suction elementary force. This specific thrust will be written as

$$dF_x = -dF_n\frac{\partial\eta}{\partial x} - dP. \quad (1.119)$$

The complete thrust can be derived through integrating the expression (1.119) by the body length.

In the case of the body's periodical motion, G.V. Logvinovich offered a simple expression for the thrusting force originating in the flow of pulses running off

$$I = m^*(x_1)V\left(\frac{\partial\eta}{\partial t} - V\frac{\partial\eta}{\partial x}\right)\frac{\partial\eta}{\partial x} \quad \text{and } x = x_1 \quad (1.120)$$

However, it is not difficult to demonstrate that the simplified formula for the thrusting force (1.120), offered by G.V. Logvinovich, is valid only for the case of the "eel-shaped" manner of swimming when the oscillation amplitude is constant along the body length. For this case, the thrusting force can be calculated by integration of

$$I = \int_{x_1}^{x_2}\frac{d}{\partial t}[m^*(x)v_n(x,t)]\frac{\partial\eta}{\partial x}dx. \quad (1.121)$$

In this expression, the operation of time-differentiation looks as

$$\frac{d}{dt} = \frac{\partial}{\partial t} - V\frac{\partial}{\partial x}. \tag{1.122}$$

Let us transform (1.121)

$$\begin{aligned} I &= \int_{x_1}^{x_2} \frac{\partial \eta}{\partial x}\left(\frac{\partial}{\partial t} - V\frac{\partial}{\partial x}\right)[v_n m^*]dx = \\ &= \int_{x_1}^{x_2}\left(\frac{\partial}{\partial t} - V\frac{\partial}{\partial x}\right)\left[\frac{\partial \eta}{\partial x} v_n m^*\right]dx - \int_{x_1}^{x_2} v_n m^*\left(\frac{\partial}{\partial t} - V\frac{\partial}{\partial x}\right)\frac{\partial \eta}{\partial x}dx = \\ &= \frac{\partial}{\partial t}\int_{x_1}^{x_2}\frac{\partial \eta}{\partial x} v_n m^* dx - V\int_{x_1}^{x_2} d\left[\frac{\partial \eta}{\partial x} v_n m^*\right] - \frac{1}{2}\int_{x_1}^{x_2} m^*\frac{\partial v_n^2}{\partial x}dx. \end{aligned} \tag{1.123}$$

By time-averaging of this expression and by integrating the second member of its right part, and also bearing in mind that $m^*(x_2) = 0$, we shall get

$$\bar{I} = V\overline{\frac{\partial \eta}{\partial x} v_n m^*}(x_1) - \frac{1}{2}\int_{x_1}^{x_2} m^*\overline{\frac{\partial v_n^2}{\partial x}}dx. \tag{1.124}$$

Now we shall transform the integral in the right part and get

$$\int_{x_1}^{x_2} m^*\overline{\frac{\partial v_n^2}{\partial x}}dx = \int_{x_1}^{x_2} d[\overline{m^* v_n^2}] - \int_{x_1}^{x_2}\overline{v_n^2}\frac{\partial m^*}{\partial x}dx. \tag{1.125}$$

Substituting (1.125) into (1.124), and remembering that

$$v_n = \frac{\partial \eta}{\partial t} - V\frac{\partial \eta}{\partial x}, \tag{1.126}$$

we shall come to

$$\bar{I} = m^*(x_1)\left[V\overline{\frac{\partial\eta}{\partial x}\frac{\partial\eta}{\partial t}} - V^2\overline{\left(\frac{\partial\eta}{\partial x}\right)^2} + \frac{1}{2}\overline{\left(\frac{\partial\eta}{\partial t}\right)^2} - V\overline{\frac{\partial\eta}{\partial x}\frac{\partial\eta}{\partial t}} + \frac{V^2}{2}\overline{\left(\frac{\partial\eta}{\partial x}\right)^2}\right]_{x=x_1} + \\ + \frac{1}{2}\int_{x_1}^{x_2}\overline{v_n^2}\frac{\partial m^*}{\partial x}dx. \tag{1.127}$$

Reducing the similar members, we shall finally obtain

$$\bar{I} = \frac{m^*(x_1)}{2}\left[\overline{\left(\frac{\partial\eta}{\partial t}\right)^2} - V^2\overline{\left(\frac{\partial\eta}{\partial t}\right)^2}\right] + \frac{1}{2}\int_{x_1}^{x_2}\overline{v_n^2}\frac{\partial m^*}{\partial x}dx. \tag{1.128}$$

The first member in the right part exactly coincides with the expression for the thrust (1.109) derived by Lighthill. Here, the time-averaging is marked by the dash above. The second member in the expression (1.128) is nothing else but the suction force with the inverse sign. By transforming the expression (1.128)

$$\bar{I} = \frac{m^*(x_1)}{2}\left[\overline{\left(\frac{\partial\eta}{\partial t} - V\frac{\partial\eta}{\partial x}\right)\left(\frac{\partial\eta}{\partial t} - V\frac{\partial\eta}{\partial x} + 2V\frac{\partial\eta}{\partial x}\right)}\right]_{x=x_1} + \\ + \frac{1}{2}\int_{x_1}^{x_2}\overline{v_n^2}\frac{\partial m^*}{\partial x}dx = Vm^*(x_1)\left[\overline{\left(\frac{\partial\eta}{\partial t} - V\frac{\partial\eta}{\partial x}\right)\frac{\partial\eta}{\partial x}}\right]_{x=x_1} + \\ + \frac{m^*(x_1)}{2}\overline{v_n^2} + \frac{1}{2}\int_{x_1}^{x_2}\overline{v_n^2}\frac{\partial m_*}{\partial x}dx. \tag{1.129}$$

or bearing in mind that

$$\bar{E} = \frac{m^*(x_1)}{2}V_n^2, \tag{1.130}$$

we shall finally write

$$\bar{I} = Vm^*(x_1)\left[\overline{\left(\frac{\partial\eta}{\partial t} - V\frac{\partial\eta}{\partial x}\right)\frac{\partial\eta}{\partial x}}\right]_{x=x_1} + \bar{E} - \bar{P}. \tag{1.131}$$

The first member in the right part is the simplified formula of G.V. Logvinovich. One can see that the complete value of the thrusting force is the total of three expressions: the simplified formula, the kinetic energy, and the suction force with the inverse sign.

Let us analyse the ratio between the two last members of the expression (1.131). First, we shall consider the "eel-shaped" law of body deformation

$$\eta = \eta_0 \sin\omega\left(t - \frac{x_2 - x}{C}\right). \tag{1.132}$$

Then we shall write out the values of the derivatives in the expression (1.131) giving us (1.133)

$$\begin{aligned} \frac{\partial\eta}{\partial t} &= \omega\eta_0 \cos\omega\left(t - \frac{x_2 - x}{C}\right), \\ \frac{\partial\eta}{\partial x} &= \frac{\omega\eta_0}{C} \cos\omega\left(t - \frac{x_2 - x}{C}\right). \end{aligned} \tag{1.133}$$

Then we shall have (1.134) and (1.135).

$$v_n = \left(\omega\eta_0 - \frac{\eta_0\omega V}{C}\right)\cos\omega\left(t - \frac{x_2 - x}{C}\right). \tag{1.134}$$

$$\overline{v_n^2} = \frac{1}{2}\omega^2\eta_0^2\left(1 - \frac{V}{C}\right)^2. \tag{1.135}$$

Inasmuch as none of the motion parameters, comprising the expression (1.135), depends on the coordinate x, we shall get

$$\overline{E} = \overline{P}, \tag{1.136}$$

and only under this condition -

$$\overline{I} = Vm^*(x_1)\left[\left(\frac{\partial\eta}{\partial t} - V\frac{\partial\eta}{\partial x}\right)\frac{\partial\eta}{\partial x}\right]_{x=x_1}. \tag{1.137}$$

Now we shall analyse the periodical law of body deformation with a random amplitude function which is the function of the coordinate x

$$\eta = \eta_0(x)\sin\omega\left(t - \frac{x_2 - x}{C}\right). \tag{1.138}$$

Like in the previous case, we perform the time-differentiation

$$\begin{aligned}
&\frac{\partial\eta}{\partial t} = \omega\eta_0\cos\omega\left(t - \frac{x_2 - x}{C}\right),\\
&\frac{\partial\eta}{\partial x} = \frac{\partial\eta_0}{\partial x}\sin\omega\left(t - \frac{x_2 - x}{C}\right) + \frac{\omega\eta_0}{C}\cos\omega\left(t - \frac{x_2 - x}{C}\right).
\end{aligned} \tag{1.139}$$

Then

$$\begin{aligned}
&v_n = \omega\eta_0\left(1 - \frac{V}{C}\right)\cos\omega\left(t - \frac{x_2 - x}{C}\right) -\\
&-V\frac{\partial\eta_0}{\partial x}\sin\omega\left(t - \frac{x_2 - x}{C}\right),
\end{aligned} \tag{1.140}$$

$$\overline{v_n^2} = \frac{\omega^2\eta_0^2}{2}\left(1 - \frac{V}{C}\right)^2 + \frac{V^2}{2}\left(\frac{\partial\eta_0}{\partial x}\right)^2. \tag{1.141}$$

The expressions for the kinetic energy and for the suction force will be respectively

$$\overline{E} = \frac{m^*(x_1)}{2}\left[\frac{\omega^{2\eta_0^2}}{2}\left(1 - \frac{V}{C}\right)^2 + \frac{V^2}{2}\left(\frac{\partial\eta_0}{\partial x}\right)^2\right] \tag{1.142}$$

and

$$\overline{P} = \frac{1}{4}\omega^2\left(1 - \frac{V}{C}\right)^2\int_{x_1}^{x_2}\eta^2(x)\frac{dm^*}{dx}dx - \frac{V^2}{4}\int_{x_1}^{x_2}\left(\frac{\partial\eta_0}{\partial x}\right)^2\frac{dm^*}{dx}dx. \tag{1.143}$$

These two expressions are obviously not equal and, hence,

$$\bar{I} \neq Vm^*(x_1)\left[\overline{\left(\frac{\partial \eta}{\partial t} - V\frac{\partial \eta}{\partial x}\right)\frac{\partial \eta}{\partial x}}\right]_{x=x_1}, \tag{1.144}$$

which was to be proved.

As to the sucking force, it should be derived only by integration of the specific suction force along the body. As a result, we receive

$$P = -\int_{x_1}^{x_2} \frac{dm^*(x)}{dx}\frac{1}{2}\left(\frac{\partial \eta}{\partial t} - V\frac{\partial \eta}{\partial x}\right)^2 dx. \tag{1.145}$$

The complete thrust is the total of the expressions (1.128) and (1.145).

The mean active power of the thrusting forces may be presented as

$$(\bar{I} + \bar{P})V = \bar{A}. \tag{1.146}$$

The kinetic energy of the flow, running into the trace from the body tail, equals

$$\bar{E} = \frac{1}{2}m^*(x_1)\overline{\left(\frac{\partial \eta}{\partial t} - V\frac{\partial \eta}{\partial x}\right)^2}_{x=x_1}. \tag{1.147}$$

The complete power, spent on the initiation of the thrusting force, will be

$$\left(\bar{I} + \bar{P} + \bar{E}\right)V = \bar{N}. \tag{1.148}$$

Then the hydrodynamic efficiency will look as

$$\bar{\eta} = \frac{\bar{A}}{\bar{N}}. \tag{1.149}$$

In one of his papers Wu (1971) made an attempt to take into account the appearance of vortexes near the oscillating body within its limits from the widest span section to the caudal fin. Fig.1.19 shows the scheme explaining the problem formulation as offered by Wu. The symbols S_b and S_w present the fish body and the vortex sheet respectively projected onto the plane $z = 0$. The other symbols are clear from the Figure. The total of the projections is nominated as

$$S_c = S_b + S_w. \tag{1.150}$$

In its general form, the motion of fish can be written as

$$z = h(x,t). \tag{1.151}$$

The velocity in the particles of liquid, due to the constant velocity U of the body's movement in the flow, can be characterised by the potential of perturbation

$$\mathbf{q} = (U + u, v, w) = \mathbf{grad}(Ux + \phi), \tag{1.152}$$

which satisfies the equation of Laplace

$$\nabla^2 \phi = 0. \tag{1.153}$$

The linearized equation of motion offered by Euler looks as

$$D\mathbf{q} = \nabla\Phi, \quad \Phi = (p_\infty - p)/\rho, \tag{1.154}$$

where

$$D = \frac{\partial}{\partial t} + U\frac{\partial}{\partial x} \tag{1.155}$$

is the linearized differential operator, Φ is Prandtl's potential of accelerations, p is the pressure near the body, p_∞ is the pressure at infinity, ρ is the density of the liquid. With that, Φ also satisfies Laplace equation

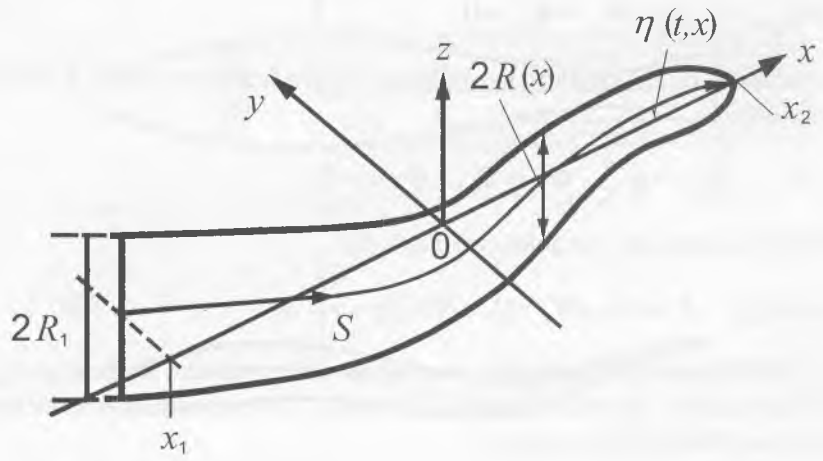

Fig. 1.19. The co-ordinate system in the body frame of reference. (Adopted from Logvinovitch, 1970).

$$\nabla^2\Phi = 0 \cdot \tag{1.156}$$

The boundary conditions in this problem equal

$$\phi_z^{\pm} = Dh \equiv v(x,t) \qquad \text{or } \Phi_z^{\pm} = Dv \quad (x, y \in S_b); \tag{1.157}$$

$$D\phi^{\pm} = 0 \qquad \text{or } \Phi^{\pm} = 0 \quad (x, y \in S_w); \tag{1.158}$$

$$D\phi^{\pm} = 0 \qquad \text{or } \Phi^{\pm} = 0 \quad \text{(on the tail edge)}; \tag{1.159}$$

$$\phi^{\pm} = 0 \qquad \text{or } \Phi^{\pm} = 0 \quad (x, y \in S_c); \tag{1.160}$$

$$\phi \to 0 \qquad \text{or } \Phi \to 0 \quad (x^2 + y^2 + z^2 \to \infty). \tag{1.161}$$

Here a new symbol is introduced

$$\phi_z^{\pm} = \partial\phi / \partial z \quad \text{when} \quad z \to \pm 0. \tag{1.162}$$

It is believed that when the body is thin and satisfies the condition

$$\delta = b_0 / l_T << 1 \qquad (l_T \equiv l_n + l), \tag{1.163}$$

where b_0 is the body width in the plane $x = 0$, it is possible to employ the two-dimensional equation of Laplace

$$\phi_{yy} + \phi_{zz=0} = 0 \quad \text{or} \quad \Phi_{yy} + \Phi_{zz} = 0. \tag{1.164}$$

Two equations (1.154) suggest the existence of two functions: ψ and Ψ which satisfy the conditions of

$$\phi_y = \psi_z, \quad \phi_z = -\psi_y, \quad \Phi_y = \Psi_z, \quad \Phi_z = -\Psi_y. \tag{1.165}$$

Transiting to complex variables, we can write

$$f = \phi + i\psi, \quad F = \Phi + i\Psi, \quad \Omega = df / d\xi = v - iw. \tag{1.166}$$

Fig.1.20 a, b presents the boundary conditions of the problem. Without going into the details of the solution, we shall write only its result. The pressure difference on the two sides of the oscillating body looks as

$$\Delta p = p^- - p^+ = \rho(\Phi^+ - \Phi^-) = 2\rho\Phi^+(x,y,t) \qquad (x, y \in S_b), \tag{1.167}$$

where

$$\Phi^+ = -D\{v(x,t)[b^2(x) - y^2]^{1/2}\}(-l_n < x < 0;\ 1 < x < l); \tag{1.168}$$

$$\Phi^+ = -[Dv(x,t)][b^2(x) - y^2]^{1/2} \qquad (0 < x < 1). \tag{1.169}$$

The spontaneous force in the z-direction per unit of body length is

$$\mathcal{L}(x,t) = \int_{-b}^{b} (\Delta p)dy = -2\rho D \int_{-b}^{b} v(x,t)(b^2 - y^2)^{1/2} = -\rho D[vA],$$

when $(-l_n < x < 0)$ и $(1 < x < l)$, (1.170)

and

$$\mathcal{L}(x,t) = -2\rho(Dv)\int_{-b}^{b} (b^2 - y^2)^{1/2} dy = -\rho[Dv]A \quad (0 < x < 1), \tag{1.171}$$

where $\rho A(x) = \rho\pi b^2(x)$ is the virtual mass of one unit of body length for the motion in the z-direction.

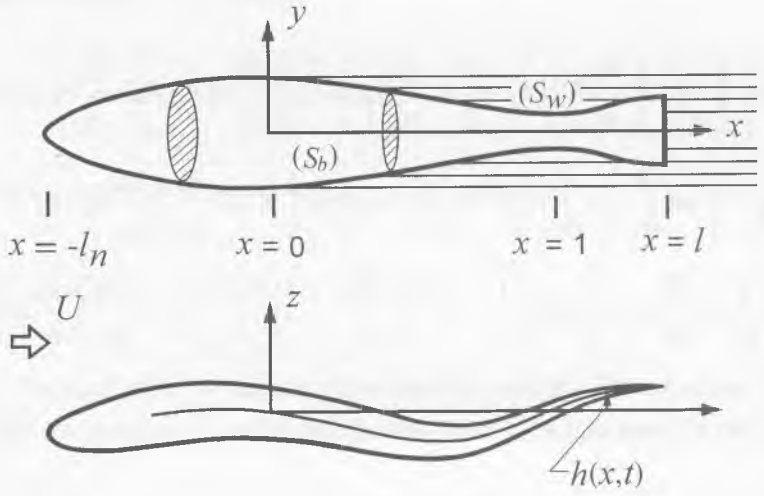

Fig. 1.20. The co-ordinate system in the body frame of reference. (Redrawn from Wu, 1971).

The complete force in the z-direction can be found by integration of (1.170) and (1.171) by the body length

$$L(t) = -\rho \int_{-l_n}^{l} D[vA]dx + \rho U \int_{0}^{1} v \frac{\partial A}{\partial x} dx. \tag{1.172}$$

The moment of forces in respect to the onset of the coordinates is

$$M(t) = \rho \int_{-l_n}^{l} xD[vA]dx - \rho U \int_{0}^{1} xv \frac{\partial A}{\partial x} dx. \tag{1.173}$$

The force of thrust is

$$T = \int_{-l_n}^{l} \mathcal{A}(x,t) \frac{\partial h}{\partial x} dx + T_s. \tag{1.174}$$

Here, T_s is the suction force on the body sections $-l_n < x < 0$ and $1 < x < l$ which looks as

$$T_s = \left(\int_{-l_n}^{l} + \int_{1}^{l} \right) \frac{1}{2} \rho v^2 \frac{dA}{dx} dx. \tag{1.175}$$

Then the total thrust may be presented as

$$\begin{aligned} T &= -\rho \left(\int_{-l_n}^{0} + \int_{1}^{l} \right) \left[\frac{\partial h}{\partial x} D(vA) - \frac{1}{2} v^2 \frac{dA}{dx} \right] dx - \rho \int_{0}^{1} \frac{\partial h}{\partial x} (Dv) A dx = \\ &= -\rho \int_{-l_n}^{l} \left[D\left(vA \frac{\partial h}{\partial x} \right) - \frac{\partial}{\partial x} \left(\frac{1}{2} v^2 A \right) \right] dx - \rho \int_{0}^{1} v \left(\frac{1}{2} v - U \frac{\partial h}{\partial x} \right) \frac{\partial A}{\partial x} dx = \\ &- \rho \frac{\partial}{\partial t} \int_{-l_n}^{l} Av \frac{\partial h}{\partial x} dx + \left[\rho A v \left(\frac{1}{2} v - U \frac{\partial h}{\partial x} \right) \right]_{x=l} - \rho \int_{0}^{1} v \left(\frac{1}{2} v - U \frac{\partial h}{\partial x} \right) \frac{\partial A}{\partial x} dx. \end{aligned} \tag{1.176}$$

Taking into account that $A(-l_n) = 0$, and effecting time-averaging, we shall get

$$\overline{T} = \frac{1}{2}\rho A(l)\overline{\left[\left(\frac{\partial h}{\partial t}\right)^2 - U^2\left(\frac{\partial h}{\partial x}\right)^2\right]}_{x=l} -$$
$$-\frac{1}{2}\rho\int_0^l\left[\left(\frac{\partial h}{\partial t}\right)^2 - U^2\left(\frac{\partial h}{\partial x}\right)^2\right]^2\frac{\partial A}{\partial x}dx. \qquad (1.177)$$

The first member coincides with the expression obtained by Lighthill (1.109), and the second one is due to the take-off of vortex sheet on the body section $0 < x < l$.

The expression for the complete power, developed by the body against the transverse waves affecting it and the appearance of the vortex sheet, looks as

$$P = -\int_{-l_n}^{l}\mathcal{L}(x,t)\frac{\partial h}{\partial t}dx =$$
$$= \rho\int_{-l_n}^{l}\left[D\left(\frac{\partial h}{\partial t}\right) - Av\frac{\partial v}{\partial t}\right]dx - \rho U\int_0^l v\frac{\partial h}{\partial t}\frac{\partial A}{\partial x}dx = \qquad (1.178)$$
$$= \rho U\frac{\partial}{\partial t}\int_{-l_n}^{l}Av\left(\frac{\partial h}{\partial t} - \frac{1}{2}v\right)dx + \rho U\left(Av\frac{\partial h}{\partial t}\right)_{x=l} - \rho U\int_0^l v\frac{\partial h}{\partial t}\frac{\partial A}{\partial x}dx.$$

The time-averaged value looks as

$$\overline{P} = \rho UA(l)\overline{\left[\frac{\partial h}{\partial t}v\right]}_{x=l} - \rho U\int_0^l\overline{\frac{\partial h}{\partial t}v}\frac{\partial A}{\partial x}dx. \qquad (1.179)$$

The kinetic energy entering the liquid per unit of time is

$$E = -\iint_S(p\vec{n})\vec{q}ds = -\int_{-l_n}^{l}v(x,t)L(x,t)dx - UT_s. \qquad (1.180)$$

There is another way to calculate the kinetic energy - from the law of energy conservation

$$E = P - TU, \qquad (1.181)$$

or by time averaging

$$\overline{E} = \frac{1}{2}\rho UA(l)\overline{v^2(l,t)} - \frac{1}{2}\rho U\int_0^1 \overline{v^2}\frac{\partial A}{\partial x}dx. \tag{1.182}$$

In his paper (Wu, 1971) Wu considers some other very important problems. In particular, that on the impact of the thickness of the fish-shaped body rendered on the hydrodynamic forces induced by this body. The body thickness is presented by the function

$$z = \pm g(y;x). \tag{1.183}$$

As a result, one can see the expression for the force per unit of body length to be conserved as (1.160) and (1.161), while the body thickness has a bearing on the pattern of the dependence between the mass and the coordinate. In this case, the expression for the virtual mass in the complex plane looks as

$$\rho A(x) = \rho\int_{-\beta}^{\beta}\left[\left(\beta^2 - \xi^2\right)^{1/2} - z(\xi)\right]\frac{\partial\eta}{\partial\xi}d\xi, \tag{1.184}$$

$$-\beta(x) < \mathrm{Re}\,\xi < \beta(x) \tag{1.185}$$

and

$$\beta(x) = \xi[b(x)]. \tag{1.186}$$

Here Re means the real part.

Another problem touched upon in paper (Wu, 1971) deals with the optimal pattern of motion in the fish-shaped body. The criterion of optimization is the minimum of power spent at fixed thrust. It came out that in this case the optimal pattern of the body's motion is when the amplitude of displacement in the body's points remains constant within its length and the relation between the phase velocity of the locomotor wave and the motion velocity of the body is necessarily slightly more than a unit.

Another problem discussed in paper (Wu, 1971) is about the impact rendered by the body asymmetry upon the hydrodynamic forces. If the body shape is such that

$$y = -b_1(x) \text{ and } y = b_2(x), \tag{1.187}$$

and with that $b_1 \neq b_2$, then the expression for the force (1.162) still remains but that for the virtual mass changes, now looking as

$$\rho A(x) = \rho\pi\left[\frac{1}{2}(b_1 + b_2)\right]^2. \tag{1.188}$$

1.2.2. Theory of swimming for fishes with large amplitudes of body oscillations

As it was mentioned, the above theories, apply to describe the swimming of bodies whose shifted amplitude is transversely low. This condition is not always valid in actual swimming of fishes and dolphins. Lighthill (1971) tried to spread the above theory for the case of swimming of thin bodies with an arbitrary oscillation amplitude.

He considered a fish swimming at a fixed horizontal level within the plane $x0z$ at y=0, where y is the vertical coordinate in the rectangular system of coordinates x; y; z. The mean direction of fish swimming is taken in the positive direction of the axis $0x$. To describe the fish movement with an arbitrary amplitude, Lighthill accepted the «Lagrangian» coordinate a which varies from 0 to l (where l is the length of the non-oscillating fish). Here, the count a begins from the tail edge where $a = 0$. Coordinate a is counted along the median line of the fish coinciding with its spinal column. Lighthill regards the coordinate of any point of the fish body (x,z) as the function x (a,t) and $z(a,t)$ from a and t, inasmuch as this points moves owing to the longing oscillations, the resulting movement of the fish forward and to any lateral movement with the fish may involuntary make (yawing). The task is illustrated by Fig. 1.21. The median line of the fish is trough not to stretch, while

$$\left(\frac{\partial x}{\partial a}\right)^2 + \left(\frac{\partial z}{\partial a}\right)^2 = 1. \tag{1.189}$$

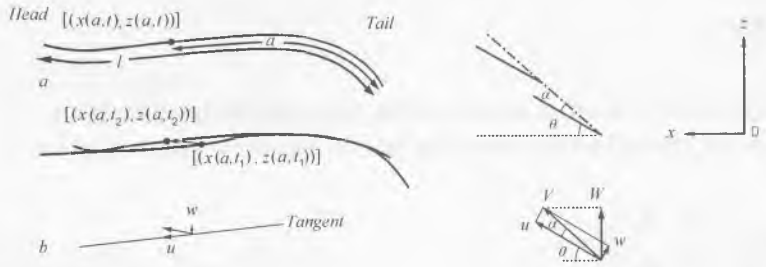

Fig. 1.21. The spinal column's configuration at two successive instants t_1 and t_2 and motion of the tip of the caudal fin. (Redrawn from Lighthill, 1960).

The vector of horizontal velocity $\left(\frac{\partial x}{\partial t}, \frac{\partial z}{\partial t}\right)$ may be presented as a component

$$u = \frac{\partial x}{\partial t}\frac{\partial x}{\partial a} + \frac{\partial z}{\partial t}\frac{\partial z}{\partial a}, \tag{1.190}$$

tangentially directed to the median line of the fish in direction of positive x and component

$$w = \frac{\partial z}{\partial t}\frac{\partial x}{\partial a} - \frac{\partial x}{\partial t}\frac{\partial z}{\partial a}, \tag{1.191}$$

The impulse per one unit of the fish body length when the fish moves in the w-direction is a vector

$$mw\left(-\frac{\partial z}{\partial a}, \frac{\partial x}{\partial a}\right), \tag{1.192}$$

where the value in parentheses is a single vector in the w-direction expressed as x- and z-components. The impulse projection upon the axis x in this case looks like

$$-mw\frac{\partial z}{\partial a}, \tag{1.193}$$

and upon the axis z respectively looks like

$$mw\frac{\partial x}{\partial a}. \tag{1.194}$$

The virtual mass of water, as before, is found by expression

$$m = \frac{1}{4}\pi\rho s^2, \tag{1.195}$$

where s is the size of the cross section of the fish body in the direction y.

In this case, Lighthill writes down the law of impulse conservation as

$$\frac{d}{dt}\int_0^l mw\left(-\frac{\partial z}{\partial a}, \frac{\partial x}{\partial a}\right)da = \tag{1.196}$$

$$= \left[-umw\left(-\frac{\partial z}{\partial a}, \frac{\partial x}{\partial a} \right) + \frac{1}{2} mw^2 \left(\frac{\partial x}{\partial a}, \frac{\partial z}{\partial a} \right) \right]_{a=0} - (P, Q).$$

The last member in the right part presents the reactive force (i. e. the force of reaction) with which the liquid affects the body. It involves two components - P - the trust and Q - the lateral force. The expression in brackets in the right part always seems simplification due to which formula (1.196) changes into

$$(P, Q) = \left[mw\left(\frac{\partial z}{\partial t}, -\frac{\partial x}{\partial t} \right) - \frac{1}{2} mw^2 \left(\frac{\partial x}{\partial a}, \frac{\partial z}{\partial a} \right) \right]_{a=0} -$$

$$- \frac{d}{dt} \int_0^l mw\left(-\frac{\partial z}{\partial a}, \frac{\partial x}{\partial a} \right) da. \qquad (1.197)$$

Expression (1.197) is the force in vector form affecting the body from the side of the liquid mean the body moves at a large amplitude. It is feasible to present this force as its separate components, i.e. the thrust

$$P = \left[mw \frac{\partial z}{\partial t} - \frac{1}{2} mw^2 \frac{\partial x}{\partial a} \right]_{a=0} + \frac{d}{dt} \int_0^l mw \frac{\partial z}{\partial a} da \qquad (1.198)$$

and the lateral force

$$-Q = \left[mw \frac{\partial x}{\partial t} + \frac{1}{2} mw^2 \frac{\partial z}{\partial a} \right]_{a=0} + \frac{d}{dt} \int_0^l mw \frac{\partial x}{\partial a} da. \qquad (1.199)$$

In case of intermittent swimming motions, the time - averaged values of P and Q looks as

$$\{P\} = \left\{ \left[mw \frac{\partial z}{\partial t} - \frac{1}{2} mw^2 \frac{\partial x}{\partial a} \right] \right\}_{a=0} \qquad (1.200)$$

and

$$-\{Q\} = \left\{ \left[mw \frac{\partial x}{\partial t} + \frac{1}{2} mw^2 \frac{\partial z}{\partial a} \right] \right\}_{a=0}. \qquad (1.201)$$

Formulas (1.187) and (1.188) generalise the results of the small amplitude theory developed earlier for the case of the fish body oscillations with an arbitrary amplitude. It is easy prove by using

$$\frac{\partial x}{\partial a} = 1; \quad \frac{\partial z}{\partial a} = \frac{\partial z}{\partial x}. \tag{1.202}$$

With that, there will be respective small - amplitude values of the thrust and the lateral force.

It is interesting to see how much the calculation thrust according to (1.200) differs from there respective calculation according to the small - amplitude formula (1.109). It can be best seen by the example of thrust calculations for Leuciscus which Lighthill personally performed (1971). We shall only supplement his calculations by that on the small - amplitude formula (1.109). The necessary kinematic parameters of fish swimming were taken by Lighthill from Bainbridge (1963). The calculations include ten time moments varying from one another by 0.04 sec. The results of the calculation showed by Lighthill are presented in Table 1.1.

The meanings of the columns in the Table became clear from Fig. 1.21 and from relations (1.190)

$$w = V\sin\alpha, \quad W = \frac{\partial z}{\partial t} = V\sin(\alpha+\theta), \quad \frac{\partial x}{\partial a} = \cos\theta. \tag{1.203}$$

In this calculations Lighthill employed formula (1.187). We shall supplement Table 1.1 with Table 1.2 calculated by the formula

$$\{P\} = \frac{1}{2}m\left\{\left[\left(\frac{\partial z}{\partial t}\right)^2 - V^2\left(\frac{\partial z}{\partial x}\right)^2\right]\right\}_{x=0}, \tag{1.204}$$

showing the thrust of the same fish obtained from Lighthill's small - amplitude theory (1971). Table 1.2 will have only those columns (except that of time) which will differ from the respective dues in Table 1.1. In accordance with the small - amplitude theory we shall think that

$$\frac{\partial x}{\partial a} = 1, \quad \frac{\partial z}{\partial a} = \frac{\partial z}{\partial x} = \theta, \quad w = V\alpha, \quad W = \frac{\partial z}{\partial t} = V(\alpha+\theta). \tag{1.205}$$

The mean value of thrust throughout the entire time interval is the mean value of members in the last column of Table 1.1. It equals 0.21 N. The means value of thrust according to the small - amplitude theory (the mean value of numbers in the last column

t, s	V, ms^{-1}	$\alpha+\theta$, deg	α, deg	W, ms^{-1}	w, ms^{-1}	$\frac{\partial x}{\partial a}$	s, m	m, kgm^{-1}	mwW, N	$\frac{1}{2} mw^2 \frac{\partial x}{\partial a}$, N	$mwW - \frac{1}{2} mw^2 \frac{\partial x}{\partial a}$, N
0.04	0.50	17	3	0.15	0.03	0.97	0.094	6.9	0.03	0.00	0.03
0.08	0.60	45	3	0.42	0.03	0.74	0.087	5.9	0.07	0.00	0.07
0.12	0.74	60	5	0.64	0.06	0.57	0.079	4.9	0.19	0.01	0.18
0.16	0.68	48	16	0.50	0.19	0.85	0.083	5.4	0.51	0.08	0.43
0.20	0.52	13	10	0.12	0.09	1.00	0.087	5.9	0.06	0.02	0.04
0.24	0.62	-36	-8	-0.36	-0.09	0.88	0.088	6.1	0.20	0.02	0.18
0.28	0.87	-60	-16	-0.75	-0.24	0.72	0.083	5.4	0.97	0.11	0.86
0.32	0.67	-46	-10	-0.48	-0.12	0.81	0.084	5.5	0.32	0.03	0.29
0.36	0.52	-25	-6	-0.22	-0.05	0.95	0.092	6.6	0.07	0.01	0.06
0.40	0.48	-3	0	-0.02	0.00	1.00	0.093	6.8	0.00	0.00	0.00

Table 1.1. Measured values of swimming parameters for *Leuciscus* observed by Bainbridge, 1963, and estimated the mean thrust as given on the theory by equation 1.200. For explanations of variables, see text. Based on data by Lighthill, 1975. (Note: 1N = $1kgms^{-2}$ = 10^5 dyne.).

of Table 1.2) equals 0.25 N. The small - amplitude theory is seen to give somewhat higher values of thrust (by 19%). Quite likely, in most calculations this difference may be neglected and we may use the formulas based upon the similar small - amplitude theory.

Based on the obtained calculation of thrust (the lost column of Table 1.1), Lighthill assessed the mean value of the coefficient of fish resistance. It proved to approximate 0.04, whole is by hour times larger than the expected value for the laminary streamlining with the Reynolds number of above 10^5 corresponding to the length of the fish and its swimming velocity. Such divergence remains a puzzle. Lighthill considered the possible calculation errors but could not explain the divergence.

However, as Lighthill said, in their personal talk Dr. Bone suggested an idea explaining the obtained divergence. He attributes the greatest importance to the non-steady-state pattern of the fish's swimming movements, regarding it as the reason for a higher

t, s	W, ms^{-1}	w, ms^{-1}	mwW, N	$\frac{1}{2} mw^2$, N	$mwW - \frac{1}{2} mw^2$, N	t, s	W, ms^{-1}	w, ms^{-1}	mwW, N	$\frac{1}{2} mw^2$, N	$mwW - \frac{1}{2} mw^2$, N
0.04	0.15	0.03	0.03	0.00	0.03	0.24	-0.39	-0.09	0.21	0.02	0.19
0.08	0.47	0.03	0.08	0.00	0.08	0.28	-0.91	-0.24	1.18	0.16	1.02
0.12	0.78	0.07	0.27	0.01	0.26	0.32	-0.54	-0.12	0.36	0.04	0.32
0.16	0.57	0.19	0.58	0.10	0.48	0.36	-0.23	-0.05	0.08	0.01	0.07
0.20	0.12	0.09	0.06	0.02	0.04	0.40	-0.02	0.00	0.00	0.00	0.00

Table 1.2. Estimated the mean thrust as given on the theory by equation 1.109. For explanations of variables, see text.

resistance coefficient, according to Dr. Bone, the lateral movements of the fish body may adversely affect the growth of the boundary layer thickness. As it will be shown below, his suggestion is not far from the truth. Indeed, when the oscillation amplitude increases from head to tail, the oscillation body acquires an essential pressure gradient affecting the thickness and structure of the boundary layer.

The above studies disregard the values of the dorsal and ventral fins on the fish body as farming the flow streamlining the fish body. In (Newman, Wu, 1973, 1975) the theory of the thin body is applied to the analysis of propulsive parameters of the fish-like body which may carry fins of different configuration. Under configuration there was also the interrelation between the body thickness, the fin span and the vortex sheet causing off the fin edge.

1.3. Theory of swimming for animals with the semilunar caudal fin

According to Lighthill, the theory of thin body is not applicable to describe the mechanism by which animals with the semilunar caudal fin create the thrust, because in such case its main hypotheses is violated. This hypotheses claims that the environment is affected by the body through the mechanisms distributed along the very body. In such case, the function of the propeller is practically completely benefited by the caudal fin. As seen from the analysis of the latter, form and profile, the caudal fin can be examined by the method of the wing theory in an unsettled flow. The analysis of the problem may involve either of the following methods introduced below (Chopra, 1976).

1. To apply hydrodynamic equations and potential theory.
2. To construct a decision by using the distribution of vortexes or sources.

1.3.1. Two-dimensional theory of the lunate tail

Lighthill (1970) was the first to consider the two-dimensional theory of the lunate tail by using the first of the above mentioned methods. He based his analysis on the concept of the potential of accelerations, introduced by Prandtl. Previously this method was successfully employed in the work (Possio, 1940) to analyse the movement of profiles in some compressed medium, as well as in (Wu, 1961) to consider the efficiency of swimming movements of a flexible thin plate. The later paper may perfectly illustrate the efficiency of the two-dimensional theory.

The physical mechanism of work in the semilunar fin, according to Lihgthill (1969), can be illustrated by Fig. 1.22 from (Karman, Burgers, 1934). The Figure shows a horizontal layer of water excited by the oscillating fish tail. At the moments when the caudal fin takes extreme positions, vortexes are formed, something like a reactive jet is formed between the rows of vortexes. Regarding this simplified picture, one can say

Fig. 1.22. Illustrating vortices cast off by the caudal-fin trailing edge as the fish moves to the left, and also the jet-like streamline pattern induced by those vortices. (Redrawn from Lighthill, 1969, after Karman & Burgers, 1934).

that the caudal fin actuates the fish by the principle of the reactive jet, while the high efficiency is provided thanks to the large square of the cross section in the jet.

In his two-dimensional theory, Lighthill considers the caudal one unit of the wing of infinite length (in the direction of the span) with the chord $c = 2a$ in the direction from $-a$ to $+a$. The displacement law was found by Lighthill as

$$z = \left[h - i\alpha\left(x - b\right)\right]e^{i\omega t}, \tag{1.206}$$

where h and a are real numbers signifying the amplitude of the heaving and pitching motion respectively, and $x = b$ is the axis of pitch. A 90^0 phase difference between the heaving and pitching motions is assumed, ω is radian frequency, t is the time.

The mean thrust per unit span is

$$\rho\overline{P} = \rho\overline{\left[\pi a U^{-2}\left|A\right|^2 + \left(\pi A\alpha\,\mathrm{Im}\,A - \frac{1}{2}\pi a^2\omega^2\alpha^2 b\right)\right]}. \tag{1.207}$$

The mean rate of working per unit span equals

$$\rho\overline{E} = \frac{\rho}{2}\,\mathrm{Re}\left[\omega\left(2\pi aA + \pi a^2 B\right)\left(-\alpha b - ih\right) + \left(\pi\alpha^2 A - \frac{1}{8}\pi A^4 C\right)\left(-\omega\alpha\right)\right]. \tag{1.208}$$

The hydromechanic efficiency is not difficult to express through (1.207) and (1.208):

$$\eta = 1 - \frac{\left[\omega^2\alpha^2\left(b - \frac{1}{2}a\right)^2 + \left(\omega h - U\alpha\right)^2\right]\left(F - F^2 - G^2\right)}{\left(\omega\alpha\left(b - \frac{1}{2}a\right)\left[\alpha\left(b + \frac{1}{2}a\right)F - hG - \frac{1}{2}\alpha a\right] + \left(\omega h - U\alpha\right)\left[hF + \alpha\left(b + \frac{1}{2}a\right)G\right]\right)\omega}. \tag{1.209}$$

The above expressions involve the following symbols

$$A = -U\left(\left[\omega\alpha\left(b-\frac{1}{2}a\right)+i(U\alpha-\omega h)\right](F+iG)+\frac{1}{2}\omega\alpha a\right), \tag{1.210}$$

$$B = 2U\omega\alpha-\omega^2(h+i\alpha b), \tag{1.211}$$

$$C = i\omega^2\alpha. \tag{1.212}$$

where U is the undisturbed fluid flow, $F+iG$ is Theodorsen's function, Re and Im are the actual and the imaginary parts respectively.

Fig. 1.23 presents the numerical estimates of the thrust coefficient specified by the expression

$$C_T = \frac{\overline{P}}{\omega^2 h^2 a}, \tag{1.213}$$

and the efficiency, depending on the parameter

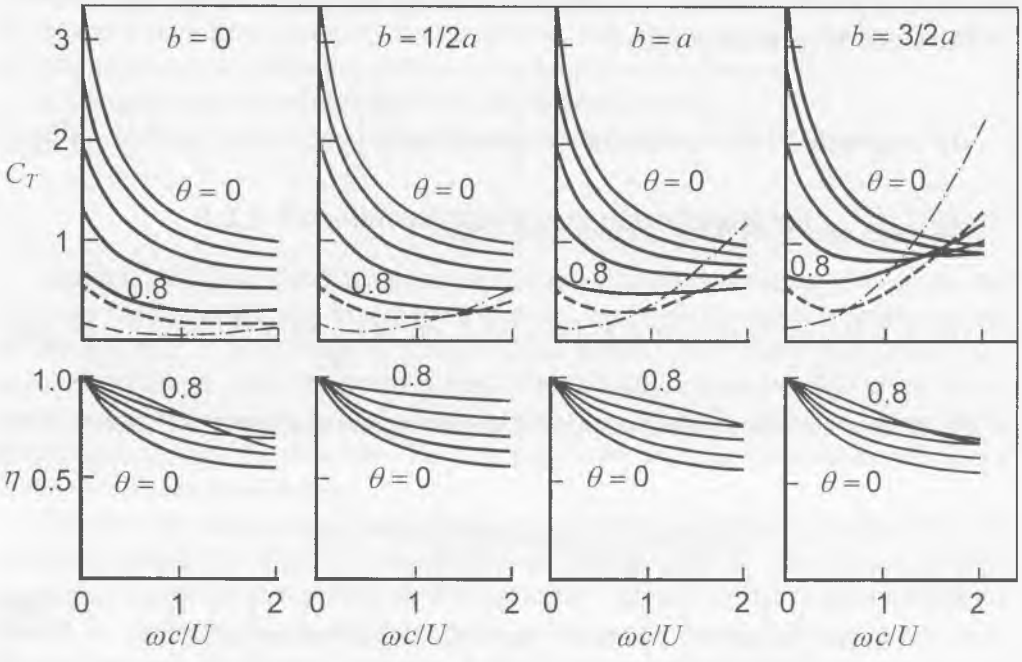

Fig. 1.23. Thrust coefficient and efficiency predicted by two-dimensional aerofoil theory, for values 0, 0.2, 0.4, 0.6 and 0.8 of a feathering parameter. (Redrawn from Lighthill, 1969).

$$\theta = \frac{U\alpha}{\omega h} \tag{1.214}$$

and the reduced frequency

$$2\sigma = \frac{2\omega a}{U} \tag{1.215}$$

for some positions of the pitch-axis : $b = 0$, $(1/2)a$, a and $(3/2)a$. The dotted line shows the contribution of the leading-edge suction of the wing for $\theta = 0.6$; the dot - and dash line shows the same for $\theta = 0.8$.

When analysed, the curves in Fig. 1.23 permit the some conclusions: One can clearly see the tendencies of the opposite trends: an increase in the efficiency and a decrease in the thrust coefficient when θ grows. At large values of θ the thrust coefficient grows when the pitch-axis shifts downstream (with an increase in b). With that, the contribution of the leading-edge suction in the total thrust is considerably growing, especially at light values of reduced frequency.

The above estimates are overstated because under consideration is only the energy of vorticity perpendicular to the motion (the consequence of a two-dimensional theory). At the same time, there is another vorticity parallel to the motion which can be considered only by the three-dimensional theory.

Lighthill regards the semilunar shape of the caudal fin to be evolutionary culmination of the motive complex. He marks that animals belonging to absolutely different evolutionary lines (for example, fishes and the cetaceans) acme up (biologically) to the semilunar tail as a means of fast movement in water. Moreover, the cross section of the semilunar tail in fishes and the cetaceans acquired the shape similar to the cross section of the aerodynamic wing. Of special importance is the monthly rounded leading edge, because the largest contribution of the thrust developed by the wing is due to its interaction with water near this leading edge.

Lighthill associates the benefits of the semilunar shape with the fact that under conventional oscillation frequencies, common for fast swimming, the tail of such shape can generate vortex rings approximating the circular shape (Fig. 1.22). Such rings carry a relatively high impulse at low energy.

1.3.2. Further progress of the semilunar fin theory

Lighthill's ideas were further advanced in some papers (Wu, 1971; Chopra, 1974, 1975, 1976; Chopra, Kambe, 1977). A two-dimensional task about the optimal shape of movement in the thin wing was also considered by Wu (1971) who stated the task in the way similar to Lighthill's one.

The respective difference of phases between the pitching and the heaving movement of the wing, depending on the reduced frequency, is demonstrated in Fig. 1.24 for various values of the load coefficient $\overline{C}_{T_0}$. The lower dotted chain curve $\alpha_p\left(\sigma_c, \overline{C}_{T_0}\right)$ shows the lower boundary corresponding to the smallest value of the reduced frequency. The solution acquires sense beginning with this smallest value.

Fig. 1.25 displays possible correlations between the coefficient of the suction (C_S) and of the thrust (C_T) as dependent on the reduced frequency.

The regard as the minimum value of this correlation to be the optimal one. Inhere, the coefficient of the suction is specified by expression

$$C_S = \frac{\overline{T}_S}{\frac{1}{4}\pi\rho U^2 a}, \tag{1.230}$$

where $\overline{T}_S$ is the time-averaged value of the suction.

Fig. 1.26 shows the dependence between the position of the pitch-axis of the wing and the reduced frequency. Fig. 1.27 demonstrates the respective dependence of the value (1-θ). The region of optimal parameters in Fig. 1.26 and 1.27 corresponds to the position of the dotted chain line.

On the whole, Wu's results well agree with those of Lighthill.

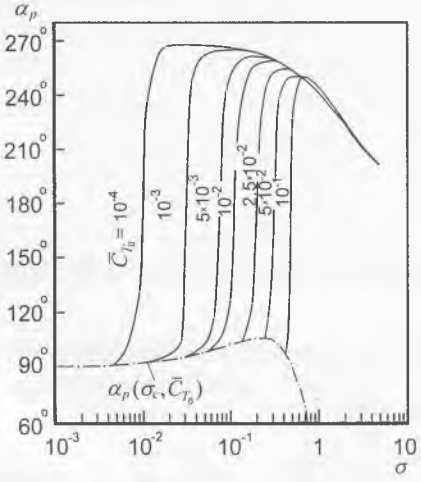

Fig. 1.24. The phase advance angle $\alpha_p(\sigma, \overline{C}_{T_0})$ of the pitching mode. (Redrawn from Wu, 1971).

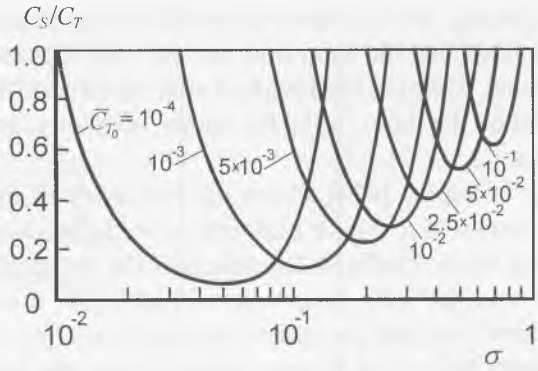

Fig. 1.25. The ratio of the thrust coefficient due to leading-edge suction to the total thrust coefficient. (Redrawn from Wu, 1971).

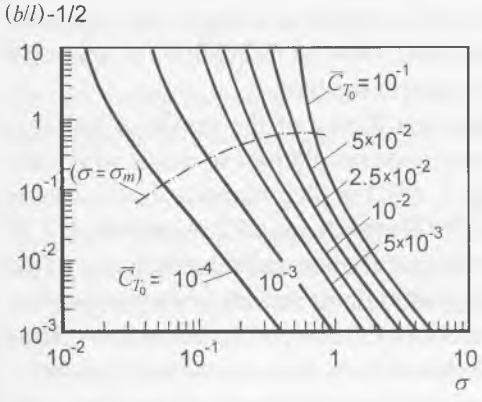

Fig. 1.26. The optimum location of pitching axis when the heaving is taken to lead the pitching by 90^0 in phase. (Redrawn from Wu, 1971).

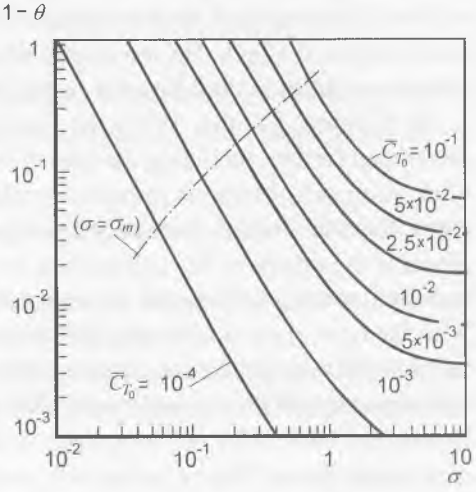

Fig. 1.27. Variation of the feathering parameter with the reduced frequency. (Redrawn from Wu, 1971).

Papers (Chopra, 1974, 1975) consider the movement of the wing with a finite aspect ratio (the three-dimensional theory). With that, the author limited his consideration to the case of the rectangular wing. However, the approach to the task in (Chopra, 1974) is absolutely different from that of Lighthill. This approach corresponds to the second method mentioned at the beginning of the section. The author accepted the concept advanced in (Karman, Burgers, 1934) which, in its turn, further develops those of Prandtl and Betz on the infinite line of action in the lifting force with the vortex intensity varying according to the wing span. Later on, Carman advanced this concept for the wing of finite span in the stationary case.

The analyses in (Chopra, 1974) is based on the assumption about the action line of the lifting force. It is assumed that the local flow around each cross section of the profile remains two-dimensional, while the local angle of attack is affected by the entire spectrum of vorticity, dependent on the time, within the lee jet, both towards the flow and across it along the plate span.

As a result, paper (Chopra, 1974) shows the efficiency of the rectangular wing, likewise in the two-dimensional case of Lighthill, to be the largest when the pitch-axis is close to the trailing edge. Under study was also the dependence between of the efficiency and thrust and the wing aspect ratio equalling 4; 6 and 8 of the reduced frequency, the parameter θ and the position of the pitch-axis ($b = 0$; $c/2$ and $3c/2$). The thrust and efficiency are shown not to depend much upon the wing aspect ratio. The pattern of dependence on Θ and σ is practically the same as in two-dimensional theory of Lighthill.

In (Chopra, 1976) the same author expanded his theory in the case of the thin wing with an infinite span of large amplitude. The analysis is simplified owing to the suggested small angles of attack. He shows that when combined, reduced frequencies of about 0.8 with the amplitude doubling the chord length, prove to the best.

In (Chopra, Kambe, 1977) the three-dimensional theory of the previous author is developed further, including the care of small-amplitude oscillations of wings with finite elongation and of various forms in the plan (Fig. 1. 28). For their numerical calculations these scientists adapted a special program of the Royal Aviation Institute. Fig. 1.29 presents the results of the calculation for the thrust coefficient and the efficiency of the rectangular wing with aspect ratio equalling 8 the solid lines, as well as the comparison with the rated data of (Chopra, 1974) (the crosses) and also with the calculation based on Lighthill two-dimensional theory (1970) (the dotted line). One can see that Lighthill's two-dimensional theory and, hence, Wu's theory (1971) do provide higher values of the thrust and efficiency as compared with the three-dimensional theory, which was mentioned above. This is particularly evident in the region of low values of the reduced frequency.

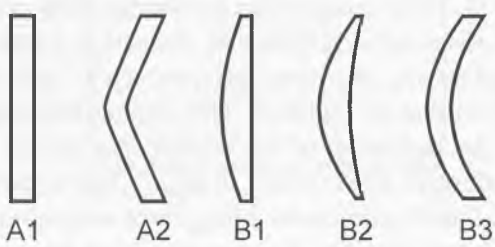

Fig. 1.28. Wing planforms for which detailed calculations have been made. (Redrawn from Chopra, Kambe, 1977).

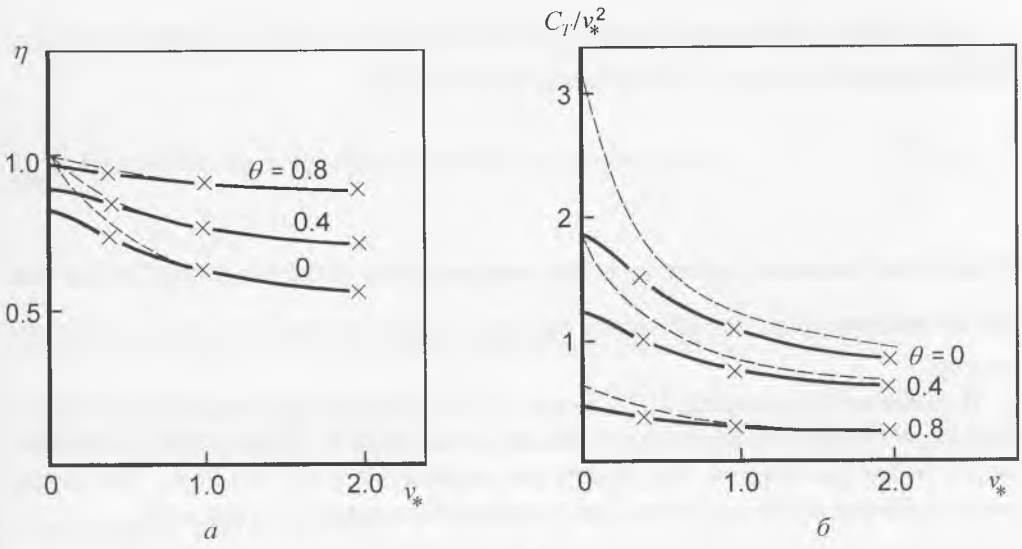

Fig. 1.29. Comparision of the values of η and C_T/v_*^2 given by the theory Chopra, Kambe, 1977 (solid lines), Chopra, 1974 (crosses) and Lighthill, 1970 (broken lines). (Redrawn from Chopra, Kambe, 1977).

The authors of (Chopra, Kambe, 1977) wanted to compare their theoretical calculations with experimental observations of animals.

They tried to consider the fact that generally speaking the oscillating amplitudes of caudal fins in fishes and dolphins can be regarded as small ones.

In any case, these authors correlated their calculations with Chopra (1976) which deals with oscillations of the rectangular wing of infinite span and arbitrary amplitude. According to the expression for the parameter

$$\theta = \frac{U\alpha}{\omega h}, \tag{1.231}$$

valid at small angles α was accepted as

$$\theta = \frac{U(tg\alpha)}{\omega h}, \tag{1.232}$$

regarding the fact that at essential α

$$tg\alpha \neq \alpha. \tag{1.233}$$

Fig. 1.30 shows the changes of two most important values η and C_T^* of the rectangular wing when the amplitude of oscillations is growing. Value

$$\varepsilon_* = \frac{h}{c_*} \tag{1.234}$$

serves as the parameter, where c_* is the complete chord of the wing. One can see that with an increase in ε_* the efficiency obviously goes down and the thrust coefficient goes up.

The authors (Logvinovitch, 1972; Kozlov, 1979, 1983) also tried to apply the theory of the wing with large elongation to calculations of the thrust for fishes with the semilunar caudal fin and for dolphins. Very briefly, the calculations are as a follows. The instant thrust coefficient of the rigid wing, approximating the caudal fin, is found by

$$c_A = -c_L\left(\frac{\partial \eta}{\partial t}\frac{1}{V} + \varphi\right) - c_{Di}. \tag{1.235}$$

Here c_L is the coefficient of the lifting force expressed by

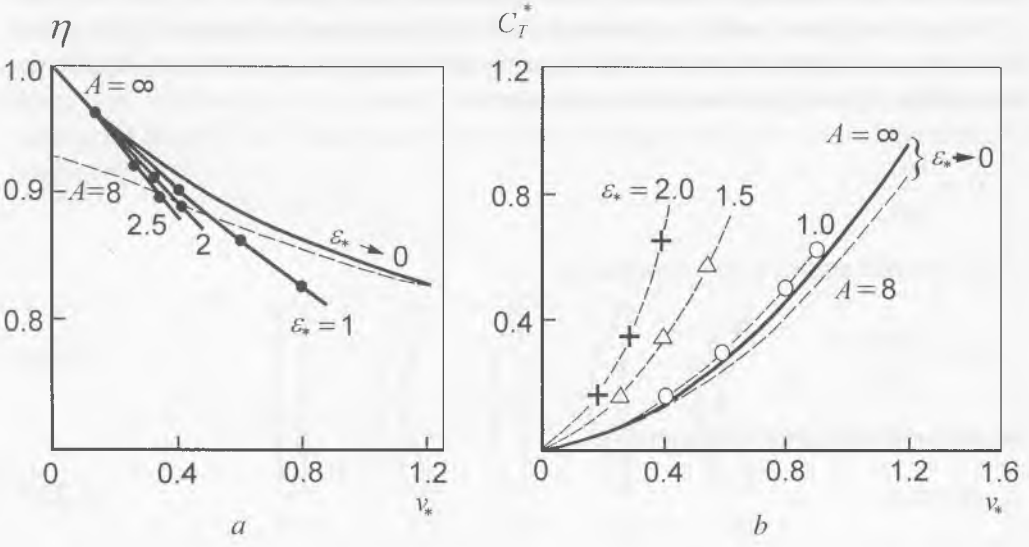

Fig. 1.30. Effect of finite amplitude on (*a*)η and (*b*)C_T^*. $\Theta = 0.6$. (Redrawn from Chopra, Kambe, 1977).

$$c_L = \frac{2\pi\lambda\alpha}{\sqrt{\lambda^2+4}+2}, \tag{1.236}$$

c_{Di} is the coefficient of the inductive resistance expressed by

$$c_{Di} = \frac{c_L^2(1+\delta)}{\pi\lambda}, \tag{1.237}$$

α is the attack angle of the wing (the caudal fin) expressed by

$$\alpha = -\frac{v_n}{V} = -\frac{1}{V}\left(\frac{\partial\eta}{\partial t} - V\frac{\partial\eta}{\partial x}\right), \tag{1.238}$$

λ is the aspect ratio of the wing

$$\lambda = \frac{(2R)^2}{S}, \tag{1.239}$$

where S is the wing area, $(1+\delta)$ is the cofactor regarding the deviation in the geometric form of the caudal fin from the optimal form in terms of the smallest inductive losses. Value δ with aspect ratio $\lambda = 1 \div 4$ does not exceed 2- 3% and in its first approximation it can be neglected. $2R$ is the wing span, v_n is the normal component of velocity in the trailing edge point of the wing, V is the animal velocity, $\eta(x, t)$ is the deviation of the median line from the coordinate axis: φ is the turning angle of the wing in relation to the direction of the instant velocity of the median line. The calculations accept $\varphi = 0$ because there are no experimental data on the value of this angle. Substituting (1.219) and (1.220) in (1.218), we shall get

$$c_A = \frac{2\pi\lambda}{\sqrt{\lambda^2+4}+2}\frac{v_n}{V}\left(\frac{\partial\eta}{\partial t}\frac{1}{V}\right) - \frac{4\pi\lambda}{\left(\sqrt{\lambda^2+4}+2\right)^2}\left(\frac{v_n}{V}\right)^2 \tag{1.240}$$

or, by averaging the expression (1.240) for the period of oscillation, we shall get

$$\bar{c}_A = \frac{2\pi\lambda}{\sqrt{\lambda^2+4}+2}\overline{\left[\left(\frac{v_n}{V}\right)\frac{\partial\eta}{\partial t}\frac{1}{V}\right]} - \frac{4\pi\lambda}{\left(\sqrt{\lambda^2+4}+2\right)^2}\overline{\left(\frac{v_n}{V}\right)^2}. \tag{1.241}$$

The expression for the average meaning of the thrust looks as

$$\overline{A} = \overline{c}_A \frac{\rho V^2}{2} S, \tag{1.242}$$

or, regarding

$$S = \frac{(2R)^2}{\lambda}, m = \rho \pi R^2, \tag{1.243}$$

it can be presented in a different way:

$$\overline{A} = \overline{c}_A \frac{2m_1^* V^2}{\pi \lambda}\Bigg|_{x=x_1}. \tag{1.244}$$

Here, x_1 is the coordinate of the trailing edge.

This form of the expression for the thrust was obtained by L. F. Kozlov. The above conclusion was also taken from L. F. Kozlov (1979).

The most comprehensive account of the tail fin kinematical parameters was given in the work by Zaytsev, Fedotov (1986). Unfortunately, the calculation was performed for the outdated assumptions on the dolphin fluke kinematics. They supposed that the angle of attack varied harmonically, the amplitude of this variation was overvalued (10°), and the fluke was considered rigid. Besides, the numerical methods used to solve the fluke movement equation were very sophisticated, which made it difficult to use the obtained results.

1.3.3. Comparison with the experiment

The authors of (Wu, 1971; Chopra, Kambe, 1977) tried to compare the results of theoretical calculations with literature data on experimental observations over parameters of fish and dolphin's swimming. They used data of works (Lang, Daybell, 1963; Fierstine, Walters, 1968; Masuda, Araga, Yoshino, 1975) only despite the fact that at the time were known other works (Bainbridge, 1963; Magnuson, Prescott, 1966; Pyatetsky, 1970*a*,*b*, 1975; Pyatetsky, Kayan, 1971, 1972*a*,*b*; 1976; Kayan, 1974; Kayan, Pyatetsky, 1977) involving the data of fish and dolphin kinematics.

Table 1.3 shows experimental data on the kinematics and hydrodynamics of the dolphin Lagenorhyncus obliquidens, taken from (Lang, Daybell, 1963), and data on the swimming of Wavyback skipjack from (Fierstine, Walters, 1968). With that, the data on the body length of the fish, the size of its caudal fin chord and the relation S_T/S_B of the projected planform area of tail to the total body surface area are not presented in (Fierstine, Walters, 1968). Therefore the data on the body length and the tail chord were taken

	L, cm	U, cms^{-1}	$\mathrm{Re} = \frac{UL}{\nu}$	$\nu_0 = \frac{\omega c_0}{U}$	$\epsilon_0 = \frac{h}{c_0}$	$\frac{S_T}{S_B}$
Lagenorhynchus obliquidens	200	510	$9.3.10^6$	0.71	1.3	0.03
Wavyback skipjack	100	310-820	$(2.8\text{-}7.5).10^6$	0.7-1.05	1.4-2.5	0.02

Table 1.3. Kinematic and hydrodynamic parameters for dolphin *Lagenorhinchus obliquidens* (Lang, Daybell, 1963) and fish *Wavyback skipjack* (Fierstine, Walters, 1968). (Adopted from Chopra and Kambe, 1977). For explanations of variables, see text.

	B1 ($b_0 = 0.8$; $\theta = 0.8$)		
	C_T	$\epsilon_0^2 C_T$	C_D
Lagenorhyncus obliquides	0.17	0.29	0.01
Wavyback skipjack	0.17-0.31	0.6-1.2	0.01-0.03
	B2 ($b_0 = 1.0$; $\theta = 0.8$)		
	C_T	$\epsilon_0^2 C_T$	C_D
Lagenorhyncus obliquides	0.19	0.32	0.01
Wavyback skipjack	0.19-0.38	0.74-1.48	0.15-0.03

Table 1.4. Hydrodynamic forces calculated from Table 1.3. (Adopted from Chopra and Kambe, 1977).

from (Masuda, Araga, Yoshino, 1975) and the relation S_T/S_B was estimated by the photographs in that paper. Besides, the available datas are badly scattered, which itself gives room for certain doubts.

The authors of (Chopra, Kambe, 1977) used the data from Table 1.3 to calculate the hydrodynamic forces (the coefficients of thrust and resistance). The results of their calculations are shown in Table 1.4 for the form of caudal fins approximated by the theoretical wings B1 and B2 (see Fig. 1.28) when the parameter $\theta = 0.8$, and the positions pitch-axis of the wing $b_0 = 0.8$ and $b_0 = 1.0$ (the pitch-axis of the wing is situated from the leading edge at the distance equalling of 0.8 and 1.0 of the chord length respectively).

When analysed, the data of Table 1.4 primarily demonstrates that the calculated values of the drag coefficient in the dolphin are essentially smaller than in the fish, but

at the same time they are three times as higher than in the respective rotation body during turbulent streamlining.

The authors of (Chopra, Kambe, 1977) analyse possible reasons behind such higher drag coefficient. They made calculations for the wing with the aspect ratio 8, while the aspect ratio in the dolphin was 5.4. The account of this fact could decrease the drag coefficient by 6%. A more accurate estimation of leading suction could also decrease this value by 10%. Besides, the calculations accepted $\theta = 0.8$. The authors accept that this value in fish and dolphin can actually be higher. Indeed, in the work of Yates, 1983 there is an assumption that the dolphin, whose kinematical data are adduced in the work of Lang and Daybell 1963 and referred in the works of Wu 1971b, Chopra and Kambe 1977, has the angle of slope of the fluke to horizontal plane is $\alpha = 0.66$. Under this value of the angle of slope of the fluke parameter $\theta = 0.9$.

If this value were raised up to 0.9, the drag coefficient could drop by two times. In this way, the estimates made by the authors of (Chopra, Kambe, 1977) are rather approximate. Nevertheless, the authors conclude that the streamlining of dolphins resembles that of a smooth surface with a respective laminar section. The streamlining of fishes is characterised by these authors as that of a rough surface.

Wu (1971) characterised more accurately the swimming of dolphins according to (Lang, Daybell, 1963). In his paper he gives a fragment of the kinematic picture of the dolphin's fluke as taken from (Lang, Daybell, 1963) and also makes the analysis of the fragment (Fig. 1.31).

Table 1.5 shows the geometric parameters of the dolphin determined by Wu according to (Lang, Daybell, 1963), as well as some additional kinematic characteristics. In the table we used the following denotations: L is the dolphin's body length, S - total body surface area, S_T projected planform area of the fluke, R - the span, l_o is the central chord, λ is the aspect ratio, h is the amplitude of the fluke oscillations.

Wu based his estimates on the suggestion that at a constant swimming velocity of the dolphin the thrust is balanced by the total drag. With that, the total drag (and hence, that of thrust) is estimated in view of the fact that the dolphin is streamlined by the flow as a rigid body having a 40% laminar section in the anterior part of the body. In this case, Wu regards the friction drag coefficient to equal $c_D = 0.0027$; the total drag being

$$D = c_D \frac{1}{2} \rho U^2 S. \tag{1.245}$$

The thrust coefficient of the fluke is found from

$$c_{T_0} = \frac{D}{\frac{1}{8}\pi\rho U^2 S_T} = 0.11. \tag{1.246}$$

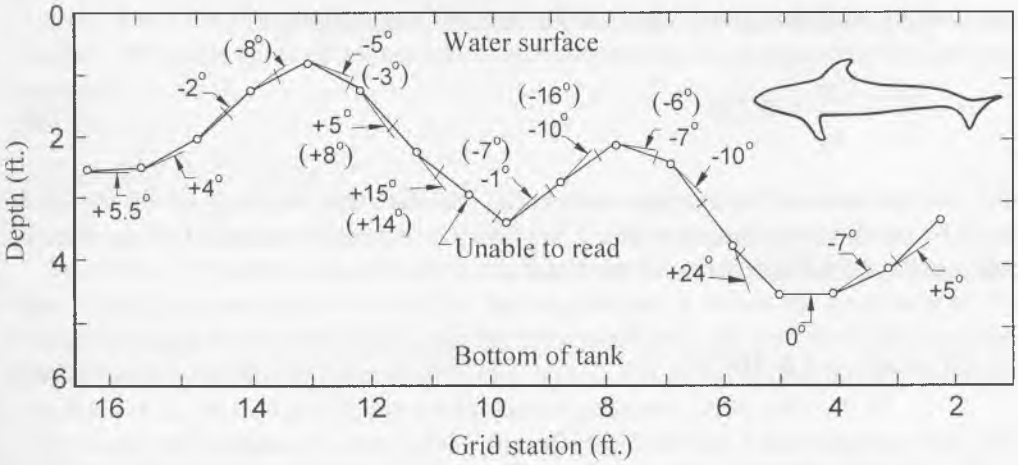

Fig. 1.31. Tail movements of a porpoise in cruising. The angles with arrows are the incidence angles of the tail relative to the path of tail-base measured by Lang & Daybell (1963); the angles in parentheses are the theoretical prediction. (Redrawn from Wu, 1971).

L, m	S, m^2	S_f, m^2	R, m	l_0, m	λ	h, m	U, ms^{-1}
2.0	1.512	0.047	0.51	0.188	5.4	0.25	5.1

Table 1.5. Kinematic and hydrodynamic parameters of dolphin *Lagenorhinchus obliquidens* (Lang, Daybell, 1963). (Adopted from Wu, 1971). For explanations of variables, see text.

Then Wu calculates the relative amplitude of oscillations in the fluke $\left(\frac{1}{2}\xi_0\right)$ comprising the expression (1.218), for the low of movement accepted by Wu

$$\frac{1}{2}\xi_0 = \frac{h}{l} = 4.15, \tag{1.247}$$

then $\xi_0 = 8.3$.

Here, the computation involves the value l which is the effective average semichord of the fluke equalling 0.06 m. The thing is that Wu's theory is developed for the wing with infinite span and a constant chord. Wu believes that his value of the average semichord

better agrees with his two-dimensional theory. This assumption seems to be most arbitrary one is Wu's estimations. Wu specifies the reduced frequency by

$$\sigma = \frac{\omega l}{U} = \frac{2\pi l}{\lambda_0} = 0.228. \tag{1.248}$$

and uses his value of the average semichord l and the value length λ_0 of the trajectory made by the fluke (according to Fig. 1.31) which he estimates to equal 1.65 m. Then he calculates the load coefficient of the fluke as

$$\overline{C}_{T_0} = \frac{C_{T_0}}{\xi_0^2} = 1.6 \cdot 10^{-3}. \tag{1.249}$$

By using the obtained values of σ and $\overline{C}_{T_0}$ and by suggesting that the movement of the fluke is optimal, Wu employs Figs. 1.24 and 1.27 and the calculated relations (1.221) -(1.232) to determine the values of $\eta = 0.99$; $Z_p = 0.104$; $\alpha_p = 263^0$; $\theta = 0.92$; and $x_0/2l = 0.793$. Here, $x_0/2l$ is the relative position of the pitch-axes of the fluke. The other symbols are given in that part of the previous paragraph where Wu's theory is described.

Wu also theoretically assessed the values of the angle between the fluke and the direction of the trajectory of its movement which are shown in Fig. 1.31 in brackets. The results of the estimates well agree with the measured values (the numbers without brackets). However we ought to consider this accordance accidental. In chapter 6 it was shown that the conception of the fluke as some flat plate leads to the angles of attack, which are a few times overvalued.

When analysed, the results of the estimates demonstrate that the phase shift α_p between the heaving and pitching movements of the fluke, as well as the position of the pitch-axis, are actually close it the optimal ones. The value of Θ, and especially that of η, seem to be overestimated. It is not surprising for the two-dimensional theory, witch was already mentioned before and is particularly obviously illustrated in Fig. 1.29.

In addition to the foreign experimental data discussed above, some experimental papers have been recently published in our own literature (Pyatetsky, Kayan, 1975; Kayan, 1979; Romanenko, 1980, 1986). These papers contain data necessary to compare experiments and the theory. The most important parameters of dolphin's swimming cited above

$$\sigma = \frac{\omega l}{U} \quad \text{and} \quad \Theta = \frac{Utg\alpha}{\omega h} \tag{1.250}$$

embrace the relations between the values ω/U and U/h which have been well examined by now. Here, h is the amplitude of the tail oscillations. A well-checked dependence (Kozlov, 1983) was obtained for the relations between w and U, in particular for *Tursiops truncatus*

$$\omega = 2\pi\left(1.05\frac{U}{L} + 0.25\right). \tag{1.251}$$

As to the U/h relation, we may unite the data from (Kozlov, 1975; Fish, 1983). The value α for the same species is vital for the calculations. It shows the amplitude of the inclination angle between the fluke and the movement axis. As well as the value of the central chord l_0 and that of the animal's body length, it is given in (Kayan, 1979) for the velocity $U = 2.3$ ms^{-1}. All of them are brought together in Table 1.6.

By using the formulas (1.250-1.251), the data from Table 1.6 and relations $h \cong 0.1L$ (Fish, 1993), we shall obtain the following estimates for the relation between the oscillation amplitude and the central chord ε, the reduced frequency σ, parameter θ and efficiency η demonstrated in table 1.7. Here, σ is calculated by using the complete central chord. The values of η corresponding to there of σ is estimated by Fig. 1.30 taken from (Chopra, Kambe, 1977). This figure shows the data for the rectangular wing of infinite span ($A = \infty$) and for the wing with the aspect ratio of 8 ($A = 8$) (the dotted line). The impact of the large amplitude of oscillations in this Figure is considered only for the wing of infinite span. If we suggest that the impact of the large amplitude will be similar for the wing of finite span with the aspect ratio $A = 4$ (the fluke of *Tursiops truncatus*), then the values of η will become still a little smaller.

Wu's theory (1971) also permits estimating the position of the pitch-axis in the fluke of *Tursiops truncatus*. These datas are given in table 1.7. The estimate shows the pitch-axis to be situated at the distance of 0.83 of the chord from anterior edge of the fin.

The analysis of the obtained estimates demonstrates the values of the parameters θ and the position of the pitch-axis of the fluke of *Tursiops truncatus* to be in good agreement with presumed theoretically the optimal values.

To conclude this section, we should like to emphasise that the theory developed in (Chopra, Kambe, 1977), if corrected for a larger amplitude of oscillations, seems to be best to completely consider the peculiarities of the semilunar caudal fin. However, this

U, ms^{-1}	α, rad	l_0, m	L, m
2.3	0.52	0.24	2.4

Table 1.6. Parameters of dolphin *Tursiops truncatus* (Adopted from Kayan, 1979). For explanations of variables, see text.

U, ms^{-1}	$\epsilon = \frac{h}{l_0}$	σ	θ, rad	η
2.3	1.0	0.82	0.7	0.79

Table 1.7. Parameters calculated from Table 1.6.

theory does not regard all and everything. For example, it disregards the impact of the thickness and flexibility of the fluke; the correction for a larger amplitude is made only for the wing of infinite span and only for the value of $\theta = 0.6$.

1.3.4. Peculiarities of scombroid swimming

As we have cited before, according to Lighthill, the scombroid way of swimming is more progressive than the eel-like one. The scombroid swimming has a higher hydromechanic efficiency. This can be attributed to the fact that unlike in the eel-like swimming, the appearance of vortex screening on the edges of the dorsal and ventral fins is less probable in the scombroid swimming. In such swimming, the relative amplitude of lateral displacement of the fish's own body is essentially lower than in eel-like swimming. Vortex screening on the fin edges is more possible in eel-like swimming. As a result, the cumulative impulse in the fish's vortex wake does not happen to occur exactly in the phase with the lateral velocity of oscillations of the caudal fin. Therefore the thrust is less increasing (due to the additional impulse of the vortex screening of the dorsal and ventral fins) than the energy losses in the wake. However, the scombroid swimming has a certain defect, as compared with the eel-like one. In the former, the so-called «recoil», return i.e. the reaction of the fish's body to the forces chiefly applied to the caudal part. This «recoil» is manifested as the anterior part of the fish body begins yawing during its active motion. This phenomenon of yawing is practically absent in the eel-like swimming when not only the caudal part but all sections of the fish's body are involved in oscillations. Such «recoil» in scombroid swimming could necessitate additional loses of energy and, hence, decrease the efficiency. These additional losses could annihilate the above advantages of the scombroid swimming as compared with the eel-like one, but there are some morphological changes typical of scombroid fishes which annihilate the phenomenon of the «recoil». Lighthill (1977) discussed it in details and estimated it quantitatively. According to him, if the «recoil» is properly regarded, the law of the body deformation in scombroid fishes can be written as

$$h = H(x)\cos\left[\omega\left(t + \frac{l-x}{C}\right)\right] + [h_1 + h_3(l-x)]\cos\omega t + [h_2 + h_4(l-x)]\sin\omega t. \qquad (1.252)$$

The first term in the right-hand part of (1.252) is the law of deformation. It could be preconditioned by the muscular contractions proper if there were no «recoil». The second and the third members respectively reflect the displacements of the body elements due to the «recoil». Here, h_1, h_2, h_3 and h_4 are constant values, $H(x)$ is the amplitude function preconditioned by muscular contractions, l is the body length of the fish, C is the velocity of the propulsive wave, x is the current co-ordinate of a body points within the system of co-ordinates associated with the fish body. If we turn to the expression for the total thrust developed by the fish, which was given before, and rewrite it as

$$\overline{T} = \overline{\left[m\left[\left(v_n \frac{\partial h}{\partial t}\right) - \frac{1}{2} v_n^2\right]\right]}_{x=l}, \qquad (1.253)$$

then the values compressing this expression, with regards of the deformation law (1.252), will look as

$$v_n = -\left[\omega\left(1-\frac{U}{C}\right)H(l) + \omega h_1 + U h_4\right]\sin\omega t + \left[U\left(\frac{\partial H}{\partial x}\right)_{x=l} + \omega h_2 - U h_3\right]\cos\omega t \qquad (1.254)$$

and

$$\frac{\partial h}{\partial t} = -\omega[H(l) + h_1]\sin\omega t + \omega h_2 \cos\omega t. \qquad (1.255)$$

It is easy to see that the values v_n and $\frac{\partial h}{\partial t}$ can be correlated when $h_1=h_2=h_3=h_4=0$, i. e. when there is no «recoil». Under such conditions, the thrust will be the maximum one.

It is true, there is another condition to be fulfilled, i. e. $\left(\frac{\partial H}{\partial x}\right)_{x=l} = 0$. Lighthill offered this condition before as that to optimise the efficiency of eel-like swimming. In reality fishes may not fulfil this condition. In this case, the condition for optimisation may be realised by the best correlation between the values v_n and $\frac{\partial h}{\partial t}$ which can be written as based upon (1.254) and (1.255) to yield

$$U\left(\frac{\partial H}{\partial x}\right)_{x=l} + \omega h_2 - U h_3 = 0 \qquad (1.256)$$

and

$$h_2=0. \tag{1.257}$$

Hence, we may have

$$h_3=\left(\frac{\partial H}{\partial x}\right)_{x=l}\neq 0. \tag{1.258}$$

Lighthill (1977a) made a quantification to assess the position of the yawing axis and the yawing amplitude of the scombroid fish body as specified by the «recoil». He regarded not only the force F applied to the caudal fin (Fig. 1.32) but also the force of resistance exercised by the fish body due to lateral yawing movements. Lighthill presents the velocity of lateral movements in different sections of the fish body in some general form

$$v_n = v_{n1}e^{i\omega t}, \tag{1.259}$$

where v_n and v_{n1} may be complex values. The resistance force against the lateral motion of the fish can be sufficiently accurately written as $k\rho s(v_{n1})v_n$
where

$$k = 8/3\pi = 0.85 \tag{1.260}$$

and

$$s = s_m\left[4\frac{x}{l}\left(1-\frac{x}{l}\right)\right]. \tag{1.261}$$

The latter expression approximates the distribution of the fish's body height along the fish's length. It is also feasible to consider the distribution of the oscillation velocity along the fish body as

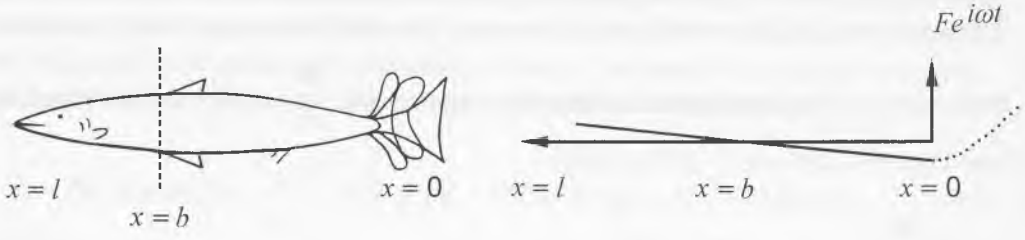

Fig. 1.32. Assumptions underlying recoil. (Redrawn from Lighthill, 1977).

$$v_{n1} = v_{n0}\left(1 - \frac{x}{b}\right). \tag{1.262}$$

Here, $x = b$ is the axis of yawing, b is the actual number, unlike v_n, which may be complex and is the amplitude of oscillations in the lateral velocity at the point $x = 0$ (on the tail edge).

Then Lighthill writes down the equation of impulses as

$$i\omega\int_0^l \rho s^2 v_{n1} dx = -\int_0^l k\rho s|v_{n1}|v_{n1} dx + F_0, \tag{1.263}$$

where $F=F_0 e^{iwt}$; the factor e^{iwt} is everywhere omitted. The left-hand part is a time-derivative of the impulse of liquid induced by the oscillating body. It is integrated by the body length. The right-hand part is the sum of the acting lateral forces, including those of resistance against the lateral motion (the integral in the right-hand part).

In the similar way one writes down the equation of the angular moment

$$i\omega\int_0^l x\rho s^2 v_{n1} dx = -\int_0^l xk\rho s|v_{n1}|v_{n1} dx + F_0. \tag{1.264}$$

Here, the moment of forces is calculated in relation to the points $x = 0$ to which the force F is applied.

The left-hand part (1.264) regards (1.262) and (1.261) and accepts the form

$$\frac{4i\omega\rho s_m^2 v_{n0} l^2}{15}\left(1 - \frac{4}{7}\frac{l}{b}\right), \tag{1.265}$$

disappearing at $b = 0.571l$.

The right-hand part can be written as

$$-\frac{k\rho s_m |v_{n0}| v_{n0}}{15l^2 b^2}\left[2lb^5 - b^6 - (l-b)^6 + 4l(l-b)^5 - 5l^2(l-b)^4\right] \tag{1.266}$$

which disappears at $b = 0.589l$.

The value of b in the interval between the obtained ones can be considered as the axis of yawing, i. e.

$$b \cong 0.58l. \tag{1.267}$$

With account of the above results, the equation of impulses (1.263) is transformed into

$$0.074i\omega\rho s_m^2 l v_{n0} + 0.051\rho s_m l |v_{n0}| v_{n0} = F_0. \tag{1.268}$$

The second term in the left-hand part is due to the impact of resistance against the lateral movement. If we neglect it, then we shall have a clearly «reactive» case when the lateral velocity, expressed by

$$v_{nR} = \frac{F_0}{0.074i\omega\rho s_m^2 l}, \tag{1.269}$$

gets shifted by the phase to 90° in relation of F_0. Such phase shift of the force and the reaction velocity should not lead to additional losses of energy. However, this condition is not valid because of the resistance term in the equation (1.268).

With account of (1.269), the complete expression (1.268) can be rewritten as

$$v_{n0}\left(1 + 0.69\frac{|v_{n0}|}{i\omega s_m}\right) = v_{nR}. \tag{1.270}$$

The actual and imaginary parts of this expression can be easily calculated and are shown in Fig. 1.33 in the function of the value

$$\zeta = \frac{v_{nR}}{-i\omega s_m} = \frac{F_0}{0.074\omega^2\rho s_m^3 l}. \tag{1.271}$$

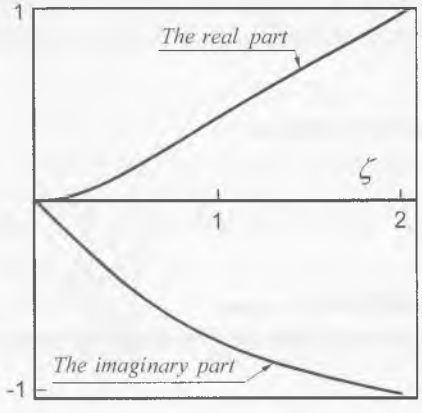

Fig. 1.33. The real and imaginary parts of the expression (1.270) *vs.* of the parameter .(Redrawn from Lighthill, 1977).

The latter is the relation between the reactive response of the fish body to the impact of the force F_o and the response in which the lateral shifts of the posterior edge at $x = 0$ have the amplitude equalling the maximum body height s_m. The imaginary part $\mathrm{Im}(v_{no})$ is always negative and therefore it is situated below the axis in Fig. 1.33. Meanwhile, the actual part $\mathrm{Re}(v_{no})$, leading to the energy dissipation, is always positive, being situated above the axis. An interesting conclusion can be drawn from Fig. 1.33. If ξ is small in comparison with 1 (for example, when $\xi \leq 0.2$), the «recoil» is almost completely reactive, i.e. $\mathrm{Re}\,(v_{no})$ is essentially smaller than $\mathrm{Im}(v_{no})$. It is quite accurate to believe that $v_{no} = v_{nR}$. Under such conditions, additional losses of energy can be neglected.

The condition $\xi \leq 0.2$ means that the movement of the «recoil» is a lateral shift with the amplitude below $0.2\, s_m$ throughout the entire body length of the fish. With that, the greatest value of the shift relates to the body point $x = 0$ (the point to which force F is applied). Hence we can make a very important conclusion: the fish prefers to have the body height s_m as high as possible because in such case the condition of the small ξ is easier to fulfil.

Lighthill believes that scombroid fishes reveal respective morphological changes aimed at minimising the phenomenon of yawing (the phenomenon of the «recoil»). First, there is an increase in the height of the anterior part of the body due to which the virtual mass greatly grows. Second, there is a decrease in the cross section of the body part between its middle and the caudal fin: this part directly adjust the caudal fin. The oscillation velocity of this part is already quite considerable but still it does not heavily intensify the thrust. When the cross section is essential, this part could have a large virtual mass and could promote the value of the «recoil». Such morphology of scombroid fishes permits them to realise the advantages of the scombroid swimming discussed above and to utmostly minimise its drawbacks («recoil»).

The above theoretical analysis made by Lighthill disregards the longitudinal velocity of fishes' motion. However, this problem when specially considered, shows that the swimming velocity with $U/\omega l$ not more than 0.1, the impact of the longitudinal velocity upon «recoil» can be neglected.

Paper (Kambe, 1978) develops Lighthill's theory about «recoil» for a more common case. Besides the facts regarded by Lighthill, some more information has been added: 1) on the rectilinear motion at constant velocity U; 2) on the resistance to the fish's rectilinear motion; 3) on the possible descent of the vortex screening in the posterior part of the fish's body from the edges of the dorsal and ventral fins.

However, it should be noted that the numerical estimates in (Kambe, 1978) do not differ much from those made by Lighthill. In particular, according to the estimates of (Kambe, 1978), the axis of yawing should assure at the distance of 0,42 from the fish nose, which particularly coincides with Lighthill's estimate for a simpler theory. The analysis made in (Kambe, 1978) also allows to conclude that the energy losses due to «recoil» are considerably smaller when there is no descent of the vortex screening from the dorsal and ventral fins. It is very urge to minimise the descent of the vortex screening

from the fins by which the author of (Kambe, 1978) explains the power of some fast-moving fishes to withdraw their fins into special hallows on their body.

The author of (Kambe, 1978) compares these estimates of the position of the yawing axis with the position of the minimums of the amplitude function of oscillations in some fishes as they were examined by Bainbridge (1963). This scientist believes the minimums of the amplitude function to be coinciding with the yawing axes. According to Bainbridge, in three fish slices under his study these minimums are situated at the distance of $0.36l$, $0.31l$ and $0.29l$ from the fish's nose respectively. This is in good agreement with the estimates of Lighthill and Kambe. Some divergence from the marking estimate ($0.42l$) is due to the asymmetry of the position of the mass along the fish's body which was disregarded by the theory. But there can be another explanation: we shall give it in the next chapter with the body deformation in actively swimming fishes and dolphins.

The described analysis of peculiarities typical of scombroid swimming in fishes demonstrates that in the first approximation it seems possible to describe it by the theory of the thin body developed by Lighthill, his followers and Russian academician G.V. Logvinovich. The phenomenon of «recoil» can be disregarded because nature has given scombroid fishes such morphological features which utterly minimise the adverse side effects. Whenever possible, it is vital to get experimental data on the genuine law of body deformation in the actively swimming animal. This law will inevitably include both the result of the animal's muscular activity and the effect of «recoil». The use of such law while estimating the energy and force parameters of animals' swimming will be the most correct one.

1.3.5. Applicability of the hypothesis on stability for estimation of the hydrodynamic forces developed by the lunate tail

The above theories of the lunate caudal fin are, to a large extent, very approximate. Even the theory advanced in (Chopra, Kambe, 1977), though it most completely reflects the characteristic features of the lunate fin, is far from perfection. This theory disregards some important peculiarities, for example, the thickness of the fin, the oscillation amplitude, etc. Therefore, to be able to provide express-estimates of the forces developed by the fin, it is often necessary to use relations obtained for the wing in the stationary flow and to consider that the forces affecting the wing are specified by the instant values of the attack angle and the instant velocity of the wing motion (the hypothesis of stability). However, it is vital to know the threshold values of the motion parameters in the caudal fin or of its approximating wing at witch the hypothesis on stability stops working.

In paper (Dovgy, Kayan, 1983) the authors made experiments with the propulsive characteristics of the rigid rectangular wing with the profile of NACA-0015 and aspect ratio $\lambda = 3$. The wing was fixed in the water flow on some special drafts which provided the wing with vertical oscillations in accordance with harmonic law

$$y=A_o\cos\omega t, \tag{1.272}$$

where A_o was the amplitude of oscillations. The drafts, were hinged in the middle section of the wing at the ends of the profile chord. The coordinates of the wing edge in this case were changing by the following laws: the anterior edge

$$y_1=A_o\cos\omega t, \tag{1.273}$$

for the posterior edge

$$y_2 = A_o\cos(\omega t-\varphi).$$

Fig. 1.34 shows the experimental data for the thrust coefficient depending on the parameter $\lambda_p = U/(\omega A_o)$ where U is the longitudinal component of the flow velocity. The data were obtained at two values of the phase sleight in oscillations of the wing edges equalling 36° and 18°, the oscillation amplitude $A_o = 0.06$ m.

The same figures presents the respective dependencies calculated theoretically (curves 1 and 2) disregarding the suction.

It is obvious that at the phase shift of 36° the calculated values, based on the hypothesis of stability, rather accurately agree with the experimental ones at the values of λ_p from 1.1-1.2 and higher. If we regard the suction, the thresholds of the hypothesis on stability will expand towards smaller values if λ_p.

By using the data in Table 1.5 - 1.7 and of work (Fish, 1983), it is easy to estimate the values of the parameter $\lambda_p = 1.16 - 1.36$ characterising the kinematics of the dolphins caudal fin for two values of *Tursioips truncatus* swimming velocity U = 2 – 6 ms^{-1}. The estimates showed that when the dolphin's swimming speed varies from 2 to 6 ms^{-1}, the value of λ_p varies from 1.16 to 1.36.

Before drawing any conclusions from the analysed estimates, it should be noted that the kinematics of the caudal fin of *Tursiops truncatus* corresponds to that of the wing

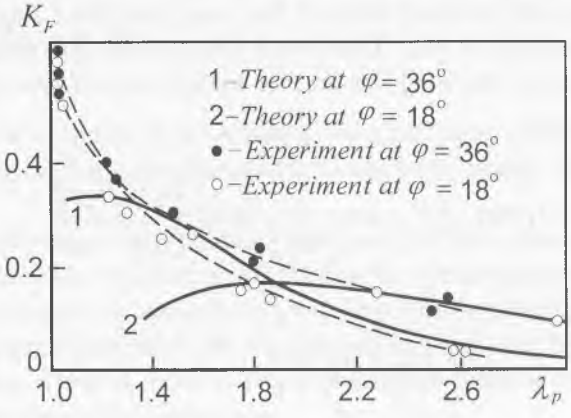

Fig. 1.34. Thrust coefficient *vs.* λ_p. (Redrawn from Dovgy, Kayan, 1981).

profile studied in (Dovgy, Kayan, 1983) when the phase shift of the wing edges equalled 36°. Hence, the theory of the wing, based upon the hypothesis of stability, is sufficiently accurately applicable to estimate the characteristics of the fin propulsor of *Tursiops truncatus* when the animal's swimming velocity is 2 ms^{-1} and higher. Unfortunately, it is impossible to make similar estimates for other species of dolphins, likewise for fishes with the lunate fin because there are no kinematic parameters necessary for such calculations.

The conclusions on the applicability of the hypothesis of stability, similar to those made above can be also drawn from the analysis of (Grebeshov, Sagoyan, 1976; Korennaya, 1981).

1.3.6. Hydrodynamic forces exerting a rigid wing moving with high hearing and pitching

This part deals with two models of wing movement: one with low amplitude of pitch and heave and the other with high amplitude (Pushkov, Romanenko, 2000). That is aimed to compare the results of different methods used to estimate achieved hydrodynamic forces although the ways of obtaining the results were the same and also aimed to compare them with the experimental data.

Plane transient movement of thin wing problem was discussed by L. I. Sedov (1966) and A. I. Nekrasov (1948). In case of low amplitude oscillations of the profile in relation to some main motion the authors obtained the expressions for hydrodynamic forces, which allow simple physical interpretation.

Given a thin wing moving in boundless volume of liquid, which rests on the infinity. The movement of the wing can be represented as the main movement with the speed U_0 and some additional movement with small drift and low speed. When the wing movement is described by the coordinates $X0Y$, which moves with the speed U_0, we consider that vortex wake comes off the back edge of the wing, and the Chaplygin–Jouckovsky condition for finite speed is true. There were obtained the following expressions for lifting force Y normal to the wing line and for suction force X oriented along the wing line,

$$Y = -m^* \frac{dv_n}{dt} - 2\rho\pi a U_0 \left(v_n - a\omega_z / 2\right) - \rho a U_0 \int_a^\infty \frac{\gamma(\xi,t)d\xi}{\sqrt{\xi^2 - a^2}}, \qquad (1.274)$$

$$X = 2\rho\pi a \left(v_n + (1/2\pi) \int_a^\infty \frac{\gamma(\xi,t)d\xi}{\sqrt{\xi^2 - a^2}} \right)^2,$$

where $m^* = \rho\pi(b/2)^2$ is virtual mass of wing, $b/2$ is a half of chord, a is amplitude of transversal oscillations, v_n is normal speed in the center of the wing, $\omega = \dfrac{\partial\vartheta}{\partial t}$ is angular velocity, $\gamma(\xi,t)$ is vortex intensity in the trace at the distance of ξ from the centre of the wing.

With the help of simple transformations equation (1.274) can be transformed in notation

$$\begin{aligned} Y &= -m^* \frac{dv_n}{dt} - \rho U_0 \Gamma, \\ X &= m^* v_n \omega_z + \rho v_n \Gamma - 2\rho\pi a u_* (v_n - u_*). \end{aligned} \tag{1.275}$$

Here the value $\Gamma = 2\pi\alpha\left(v_n - \dfrac{a\omega_z}{2} - u_*\right)$ may be considered as added circulation (Nekrasov, 1948) and the value $u_* = \dfrac{-1}{2\pi}\int\limits_a^\infty \dfrac{\gamma(\xi,t)d\xi}{\sqrt{\xi^2 - a^2}}$ as some effective velocity induced by presence of the vortex wake behind the wing.

The first member of the suction force notation (1.275) coinAides with the solution of the wing movement plane problem in the absence of the circulation, the second member is due to circulation and may be treated as Jouckovsky force projection $Y = \rho U\Gamma$, where U is absolute velocity of profile centre movement. The third component by its structure is analogous to the expressions for inductive reactance X_i of the stationary moving finite span wing.

In fact, the scheme of the Prandtl carrying line leads to the equation

$$X_i = \rho\pi \int\limits_{-l}^{l} b u_{ni}(v_n - u_{ni})dz, \tag{1.276}$$

where b is the chord of the wing in section z, l is a half-span of the wing, v_n is normal velocity of the wing, $u_{ni} = u_{ni}(z)$ is the velocity induced by vortex wake in the points of the carrying line.

Let us consider the task of nonstationary motion of the finite span wing as it is defined in plane task. Let the plane projection of the wing be symmetrical relatively to central line OZ (fig. 1.35). In case of nonstationary motion of finite span wing the effect of the trace on hydrodynamics features of the wing can (as in plane task) be taken into account by introducing some effective induced velocity. Suppose plane sections method can be applied and relations like (1.275) are right

$$Y = -m^* \frac{dv_n}{dt} - \rho U_0 \int_{-l}^{l} \Gamma(z) dz,$$
$$X = m^* v_n \omega_z + \rho v_n \int_{-l}^{l} \Gamma(z) dz - X_i. \qquad (1.277)$$

Here m^* is virtual mass of the wing, $X_i = \rho\pi \int_{-l}^{l} b(z) f_*(z)(v_n - f_*(z)) dz$ is inductive "reactance", f_* is some effective velocity induced by the vortex wake that stays in the trace, v_n is normal velocity of the wing in the points of its symmetry axis $0Z$, $b(z)$ is the chord of the wing section $z=const$, l is half span of the wing.

As v_n does not depend on z then it is possible to make upper estimation for X_i:

$$X_i \le \rho\pi S \frac{v_n^2}{4}, \qquad (1.278)$$

where S is the square of the wing. The last expression shows that in case of non-steady-state motion of finite span wing the coefficient of inductive resistance can not exceed $C_{Xi} \le \pi\alpha^2 / 2$, where $a = v_n/U_0$ - is the instant angle of attack, U_0 is the velocity of the main movement.

Comparing the obtained upper estimation value for C_{Xi} with the standard characteristics of the wings with aspect ratio λ=2-5 we can see that actual values of C_{Xi}

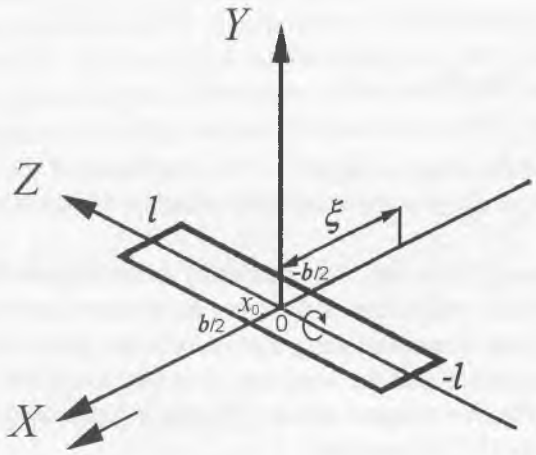

Fig. 1.35. The co-ordinate system in the wing frame of reference.

are slightly less than the estimation. So for the wings of such aspect ratio the vortex wake staying behind the wing during its stationary motion with some angle of attack α, in fact ensures the maximum value $C_{Xi} = \pi\alpha^2 / 2$ by means of the inductive slopes of the flow, which it creates. Therefore the additional slopes of the flow created by the vortices caused by the non-steady-state motion of the wing can not increase the value of C_{Xi} due to the estimation (1.278).

In order to get the value of the suction force X and projection of the hydrodynamic forces T on the axis OX of the oscillating finite span wing we can use the upper estimation mentioned above.

Taking into account (1.277) and profile resistance, it is possible to state:

$$T = m^* v_n \omega_z - \left(Y + m^* \frac{dv_n}{dt} \right) \frac{v_n}{U_0} - Y\vartheta - X_i - \frac{\rho U_0^2 S}{2} C_p, \tag{1.279}$$

where C_p is the coefficient of profile resistance, and the inductive resistance X is defined by (1.278).

If $V_y = dy/dt$ – transverse velocity of the wing in its centre, then $v_n = V_y - U_0\vartheta$ and

$$X = m^* v_n \omega_z - \left(Y + m^* \frac{dv_n}{dt} \right) \frac{v_n}{U_0} - X_i,$$

$$T = m^* v_n \omega_z - Y \frac{V_y}{U_0} - m^* \frac{dv_n}{dt} \frac{v_n}{U_0}. \tag{1.280}$$

So if we know the value of m^* and Y we can estimate the suction force and the projection of the hydrodynamic forces on the axis $0X$. Every time as we evaluate X and T we can use the known numerical solutions (Belotserkovskii, 1971) for Y and m^*.

Let us consider the motion of the rectangular wing. The transverse oscillation

$$y = a\sin\omega t, \tag{1.281}$$

and angular oscillation in relation to the point, which is quarter chord far from the front edge,

$$\vartheta == \vartheta_0 + \vartheta_1 \cos\omega t. \tag{1.282}$$

are added to the basic motion with the speed U_0 along $0X$ axis. We get for T

$$T = X_0 - Y\vartheta - X_i - \frac{\rho U_0^2 S}{2} C_p, \tag{1.283}$$

or for thrust coefficient

$$k_T = \frac{2T}{\rho S\left(U_0^2 + (a\omega)^2\right)} = k_{X0} - k_{TF} - k_i - \frac{U_0^2 C_p}{\left(U_0^2 + (a\omega)^2\right)}. \tag{1.284}$$

Here X_0 and k_{x0} are the suction force and suction force coefficient respectively without accounting inductive resistance, k_{TF} is drag force coefficient, k_i is inductive resistance coefficient, C_p is the shape coefficient, ϑ is angle between $0Y$ axis and normal to the wing plane.

Every time as we evaluate X and T we can use the known numerical solutions (Belotserkovskii, 1971). Linear approximation of the lifting force value is defined by expression

$$Y = \frac{\rho U_0^2}{2} S\left(- C_y^{\alpha} \frac{v_n}{U_0} - C_y^{\dot{\alpha}} \frac{\dot{v}_n b}{U_0^2} + C_y^{\omega_z} \frac{\omega_z b}{U_0} + C_y^{\dot{\omega}_z} \frac{\dot{\omega}_z b^2}{U_0^2} \right). \tag{1.285}$$

Here $C_y^{\alpha}, C_y^{\dot{\alpha}}, C_y^{\omega_z}, C_y^{\dot{\omega}_z}$ - coefficients of hydrodynamic derivatives

Now we are going to find the law of wing motion relatively to its centre to define the $0X$ components of the hydrodynamic forces

Vertical speed of the wing centre is

$$V_y = a\omega \cos\omega t + (b/4)\omega\vartheta_1 \sin\omega t\,. \tag{1.286}$$

Normal speed in the wing centre is

$$v_n = V_y - U_0\vartheta = (a\omega - U_0\vartheta_1)\cos\omega t + (b/4)\omega\vartheta_1 \sin\omega t - U_0\vartheta_0. \tag{1.287}$$

More essential relations:

$$\begin{aligned} \dot{v}_n &= -(a\omega - U_0\vartheta_1)\omega \sin\omega t + (b/4)\omega^2\vartheta_1 \cos\omega t, \\ \omega_z &= \dot{\vartheta} = -\vartheta_1\omega \sin\omega t, \\ \dot{\omega}_z &= -\vartheta_1\omega^2 \cos\omega t. \end{aligned} \tag{1.288}$$

Coefficients of hydrodynamic derivatives depend upon Strouhal number which looks like

$$Sh = \frac{\omega b}{U_0}\,. \tag{1.289}$$

They are represented in the Table 1.8.

Let us define separately drag force, suction force and inductive resistance. To define the drag force we have:

$$-Y\vartheta = -\frac{\rho U_0^2}{2} S\vartheta \left(-C_y^{\alpha} \frac{v_n}{U_0} - C_y^{\dot{\alpha}} \frac{\dot{v}_n b}{U_0^2} + C_y^{\omega_z} \frac{\omega_z b}{U_0} + C_y^{\dot{\omega}_z} \frac{\dot{\omega}_z b^2}{U_0^2} \right). \tag{1.290}$$

Using equations (1.281), (1.282), (1.284) and (1.286)-(1.288) and accounting smallness of ϑ_i^2 we get equations for wing oscillation period average drag force coefficient

$$\bar{k}_{TF} = \frac{C_y^{\alpha} \lambda_p^2}{\lambda_p^2 + 1} \left[\vartheta_0^2 - \frac{1}{2} \vartheta_1 \left(\frac{1}{\lambda_p} - \vartheta_1 \right) \right], \tag{1.291}$$

where

$$\lambda_p = \frac{U_0}{a\omega}. \tag{1.292}$$

According to (1.280), suction force (without inductive resistance) can be represented as

$$X_0 = m^* v_n \omega_z - \left(Y + m^* \frac{dv_n}{dt} \right) \frac{v_n}{U_0}. \tag{1.293}$$

Using the same equations and conditions as in derivation of equation (1.291) and accounting $C_y^{\dot{\omega}_z} << C_y^{\alpha}$ (see Table 1.8) we get suction force coefficient

Wing planform	λ	Sh	C_y^{α}	$C_y^{\dot{\alpha}}$	$C_y^{\omega_z}$	$C_y^{\dot{\omega}_z}$
infinite	∞	0.5	4.352	-0.761	1.089	-0.583
infinite	∞	1.0	3.757	0.624	0.939	-0.237
rectangular	4	0.25	3.47	0.1	0.933	-0.492
rectangular	4	0.5	3.26	0.473	0.875	-0.243
rectangular	4	1.0	2.96	0.895	0.8	-0.128
triangular	4	0.25	3.33	0.077	1.248	-0.163
triangular	4	0.5	3.24	0.182	1.22	-0.121
triangular	4	1.0	3.07	0.352	1.153	-0.061

Table 1.8. Coefficients of hydrodynamic derivatives. (Adopted from Belotserkovskii, 1971).

$$\bar{k}_{X0} = \frac{C_y^{\alpha} \lambda_p^2}{\left(\lambda_p^2 + 1\right)} \left[\vartheta_0^2 + \frac{1}{2} \left(\frac{1}{\lambda_p} - \vartheta_1 \right)^2 \right]. \tag{1.294}$$

To estimate inductive resistance we use relations (1.279), (1.281), (1.282), (1.284), (1.286) and (1.287) and get the inductive resistance coefficient

$$\bar{k}_i = \frac{\pi}{2} \frac{\lambda_p^2}{\left(\lambda_p^2 + 1\right)} \left[\vartheta_0^2 + \frac{1}{2} \left(\frac{1}{\lambda_p} - \vartheta_1 \right)^2 \right]. \tag{1.295}$$

Inserting (1.291), (1.294) and (1.295) into (1.284) we get expression for time average thrust coefficient

$$\bar{k}_T = \frac{\lambda_p^2}{(\lambda_p^2 + 1)} \left[\frac{C_y^{\alpha}}{2} \left(\frac{1}{\lambda_p} - \vartheta_1 \right) \frac{1}{\lambda_p} - \frac{\pi}{4} \left(\frac{1}{\lambda_p} - \vartheta_1 \right)^2 - \frac{\pi}{2} \vartheta_0^2 - C_p \right]. \tag{1.296}$$

The last two members of the right part in the square brackets do not depend on the varying wing parameters but only on its stationary characteristics. They can be merged

$$C_{X0} = \frac{\pi}{2} \vartheta_0^2 + C_p. \tag{1.297}$$

Here C_{X0} is the coefficient of wing resistance under condition of stationary motion with angle of the pitch ϑ_0

Fig. 1.36 shows the theoretical dependence of the value k_T on λ_p for the right-angled wing of NACA 0015 airfoil (aspect ratio is 4) with a/b=0.285, ϑ_o=3.7°, ϑ_1=3°, C_{X0}=0.012.

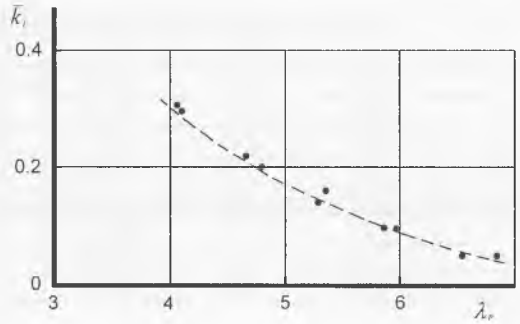

Fig. 1.36. Thrust coefficient *vs.* λ_p for the heaving and pitching motions of the wing (the profile NACA-0015).

This value of C_{X0} is taken from (Grebeshov, Sagoyan, 1976) and dependence of C_y^{α} on Strouhal number is taken from (Belotserkovskii, 1971) (see Table 1.8). In the same picture are plotted the experimental points for corresponding wing motion taken from (Grebeshov, Sagoyan, 1976). As we can see, the theoretical evaluations correspond to the experimental data. In work (Grebeshov, Sagoyan, 1976) there are shown the results of the experimental studying of the two wings of different relative thickness. There is the aerofoil TSAGI KV-1-7 wing, whose relative thickness is 7% and the aerofoil NACA-0015 wing with relative thickness 15%. However we compare the theoretical estimations and the experimental propulsive characteristics of NACA-0015 wing of greater relative thickness just because it satisfies the condition of airflow without breakaway in large range of the attack angle values, which was assumed while deriving the equations of estimations. According to the experimental data the hydrodynamic characteristics of both wings are close to each other only if the angles of attack are less then 8°. When the instant angle of attack is large, the suction force of the thin wing is reduced by the partial or complete airflow breakaway.

Now let us discuss the case of the harmonic plane-parallel oscillations of the wing of finite span. Let the plane-parallel oscillation $y = \alpha\sin\omega t$ with amplitude of α and cyclic frequency of ω be superimposed on the basic motion of the wing along the $0X$ axis at the angle of attack of ϑ_1 and the velocity of U_0. Let us define the oscillation period average thrust with equation (1.296) at $\vartheta_1=0$:

$$\bar{k}_T = \frac{\lambda_p^2}{(\lambda_p^2+1)}\left[\frac{1}{2}\left(C_y^{\alpha}-\frac{\pi}{2}\right)\frac{1}{\lambda_p^2}-C_{X0}\right]. \qquad (1.298)$$

Figure 1.37 shows the theoretical dependence of value k_T on λ_p according to equation (1.298) for the same wing at $\vartheta_0=3.7°$. The experimental points from the work (Grebeshov, Sagoyan, 1976) were also plotted in the same chart. It can be seen that in this case the experimental and computed data match well.

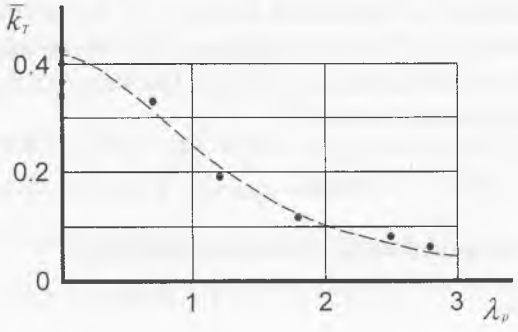

Fig. 1.37. Thrust coefficient *vs.* λ_p for the heaving motions of the wing (the profile NACA-0015).

The case of large oscillations of the wing. Let us consider the motion of the finite span wing into the unlimited volume of a liquid. Let the plane projection of the wing be of symmetric shape relative to *0Z*-axis. Let the motion of the wing be defined as periodic oscillation $y = y(t)$ and $\vartheta = \vartheta(t)$ in the coordinate system of *0XYZ*, which moves at the constant speed of U_0 in the direction of *0X*, see fig. 1.35. Here ϑ is the angle of pitch. Let us assume that under the transverse and angle oscillations at high amplitude the instant values of the angle of the attack are of small values and that there is no breakaway. In this case due to the laws of physics the equations like (1.277) for the components of hydrodynamic forces are valid:

$$Y = -m^* \frac{dv_n}{dt} - \rho U \cos\alpha \int_{-l}^{l} \Gamma(z)dz,$$

$$X = m^* v_n \omega_z + \rho v_n \int_{-l}^{l} \Gamma(z)dz - X_i. \qquad (1.299)$$

The lifting force *Y*, which is normal to the plane of the wing, has two components: the component depending on the media inertia and the circulation component. The vector of suction force *X* is perpendicular to *0Z*-axis in the plane of the wing. The value of *X* is determined by the values of inertia component $m^* v_n \omega_z$, of circulation component $\rho v_n \int_{-l}^{l} \Gamma(z)dz$ and of inductive resistance X_i. The circulation components in the expressions of the lifting force and the suction force are the corresponding projections of the Jouckovsky force $\rho U \int_{-l}^{l} \Gamma(z)dz$ which is normal to the vector of the instant velocity of the wing motion *U*. In expression (1.299): *U* is the absolute velocity of the wing movement respecting to motionless liquid, v_n is the normal to the wing plane component of the velocity *U*; m^* is the virtual mass, Γ is the circulation in the section of the wing *Z*, ρ is density of the liquid, $\omega = d\vartheta / dt$. The values of *U*, v_n are determined in the points of the wing symmetry axis *0Z*

$$v_n = V_y \cos\vartheta - U_0 \sin\vartheta = U \sin\alpha, \qquad (1.300)$$

here $V_y = dy/dt$, α is the instant angle of attack of the wing.

The *0X*-components of the hydrodynamic forces are

$$T = X\cos\vartheta - Y\sin\vartheta - \frac{\rho S U^2}{2} C_p \cos\vartheta . \qquad (1.301)$$

On the basis of (1.299) and (1.301) we can take the expression for T into another expression:

$$T = m^* \frac{d(v_n \sin\vartheta)}{dt} + \rho V_y \int_{-l}^{l} \Gamma(z)dz - X_i \cos\vartheta - \frac{\rho S U^2}{2} C_p \cos\vartheta . \qquad (1.302)$$

Therefore under periodic oscillations of the wing, period average T depends mainly on circulation member and on inductive resistance.

Under linear approximation like in case of small oscillations of the wing the lifting force Y can be estimated with equation

$$Y = -m^* \frac{dv_n}{dt} - \rho U \cos\alpha \int_{-l}^{l} \Gamma(z)dz = \qquad (1.303)$$

$$= \frac{\rho U^2}{2} S\left(- C_y^{\alpha} \frac{v_n}{U} - C_y^{\dot{\alpha}} \frac{\dot{v}_n b}{U^2} + C_y^{\omega_z} \frac{\omega_z}{U} + C_y^{\dot{\omega}_z} \frac{\dot{\omega}_z b^2}{U^2} \right).$$

Let us consider, as we did above, that the coefficients of the hydrodynamic derivatives depend on the Strouhal number (see Table 1.8) and keep constant during the period of oscillation.

Taking into account (1.302) and (1.303), and considering $U\sin\theta = V_y$ we get

$$T = m^* \frac{d(v_n \sin\vartheta)}{dt} + \frac{\rho S}{2}\left(C_y^{\alpha} v_n V_y + b\left\{ C_y^{\dot{\alpha}} - \frac{2m^*}{\rho S b} \right\} \dot{v}_n \sin\theta - b C_y^{\omega_z} \omega_z V_y - b^2 C_y^{\dot{\omega}_z} \dot{\omega}_z \sin\theta \right) -$$

$$- X_i \cos\vartheta - \frac{\rho S U^2}{2} C_p \cos\vartheta . \qquad (1.304)$$

Here $\theta = \alpha + \vartheta$ is the angle of the slope of the wing motion trajectory.

Let us find the period average $\overline{T}$ in cases when

1) $y = a\sin\omega t, \quad \vartheta = \vartheta_1 \cos\omega t;$

2) $y = a\sin\omega t, \quad \alpha = \alpha_1 \cos\omega t;$

are true. If $y=a\sin\omega t$, $\vartheta=\vartheta_1\cos\omega t$ then equations $\overline{\dot{v}_n \sin\theta} = 0$; $\overline{\omega_z V_y} = 0$ take place. In fact

$$\overline{\dot{v}_n \sin\theta} = \overline{\frac{d(v_n \sin\theta)}{dt}} - \overline{v_n \cos\theta\dot{\theta}} = \overline{-U_0\alpha\dot{\theta}} = \overline{U_0\vartheta\dot{\theta}};$$

$$\theta = arctg\frac{V_y}{U_0},\ \dot{\theta} = \frac{U_0\dot{V}_y}{U_0^2+V_y^2}$$

and $\int_0^\tau (-U_0\alpha\dot{\theta})dt = \int_0^\tau (U_0\vartheta\dot{\theta})dt = 0$.

Here τ is the period of the wing oscillation. Under the motion law: $y = a\sin\omega t$, $\vartheta=\vartheta_1\cos\omega t$ equality $\omega_z V_y = 0$ is evident.
If $y = a\sin\omega t$, $\alpha=\alpha_1\cos\omega t$ then

$$\omega_z V_y = \dot{\vartheta}V_y = (\dot{\theta}-\dot{\alpha})V_y = \frac{U_0 V_y \dot{V}_y}{U_0^2+V_y^2} - \dot{\alpha}V_y,$$

$$\overline{\omega_z V_y} = \int_0^\tau \frac{U_0 V_y \dot{V}_y dt}{U_0^2+V_y^2} = 0, \quad \int_0^\tau \dot{\alpha}V_y dt = 0.$$

Thus in the case of the discussed wing motion, the period average T is defined by quasi-stationary approximation

$$\overline{T} = \frac{\rho S}{2}\left(C_y^\alpha \overline{v_n V_y} - C_y^{\dot{\omega}_z} b^2 \overline{\dot{\omega}_z \sin\theta}\right) - \overline{X_i \cos\vartheta} - \frac{\rho S}{2} C_p \overline{U^2 \cos\vartheta}. \qquad (1.305)$$

Also, on the base of (1.278) we can write

$$\overline{T} = \frac{\rho S}{2}\left(C_y^\alpha \overline{v_n V_y} - C_y^{\dot{\omega}_z} b^2 \overline{\dot{\omega}_z \sin\theta}\right) - \frac{\rho\pi S}{4}\overline{v_n^2 \cos\vartheta} - \frac{\rho S}{2} C_p \overline{U^2 \cos\vartheta}. \qquad (1.306)$$

When T is estimated under the law of oscillation is $y = a\sin\omega t$, $\vartheta=\vartheta_1\cos\omega t$, we can use the equation

$$v_n = V_y \cos\vartheta - U_0 \sin\vartheta.$$

With Taylor expansions of the functions $\cos\vartheta$ and $\sin\vartheta$ we get the equation for the mean value of $v_n V_y$

$$\overline{v_n V_y} \cong U_0^2 \vartheta_1^2 \frac{a\omega}{U_0 \vartheta_1} \left(\begin{array}{l} \frac{1}{2}\left(\frac{a\omega}{U_0 \vartheta_1} - 1 \right) - \frac{3}{8}\frac{\vartheta_1^2}{2!}\left(\frac{a\omega}{U_0 \vartheta_1} - \frac{1}{3} \right) + \\ + \frac{5}{16}\frac{\vartheta_1^4}{4!}\left(\frac{a\omega}{U_0 \vartheta_1} - \frac{1}{5} \right) \end{array} \right). \qquad (1.307)$$

Taking into account (1.292) we can formulate (1.307) as

$$\overline{v_n V_y} \cong U_0^2 \frac{1}{\lambda_p} \left(\begin{array}{l} \frac{1}{2}\left(\frac{1}{\lambda_p} - \vartheta_1 \right) - \frac{3}{8}\frac{\vartheta_1^2}{2!}\left(\frac{1}{\lambda_p} - \frac{1}{3}\vartheta_1 \right) + \\ + \frac{5}{16}\frac{\vartheta_1^4}{4!}\left(\frac{1}{\lambda_p} - \frac{1}{5}\vartheta_1 \right) \end{array} \right). \qquad (1.308)$$

To estimate the value of $b^2 \overline{\dot{\omega}_z \sin\theta}$, which is the part of the equation (1.306), we need the following equations.

$$\dot{\omega}_z = \frac{d^2(\vartheta)}{dt^2} = \frac{d^2(\vartheta_1 \cos\omega t)}{dt^2} = -\vartheta_1 \omega^2 \cos\omega t,$$

$$\sin\theta = \sin(\vartheta + \alpha) = \sin\vartheta\cos\alpha + \cos\vartheta\sin\alpha \cong \sin\vartheta + \alpha\cos\vartheta,$$

$$\theta = arctg\frac{V_y}{U_0},$$

$$\alpha = arctg\frac{V_y}{U_0} - \vartheta \cong \frac{V_y}{U_0} - \frac{1}{3}\left(\frac{V_y}{U_0}\right)^3 + \frac{1}{5}\left(\frac{V_y}{U_0}\right)^5 - \frac{1}{7}\left(\frac{V_y}{U_0}\right)^7 - \vartheta_1 \cos\omega t,$$

$$\cos\vartheta \cong 1 - \frac{\vartheta^2}{2} + \frac{\vartheta^4}{24}.$$

Here we use the Taylor approximation for the functions $arctg\frac{V_y}{U_0}$ and $\cos\vartheta$. We take into account only four members of the series for the first function and only three members

for the second one. Also we used the condition under which the attack angle is very small. Eventually we get

$$\overline{b^2\dot{\omega}_z \sin\theta} \cong$$
$$\cong -\frac{\vartheta_1 U_0^2}{2}(Sh)^2\left[\frac{1}{\lambda_p}\left(1-\frac{1}{4\lambda_p^2}+\frac{1}{8\lambda_p^4}-\frac{5}{64\lambda_p^6}\right)-\frac{3\vartheta_1^2}{8\lambda_p}\left(1-\frac{5}{18\lambda_p^2}+\frac{7}{48\lambda_p^4}-\frac{3}{32\lambda_p^6}\right)+\right.$$
$$\left.+\frac{1}{4}\vartheta_1^3\left(1-\frac{5}{48}\vartheta_1^2\right)\right]. \qquad (1.309)$$

Likewise, for the expressions $\overline{v_n^2 \cos\vartheta}$ and $\overline{U^2 \cos\vartheta}$, which are the parts of the second and third members of the right-hand side of the equation (1.306) we get

$$\overline{v_n^2 \cos\vartheta} \cong \frac{1}{2}U_0^2\left[\left(\frac{1}{\lambda_p}-\vartheta_1\right)^2-\frac{9}{8}\vartheta_1^2\left(\frac{1}{\lambda_p^2}-\frac{14}{9}\frac{\vartheta_1}{\lambda_p}+\frac{5}{9}\vartheta_1^2\right)+\right.$$
$$\left.+\frac{15}{32}\vartheta_1^4\left(\frac{1}{\lambda_p^2}-\frac{10}{9}\frac{\vartheta_1}{\lambda_p}+\frac{7}{27}\vartheta_1^2\right)\right] \qquad (1.310)$$

and

$$\overline{U^2 \cos\vartheta} \cong U_0^2\left(1+\frac{1}{2\lambda_p^2}-\frac{3\vartheta_1^2}{16\lambda_p^2}-\frac{\vartheta_1^2}{4}\right). \qquad (1.311)$$

In this case we also use only two first members of the Taylor approximation for functions $\sin\vartheta$ and $\cos\vartheta$. Error does not exceed 1.6% under the real parameters of the dolphin fluke (Romanenko, Pushkov, 1998).

The first members of the expressions (1.308), (1.310) and (1.311) define the solution of the task under the low amplitude theory conditions. Their substitution into expression (1.306) gives the equation that exactly coincides with expression (1.296) under the $\vartheta_0=0$ condition.

It is useful to estimate separately the part of the suction force in the expression (1.306). If we assume the angle of attack to be small and we do not take into account

inductive resistance, then on basis of expressions (1.299), (1.300) and (1.303) the suction force can be presented

$$X_x = X_O \cos\vartheta = m^* v_n \omega_z \cos\vartheta - m^* \dot{v}_n \alpha \cos\vartheta + \frac{\rho S}{2}\left(C_y^{\alpha} v_n^2 + C_y^{\dot{\alpha}} \dot{v}_n b\alpha - C_y^{\omega_z} \omega_z b v_n - C_y^{\dot{\omega}_z} \dot{\omega}_z b^2 \alpha\right)\cos\vartheta. \tag{1.312}$$

If we find the time-mean value of this expression at the oscillation period it will lead us to

$$\overline{X}_x = \frac{\rho S}{2}\left(C_y^{\alpha} \overline{v_n^2 \cos\vartheta} - C_y^{\dot{\omega}_z} \overline{b^2 \dot{\omega}_z \alpha \cos\vartheta}\right). \tag{1.313}$$

Here $\overline{v_n^2 \cos\vartheta}$ defined by expression (1.310), and

$$\overline{b^2 \dot{\omega}_z \alpha \cos\vartheta} \cong -\frac{\vartheta_1 U_0^2}{2}(Sh)^2 \left[\left(\frac{1}{\lambda_p} - \vartheta_1\right)\left(1 - \frac{3}{8}\vartheta_1^2 + \frac{5}{192}\vartheta_1^4\right) - \frac{1}{4\lambda_p^3}\left(1 - \frac{1}{2\lambda_p^2}\right) + \frac{5}{48}\frac{\vartheta_1^2}{\lambda_p^3}\left(1 - \frac{21}{40\lambda_p^2}\right)\right]. \tag{1.314}$$

To derive this equations we used the expression for the attack angle

$$\alpha = arctg\frac{V_y}{U_0} - \vartheta, \tag{1.315}$$

and Taylor approximation of the functions $arctg\dfrac{V_y}{U_0}$ and $\cos\vartheta$ with only three first members.

Now let us estimate the value of the thrust when $y=a\sin\omega t$, $\alpha=\alpha_1\cos\omega t$. Under this law of the wing motion we get

$$\overline{v_n V_y} = \alpha_1 a\omega \frac{\omega}{\pi} \int_0^{\pi/\omega} \cos^2 \omega t \sqrt{U_0^2 + (a\omega)^2 \cos^2 \omega t}\, dt \cong$$

$$\cong \frac{1}{2}\alpha_1 a\omega \left(1 + \frac{1}{4} \frac{(a\omega)^2}{2U_0^2 + (a\omega)^2} - \frac{1}{16} \frac{(a\omega)^4}{\left[2U_0^2 + (a\omega)^2\right]^2} + \ldots \right) \sqrt{U_0^2 + (a\omega)^2 / 2}. \qquad (1.316)$$

The expression (1.316) was obtained on the base of

$$\cos^2 \omega t \sqrt{U_0^2 + (a\omega)^2 \cos^2 \omega t} \cong \frac{1}{2}(1 + \cos 2\omega t) \sqrt{U_0^2 + \frac{(a\omega)^2}{2}} \sqrt{1 + \frac{(a\omega)^2 \cos 2\omega t}{2U_0^2 + (a\omega)^2}} \cong$$

$$\cong \frac{1}{2}(1 + \cos 2\omega t) \sqrt{U_0^2 + \frac{(a\omega)^2}{2}} \left\{ 1 + \frac{1}{2}\left[\frac{(a\omega)^2 \cos 2\omega t}{2U_0^2 + (a\omega)^2} \right] - \frac{1}{8}\left[\frac{(a\omega)^2 \cos 2\omega t}{2U_0^2 + (a\omega)^2} \right]^2 + \ldots \right\}. \qquad (1.317)$$

Taking into account (1.292) we can write

$$\overline{v_n V_y} \cong \frac{1}{2} U_0^2 \alpha_1 \frac{1}{\lambda_p} \left[1 + \frac{1}{4} \frac{1}{\left(2\lambda_p^2 + 1\right)} - \frac{1}{16} \frac{1}{\left(2\lambda_p^2 + 1\right)^2} + \ldots \right] \sqrt{1 + \frac{1}{2\lambda_p^2}}\,. \qquad (1.318)$$

Similarly we can obtain the expressions

$$\overline{b^2 \ddot{\omega}_z \sin\theta} \cong -\frac{\alpha_1 U_0^2}{2} (Sh)^2 \left[\frac{1}{\lambda_p} \left(1 - \frac{3}{8\lambda_p^2} + \frac{5}{48\lambda_p^4} - \frac{35}{384\lambda_p^6} \right) \right], \qquad (1.319)$$

$$\overline{v_n^2 \cos\vartheta} \cong \frac{U_0^2 \alpha_1^2}{2} \left(1 + \frac{3}{8\lambda_p^2} - \frac{5}{48\lambda_p^4} + \frac{49}{1152\lambda_p^6} - \frac{119}{1280\lambda_p^8} \right) \qquad (1.320)$$

and

$$\overline{U^2 \cos\vartheta} \cong U_0^2 \left(1 + \frac{1}{4\lambda_p^2} - \frac{1}{16\lambda_p^4} \right). \qquad (1.321)$$

To derive the expressions (1.319) – (1.321) as previously we used the Taylor approximations of the functions $arctg\frac{V_y}{U_0}$ and $\cos\vartheta$.

Thus, when the angle of an attack or the angle of a pitch are varied harmonically, we get the various estimations of the component of the hydrodynamic force *T*.

A relationship between the hydrodynamic forces and the location of the pitch-axes. Previously we explored a problem when the parameters of kinematics of a wing center are assigned. However, the problem when the parameters of kinematics of the arbitrary wing point are assigned is more important because a fluke pitch-axes of dolphin is arranged in trailing edge (Wu, 1971; Zaytsev, Fedotov, 19860. (This agrees with estimates of the Ch. 6).

We shall analyse the problem when the parameters of the wing kinematics can be specified relatively to a point x_0 which is located at a distance of *x* from the wing center (Fig. 1.35). A wing movement determined by the parameters of movement of the point x_0 is:

amplitude of oscillaton

$$y_0 = y(t) \tag{1.322}$$

and an angle of fluke axis relatively to horizontal axis

$$\vartheta_0 = \vartheta(t). \tag{1.323}$$

To make an estimate of the hydrodynamic forces developed by the wing we can use the formula (1.304) but all involved expressions are bound to be written relatively to the wing center:

$$T_c = m^* \frac{d(v_{nc}\sin\vartheta)}{dt} + \frac{\rho S}{2}\left(C_y^{\alpha} v_{nc} V_{yc} + b\left\{ C_y^{\alpha} - \frac{2m^*}{\rho S b} \right\} \dot{v}_{nc}\sin\theta_c - bC_y^{\omega_z}\omega_z V_{yc} - b^2 C_y^{\dot{\omega}_z}\dot{\omega}_z \sin\theta_c \right) -$$
$$- X_f \cos\vartheta - \frac{\rho S U^2}{2} C_p \cos\vartheta. \tag{1.324}$$

Here index "*c*" symbolizes that the parameter is bound to be written relatively to the wing center.

All involved expressions in (1.324) are in the form

$$V_{xc} = U_0 - \omega_z x \sin\vartheta, \tag{1.325}$$

$$V_{yc} = V_{y0} + \omega_z x \cos\vartheta\,, \tag{1.326}$$

$$v_{nc} = V_{y1}\cos\vartheta - U_0 \sin\vartheta + \omega_z x = U_c \sin\alpha_c\,, \tag{1.327}$$

$$\dot{v}_{nc} = \frac{dv_{nc}}{dt}\,, \tag{1.328}$$

$$\theta_c = \alpha_c + \vartheta = arctg\frac{V_{yc}}{V_{xc}}\,, \tag{1.329}$$

$$U_c^2 = \left(V_{yc} + \omega_z x\cos\vartheta\right)^2 + \left(U_0 - \omega_z x\sin\vartheta\right)^2, \tag{1.330}$$

$$y_0 = a\sin\omega t\,, \tag{1.331}$$

where $V_{y0} = \dot{y}_0(t)$, $\omega_z = \dot{\vartheta}(t)$ and x is the separation between x_0 and the wing center (in metres).

Formula (1.324) is the same for the different parameters and the wing forms. The wing form is defined by values of the coefficients of hydrodynamic derivatives and virtual mass. Formula admits the computer solution only. However, it has been possible to calculate in a crude way the thrust by using formula (1.324) after rearrangement. As before by applying the averaging t over the ray period with the proviso that $\vartheta = \vartheta_1 \cos\omega t$ an approximate formula is derivable from (1.324). A variant of $\alpha = \alpha_1 \cos\omega t$ we exclude from consideration because an angle of attack of dolphin flukes is not harmonical (chapter 6).

The time - averaged thrust is

$$\overline{T_c} = \frac{\rho S}{2}\left\{C_y^{\alpha}\overline{v_{nc}V_{yc}} + \left[-\frac{x}{b}\left(C_y^{\dot{\alpha}} - \frac{2m^*}{\rho Sb}\right) - C_y^{\bar{\omega}_z}\right]b^2\overline{\dot{\omega}_z \sin\theta_c} - \frac{\pi}{2}\overline{v_{nc}^2\cos\vartheta} - C_p\overline{U_c^2\cos\vartheta}\right\} \tag{1.332}$$

Here as before the coefficient of inductive resistance can be represented by expression (1.278).

A rigorous analysis of formula (1.276) shows that:
in the case of the two-dimensional wing the inductive resistance is equal

$$X_{ic} = \rho\pi b u_* (v_{nc} - u_*), \tag{1.333}$$

for triangular wing (l – semi-span)

$$X_{ic} = \rho\pi l b u_* (v_{nc} - u_*) \tag{1.334}$$

and for rectangular wing

$$X_{ic} = 2\rho\pi l b u_* (v_{nc} - u_*) \tag{1.335}$$

where $u_* = v_{nc} - C_y^{\alpha}\frac{v_{nc}}{2\pi} + C_y^{\omega_z}\frac{\omega_z b}{2\pi} - \frac{\omega_z b}{4} + \frac{\dot{v}_{nc} b}{4U_c} - C_y^{\alpha}\frac{\dot{v}_{nc} b}{2\pi U_c} + C_y^{\dot{\omega}_z}\frac{\dot{\omega}_z b^2}{2\pi U_c}$.

The estimation of the inductive resistance calculated by formula (1.278) exceeds the one calculated by formula (1.333 – 1.335) by 20%.

All involved expressions (averaged) in (1.324) are in the form

$$\overline{v_{nc} V_{yc}} \cong \overline{v_n V_y} + \frac{\vartheta_1^2 \omega^2 x^2}{2}\left[1 - \frac{\vartheta_1^2}{8}\left(1 - \frac{\vartheta_1^2}{24}\right)\right], \tag{1.336}$$

where the first term at the right part of formula is (1.308).

$$b^2 \overline{\dot{\omega}_z \sin\theta_c} \cong b^2 \overline{\dot{\omega}_z \sin\theta} \cong -\frac{\vartheta_1^2 U_0^2}{2}(Sh)^2, \tag{1.337}$$

$$\overline{\omega_z V_{yc}} = 0, \tag{1.338}$$

$$\overline{v_{nc}^2 \cos\vartheta} \cong \overline{v_n^2 \cos\vartheta} + \frac{\vartheta_1^2 \omega^2 x^2}{2}\left[1 - \frac{\vartheta_1^2}{8}\left(1 - \frac{\vartheta_1^2}{24}\right)\right], \tag{1.339}$$

where the first term at the right part of formula is (1.310).

$$\overline{U_c^2 \cos\vartheta} \cong \overline{U^2 \cos\vartheta} + \frac{\vartheta_1^2 \omega^2 x^2}{2}\left[1 - \frac{\vartheta_1^2}{8}\left(1 - \frac{19}{48}\vartheta_1^2\right)\right], \tag{1.340}$$

where the first term at the right part of formula is (1.311).

The expressions (1.332 – 1.340) should be put to better use of coordinate x normalized to the wing chord

$$x = bX \ , \text{where } X = \frac{x}{b} \tag{1.341}$$

The virtual mass of the infinite profile per unit length (Logvinovitch, 1970)

$$m^{\bullet} = \frac{\rho\pi b^2}{4}. \tag{1.342}$$

The virtual mass of the rectangular wing

$$m^{*} \approx 0.9\rho l \frac{\pi b^2}{2}. \tag{1.343}$$

The virtual mass of the triangular wing (Romanenko, 1986)

$$m^{\bullet} = \frac{\rho\pi b^2 l}{6}. \tag{1.344}$$

It is useful to estimate the contribution of suction force to the total thrust:

$$X_{xc} = m^{*} v_{nc}\omega_z \cos\vartheta - m^{*}\dot{v}_{nc}\alpha_c \cos\vartheta + \frac{\rho S}{2}\left(C_y^{\alpha} v_{nc}^2 + C_y^{\dot{\alpha}}\dot{v}_{nc} b\alpha_c - C_y^{\omega_z}\omega_z b v_{nc} - C_y^{\dot{\omega}_z}\dot{\omega}_z b^2\alpha_c\right)\cos\vartheta. \tag{1.345}$$

The time – averaged suction force is

$$\overline{X}_x = \frac{\rho S}{2}\left(C_y^{\alpha}\overline{v_n^2\cos\vartheta} - C_y^{\dot{\omega}_z}\overline{b^2\dot{\omega}_z\alpha\cos\vartheta}\right) + + \left[\frac{\rho S}{2}\left(C_y^{\alpha}X + C_y^{\omega_z}\right) - \frac{m^{\bullet}}{b}\right]\frac{\vartheta_1^2 U_0^2 (Sh)^2}{2} X\left(1 - \frac{\vartheta_1^2}{8}\right). \tag{1.346}$$

The time – averaged expressions at the right part of formula are (1.310) and (1.315) correspondingly.

Coefficients of hydrodynamic derivatives included in the expressions of the thrust and suction force are in the Table 8.

To test the validity of the theory and derived solution for thrust (1.332) we estimated the thrust of two-dimensional wing and compared it with data of works (Schehovtsov, 1999; Zaytsev, Fedotov, 1986) (the wing profile drag is not taken into consideration). In the work (Schehovtsov, 1999) a non-linear, non-stationary, two-dimensional numerical model was constructed using the improved method of discrete vortices. Authors of the work (Zaytsev, Fedotov, 1986) examined by the numerical method of the vortical surfaces the problem of a rigid finite span wing moving with high amplitude of transversal and angular oscillations. The calculations were performed at following conditions: $Sh = 1$, $\frac{a}{b} = 1$, $\alpha_1 = 10^0$. Our data (curve 3 on Fig. 1.38) are positioned below the data of Zaytsev, Fedotov (1) and Schehovtsov (2) in the interval $0.4 \le \frac{x}{b} \le 1.5$. This is attributable to values of coefficients of hydrodynamic derivatives which are defined in the context of small amplitude theory. In line with this theory wing surface and vortical wake are arranged in the same plane. When the wing moves at a high amplitude of transversal and angular oscillations its trajectory is distorted and instantaneous velocity is changed markedly. Therefore in deciding on the coefficients of hydrodynamic derivatives (Table 8) it is appropriate to use Strouhal number in the form

$$Sh_U = \frac{\omega b}{U}, \tag{1.347}$$

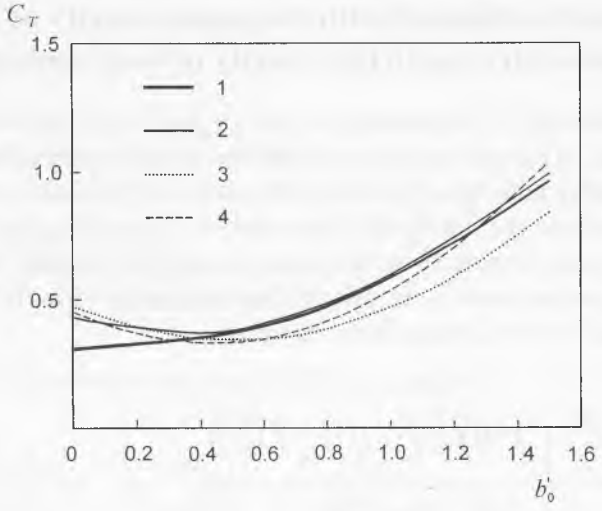

Fig. 1.38. Comparison of the values of thrust coefficients calculated by the different methods. See text for details.

where $U = \sqrt{U_0^2 + \omega^2 a^2}$.

Such approach to the problem brings our data and results of works (Schehovtsov, 1999; Zaytsev, Fedotov, 1986) into better agreement. The curve 4 (our data) differs from curves 1 and 2 by 10 – 13% in interval $0.3 \le \frac{x}{b} \le 1.5$.

Good agreement between results of Zaytsev, Fedotov and Schehovtsov is doubted. Curve 1 is bound to position below that of curve 2 because the thrust of the finite span wing is less than that of two-dimensional wing. This is evident from Fig. 1 in the work of Zaytsev, Fedotov as well as from works (Lighthill, 1970; Chopra, Kambe, 1977).

Unlike the rigid wing used in the model, the fluke of a dolphin is elastic and of a half moon shape. Elasticity leads to deflection of the fluke under active swimming. The airflow of the fluke is different from the airflow of the rigid plane wing because of the elasticity of the dolphin's fluke, which transforms the fluke into an arc. In (Katz, Weihs, 1979; Bose, Lien, 1989) it is shown that such deflection of the fluke gives the thrust a 20% decrease. The shape of the wing also influences the thrust. Work (Chopra, Kambe, 1977) deals with low amplitude theory of the motion of rigid wings of finite aspect ratio. These wings have different shapes of leading and trailing edges from straight to parabolic. They perform linear and angular oscillations. One of the wings is very similar in shape to the fluke of a dolphin. Analysis showed that such a wing produces a thrust that is approximately 12% stronger than the one of the rectangular wing when all the other conditions are the same.

1.4. Threshold values of the thrust and efficiency of dolphin's and fishes' propulsors estimated with the phase velocity of the locomotor wave striving to the velocity of body motion

The above formulas for estimation of energy and force parameters of animals' swimming depend, in particular, on the relation between the values U and C. Moreover, it has been repeatedly noted that the positive thrust is only possible when $C > U$. It is of interest to analyse how the thrust will change when C is striving to U ($C \to U$). As it follows from physical considerations the thrust in such cases should strive to zero. The same conclusion can be made more strictly if we turn to the formula for the efficiency derived by Lighthill from his theory of the thin body:

$$\eta = 1 - \frac{1}{2} \frac{\left(1 - \frac{U}{C}\right)^2 f^2 (l) \overline{(g')^2} + U^2 (f')^2 \overline{(g^2)}}{\left(1 - \frac{U}{C}\right) f^2 (l) \overline{(g')^2}}. \qquad (1.348).$$

The formula yields that the denomination in the second term strives to zero at $C \to U$, while the efficiency strives to infinity. For the efficiency to remain limited (within 0-1), it ix necessary to demand that the numerator also strives to zero, the numerator being nothing else best the thrust multiplied by the swimming velocity.

In this way, if the theory is correct, at $C \to U$ the thrust must turn into zero meaning if $U \neq 0$. Let us try to analyse the above theories of fishes' and dolphins' swimming from this point of view.

Let us begin with Lighthill's theory. We shall again remind his expression for the thrust,

$$\bar{T} = \frac{1}{2}\rho A(l)\left[\overline{\left(\frac{\partial h}{\partial t}\right)^2 - U^2\left(\frac{\partial h}{\partial x}\right)^2}\right]_{x=l}. \qquad (1.349).$$

and we shall accept the law of deformation as

$$h(x,t) = h_0(x)\cos\omega\left(t - \frac{x}{C}\right). \qquad (1.350)$$

Then we'll write down in detail all derivatives comprising the relation (1.349):

$$\frac{\partial h}{\partial t} = -h_0\omega\sin\omega\left(t - \frac{x}{C}\right),$$

$$\overline{\left(\frac{\partial h}{\partial t}\right)^2} = \frac{h_0^2\omega^2}{2},$$

$$\frac{\partial h}{\partial x} = \frac{\partial h_0}{\partial x}\cos\omega\left(t - \frac{x}{C}\right) + \frac{h_0\omega}{C}\sin\omega\left(t - \frac{x}{C}\right), \qquad (1.351)$$

$$\overline{\left(\frac{\partial h}{\partial x}\right)^2} = \frac{1}{2}\left(\frac{\partial h_0}{\partial x}\right)^2 + \frac{h_0^2\omega^2}{2C^2}.$$

By substituting the derivatives into (1.349) we shall get

$$\bar{T} = \frac{1}{2}\rho A(l)\left[\frac{h_0^2\omega^2}{2} - \frac{U^2}{2}\left(\frac{\partial h_0}{\partial x}\right)_{x=l}^2 - \frac{U^2 h_0^2\omega^2}{2C^2}\right] \qquad (1.352)$$

and finally, at $U = C$:

$$\overline{T} = -\frac{1}{4}\rho A(l)U^2\left(\frac{\partial h}{\partial x}\right)^2_{x=l}. \tag{1.353}$$

All quantities of the right-hand part of the expression (1.353) are positive and, hence, the thrust is negative.

It is not difficult to show and it is shown in § 1.2 that the theory of G. V. Loginovich gives such an expression for thrust which is similar to that of Lighthill (1.349). Hence, when $C = U$ the thrust is negative in this case too.

Now, let us estimate Wu's expression for total thrust (1.177) at $C \to U$ and the accepted law of body deformation (1.350). The first term coincides with the expression for thrust obtained by Lighthill (1.349). In this case it yields a negative value. The second term, when given the derivatives, regarding in the law of deformation at $C = U$, will look as

$$-\frac{1}{2}\rho\int_0^1\left\{\left(\frac{\partial h}{\partial t}\right)^2 - U^2\left(\frac{\partial h}{\partial x}\right)^2\right\}\frac{\partial A}{\partial x}dx = \frac{1}{4}\rho\int_0^1\left[U^2\left(\frac{\partial h_0}{\partial x}\right)^2\frac{\partial A}{\partial x}\right]dx. \tag{1.354}$$

This expression is also negative, if we consider - that $\frac{\partial A}{\partial x} < 0$ in the section $0 < x <$ 1. Hence, the general expression for thrust, obtained by Wu, is negative at $C = U$ and the accepted law of the deformation.

Let us try to estimate the threshold value of the pull derived from the theory of the wing (1.244) when $C = V$. Believing that the law of deformation looks as (1.350), and bearing in mind

$$v_n = \frac{\partial h}{\partial t} - V\frac{\partial h}{\partial x}, \tag{1.355}$$

we shall get

$$\overline{A} = \frac{2m^*(x_1)\omega^2 h_0^2}{\sqrt{\lambda^2+4}+2}\left(1-\frac{V}{C}\right) - \frac{4m^*(x_1)\omega^2 h_0^2}{\left(\sqrt{\lambda^2+4}+2\right)^2}\left(1-\frac{V}{C}\right) - \frac{4m^*(x_1)V^2}{\left(\sqrt{\lambda^2+4}+2\right)^2}\left(\frac{\partial h_0}{\partial x}\right)^2. \tag{1.356}$$

When $V = C$, this relation (1.356) looks as

$$\overline{A} = -\frac{4m^*(x_1)V^2}{\left(\sqrt{\lambda^2+4}+2\right)^2}\left(\frac{\partial h_0}{\partial x}\right)^2. \tag{1.357}$$

The pull proves to be negative, like in the previous cases.

We have estimated the threshold expressions for the pull and thrust obtained by solving some three-dimensional problems. Is it possible that the things differ when the problems to solve are two-dimensional? Let us verify it. To this end, we shall take Table 3 from (Uldrick, 1968) and will sample some values of the thrust coefficient c_T calculated for the profile with the relative thickness of $\varepsilon = 0.3$ at two values of the wave number $\alpha = \pi$ and $\alpha = \pi/2$. This sampling is presented in Table 1.9. The first column gives the values of the reduced frequency.

In case $\alpha = \pi$, the thrust coefficient C_T should pass through zero at $\sigma = \pi$. This value of the reduced frequency corresponds to the equation $U = C$, and indeed, under such conditions we have

$$\alpha = \sigma, \frac{\omega}{C} = \frac{\omega}{U} \rightarrow U = C. \tag{1.358}$$

By linear interpolation we can easily show that the thrust coefficient turns into zero at $\sigma = 3.17$ i.e. at a slightly higher value than π. This is still more evident at $\alpha = \pi/2$. In such case, the thrust coefficient should transit through zero at $\sigma = 1.57$. In Table 1.9 the transit through zero occurs $\sigma > 2$.

In this way, practically all of the existing theories on dolphins' and fishes' swimming, no matter which problems they consider, namely two-dimensional or three-dimensional ones, yield the negative value of thrust at $U = C$. It is true this concerns only the problems regarding the body thickness or body volume, in this or that extent. Some experiments were made to study how oscillating profiles with different thickness behave in the water flow at constant velocity. The experiments also yielded the reparative value of thrust at $U = C$. This should not take place in terms of physics. The thrust in such case should equal zero. The body is moving in the channel of liquid and $U = C$. There should be no reaction from the part of liquid. One can see a kind of paradox here which remains to be explained.

σ	C_T ($\alpha = \pi$)	C_T ($\alpha = \pi/2$)
1	-0.00267	-0.00206
2	-0.00211	-0.00027
4	0.00149	0.00586
6	0.00765	0.01554
8	0.01627	0.02884

Table 1.9. Thrust coefficients. (Adopted from Uldric, 1968). For explanations of variables, see text.

There is still another case which has no obvious contradictions. We mean the case of the "anguilliform" swimming when the amplitude of the propulsive wave is constant within the body limits or at least, on the tail.

In this case, the threshold value of thrust in the above expressions

$$\frac{\partial h_0}{\partial x} = 0 \tag{1.359}$$

or

$$\left(\frac{\partial h_0}{\partial x}\right)_{x=l} = 0. \tag{1.360}$$

and the thrust turns into a zero at $U = C$.

However, in reality there are neither dolphins, nor fishes, when the condition of the constant amplitude of the propulsive wave is fulfilled. The condition of (1.360), perhaps, is fulfilled but it is very difficult to verify it in experiments.

It is interesting to assess the threshold value of thrust when the law of deformation regards the phenomenon of "recoil" theoretically examined by Lighthill. Let us accept the law of deformation in the form regarding the phenomenon of "recoil" and offered by Lighthill

$$h = H(x)\cos\left[\omega\left(t + \frac{l-x}{C}\right)\right] + [h_1 + h_3(l-x)]\cos\omega t + [h_2 + h_4(l-x)]\sin\omega t. \tag{1.361}$$

Then let us compute the derivatives comprising the expression for thrust (1.349), so that we shall get

$$\begin{aligned}
\frac{\partial h}{\partial t} &= -\omega H(x)\sin\left[\omega\left(t + \frac{l-x}{C}\right)\right] - \omega[h_1 + h_3(l-x)]\sin\omega t + \omega[h_2 + h_4(l-x)]\sin\omega t, \\
\frac{\partial h}{\partial x} &= \frac{\partial H}{\partial x}\cos\left[\omega\left(t + \frac{l-x}{C}\right)\right] + \frac{\omega H(x)}{C}\sin\left[\omega\left(t + \frac{l-x}{C}\right)\right] - h_3\cos\omega t - h_4\sin\omega t.
\end{aligned} \tag{1.362}$$

Substituting these derivatives into (1.349) and averaging them in time, at $U = C$ and $x = l$ we shall have

$$\overline{T} = \frac{1}{2}\rho A(l)\left[\begin{array}{l}\dfrac{\omega^2}{2}\left(h_1^2 + h_2^2\right) - \dfrac{U^2}{2}\left(h_3^2 + h_4^2\right) + \omega^2 H h_1 - \\ -\dfrac{U^2}{2}\left(\dfrac{\partial H}{\partial x}\right)^2 + \dfrac{U^2 h_3}{2}\left(\dfrac{\partial H}{\partial x}\right) + \dfrac{U\omega H h_4}{2}\end{array}\right]. \quad (1.363)$$

This expression contains several terms, sign in which is hard to determine because they include the values h_1; h_2; h_3 and h_4, so far unknown. They can be found only in experiments with animals. Nevertheless, this is a possibility to turn the thrust into zero when $U = C$. Thus the expression in brackets in its right-hand part (1.363) should turn into zero.

In this way, the phenomenon of "recoil" generally speaking, may include the above contradiction. However, there are also some other possibilities but they will be discussed later.

1.5. Evolution of fish locomotion function: whether it was influenced by the sound factor

In the process of the evolution the lowest aquatic vertebrates acquired the undulate mode of motion. Most species flex their body in horizontal plane and only few bottom dwelling species of fish such as skate and plaice flex their bodies in vertical plane. But the ancestors of these fishes swam as other fishes and their larvae swim this way. Therefore this way of swimming is a secondary development. What were the reasons for it to appear? There is a possible explanation given by acoustics.

Water, the natural environment for water vertebrates, is a good conductor of sound, and an oscillating fish body produces acoustic wave of low frequency or infrasound. The efficiency of sound emission depends on such characteristic of the generator as the orientation of the plane of oscillations and the position of the generator in relation to the surface of the water and the bottom (i.e. the boundaries of the medium).

The oscillating body of a fish can be considered as an acoustic dipole (depicted as an arrow): vertical for skates and plaies and horizontal for other fishes (Fig. 1.39). In any case the acoustic waves propagate through water and reaching the boundary of the substances reflect from it. For the fishes, which swim in the upper layers the nearest boundary is the surface of the water, and for bottom dwelling fishes such boundary is the bottom. In the first case the wave is reflected from the boundary, which separates the more dense medium (water), from the less dense medium (air), and in the second case the boundary separates the less dense medium (water) from the more dense (bottom). When one calculates the total efficiency of the acoustic radiation the reflected waves can be displaced by additional (virtual) acoustic dipoles in the endless mass of water.

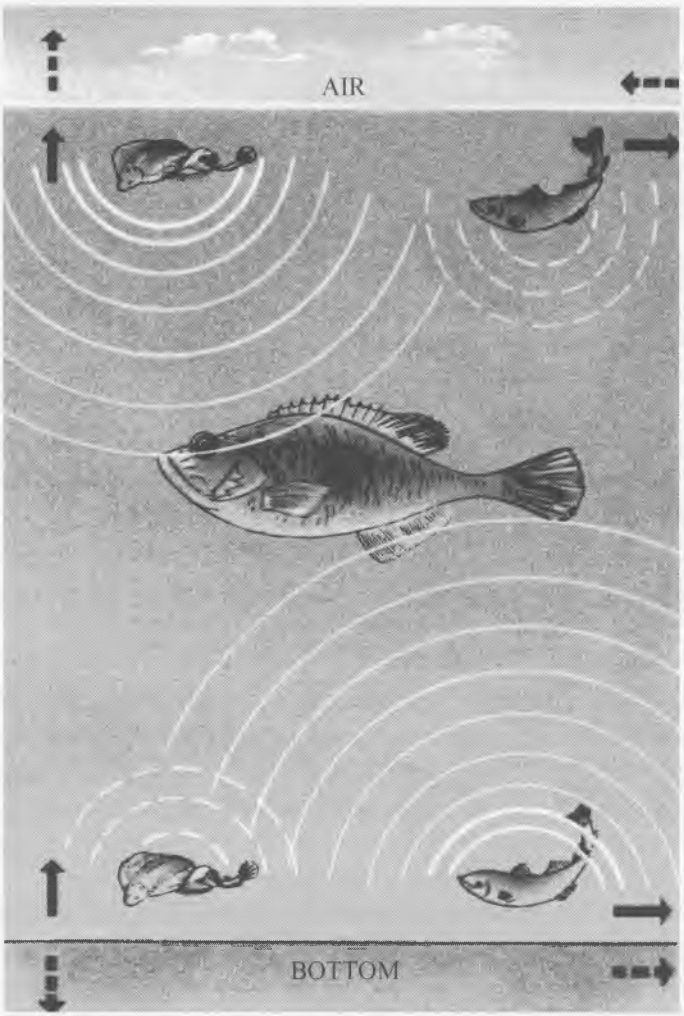

Fig. 1.39. A schematic representation of the acoustical pattern.

Considering dipoles one can see that at the two different boundaries the medium the virtual dipoles are oriented in the opposite directions, and the total efficiency of the acoustic radiation is equal to the sum of the fields of both real and virtual dipoles. As the dipoles (both real and virtual) have the same direction (vertical dipoles near the surface and horizontal ones near the bottom) the mutual acoustic field will be equal to the sum of the fields of both dipoles. At the same time near the surface horizontal dipoles have different orientation, and so do vertical dipoles near the bottom. Therefore their mutual field is equal to the difference of their fields. So near the surface the fishes

with the horizontal plane of oscillations radiate less sound than the fishes with the vertical plane of oscillations.

Let us discuss a mathematical model of the tail fin as a generator of acoustic waves. We have already mentioned that the oscillating fin can be considered as a dipole. The combination of the main dipole and the "reflected" dipole is called quadrupole. If the moment of the main dipole is parallel to the reflecting surface quadrupole is transverse, if the moment is perpendicular to the reflecting surface quadrupole is longitudinal.

We set up a model of a transverse quadrupole in case when the reflecting surface is the boundary between the water and the air. (See figure 1.40).

The pressure field of the main dipole is given by (Skuchik 1976):

$$P_1 = B\frac{\cos\theta}{r}\left(1+\frac{1}{jkr}\right)e^{-jkr}e^{j\omega t}, \tag{1.364}$$

while the field of the reflected dipole is given by:

$$P_2 = B\frac{\cos\theta}{r+d\cos\varphi}\left(1+\frac{1}{jk(r+d\cos\varphi)}\right)e^{-jk(r+d\cos\varphi)}e^{j\omega t}, \tag{1.365}$$

where P_1 and P_2 are the acoustic pressure, r is the distance between the quadrupole and the viewpoint, $k = 2\pi/\lambda$ is the wavenumber, λ is the length of acoustic wave, $\omega=2\pi f$, f is the frequency of the oscillations of the tail, j – imaginary unit, θ – the angle between the Y-direction and the direction to the viewpoint, φ – the angle between the Z-direction and the direction to the viewpoint, $d/2$ – depth of the main dipole, and B is given by:

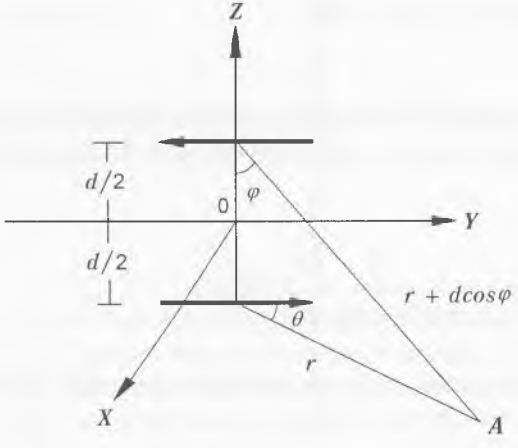

Fig. 1.40. A schematic representation of the transverse quadrupole under conditions when reflective interface is the demarcation line between the atmosphere and water.

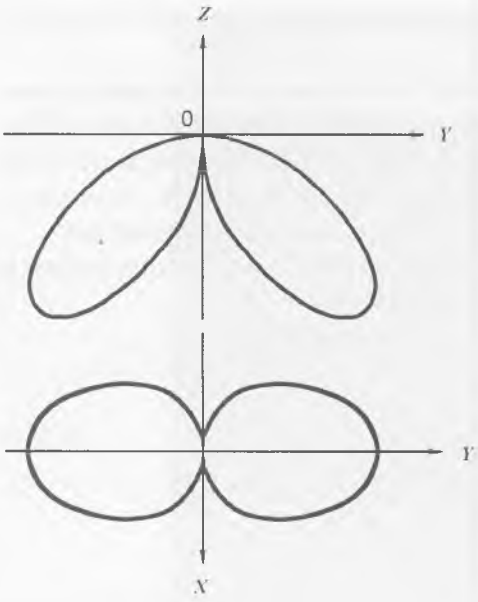

Fig. 1.41. A diagram of the sound directivity of the transverse quadrupole under conditions when reflective interface is the demarcation line between the atmosphere and water.

$$B = -\frac{3k}{4\pi}\omega m V_0, \tag{1.366}$$

where m is the virtual mass of the tail, V_0 – the velocity of the particles of the liquid in the direction of oscillations. The time –varying terms can be omitted from the expressions (1.364) and (1.365) as they do not influence the calculations. We are interested in the so-called nearest field, i.e. the field of the quadrupole at the distances much less than the length of the sound wave. In this case:

$$kr << 1. \tag{1.367}$$

As the dipole components of the transverse quadrupole have opposite directivity the resulting field is equal to the difference of fields of its components. Taking into account (1.367) we obtain:

$$P_1 - P_2 = B\left(\frac{1}{jkr^2} - \frac{1}{jk(r + d\cos\varphi)^2}\right)\cos\theta. \tag{1.368}$$

We omitted the first members in the brackets in the expressions (1.364) and (1.365) and also replaced the exponential functions by 1 according to (1.367). After some alterations we obtain:

$$P_1 - P_2 = B\frac{\cos\theta}{jkr^2}\left(1 - \frac{1}{1 + 2\frac{d}{r}\cos\varphi + \frac{d^2}{r^2}\cos^2\varphi}\right). \tag{1.369}$$

After we put over the common dominator:

$$P_1 - P_2 = B\frac{\cos\theta}{jkr^2}\left(\frac{\frac{d}{r}\cos\varphi\left(2 + \frac{d}{r}\cos\varphi\right)}{1 + 2\frac{d}{r}\cos\varphi + \frac{d^2}{r^2}\cos^2\varphi}\right). \tag{1.370}$$

This expressions are true for any r and d under the condition (1.367). But if the distance between the quadrupole and the point of view is much bigger than the depth, i.e.

$$r >> d, \tag{1.371}$$

the expressions (1.370) can be simplified:

$$P_1 - P_2 = \frac{2jBd\cos\varphi\cos\theta}{kr^3}. \tag{1.372}$$

For the amplitude value one has:

$$|P_1 - P_2| = \frac{2Bd\cos\varphi\cos\theta}{kr^3}. \tag{1.373}$$

In order to find the maximum of directivity diagram we put $\varphi = \theta = 45°$(Fig. 41). In this direction the amplitude of pressure is equal to:

$$|P_1 - P_2| = \frac{Bd}{kr^3}. \tag{1.374}$$

Now let us discuss the case of the longitudinal quadrupole, which describes vertical oscillations of the fish tail, when the fish is swimming near the surface (see fig. 1.42). The pressure field is given by (1.364). The field of reflected dipole differs from (1.365) and is given by:

$$P_2 = B\frac{\cos\theta}{r + d\cos\theta}\left(1 + \frac{1}{jk(r + d\cos\theta)}\right)e^{-jk(r + d\cos\theta)}. \tag{1.375}$$

The difference is: $\varphi = \theta$.

The total field can be presented by the following expression:

$$P_1 + P_2 = B\cos\theta\left[\frac{e^{-jkr}}{r} + \frac{e^{-jkr}}{jkr^2} + \frac{e^{-jk(r+d\cos\theta)}}{r+d\cos\theta} + \frac{e^{-jk(r+d\cos\theta)}}{jk(r+d\cos\theta)^2}\right]. \quad (1.376)$$

Let us consider the nearest field, where the condition (1.367) is true. After some alternations we obtain:

$$P_1 + P_2 = \frac{B\cos\theta}{jkr^2}\left(\frac{2+2\frac{d}{r}\cos\theta + \frac{d^2}{r^2}\cos^2\theta}{1+2\frac{d}{r}\cos\theta + \frac{d^2}{r^2}\cos^2\theta}\right). \quad (1.377)$$

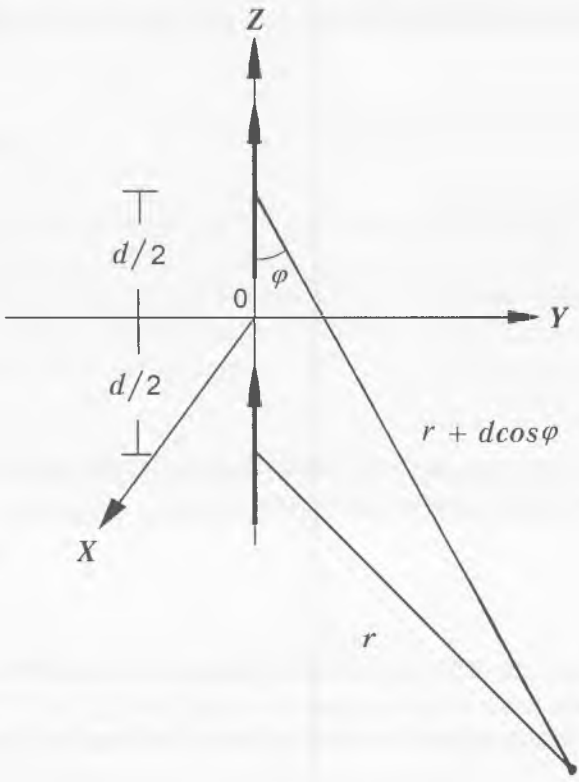

Fig. 1.42. A schematic representation of the longitudinal quadrupole under conditions when reflective interface is the demarcation line between the atmosphere and water.

For the distances, where (1.371) is true the expression can be simplified:

$$P_1 + P_2 = \frac{2B\cos\theta}{jkr^2}. \tag{1.378}$$

The amplitude of pressure is given by:

$$|P_1 + P_2| = \frac{2B\cos\theta}{kr^2}. \tag{1.379}$$

Therefore maximum of the directivity diagram for the quadrupole radiation occurs when $\theta = 0$ (Fig. 1.43*a*,*b*). The final expression for the amplitude of pressure in case of maximum can be expressed as follows:

$$|P_1 + P_2| = \frac{2B}{kr^2}. \tag{1.380}$$

Let us compare the fields of pressure for the transverse quadrupole and longitudinal quadrupole near the boundary of the water and the air. Pressure amplitude ratio is found to be:

$$\frac{|P_1 + P_2|}{|P_1 - P_2|} = \frac{r}{d}. \tag{1.381}$$

This expression shows that the farther the viewpoint from the source of radiation and the nearer the source of radiation to the water surface the bigger the value of the amplitude ratio is.

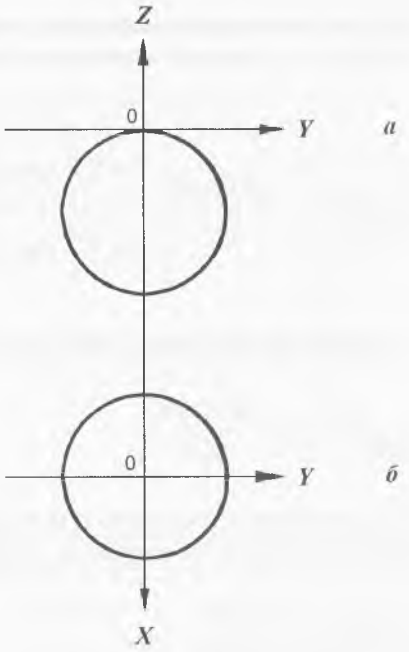

Fig. 1.43. A diagram of the sound directivity of the longitudinal quadrupole under conditions when reflective interface is the demarcation line between the atmosphere and water.

Near the bottom the situation is quite the opposite: the radiation of the transverse quadrupole is more intensive than the one of the longitudinal quadrupole. Let us show it. The scheme of transverse quadrupole near the solid reflecting surface (bottom) is given in fig. 1.44. The pressure field of the main dipole is given by expression (1.364). The field of the reflected dipole is given by (1.365). As the moments of both dipoles have the same orientation, the mutual field is equal to the sum of the fields of single dipoles.

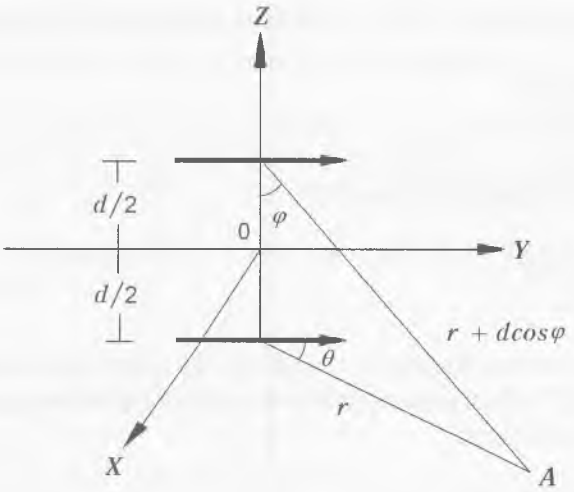

Fig. 1.44. A schematic representation of the transverse quadrupole under conditions when reflective interface is the demarcation line between the water and the bottom of the water bodies.

$$P_1 + P_2 = \frac{B\cos\theta}{jkr^2}\left(\frac{2+2\frac{d}{r}\cos\varphi+\frac{d^2}{r^2}\cos^2\varphi}{1+2\frac{d}{r}\cos\varphi+\frac{d^2}{r^2}\cos^2\varphi}\right). \qquad (1.382)$$

In case the additional condition (1.371) is true, we obtain from previous expression:

$$P_1 + P_2 = \frac{2B\cos\theta}{jkr^2}. \qquad (1.383)$$

The condition of maximum is the same as it was for the expression (1.379): $\theta = 0$. The absolute value of the amplitude of pressure is given by:

$$|P_1 + P_2| = \frac{2B}{kr^2}. \qquad (1.384)$$

The scheme of the longitudinal quadrupole in the presence of solid reflecting boundary (bottom) is shown in fig.1.45. In this case the field of longitudinal quadrupole is the difference of the fields of the dipoles:

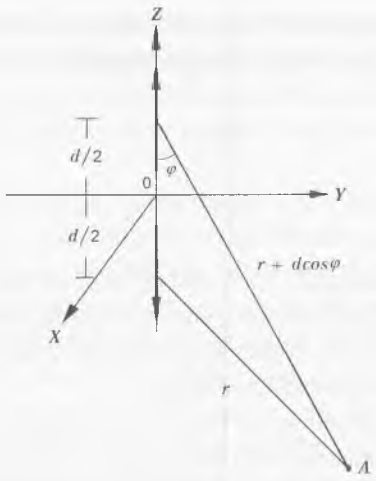

Fig. 1.45. A schematic representation of the longitudinal quadrupole under conditions when reflective interface is the demarcation line between the water and the bottom of the water bodies.

$$P_1 - P_2 = B\frac{\cos\theta}{jkr^2}\left(\frac{\frac{d}{r}\cos\theta\left(2+\frac{d}{r}\cos\theta\right)}{1+2\frac{d}{r}\cos\theta+\frac{d^2}{r^2}\cos^2\theta}\right). \tag{1.385}$$

When the additional condition (1.371) is true we can simplify the expression to the following:

$$P_1 - P_2 = \frac{2Bd\cos^2\theta}{jkr^3}. \tag{1.386}$$

It follows from expression (1.386) that the maximum of the directivity diagram occurs when $\theta = 0$, and the directivity diagram is narrower than it was in the previous cases.

It would be interesting to compare the levels of radiation of the longitudinal and transverse quadrupoles near the surface and near the bottom. In the first case the relation of the level of the weaker radiation of the transverse quadrupole to the level of more intensive radiation of longitudinal quadrupole is obtained by:

$$\frac{|P_1 - P_2|}{|P_1 + P_2|} = \frac{d}{2r}. \tag{1.387}$$

In the second case the relation of the level of the weaker radiation of the longitudinal quadrupole to the level of the more intensive radiation of the transverse quadrupole is given by:

$$\frac{|P_1 - P_2|}{|P_1 + P_2|} = \frac{d}{r}. \tag{1.388}$$

While comparing expressions (1.387) and (1.388) we may notice that the difference in the radiation of the longitudinal and transverse quadrupoles near the surface is two fold bigger than near the bottom. Either way the farther the viewpoint from the source, the more is the difference in the radiation level.

In order to understand the biological function of acoustic waves radiated by fish it is necessary to take into account so-called near field, which occurs in the distances much smaller than the length of the acoustic wave, i.e. several meters or dozens of meters. While moving near the bottom plaices and skates radiate almost no sound, but the fish with horisontal plane of oscillations generate intensive acoustic waves. What is the advantage of soundless swimming? It seems that such way of locomotion can be a specific way of coverage. Of course if a plaice or a skate swam near the surface the predator would hear them much better, and the same for the ordinary fish if it swam near the bottom. There is a numerical evaluation of the acoustic field. For a fish of 5 –10 cm in length swimming at a depth of 0.5 m the value of the acoustic field at a distance of 5 m is of order 10^{-9} Pa (for vertical oscillations) and of order 10^{-10} Pa (for horizontal oscillations). According to V. R. Protasov such values are distinctive for the hearing sensitivity of the fish with sound bladder. If we assume the hearing sensitivity of a predator equal to 10^{-10} Pa, near the surface it should hear the fish with horizontal plane of oscillations at a distance of 5 meters, and the fish with vertical plane of oscillations at a distance of 20 meters. Near the bottom the situation changes, as the radiation of the vertical dipole is weakening because of the reflection from the solid bottom, and the radiation of horizontal dipole is increasing.

These speculations lead to the conclusion, that in the presence of predators the sound is one of the evolutional factors. This factor could have been decisive for low vertebrates to evolve the way of swimming. To evolve the ability to swim by horizontal oscillations of the body they had to live in the upper layers of the water basins. This requirement does not contradict the modern data on the origin of life, according to which the upper layers were the richest in oxygen and warmth.

It seems natural that the ancient aquatic animals could bend their bodies in different planes unlike most of the modern fishes, which can bend their bodies only in horizontal plane. As the time went by the animals, which moved loudly, were exterminated by predators, and only the most quiet, moving by horizontal oscillations of the body, could survive.

Unfortunately there are not any paleontologic evidence of animals which were able to make undulate oscillations in different planes. The method of comparative morphology also gives no evidence that the low vertebrates had different forms of locomotion. There is only one exception: lancelet, whose larva reminds the plaice by its form and the way of moving.

There are some doubts about the correctness of this hypothesis as there are some species of skates, which live in the upper layers of the ocean, and there are some bottom dwelling fishes (gobs, sea hens, rockfishes) which move by the oscillations of their bodies in horizontal plane. But after deeper consideration one should admit that they do not contradict the hypothesis for the role of the sound as a factor of evolution. In fact, most of the pelagic fishes flex their bodies in horizontal plane and the fishes which flex their bodies in vertical plane are mainly bottom dwelling. And what is more, most of the fishes whose way of swimming does not agree with the hypothesis are either predators (rockfishes) or have special means of defense like poison bearing pikes or protective coloring and thus they do not need to swim quietly.

Brief conclusions

Analysis of the theoretical models of swimming showed that till now there is no model, which can express fully enough kinematical and hydrodynamic features of fish and dolphin swimming. Partly this can be explained by shortage of experimental data. There are some advanced models of dolphin swimming (Chopra and Kambe, 1977, Zaytsev and Fedotov, 1986 and our model described above), but they do not reflect in full the features of the tail fin operation. It is necessary to develop further experimental researches and to create on this base more advanced theoretical models.

CHAPTER 2. THE LAW OF BODY DEFORMATION IN ACTIVELY SWIMMING FISH OR DOLPHIN

Mathematical approximation of the propulsive wave in an actively swimming dolphin is vital for estimations of energy and force parameters of the animal's swimming. Mathematical approximation should sufficiently well satisfy all of the main kinematic parameters of swimming.

2.1. Analysis of the existing hypothesis of fish or dolphin body deformation law

Up to now there are not any reliable data on the law of deformation of the body of actively swimming fish or dolphin. Various researchers believed different analytical functions to be the best approximation of this law. In particular, Siekman (1962) considered that the function

$$y(x,t) = (c_0 + c_1 x + c_2 x^2)\cos(\omega t - kx), \tag{2.1}$$

describes the deformation law of the fish body best. Here c_0, c_1 and c_2 are constant coefficients, $k = \omega/C$ is the wave number, ω is the circular frequency, f is the cyclic frequency, t is the time. C is the fixed phase velocity of the propulsive wave spreading along the animal body from its head to its tail. The values of the constant coefficients are $c_0 = 0.023$, $c_1 = 0.042$, $c_2 = 0.034$.

Kelly (1961) gives another numerical values of the coefficients (for a swimming salmon): $c_0 = 0.016$, $c_1 = 0.028$, $c_2 = 0.035$.

Logvinovitch (1970b) (as a rough approximation of the law of body deformation of a swimming fish) uses the function

$$\eta = \eta_0 \sin\omega\left(t - \frac{x_2 - x}{C}\right). \tag{2.2}$$

Here η and η_0 are the amplitudes of bias of the some point of the body and of the tail correspondingly.

Kozlov (1983) (as possible variants to approximate the law of body deformation of an actively swimming fish) considers the following functions:

$$\eta = \eta_0 \frac{x_2 - x}{L_p} \sin\left(\frac{Ct}{L} - \frac{x_2 - x}{L}\right) \tag{2.3}$$

and

$$\eta = \eta_0 \sin\left[\frac{\pi}{2}\frac{x_2 - x}{L_p}\right]\sin\left(\frac{Ct}{L} - \frac{x_2 - x}{L}\right), \tag{2.4}$$

$$L = \frac{L_p}{2\pi n}, \tag{2.5}$$

Here n is the number of wavelengths that go along the fish body, L_p and L represent the body length measured in the absolute units and in the units of locomotive wavelength correspondingly.

But functions (2.2) – (2.4) do not take into account at least one obvious feature of fish swimming. This feature is oscillation of the forepart of the body that amounts to 20 – 40% of the amplitude of the tail oscillation. Besides, the choice of function is not based on any experimental data.

Such variety of functions proposed as possible laws of the swimming fish body deformation indicates lack of reliable experimental data on kinematics of this animal.

The laws of deformation of the body of actively swimming dolphins (*Phocoena Phocoena L. and Delphinus delphis L.*) is proposed by Semyonov, Babenko and Kayan (1974):

$$A = A_n e^{\beta x}\cos\omega\left(t - \frac{x}{C}\right). \tag{2.6}$$

Here A is the vertical bias of some point of the body, x is the distance along the body, t is the current time, C is the fixed speed of the locomotive wave propagation along the body, $\omega = 2\pi f$ is the circular frequency, A_n is the amplitude of the transversal oscillation of the head part of the body, β is the factor that characterizes the growth of the oscillation amplitude along the body from head to tail, which depends on the speed of the movement. Lighthill (1970) proposed the similar expression for the fish movement description.

But it is easy to show that β is not an independent parameter of the animal movement. It can be evaluated on the account of the boundary condition of the body oscillation problem. Indeed, we have in the point $x = l$

$$A_l = A_n e^{\beta l}. \tag{2.7}$$

Up to now we have not taken into account the time factor. Here l is the dolphin body length. Hence we can conclude that

$$\beta = \frac{1}{l} \ln \frac{A_t}{A_n}. \tag{2.8}$$

If we insert this expression into above mentioned one, we obtain

$$A = A_n \left(\frac{A_t}{A_n} \right)^{\frac{x}{l}} \cos \omega \left(t - \frac{x}{C} \right). \tag{2.9}$$

From this expression one can conclude that the rate of the oscillation amplitude growth along the dolphin body is unambiguously defined by the relation of the amplitudes of the nose oscillation and of the tail oscillation, which does not seem very likely.
Lighthill (1970b) proposed the following law of deformation of the body of actively swimming mackerel:

$$\begin{aligned} h(x,t) &= H(x) \cos \left[\omega \left(t + \frac{l-x}{C} \right) \right] + \\ &+ [h_1 + h_3(l-x)] \cos \omega t + [h_2 + h_4(l-x)] \sin \omega t, \end{aligned} \tag{2.10}$$

where h_1, h_2, h_3, h_4 are constant. The amplitude function $H(x)$ is not explicitly defined here. We think this form of the law of deformation is the most applicable for description of fish swimming. First, it takes into account "recoil" unlike the other variants. Second, under the certain values of the constant h_1, h_2, h_3, h_4 it can provide the zero thrust when $C \to U$ and exclude the contradiction mentioned above. However, in order to use this law of deformation, we must explicitly specify the amplitude function of the propulsive wave generated with muscles and define the values of coefficients characterizing the "recoil". It is rational to define the amplitude function like

$$H(x) = h_{t0} \left[K_n - 1 + e^{\alpha \left(\frac{x}{l} \right)^{\gamma}} \right]. \tag{2.11}$$

Here $K_n = h_{n0} / h_{t0}$, h_{n0} is the amplitude of the tail edge bias under the absence of the "recoil" condition, h_{n0} is the amplitude of the head (tip of nose) bias under the same condition, l is the fish body length, γ is the exponent that characterizes the power of the wave amplitude growth, α is a coefficient.

This amplitude function (2.11) includes all possible variants of the monotonically increasing function. Finally, the law of deformation of the mackerel like fish body can be written as

$$h(x,t)=h_{t0}\left[K_n-1+e^{\alpha\left(\frac{x}{l}\right)^{\gamma}}\right]\cos(\omega t-k_0 x)+ \\ +(h_1+h_3 x)\cos\omega t+(h_2+h_4 x)\sin\omega t. \qquad (2.12)$$

In this case the point of the coordinate origin coincides with the tip of the nose, x-axis goes from the head to the tail. Here $k_0=\omega/C_0$, C_0 is the speed of the propulsive wave, generated with muscles. It is a constant value under the constant speed of animal swimming. All parameters of the expression (2.12) can be defined experimentally.

2.2. Comparison with experiment

There are several experimental works containing the comprehensive data on the fish kinematics. They are of Bainbridge (1963), Videler and Hess (1984), Hess and Videler (1984), Videler (1993). In the first of these works there are data on kinematics of the three fish species: the roach (*Leuciscus leuciscus*), bream (*Abramis brama*) and goldfish (*Carassius auratus*). The author carefully measured the amplitudes of bias and speed of the propulsive wave at six points of the fish body. To be more exact, it was not the speed, that he measured, but the wavelength. However, when the wavelength is known, we can calculate the speed easily. The work of Bainbridge contains all the data, which are necessary to define the unknown values in the deformation law expression (2.12), and thus it makes possible to examine the adequacy of this law to real fish kinematics.

The values of bias of different points of body for the roach, bream and silvery crucian during active swimming are shown in fig. 2.1

The data on the locomotive wavelength are gathered in table 2.1 in the same order.

The amplitude and phase functions for the pollack and mackerel are adduced in the works of Videler and Hess (1984), Hess and Videler (1984) and shown in figures 2.2 and 2.3.

In paper (Grillner, Kashin, 1976) there are the data on the amplitude functions of three more fish species but there are no information about the respective lengths of the propulsive waves on their bodies, those data are given in Fig. 2.4.

When analysed, the data from Fig. 2.1 2.2 and 2.4 demonstrate that in most cases the amplitude function is characterised by the presence of a minimum at the distance of about $0.3l$ from the nose tip of the fish. The minimum may be more or less deep and sometimes it may be completely absent, as shown in the curve 1 in Fig. 2.4. It means that the phenomenon of «recoil» in different fishes is manifested differently.

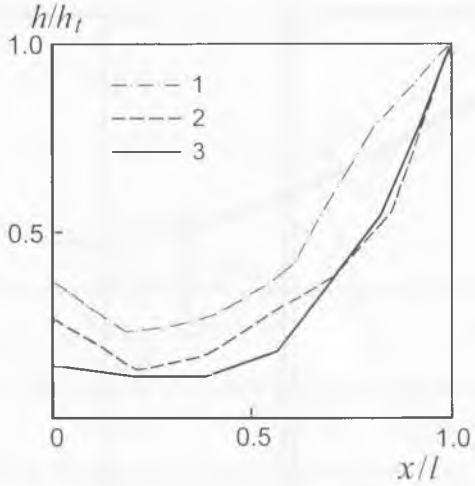

Fig. 2.1. The amplitude function of the lateral movements at six positions along the length of the body of a goldfish (1), bream (2) and dace (3) swimming steadily. (Based on data by Bainbridge, 1963).

1	x, m	0	0.048	0.095	0.14	0.208	0.25
	λ_n, m	0.141	0.147	0.16	0.15	0.155	0.155
2	x, m	0	0.04	0.072	0.133	0.162	0.19
	λ_n, m	0.125	0.125	0.116	0.115	0.12	0.115
3	x, m	0	0.03	0.064	0.096	0.126	0.16
	λ_n, m	0.115	0.115	0.116	0.11	0.113	0.115

Table 2.1. Length of propulsive wave (l_n) for a dace (1), bream (2) and goldfish (3) along a body (x). (Adopted from Bainbridge, 1963).

As to the length of the propulsive wave, according to the above data, it is practically constant within the limits of the fish body. Hence, in this case the real velocity of the propulsive wave in its first approximation can also be regarded as a constant value.

Fig. 2.5 schematised experimental amplitude function of an actively swimming fish with all the necessary symbols. h_n and h_t are the amplitudes of shift in the nose tip and

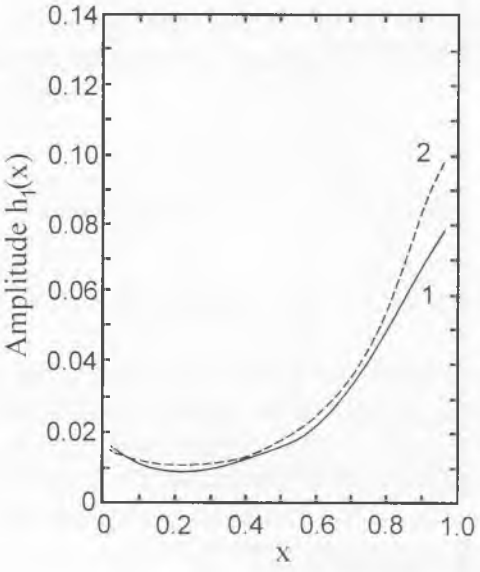

Fig. 2.2. The amplitude function of the lateral movements of the body for 'average' saithe (1) and 'average' mackerel (2) swimming steadily. (Redrawn from Videler and Hess, 1984).

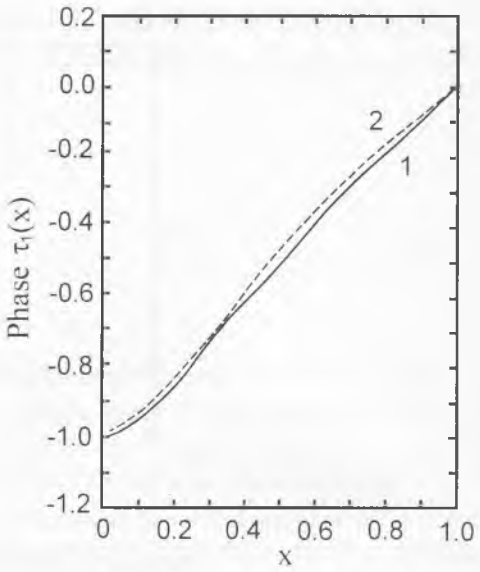

Fig. 2.3. The phase function of the lateral movements of the body for 'average' saithe and 'average' mackerel swimming steadily. (Redrawn from Videler and Hess, 1984).

the tail respectively as measured experimentally; b_{min} and h_{min} are the positions of the minimum of the amplitude function and the amplitude of shift in the minimum: b_{00} is chosen as equal to $0.42l$ according to Ligthhill's theory of «recoil». Then h_{00} is determined by the experimental amplitudinal function for this point. All of the above values are regarded to be known.

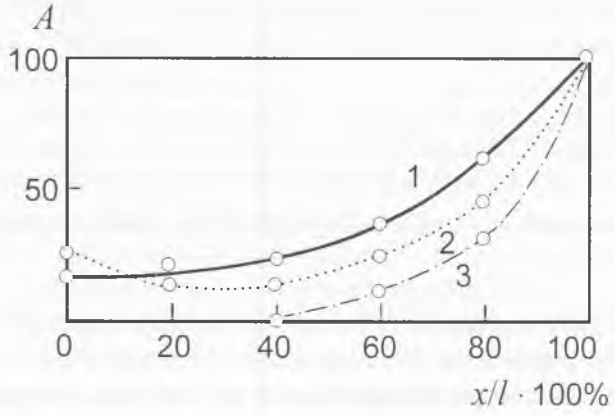

Fig. 2.4. The amplitude function of the lateral movements of the body of a *Anguilla vulgaris* (1), *Cyprinus carpio* (2) and *Myoxocephalus sp.* (3). (Redrawn from Grillner, Kashin, 1976).

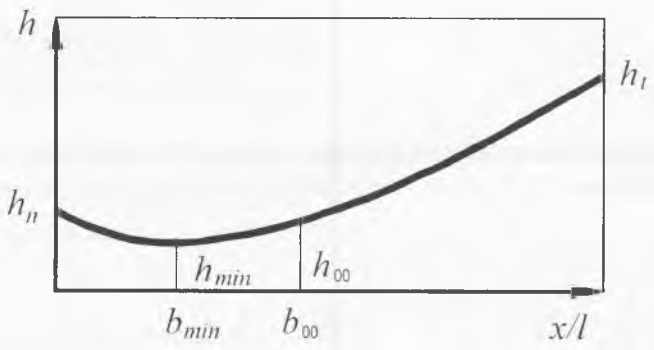

Fig. 2.5. A schematic sketch of the amplitude function of the lateral movements of the active swimming fish.

The unknown values in the expression (2.12) are those of k_0, h_n h_t, α, g, h_1, h_2, h_3 and h_4. To determine them unambiguously, it is necessary to have nine independent equations.

To derive first equation, we shall write down separately the amplitude function of the wave generated by muscular contractions, namely

$$H(x) = h_t \left[\frac{h_n}{h_t} - 1 + e^{\alpha \left(\frac{x}{l} \right)^\gamma} \right]. \tag{2.13}$$

When $x = l$, we shall have

$$1 = \frac{h_n}{h_t} - 1 + e^{\alpha}. \tag{2.14}$$

Hence we shall get

$$\alpha = \ln\left(2 - \frac{h_n}{h_t} \right). \tag{2.15}$$

The second and the third equations will be derived from the condition when $x = b_{00}$ (on the axis of yawing)

$$(h_1 + h_3 b_{00})\cos \omega t + (h_2 + h_4 b_{00})\sin \omega t = 0. \tag{2.16}$$

Therefrom we shall get

$$h_1 = -h_3 b_{00} \tag{2.17}$$

and

$$h_2 = -h_4 b_{00}. \tag{2.18}$$

Let us rewrite the law of deformation with regards of the relations (2.15), (2.17) and (2.18). We shall have

$$h(x,t) = h_t \left[\frac{h_n}{h_t} - 1 + \left(2 - \frac{h_n}{h_t} \right)^{\left(\frac{x}{l}\right)^\gamma} \right] \cos(\omega t - k_0 x) + \tag{2.19}$$

$$+ h_3 (x - b_{00}) \cos \omega t + h_4 (x - b_{00}) \sin \omega t.$$

In this form the law of deformation contains six unknown values. Let us make use of

$$H(x,t) = h_t \left[\frac{h_n}{h_t} - 1 + \left(2 - \frac{h_n}{h_t} \right)^{\left(\frac{x}{l}\right)^\gamma} \right] \tag{2.20}$$

and the formula from trigonometry for the difference cosine between two angles. Then it is possible to write

$$h(x,t) = H(x)\cos\omega t \cos k_0 x + H(x)\sin\omega t \sin k_0 x +$$

$$h_3(x - b_{00})\cos\omega t + h_4(x - b_{00})\sin\omega t \tag{2.21}$$

or

$$h(x,t) = [H(x)\sin k_0 x + h_4(x - b_{00})]\sin\omega t + [H(x)\cos k_0 x + h_3(x - b_{00})]\cos\omega t. \tag{2.22}$$

The last expression is convenient to write as

$$h(x,t) = h(x)\sin(\omega t + \alpha), \tag{2.23}$$

where

$$h(x) = \sqrt{[H(x)\sin k_0 x + h_4 (x - b_{00})]^2 + [H(x)\cos k_0 x + h_3 (x - b_{00})]^2} \tag{2.24}$$

and

$$\alpha = arctg \frac{H(x)\cos k_0 x + h_3(x - b_{00})}{H(x)\sin k_0 x + h_4(x - b_{00})}. \tag{2.25}$$

Such form of presentation facilitates the composition of the remaining equations necessary to determine the unknown parameters. With $x = 0$, from (2.20) and (2.21) we shall get

$$h_n = \sqrt{h_4^2 b_{00}^2 + [h_{n0} - h_3 b_{00}]^2}. \tag{2.26}$$

With $x = b_{00}$ from (2.20) we shall get

$$h_{00} = h_t \left[\frac{h_n}{h_t} - 1 + \left(2 - \frac{h_n}{h_t} \right)^{\left(\frac{b_{00}}{l} \right)^\gamma} \right]. \tag{2.27}$$

With $x = l$, from (2.24) we shall get

$$h_t^2 = [h_{t0} \sin k_0 l + h_4(l - b_{00})]^2 + [h_{t0} \cos k_0 l + h_3(l - b_{00})]^2. \tag{2.28}$$

With $x = b_{mm}$, we shall similarly have

$$\begin{aligned} h_{min}^2 &= [H(b_{min})\sin k_0 b_{min} + h_4(b_{min} - b_{00})]^2 + \\ &+ [H(b_{min})\cos k_0 b_{min} + h_3(b_{min} - b_{00})]^2. \end{aligned} \tag{2.29}$$

The two other equations, which are still lacking, may be derived from the equation of the phase. The latter can be written as

$$\omega t + \alpha = \varphi_0 = const. \tag{2.30}$$

Upon its differentiation in time, we shall have

$$\omega + \frac{\partial \alpha}{\partial x} \frac{\partial x}{\partial t} = 0. \tag{2.31}$$

Therefrom we shall have

$$\frac{\partial x}{\partial t} = C = -\frac{\omega}{\frac{\partial \alpha}{\partial x}}. \tag{2.32}$$

Here C is the phase velocity of the real propulsive wave propagating along the fish body during its motion. This is the very velocity, which can be measured experimentally or calculated by the results of the length measurements of the real propulsive wave.

Hence, the value $-\dfrac{\partial\alpha}{\partial x}$ (with the negative sign) is nothing else but the real wave number k (unlike the wave number k_0 of the muscular propulsive wave).

The value $-\dfrac{\partial\alpha}{\partial x}$ is easy to obtain from the relation (2.25) to

$$\frac{\partial\alpha}{\partial x}=\frac{-H^2(x)k_0-\left[\dfrac{\partial H(x)}{\partial x}(x-b_{00})-H(x)\right]\left[h_3\sin k_0x-h_4\cos k_0x\right]}{h^2(x)}-$$
$$-\frac{H(x)(x-b_{00})k_0\left[h_3\cos k_0x+h_4\sin k_0x\right]}{h^2(x)}. \tag{2.33}$$

With $x = 0$, we shall have

$$\frac{-h_n^2k_0-h_nh_4+h_nb_{00}k_0h_3}{h^2(x)}=k=\frac{2\pi}{\lambda_{x=0}}. \tag{2.34}$$

Here, $\lambda_{x=0}$ is the measured length of the propulsive wave at the point $x = 0$. In the same way we shall get

$$\frac{-H^2(b_{00})k_0+H(b_{00})\left[h_3\sin k_0b_{00}-h_4\cos k_0b_{00}\right]}{h_{00}^2}=\frac{2\pi}{\lambda_{x=b_{00}}}, \tag{2.35}$$

when $x = b_{00}$.
However, regarding the equation (2.16), we can write

$$h_{00}=H(b_{00}). \tag{2.36}$$

Then we shall finally have

$$-k_0+\frac{h_3\sin k_0b_{00}-h_4\cos k_0b_{00}}{h_{00}}=\frac{2\pi}{\lambda_{x=b_{00}}}. \tag{2.37}$$

So, we have obtained nine independent equations, namely (2.15), (2.17), (2.18), (2.26) - (2.29), (2.34) and (2.37), to determine nine unknown values. An attempt had been made to solve this system of equations but it came out that it was impossible to reach good agreement between the calculated functions of the amplitude and the velocity of the propulsive wave, on the one hand, and the measured ones on the other hand. This phenomenon is illustrated in Fig. 2.6 and 2.7.

Fig. 2.6 compares the calculated and the measured values of the amplitudes of the shifted points in case of a dace. Fig. 2.7 compares the calculated and the measured values of the phase velocity of the propulsive wave. One can see that with the good agreement between the amplitudinal functions there is a considerable divergence between the functions of the wave velocity. It is possible to get a solution when there will be a good coincidence between the calculated and the measured values of the wave velocity but then there will be a large divergence between the existing amplitudinal functions. It's impossible to get simultaneously agreement between the amplitudinal functions and the wave velocities. Similar results of comparison between the calculated and the measured parameters were also obtained for a bream (Figs. 2.8 and 2.9). It testifies to the fact that the law of deformation as presented in (2.12) is not satisfactory to reflect the real processes in fish swimming.

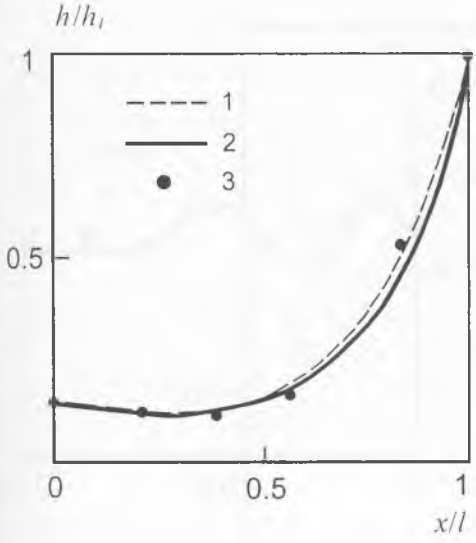

Fig. 2.6. The amplitude function of the lateral movements of the body for a dace. 1 – theory on the assumption that phase velocity is constant, 2 - theory on the assumption that phase velocity is not constant, 3 – experimental data. (Based on data by Bainbridge, 1963).

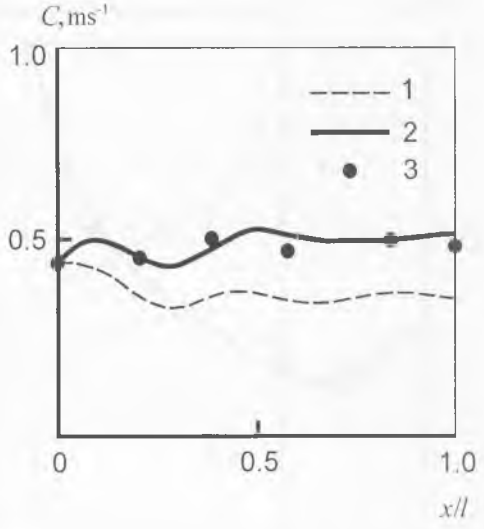

Fig. 2.7. The phase velocity function of the lateral movements of the body for a dace. 1 – theory on the assumption that phase velocity is constant, 2 - theory on the assumption that phase velocity is not constant, 3 – experimental data. (Based on data by Bainbridge, 1963).

2.3. Propulsive wave phase velocity. Dependence on the location

In the work (Romanenko, 1980a) there was given a hypothesis that the phase velocity of the propulsive wave of the dolphin body depends on the co-ordinate. This hypothesis got the tentative verification in the experiments on dolphins (Romanenko, 1980*1*). As for fishes, the above cited Bainbridge's work (1963) attests that the factual velocity of spreading of the propulsive wave along the fish body is constant. But according to Lighthill the body of a fish is involved in two simultaneous motions: the first one is generated by muscular system and the other is the yawing due to recoil effect. The propulsive wave, which is the sum of the two motions, is observed in experiments. The phase velocity of the muscular propulsive wave of fish body may depend on the co-ordinate. But the yawing motion compensates this dependence and it results in constant or almost constant velocity of the propulsive wave. Actually some authors (Hess, Videler, 1984; Videler, Hess, 1984) show that some fish (saithe, mackerel) propulsive wave speed depends on coordinate. Fig. 2.10 shows that saithe and mackerel propulsive wave speed function calculated on data base of fig. 2.3 with the help of the formula

$$C(x) = \frac{\Delta x}{\Delta t}. \qquad (2.38)$$

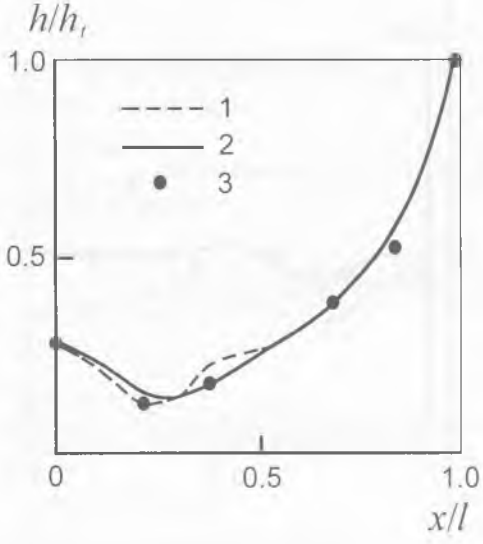

Fig. 2.8. The amplitude function of the lateral movements of the body for a bream. 1 – theory on the assumption that phase velocity is constant, 2 - theory on the assumption that phase velocity is not constant, 3 – experimental data. (Based on data by Bainbridge, 1963).

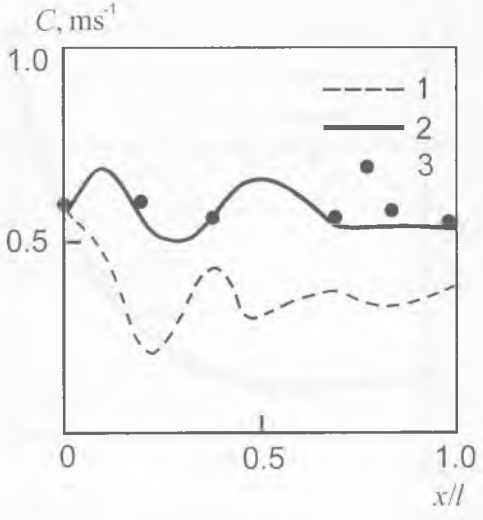

Fig. 2.9. The phase velocity function of the lateral movements of the body for a bream. 1 – theory on the assumption that phase velocity is constant, 2 - theory on the assumption that phase velocity is not constant, 3 – experimental data. (Based on data by Bainbridge, 1963).

This formula can be get from the phase equation

$$\omega[t-\tau(x)]=const. \tag{2.39}$$

Upon its differentiation in time we shall have

$$1-\frac{\partial\tau}{\partial x}\frac{\partial x}{\partial t}=0. \tag{2.40}$$

We can designate

$$\frac{\partial x}{\partial t}=C(x). \tag{2.41}$$

Then

$$C(x)=\frac{\Delta x}{\Delta t}. \tag{2.42}$$

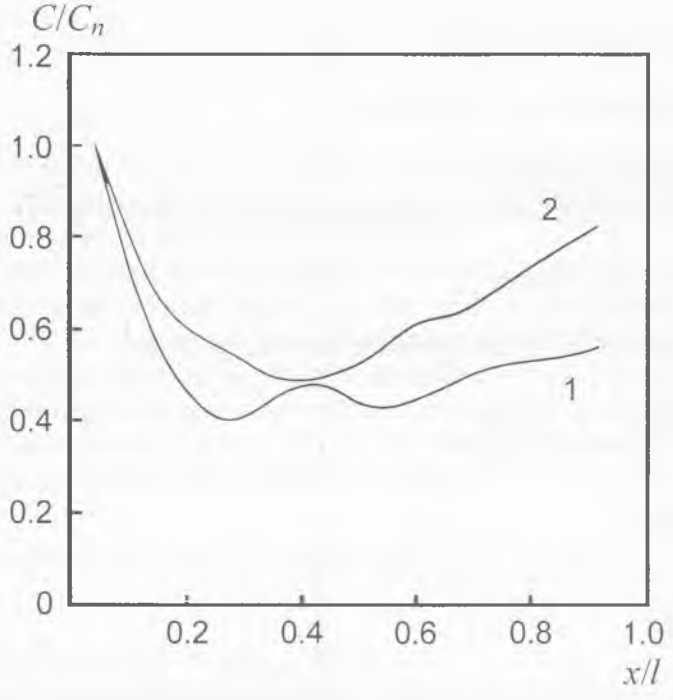

Fig. 2.10. The phase velocity function of the lateral movements of the body for 'average' saithe (1) and 'average' mackerel (2) swimming steadily. (Converted from fig. 2.3.).

The analysis shows that we can achieve tolerable concordance between the theory and the experiment if we present the dependence of the phase velocity of the propulsive wave in the form

$$C = C_t\left[1 + a_0\left(1 - e^{-b_0 x}\right)\right] \tag{2.43}$$

for fishes with small yawing motions (as roaches) and in the form

$$C = C_t\left[1 + a_0\left(1 - e^{-b_0 x}\right)e^{-b_0 x}\right] \tag{2.44}$$

for fishes with large yawing motions (as breams). Here C_t is the phase velocity at the head region, a_0 and b_0 are the coefficients, which characterise the varying of the velocity. Generally speaking, they can be positive or negative. Such notation with only two arbitrary constants describes the wide class of dependencies. This class includes the constant velocity of the wave when $a_0 \to b_0 \to 0$, the linear dependence on co-ordinate when $a_0 \neq 0$, $b_0 \to 0$, and more complicated dependencies when $a_0 \neq 0$, $b_0 \neq 0$.

Dependence of the wave phase velocity on the coordinate denotes dependence of the wave number k_0 on the co-ordinate. In this case the deformation law (2.12) and (2.19) can be written as

$$\begin{aligned} h(x) &= H(x)\cos\left[\omega t - k(x)x\right] + \\ &+ h_3(x - b_{00})\cos\omega t + h_4(x - b_{00})\sin\omega t, \end{aligned} \tag{2.45}$$

where $H(x)$ looks like (2.20)

We shall define the kind of the dependence $k(x)$ with phase equation

$$\omega t - k(x)x = \varphi_0 = const. \tag{2.46}$$

Differentiation of this equation with respect to time gives

$$\omega - \frac{\partial k(x)}{\partial x}\frac{\partial x}{\partial t}x - k(x)\frac{\partial x}{\partial t} = 0. \tag{2.47}$$

In this equation

$$\frac{\partial x}{\partial t} = C(x). \tag{2.48}$$

Substitution of (2.48) in (2.47) gives the differential equation to define $k(x)$

$$\omega - \frac{\partial k(x)}{\partial x} C(x) x - k(x) C(x) = 0. \tag{2.49}$$

The solution of the equation for the dace looks like

$$k(x) = \frac{k_0}{x(1+a_0) b_0} \ln \frac{\left[1 + a_0 \left(1 - e^{-b_0 x}\right)\right]}{e^{-b_0 x}} \tag{2.50}$$

and for the bream looks like

$$k(x) = \frac{k_0}{2b_0 x} \ln\left(1 + a_0 e^{-b_0 x} - a_0 e^{-2b_0 x}\right) +$$
$$+ \frac{k_0 a_0}{2b_0 x \sqrt{4a_0 + a_0^2}} \ln \frac{\left(\sqrt{4a_0 + a_0^2} - a_0 + 2a_0 e^{-b_0 x}\right)\left(\sqrt{4a_0 + a_0^2} - a_0\right)}{\left(\sqrt{4a_0 + a_0^2} + a_0 - 2a_0 e^{-b_0 x}\right)\left(\sqrt{4a_0 + a_0^2} + a_0\right)} + k_0, \tag{2.51}$$

where

$$k_0 = \frac{\omega}{C_t}. \tag{2.52}$$

Finally, the deformation law in the discussed case looks like (2.45) with $k(x)$ defined by equations (2.50) when the amplitude functions are the dace-like ones and (2.51) when the amplitude functions are the bream-like ones.

Let us examine, whether this deformation law gives us a good accordance between the experimental amplitude and phase functions and the corresponding calculated functions. But first let us correct the set of equations, which gives the values of the deformation law parameters. Accounting the dependence of the phase velocity on the coordinate, which adds two more unknown parameters a and b, we get the complete set of equations. The equations (2.15), (2.17), (2.18), (2.26), (2.27) and (2.34) remain the same. The equations (2.28), (2.29) and (2.37) become

$$h_t^2 = \left[h_{t0} \sin \varphi(l) + h_4 (l - b_{00})\right]^2 + \left[h_{t0} \cos \varphi(l) + h_3 (l - b_{00})\right]^2, \tag{2.53}$$

$$h_{min}^2 = \left[H(b_{min}) \sin \varphi(b_{min}) + h_4 (b_{min} - b_{00})\right]^2 +$$
$$+ \left[H(b_{min}) \cos \varphi(b_{min}) + h_3 (b_{min} - b_{00})\right]^2, \tag{2.54}$$

$$-\frac{\partial\varphi(b_{00})}{\partial x}+\frac{h_3\sin\varphi(b_{00})-h_4\cos\varphi(b_{00})}{h_{00}}=\frac{2\pi}{\lambda_{x=b_{00}}}, \tag{2.55}$$

here

$$\varphi(x)=k(x)x\ . \tag{2.56}$$

Besides two new equations appear because now we have eleven (not nine) unknowns. One of these equations we get from the formula of the amplitude function like (2.24) which accounts the dependence of the wave number on the coordinate at the point of minimum

$$\frac{\partial h}{\partial x}=0 \text{ under } x = b_{min}. \tag{2.57}$$

If (2.57) is expanded then

$$\begin{aligned} &H(b_{min})\frac{\partial H(b_{min})}{\partial x}+\left[\frac{\partial H(b_{min})}{\partial x}(b_{min}-b_{00})+H(b_{min})\right]\left[h_4\sin\varphi(b_{min})+h_3\cos\varphi(b_{min})\right]+\\ &+H(b_{min})\frac{\partial\varphi(b_{min})}{\partial x}(b_{min}-b_{00})\left[h_4\cos\varphi(b_{min})-h_3\sin\varphi(b_{min})\right]+(b_{min}-b_{00})\left(h_3^2+h_4^2\right)=0. \end{aligned} \tag{2.58}$$

We can get the second equation from the formula (2.33) under condition $x = b_0$, accounting (2.53) or (2.54).

$$\frac{\partial\alpha}{\partial x}(b_{min})=\frac{2\pi}{\lambda_{x=b_{min}}}. \tag{2.59}$$

We do not write it here because of its length.

In figures 2.6 and 2.7 we can compare the theoretical values with the results of the experiment for the case of the dace and for the case of the bream Fig 2.8, Fig 2.9 (in both cases curves 2). It is clear that in those cases when we did not make the assumption of the constant phase velocity the assent is much better (see curves 1 of the same figures).

The dependencies of the muscular propulsive wave on the coordinate have been accepted in the shape that is shown in figures 2.11 and 2.12 for the dace and for the bream correspondingly. The experimental values of the phase velocity of the real propulsive wave, which have been calculated for the above-cited data, are also shown in the same figures.

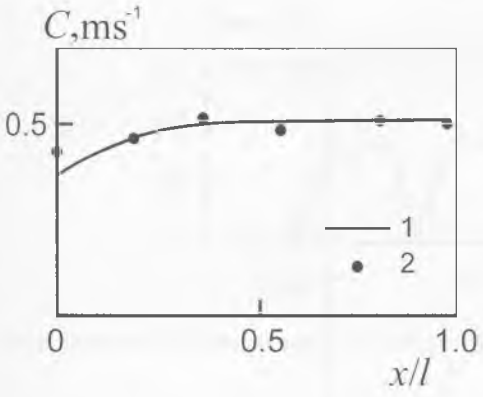

Fig. 2.11. The theoretical phase velocity function of the muscle propulsive wave of a dace (1) and experimental data. (Based on data by Bainbridge, 1963).

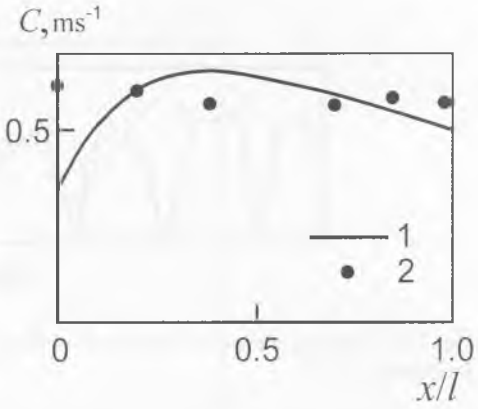

Fig. 2.12. The theoretical phase velocity function of the muscle propulsive wave of a bream (1) and experimental data. (Based on data by Bainbridge, 1963).

The values of the parameters of the muscular propulsive wave are cited in table 2.2. These values correspond to the calculated curves in figures 2.6 – 2.9. The second line in table 2.2 corresponds with the dace and the third line corresponds with the bream.

The analysis of the data, that is shown in figures 2.6 – 2.9, 2.11, 2.12 and in table 2.2, allows to outspeak some considerations and conclusions.

The deformation law (2.45) with dependence of the muscular wave phase velocity (2.43) and (2.44) give the fair picture of swimming of the fishes, whose amplitude function has a minimum generated by the yawing caused by recoil effect. The less the yawing, the better the theory matches the experiment. In fact, the calculated curves of the amplitude function and especially of the speed function are of oscillating formation. The calculated curves for the bream, which have more recoil, are more oscillating. These oscillations are rather due to the imperfection of the theoretical model. The weak point of the model, perhaps, is the harmonic approximaion of the fish body oscillations, which can actually be nonharmonic. Figure 2.13, which demonstrates the oscillations of the bream's caudal fin, is an illustration to this fact.

The theoretical model is also imperfect because it implies the linear mode of yawing.

k_0, m^{-1}	h_{n0}, m	h_{f0}, m	γ	h_4	h_3	a_0	b_0, m^{-1}
54.4	0.0038	0.0331	4	-0.005	-0.0053	0.4	25
86.2	0.0038	0.0203	2.8	-0.01	-0.0191	3.3	10

Table 2.2. Parameters of a muscle propulsive wave for a dace (second line) and bream (third line). For explanations of variables, see text.

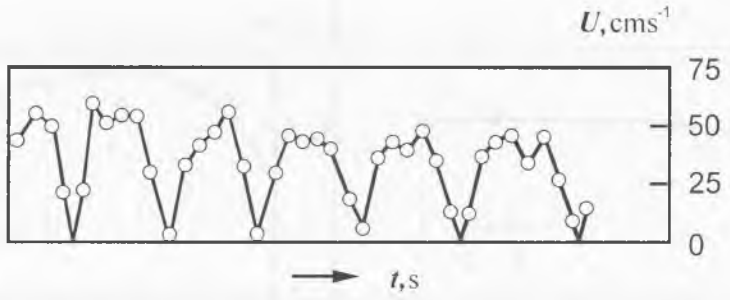

Fig. 2.13. Speed of transverse movement of the caudal fin of a bream swimming steadily. (Redrawn from Bainbridge, 1963).

It is presumed that the muscular propulsive wave runs along all the body of a fish, but the head region, where there are not any muscular structures, is unlikely to assist in the wave generation (Fig. 2.10).

However, the discussed model still maps the basic features of the fish swimming.

There is a possibility to registrate the phenomena that accompany the muscular propulsive wave. Now there is only one work (Grillner, Kashin, 1976), that contains the results of the study of the myographic wave and the simultaneously actual muscular propulsive wave of the fish. There are a few data about only one species (the eel). But these data allow to think that the myographic wave (and therefore, muscular wave) have the velocity, which varies within the range of the body.

This work contains the important conclusion, that the myographic wave spreads approximately 40% faster than the mechanical wave, which is actually observed (see fig. 2.14). This fact qualitatively corresponds to the results that are represented in fig. 2.12. It shows the calculated dependence of the phase velocity of the muscular locomotive wave of the body on its location in the comparison with the experimentally-measured velocity of the observed propulsive wave. It is obvious, that the velocity of the muscular wave at the body segment $0.2<x/l<0.8$ had to be 15 – 20% higher than the velocity of the observed propulsive wave. However, the data of the single work (Grillner, Kashin, 1976) cannot be the unconditional confirmation of the above mentioned theoretical conclusions. This data can only outline the way and the method of the further experimental investigations.

One more remark. According to Lighthill, the axis of the yawing has to be located at the distance $0.58l$ from the fish tail. But according to our data, the dace axis of yawing has to be located at the distance $0.5l$ from the fish tail, and the bream axis of the yawing has to be located at the distance $0.42l$ from the fish tail. In any case, the axis of the yawing must not coincide with the minimum of the amplitude function opposite to Lighthill's statement. The coincidence exists only when the amplitude of the oscillation is constant along the whole fish body. The difference of the estimations of the yawing axis locations can be explained

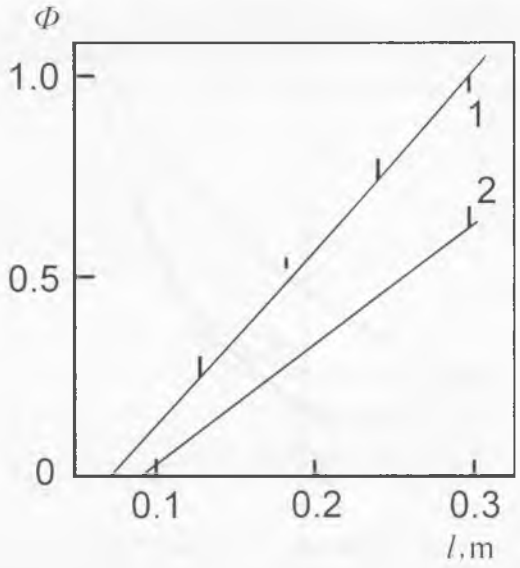

Fig. 2.14. The phase angle of the propulsive wave (1) and miographic wave (2) at different positions along the length of the body of an eel. (Redrawn from Grillner, Kashin, 1976).

by the imperfection of the theoretical model used by Lighthill. This model does not take into account that the propulsive wave phase velocity is not necessary constant.

2.4. The law of body deformation in actively swimming dolphin

Available experimental data on dolphins (*Tursiops truncatus*) (Romanenko 1980a, 1980b, 1986a) reliably establish at least the linear dependence of the propulsive wave phase velocity on coordinate and monotone growth of the amplitude function. But Yanov (1990, 1997, 1998) distinguished a more complex dependence of the amplitude and phase functions in the same dolphin species. In figure 2.15 there is an amplitude function of the *Tursiops truncatus* dolphin (1) experimentally measured by Yanov (1990, 1997) for a dolphin swimming with a constant speed of 3.12 ms^{-1} and its approximation (3) with the expression

$$h(x) = h_{xa}\left[0.21 - 0.66\frac{x}{l} + 1.1\left(\frac{x}{l}\right)^2 + 0.35\left(\frac{x}{l}\right)^8\right]. \qquad (2.60)$$

There is also an approximation made by Romanenko (1986a) based on the measurements in three points of the dolphin body under the constant speed 4.3 ms^{-1} (2), and the law of deformation (4) proposed by Semyonov, Babenko, and Kayan (1974). We can see that the variant of Semyonov, Babenko, and Kayan gives the worst accordance

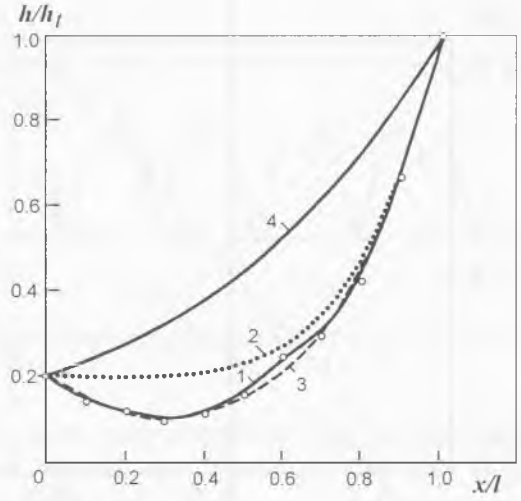

Fig. 2.15. The amplitude function of the transverse movements of the dolphins' body. 1 - experimental data. (Adopted from Yanov, 1990, 1997), 2 – 4 – the versions of the mathematical approximations of the amplitude functions.

to the experiment. Taking into account that in some cases the difference between the representation of kinematical data by Romanenko and Yanov's is minor, we will base our calculations on the law of deformation

$$h(x,t)=h_t\left[\frac{h_n}{h_t}-1+\left(2-\frac{h_n}{h_t}\right)^{\left(\frac{x}{l}\right)^{\gamma}}\right]\sin[\omega t-k(x)x] \qquad (2.61).$$

Here, the function $k(x)$ in its first approximation may be taken as

$$k(x)=\frac{k_0\ln(1+b_0x)}{bx}. \qquad (2.62).$$

This function is corresponding to the linear dependence between the phase velocity of the propulsive wave and the coordinate

$$C(x)=C_n(1+b_0x). \qquad (2.63)$$

In the formula (2.62)

where C_n is the phase velocity of the propulsive wave in the area of the animal's head (nose).

The presentation of the law of body deformation as (2.61) should not, in the first place, lead to the physical contradiction mentioned in §1.4. To verify this, we shall substitute (2.61), with regards of (2.62) and (2.63), into the formula for the thrust, obtained by Lighthill:

$$\overline{T} = \frac{1}{2}\rho A(l)\left[\overline{\left(\frac{\partial h}{\partial t}\right)^2 - U^2\left(\frac{\partial h}{\partial x}\right)^2}\right]_{x=l} \tag{2.64}$$

and we shall have

$$\overline{T} = \frac{1}{4}\rho A(l)\omega^2 h_t^2\left[1 - \frac{U^2}{C_n^2(1-b_0 l)^2} - \frac{U^2\left[\ln\left(2-\frac{h_n}{h_t}\right)\right]^2\gamma^2}{\omega^2 l^2}\left(2-\frac{h_n}{h_t}\right)^2\right]. \tag{2.65}$$

This expression must transform to zero at some correlation between U and $C(x)$. We just cannot simply equate U and $C(x)$ because $C(x)$ varies within the limits of the animal's body, from the value of C_n on the nose tip to $C_n(1+b_0 l)$ on the tail edge. Therefore we shall try to find out at what correlation between U and $C(x)$ the expression (2.65) turns into zero. Let us equate to zero the expression in brackets

$$1 - \frac{U^2}{C_n^2(1-b_0 l)^2} - \frac{U^2\left[\ln\left(2-\frac{h_n}{h_t}\right)\right]^2\gamma^2}{\omega^2 l^2}\left(2-\frac{h_n}{h_t}\right)^2 = 0. \tag{2.66}$$

Therefrom we shall get

$$\frac{U}{C_n(1+b_0 l)} = \sqrt{1 - \frac{U^2\left[\ln\left(2-\frac{h_n}{h_t}\right)\right]^2\gamma^2\left(2-\frac{h_n}{h_t}\right)^2}{\omega^2 l^2}}. \tag{2.67}$$

One can see that there is a certain real correlation between U and $C_n(1+b_0 l)$ at which the thrust turns into zero. With that, when $U \neq 0$ and $\gamma \neq 0$, it is always the case that $U < C_n(1+b_0 l)$.

In this way, the suggestion that the phase velocity of the propulsive wave depends upon the coordinate as (2.52) does allow indeed to avoid the above contradiction.

2.4.1. Estimation of the parameters comprising the law of body deformation in the dolphins

It is possible to estimate the most important values γ and b_0, comprising the law of body deformation (2.61) for dolphins, without any experiments. To this end, we shall employ the relation (2.67). If we could know the exact correlation between U and $C_n(1+b_0 l)$, at which the thrust must turn into zero, we would be able to get some unambiguous relation between γ and b_0. But we only know that U must occur within the interval of values C_n - $C_n(1+b_0 l)$ for the thrust to turn into zero. Therefore we shall divide the above interval into four equal parts and shall calculate the dependence between γ and b_0 for five values of U, namely

$$U_1 = C_n, \tag{2.68}$$

$$U_2 = \frac{C_n(4+b_0 l)}{4}, \tag{2.69}$$

$$U_3 = \frac{C_n(2+b_0 l)}{4}, \tag{2.70}$$

$$U_4 = \frac{C_n(4+3b_0 l)}{4}, \tag{2.71}$$

$$U_5 = C_n(1+b_0 l). \tag{2.72}$$

By substituting (2.68) - (2.72) into (2.66) we shall get the following correlations:

$$\gamma = \frac{\omega l \sqrt{b_0 l(2+b_0 l)}}{U(1+b_0 l)\left(2-\frac{h_n}{h_t}\right)\ln\left(2-\frac{h_n}{h_t}\right)}, \tag{2.73}$$

$$\gamma = \frac{\omega l \sqrt{3b_0 l(8 + 5b_0 l)}}{4U(1 + b_0 l)\left(2 - \frac{h_n}{h_t}\right)\ln\left(2 - \frac{h_n}{h_t}\right)}, \tag{2.74}$$

$$\gamma = \frac{\omega l \sqrt{b_0 l(4 + 3b_0 l)}}{2U(1 + b_0 l)\left(2 - \frac{h_n}{h_t}\right)\ln\left(2 - \frac{h_n}{h_t}\right)}, \tag{2.75}$$

$$\gamma = \frac{\omega l \sqrt{b_0 l(8 + 7b_0 l)}}{4U(1 + b_0 l)\left(2 - \frac{h_n}{h_t}\right)\ln\left(2 - \frac{h_n}{h_t}\right)}, \tag{2.76}$$

$$\gamma = 0. \tag{2.77}$$

The obtained expressions, besides the values of γ and b_0, which are interesting for us, also contain the parameters of U/l, l and h_n/h_t. All these values in their first approximation can be regarded as known ones or as easy to be defined. For instance, the dolphin's body length l is easy to measure. The value U/l can be taken as a parameter. The value h_n/h_t is easy to be estimated by kinogrammes published in some papers (Kokshaysky, 1974). Such estimates show the value h_n/h_t to equal about 0.2 as to the circular frequency of body oscillations ($\omega = 2\pi f$), it can be found as based on the dependence

$$f = 1.1\frac{U}{l} + 0.15, \tag{2.78}$$

obtained by Kayan and Pyatetsky (1977) for *Tursiops truncatus*.

Kozlov (1963) adduced another expression, which matches the previous one

$$f = 1.05\frac{U}{l} + 0.25. \tag{2.79}.$$

In case of *Phocaena phocaena* the same authors (Pyatetsky, Kayan, 1972) present a similar relation which looks as

$$f = 0.46\frac{U}{l} + 0.26\,. \qquad (2.80)$$

Fig. 2.16 demonstrates the dependencies $\gamma(b_0)$ for *Tursiops truncatus*. Fig.2.17 shows similar dependencies for *Phocaena phocaena*. The parameter of the curves is the relation *U/l*. All curves are built for the relation *U/l* = 2. The body length of *Tursiops truncatus* is accepted as 2.2 m and that of *Phocaena phocaena* as 1 m.

When analysed, the obtained correlations and the curves based on this allow to draw some conclusions and suggestions.

1. The values of the parameters γ and b_0 are specific for various species. It is particularly evident in Figs. 2.16 and 2.17. The main reason behind this fact is in that the empirical relations (2.78) and (2.79) are species-specific. These dependencies correlate the frequency of body oscillations and the relative velocity of swimming.

2. According to the data in Figs. 2.16 and 2.17, it can be suggested that the extent of increase in the amplitude of the propulsive wave on the body of *Tursiops truncatus* must be much higher than on the body of *Phocaena phocaena*.

3. The dependence of the parameters g and b_0 on the relative velocity of swimming seems to be rather insignificant.

4. In the parameters γ and b_0 there should be a considerable dependence upon the age (the dependence upon the body length).

The conclusions are of qualitative nature because they were suggested as based on the fact that the relations (2.73)-(2.77) remain the same even in the actual regimes of the animals' swimming, not only in the threshold case of the zero thrust for which these relations were derived.

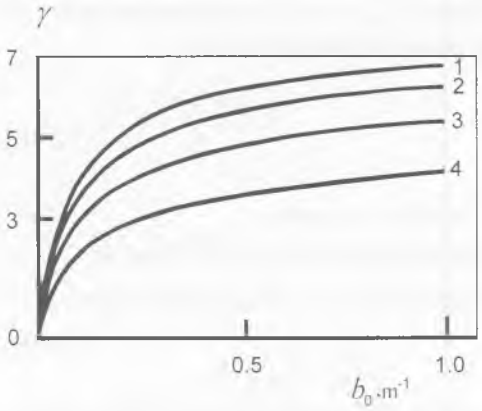

Fig. 2.16. The theoretical values of γ *vs.* b_0 for *Tursiops truncatus*. 1 – 4 – was computed from the formulas (2.73 – 2.76).

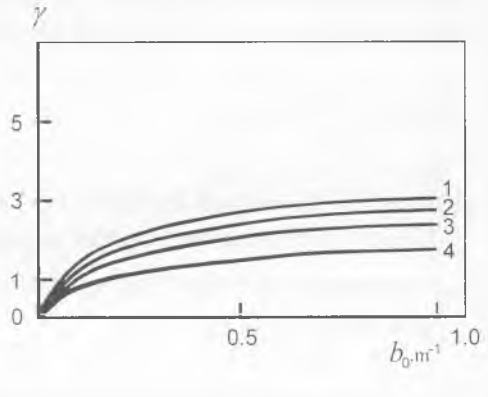

Fig. 2.17. The theoretical values of γ *vs.* b_0 for *Phocoena phocoena*. 1 – 4 – was computed from the formulas (2.73 -- 2.76).

b_0, m^{-1}	γ	
	$U/l = 1$	$U/l = 2$
0	0	0
0.1	3.08	2.89
0.2	3.94	3.70
0.3	4.43	4.17
0.4	4.76	4.48

Table 2.3. Values of γ *vs.* b_0. For explanations of variables, see text.

If the expressions (2.73)-(2.77) remain valid in the actual regimes of dolphins' swimming, it is feasible to select among them only just one, which is most probable. It is evident that the zero thrust should not appear at the external values of U within the interval of C_n-$C_n(1+b_0 l)$ most likely, the zero thrust must occur at some average value of U within the above interval. This average value may be

$$U = \frac{C_n(2 + b_0 l)}{2}. \tag{2.81}$$

From Table 2.3 we present the values of γ in the function of b_0 calculated for (2.75) and for two values of the parameter U/l in case of *Tursiops truncatus* swimming.

It is easy to perform analogous analysis for the law of deformation (2.60), considering dependence of the phase velocity on the coordinate like (2.62).

Brief conclusions

The fact that on the initial stages of the research there were proposed so many variants of the fish or dolphin body deformation laws (which are considered in this chapter) witnesses the lack of the reliable experimental facts on the kinematics of these animals. Data that allow us to construct a reliable model of fish and dolphin kinematics appeared only in recent years. These discoveries are the "recoil" phenomenon and the dependence of the propulsive wave phase velocity on the coordinate in the coordinate system based on the animal body. Till now all the models of fish and dolphin swimming proceed from the idea that the phase velocity of propulsive wave is constant. We think that unlike all others problems of fish and dolphin swimming, the problem of the body deformation law is close to the full solution.

CHAPTER 3. DISTRIBUTION OF THE DYNAMIC PRESSURE ON THE BODY OF FISH AND DOLPHIN CAUSED BY ITS OSCILLATIONS

As we have already mentioned before, James Gray, an English zoologist, in 1936 suggested that Cetacea, and dolphins in particular, reveal some stabilization of their streamline flow and , hence, an increase in the critical Reynolds number in the transition from laminar overflow to turbulent one, owing to the favourable (negative) gradient of pressure occuring along the animal's body in its active locomotion in water. Gray believed that the negative pressure gradient was caused by the oscillating movement of the dolphin's tail throwing the water masses backward. He assirted that there was a peculiar sucking of the animal's boundary layer. Such mechanism , indeed, takes place in reality, but it does not determine the formation of the pressure gradient along the animal's body. A strict mathematical analysis of this phenomenon (Romanenko, 1986a) shows that its main mechanism is quite different from that suggested by Gray. Moreover, even if the dolphin had no caudal fin and the water masses were not thrown backward, but the body was making its vertical oscillations, the negative pressure gradient along the body would be still formed there.

3.1. The role of fish or dolphins' body oscillations in formation of the dynamic pressure gradient

Let us discuss in more details the mechanism responsible for the formation of the pressure gradient on the animal's body due to its oscillations. Let us consider the animal's body as a long, elliptical or circular cylinder making bending oscillations in one plane. In this case, to calculate the dynamic pressure on the body surface (p-p_∞), we may use the familiar expression for a circular cylinder transversely overflown by a stream (Logvinovich, 1969).

$$p - p_\infty = \frac{\rho v_n^2}{2}\left(1 - 4\sin^2\theta_0\right) + \frac{\rho\cos\theta_0}{R}\frac{d\left(R^2 v_n\right)}{dt}. \tag{3.1}$$

Here, R and θ_0 are cylindrical coordinates, t is the time, v_n is the velocity of the body's transverse movement as specified by the expression

$$v_n = \frac{\partial h}{\partial t} + U\frac{\partial h}{\partial x}, \tag{3.2}$$

where $h(x,t)$ is the instantaneous value of transverse oscillations of the body, U is the body's velocity towards its longitudinal axis x. Fig. 3.1 shows the position of the dolphin in the accepted system of coordinates.

The formation of the boundary layer on the overflown body is governed not by the excessive pressure itself but by its gradient which, with account of expression (3.1), may be presented as

$$\frac{dp}{dx} = \rho v_n \frac{dv_n}{dx}\left(1 - 4\sin^2\theta_0\right) + \frac{d}{dx}\left[\frac{\rho\cos\theta_0}{R}\frac{d\left(R^2 v_n\right)}{dt}\right]. \tag{3.3}$$

After normalization of the expression (3.3) on the dynamic pressure we obtain the expression of the dynamic pressure gradient in the following form:

$$\frac{2}{\rho U^2}\frac{dp}{dx} = \frac{2}{U^2}\left\{v_n \frac{dv_n}{dx}\left(1 - 4\sin^2\theta_0\right) + \frac{d}{dx}\left[\frac{\rho\cos\theta_0}{R}\frac{d\left(R^2 v_n\right)}{dt}\right]\right\}. \tag{3.4}$$

In addition to the instantaneous values it is useful to know the values of the time-averaged dynamic pressure and its gradient. Averaging on time expression (3.1) we obtain

$$\overline{p - p_\infty} = \frac{\overline{\rho v_n^2}}{2}\left(1 - 4\sin^2\theta_0\right). \tag{3.5}$$

The normalized form looks like

$$\frac{\overline{p - p_\infty}}{\frac{1}{2}\rho U^2} = \frac{\overline{v_n^2}}{U^2}\left(1 - 4\sin^2\theta_0\right) \tag{3.6}$$

The pressure gradient is

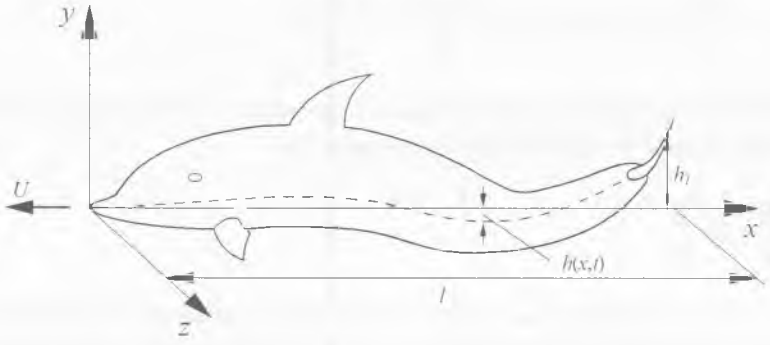

Fig. 3.1. The co-ordinate system of a swimming dolphin.

$$\overline{\frac{dp}{dx}} = \rho\left(\overline{v_n \frac{dv_n}{dx}}\right)\left(1-4\sin^2\theta_0\right) \tag{3.7}$$

After normalization:

$$\frac{2}{\rho U^2}\overline{\frac{dp}{dx}} = \frac{2}{U^2}\left(\overline{v_n \frac{dv_n}{dx}}\right)\left(1-4\sin^2\theta_0\right) \tag{3.8}$$

Critical Reynolds number is unambiguously connected with the shape parameter of the profile of speed in the boundary layer. It looks like

$$\Lambda = -\frac{\delta^2}{\nu\rho U}\frac{dp}{dx}. \tag{3.9}$$

Here ν is the kinematical viscosity; δ is the boundary layer thickness. Taking into account expressions (3.3) and (3.7) we can easily obtain the instantaneous and time-averaged values of the shape parameter of the profile of speed:

$$\Lambda = -\frac{\delta^2}{\nu U}\left\{v_n \frac{dv_n}{dx}\left(1-4\sin^2\theta_0\right)+\frac{d}{dx}\left[\frac{\rho\cos\theta_0}{R}\frac{d\left(R^2 v_n\right)}{dt}\right]\right\} \tag{3.10}$$

and

$$\overline{\Lambda} = -\frac{\delta^2}{\nu U}\left(\overline{v_n \frac{dv_n}{dx}}\right)\left(1-4\sin^2\theta_0\right). \tag{3.11}$$

The pressure gradient influences both the laminar boundary layer stabilization and the fine structure of the turbulent layer. In particular the negative gradient of the dynamic pressure of the sufficient value can cause the back transition from the turbulent streamline to laminar one (Lander, 1964; Repik, 1970; Nazartchuk, Kovetskaya, Panchenko, 1974) or at least the significant reduction of the turbulization degree, which leads to the friction drag reduction. This effect depends on the value of the shape parameter, which is

$$B = \frac{\nu}{\rho U^3}\frac{dp}{dx}. \tag{3.12}$$

The referenced above works analyze how the negative gradient of pressure influences the back transition from the turbulent streamline to the laminar one. They show that the

negative gradient of the dynamic pressure of the sufficient value can "laminarize" the turbulent boundary layer. With this going on, the phenomena, which are the evidence of the "laminarization" process, are observed. The value of the shape parameter of the speed profile ($H = \delta_1 / \delta_2$, δ_1 and δ_2 are the thickness of displacement and the thickness of the impulse loss correspondingly) rises. The profile of the speed in the boundary layer tends to Blasius's one. The intensity of speed and pressure pulsation in the boundary layer decreases. The drag coefficient decreases. The back transition from the turbulent streamline to laminar one occurs when the value of the shape parameter B is

$$B = \frac{\nu}{\rho U^3}\frac{dp}{dx} \cong -(2 \div 3).10^{-6}. \tag{3.13}$$

Taking into account expressions (3.3) and (3.7) we can represent (3.13) in the instantaneous and time-averaged forms,

$$B = \frac{\nu}{U^3}\left\{v_n \frac{dv_n}{dx}\left(1-4\sin^2\theta_0\right)+\frac{d}{dx}\left[\frac{\rho\cos\theta_0}{R}\frac{d\left(R^2 v_n\right)}{dt}\right]\right\} \tag{3.14}$$

and

$$\overline{B} = \frac{\nu}{U^3}\overline{\left(v_n \frac{dv_n}{dx}\right)}\left(1-4\sin^2\theta_0\right). \tag{3.15}$$

We shall adduce the numerical estimates of the dynamic pressure gradient distribution on the body of the actively swimming dolphin and the value of the shape parameter Λ and B in the 7th chapter.

3.1.1. Angle dependence of dynamic pressure distribution on animal body

Let us consider formula (3.3), which characterizes the time-averaged value of the redundant pressure on the dolphin body. Let us analyze the dependence of pressure on the angle θ_0. This dependence is defined by the factor

$$1-4\sin^2\theta_0. \tag{3.16}$$

It is represented in figure 3.2*a* for the middle cross section of the dolphin body. We can see that on the lateral surfaces of the dolphin body the redundant pressure is negative, and on the top and bottom surfaces the pressure is positive, the maximal value of the negative pressure is three times higher than the positive one.

The cross section of the dolphin body abaft the middle is not circular, the closer to the tail fin, the more it differs from a circle. The exact calculation of the redundant pressure for this part of the dolphin body is difficult, but its results seem to differ very little from those for the circle cross-section, because formula (3.1) is correct not only for the circle cylinder, but also for the elliptical cylinder (Logvinovitch, 1969), and the caudal cross section is near elliptical. The distribution of the dynamic pressure on the tail stem is shown in figure 3.2.*b*. The area of the positive values decreases, and the area of the negative values increases.

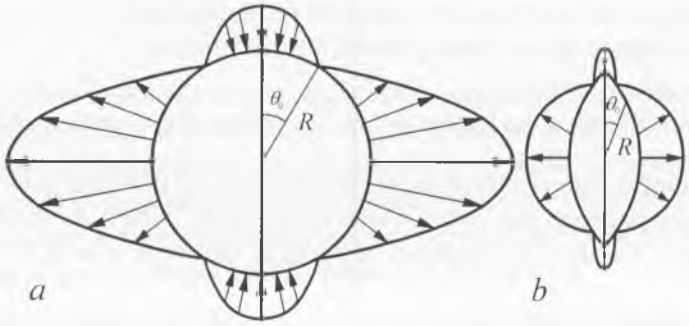

Fig. 3.2. Distribution of the dynamic pressure over the surface of a dolphin's body (*a*) and a caudal peduncle (*b*).

The distribution of the dynamic pressure on the body of a fast swimming tuna-like fish must be analogous, because its body cross-section is dolphin-like (especially in the caudal part of the body). As for common fish, whose body is laterally flat, distribution of the dynamic pressure is not very advantageous because the pressure gradient on the lateral surfaces is positive and only in the narrow dorsal and ventral areas this gradient is negative.

3.2. The pressure gradient generated by the tail fin

Till now we have discussed the gradient of dynamic pressure on the body of actively swimming dolphin caused by its undulation. But at the same time there is Gray's (1936) mechanism based on the tail fin oscillation. To be more exact, there are at least two independent mechanisms: the first one is caused by the vortex wake behind the edge of the tail fin, which influences the flow around the body, and the second one is caused by the additive field of the velocities induced by the oscillating tail fin dipole (Romanenko, Pushkov, 2001).

3.2.1. The vortex wake influence

In order to estimate the velocities and pressures induced by the vortex wake, we shall consider the movement of the flat wing of finite span (fin) in the coordinate system *OXYZ*, that moves at the velocity of *U*, equal to the dolphin velocity, in the direction of *OX*-axis (see fig. 3.3). Oscillation of the angle between the wing plane and plane OXYZ $\theta = \theta_0 \cos\omega t$ is superposed on transversal oscillation of the wing $y = h\sin\omega t$.

Let us consider the wing to be a carrying line *AB*. While moving, the vortex wake behind the wing forms vortex wisps and makes a track of vortex frames. At the first approximation, we consider these frames to be rectangles (fig. 3.3).

In order to evaluate the pressure gradient we can suppose:

- the transversal size of the frames is $l = \frac{\pi R}{2}$, where *R* is a semi-span of the wing in accordance to elliptical distribution of the circulation along the wing span,

- the distance between the vortex frame components, which are transversal to the wing movement, and the OXZ-plane to be equal to the amplitude of the wing vertical oscillation *h*.

We shall evaluate $\partial p/\partial x$ at the moment when the wing passes through:

A. the plane *OXZ*

B. the point of maximal deviation from the plane *OXZ*.

The vortex wake shown in fig. 3.3 corresponds to the moment of passing through *OXZ*- plane. Using Bernoulli law we can write for Δp in a certain point *X* on *OX*-axis as a first approximation

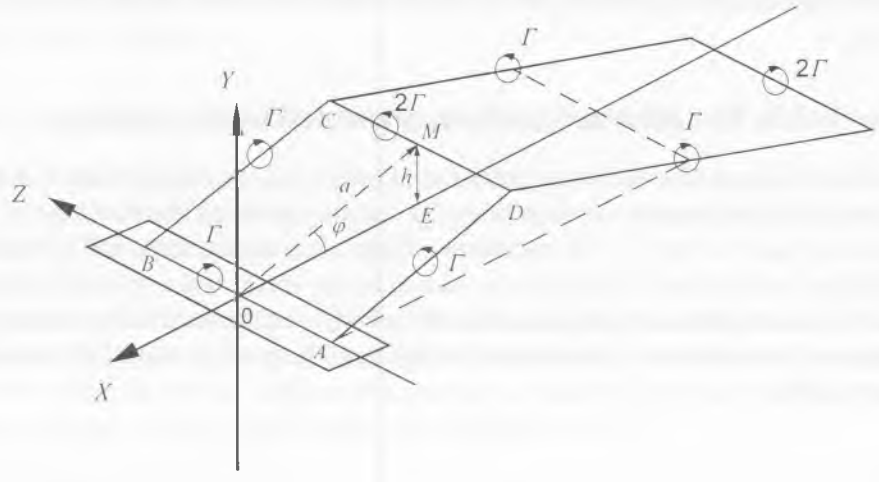

Fig. 3.3. A schematic sketch of a wing.

$$\Delta p \approx \rho U V_{ix}, \tag{3.17}$$

where V_{ix} is the component of induced velocity in OX-axis direction.

To define the order of $\Delta p/\Delta x$ let us estimate the value of V_{ix}, induced by the vortex trail which is formed during the half period T of the wing oscillation. Using the Biot-Savart formula for the velocity induced by an arbitrary interval of the vortex line with circulation Γ in a certain point, we get

$$V = \frac{\Gamma}{4\pi h_0}(\cos\alpha + \cos\beta). \tag{3.18}$$

Here h_0 is the shortest distance from the vortex line segment to the observation point, α and β are the angles, which abut upon the segment and are formed by the lines, which connect the point of observation with the ends of the vortex line segment. The value of V_{ix} is the sum of OX-components of the velocities, which are induced in the point X by all straight segments of the vortex frames formed over a half period of the wing oscillation at the moment of passing through XOZ–plane (for the case A).

$$V_{ix} = \frac{\Gamma l_0}{4\pi\left[(x\sin\varphi)^2 + \frac{l_0^2}{4}\right]}\left(\frac{a + x\cos\varphi}{\sqrt{(x + a\cos\varphi)^2 + h^2 + \frac{l_0^2}{4}}} - \frac{x\cos\varphi}{\sqrt{x^2 + \frac{l_0^2}{4}}}\right)\sin\varphi +$$

$$+\frac{\Gamma l_0}{4\pi\left[\left(x + \frac{UT}{2}\right)^2\sin^2\varphi + \frac{l_0^2}{4}\right]}\left[\frac{\left(x + \frac{UT}{2}\right)\cos\varphi}{\sqrt{\left(x + \frac{UT}{2}\right)^2 + \frac{l_0^2}{4}}} - \frac{\left(x + \frac{UT}{2}\right)\cos\varphi - a}{\sqrt{\left(x + \frac{UT}{4}\right)^2 + h^2 + \frac{l_0^2}{4}}}\right]\sin\varphi + \tag{3.19}$$

$$+\frac{\Gamma l_0 h}{2\pi\left[\left(x + \frac{UT}{4}\right)^2 + h^2\right]\sqrt{\left(x + \frac{UT}{4}\right)^2 + h^2 + \frac{l_0^2}{4}}}.$$

Here the first and the second terms are defined by the velocities induced by the longitudinal vortex lines at the point X. The third term is defined by the velocity induced by the transversal vortex CD (see fig. 3.3).

We can obtain the value of V_{ix} for the case B in the same way:

$$V_{ix} = \frac{\Gamma l_0 \sin\varphi}{4\pi\left[\left(x+\frac{UT}{4}\right)^2 \sin^2\varphi + \frac{l_0^2}{4}\right]}\left[\frac{a+\left(x+\frac{UT}{4}\right)\cos\varphi}{\sqrt{\left(x+\frac{UT}{2}\right)^2 + h^2 + \frac{l_0^2}{4}}} - \frac{\left(x+\frac{UT}{4}\right)\cos\varphi - a}{\sqrt{x^2+h^2+\frac{l_0^2}{4}}}\right] +$$

$$+ \frac{\Gamma l_0 h}{4\pi\left(x^2+h^2\right)\sqrt{x^2+h^2+\frac{l_0^2}{4}}} + \frac{\Gamma l_0 h}{4\pi\left[\left(x+\frac{UT}{2}\right)^2 + h^2\right]\sqrt{\left(x+\frac{UT}{2}\right)^2 + h^2 + \frac{l_0^2}{4}}}. \qquad (3.20)$$

Here longitudinal vortex lines define the first term, the second and the third terms are defined by transversal vortex lines. φ in the expressions (3.19) and (3.20) is the angle between the vortex frame and *OXZ*- plane, a - is a half of the longitudinal dimension of the complete vortex frame, $h = a\sin\varphi$. The value of circulation is defined by the connexity equation

$$C_y \rho \frac{U_i^2}{2} S = \rho U_i \Gamma l_0 = F, \qquad (3.21)$$

where C_y is the lifting force coefficient, ρ is water density, $U_i = \sqrt{U^2 + h^2\omega^2}$ is the amplitude of the absolute velocity of the wing movement, S is the square of the wing.

These expressions for V_{ix} define the value of the gradient $\partial p/\partial x$:

$$\frac{\partial p}{\partial x} \approx \rho U \frac{\partial V_{ix}}{\partial x}. \qquad (3.22)$$

When we define F, we must take into account that the coefficient of the lifting force C_y and its derivative with respect to the angle of attack C_y^α depend on Strouhal number $Sh=\omega b/U$, where b is the chord of the wing.

3.2.2. The influence of the tail fluke as an acoustic dipole

In section 1.5 of ch. 1 we have already analyzed the simple acoustic model of swimming fish, where the oscillating tail fin was considered to be an acoustic dipole, which produced a field of velocity and pressure in the circumjacent water media. The radial component of particles velocity, which is generated by the dipole, can be expressed (Skudrzyk, 1976) like

$$V_r = \frac{B}{\rho c r}\left[1 + \frac{2}{jkr} + \frac{2}{(jkr)^2}\right]\cos\theta e^{-jkr}, \tag{3.23}$$

where

$$B = -\frac{k^2 \rho c D}{4\pi}, \tag{3.24}$$

D is the moment of the dipole, which can be written like

$$D = 2Qr_0. \tag{3.25}$$

Here $Q = v_n S_t$ is the space velocity of both dipole sources, v_n is the component of liquid particles velocity, which is normal to the fluke, S_t is the surface area of the one side of the tail fluke. r_0 is the effective radius of the tail fluke, $2r_0$ is the distance between the two dipole sources, which can be evaluated as

$$2r_0 = 2\sqrt{\frac{S_t}{\pi}}, \tag{3.26}$$

r is the distance between the dipole center and the observation point, c is sound speed in water, j is an imaginary unit. θ is the angle between the dipole axis and the direction to the observation point.

We are interested in the case of $kr << 1$, when the observation point is located near the dipole. In this case we can neglect the first two terms in the brackets on the right side of (3.23) and consider the multiplier e^{-jkr} to be equal to 1. Then formula (3.23) transforms to

$$V_r = \frac{v_n S_t^{1.5}}{r^3 \pi^{1.5}}\cos\theta. \tag{3.27}$$

Using formula (3.23) we can write the expression for the dynamic pressure gradient, normalized by dynamic push

$$\frac{2}{\rho U^2}\frac{dp}{dr} = -\frac{6 v_n S_t^{1.5}}{U r^4 \pi^{1.5}}\cos\theta. \tag{3.28}$$

We can consider the expression

$$v_n \approx \alpha U_t, \tag{3.29}$$

to be right in application to the dolphin fluke. Here U_i is the instant velocity of the flowing around the dolphin fluke, which is defined by the expression

$$U_i = \sqrt{U^2 + \left(\frac{\partial y}{\partial t}\right)^2}. \tag{3.30}$$

We believe that the dolphin fluke moves by the harmonic law. Then we get

$$U_i = U\sqrt{1 + \frac{\omega^2 h^2 \cos^2 \omega t}{U^2}}. \tag{3.31}$$

Here $\omega=2\pi f$, f is the frequency and h is the amplitude of the fluke oscillation. The final formula for numerical estimation of dynamic pressure gradient is derived from (3.29) – (3.31):

$$\frac{2}{\rho U^2}\frac{dp}{dr} = -\frac{6\alpha S_i^{1.5}}{r^4 \pi^{1.5}}\sqrt{1 + \frac{\omega^2 h_0^2}{U^2}\cos^2 \omega t}\cos\theta. \tag{3.32}$$

3.3. Comparison of the results of mathematical modelling and the experimental data on fish

There are very few works on the measurement of the dynamic pressure distribution on bodies of aquatic animals. We know only one work on the dynamic pressure distribution on a living and dead fish body (Dubois, Cavogna, Fox 1974). The measurements were made with subcutaneous liquid manometers. The results are shown in fig. 3.4 and 3.5. The locations of the manometers are shown on the fish (*Pomatomus saltatrix*) silhouette. The dynamic pressure distributions on the dorsal side (*a*) and lateral side (*b*) of a living fish body are shown in fig. 3.5. The point 1 on the upper plot shows the value of the dynamic pressure on the body of the dead fish. It can be seen that the pressure gradient between the last measurement points on the body of the dead fish is positive, while the pressure gradient on the body of the living fish between the same points is negative. It is remarkable that the negative pressure gradient on the body of the living fish is observed only on the dorsal side of the body. Gradient on lateral side is positive on either fish (living or dead). The explanation of this fact is given at the end of section 3.1.1. It illustrates fig. 3.6, which is similar to the fig. 3.2.*b*. The only difference is that dynamic pressure on dorsal and lateral sides are of inverse signs. The reason for it is that the fish body undulation plane, unlike the dolphin, is horizontal whereas fish body shape in the tail region is approximately dolphin-like.

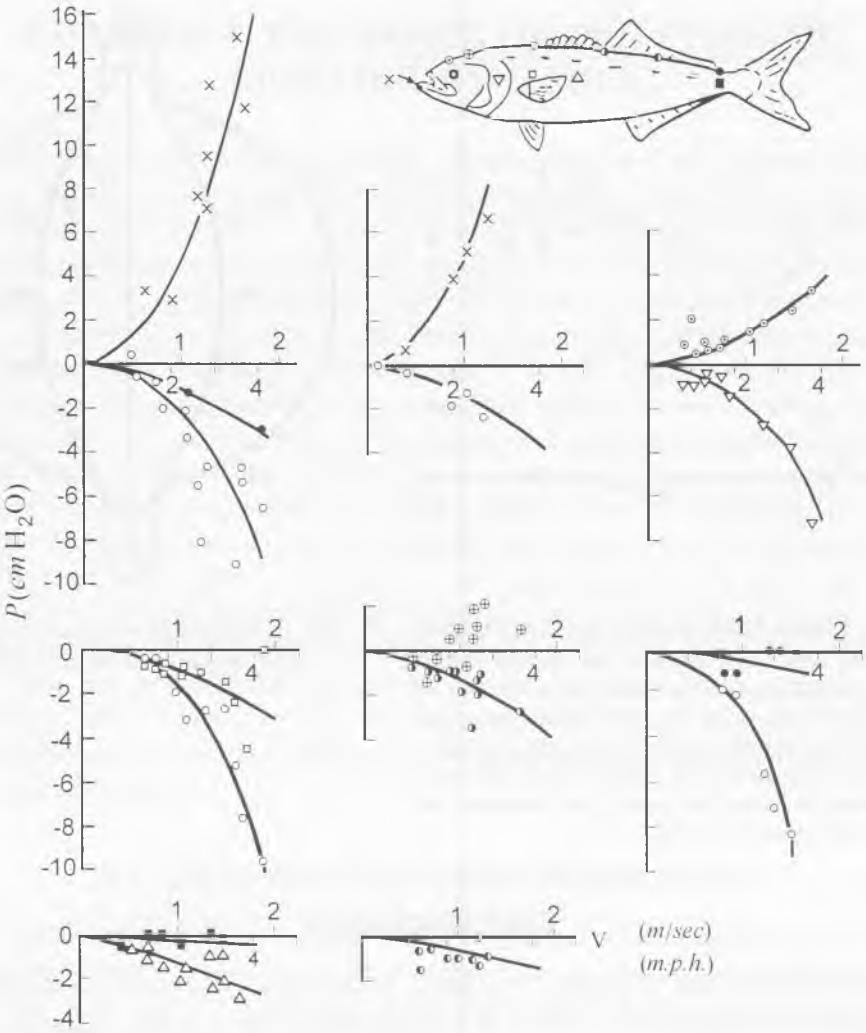

Fig. 3.4. This series of 8 graphs reflects the change of pressure seen on the various surface points with increasing speed. Symbols on the drawn bluefish indicate the position from which the pressure was recorded. Each of the 8 graphs contains the data obtained on an individual fish. One notes the general tendency for the positive pressure on the front of the fish to increase in a quadratic fashion with increasing speed. Pressures at the region of widest girth and the back portion become increasingly negative with speed. In the dorsal region, just behind the eye both negative and positive values were recorded, indicating its proximity to the position where pressures switch from positive to negative. (Redrawn from Dubois, Cavagna, Fox, 1974).

The quantitative estimate of the value and distribution of dynamic pressure gradient on the body of the active swimming dolphin we shall give in chapter 7 and there we shall compare it with the experiment.

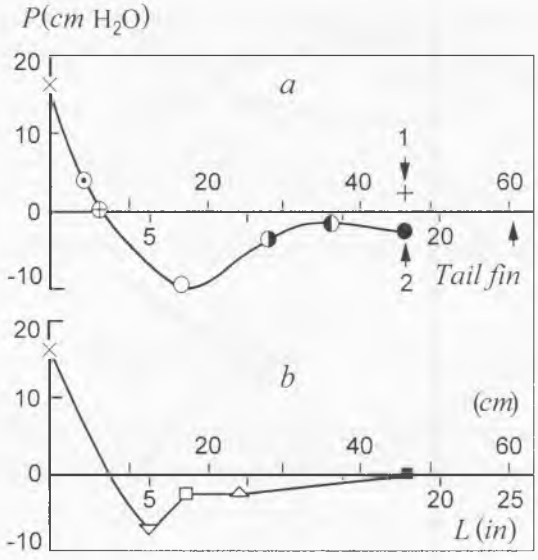

Fig. 3.5. Pressure profile from the back and side of the bluefish at 4 m.p.h. The distances were normalized to an average overall length of the fish of 24 in. Symbols are referable to the drawing in Fig. 3.4. One notes the marked contrast of the positive pressure recorded on the top of the tail of the dead bluefish with the negative pressure recorded on the same point of live fish. (Redrawn from Dubois, Cavagna, Fox, 1974).

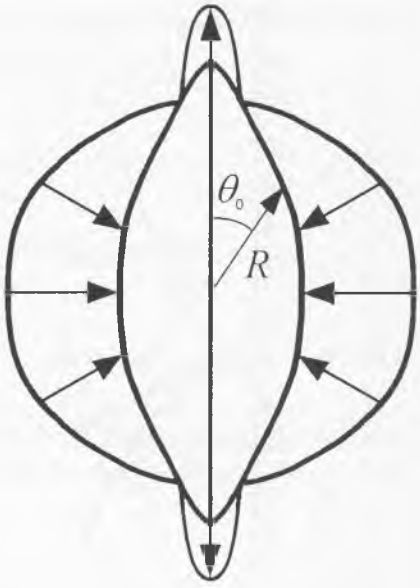

Fig. 3.6. Distribution of the dynamic pressure over the surface of the fish caudal peduncle.

Brief conclusions

The idea that there is a negative gradient of the dynamic pressure on the dolphin body, which influences the structure of the boundary layer, was first suggested by an English zoologist J. Gray in 1936. However this hypothesis did not arouse any interest of the scientific society. The strict theory of the subject is for the first time adduced in this chapter. It has been shown Gray's assumption was right in general. Furthermore, it turned out that this effect occurs in fish hydrodynamics as well.

CHAPTER 4. THE BASICS OF THE STATISTIC BIOHYDRODYNAMICS

Scientists have always been interested in hydrodynamics of fast-swimming aquatic animals. But this area is more difficult to investigate than hydrodynamics of a rigid body. The shape of an animal's body alters while it is swimming; the velocity of the swimming varies continuously. Many fish species have their bodies covered with scales and mucus, and the pinnipeds have fur. The temperature of a body is not always equal to the temperature of a liquid flow. All these facts greatly complicate research of characteristics of flow around an animal's body. If we take into account the methodical difficulties of the experimental study of the flow around animal's bodies, we shall understand the reasons why practically nothing is known about its hydrodynamics. Nevertheless it is obvious, that the phenomena we can observe in the boundary layer of an animal's body are identical to those in the boundary layer of a rigid body. Therefore the study of the biohydrodynamics should be based upon the achievements of the theoretical and experimental investigation of the hydrodynamics of a rigid body.

In this part we shall briefly present some basic information about the laminar and turbulent boundary layer on the flat plate and on the bodies of rotation; about physical mechanisms that influence the structure of boundary layer (mainly after Hintse, 1963; Schlichting, 1969; Petrovsky, 1966; Loytsyansky, 1973; Monin, Yaglom, 1965). All this information gives us the opportunity to define problems of the biohydrodynamics to the best advantage.

4.1. The basics of the theory of boundary layer

L. Prandtl showed the way to theoretical investigations of the liquid flow with friction for some important practical cases. He introduced the concept of the boundary layer as a very thin layer near the body in the flow, where the friction is of substantial value. Beyond this layer the friction is negligible.

The boundary layer is a result of the adhesion of liquid to the surface of the rigid body. In this case velocity of the liquid varies from zero on the surface of the body to the full value in the outer flow. For real liquid having the resistance the formation of the boundary layer is characteristically. It makes it different from ideal liquid because the latter doesn't have resistance. The concept of the ideal liquid was treated as the main one. The theory of ideal liquid could not explain the resistance of the body that moves in gas or liquid. According to this theory the body that moves uniformly in infinite medium has no resistance (D'Alember paradox).

The friction force in a real liquid is caused by its viscosity. This force is defined by Newton friction law

$$\tau = \mu \frac{dU}{dy}, \tag{4.1}$$

where τ is the tangential stress between the layers of liquid or on the side of the body in flow, μ is the dynamic viscosity factor, dU/dy is gradient of the velocity in the direction of the perpendicular to the flow.

At the beginning the theory of the boundary layer dealt with the laminar flows of incompressible liquid. Subsequently the theory of the boundary layer has been expanded on the more important case of incompressible turbulent flows.

Existence of two types of flows, so called laminar and turbulent, was first observed at the beginning of the 19th century. But the theory of turbulence appeared only after the works of O. Reynolds' were published. In this works the main attention was paid to the conditions under which the laminar flow of liquid became the turbulent one. O. Reynolds has established the common criterion of the dynamic similarity of viscous liquid flows. Beside the geometrical similarity of flows, such criterion involves the coincidence of the values of the so-called "Reynolds number"

$$\mathrm{Re} = \frac{Ul}{\nu}, \tag{4.2}$$

where U and l are the characteristic scales of velocity and length in the flow in the question, ν is the coefficient of kinematic viscosity defined by equation

$$\nu = \frac{\mu}{\rho}, \tag{4.3}$$

where p is the liquid density.

From the dynamic point of view Reynolds number can be interpreted as relation of the forces of inertia to the forces of viscosity that act in the liquid. Inertia forces cause mixing of different volumes of liquid, moving with different velocities. These forces actualize delivery of energy from large-scale components of motion to small-scale ones. By that the inertia forces advance generation of small-scale severe non-uniformity in the flow. The viscosity forces on the contrary cause smoothing of the small-scale non-uniformity.

Small values of the Reynolds number and considerable influence of the viscosity forces are typical for the laminar flows. The situation in the turbulent flows is opposite.

The concept of Reynolds number simplifies the analysis of geometrically similar flows, such as a boundless flow around a rigid body of specified shape. If the Reynolds numbers are equal, then the flows, which are geometrically similar, are also mechanically similar. It means they have geometrically similar patterns of the flow lines and they can be

described by the same functions of dimensionless coordinates. It is so-called Reynolds law of similarity. This law is of great importance for theoretical study of the flows, which take place under similar conditions. It is used to unify observations processing and to simulate the flows, which are met in practical tasks. But Reynolds law is applicable only for the stable flows of incompressible liquid where there is no substantial influence of external forces. If these conditions are not fulfilled, then the similarity law tends to be more complicated. For mechanical similarity not only Reynolds numbers should be equal but also some additional dimensionless criteria of similarity should be true. For example, in case of compressible medium motion such additional similarity criterion is Mach number, which is defined as the ratio of the flow speed to the speed of sound in the medium. While studying the motion of non-uniform temperature liquid we use the dimensionless Prandtl number and Peclet number. If there is a heat current across the surface of the submerged body then Nusselt number (or Stanton number) is introduced. In the case of free convection the Grasshof number (or the Rayleigh number) serves as the similarity criterion. When there is a free surface flow, the similarity criterion is the Froude number. Strouhal number is a very important criterion of similarity in case of a flow around cylindrical bodies. (Monin, Yaglom, 1965).

Investigation of the flow of liquid or gas is generally involves evaluation of the seven functions: u, v, w, p, ρ, T, μ. They are respectively three components of velocity, pressure, density, temperature and viscosity of the medium. In order to find them we should write seven equations. The first three of them are the differential equations of Navier-Stockes, which form the basis of the whole mechanics of fluid and gas. Then there is the equation of continuity, the equation of state, the energy equation and the equation that associates the viscosity coefficient and the temperature. We do not cite them in full because they are too lengthy. Furthermore, the exact analysis of such equation set is not our task. We confine ourselves to the most general conception of the mathematical description of the phenomenon we study. The set of equations is greatly simplified, if we discuss the incompressible flows (ρ = const), that occur in animal's swimming. In this case three out of the seven unknown values turn out to be constant. Four values (u, v, w, p) stay variable. There are four equations, which allow us to find them: three Navier-Stokes equations and the equation of continuity. If Navier-Stokes equation is presented by vectors, then the whole set of equations reduces to only two equations:

$$\rho \frac{D\vec{U}}{Dt} = \vec{K} - gradp + \mu\Delta\vec{U} \tag{4.4}$$

and

$$div\vec{U} = 0, \tag{4.5}$$

where $\frac{D\bar{U}}{Dt} = \frac{\partial \bar{U}}{\partial t} + \frac{d\bar{U}}{dt}$, $div\bar{U} = \frac{\partial u}{\partial x} + \frac{\partial v}{\partial y} + \frac{\partial w}{\partial z}$, Δ — is Laplace operator, and $\bar{K}$ — is the body force.

Navier-Stokes equation derivation is based on some empiric assumptions. Therefore we can not be sure if they describe correctly the motion of the viscous liquid. This fact means that Navier-Stokes equations need checking which can be performed only by experimental means.

Up to now there has been found no general solution of the complete Navier-Stockes equation because of mathematical difficulties. But some partial solutions are known. For example, we know the solution for the laminar flow in tube, for the flows in boundary layer. These partial solutions coincide with experimental results quite well. So the general applicability of the Navier-Stokes equations is evident.

Now we are going to discuss the fundamental facts of the theory of boundary layer.

4.1.1. The laminar boundary layer

When liquid or gas flows around various bodies, sticking phenomenon is observed, which leads to zero velocity of liquid or gas particles on the body surface. The speed of the flow $U(x,y)$ varies in thin layer from zero on the body surface to the maximal value (U_∞) in a distance from the body. This thin layer of liquid (or gas) is called boundary layer or friction layer $\delta(x)$. The laminar boundary layer on the flat plate in the flow of longitudinal direction is schematically shown in fig. 4.1. In the transversal direction the scale is magnified for the better layout. The thickness of the layer (denoted as δ) locked by friction gradually increases along the plate starting from the forward edge. The thickness of a boundary layer is usually the distance from the wall where the flow speed differs by 1% from the external flow speed. In this case the thickness of a boundary layer is defined by equation

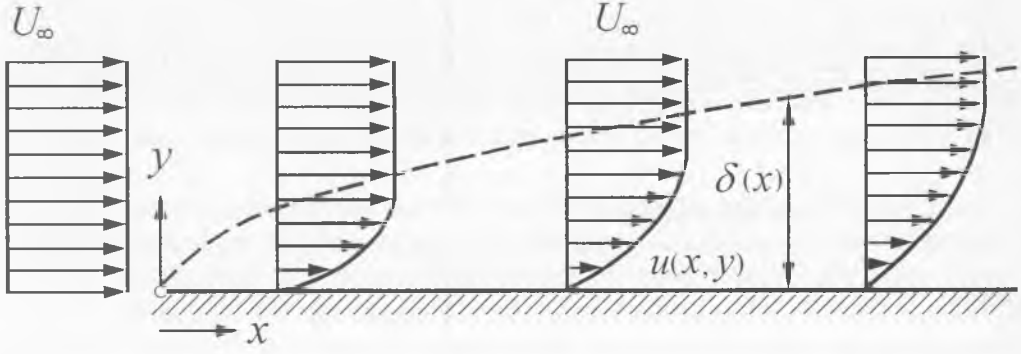

Fig. 4.1. A schematic sketch of a boundary layer along a plane surface. (Redrawn from Schlichting, 1974).

$$\delta \approx 5.0\sqrt{\frac{\nu x}{U_\infty}}, \tag{4.6}$$

where U_∞ is the speed of the flow at the infinite long distance from the plate; x is the distance from the front edge of the plate; $\nu=\mu/\rho$ is the coefficient of kinematic viscosity, μ is viscosity; ρ is density.

So-called displacement thickness δ_1 (fig. 4.2) is often used instead of the boundary layer thickness.

$$\delta_1 = \int_{y=0}^{\infty}\left(1-\frac{U}{U_\infty}\right)dy. \tag{4.7}$$

The displacement thickness is the distance between the wall and the current streamlets of the external flow moved away because of the accumulation of increasing quantity of the locked liquid in the boundary layer. The equation that describes the displacement thickness can be written like (4.6):

$$\delta_1 \approx 1.72\sqrt{\frac{\nu x}{U_\infty}}. \tag{4.8}$$

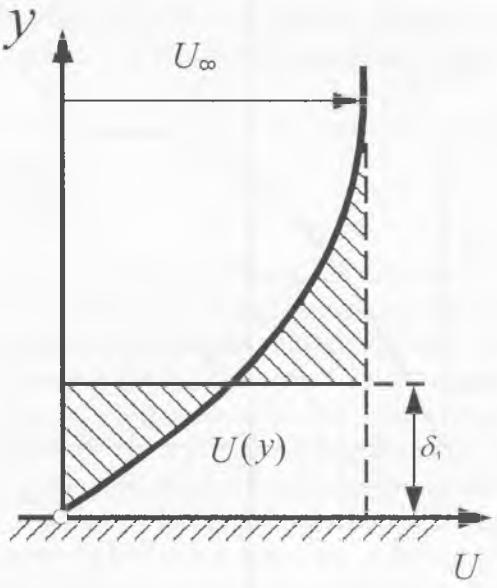

Fig. 4.2. Displacement thickness, δ_1, in a boundary layer. (Redrawn from Schlichting, 1974).

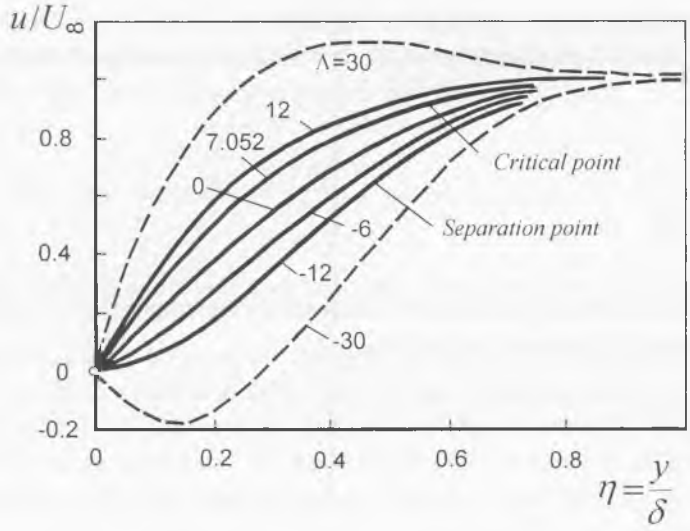

Fig. 4.4. A family of a velocity distributions. Λ - is parameter. (Redrawn from Schlichting, 1974).

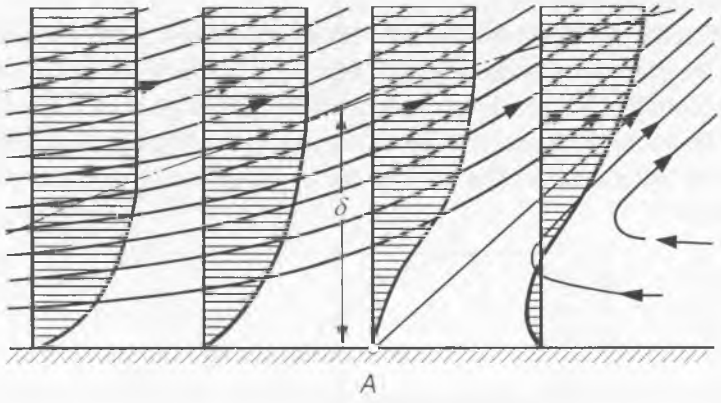

Fig. 4.5. Diagram illustrating flow in a boundary layer near point of separation, *A*. δ - is a velocity thickness of the boundary layer. (Redrawn from Schlichting, 1974).

layer near the surface caused by the friction is the reason why the particles can not overcome increasing pressure and halt. This leads to significant thickening of the boundary layer. Then the return flow near the wall is generated due to the positive pressure gradient. It makes the liquid to be carried out of the boundary layer into the outer flow. One of the threads of the current that makes a certain angle with the wall starts in the separation point.

The phenomenon of the boundary layer separation is especially typical to the bodies with dulling stern. When a liquid flows around such a body, the positive pressure gradient is generated at its stern area. This causes the boundary layer separation and the formation of the vortex zone behind the stern, which leads to an increase of the so-called pressure resistance.

Let us discuss the mechanisms, which make the pressure resistance of the flow of liquid around a cylinder arise. Fig. 4.6 shows the chart of the liquid flow around a cylinder with the separation of the boundary layer and formation of the vortices, fig. 4.7 shows the pressure distribution on the surface of such cylinder. We can see that the pressure has maximum at the front critical point ($\varphi = 0^{\circ}$). The pressure has minimum at the angles of 90° and of 270°. At the point that corresponds to angle of 180° the pressure

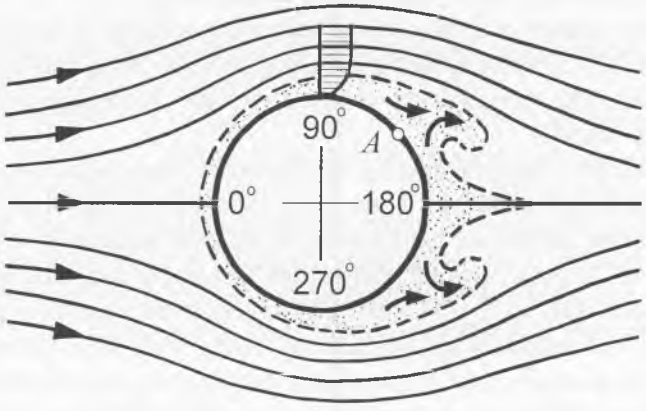

Fig. 4.6. Flow pattern about a circular profile. (Redrawn from Schlichting, 1974).

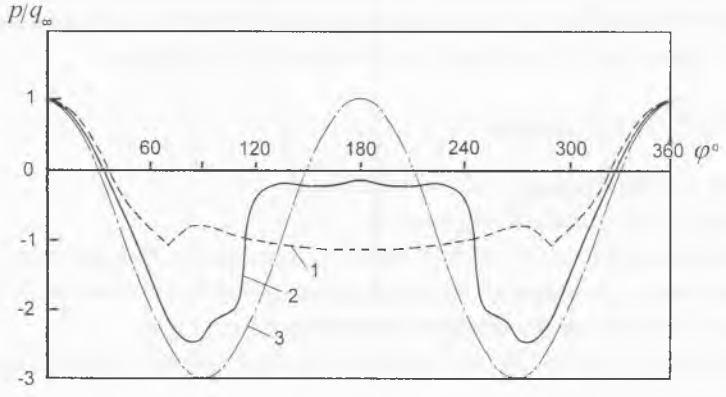

Fig. 4.7. Pressure distribution near a circular profile. 1 – at Reynolds number smaller than a critical value, 2 - at Reynolds number greater than a critical value, 3 – in a perfect (inviscid) fluids.

increases the same as it does at the front critical point, but it does not obtain the same value. Only in theory the pressure values are the same at the both critical points (the front and the rear points). This difference of the values of pressure at the opposite points of the direct axis is the reason for the pressure resistance to arise. If we integrate the pressure along the whole surface of the cylinder we'll get the absolute value of the pressure resistance.

Pressure resistance is also called shape resistance. The pressure resistance of the cylinder under laminar flow is noticeably greater than the friction resistance and is much greater than the pressure resistance under turbulent flow. It is explained by the fact that the condition of the separation of boundary layer on the cylinder changes a lot when the boundary layer becomes turbulent. The point of separation moves downstream, stagnant space of the flow behind the cylinder becomes narrow and pressure distribution converges to the pressure distribution under a condition of a flow without friction.

The pressure resistance of a streamlined body is a small part of the friction resistance (does not exceed-20 – 30%) because the boundary layer separation is either nonexistent or relatively small. This phenomenon characterizes the swimming of fishes, dolphins and other aquatic animals.

Before now we have been discussing the stationary boundary layer. But the motion of the sea animals is non-stationary. Therefore it is helpful to analyze how the unsteady-state of their motion influences the features of the flow outline. It is a very difficult mathematical task. An experimental study of the features of non-stationary flow of the sea animals is more likely to give a clue to the problem of their swimming. Nevertheless, we want to know beforehand what we ought to expect from these experiments. This is the reason why the attempts of the mathematical consideration of the simplified versions of the non-stationary boundary layers proved to be very fruitful (Lin, 1957, Faddejev et all, 1969, Jurava, Faddejev, 1973; Schlichting, 1969)

Let us briefly discuss two tasks. One of them is given in Schlichting's (1969) book. It is the analysis of the flow of viscous incompressible fluid along flat surface; velocity of the fluid is composed of stationary and oscillating components:

$$U(x,t) = \overline{U}(x) + U_1(x)\sin\omega t\,, \tag{4.15}$$

where $\omega=2\pi f$, f is the frequency of the oscillation.

The solution of this problem shows that:

1. The longitudinal velocity of the liquid is composed of the stationary component and of the oscillating component, whose phase is shifted in relation to the phase of the outer flow and depends on the distance from the wall y.

2. The boundary layer of the oscillating component of the longitudinal velocity is defined by equation

$$\delta_0 = \sqrt{\frac{2\nu}{\omega}}, \tag{4.16}$$

where ν is the viscosity.

3. There is the additional gradient of the pressure given by the function

$$F(x, y) = \frac{1}{2} U_1 \frac{dU_1}{dx} \overline{F}\left(\frac{y}{\delta_0}\right). \tag{4.17}$$

Fig. 4.8 shows the plot of the function $\overline{F}\left(\frac{y}{\delta_0}\right)$, which is included into equation (4.17). It is evidently that this function obtains the greatest value by the wall, and therefore the pressure gradient does the same.

4. The profile of velocity in the boundary layer differs from the profile under the stationary flow conditions. This distinction depends on the amplitude U_1 and on its derivative dU_1/dx according to equation (4.17). In particular, when U_1=const, even oscillation of the outer flow at high amplitude can cause no alteration of average profile of the velocity because $dU_1/dx = 0$, and therefore the pressure gradient is also zero.

Perhaps some features of the oscillating outer flow along the flat surface anyhow can take place in case of the sea animals. Measurement of the velocity profile on the

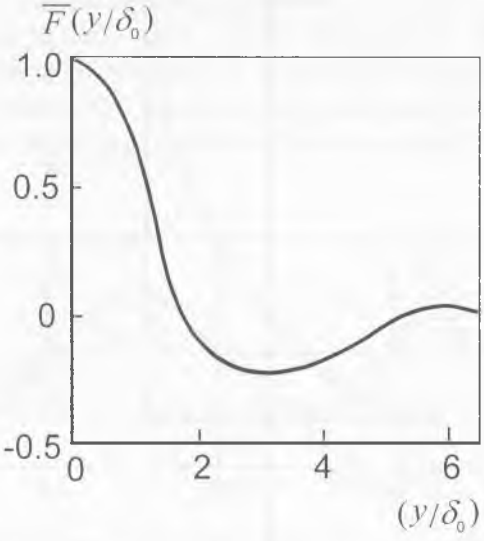

Fig. 4.8. Graphical representations of a function $\overline{F}$. (Redrawn from Schlichting, 1974).

boundary layer along the body of a fish or a dolphin, which swims freely in water, seems to be valuable.

Another problem is the estimation of the possible influence of the stream non-stationarity on the friction resistance of the ellipsoid of revolution with elongation equal 6 (Jurava, Faddejev, 1973). In order to solve the problem there was calculated the non-stationary boundary layer on such ellipsoid under alteration of its progressive motion speed as

$$U = U_0\left[1 + \Delta U \sum_{i=1}^{3} \xi_i \sin \omega t\right], \tag{4.18}$$

where U_0 is the non-stationarity period average speed of progressive motion, ΔU is the speed alteration amplitude, ξ_i are the factors that define figuration of the speed plot $U_0(t)$. The three different laws of alteration of ellipsoid speed are shown in fig. 4.9.

The calculation demonstrates that non-stationarity of the ellipsoid progressive movement has quite small influence on the non-stationarity period average friction resistance.

4.1.2. Transition of a laminar flow into a turbulent one

In the previous paragraph we discussed a laminar flow. This flow exists only under subcritical values of the Reynolds number. This flow in the boundary layer is not affected by any disturbances. Whatever caused these disturbances, they damp inevitably and the vortices do not grow up. When the Reynolds number increases and reaches the critical value, the laminar flow is not steady already. Then some of the disturbances do not damp. There is such a range of frequencies in the spectrum of disturbances oscillations of which frequencies swell with the lapse of time and it eventually leads to turbulization of the boundary layer. Transition from the laminar flow to the turbulent flow is not an

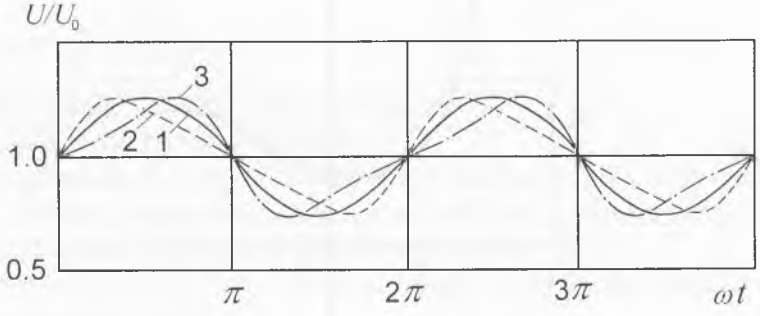

Fig. 4.9. Ellipsoid movement. 1 – harmonic, 2 – fast acceleration and slow braking, 3 – slow acceleration and fast braking. (Redrawn from Zhurava, Faddeev, 1973).

instant one. There is an interval of the Reynolds numbers from the number, which corresponds to the limit of steadiness (neutral point), to the number that corresponds to eventual transition of the flow mode. The difference between the Reynolds numbers that correspond to the neutral point and to the point of transition is shown in fig. 4.10. When the turbulence proper to the incident flow increases, the point of transition and the neutral point converge. When the turbulence decreases, the point of transition moves from the neutral point to the marginal point, which corresponds to the marginal value of the Reynolds number. In case of a flat plate this marginal value ranges from 2.8 to 4.10^6. When the Reynolds number is greater than specified, only the turbulent flow can exist in the boundary layer of the plate without gradient of the pressure. The dependence of the marginal value of the Reynolds number on the level of the incident flow turbulization is shown in fig. 4.11. When the turbulence proper to the incident flow is very small, formation and fast increasing of the almost sinusoidal oscillation in the boundary layer precedes the change of the flow mode from laminar to turbulent. Just before the point of transition the amplitude of this oscillation reaches very large value. At the point of transition the regular oscillation suddenly passes into irregular high-frequency fluctuation, which is a feature of a turbulent flow. If the turbulization proper to the flow is large enough (approximately 1%), then transition to turbulent mode of the flow is caused by accidental variations without any introductory sinusoidal oscillations. It is remarkable that the wavelength of the non-steady oscillation is large in comparison with the boundary layer width. The wavelength of the non-steady fluctuation is λ_{min} is at least 6δ, where δ

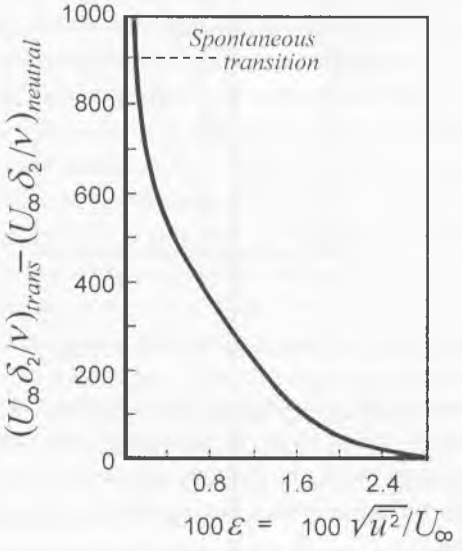

Fig. 4.10. Transition of a laminar flow into a turbulent one in a boundary layer along a plane surface. (Redrawn from Schlichting, 1974).

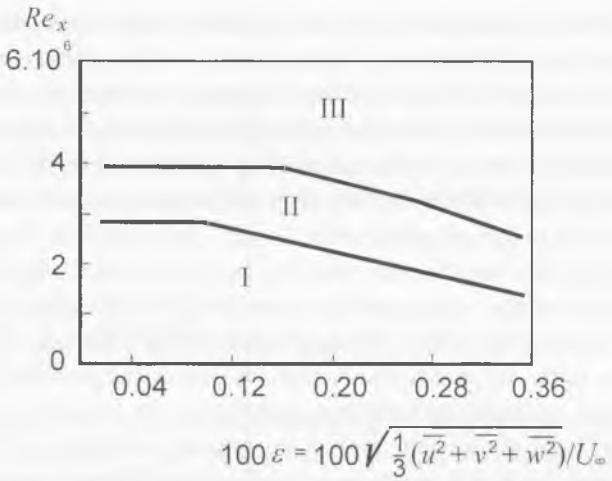

Fig. 4.11. Critical Reynolds number *vs.* a turbulence in the free stream. I – laminar flow, II – transition, III - turbulent flow. (Redrawn from Schlichting, 1974).

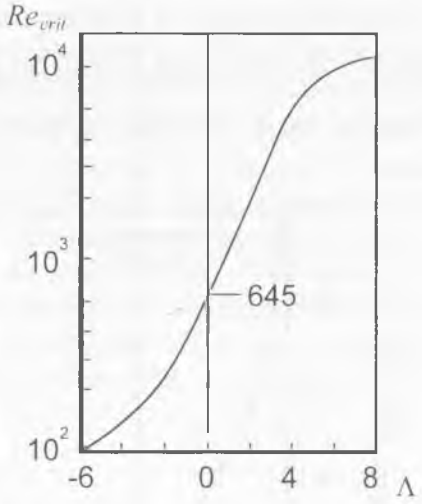

Fig. 4.12. Critical Reynolds number *vs.* Λ. (Redrawn from Schlichting, 1974).

is the boundary layer width. We can detect these unsteady sinusoid-like waves in the boundary layer of animals as they swim in practically motionless water medium. It is necessary that the turbulence proper to the medium to be less than a certain limit. This condition can be fulfilled if we conduct measurement on an animal in unruffled and relatively small reservoir.

The transition from laminar to turbulent mode of flow can be either accelerated or decelerated if we create positive or negative gradient of pressure along the surface

correspondingly. If the gradient of the pressure is negative, the stability of laminar flow increases; if the gradient of the pressure is positive, the stability decreases. Dependence of the critical Reynolds number on the configuration parameter of the velocity profile in the boundary layer is shown in figure 4.12. It is defined by

$$\Lambda = \frac{\delta^2}{\nu}\frac{dU}{dx} \tag{4.19}$$

and connected with the pressure gradient by Bernoulli equation:

$$\frac{dp}{dx} = -\rho U \frac{dU}{dx}. \tag{4.20}$$

Thus, the gradient of the pressure influences configuration of the velocity profile. Engineers who design the wing profiles and shapes of submarine vessels use this influence. The longer the boundary layer of such profiles stays laminar, the better. To gain this effect they try to move the site of the profile, where the thickness is maximal, as far backwards as possible. Doing so they increase the interval with negative gradient of the pressure and therefore increase the stability of the laminar flow.

4.1.3. Turbulent boundary layer

If the Reynolds number is greater than the critical value, then the flow in boundary layer is turbulent. In this case the velocity and the pressure in a fixed point of space vary very frequently and very non-uniformly. These variations of speed and pressure called pulsations, are the most typical symptoms of turbulence. But it does not mean that in the laminar flow there is no pulsation of speed and pressure. Reasons that cause pulsation in a turbulent flow are the same as in a laminar flow. These reasons are asperity, temperature non-uniformity, non-uniformity of density, and so on. But in a laminar flow the arising pulsation quickly damps and does not spread on nearby domains of the flow, whereas in a turbulent flow pulsation spreads on the whole flow, transforms into small-scale irregularity and damps due to viscosity. The level of pulsation in laminar flow may be greater than the level of the turbulent pulsation, but the spectrum of the laminar pulsation lies in the low-frequency area. We will return to the exact definition of relation of the levels and spectra of pulsation in laminar and turbulent flows after the concept of turbulence intensity will be introduced.

For illustration we can represent turbulent motion as the set (superposition) of vortices of different size. The upper limit of the vortex size is defined mainly by characteristic size of the flow or of the arrangement where liquid flows. In a boundary layer the maximal vortex size is of the same order as the thickness of the boundary layer, in a tube it is as the tube diameter. The lowest extreme is defined by the influence of viscosity. If the

other parameters are equal, it decreases as the mean velocity of the flow increases. Inside of these smallest vortices the flow is already not turbulent but viscous. The leading part now belongs to the molecular effects. However it does not mean that the smallest size of the vortices is comparable with the average free path of a molecule. To explain this, we adduce some figures (Hintse, 1963). If the velocity of a gas flow does not exceed 100 ms^{-1}, then the smallest size of the vortex is approximately 1 mm. This value is still very large as compared with the average free path of a molecule that has the order of 10^{-4} mm. The value of the speed pulsation is approximately 10% of the average speed. This value lies in the interval from 0.01 to 10 ms^{-1}. These figures should be compared with the average speed of molecules, which in case of air has the order of 500 ms^{-1}. The frequency of the turbulent pulsation varies in the range of $1 \div 10^4$ Hz, while the frequency of contacts of air molecules is 5.10^9 Hz. We can see that the interval of the turbulence values is rather far from the range of the corresponding molecular values. The same can be stated for the pulsation in a liquid flow. We can represent the flow pulsation as the eddy movement, which overlays the average movement. Let us denote the time average x-components of the velocity as $\overline{U}$ and the pulsatory velocity as u, the y-components of the velocity as $\overline{V}$ and v, the z-components of the velocity as $\overline{W}$ and w, and the pressures as $\overline{P}$ and p. Then in case of incompressible liquid we get the equalities

$$U = \overline{U} + u, \quad V = \overline{V} + v, \quad W = \overline{W} + w, \quad P = \overline{P} + p. \tag{4.21}$$

The time average velocity is

$$\overline{U} = \frac{1}{t_1} \int_{t_0}^{t_0+t_1} U dt. \tag{4.22}$$

The averaging interval has to be long enough to make the mean value independent on time. Then the time average pulsatory values are zeros, i.e.

$$\overline{u} = 0, \quad \overline{v} = 0, \quad \overline{w} = 0, \quad \overline{p} = 0. \tag{4.23}$$

The pulsatory components of velocity and pressure in the boundary layer affect the mean parameters of the boundary layer. First of all, the deformation resistance quasi increases. In other words, the pulsation leads to virtual increasing of the viscosity of the average motion. We can write Newton's law of friction for turbulent boundary layer like

$$\tau = (\mu + A_\tau) \frac{d\overline{U}}{dy}, \tag{4.24}$$

where A_τ is the factor of turbulent exchange that imply the additional viscosity. The tangential turbulent quasi stress is defined by the pulsation of the velocity with the following equation

$$\tau = -\overline{\rho uv} + \mu\frac{\overline{dU}}{dy}. \tag{4.25}$$

Thus under the turbulent flow conditions, the tangential stress is composed of the two parts: the laminar one and the turbulent one. Directly at the wall

$$A_\tau = 0. \tag{4.26}$$

So, if y is sufficiently small value, then the viscous friction stress is much greater than the Reynolds stress ($-\overline{\rho uv}$). The layer of liquid, where the condition

$$\mu >> A_\tau \tag{4.27}$$

is fulfilled, is usually called the viscous under-layer. For a long time instead of the term "viscous under-layer", there was used another one - "laminar under-layer", as it was supposed that the flow within this under-layer is laminar. But the direct ultramicroscoping observation of the suspended particle motion in the liquid near the wall showed that the flow is not laminar and it is accompanied by the appreciable turbulent pulsation despite the fact that the profile of the mean velocity within the layer coincides with the profile of the laminar flow velocity. Therefore, now the term "laminar under-layer" does not seem apposite. Instead of "laminar under-layer" we use the term "viscous under-layer" (Monin, Yaglom, 1965).

The pulsatory motion significantly influents the velocity profile in turbulent boundary layer. The Blasius profile takes place in laminar boundary layer and in viscous under-layer, but here, if the Reynolds number is less than 10^6, then the velocity distribution is defined by equation

$$\frac{U}{U_\infty} = \left(\frac{y}{\delta}\right)^{1/7}. \tag{4.28}$$

If the Reynolds number is greater than 10^6, and the laminar tangential stress is small in relation to the turbulent one, the other law is reasonable:

$$\frac{U}{V^*} = 5.85\ln\eta + 5.56, \tag{4.29}$$

where $\eta = \frac{yV^*}{\nu}$, $V^* = \sqrt{\frac{\tau_0}{\rho}}$, is so called dynamic velocity, which corresponds to the tangential stress τ_0 at the wall.

The thickness of the turbulent boundary layer is

$$\delta(x) = 0.37x\left(\frac{U_\infty x}{\nu}\right)^{-1/5}. \tag{4.30}$$

and the displacement thickness and the thickness of impulse loss is coupled with the thickness of the boundary layer by the equations

$$\delta_1(x) = \frac{1}{8}\delta(x) \tag{4.31}$$

and

$$\delta_2(x) = \frac{7}{72}\delta(x). \tag{4.32}$$

The factor of the friction resistance for the flat plate with the boundary layer, which is turbulent from the leading edge, looks like

$$c_l = \frac{0.074}{\sqrt{\mathrm{Re}_l}}. \tag{4.33}$$

We can use the law only when the Reynolds number ranges from 5.10^5 to 10^7. If there is a laminar interval of the flow along the plate, then the equation, which describes the factor of friction resistance, looks like

$$c_l = \frac{0.074}{\sqrt{\mathrm{Re}_l}} - \frac{A}{\mathrm{Re}_l}. \tag{4.34}$$

Prandtl-Schlichting law

$$c_l = \frac{0.455}{(\lg \mathrm{Re}_l)^{2.58}} - \frac{A}{\mathrm{Re}_l} \tag{4.35}$$

is used if the Reynolds number has order of 10^9.The value of A in this and in previous equations depends on the critical Reynolds number. It is shown in the table 4.1.

The relations described above are reasonable for a completely plain plate. Any asperity increases the friction resistance. The graphs in fig. 4.13 and fig. 4.14 show the laws of the friction resistance of the plates with the roughness of sand size. There are shown the

Re_{crit}	3.10^5	5.10^5	10^6	3.10^6
A	1050	1700	3300	8700

Table 4.1. Values of a parameter A. (From Schlichting, 1969).

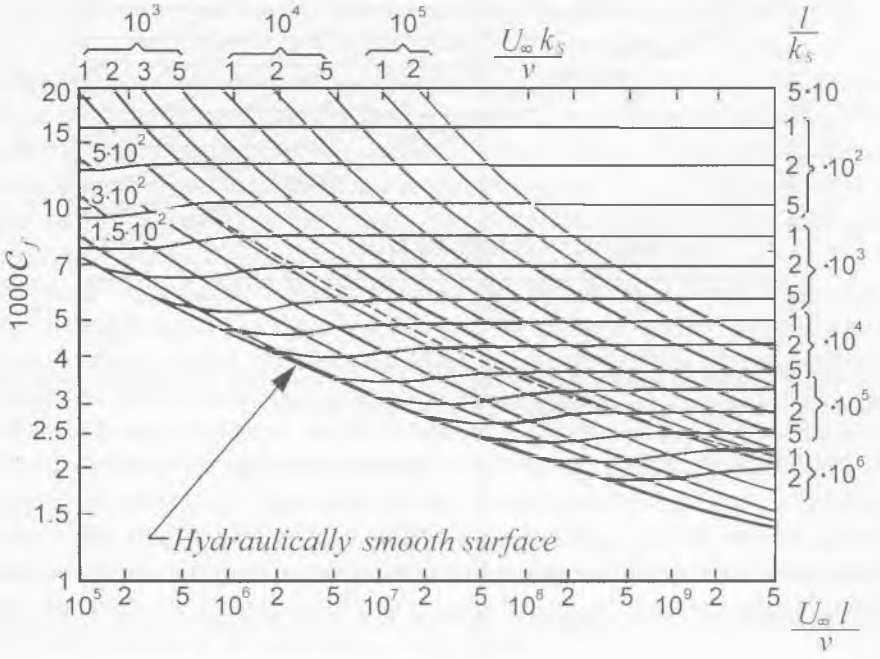

Fig. 4.13. Full friction resistance factor of the plate with the roughness of sand size *vs.* the Reynolds numbers and the relative roughness. (Redrawn from Schlichting, 1974).

dependencies of the full and local friction resistance factors on the Reynolds numbers and on the relative roughness. In order not to affect the friction resistance, the roughness must be less than a certain value. The allowable values of the roughness for different values of the Reynolds numbers are shown in the table 4.2. The height of the roughness is given in relation to the plate length.

For example: The roughness of a newly launched vessel is on average 0.3 mm. Under the high Reynolds number, which characterizes vessels, such roughness increases the friction resistance approximately by 30÷45% in relation to the resistance of the hydraulically smooth surface. The biofouling of a vessel increases the resistance approximately by 50%.

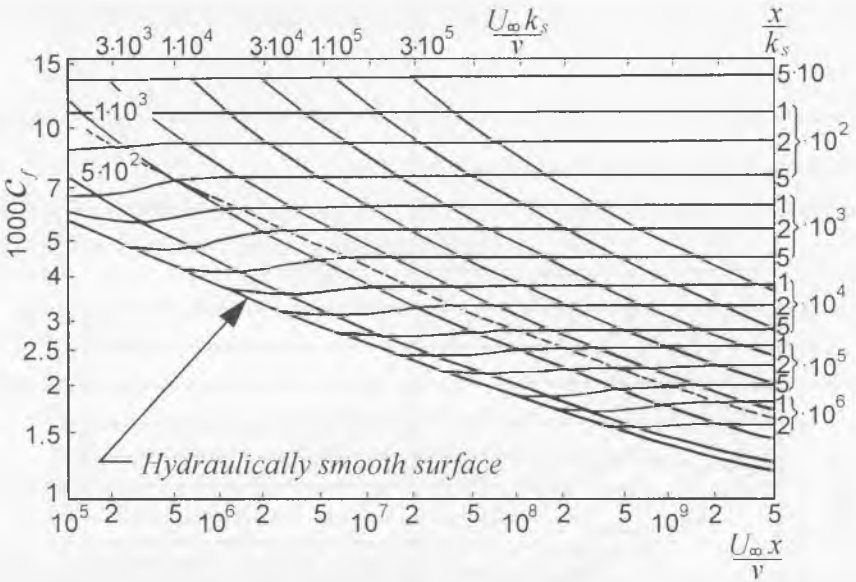

Fig. 4.14. Local friction resistance factor of the plate with the roughness of sand size *vs.* the Reynolds numbers and the relative roughness. (Redrawn from Schlichting, 1974).

Re	10^5	10^6	10^7	10^8	10^9
h/l	10^{-3}	10^{-4}	10^{-5}	10^{-6}	10^{-7}

Table 4.2. Allowable values of the roughness for different values of the Reynolds numbers. (From Schlichting, 1969).

4.1.4. The statistical features of hydrodynamic fields

Hydrodynamic fields and turbulent fields in particular are kind of stochastic fields. The stochastic field is the field of random multivariable function. The turbulent field is a field of pressures and velocities. Pulsation of pressure is a scalar continuous random function of space and time $p(x,y,z,t)$, pulsation of velocity is a vector $\overline{U}(x,y,z,t)$ continuous random function. If we consider coordinates of the vector $\overline{U}$, we can describe the vector field with three scalar fields. If averaged characteristics of stochastic field do not depend on time, then the field is a stationary field. If averaged characteristics of stochastic field depend on time, then the field is a non-stationary field.

A field can be either uniform or non-uniform. If averaged characteristics of stochastic field do not depend on coordinate of point, then the field is uniform. Averaged characteristics of a non-uniform stochastic field do depend on coordinates of a point.

A field can be either isotropic or non-isotropic. Statistical characteristics of an isotropic field do not depend on the vector of difference direction of points' coordinates. Statistical characteristics of a non-isotropic field do depend on the the vector of difference direction of points' coordinates (Monin, Yaglom, 1965).

In case of a real viscous liquid, viscosity of the liquid causes transformation of kinetic energy into warmth. Therefore, the turbulent flow is dissipative by nature. If there is no external continuous power supply, which is needed for continuous stimulation of turbulent movement, then the movement is degenerated. Another effect of viscosity makes the turbulence become more uniform and less dependent on direction. In extreme case the turbulence in all domains of the flow field is numerically of the same structure. Then the turbulence is called uniform. If the statistical characteristics of the turbulence do not depend on direction and the turbulence is quite irregular, then the turbulence is called isotropic. In this case average shear stress does not exist. Therefore there is no gradient of the average velocity. If the mean velocity exists, it is constant on the whole flow field.

If the mean velocity has nonzero gradient, the turbulence is anisotropic. Since the gradient of the average velocity is bundled with the existence of the mean shear stress, this kind of flows is often denoted as turbulence in a shear flow. The wall turbulence and anisotropic free turbulence belong to this kind of flows.

If the turbulence is isotropic and if we count the number of amplitudes of the certain value in the velocity (or pressure) pulsation oscillogram then we get the curve of the Gaussian distribution. For a common case of the turbulent shear flow (i.e. anisotropic turbulence) this distribution is more or less asymmetrical, i.e. the random process of such turbulence strictly speaking is not a Gaussian process. But it does not mean that in this case the methods of analysis of the normal processes are not applicable. We can analyze such process, if we normalize it with filters.

The general feature of the turbulent flow is its intensity. Let us denote the instant velocity value by

$$U = \bar{U} + u, \tag{4.36}$$

where the score above denotes the mean value. For a turbulent velocity pulsation the equality $\bar{u} = 0$ is right. The same equality is also right for the pressure pulsation. We can use the mean value of the pulsation magnitude as the measure of the pulsation intensity $|u|$. But usually the mean-square value is used as the intensity of turbulent pulsation

$$\sqrt{\overline{u^2}} \tag{4.37}$$

or

$$\sqrt{\overline{p^2}}. \tag{4.38}$$

Then the relative intensity, which sometimes is called "degree of turbulence" or "level of turbulence", is defined with equation

$$\frac{\sqrt{\overline{u^2}}}{U} \tag{4.39}$$

or

$$\frac{\sqrt{\overline{p^2}}}{q}, \tag{4.40}$$

where $q = \frac{\rho U^2}{2}$ is dynamic pressure, U is the flow velocity, ρ is density of the medium.

The average values can be defined in different ways. If the turbulent flow is a stationary one, we can use the time averaging. If the turbulence of the flow is a uniform one, we can use the space average. But if the flow is neither stationary nor uniform, then it is not always possible to average over the space or over the time. In similar cases we can suppose that the average is defined on the great number of tests, which are performed under the same initial and boundary conditions. In these cases the average is an ensemble average.

Let us consider the mechanics of the energy transfer from the average movement to the pulsation of the velocity and pressure. The power of the average movement is transferred directly to the longitudinal pulsation of the velocity only. The transversal pulsation of the velocity gets its power from longitudinal pressure pulsation, which redistributes power between the pulsation of different directions. Thus the trend to the isotropic pulsation motion is formed. For example, if two neighbouring elements of the liquid (like fig. 15) move along the average flow direction towards each other, then the positive pressure pulsation arises in the domain between them on account of their energy. This growth of the pressure leads to liquid drain in transversal directions and to transversal velocity pulsation components arise, (Monin, Yaglom, 1965).

As we mentioned above, the level of the velocity and pressure pulsation in the laminar boundary layer is not zero. However it is significantly less than one in the turbulent boundary layer. We know from experience that under the same flow velocity the mean square pressure in the laminar boundary layer is at least six times less than the corresponding pressure in the turbulent layer

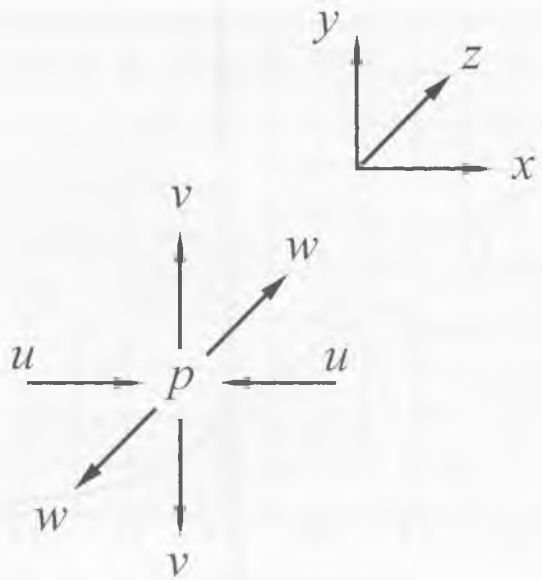

Fig. 4.15. Mechanics of the energy transfer from the average movement to the pulsation of the velocity and pressure. (Redrawn from Monin, Yaglom, 1965).

$$\frac{\left(\sqrt{\overline{p^2}}\right)_{turb}}{\left(\sqrt{\overline{p^2}}\right)_{lam}} > 6. \tag{4.41}$$

For the adequate estimation of turbulence intensity it is important to know that in general the pulsation of the velocity amounts to 5÷10% of the average velocity of the incident flow. The mean square pressure pulsation suits the equation

$$\frac{\sqrt{\overline{p^2}}}{q} = c_1 \mathrm{Re}_x, \tag{4.42}$$

where $\mathrm{Re}_x = \frac{Ux}{\nu}$. The value of the factor c_1 in the domain of the automodel boundary layer estimated for the experimentally derived data at the Reynolds number of $1.5 \div 10^6$ and above is in the range of $c_1 = 0.6 \div 0.8$.

The distribution of the velocity and the distribution of the tangential stress turbulent pulsation of the longitudinal flow over the boundary layer thickness are shown in fig.

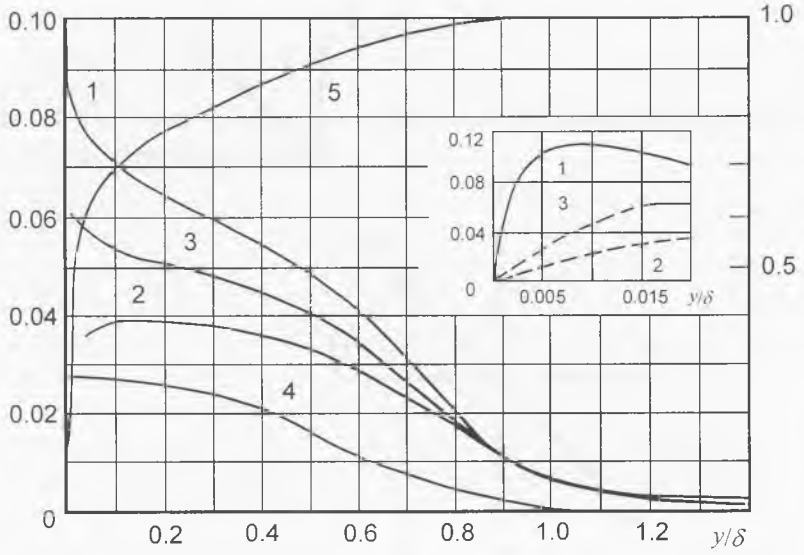

Fig. 4.16. Distribution of the turbulent velocity pulsation in a boundary layer on a flat plate: 1 - $\frac{\sqrt{\overline{u^2}}}{U_\infty}$; 2 - $\frac{\sqrt{\overline{v^2}}}{U_\infty}$; 3 - $\frac{\sqrt{\overline{w^2}}}{U_\infty}$; 4 - $\frac{\overline{uv}}{U_\infty^2}$; 5 - $\frac{\overline{u}}{U_\infty}$. (Redrawn from Schlichting, 1974).

4.16. These distributions take place without longitudinal pressure gradient on the flat plate. The value of the turbulent tangential stress on the wall coincides with the local friction coefficient

$$\frac{\tau}{\rho U_\infty^2} = -\frac{\overline{uv}}{U_\infty^2} \approx 0.0015. \qquad (4.43)$$

We have introduced the concept of the turbulent vortices of different scales. Numerical definition of the turbulence scale is bound with the correlation of the velocity (pressure) pulsation in the studied region of the flow. The coefficient of correlation between the velocity and pressure pulsation is the measure of this bounding. If we find the space distribution of the correlation coefficient, we can estimate the space structure of turbulent perturbations and at the each stage of vortex disintegration we can find its scale. In case of stationary uniform field the correlative function is a function of four variables: $R\ (x_1\text{-}x_2,\ y_1\text{-}y_2,\ z_1\text{-}z_2,\ t_1\text{-}t_2)$. Here $x_1\text{-}x_2 = \xi$, $y_1\text{-}y_2 = \eta$, $z_1\text{-}z_2 = \zeta$ are the distances between the points of measurement along the coordinate axes, and $t_1\text{-}t_2 = \tau$ is the time interval between the moments of measurement (the time delay). In general the spatio-temporal correlation coefficient of the velocity or pressure pulsation is considered to be described by equations like

$$R_p(\xi,\eta,\zeta,\tau) = \frac{\overline{p_1(x_1,y_1,z_1,t_1)p_2(x_2,y_2,z_2,t_2)}}{\sqrt{\overline{p_1^2}}\sqrt{\overline{p_2^2}}}, \tag{4.44}$$

$$R_{uu}(\xi,\eta,\zeta,\tau) = \frac{\overline{u_1(x_1,y_1,z_1,t_1)u_2(x_2,y_2,z_2,t_2)}}{\sqrt{\overline{u_1^2}}\sqrt{\overline{u_2^2}}}, \tag{4.45}$$

$$R_{vv}(\xi,\eta,\zeta,\tau) = \frac{\overline{v_1(x_1,y_1,z_1,t_1)v_2(x_2,y_2,z_2,t_2)}}{\sqrt{\overline{v_1^2}}\sqrt{\overline{v_2^2}}}, \tag{4.46}$$

$$R_{ww}(\xi,\eta,\zeta,\tau) = \frac{\overline{w_1(x_1,y_1,z_1,t_1)w_2(x_2,y_2,z_2,t_2)}}{\sqrt{\overline{w_1^2}}\sqrt{\overline{w_2^2}}}, \tag{4.47}$$

$$R_{uv}(\xi,\eta,\zeta,\tau) = \frac{\overline{u_1(x_1,y_1,z_1,t_1)v_2(x_2,y_2,z_2,t_2)}}{\sqrt{\overline{u_1^2}}\sqrt{\overline{v_2^2}}}, \tag{4.48}$$

$$R_{uw}(\xi,\eta,\zeta,\tau) = \frac{\overline{u_1(x_1,y_1,z_1,t_1)w_2(x_2,y_2,z_2,t_2)}}{\sqrt{\overline{u_1^2}}\sqrt{\overline{w_2^2}}}, \tag{4.49}$$

$$R_{vw}(\xi,\eta,\zeta,\tau) = \frac{\overline{v_1(x_1,y_1,z_1,t_1)w_2(x_2,y_2,z_2,t_2)}}{\sqrt{\overline{v_1^2}}\sqrt{\overline{w_2^2}}}. \tag{4.50}$$

In real experimental studies our devices can measure only a one-dimensional function of a single variable and so we differentiate the following one-dimensional functions, which characterize the stationary uniform field:

1. The function of temporal correlation, which is in fact the autocorrelation function of a signal measured in a single point of the field:

$$R_p(0,0,0,\tau)=\frac{\overline{p_1(x_1,y_1,z_1,t_1)p_2(x_1,y_1,z_1,t_1+\tau)}}{\sqrt{\overline{p_1^2}}\sqrt{\overline{p_2^2}}}. \tag{4.51}$$

2. The single-coordinate function of spatial autocorrelation:

$$R_p(\xi,0,0,0)=\frac{\overline{p_1(x_1,y_1,z_1,t_1)p_2(x_2,y_1,z_1,t_1)}}{\sqrt{\overline{p_1^2}}\sqrt{\overline{p_2^2}}}, \tag{4.52}$$

and all that.

In the same way we can write the equations for the case of velocity pulsation. The autocorrelation function can be characterized by the correlation window (or the correlation time) τ_0. If the temporal interval between the two moments of the velocity (or pressure) measurements is greater than τ_0, then we can consider these measurements to be uncorrelated.

The spatial mutual correlation can be characterized by the correlation window or by the correlation radius: $d_0=\sqrt{\xi_0^2+\eta_0^2+\zeta_0^2}$. The correlation radius is defined by the certain distance. If the span between the measurement points is greater than this distance, then we can consider the pulsations to be uncorrelated.

If the field is anisotropic the correlation windows, measured in different directions, are different.

The autocorrelation function defines the total turbulent power or the mean square pulsation pressure in the common frequency band, while the Fourier transformation of the autocorrelation function gives the resource to calculate the spectral density of the pulsation power. The spatial correlation in some frequency band gives us the possibility to view average vortex size that corresponds to this frequency band. Drop in the correlation, as the span between the measurement points increases, lets us view the average spread of coherent action of turbulent liquid mass. If we fix the lags for optimal delays and the certain frequency, we can evaluate the convective speed of transfer of vortices of a certain scale. We can ascertain degree of vortex degeneration, using the correlation maxima envelope. Knowing the time-spatial correlation function, we can easily obtain the scales of the turbulent vortices. Usually we confine ourselves to longitudinal scale and two transversal scales, which are defined by the integrals

$$L_x=\int_0^\infty\frac{\overline{u_1(x_1,y_1,z_1,t)u_2(x_1+\xi,y_1,z_1,t)}}{\sqrt{\overline{u_1^2}}\sqrt{\overline{u_2^2}}}d\xi, \tag{4.53}$$

$$L_y = \int_0^\infty \frac{\overline{u_1(x_1, y_1, z_1, t)u_2(x, y_1 + \eta, z_1, t)}}{\sqrt{\overline{u_1^2}}\sqrt{\overline{u_2^2}}} d\eta. \tag{4.54}$$

$$L_x = \int_0^\infty \frac{\overline{u_1(x_1, y_1, z_1, t)u_2(x, y_1, z_1 + \zeta, t)}}{\sqrt{\overline{u_1^2}}\sqrt{\overline{u_2^2}}} d\zeta. \tag{4.55}$$

These scales are applied to the large-scale vortices. They are "large scales". The shape of the spatial correlation function around the point, where the differentiation is almost equal to zero, contains information on the scales of the small vortices. The shape of the spatial correlation function around the point with almost zero differentiation is defined by the equation

$$R_u(\xi,0,0,0) \cong 1 - \frac{\xi^2}{\lambda_x^2}, \tag{4.56}$$

where λ_x is the small scale of the turbulence in the longitudinal direction, and also the smallest vortex size. The transversal direction scales are defined like this. Relation between the turbulence scales depends on the degree of the turbulence degeneration. At the final stage of degeneration λ and L have the values of the same order. They are bundled by the equation

$$\lambda = 2\sqrt{\nu t} = \sqrt{\frac{2}{\pi}} L. \tag{4.57}.$$

At the initial stage of degeneration λ and L are bundled by the equation

$$\frac{L}{\lambda} \approx \frac{\lambda\sqrt{\overline{u^2}}}{\nu}, \quad \frac{\lambda}{L} \approx \frac{1}{\sqrt{\frac{L\sqrt{\overline{u^2}}}{\nu}}}. \tag{4.58}$$

The values $\frac{\lambda\sqrt{\overline{u^2}}}{\nu}$ and $\frac{L\sqrt{\overline{u^2}}}{\nu}$ play the role of the turbulence Reynolds numbers for the discussed kind of motion (Loytsyansky, 1973).

Measurements in the boundary layer show that apart from the region close to the wall the value of L is approximately proportional to the thickness of the boundary layer (Petrovsky, 1966). For the majority of measurements $L \approx 0.4\delta$.

We can estimate the scale L of middle-sized vortices by equation $L \approx U/f$, where U is the flow speed, f is frequency.

In a turbulized flow the power of the mean movement is transformed to heat by power transfer from a large-scale turbulence to a small-scale one. Fig. 4.17 shows the frame of this process.

The vortices of different scales have different energy. The curve of the energy density distribution has a maximum. The maximal energy does not fit the greatest vortex. The spectral density of the turbulent energy under the high Reynolds number is shown in fig. 4.18. It depends on the wave number, which is defined by the equation

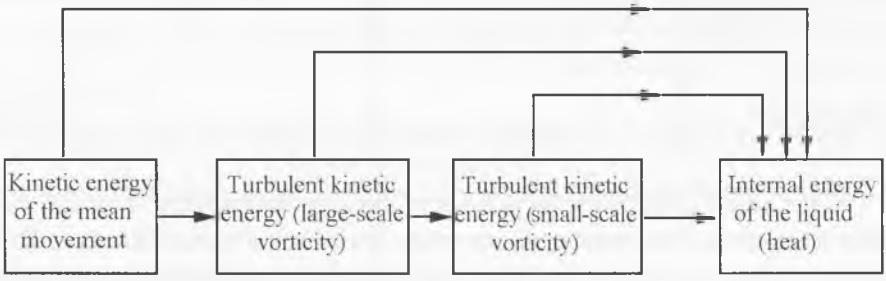

Fig. 4.17. Scheme of the energy transfer from the average movement and a large-scale turbulence to a small-scale on. (Redrawn from Petrovsky, 1966).

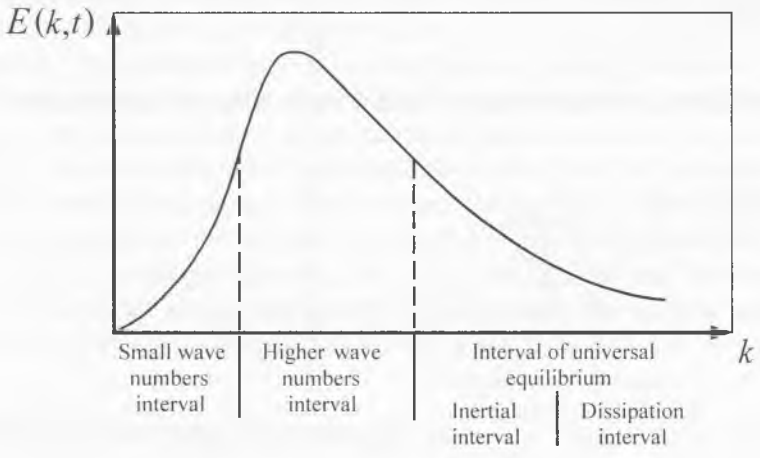

Fig. 4.18. Spectral density of the turbulent energy under the high Reynolds number vs. a wave number k. (Redrawn from Hintse, 1963).

$$k = \frac{2\pi f}{\overline{U}}, \tag{4.59}$$

where f is the frequency that characterizes the vortex of a given size, $\overline{U}$ is the mean velocity of the flow. We can split the whole range into a few intervals.

1. The small wave numbers interval. At the beginning of this interval the spectral density is proportional to k^4, and at the end - to k. The share of this part is about 20% of the turbulent energy.

2. The higher wave numbers interval. The most powerful vortices are in this interval. This interval is the interval of the maximal spectral density of the energy.

These two intervals represent the macrostructure of the turbulence, which depends upon the turbulent flow formation mode, i.e. on the external conditions. The higher wave numbers define the turbulence microstructure, which does not depend on the external conditions. These higher values form the so-called interval of universal equilibrium. This interval, in turn, is divided into two:

1. The inertial interval, where the Kolmogorov spectral law effects

$$E(k,t) \approx k^{-5/3}. \tag{4.60}$$

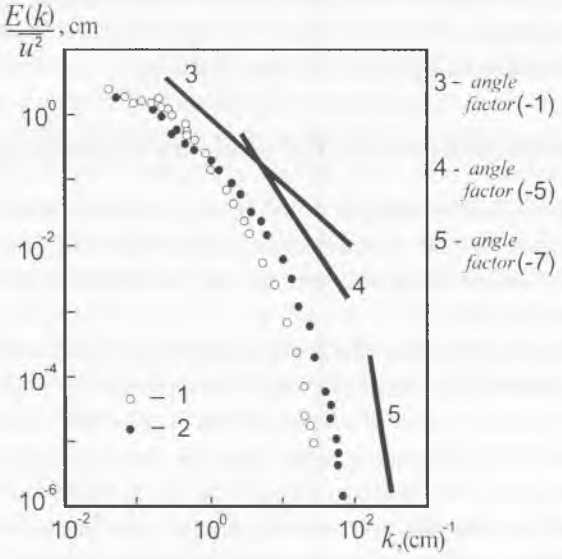

Fig. 4.19. The energy spectrum of the longitudinal velocity pulsation in the turbulent boundary layer at a flat plate *vs.* a wave number k: 1 - $\frac{y}{\delta}$ = 0.8; 2 - = 0.05. (Redrawn from Hintse, 1963).

2. The dissipation interval, where the Heisenberg spectral law effects

$$E(k,t) \approx k^{-7}. \qquad (4.61).$$

The vortices that correspond to the inertial subregion are actuated because of energy transfer by the inertia forces from the large vortices.

Cited above schematic structure of the turbulence is hypothetical in many ways. It is developed in the works of Kolmogorov, Heisenberg, Karman, Lin, Betchelor, Taunsend and others. This structure is proved by experiments, especially in the interval of universal equilibrium. In this interval the turbulence does not depend on external conditions and is locally isotropic even if the whole turbulent flow is not isotropic (in reality this case occurs more often). Due to its relative simplicity, the isotropic turbulence is studied better than any other case both theoretically and experimentally. But even if we deal with nonisotropic microstructure of real turbulence, or if the turbulence is nonisotropic in the major part of its spectrum, then we can consider this turbulence isotropic at a first approximation. The difference between the theoretical and experimental results in this case is often so small, that at the first approximation it can be neglected. This discrepancy is sometimes even less than the scattering of the experimental data.

The readout of the experiments is mainly the microstructure of the turbulence, because the measurements under very small wave numbers are difficult. Therefore the measured energy spectrum of the turbulence differs from the spectrum in fig. 4.18. The energy spectrum of the longitudinal velocity pulsation in the turbulent boundary layer at a flat plate is given for example in fig. 4.19 (Hintse, 1963).

4.2. Methods and devices for analysis of random processes

We discussed above the foundation of the hydrodynamics. It was information about the boundary layer and its fine structure. The most reliable information on features of the flow around the bodies of aquatic animals can be obtained as a result of boundary layer fine structure studying.

It does not seem possible to describe the boundary layer fine structure in deterministic terms, so we have to treat it as a random field. Furthermore, the pulsation of the velocity and pressure in the boundary layer of a living object is generally a non-stationary random field. We considered in the foregoing some specific characteristics of a hydrodynamic random field. To describe the methods and results of the biohydrodynamic researches, we have to analyse the random process in general, its characteristics, methods and devices for its studying, and we will do it in this part of the chapter, where the results of G. Ya. Mirsky, V. E. Gmurman, A. K. Novikov, V. V. Olshevsky and others are used. The basic random processes theory and correlation analysis determinations are taken from the works Mirsky (1972) and Novikov (1971).

4.2.1. Brief information about random processes and their characteristics

A process, which parameters vary in time by chance, is called the random (stochastic) process. The parameters can be of physical, chemical, physiological and other nature. The random function of time or space or both of them describes the random process. We can represent the random function as infinite set (ensemble) of functions, where each of them is a possible realization of this random function.

Let us introduce the next denotations: $X(t)$, $Y(t)$, $Z(t)$ are random functions; $x(t)$, $y(t)$, $z(t)$ are realizations. Thus, a random process, which is described by random function $X(t)$, is the set of realizations $x_1(t)$, $x_2(t)$,... $x_\infty(t)$.

Generally speaking, the stochastic characteristics of one realization do not give the complete vision of the corresponding stochastic characteristics of the random function as a whole. Nevertheless, under certain conditions we can get satisfactory notion of the random function on the base of the single realization.

The random processes can be both stationary and non-stationary. Process is called stationary, when the stochastic characteristics (time averaged) of the process do not fluctuate, when the time is shifted, i.e. the time t is substituted with the time $t+\tau$, where τ is a voluntary time interval. If stochastic characteristics of the process are functions of time and depend on the initial time, such process is called non-stationary process.

The turbulent noise in a steady-state turbulent flow is an example of a stationary process. The noise given by hydrophone when a vessel is passing by, is an example of a non-stationary process.

The ergodic hypothesis, treated in the classical sense, is acceptable with respect to many real random processes. The stochastic characteristics of an ergodic process can be obtained as a result of time averaging of one realization, whose duration is large enough. The ergodic property is very important for the technique of instrumental analysis of random processes, since it gives a possibility to replace ensemble averaging with time averaging. A stationary turbulent noise in particular is considered an ergodic process.

A random process is determined by a set of numerical and functional characteristics.

The probability distribution function is the probability that the value of the random process, which is described by random function $X(t)$, at the fixed moment $t = t_1$ is less than voluntary: x. This function is also called an integral distribution law of a continuous random process. It is defined by equation

$$F(x,t_1)=P[X(t_1)<x_1], \tag{4.62}$$

where $P[\ ]$ means the probability of what is shown within the brackets.

The probability density function is the probability of the event that any value of a random process at the moment t is between x and $x+dx$

$$w(x,t_1)=\frac{\partial F(x,t_1)}{\partial x}. \tag{4.63}$$

The main features of the probability density function are

$$w(x,t) \geq 0 \tag{4.64}$$

at any x

$$\int_{-\infty}^{\infty} w(x,t)dx = F(x,t), \tag{4.65}$$

$$\int_{-\infty}^{\infty} w(x,t)dx = 1. \tag{4.66}$$

If possible values of a random variable belong to the interval $[a, b]$, then

$$\int_{a}^{b} w(x,t)dx = 1. \tag{4.67}$$

The corresponding plot of the integral distribution law of a continuous random process and the probability density function is shown in fig. 4.20.

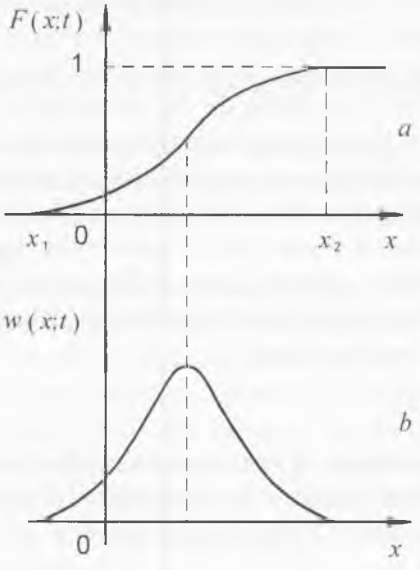

Fig. 4.20. The integral distribution law of a continuous random process (*a*) and the probability density function (*b*). (Redrawn from Gmurman, 1963).

The average of a random function is a certain mean function, around which all-possible realizations of a random function gather.

The average of the random function $X(t)$ can be evaluated by the equation

$$m_X(t) = M[X(t)] = \int_{-\infty}^{\infty} xw(x,t)dx, \tag{4.68}$$

where $w(x,t)$ is the density of probability, M is the denotation of probabilistic average. The probabilistic average of a stationary random process does not depend on time. It is a constant number. If a random process is not only stationary but also ergodic with respect to probabilistic average, then the ensemble average of such process is equal to time average, defined by one realization

$$M[X(t)] = \overline{x(t)}. \tag{4.69}$$

The time average $\overline{x(t)}$ is evaluated with equality

$$\overline{x(t)} = \lim_{T\to\infty} \frac{1}{2T} \int_{-T}^{T} x(t)dt, \tag{4.70}$$

where $2T$ is the interval of integration.

If the studied random process is either the electric potential or the electric current, then the mean value is the direct component of either the voltage or the current.

Dispersion is the characteristic of variation of possible realizations of random function around the mean value. It is defined by expression

$$D[X(t)] = M\left\{[X(t) - m_X(t)]^2\right\} = \int_{-\infty}^{\infty} [x - m_X(t)]^2 w(x,t)dx. \tag{4.71}$$

If the random process is stationary and ergodic, then the expression for dispersion looks like

$$D[X(t)] = \overline{x^2(t)} - [\overline{x(t)}]^2. \tag{4.72}$$

This dispersion is a constant number.

If the studied random process is either the electric potential or electric current (load resistance is equal to 1 Ohm), then the expression member $\overline{x^2(t)}$ is the complete mean process power, the expression member $\overline{[x(t)]^2}$ corresponds to the power of the direct

component, and the dispersion $D[X(t)]$ corresponds to the power of the alternating component.

The mean-square value is often used in practice. It is the positive value of the square root of dispersion

$$\sigma_X = \sqrt{D[X(t)]}. \tag{4.73}$$

It is clear that if the process corresponds to the electric potential, then the value of σ_X is the mean-square (effective) value of the alternating component of this potential.

Now we can proceed to definition of normal random process, which covers a wide range of phenomena. This process is often observed in radio and hydrodynamic devices.

Random variable is called normal, if its probability density is

$$w(x) = \frac{1}{\sigma_X \sqrt{2\pi}} e^{-\frac{x^2}{2\sigma_X^2}}. \tag{4.74}$$

We can observe a similar distribution law in all the cases when we treat the studied process as a sum of many independent (or weakly dependent) random variables if there is no component that greatly exceeds the others.

The three curves for the three values of σ_x are shown in fig. 4.21. They give the examples of normal curves (Gaussian curves).

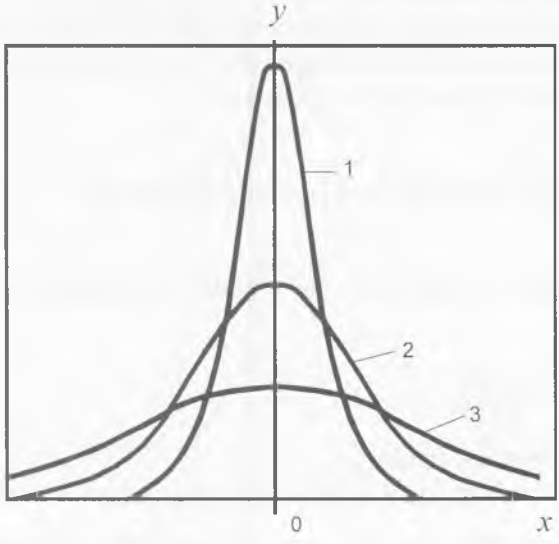

Fig. 4.21. The probability density function for the three values of σ_x: 1 - σ_x = 1; 2 - σ_x = 2; 3 - σ_x = 4. (Redrawn from Gmurman, 1963).

There are many other distribution laws besides the normal law. There are Poisson distribution, Cauchy distribution, gamma distribution laws, Rayleigh distribution, distribution chi-square (χ^2), etc. When we are studying a non-normal distribution, we need to estimate this difference numerically. Special characteristics are introduced for this purpose, such as skewness and kurtosis of distribution. These values are zeroes for a normal distribution. Therefore, if these characteristics of a studied distribution are small, then we can assume that the distribution is almost-normal. The coefficients of skewness and of kurtosis are defined correspondingly by expressions

$$A = \frac{\int_{-\infty}^{\infty} [x(t) - m_X(t)]^3 w(x,t) dx}{\sigma_X^3}, \tag{4.75}$$

$$E = \frac{\int_{-\infty}^{\infty} [x(t) - m_X(t)]^4 w(x,t) dx}{\sigma_X^4}. \tag{4.76}$$

The coefficient of skewness describes asymmetry of the distribution curve. The skewness is positive when the longer part of the distribution curve is located to the right from the probabilistic average (fig. 4.22, *a*), the skewness is negative when the longer part of the distribution curve is located to the left from the probabilistic average (fig. 4.22, *b*).

The coefficient of kurtosis gives the estimation of abruptness of a distribution curve. If the coefficient of kurtosis is positive, then the curve peak (fig. 4.23, 2) is higher and sharper than the normal distribution peak (fig. 4.23, 1), if the coefficient of kurtosis is negative, then the curve peak (fig. 4.23, 3) is lower and more flat than the normal distribution peak.

Let us point out some features of normal random process.

1. Normal process is completely defined by the law of probabilistic mean and correlation function time variation.
2. The sum of two normal processes is also a normal process.
3. Uncorrelated normal processes are independent.
4. Linear transformation of a normal process does not alter its nature.
5. Probability distribution of the derivative of a stationary normal process, which is defined by a continuous differentiable function, is also normal.
6. Nonlinear transformation breaks the normal property of a process.
7. If a non-Gaussian process is passing through a narrow-band linear system, it becomes a normal process. It can be the way of normalization of a non-Gaussian process if its spectrum is smooth.

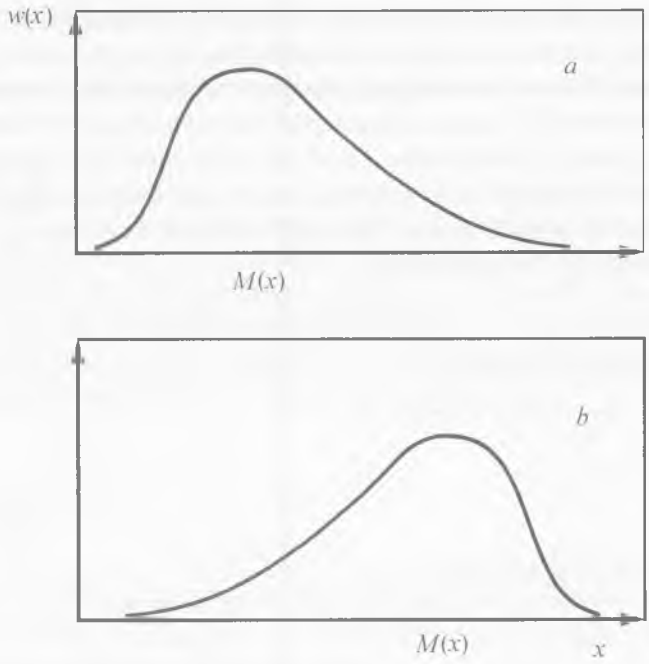

Fig. 4.22. The asymmetrical distribution curves: the skewness is positive (*a*) and negative (*b*). (Redrawn from Gmurman, 1963).

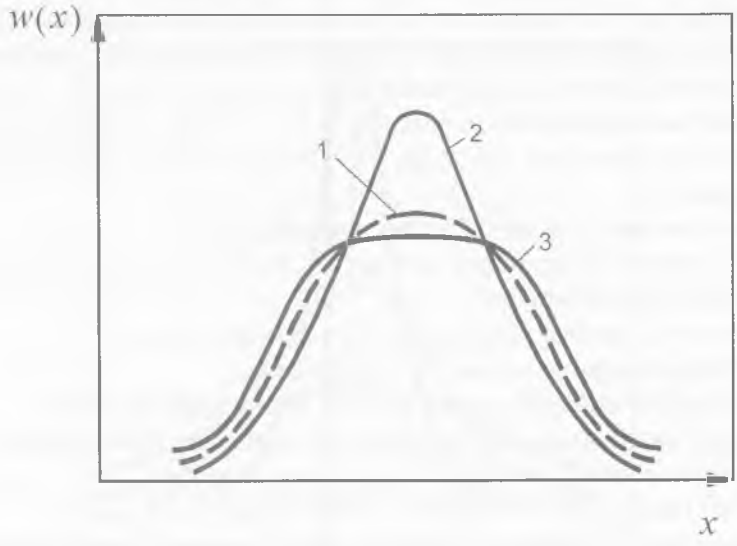

Fig. 4.23. The distribution curves with a different coefficient of kurtosis: 1 – the kurtosis is equal to zero; 2 - the kurtosis is positive; 3 - the kurtosis is negative. (Redrawn from Gmurman, 1963).

Correlation function characterizes the level of linear relationship between the random process samples taken at different time moments. In general case, it is the two-argument function of t_1 and t_2

$$K_X(t_1,t_2)=M\{[X(t_1)-m_X(t_1)][X(t_2)-m_X(t_2)]\}. \tag{4.77}$$

Index X in the left part of the equality (4.77) indicates which random function correlation function corresponds to. Correlation function (4.77), obtained by ensemble averaging, is often called a covariance function. A time correlation function, obtained by time averaging of a single realization, is called a correlation function. The equation for such function looks like

$$K_X(\tau)=\lim_{T\to\infty}\frac{1}{2T}\int_{-T}^{T}\overset{\circ}{x}(t)\overset{\circ}{x}(t+\tau)dt. \tag{4.78}$$

Here the difference $\overset{\circ}{x}(t)=x(t)-m_X(t)$ is the centered random function, $\tau = t_2 - t_1$ is the lag.

If the random process is stationary and ergodic, then the correlation function coincides with the covariance function (4.77).

Correlation function (4.78) characterizes relationship between the separate samples of a single random process. Thus it sometimes is called autocorrelation function.

Interaction between values of two random processes $X(t)$ and $Y(t)$ is characterized by joint correlation function, that is defined by equation

$$K_{XY}(t_1,t_2)=M\{[X(t_1)-m_X(t_1)][Y(t_2)-m_Y(t_2)]\}. \tag{4.79}$$

The normalized autocorrelation function and normalized joint correlation function look like

$$R_X(t_1,t_2)=\frac{K_X(t_1,t_2)}{\sqrt{K_X(t_1,t_1)K_X(t_2,t_2)}} \tag{4.80}$$

and

$$R_{XY}(t_1,t_2)=\frac{K_{XY}(t_1,t_2)}{\sqrt{K_X(t_1,t_1)K_Y(t_2,t_2)}} \tag{4.81}$$

When a process is ergodic and stationary, the normalized autocorrelation function and normalized joint correlation function look like

$$R_X(\tau) = \frac{K_X(\tau)}{\sigma_X^2}, \tag{4.82}$$

$$R_{XY}(\tau) = \frac{K_{XY}(\tau)}{\sigma_X \sigma_Y}. \tag{4.83}$$

Autocorrelation function of an ergodic and stationary process has the features, that are listed below (Novikov, 1971):

1. Autocorrelation function is an even function

$$K_X(\tau) = K_X(-\tau). \tag{4.84}$$

2. The value of $K_x(0)$ gives dispersion of the process. Dispersion does not depend on time due to stationarity of $x(t)$,

$$K_X(0) = \overline{x^2(t)} = \overline{x^2(t+\tau)}. \tag{4.85}$$

3. None of values of $K_x(\tau)$ can exceed $K_x(0)$.

4. For a purely random process

$$K_X(\tau) \to 0 \text{ when } \tau \to \infty. \tag{4.86}$$

5. Normalized correlation function

$$R_X(\tau) = \frac{K_X(\tau)}{K_X(0)} \tag{4.87}$$

has the following features

$$R_X(0) = 1 \text{ and } -1 < R_X(\tau) < 1. \tag{4.88}$$

6. Correlation function of the sum (difference) of independent processes is equal to the sum (difference) of correlation functions of the addends

$$R_{(X+Y)}(\tau) = R_X(\tau) + R_Y(\tau). \tag{4.89}$$

7. Correlation function of a derivative process is equal to the second derivative of sign inverted correlation function of original process

$$K'_X(\tau) = -K''_X(\tau). \tag{4.90}$$

8. We can treat autocorrelation function as the Fourier transform of spectral function $G(\omega)$, which is called a spectral density of power or an energy spectrum (Wiener-Khinchin theorem):

$$K_X(\tau) = \frac{1}{2\pi} \int_{-\infty}^{\infty} G_X(\omega) e^{i\omega\tau} d\omega, \tag{4.91}$$

$$G_X(\omega) = \int_{-\infty}^{\infty} K_X(\tau) e^{-i\omega\tau} d\tau. \tag{4.92}$$

9. If values $x(t)$ and $x(t+\tau)$ become practically uncorrelated when τ becomes greater than τ_0, then the time interval τ_0 is called correlation window. According to the nature of the task we use one of the following definitions of the correlation window:

integral correlation window

$$\tau_{0i} = \int_0^{\infty} R_X(\tau) d\tau, \tag{4.93}$$

absolute correlation window

$$\tau_{0a} = \frac{1}{2} \int_{-\infty}^{\infty} |R_X(\tau)| d\tau = \int_0^{\infty} |R_X(\tau)| d\tau, \tag{4.94}$$

quadratic correlation window

$$\tau_{0q} = \int_0^{\infty} R_X^2(\tau) d\tau, \tag{4.95}$$

correlation window at the level of ε; if $\tau > \tau_0(\varepsilon)$, then

$$|R_X(\tau)| < \varepsilon. \tag{4.96}$$

Usually $\mu = 1/e \approx 0.37$. This value is convenient for calculation. Sometimes $\mu = 0.1$. The choice of either of the two equations is made on the basis of convenience and simplicity of calculation.

The correlation window is bundled with the effective width of spectrum by the general relation

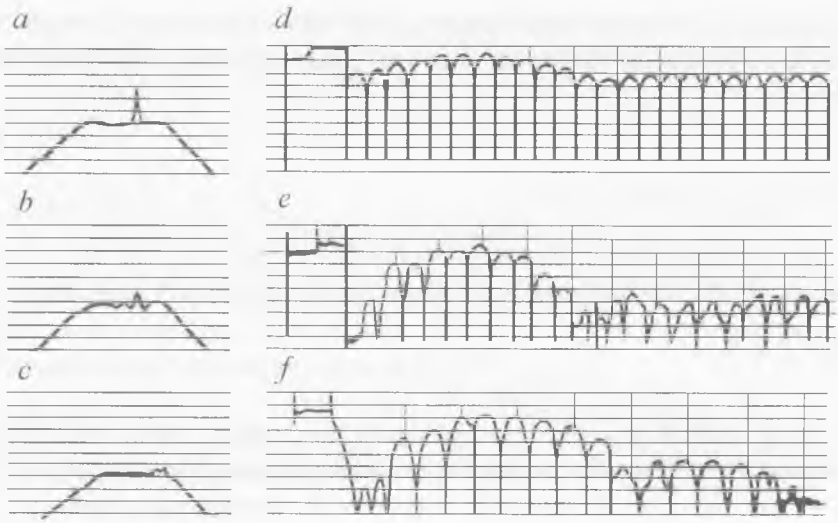

Fig. 4.24. Spectrograms (*a*,*b*,*c*) and autocorrelation functions (*d*,*e*,*f*) of the compound process (harmonic process and noise) is shown in the logarithmic scale. (Redrawn from Novikov, 1971).

$$\Delta F \tau_0 = \eta = \text{const.} \tag{4.97}$$

While estimating we consider η to be equal to 1.

Another definition of correlation window is very convenient when correlation function is oscillating. Here the correlation window is abscissa τ_0 of the first zero of the correlation function envelope.

10. Autocorrelation function of a harmonic signal is also harmonic function of the same period. Autocorrelation function of any periodic process is also a periodic function with the period that equals to the process period.

11. Autocorrelation function of the sum of a periodic and noise processes is the sum of correlation functions of both processes. Correlation window τ_0 of noise is limited and defined by its bandwidth and by the shape of noise spectrum, while correlation window of a periodic process is limitless. Therefore if a delay exceeds τ_0 then the resultant autocorrelation function only depends on the periodic process. We can see this in fig. 4.24, where the sample of absolute value of autocorrelation function of compound process is shown in logarithmic scale. Thus in this case the correlator acts as a filter with a very narrow bandwidth. It permits us to detect all hidden periodicities analyzing only one realization of the process. Unlike analysis with real narrow-band filter, the correlation analysis does not require the slow readjustment of the filter when the analyzed signal frequency slightly varies.

The examples of autocorrelation functions of some noise processes are shown in fig. 4.25

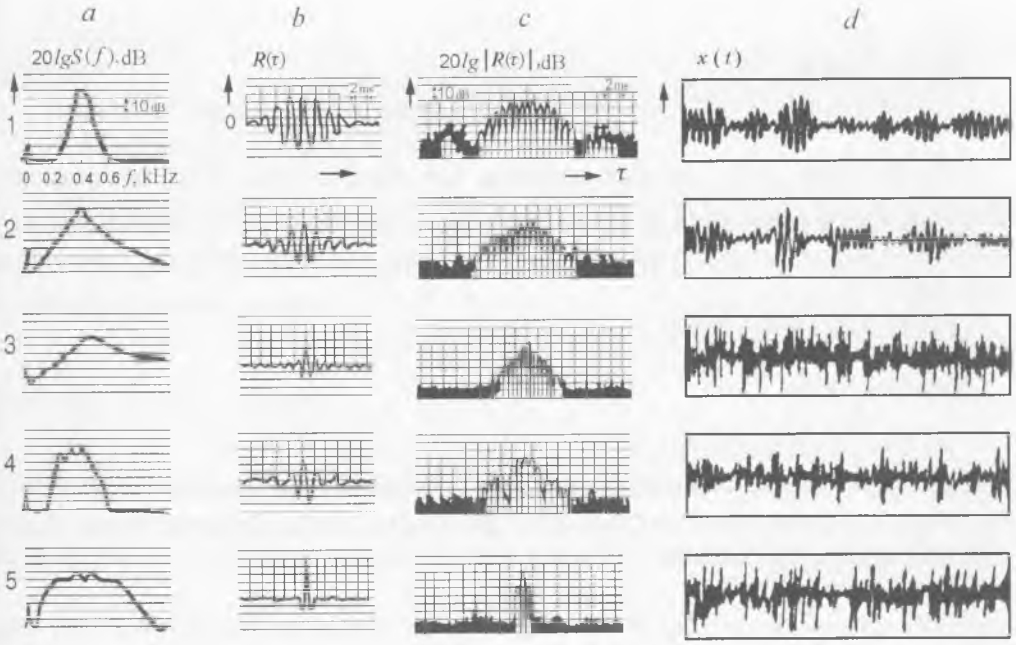

Fig. 4.25. Spectrograms of the noise in the logarithmic scale (*a*), autocorrelation functions in the linear (*b*), logarithmic scale (*c*) and oscillograms (*d*) at the output of the different filters. (Redrawn from Novikov, 1971).

Cross-correlation function of stationary ergodic random processes has the following features:

1. It is not even, but

$$K_{XY}(\tau) = K_{YX}(-\tau). \tag{4.98}$$

In practice it means that interchange of processes implies the lag sign reversal.

2. The absolute value of cross-correlation function satisfies the relation

$$|K_{XY}(\tau)| \le \sqrt{K_X(0)K_Y(0)}. \tag{4.99}$$

Statistic relationship between processes in the frequency domain is defined by their cross spectrum, which is Fourier transform of their cross-correlation function

$$K_{XY}(\tau) = \frac{1}{2\pi}\int_{-\infty}^{\infty} G_{XY}(\omega)e^{i\omega\tau}d\omega, \tag{4.100}$$

$$G_{XY}(\omega) = \int_{-\infty}^{\infty} K_{XY}(\tau)e^{-i\omega\tau}d\tau. \tag{4.101}$$

Complex spectrum of random process realization is defined by equation

$$S(\omega)=\int_{-\infty}^{\infty} x(t)e^{-i\omega t}dt. \tag{4.102}$$

Absolute value $|S(x)|$ is called spectrum. The function $S(\omega)$, which is calculated according to the equation (4.102), is a spectrum of a realization of random process. When we study a random process with some apparatus, we get a current spectrum of the realization

$$S(\omega,t)=\int_{0}^{t} x(t)e^{-i\omega t}dt. \tag{4.103}$$

This spectrum is a random function. In order to characterize random process integrally the concept of power distribution (power spectrum) is used. This spectrum is not a random function of frequency. Power spectrum (energy spectrum) is a frequency distribution of mean power.

Power spectral density $G_X(\omega)$ is associated with correlation function $K_X(\tau)$ by the couple of Fourier transforms (4.100) and (4.101). Power spectrum can be expressed through current spectrum

$$G(\omega)=\lim_{T\to\infty}\frac{1}{T}M\left[S^2(\omega,T)\right] \tag{4.104}$$

The concept of instant power spectrum is also used:

$$\lambda(\omega,t)=\frac{\partial}{\partial t}S^2(\omega,t), \tag{4.105}$$

where $S(\omega,t)$ is absolute value of the current spectrum.

Power spectral density is related with instant power spectrum by the equation

$$G_X(\omega)=M[\lambda(\omega,t)]. \tag{4.106}$$

The power spectral density of a stationary random process has the following main features:

1. Power spectral density is nonnegative

$$G_X(\omega)\geq 0. \tag{4.107}$$

2. When dispersion of a random process is limited,

$$\lim_{\omega \to \infty} G_X(\omega) = 0. \tag{4.108}$$

3. Spectral density is a real function of ω.

4. Spectral density is an even function

$$G_X(\omega) = G_X(-\omega). \tag{4.109}$$

5. The power spectral density integral equals to dispersion (mean power) of the stationary random process

$$\int_{-\infty}^{\infty} G_X(\omega) d\omega = D[X(t)] \tag{4.110}$$

6. Variation of the scale m of argument τ leads to inverse variation of the frequency scale and of the power spectral density magnitude, i.e. if $K_2(\tau) = K_1(m\tau)$, then, respectively,

$$G_2(\omega) = \frac{1}{m} G_1\left(\frac{\omega}{m}\right). \tag{4.111}$$

7. Power spectral density $G_Y(\omega)$ of a process at the output of constant parameters linear system is related with power spectral density $G_X(\omega)$ of the process at the input of the system by expression

$$G_X(\omega) = W^2(\omega) G_X(\omega), \tag{4.112}$$

where $W(\omega)$ is the absolute value of the system transfer function.

The cross spectral density of stationary ergodic processes $X(t)$ and $Y(t)$ is Fourier transform of cross-correlation function of these processes. It has the following features:

1. It possesses complex values

$$G_{XY}(\omega) = Q_{XY}(\omega) - i\rho_{XY}(\omega). \tag{4.113}$$

Its real part $Q_{XY}(\omega)$ is an even function of ω, and its imaginary part $P_{XY}(\omega)$ is uneven function

$$Q_{XY}(\omega) = \mathrm{Re}[G_{XY}(\omega)] = \int_{-\infty}^{\infty} K_{XY}(\tau) \cos \omega\tau d\tau, \tag{4.114}$$

$$\rho_{XY}(\omega) = \mathrm{Im}[G_{XY}(\omega)] = \int_{-\infty}^{\infty} K_{XY}(\tau)\sin\omega\tau d\tau. \tag{4.115}$$

2. Integration of the cross spectral density $G_{XY}(\omega)$ over infinite domain of ω gives a cross dispersion of the random processes:

$$\int_{-\infty}^{\infty} G_{XY}(\omega)d\omega = D[X(t), Y(t)] = K_{XY}(0). \tag{4.116}$$

3. Variation of the scale of the argument τ of the cross-correlation function $K_{XY}(\tau)$ affects the cross spectral density $G_{XY}(\omega)$ likewise the variation of the autocorrelation function $K_X(\tau)$ argument scale affects the power spectral density $G_X(\omega)$.

4. The cross spectral densities $G_{XY}(\omega)$ and $G_{YX}(\omega)$ are the complex conjugate values. They are bound by the relations

$$G_{YX}(\omega) = G_{XY}(-\omega), \tag{4.117}$$

$$G_{XY}(\omega) = G_{YX}(-\omega). \tag{4.118}$$

The probabilistic characteristics, which are listed above, are nonrandom values or functions. They are defined either by virtue of ensemble of infinite large number of realizations or by virtue of a single realization of limitless duration, if the process is stationary and ergodic. In practice either the number of realizations or the duration of a single realization of a random process is always limited. Therefore in reality any statistic characteristic, obtained with any device, differs from the probabilistic characteristic, which is the object of measurement. The measured probabilistic characteristic is assumed to be a search value and is called an estimation of a true probabilistic characteristic.

There are various types of estimations according to the methods of analysis instrumentation (Mirsky, 1972).

1. Unbiased estimation gives a value, whose mean coincides with the true value of a search characteristic. Thus, if $F^*(x)$ is an estimation of a distribution function, and $F(x)$ is the true distribution function, then under the condition

$$M[F^*(x)] = F(x), \tag{4.119}$$

the estimation $F^*(x)$ is unbiased. The difference

$$\Delta F(x) = M[F^*(x)] - F(x) \tag{4.120}$$

is called the bias of an estimation. If this difference is nonzero, then the estimation is called biased.

2. Efficient estimation gives a value, whose dispersion is minimal, i.e. the dispersion of this value is less than the dispersion of a value given by any other estimation under fixed number of realizations or fixed duration of analysis.

3. Sufficient estimation is an estimation, which uses all the information about evaluated probabilistic characteristic contained in the experiments.

4. Consistent estimation is an estimation, which converges in probability to the evaluated probabilistic characteristic when either the number of experiments or the duration of measurements grows unlimited.

Estimation of a certain parameter, which is a number, is called a point estimate. In parallel to this, if an estimation of a probabilistic characteristic is a curve, this estimation is called a point estimation too. In practice the point estimation is often considered as a probabilistically true value. For example, the estimation of a probabilistic mean m^*_x, which is obtained with hardware analysis, is considered to be the true value of m^*_x. Unavoidable fallibility accompanies this operation

$$\Delta m_X = m_X^* - m_X \tag{4.121}$$

Thus there is a question about accuracy and reliability of this estimate. The gauge of reliability is so called belief probability β, which is the probability that the absolute value of the discrepancy continues to be less than some value V, which defines the accuracy of the estimate

$$P[|\Delta m_X| < v] = \beta. \tag{4.122}$$

Equality

$$P\left[m_X^* - v < m_X < m_X^* + v\right] = \beta, \tag{4.123}$$

shows that probabilistically true value belongs to the interval from $m^*_x - v$ to $m^*_x + v$ with probability β. This interval is called confidence interval, and its bounds are called confidence limits.

Dispersion and mean-square deviation of an estimate, which are absolute errors, are often used in the theory of random processes as indicators of accuracy. Sometimes normalized mean-square errors are used too. The normalized mean-square error is the ratio of the mean-square deviation to the true value of the measured characteristic. Sometimes the reduced error, which is the ratio of the absolute mean-square deviation to the maximal value of the measured characteristic, is also used.

Let us discuss some methods of measuring of the mean value, dispersion, mean-square deviation, spectrum and correlation functions of a random process.

It is easy to define the mean value (probabilistic average) on the base of one realization, keeping in mind that the ensemble mean of an ergodic process equals to the time average of one realization

$$M[X(t)] = \lim_{T\to\infty} \frac{1}{2T} \int_{-T}^{T} x(t)dt, \tag{4.124}$$

if this limit exists. It is assumed that realization has limitless duration. In fact any realization is limited in time. The measurement based on the formula

$$m_X^* = \frac{1}{T} \int_{0}^{T} x(t)dt, \tag{4.125}$$

which gives the estimate of the probabilistic average.

Averaging analog device, which works according to formula (4.125), is called an ideal integrator. We can use an integrator, which is designed on the base of a direct current amplifier with deep negative feedback. Another averaging device is a passive low-pass filter.

Let us compare the integrator with the filter as it was done by Mirsky (1972).

1. In comparison with a filter, an integrator is more effective as an averaging device. This is because all the information, which we get with an integrator during the whole period of measuring, is useful, while a low-pass filter forgets the information located beyond the interval of a few response times of a filter. Thus, the integrator accuracy is limited only by the true measuring duration, and low-pass filter accuracy is limited by its response time. Duration of measuring with averaging filter T_f and duration of integration with integrator T_i are in relation

$$T_f > 2T_i. \tag{4.126}$$

This fact is of great importance when we analyze periodically non-stationary processes with period of nonstationarity of tenth fraction of a second.

2. If the response time increases (the bandpass is narrowed) and the measuring time lengthens (if it is possible), then the error of averaging decreases to almost the error of integration over a great interval.

3. The estimate given by the integrator is always unbiased. The estimate given by low pass filter is practically unbiased when $\alpha T > 4$. Here α is the reciprocal value of the filter time constant (Mirsky, 1972).

4. The structure of the low pass filter is simpler than the one of the integrator.

Besides analog methods of averaging there are discrete methods, when the sum of discrete values of a realization, taken over certain intervals, is divided by the number of samples. The mean power of random process is defined by the expression

$$P_X = \lim_{T\to\infty} \frac{1}{2T} \int_{-T}^{T} x^2(t)dt, \tag{4.127}$$

if the limit exists. This characteristic is the averaged square of $x(t)$ but not directly $x(t)$. Therefore, to measure the average power, we have to quadrate the value of the studied random process and then perform the averaging. But the actual measurement is performed during a finite time interval.

The device, which registers the random process, almost always gives on its output the electrical voltage, which replicates the shape of the random process. That is why for short hereinafter we will speak about the value of the random process as about the voltage of a realization.

The mean square of the realization voltage is measured in accordance with

$$\sqrt{\overline{x^2(t)}} = \sqrt{\frac{1}{2}\int_{0}^{T} x^2(t)dt}. \tag{4.128}$$

Unlike the measurement of mean power, here we have to use the extracting of root procedure. This operation is often included in the indicator scale calibration.

The measurement of dispersion is defined by the expression

$$D[X(t)] = \overline{x^2(t)} - \overline{[x(t)]}^2. \tag{4.129}$$

It is reduced to the measurement of alternating component mean power. That is why the device, which measures the dispersion or the mean square, has an element, which centers the realization of the studied process. It is a low-cut filter. The rest of the functional arrangement of this device does not differ from the arrangement of the mean power of the whole process measurement.

The instantaneous spectrum is in fact the output voltage of a real filter. Unlike the analysis of periodic process, the instantaneous spectrum of noise is a random function, which consists of the determinate part and the fluctuating process if the analysis time is a limited interval.

The random process has to be characterized by the power spectrum instead of the amplitude spectrum. Only the power spectrum and the correlation function have the physical sense for the random processes and they can be evaluated theoretically.

The device, which is called the spectrum analyzer, is used for the spectrum measurement. There are several methods of the analysis.

The first is the method of filtration. It is the most well known method. It consists in extraction of the narrow bands of the studied process spectrum with the device, which has selective amplitude-frequency characteristic. The main part of the analyzer is a band-pass filter, which has narrow (in comparison with the spectrum width) pass band.

The second method is obtaining the spectral density with Fourier transform of the random process realization.

The third is the evaluation of the power spectral density on the base of correlation function measuring in accordance with the Wiener-Khinchin theorem.

The fourth method is bundled with using of signum functions.

The fifth method is based on the hardware which uses the concept of the orthogonal functions.

Let us discuss in detail the first method. The others are described in the book of Mirsky (1972).

The functional arrangement of the power spectral density meter, which corresponds to the first method, is shown in fig. 4.26.

While doing the hardware analysis, we ought to consider the uncertainty principle. It is expressed by the relation

$$\Delta f.T = \text{const.} \tag{4.130}$$

Here Δf is the bandpass of the filter, T is the measurement time. It means that the narrower the filter bandpass the larger the measurement time.

There are three ways of the hardware spectrum analysis with bandpass filters: the parallel, the sequential, and the combined.

The parallel analysis is performed with the set of narrow-band filters, each filter is tuned to a certain frequency. When the signal is supplied to all inputs simultaneously, every filter extracts the band of spectrum, which corresponds to its tuning.

The sequential analysis is performed with the single narrow-band filter, whose resonance frequency can be tuned in a wide range of frequencies.

When the combined analysis is used, parallel and sequential methods are coupled in a single device. The studied spectrum separates into several subbands and the sequential analysis is simultaneously performed within these subbands.

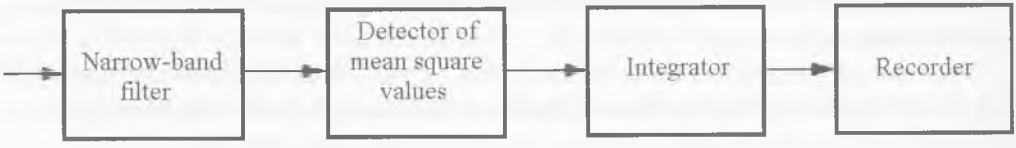

Fig. 4.26. The functional arrangement of the power spectral density meter, which corresponds to the first method. (Redrawn from Mirsky, 1972).

In practice of the experimental hydrodynamic researches they often measure the spectrum of the mean square values, not the spectral power density. In this case the linear detector of the mean square values is used in the analyzer. Satisfactory results can be obtained also when the detector of mean values (the envelope detector) is used. Its indicated values in case of the sine signal and noise differ only by 1 dB. It means that the device with this detector can be graduated with the sine signal and then can be used for the measurement of the spectrum of noise mean square values. The third kind of detectors, so called peak rectifier, is not available for the analyzer as its output voltage strongly depends on analyzed process features.

Thus, the analyzer, which can measure the spectra of both periodical and random processes, has to contain the narrow-band (Δf) filter, the linear detector of mean square (or of mean) values, integrator with a certain time of integration, and the recorder. This analyzer differs from a common harmonic analyzer only by the presence of an integrator. In practice, the recorder, which is connected to the output of the adjustable filter-analyzer, can contain a detector and an integrator. Registration of the spectrum is performed, as a rule, by the logarithmic level plotter. It directly gives the levels of the power spectrum, as

$$20\lg S(\omega) = 10\lg G(\omega), \tag{4.131}$$

where $S(\omega)$ is the spectrum of mean square values, $G(\omega)$, is the power spectrum.

We must pay attention to the features of processing of the measured spectra of the real processes, which are usually the sum of periodic and random processes. When the spectrum is discrete, the values of maximal measured levels of discrete components do not depend on analyzer band Δf. When the spectrum is solid, the registration of the same analyzer of mean square values is proportional to $\sqrt{\Delta f}$. Ordinates of the discrete components and of the solid spectrum have different dimensions. Dimension of ordinates of the discrete components is Nm^{-2} for pressure or ms^{-1} for speed while the dimension of ordinates for the solid spectrum is the dimension of the measured value divided by $(Hz)^{1/2}$. Differences of the features of discrete and solid spectra, which appear in their different dimensions, exist in practice, when the spectrograms of the process measured simultaneously with different analyzers having different analysis bands. Then the levels of discrete components in both spectrograms are the same while the solid part of the spectrum varies as $\sqrt{\Delta f}$.

We should account this difference when the levels of the spectrum are recounted to the band of 1 Hz (subtraction of 20 $\lg\sqrt{\Delta f}$). This is necessary when the spectra of processes, measured with different hardware, are compared. The only levels to be recounted are the ones of the solid spectra. These levels are easily discriminated in

spectrograms, measured with sufficiently narrow-band analyzer. However, when the band of analyzer is wide (an octave or half an octave), the recount can cause errors. Errors take place when the spectrum contains discrete components, which are undetectable under the wide band of analyzer.

4.2.2. Characteristics of non-stationary processes analysis

Heretofore we have discussed the stationary ergodic random process. Let us remind that stationary process is the process, whose mean value and dispersion do not depend on time, and correlation function depends only on time difference τ. The fact, that the absolute magnitude of the correlation function goes to zero when the time span grows infinitely, is the test of ergodicity.

Real processes, strictly speaking, are not exactly stationary and ergodic. However, the studied processes under the acceptable conditions can be considered as stationary and ergodic ones. We can obtain the rough estimate of stationarity on single realization $x(t)$ of the random process $X(t)$. To do it, we have to separate the realization $x(t)$ into n interval, then estimate the mean values on each interval $m^*_{x1}, m^*_{x2}, \ldots, m^*_{xn}$, and m^*_x on the whole realization, then evaluate the dispersion of the estimate $D[m^*_x]$. To consider the process as a stationary process the relative mean square value of the estimate dispersion should be less than a certain acceptable value of α. Then the stationarity criterion

$$\frac{\sqrt{D[m^*_X]}}{m^*_X} < \alpha \qquad (4.132)$$

is satisfied.

Besides, we ought to determine the dispersions (mean square deviations) of the process on different intervals of realization, i.e. for the multiple origins. The founded mean square deviation can not exceed the set value.

In order to decide if the ergodic hypothesis is true, it is rational to obtain the plot of the autocorrelation function and to test whether its absolute value goes to zero when the time span grows. If the studied process does not meet these criteria, this process is a non-stationary and non-ergodic process. We ought to analyze it with methods, designed for this kind of processes. The theory and practice of non-stationary process analysis are far from perfection. However, much has been done in this direction.

Non-stationary random processes are the widest class of processes, which occur in different researches. Even a stationary process, which is limited in time, strictly speaking is a non-stationary process. Besides, any modulated random process is also a non-stationary process.

There are a wide variety of types of non-stationary processes. We discuss only some of these types, which most frequently occur in practice of biohydrodynamic researches.

1. Additive non-stationary process

$$y(t) = x(t) + f(t), \tag{4.133}$$

where $x(t)$ is a stationary random process, $f(t)$ is a deterministic function. If $f(t)$ is a periodic function, then the processes $x(t)$ and $f(t)$ in both of the spectral analysis and correlation analysis are easily separated. Experimental study of such a process is not difficult. In practice such processes occur at the output of measuring system (the multifrequency signal on the noise background).

2. Multiplicative non-stationary process

$$y_1(t) = x(t)f(t) \tag{4.134}$$

or

$$y_2(t) = x(t)z(t), \tag{4.135}$$

where $x(t)$, $z(t)$ are stationary random processes, $f(t)$ is a deterministic function. Noise modulated by periodic process occurs most frequently. For example, the cavitation noise of the screw propeller is modulated by the periodic oscillations, whose main frequency is defined by the rotary speed of the screw propeller.

The other demonstrative example of a multiplicative non-stationary process is the noise, which is emitted by a moving source, such as moving submarine, fish, dolphin, and so. If this noise is received by a motionless hydrophone, then the sound pressure at the hydrophone can be presented by

$$P(t) = P_0(t)\frac{h}{\sqrt{h^2 - (vt)^2}}, \tag{4.136}$$

where h is the distance between the source of sound and the hydrophone, v is the velocity of the source motion, t is the time (it is accepted that $t = 0$ when the source is exactly opposite the hydrophone), $P_0(t)$ is the emitted stationary signal. In this case using of automatic control of the received signal level eliminates the non-stationarity.

3. Quasi-stationary process (almost stationary one). All stationary processes, which are defined on a finite time interval, are quasi-stationary processes. If the interval when a process actually exists is greater than its correlation window, such process is analyzed with the methods developed for stationary processes. The more this relation, the closer such a process to a stationary one.

4. Periodic and almost periodic non-stationary random processes. The statistical characteristics of these processes vary periodically or almost periodically. The processes,

Fig. 4.27. The oscilloscope pattern of the pressure pulsations in the boundary layer of an active swimming dolphin.

which take place in a boundary layer of dynamically moving aquatic animals (fish, dolphins, squids, pinnipeds) are just the same processes. While in active swimming the pressure and velocity pulsation in the boundary layer of these animals is modulated by the body undulation so that the spectrum of pulsation varies periodically according to the phase of the undulation. The oscilloscope pattern of such process is shown in fig. 4.27. There is the pattern of pressure pulsation in the boundary layer of a dolphin while in active swimming.

Analysis of such processes is very difficult when the period of non-stationarity is comparable with its correlation window. In this case we can define statistical characteristics of the process only on the ensemble of realizations with the exact adjustment of the realizations origins. When the period of non-stationarity is significantly greater than the correlation window, we can consider that the process is stationary on the interval, which is sufficiently less than this period and sufficiently greater than the correlation window. In this case we can use the methods of analysis, which are developed for stationary ergodic processes. We can a priori consider that a process is to a first approximation ergodic, or we can test the ergodicity by the methods described above. As a rule, the period of non-stationarity of the random processes, which evolve in the boundary layer of the sea animals, is sufficiently greater than the correlation window. The period of non-stationarity is of 200 – 300 ms, the correlation window is 3 – 4 ms.

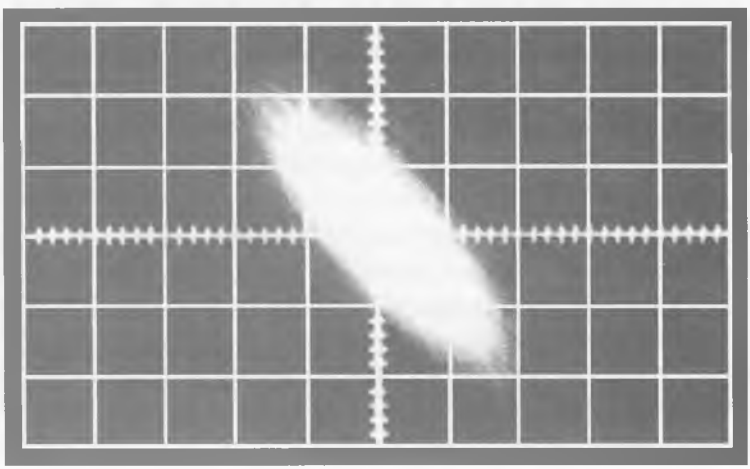

Fig. 4.28. The oscilloscope pattern of the correlation ellipse.

This relation permit to believe that the process is quasi stationary and to analyze experimental data on single realization.

Optimization of the procedure of statistical measurements is very important for minimization of the summary error of non-stationary process analysis (Olshevsky, 1973). Errors of the statistical measurements can be classified on their exercise or on their specific features. We ought to separate the errors of fluctuation and the errors of biased estimation. Errors of fluctuation are random errors, their values alter from one measurement to another. Bias errors are systematical errors and occur again in every measurement. However it does not mean that the bias of an error is known and can be anyhow compensated and reduced to zero. The summary error of the statistical measurement has minimum at the certain value of the smoothing (averaging) interval. This value equals to the time interval of the process realization, which is less than the period of non-stationarity and greater than the correlation window size. The fluctuation error decreases as the smoothing interval grows, but the bias of estimation increases because the process more and more differs from quasi stationary. When the smoothing interval decreases, the bias of estimation also decreases, however the fluctuation error grows. Practically, we ought to measure the needed statistical characteristic (for example, correlation function) several times with different smoothing intervals and then decide, which has the least error.

We give here only a general view of the optimization of the statistical measurement procedure. In reality this optimization (especially the adaptive optimization) is very difficult. It is reduced to multi-stage processing of the studied process.

There are special purpose devices for the analysis of the random processes. We often need an express estimation of mutual correlation coefficient for two processes. It can be done with a usual oscilloscope. The first studied signal is supplied to the vertical deflector, and the other to the horizontal deflector of a cathode-ray tube. In this case the

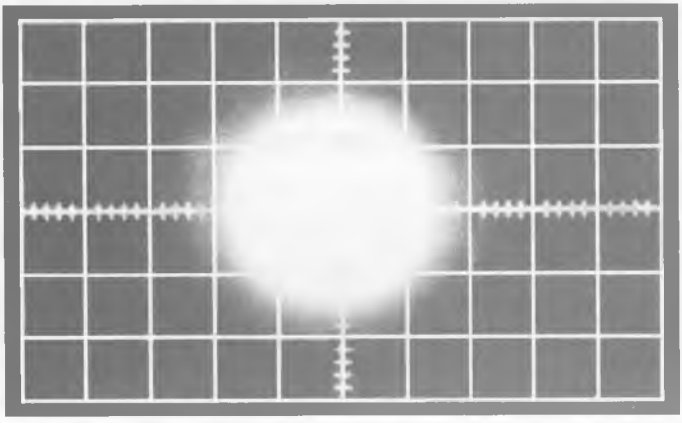

Fig. 4.29. The oscilloscope pattern of the correlation ellipse when the correlation coefficient is close to zero.

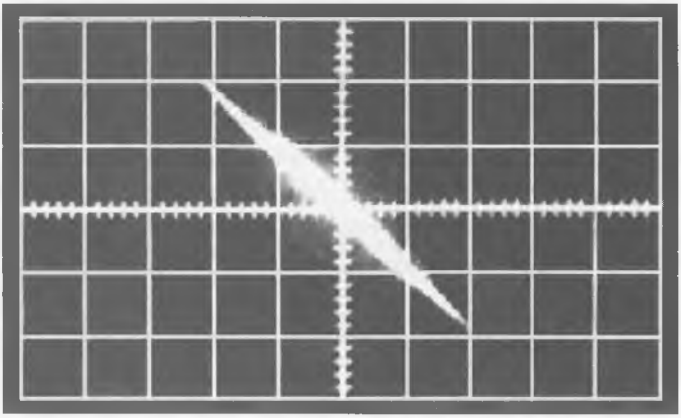

Fig. 4.30. The oscilloscope pattern of the correlation ellipse when the correlation coefficient is near one.

deflections of the light spot on the tube screen induced by these signals are perpendicular to each other. As a result, the light spot on the screen delineates Lissajous figures. The photograph of this pattern, with a long exposition, gives a figure, which is the correlation ellipse (fig. 4.28). If a and b denote correspondingly the longer axis and the shorter axis of this ellipse, then the correlation coefficient is defined by the expression

$$R \approx \frac{a^2 - b^2}{a^2 + b^2}. \tag{4.137}$$

When the correlation coefficient is close to zero, the distinction between the ellipse and a circle is very small (fig. 4.29). In this case the precise measurement of the values of a and b is very difficult. Therefore, it is difficult to measure the correlation coefficient too. The same difficulties exist when the correlation coefficient is near one. Then the ellipse becomes an almost straight line of varying thickness (fig. 4.30).

Brief conclusions

This chapter does not directly concern the research of the fish and dolphin hydrodynamics. Its aim is to give the initial knowledge of the statistical hydrodynamics to those, who research the fine structure of the boundary layer on fish and dolphins. The fact, that in chapter 6 we could reference only a few experimental works, shows that in this field there are wide prospects for further researches.

CHAPTER 5. DEVICES AND METHODS FOR EXPERIMENTAL KINEMATIC AND HYDRODYNAMIC STUDIES

The hydrodynamics of fast-swimming animals has been of great interest to scientists for a very long time. It was almost fifty years ago that certain questions were formulated which we still wish to be answered. We mean the pattern of streamline flow of fast-swimming fishes and dolphins, as well as their drag coefficient when moving under water. During these fifty years, various methods of research have been tested, but the results proved to be more than just modest. The reason seems to be in the fact that the methods applied so far should be qualified as indirect ones, they cannot answer these questions unambiguously. Among the above methods we can mention, for example, the morpho-functional study, visualization of streamline flows around the animal's body, calculations of thrust and of drag according to cine film records. Such methods provide only qualitative evidence about the phenomenon under examination. As to quantitative data, they can be obtained by direct instrumental measurements of the processes in question. In particular, the pattern of the animal's streamline flow may be examined by direct measuring of the boundary layer structure.

5.1. Devices and methods for biohydrodynamic studies

5.1.1. Receptors of pressure pulsations meant to work on dolphins

The methods of studying the pressure pulsations in the dolphin's boundary layer principally differ from those for similar studies effected on rigid bodies. In case of the latter, the pulsation sensors are usually flushed with the streamlined surface. With this, all constructive elements of the sensor are installed inside the streamlined body. As to the dolphins, to install a pulsation sensor as flushed with their skin is simply impossible. At best, one can implant a sensor under the dolphin's skin, but in such case the sensor will be separated from the boundary layer by the layer of skin, no matter how thin it may be. This will, undoubtedly, considerably diminish the sensitivity of the sensor and change the effective diameter of its receiving surface. Such process will be hard to control. There is only one possibility left - to be oriented by sensors of pressure pulsations which are in various ways installed on the skin surface of a dolphin. Several versions of such devices were designed and employed to study the hydrodynamics of dolphins (Romanenko, 1971, 1976a).

The first version of such receptor is that of pulsations, flushed with some streamlined coverplate glued (or attached in any other way) to the skin of the dolphin at the point of measurements. In this case, all constructive elements of the receptor are mounted in the body of the coverplate. The scheme of such receptor with its coverplate, fixed on a dolphin's skin, is displayed in fig. 5.1. Here, 1 is the receptor of pulsations, 2 is the

cable, 3 is the coverplate (the streamliner). This version has all positive features typical for standard receptors of pulsations used on rigid bodies, namely: its receiving surface may be made sufficiently small and flushed with the streamlined surface, etc. However, the use of such receptors on dolphins involves a number of difficulties. First, the streamlined coverplate has an input edge which may affect the pattern of streamlining at the point where the receptor of pressure pulsations is situated, this impact may be hard to control. Besides, the area of contact between the coverplate and the dolphin's skin should be large enough to provide for its good streamlining. As a result, in the vicinity of the sensitive element, within a large area, it will not be the skin under streamlining but the coverplate, i.e. the rigid body, and the streamlining conditions for such rigid body differ from those for the skin. Then, if the coverplate is large, it may hinder the bending of the body (the skin) at the point of its location.

Nevertheless, such version of the receptor was designed and considered, along with other versions, as a possibility for practical use on dolphins. Fig. 5.2 shows the scheme of such receptor of pulsations. Its construction employs the principle of pressure transformation with the view of increasing the sensitivity. The receptor is designed in the following way. A piezoceramic plate 3 is pinched between two halves of the metal carcass 1. The lower end of rod 2 touches the end of plate 3 and its other end passes through the layer of hermetic composition 4, being polished flushed with the upper streamlined surface of carcass 1. This polished butt end of rod 2 serves as a receiving surface of the device. Fig. 5.3 separately demonstrates the piezoceramic plate 3, which is a sensitive element. The plate has electrodes 5 and 6. It is polarized on the surface in such a way that the polarization vector $\bar{P}$ in the clearance δ between the electrodes could be directed as shown in fig. 5.3.

One electrode (fig. 5.2) is in immediate electric contact with the carcass. Electrode 5 is connected with the central conductor of the coaxial cable 7 linking the receptor of pulsations with the measuring circuit. The cable screen is directly connected with the carcass.

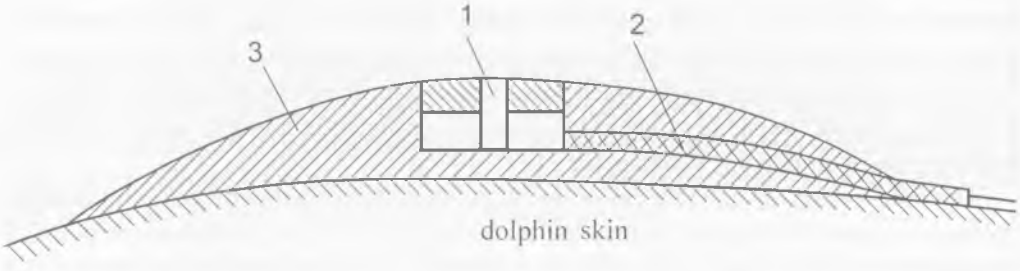

Fig. 5.1. The scheme of a meter of pressure pulsations with its coverplate, fixed on the dolphin's skin (the first version): 1 – meter, 2 – electrical cable, 3 – coverplate.

When fully assembled, the receptor of pulsations is polymerized into epoxy resin in the way displayed in fig. 5.1. Here, 3 is the coverplate (the streamliner) made of epoxy resin.

The receptor of pulsations works as follows. Pressure pulsations impact the rod butt 2 polished flushed with the streamlined surface, and through this rod butt they are transferred to the end of plate 3. Due to their impact, the plate gets bended. Since one end of plate 3 is pinched, the impact of the force upon its free end will induce mechanical strains inside it. The strains will be maximum near the point of pinching (where the clearance between the electrodes is). As a result, an electric potential will emerge on the electrodes. By cable 7 the potential will be transferred to the measuring circuit. The sensitivity of such receptor of pulsations depends upon the type of piezoceramics employed and may be of scores of mcv/Pa.

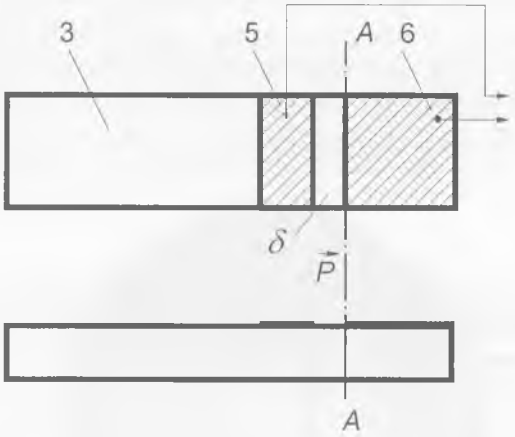

Fig. 5.2. The sensitive element: 3 – a piezoceramic plate; 5,6 – the electrodes.

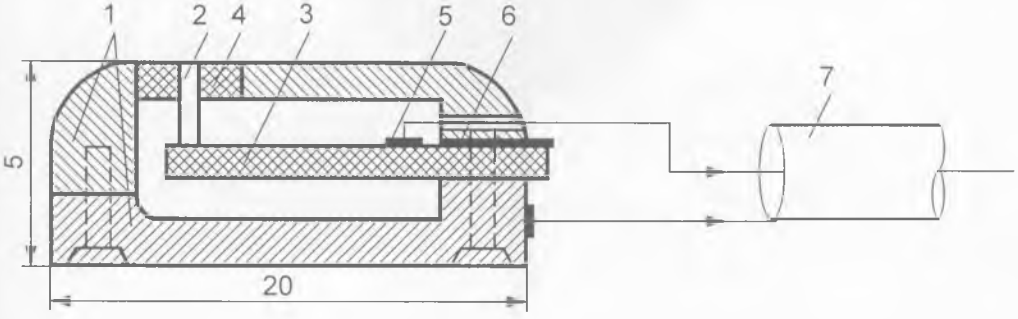

Fig. 5.3. The scheme of a meter of pressure pulsations: 1 - a metal carcass; 2 – a rod; 3 – a piezoceramic plate; 4 – a hermetic composition; 5,6 – the electrodes; 7 – a cable.

Fig. 5.4 shows a picture of such receptor of pressure pulsations.

The second version of this device differs from the first one which has a serious drawback. The first receptor of pulsations can register them only on the streamlined surface alone. It is impossible, for instance, to measure pulsations at any point of the boundary layer or beyond its limits, while such data may be extremely important when examining the pattern of dolphins' streamlining. It was this very drawback that compelled us to design another construction of the pulsations receptor. The new device is presented in fig. 5.5. Here, 1 is the sensor made as a thin round-sected rod of piezoceramics.

Fig. 5.6 separately demonstrates the sensor with the following dimensions: 1.5 mm in diameter, 7 mm in length. The rod has two ring-shaped electrodes 2, the piezoceramics in the clearance between them was polarized on the surface (vector $\vec{P}$). The rod is jammed over the area of the larger electrode between the two halves 3 of the streamlined brass body; the latter is 5 cm long and 0.5 cm in diameter. With that, the larger electrode is separated from the body by means of a Teflon lining 7. The smaller electrode is linked with the body and the larger one - with the entrance of a special electronic device 10 having a high input impedance 11. The electronic device is installed inside the receiver body. The exit of the device is connected with the central core 5 of the screened cable 4

Fig. 5.4. A picture of a meter.

and then with the elements of the registering system. The input impedance 11 is about 100 megohoms. When assembled, both halves of the body are fastened by screws 8 and 9. The internal cavity of the body is filled with a pressurizing mixture which is a melt of wax and rosin in proportion of 1 to 1. The same melt covers the place where the rod is jammed by the body 6. The end of the rod 1, protruding outside, is not covered with the melt. This section is about 1.5 mm in size and can be regarded as the size of the receiving surface.

Such pulsation receiver can be installed in any point of the boundary layer and even beyond it. With that, the sensitive end of the rod 1 should be directed towards the flow.

The sensor of the pulsation receiver may be made not as a circular rod but as a tetragonal one (fig. 5.7) with its receiving end rounded. In this case, the electrodes are installed on the two opposite longitudinal facets of the rod. Polarization is effected throughout the rod thickness. To manufacture such sensor is much easier than the circular one with its ring-shaped electrodes.

The described pulsation receiver can also work without the installed entrance electronic device. In this case, the larger electrode of the sensor is connected directly with the central conductor of the screened cable. As a result, the sensitivity becomes considerably decreased (by 2 or 3 times). But the technology of making the receiver gets greatly simplified.

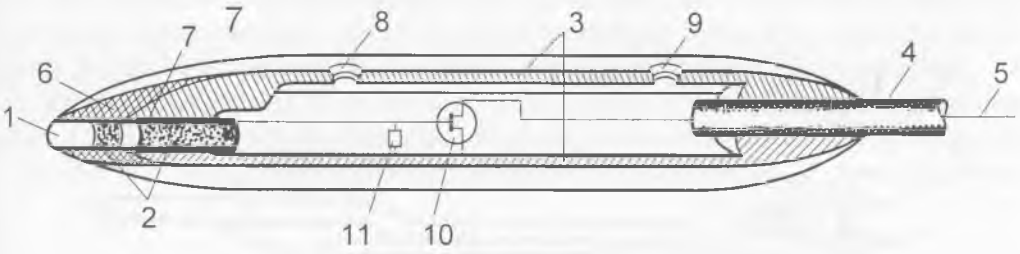

Fig. 5.5. The scheme of a meter (the second version): The designations are in the text.

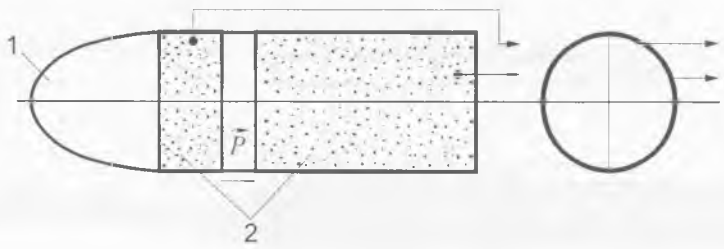

Fig. 5.6. The sensitive element: 1 – a piezoceramic rod of a circular section; 2 – the electrodes.

There is another (third) version of the pressure pulsation receiver (fig. 5.8). It is designed in the same way as the previous one. The difference is in the shape of the sensor, which is made as a thin piezoceramic platelet 1 with two electrodes 2 (as in the first version). The piezoceramics is polarized along the surface in the clearance between the electrodes $\bar{P}$. The platelet is jammed in the streamlined body 3 at the level of the clearance between the electrodes (along the line *AA*); it works for deflection. The protruding end of the platelet is rounded, the rest of the technology is similar to that described above. The larger electrode of the platelet is connected with the conductor 5 of the screened cable 4.

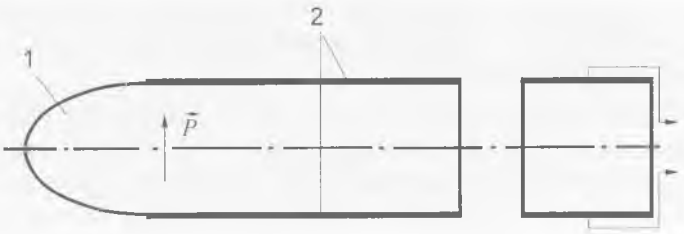

Fig. 5.7. The sensitive element: 1 – a piezoceramic rod of a square section; 2 – the electrodes.

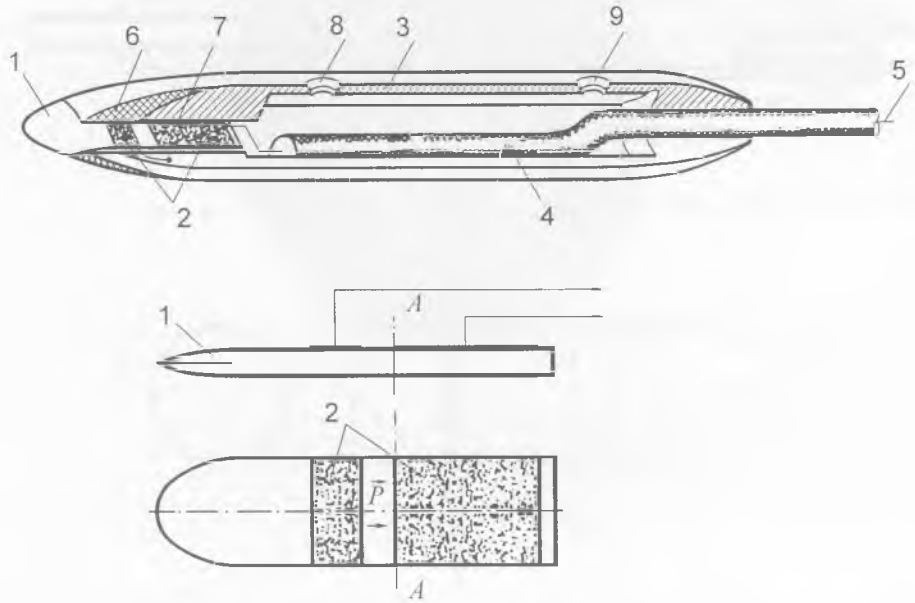

Fig. 5.8. The scheme of a meter and sensitive element (the third version). The designations are in the text.

Application of the thin platelet as a sensor greatly (more than by one order) heightens the sensitivity of the receiver, because one uses the transformed mechanical strains. The platelet employed as a sensor is of the following dimensions: 0.5 mm thick, 2 mm wide and the length from the receiving end to the clearance is 3 mm. The total length of the platelet is 7 mm.

This version of the pressure pulsation receiver, like those described above, may be manufactured both with a built-in matching electronic device and also without it.

The holders of the receivers are rather intricate in their construction; their outside diameter is 5 mm. This is preconditioned by the necessity to assemble a matching electronic device into such body. However, when the receiver can work without its electronic device, the technology of making the receiver can be simplified. In the latter case, the receiver body is only of 2 mm in its outside diameter and is shaped as a pipe. Such receiver permits more detailed studies of the boundary layer structure.

Fig. 5.9 shows pictures of the pulsation receiver with its sensor shaped as a circular rod and as a platelet.

The make-up of pressure pulsation receivers easily allows to isolate the device from pressure pulsations by using a special cap filled with air and invested onto the receiver. In such cases, the receiver will register only interference of all kinds (vibrations, the microphonic effect of the screened cable, radio disturbances, the turbulent noise on the irregularities of the receiver body, the electrical activity of the muscles, etc.). In this way, one may estimate the overall level of various interference so that to compare it with the level of pressure pulsations. This possibility is very important in terms of metrology.

If pulsation receivers are isolated by caps filled with water, they will register the overall level of an interference admixed with the acoustic noise generated by the boundary layer. By precluding such interference during the analysis, we may get some idea about

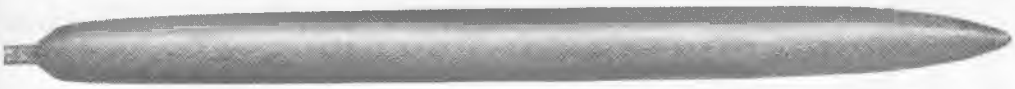

Fig. 5.9. A picture of a meter with sensitive element with its sensor shaped as a circular rod.

Fig. 5.10. A picture of a meter with sensitive element with its sensor shaped as a platelet.

the acoustic component of the turbulent noise. This may prove very important when examining the noisiness in the propellent complex of the biological object. Nevertheless, such possibility exists only when the pulsation receiver is sufficiently sound sensitive.

To illustrate the working capacity of the pressure pulsation receivers discussed above, fig. 5.11 displays three spectra of pressure pulsations. The upper spectrogram was

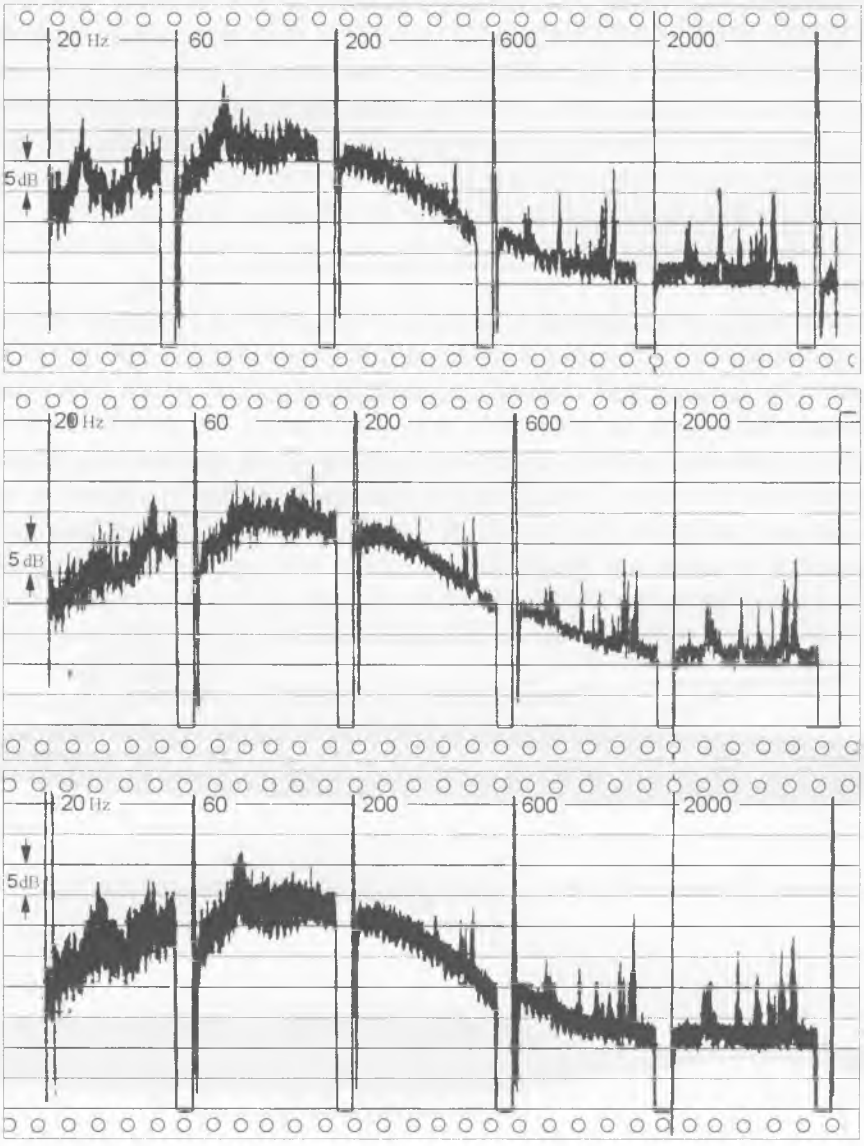

Fig. 5.11. Spectra of pressure pulsations.

obtained by using a traditional pulsation receiver installed as flushed with the streamlined surface. The middle spectrogram was derived by using a pulsation receiver with its sensor made of a piezoceramic platelet. The lower spectrogram shows superposed spectra. One can see that the spectra practically coincide. With that, the parameters of the flow under measurement remained unchanged.

Fig. 4.27 presents an oscillogram of pressure pulsations registered in the dolphin's boundary layer by means of a pressure pulsation receiver with its sensor as a platelet.

5.1.2. Receptors of velocity pulsations

At present, the most frequent method to measure turbulent velocity pulsations is still that of using a hot-wire anemometer (Hintse, 1963).

A hot-wire anemometer is such a device in which the sensitive element is a fine platinum wire heated by electric current. The wire is placed into the onflowing stream of gas or liquid. Since the temperature of the wire is higher than that of the stream, the latter cools the wire. The extent of such cooling depends on the velocity of the stream and on the physical properties of the wire and the medium. Measuring the extent of cooling in this or that way, and knowing the physical properties of the medium and of the heated element, we can rather reliably identify the stream velocity.

The extent of cooling can be measured by two methods: directly by using a thermocouple or a thermistor, and by measuring the resistance of the wire. The value of such resistance is unambiguously associated with the temperature.

The hot-wire anemometers are employed to measure both permanent and variable (pulsating) streams. However, the hot-wire anemometers have very serious limitations. First, their work involves an intricate scheme for wire heating. Besides, the wire should be very fine (about 5 mcm in diameter) and short (0.5 - 1 mm long). The thickness of the wire determines its thermal inertia, which must be the minimum possible; its length determines the frequency range of pulsations, which can be measured with its help. These difficulties are purely technical. But there are others, which are quite principal. Among them is the nonlinear pattern of dependence between the velocity and the temperature. In addition, the thermal inertia of the wire implies essential limitations too, because it worsens the parameters of the hot-wire anemometers, limiting them within the high-frequency range of the stream velocity pulsations. As a rule, the hot-wire anemometers are used to measure the turbulence in gases.

The hot-wire anemometer proves to be less suitable to measure dropping liquids. The thing is that the working temperature of the wire should be very low there because of possible evaporation and scaling.

Besides, there can also be the case of electrolysis, which may lead to numerous troubles. The force impact of the stream of liquid upon the wire is much greater than

that of gas. Therefore the wire should be sufficiently strong (hence, its diameter should be larger), and this may enhance the thermal inertia.

Nevertheless, the hot-wire anemometer may well suit to measure velocity pulsations in the boundary layer of the dolphin (Kozlov, Shakalo, 1970; Shakalo, 1969, 1972). Special steps were taken to preclude any water electrolysis (the diminished voltage on the wire). From time to time, the wire was ultrasonically cleaned from pollution.

Besides such wire hot-wire anemometers, filmy ones are occasionally used too. The sensitive element there is made of a very fine platinum wire specially heated for the occasion. The film is 1 mm long and 0.22 mm wide. It is fused on some glass or ceramic backing shaped as a wedge. As far as we know, such hot-wire anemometers have not yet been employed in biohydrodynamics. But it seems likely that their potentials are not worse than in those made of wire.

The experience gained in using the hot-wire anemometers for biohydrodynamic measurements proves to be rather positive. Nevertheless, the above limitations in working with them and their limitations mentioned above, make it necessary to look for new methods to estimate the turbulence in liquids.

To our mind, rather interesting is the method of electromagnetic induction which has already found its recognition for measuring turbulent pulsations of velocities in conductive liquids (Hintse, 1963). The method is based upon the phenomenon of induction of an electric field in some conductive liquid streaming in an electromagnetic (or magnetic) field. The intensity of this induced field is unambiguously determined by the velocity component perpendicular to the electromagnetic field. It proves to be directly proportional to this component and to the intensity of the electromagnetic field

$$V = \frac{\mu}{c} HU \,, \tag{5.1}$$

where μ is the relative magnetic permeability of the liquid, c is the velocity of light, H is the intensity of the electromagnetic field, U is the velocity component perpendicular to the electromagnetic field.

The direction of the induced field is perpendicular both to the velocity component U and to the magnetic field. It can be found by the well-known rule of the left hand.

To measure the value of the induced electric field, it is necessary to introduce two electrodes to the liquid in such a way that the line connecting the electrodes should be perpendicular both to the direction of the velocity pulsations under measurement and to the magnetic force lines simultaneously. In this case, the potential difference on the electrodes E is found in the following way

$$E = Vs = \frac{\mu}{c} HUs, \tag{5.2}$$

where s is the value of the clearance between the electrodes.

The main advantages of this method are the following: the linear dependence E on the value of velocity pulsations; complete independence on the properties of the liquid (its density, viscosity, temperature, electroconductivity, composition). Electrodes should be made of such materials which prove resistant to the chemical effects of the liquid and do not get polarized. If there is any danger of polarization, the electromagnetic field should be alternative. But in such case there is another danger - that of an electromagnetic interference, when weak potentials are measured. The electromagnetic impact may involve either the entire field of the stream or only that of its section which is under measurement. The first electromagnetic field impact is convenient when measuring the streams, which are uniform throughout the entire flow field. When measuring some non-uniform streams (in the boundary layers), the second method is more preferable because it is not necessary to consider the impact of locally induced currents caused by the non-uniformity of the stream.

Devices for measuring velocity pulsations, when they are based upon the method of electromagnetic induction, are difficult to be made sufficiently small. This is the principal drawback of such method. Nevertheless, Varich (1969, 1970a,b; 1971) designed and used such a meter of velocity pulsations when examining the streamlining of live crabes. His method was based upon electromagnetic induction. The meter was a square permanent magnet 1mm thick and 5 mm wide. Its field contained platinum electrodes, each 1 mm thick. The distance between the electrodes was 4 mm. Such meter permitted to register velocity pulsations without any errors. The scope of the pulsations was much above 4 mm. With the help of such meter one can hardly get a very good idea about the pattern of streamlining around a live object. Such meter should be rather used to assess some averaged velocity of the stream. When measuring velocity pulsations, the distance between the electrodes and their size should never exceed 0.5 - 1 mm.

A smart method to estimate velocity pulsations in a conductive liquid was offered by S. Eskinasi (1958). The essence of his method is in that two electrodes are used to register pulsations. The electrodes are installed in the stream of conductive liquid and a small potential difference is applied to them. This difference is supposed to provide such current between the electrodes that never exceeds 10 - 30 mca. With a low current, the electrodes do not yet have bubbles of hydrogen (there is no electrolysis). The velocity pulsation in the stream leads to conductivity fluctuations of the electrolyte in the clearance between the electrodes and, hence, to fluctuations in the streaming current, which are the ones to measure. For the sake of concrete geometry of the electrodes within their clearance, the current through the clearance reveals the function of the applied potential and of the transfer velocity of the conducting medium.

The author (Romanenko, 1974, 1976) also designed an electrochemical method to assess velocity pulsations. In our mind, it seems very promising not only for hydrodynamic studies but especially for biohydrodynamic ones.

The method is based upon Debye's effect (1933). It regards the difference between dynamic reactions of solvated ions of the electrolyte to the movement of the medium particles. Anions and cations differ by their effective masses and their friction coefficients. As a result, when a medium has some velocity pulsations, a potential difference appears there (the so-called vibrational potential) between two points divided by the final distance towards the action of pulsations. This potential difference can be registered by means of two electrodes placed in the field of velocity pulsations.

The theory of the effect was explained by Debye himself. However, his theoretical conclusions somewhat contradict the experiment. The thing is that according to Debye, the effect must not exist in clean liquids, while the experiment demonstrates that in clean liquids this effect is manifested even better than in electrolytes.

An attempt to explain this phenomenon was made by Weinmann (1950, 1960). He offered a phenomenological theory of the effect, having suggested that in addition to Debye's effect there is another one, associated with the density gradient of the liquid within the field of velocity pulsations. Weinmann offered his theory as applied to the acoustic field. However, this theory seems to be also applicable to hydrodynamic velocity pulsations when some density gradients may exist within their field.

Weinmann gives a general formula for this effect, which looks as follows:

$$|\Phi_{\max}| = \frac{a_0 \left[(Sc\nu M_H / e)^2 + (\Phi_\infty / a_0)^2 \right]^{1/2}}{\left[1 + S^2 \right]^{1/2}}, \tag{5.3}$$

where

$$S = \frac{4\pi L}{\varepsilon \omega} \tag{5.4}$$

and

$$L = \sum_j \left(\frac{e_j^2 n_j}{\rho_j} \right), \tag{5.5}$$

e_j are the ion charges, n_j is the equilibrium concentration (of ions/cm^3), ρ_j is the friction coefficient, M_H is the hydrogen atom mass, e is the electron charge, L approximately equals the specific conductivity of the electrolyte, $\nu \equiv 12$ is the quantitative characteristics of pure Debye's effect, Φ_∞ is the peak potential with infinite dilution of the electrolyte, a_0 is the vibrational velocity of liquid particles, $\omega = 2\pi f$, f is the frequency of vibrations, c is the sound velocity.

Formula (5.3) differs from Debye's one with Hermans' amendment (1938) only by its member $(\Phi_\infty / a_0)^2$. Experiments yield 15 mcv/cm/sec for the value Φ_∞ / a_0 in water. With the growing concentration of the electrolyte, the calculated value $|\Phi_{max}|$ changes in good agreement with the experiment. In this way, the phenomenological theory of Weinmann quite well explains the experimental results, providing an unambiguous dependence of the vibrational potential value upon the vibrational velocity. With that, in case of clean water, as it was mentioned above, the vibrational potential equals 15 mcV/cm/sec. In case of electrolytes, this value will be smaller.

If Weinmann's theory is valid not only for acoustic phenomena but also for hydrodynamic ones, this may open certain possibilities. The thing is that the level of velocity pulsations in a turbulent liquid stream comprises 5 - 10% of its average velocity. For example, with the stream velocity of 10 ms^{-1}, the velocity pulsations may reach values of about 1 ms^{-1} and the value of the vibrational potential proves to be quite measurable.

As it was mentioned before, the vibrational potential can be measured by means of two electrodes placed in the field of velocity pulsations and attached to an ordinary amplifier and a recording device. But the vibrational potential may be also measured in one point relatively to the surrounding liquid by using only one electrode placed into the point of measurement. The role of the second electrode may be played by a metal rod of the measuring electrode isolated from it but still having its electric contact with the surrounding liquid. On its own surface it averages the potential of the liquid.

It was exactly in this form that we designed and manufactured our meter of velocity pulsations offered in this paper and displayed in fig. 5.12.

A central electrode 1 is a sensor. It is made from platinum wire (diameter equal to 0.3 mm). A tube 2 is a holder. It is made from brass (external diameter equal to 3 mm). The sensor is insulated from the holder and it is attached by the copper wire 3 to a central wire of a cable 4. The velocity pulsation meter must be positioned in the flow so that its sensor is opposed to the flow.

Fig. 5.13 shows velocity pulsation spectrum which has been recorded in the boundary layer of a rigid body positioned in a hydrodynamic tube. The velocity of flow over the body was 5, 15 and 25 ms^{-1}. The sensor was positioned at 1.5 mm relatively a flow over the surface. The thickness of the boundary layer was 6 – 8 mm.

The velocity pulsation meter offers a few advantages over the thermoanemometer. It is very simple, strong and has no need of a complex electronic circuit. An input impedance of meter is defined as a conductivity of water. In operation the meter is connected with

Fig. 5.12. The scheme of a meter of velocity pulsations. The designations are in the text.

obvious wide-band amplifier. A sensitivity of the meter is the order of one or more of mcV/cm/s. Band of operation frequency is without limit practically.

In their publication of 1965, Siddon and Ribner describe a device, which they call a piezoelectric anemometer. The authors believe their device to respond to transversal velocity pulsations. Their anemometer is meant to measure velocity pulsations in gas streams. However, when covered with hermetic compositions, it seems to be applicable to liquids too. Fig. 5.14 shows its scheme. The receiving element is a foil platelet 1 (*a*) of rectangular or circular shape (*b*). The platelet is fixed on an end-convergent support 2 glued with a piezoelectric sensitive element 3. The support has a preventive (safety) cap 4.

The elementary theory of its construction is as follows: let the foil element be approached with a stream of velocity V at the attack angle α (u and v – longitudinal traverse and cross traverse velocity pulsations respectively). In the turbulent stream, V

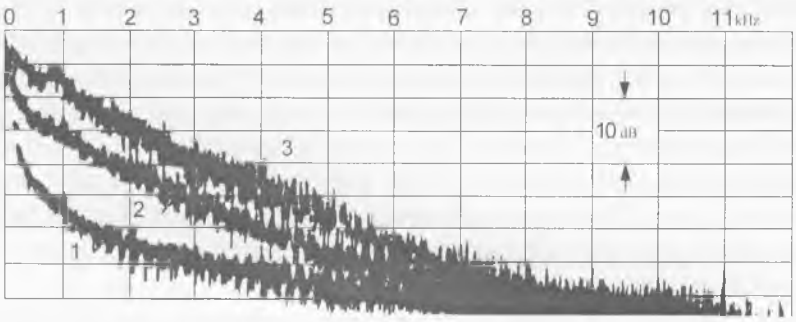

Fig. 5.13. Spectra of velocity pulsations in the boundary layer. The speed of flow: 1 – 5 ms^{-1}, 2 - 15 ms^{-1}, 3 - 25 ms^{-1}.

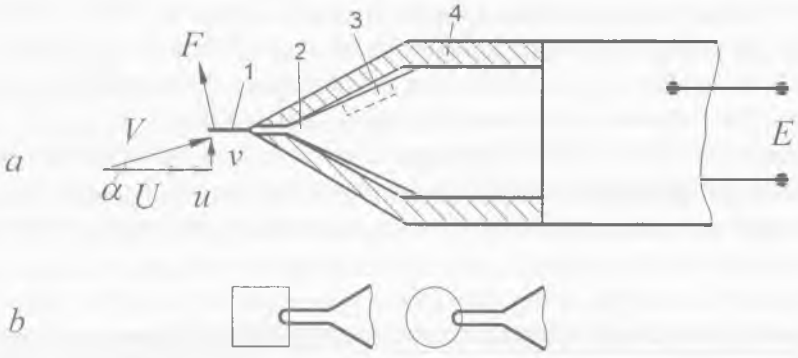

Fig. 5.14. Scheme of piezoelectric anemometer. (Redrawn from Siddon, Ribner, 1965). The designations are in the text.

and α randomly change. Suggesting that the frequency is not very high, we may assume that there is a quasi-stationary linear approximation for the lifting force which is valid at any moment of time:

$$F = \frac{1}{2}\rho V^2 S \frac{dC_F}{d\alpha}\alpha, \tag{5.6}$$

where ρ is the density of the environment, V is the stream velocity, S is the area of the foil platelet, $dC_f/d\alpha$ is the coefficient of the lifting force changed with the attack angle. Then, following the accepted approximation, α we can substitute by v/V and V by U. Then we obtain:

$$F = \frac{1}{2}\rho US\left[\frac{dC_F}{d\alpha}\right]v = kE. \tag{5.7}$$

In this way, in the region with the common signal linear in terms of the lifting force, the voltage E is proportional to v, with the coefficient of proportionality depending upon the local velocity of the stream U.

In the real construction, the receiving element was made as a disk with the diameter of about 1.8 mm. The support (holder, bracket) was conical and made of aluminum.

The authors tested their anemometer in a circular air jet and compared the data with those from a thermal flow-meter. The spectra registered by the piezoelectric anemometer and by the thermal flow-meter proved to coincide within the range of frequencies from 40 to 4000 Hz. Based on this, it is believed that the piezoelectric flow-meter does register transverse velocity pulsations in the stream.

5.1.3. Estimation of the effective size of the receiving element in the meter of velocity and pressure pulsations

The size of the receiving element in the meter of velocity and pressure pulsations is one of its most essential parameters. Likewise in acoustics, to receive a non-disturbed acoustic signal with an intricate frequency spectrum, is only possible when using a sound receiver which is small in size, as compared with the wave length of the very high-frequency component of the spectrum. In case of hydrodynamic measurements, the size of the sensitive element of the pulsation meter should be smaller than the minimum scale of turbulence to be registered. To be more exact, the size of the sensitive element of the meter must be less than one half of the measured scale of turbulence. When this condition is observed, the impact of velocity or pressure pulsations does not change the sign throughout the entire surface of the receiving element and the sensitivity

of the latter is found to be the utmost. In view of this, one should chose such size for the receiver that it could meet the inequality below:

$$d << \frac{1}{2}\frac{U}{f}, \tag{5.8}$$

where U is the velocity of the oncoming stream, f is the frequency of pulsations under measurement. For frequencies

$$f >> \frac{U}{2d} \tag{5.9}$$

several characteristic scales of turbulence can be displayed within the limits of the maximum size of the receiver. Its sensitivity to pulsations is diminishing because the acting pulsations change their sign within the receiving element. With that, the receiver will average the impact of all scales of turbulence, while the cumulative voltage at its output may only decrease. In this way, it is extremely important to assess the effective size of the sensitive element of the receiver, so that to preclude any serious errors in measurements.

In case of the hot-wire anemometer and the electrochemical receiver of velocity pulsations described above, the effective size practically coincides with the length of the platinum wire directly contacting the medium.

The receiver of velocity pulsations based upon the phenomenon of electromagnetic induction the effective size is determined by the distance between the electrodes and by the size of the electrodes themselves.

The effective size of the piezoelectric anemometer of Siddon and Ribner (1965) depends on the size of the foil platelet.

In the above described piezoelectric meter of pressure pulsations (the second version) the effective size practically coincides with the transversal section of the small piezoceramic rod which is the sensitive element, irrespective of its shape(circular or square).

To define the effective dimensions in the piezoelectric meter of pulsations (the first and the third versions) is not so simple. Let us try it (Romanenko, 1971b, 1976). We shall begin with the first meter. Here, rod 2 serves as the receiving element (see fig. 5.2.) which with one of its end is touching the piezoceramic plate 3, while its other but end is glued into the hermetic 4 as flushed with the streamlined surface of the carcass 1. At the first sight, it may seem that the size of the receiving element should coincide with the rod diameter. But in reality it comes out that in this case the effective size of the receiving element is considerably larger, depending not only on the diameter of the small rod but also on that of the hermetic.

The scheme of such a receiver can be presented as in fig. 5.15. If we use the terms of the elasticity theory, it is possible to say that the piezoceramic plate 1 is pinched with one of its ends while the second one is hinged with the rod 2 which is rigidly fixed along its counter with the inner counter of the hermetic 3. (such fixation is equal to that of the internal counter of the plate in the hermetic 3). The external counter of the hermetic plate 3 is also pinched (q is the external pressure affecting the plate). It is feasible to divide the scheme in fig. 5.15 into two parts, as it is done in fig. 5.16 *a*, *b*.

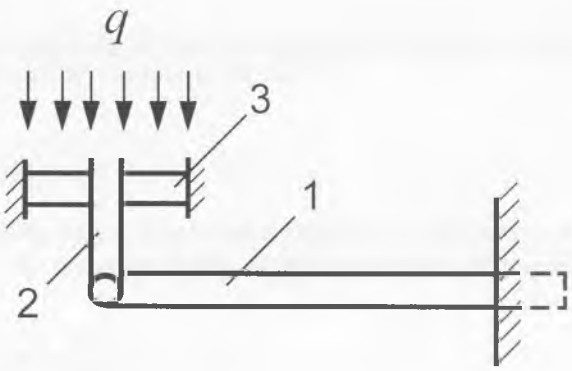

Fig. 5.15. Scheme of a meter. The designations are in the text.

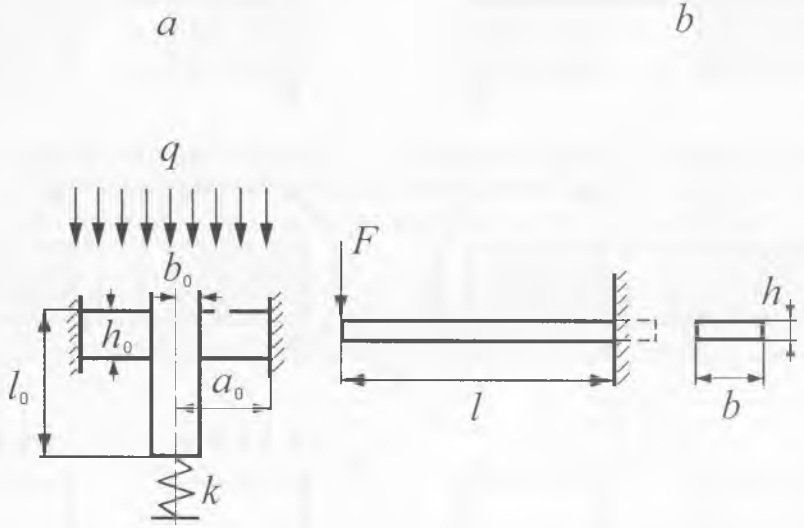

Fig. 5.16. The parts of a meter scheme: h_0 – thickness of a hermetic composition, l_0 – length of a rod, b_0 – radius of a rod, a_0 – radius of a hermetic composition, k – rigidity of a spring, F – force, l – length of plate, h – thickness of plate, b – width of plate.

In its turn, the scheme in fig. 5.16, *a* may be logically divided into elements as it is done in fig. 5.17 (1 - 6). Here, F is the force, q is the pressure, M_1 and M_2 are the bending moments. Each element in fig. 5.17 is easy to calculate (Timoshenko, Voinovsky - Kriger, 1963). The calculation scheme is as follows. In the general case, the equilibrium equation of the plate bended by the external forces can be written in the following way (Landau, Lifshits, 1965).

$$\Delta^2 w - \frac{q}{D} = 0, \tag{5.10}$$

where D is the cylindrical rigidity of the plate defined by the expression

$$D = \frac{Eh_0^3}{12\left(1-\sigma^3\right)}, \tag{5.11}$$

where σ is Poisson's coefficient, E is Young's module, h_0 is the thickness of the plate.

Equation (5.10) in polar coordinates may be written as:

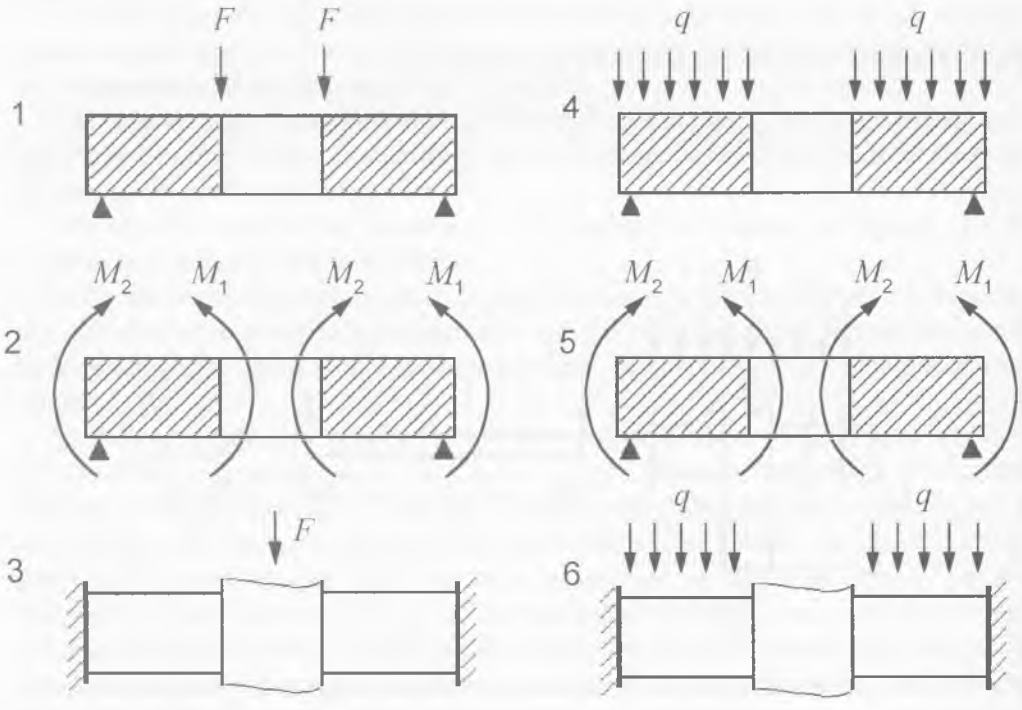

Fig. 5.17. Elements of part *a* of a meter scheme. The designations are in the text.

$$\frac{1}{r}\frac{d}{dr}\left(r\frac{d}{dr}\left[\frac{1}{r}\frac{d}{dr}\left(r\frac{dw}{dr}\right)\right]\right)=\frac{q}{D}. \tag{5.12}$$

A single integration by r from 0 yields:

$$r\frac{d}{dr}\left[\frac{1}{r}\frac{d}{dr}\left(r\frac{dw}{dr}\right)\right]=\frac{1}{D}\int_0^r qrdr. \tag{5.13}$$

The integral in the right part shows the value proportional to the crosscutting force Q multiplied by the periphery length of the radius r:

$$2\pi rQ=2\pi\int_0^r qrdr. \tag{5.14}$$

With regards of (5.14), equation (5.13) can be written as follows:

$$\frac{d}{dr}\left[\frac{1}{r}\frac{d}{dr}\left(r\frac{dw}{dr}\right)\right]=\frac{Q}{D}. \tag{5.15}$$

For element 1 in fig. 5.17:

$$Q=\frac{F}{2\pi r}. \tag{5.16}$$

By a triple integration of equation (5.15) with regards of (5.16), we can get the shape of bending in the supported plate with a hole in its center, as affected by force F applied to its internal counter. In its general form, the solution will look as follows:

$$w_1=\varphi_1(r,F,C_1,C_2,C_3). \tag{5.17}$$

The integration constants are found through a_0 and b_0 from the boundary conditions on the external counter:

$$(w_1)_{r=a_0}=0 \tag{5.18}$$

and

$$-D\left(\frac{d^2w}{dr^2}+\frac{\sigma}{r}\frac{dw_1}{dr}\right)_{r=a_0}=0, \tag{5.19}$$

as well as on the internal counter:

$$-D\left(\frac{d^2w}{dr^2}+\frac{\sigma}{r}\frac{dw_1}{dr}\right)_{r=b_0}=0. \tag{5.20}$$

Then the bending may be presented as

$$w_1=\varphi_1(r,F,a_0,b_0). \tag{5.21}$$

For case 2 in fig. 5.17, the crosscutting force $Q=0$, and equation (5.15) gets simplified:

$$\frac{d}{dr}\left[\frac{1}{r}\frac{d}{dr}\left(r\frac{dw_2}{dr}\right)\right]=0. \tag{5.22}$$

Its integration permit to obtain a bending due to the bending moments M_1 and M_2:

$$w_2=\varphi_2(r_1,C_1,C_2,C_3). \tag{5.23}$$

From the conditions on the external and internal counters we find C_1, C_2 and C_3 through M_1, M_2, a_0 8 b_0. Then

$$w_2=\varphi_2(r_1,M_1,M_2,a_0,b_0). \tag{5.24}$$

The value of bending in case 3 in fig. 5.17 can be derived as the total of bending w_1 and w_2:

$$w_3=w_1+w_2, \tag{5.25}$$

with that, M_1 and M_2 are found from the conditions:

$$\left(\frac{dw_2}{dr}\right)_{r=a_0}=-\left(\frac{dw_1}{dr}\right)_{r=a_0} \tag{5.26}$$

and

$$\left(\frac{dw_2}{dr}\right)_{r=b_0} = -\left(\frac{dw_1}{dr}\right)_{r=b_0}. \tag{5.27}$$

We are only interested in w_3 with $r = b_0$; after a number of transformations, the bending w_3 may be presented as:

$$(w_3)_{r=b_0} = K_p \frac{Fa_0^2}{Eh_0^3}, \tag{5.28}$$

where

$$K_p = \frac{3(1-\sigma^2)}{\pi}\left[\frac{\alpha^2-1}{4\alpha^2} - \frac{1}{\alpha^2-1}(\ln\alpha)^2\right] \tag{5.29}$$

and

$$\alpha = \frac{a_0}{b_0}. \tag{5.30}$$

A similar scheme of solution is used for cases 4, 5 and 6 in fig. 5.17. In case 6 the bending looks as follows:

$$(w_6)_{r=b_0} = K_q \frac{qa_0}{Eh_0^3}, \tag{5.31}$$

where

$$K_q = \frac{3(1-\sigma^2)}{16}\left[-3 + \frac{4}{\alpha^2}(1-\ln\alpha) - \frac{1}{\alpha^4} + \frac{16}{\alpha^2-1}(\ln\alpha)^2\right]. \tag{5.32}$$

Coming back to fig. 5.16 *a*, we may say that the effect of the distributed force and reaction from the support onto the lower end of the central rod equals the superposition of the effect of the forces in cases 3 and 6 in fig. 5.17. Then we may write that the bending in the case in fig. 5.16*a* equals:

$$w_{r=b} = w_6 - w_3. \tag{5.33}$$

With $r = b_0$, this bending in its value equals the contraction of the rod and the spring:

$$w=AF_0, \tag{5.34}$$

where F_0 is the resulting force contracting the system the rod - the spring:

$$A=\frac{l_0}{E_0S_0}+\frac{1}{k}, \tag{5.35}$$

l_0, S_0, E_0 are respectively the length, the cross-section and Young's modulus of the rod; k is the rigidity of the spring.

The force F_0 can be presented as:

$$F_0=qS_0+F. \tag{5.36}$$

Let us equate the right parts (5.33) and (5.34) and we shall get:

$$\frac{qa_0^4}{Eh_0^3}K_q-\frac{Fa_0^2}{Eh_0^3}K_p=AqS_0+AF. \tag{5.37}$$

Using this, we shall find F:

$$F=q\frac{\frac{a_0^4}{Eh_0^3}K_q-AS_0}{\frac{a_0^2}{Eh_0^3}K_p+A}. \tag{5.38}$$

Let us return to equation (5.36). The force F_0, affecting the system the rod - the spring and responsible for their contraction, is composed by the force qS_0, affecting the area of the rod butt end, and the force F with which the internal counter of the plate, receiving the pressure q by all of its surface, impacts the rod. In this way, the primary reason behind the appearance of the force F_0 is the pressure q. In view of this, it would be useful to present the force F_0 as a product of q multiplied by some effective circular surface:

$$S=\pi a_{eff}^2 \tag{5.39}$$

with a free external counter (unlike the real surface πa_0^2 with its pinched external counter). Then

$$F_0=F+qS_0=q\pi a_{eff}^2. \tag{5.40}$$

Using this, we can calculate a_{eff}:

$$a_{eff} = \frac{a_0}{\sqrt{\pi}} \sqrt{\frac{a_0^2 K_q + S_0 K_p}{a_0^2 K_p + E h_0^3 A}}. \tag{5.41}$$

The value a_{eff} is exactly the real radius of the sensitive receiving surface of the receiver of pressure pulsations, which does not coincides either with the radius of the rod, nor with that of the hermetic composition. In our calculation, the latter played the role of the plate with a hole in its center. If this fact is neglected, there can be serious errors in measuring the spectra of pressure pulsations.

We paid much time to calculate the unit displayed in fig. 5.17 *a*, because of the general pattern of this calculation (in some sense, even universal), since such unit can be encountered practically in all piezoelectric meters of pressure pulsations flushed with the streamlined surface.

Let us now analyze the calculation of the effective dimension of the receiving surface of the third version of the pulsation meter. Schematically, the fixation of the sensitive element of such meter can be presented as in fig. 5.18. Here, *l*, *b* and *h* are respectively the length, width and thickness of the piezoceramic plate, *q* is the pressure affecting the plate area, *X* is the coordinate. At the first sight it may seem that the receiving surface involves the entire area equal to *lb*. In fact, the pressure effectively impacts only the free end of the plate and the sections adjacent to its free end. Let us demonstrate it.

The sensitive element of the receiver of pressure pulsations is the section of pieziceramics which is polarized on its surface and occurs in the clearance between the electrodes (see fig. 5.8). The piezoceramic plate is pinched along the line *AA*. Thus, the polarized section immediately joins the line of pinching. It is known that in case the pinched plate bends accurately, the mechanical strain in the point of pinching is maximum on the plate surface and is determined by the expression

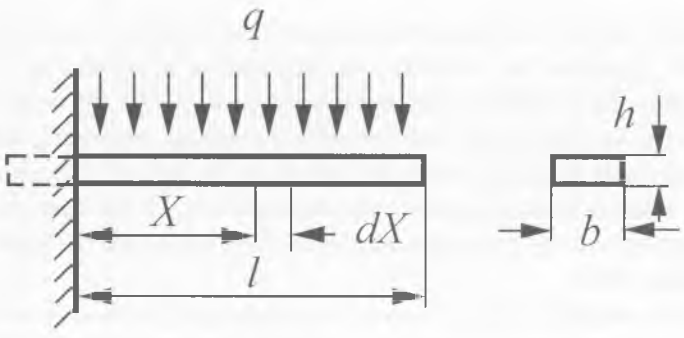

Fig. 5.18. Scheme of a fastening of a sensitive element.

$$Y_{max} = \frac{Mh}{2I}, \tag{5.42}$$

where M is the moment of the bending force applied to the plate, $I = bh^3/12$ is the moment of inertia relative to the plate axis in case its cross-section is rectangular.

The elementary moment of the pressure force in the section dX can be written as:

$$dM = qbXdX. \tag{5.43}$$

The moment of the complete force of pressure on the entire plate will be obtained by integration of (5.43) within the limits from 0 to l:

$$M = qb\int_0^l XdX = \frac{qbl^2}{2}. \tag{5.44}$$

One can see that the moment of force squarely depends on the coordinate X. It means that the contribution to the common moment of force from the sections of the plate adjacent to the point of pinching (the small values of X) are lower than that from the sections whose coordinates are close to l. It is easy to show that 75% of such contribution to the common moment of force is made by the force of pressure on the half of the plate adjacent to the free end, and only 25% - by that half of the plate which is adjacent to the point of pinching. If we want to get certain accuracy, we may find that part of the plate length, which is effective in receiving the pulsations. If our accuracy is to be of 10%, we may say that the effective part of the plate makes up about 2/3 of its length. In such case, when designing the receiver of pulsations, it is feasible to choose the width of the plate equal 2/3 of its length (from the point of pinching). Then the effective receiving surface will be of square shape.

5.1.4. Methods to calibrate receivers of velocity and pressure pulsations

Calibration of velocity and pressure pulsation receivers is a most essential operation which primarily governs the reliability of information about the absolute values of excitations within the boundary layer and beyond its limits (in the oncoming stream).

The hot-wire anemometers and velocity pulsation receivers based upon the phenomenon of electromagnetic induction are easy to be calibrated in a stationary stream of water if its velocity is known and its turbulence is low. In this case, the sensitivity is found as a relation between the output direction of the meter and the value of the stream velocity (Hintse, 1963).

The electrochemical receiver of velocity pulsations and the piezoelectric anemometer described above cannot be calibrated in a stationary stream of water. Their calibration

can be effected only by comparison with any calibrated receiver in a turbulent stream. To this end, the calibrated receiver and that to be calibrated are placed in the same turbulent stream and the indices so obtained are then compared.

Some qualitative idea about the working capacity and sensitivity of any velocity pulsations receiver, irrespective of its type, can be found by placing it into a turbulent stream of water and by registration of the input voltage. The thing is that the extent of turbulence in a turbulent stream at a distance from the grate and in the turbulent boundary layer on the flat wall usually comprises about 5 - 10% of the velocity in the oncoming stream. In this way, having got the measurements in these conditions, by using a velocity pulsation receiver of unknown sensitivity, and knowing the stream velocity in the point of measurements, it is possible to calculate the sensitivity of the receiver with the accuracy of 20 - 30%. In some cases it may prove sufficient.

To estimate the sensitivity of a piezoelectric anemometer and of a receiver of pressure pulsations (the third version), one can employ the method of static impact by a force of known value (Romanenko, 1976). This is demonstrated in fig. 5.19 where 1 is the piezoelectric anemometer or the receiver of pressure pulsations (the third version); 2 is the electrometric device calibrated in units of electric voltage, it has its input resistance

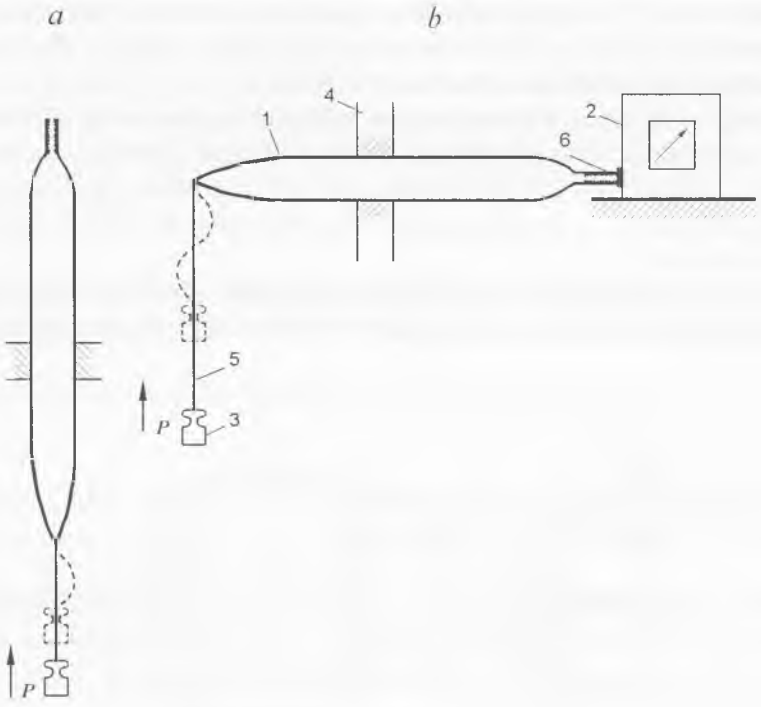

Fig. 5.19. Scheme of a meter calibration by the method of static impact by a force of known value: *a* – for a second version meter, *b* - for a third version one. The designations are in the text.

(impedance) of about 10^{12} - 10^{13} ohm, 3 is the load of known mass P, 4 is the support of the piezoanemometer, 5 is the thread, 6 is the screened cable. If at a certain moment of time the load is quickly removed (i.e. the load is lifted up to such an extent that to weaken the thread on which it was hung), and then, in order to measure the electric potential on the piezoelement by using the connected device, one can estimate the sensitivity of the piezoanemometer. In this way we can compare the sensitivity of different piezoanemometers. There are many more methods to calibrate receivers of pressure pulsations than those to calibrate receivers of velocity pulsations. In terms of their working principles, the latter, in fact, do not differ at all from conventional acoustic receivers (hydrophones) for which a great number of calibration methods were elaborated (Romanenko, 1967, 1974, *a*).

In the first place, it is worth to mention the method of static impact similar to that just described here (see fig. 5.19, *a*, *b*). This method is applicable for estimation of sensitivity in receivers of pressure pulsations of the first two versions. There is only one thing necessary to see here - the static impact force should be directed perpendicularly to the receiving surface (for the first version of the receiver), or along the axis of its support (holder) (for the second version of the receiver).

Rather successful is also the method to compare the values from receivers calibrated in turbulent streams. The most suitable among acoustic methods is that of pistonphones; the one based upon drops in static pressure, as well as the method of shock waves. We are just starting to describe these three methods below.

Method of pistonphones. This method was elaborated and is used to calibrate acoustic receivers (microphones and hydrophones) within the low frequency spectrum (from some parts of hertz to 200 - 250 Hz) (Myasnikov, 1937). However, without any changes and with equal success, it can be employed for calibration of some types of pressure pulsations receivers.

Fig. 5.20, *a, b* displays the scheme of pistonphone devices. One of them is excited electrodynamically, the other - mechanically. In the first case, piston 2 is connected with

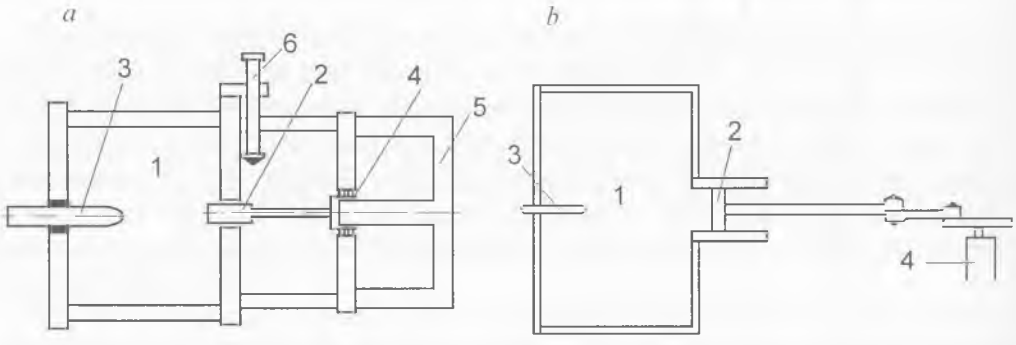

Fig. 5.20. Scheme of a pistonphone devices: *a* – electrodynamic excitation, *b* – mechanical one.

a mobile coil (4) within the clearance of the permanent magnet (or an electric magnet) 5. The excitation current from a special generator (fig. 5.20 does not show it) enters the coil and induces its oscillations which are transferred to the piston. A calibrated receiver of pressure pulsations 3 is installed inside the chamber. The latter should be hermitic.

In the second case, the variable acoustic pressure in chamber 1 is due to the oscillations of piston 1 which, in its turn, is excited by an electromotor and an eccentric. The pulsations receiver is installed in the same way as in the previous case.

The sensitivity of the receiver is found as the relation between the electric voltage on its output and the amplitude of pressure within the chamber. The amplitude is established according to the formula:

$$P = \gamma P_0 \frac{\Delta v}{V_0}, \tag{5.45}$$

where P is the atmospheric pressure, V_0 is the volume of the chamber, Δv is the changes in the chamber volume due to oscillations of the piston, $\gamma = 1.4$ in case of the air. The changes in the volume are equal to the product of the piston area multiplied by the amplitude of its displacement. The displacement amplitude is measured either by an ordinary measuring rule (if the amplitude is sufficiently high), or by a microscope 6 (see fig. 5.20, *a*).

However, formula (5.45) is valid only within a comparatively narrow range of frequencies. The lower boundary of the range is specified by the condition:

$$3.9\sqrt{f}\frac{V_0}{S} > 10, \tag{5.46}$$

due to the fact that within the range of low frequencies the adiabatic low of air deformation in the chamber gives way to the isothermal one. Here, S is the internal surface of the chamber.

The upper boundary of the range is governed by the condition

$$kl << 1, \tag{5.47}$$

which requires the smallest-possible dimensions of the chamber, as compared with the wave length. Here, $k = 2\pi/\lambda$, l is the chamber length, λ is the length of the acoustic wave in the air.

The frequency limits to apply formula (5.45) can be expanded almost by two orders, if it is supplemented by respective correction for regarding the thermodynamic and wave phenomena (Romanenko and Boguslavskaya, 1968; Romanenko, 1976). Then the formula (5.45) will look as follows:

$$P = kc\gamma P_0 \frac{\Delta v}{V_0}, \tag{5.48}$$

where

$$k = \left[\sqrt{1 + (\gamma - 1) \frac{1 - e^{-\chi}\sqrt{2}\cos\left(\chi + \frac{\pi}{4}\right) + \frac{(\gamma-1)^2}{2\chi^2}\left(1 - 2e^{-\chi}\cos\chi + e^{-2\chi}\right)}{\chi}} \right]^{-1}, \tag{5.49}$$

$$c = kl \frac{\cos kl(1-\alpha)}{\sin kl}. \tag{5.50}$$

Here,

$$\chi = 4l\sqrt{f}, \quad \alpha = \frac{x}{l}, \tag{5.51}$$

x is the coordinate of the sensitive element of the receiver of pressure pulsations as found along the axis of the cylindrical chamber from the median position of the piston.

Some companies manufacture miniature pistonphones to calibrate microphones at one fixed frequency. In particular, the Brull and K^0 (Denmark) manufacture pistonphones for 250 Hz, the RFT Company (Germany) makes pistonphones for the frequency of about 200 Hz. Such pistonphones have autonomous feeding, are very convenient in use and without any changes can be employed to calibrate receivers of pressure pulsations similar to those described above (the second version). It is only necessary to provide an additional simple intermediate device permitting to install into the chamber a calibrated receiver instead of the microphone. The intermediate device should contain a stuffing box guaranteeing the hermetic fixation of the receiver in the pistonphone.

Fig. 5.21 shows a pistonphone made by the RFT Company and three intermediate elements. The calibrated receiver of pressure pulsations is fixed in one of them. The three intermediate elements are supposed to fix one of the three different receivers of pressure pulsations which vary from one another by the diameter of their support.

Fig. 5.22 shows the same pistonphone with a receiver installed into its calibration chamber.

When calibration is effected by the method of pistonphones, calibration errors in receivers of pressure pulsations are not large, only of several percents, But when the

sensor of the receiver is made of piezoceramics and directly contacts the medium around it (for instance, the second version of the receiver), the calibration error, within frequencies of units and tens of hertz, may become considerable due to the pyroelectric effect. Pyroelectricity is determined as some change in the polarization of the dielectric caused by the change in its temperature. Pyroelectricity is rather typical of piezoceramics which is usually employed to make sensors for receivers of pressure pulsations.

During calibration by pistonphones, their chambers alter not only their pressure but temperature too. Such changes in the temperature are related with those in the pressure:

$$\Delta T = \frac{\beta T_0}{\rho_1 C_{p1}} \Delta p, \tag{5.52}$$

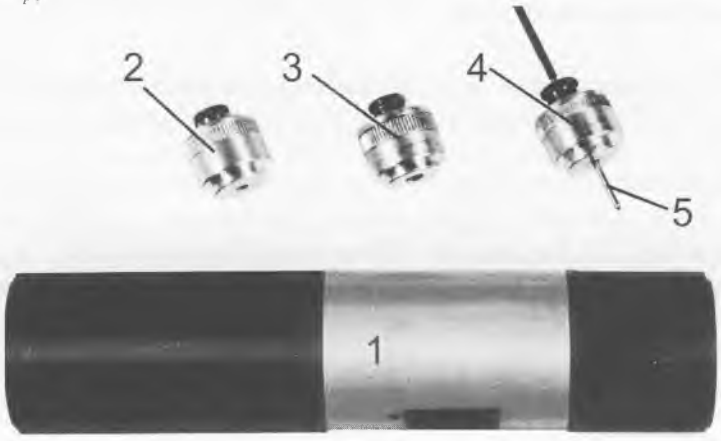

Fig. 5.21. Pistonphone (1) (production of the RFT Company, Germany); 2,3,4 – intermediate devices, 5 – meter.

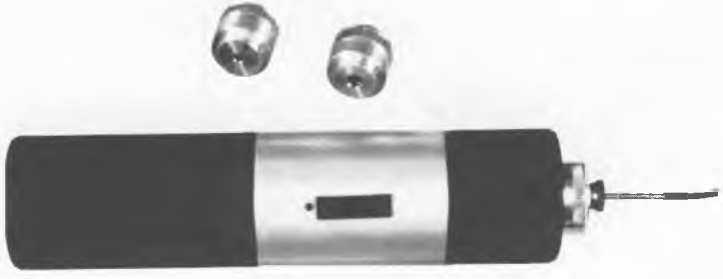

Fig. 5.22. Pistonphone with a meter installed into its calibration chamber.

where β is the coefficient of volumetric expansion of the medium within the chamber of the pistonphone (as a rule, it is the air); T_0 is the mean temperature of the medium, ρ_1 is the density; C_{p1} is the specific heat capacity of the medium at constant pressure; Δp is the change in the pressure.

As seen from estimations, in the air at T_0 = 20°C $\Delta T \cong 10^{-4}\Delta p$. Changes in the temperature of the medium, due to those in the pressure, will yield a potential difference on the electrodes of the piezoreceiver, if the piezoelement has sufficient time to get heated to the temperature of the medium. To simplify the presentation, let us imagine that the receiver sensor is shaped as a flat platelet with the thickness h. The platelet has a bilateral contact with the medium. If the platelet, being an electric capacity C, is loaded to an infinitely large resistance, then the potential difference ΔU, developing on its electrodes at a temperature increase by ΔT, will equal

$$\Delta U = \frac{4\pi h}{\varepsilon}\gamma_0 \Delta T.10^{12} V, \tag{5.53}$$

where ε is the dielectric permeability of the piezoceramics, γ is the pyroelectric constant. For example, if the facings of the piezoceramic platelet have ε = 1200 and h = 0.1 cm, when it is heated by 1°C, the potential difference will be about 20 V.

Using the relations (5.52) and (5.53), in order to find the pyroelectric sensitivity of the piezoelement in terms of pressure, we shall get

$$M_{pyro} = \frac{\Delta U}{\Delta p} = \frac{4\pi h \beta T_0 \gamma_0}{\varepsilon \rho_1 C_{p1}}.10^{19} V / Pa. \tag{5.54}$$

The expression (5.54) shows the limit sensitivity, i.e. the sensitivity in the condition that the pyroelement at each moment accepts the temperature of the medium (there is no heat inertia and heat convection when the heat is transferred from the medium to the piezoelement). The real sensitivity depends on the frequency of pressure changes. The process may be presented as follows:

$$M_{pyro} = \frac{4\pi h \beta T_0 \gamma_0.10^{19}}{\varepsilon \rho_1 C_{p1}} \frac{m}{\sqrt{m^2 + \omega^2}} V / Pa, \tag{5.55}$$

where

$$m = \frac{\alpha S}{\rho_2 V C_{p2}}, \tag{5.56}$$

α is the coefficient of heat transfer which, in case of quiet air, equals 2 - 8 kcal/ sq m sec/ grade; ρ_2, C_{p2}, S and V are the density, specific heat capacity, the surface and volume of the piezoelement respectively. Fig. 5.23 shows the erxperimentally measured (curve 1) relation between the pyroelectric sensitivity of the piezoelement in terms of pressure in total with the piezoelectric sensitivity and the piezoelectric sensitivity as a function of frequency. The material of the piezoelement is piezoceramics. The piezoelement is shaped as a platelet 0.01 cm thick. We have hatched the area of theoretically possible values determined by the relation (5.55) when α changes from 2 to 8 and the expression for the piezoelectric sensitivity is known

$$M_{pyro} = \frac{4\pi d_{u.p}}{\varepsilon} h.300.10^7 V / Pa, \tag{5.57}$$

where $d_{u.p}$ is the piezomodulus of piezoceramics at all-round pressure.

If we remember that the formula (5.57) does not take into account the phenomenon of convection and that the phase shift between the pyroelectric potential and the piezoelectric potential is possible, then the accordance of the experimental data with the results of calculation can be considered satisfactory. The pyroelectric sensibility was measured in the air, and the sensibility was measured in the water by pistonphone technique. In this case we assume as the first approximation that the pyroeffect is absent in water. But sometimes we cannot neglect the existence of the pyroeffect in case when

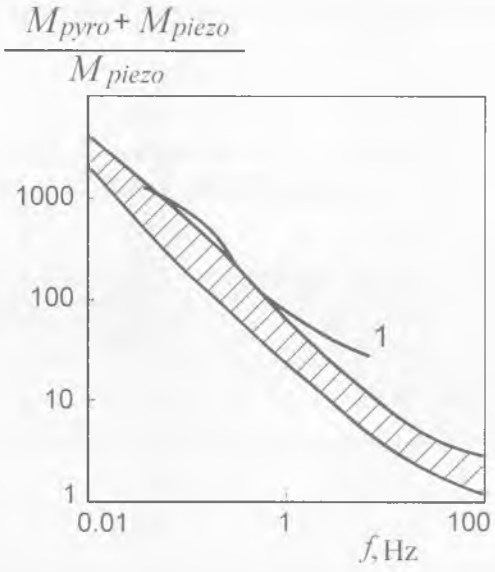

Fig. 5.23. Relation between the pyroelectric sensitivity of the piezoelement in terms of pressure in total with the piezoelectric sensitivity and the piezoelectric sensitivity as a function of frequency.

the pyroelement is submerged in liquid. We adduce the calculated maximal possible values of relation

$$\frac{M_{pyro} + M_{piezo}}{M_{piezo}} \tag{5.58}$$

for the piezoelement submerged in various ambient liquids in table 5.1. The calculation was performed for three variants of the piezoelement application. In the first variant the piezoelement is under uniform pressure (the piezomodule $d_{u.p}$ acts). In the second variant the piezoelement is under one-side pressure in the direction that the piezomodule d_{31} acts. In the third variant the module d_{33} acts. We can see that pyroeffect is completely absent only when the piezoelement is in the ambient water under the temperature of 4°C. If water temperature is 25°C, then neglecting the pyroeffect can lead to the graduation error of 15% for the module $d_{u.p}$. If the working liquid is, for example, olive oil, then the error can reach 90%.

Let us now return to the specific features of calibration of pressure pulsation receivers by the method of pistonphones. An analysis of possible errors due to the pyroelectric effect demonstrates that such method of receiver calibration in the air is only possible at frequencies above 100 Hz (see fig. 5.23). If it is necessary to calibrate receivers of pressure pulsations by this method within the range of frequencies of units and parts of

liquid	at $d_{u.p}$	at d_{31}	at d_{33}
water at 4^0 C	1	1	1
water at 20^0 C	+0.88	+1.065	+0.98
water at 25^0 C	+0.85	+1.08	+0.97
acetone	-1.1	+2.15	+0.58
glycerine	+0.57	+1.23	+0.92
alcohol	-0.30	+1.70	+0.75
olive oil	-0.1	+1.61	+0.78
sulphuric acid	+0.45	+1.30	+0.89
kerosene	-0.53	+1.85	+0.70
carbon bisulphide	-1.20	+2.23	+0.55
turpentine	-0.25	+1.68	+0.75
ether	-1.55	+2.43	+0.48

Table 5.1. Instrumental calibration error of the piezoelement submerged in various ambient liquids.

a hertz, then the receiver should be submerged into water at 4^0C. The procedure is as follows. The receiver of pressure pulsations is submerged into a glass with water and then together with the glass it is placed into the chamber of the pistonphone (if the dimensions of the chamber permit it).

The method based upon the drop of static pressure. This method was elaborated for calibration of miniature cylindrical hydrophones but it can be successfully used to calibrate receivers of pressure pulsations too. The technique is based upon a quick discharge of static pressure under which was the sensor of the receiver previously installed in a small thick-walled chamber covered with a diaphragm (Roi, Frolov, 1961). The chamber is supplied with air under a given pressure. At a certain pressure, the diaphragm gets broken and the pressure drops down to the atmospheric level. The electric voltage, developing at the exit of the receiver, is oscillographed. The sensitivity of the receiver is found as the relation between the maximum voltage and the pressure in the chamber before the perforation of the diaphragm.

The chamber (fig. 5.24) has a volume of several cubic cm. The upper lid of the chamber is the diaphragm 1 squeezed at its edge by a in-screwed ring with a rubber sealing 2. The diaphragm can be made of a film 35 mm wide. When the free part of the diaphragm is 23 mm in diameter, it gets broken at pressure of 10 to 13 at. Compressed air is supplied to the chamber from a cylinder through a reducer; the process is rather slow so that before the perforation of the diaphragm the pressure in the chamber could be measured. During the pressure rise in the chamber, the electric charge from the piezoelement of the receiver under calibration 3 should be able to flow down through

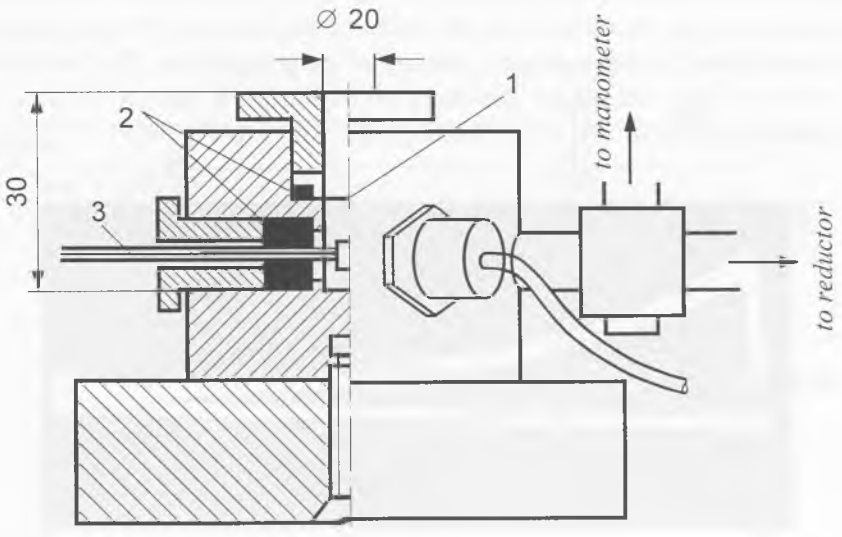

Fig. 5.24. Scheme of a chamber. (Redrawn from Roy, Frolov, 1961).

the input resistance of the oscillograph connected with the receiver. However, the input resistance should be sufficient high, so that during the pressure drop after the perforation of the diaphragm the electric voltage at the output of the receiver would not drop because of the flowing piezocharges. In view of this, the pressure must be dropped as quickly as possible. This is the reason explaining the diminished internal volume of the chamber. With the chamber volume mentioned above, the pressure drop usually occurs at 200 mAs. Hence, we shall have the following time constant RC: C is the capacity of the piezoelement, including the lead and the entrance to the oscillograph, R is the resultant resistance of parallely switched-in resistances of the oscillograph entrance and of the leakage from the receiver. This constant should be at least by one order greater than 200 mAs.

After the diaphragm gets perforated, the pressure becomes slightly lower than that of the atmosphere, due to the inertia of the scattering flow of gas. After some oscillations, the pressure strives to that of the atmosphere. Voltage oscillations during the period of about 500 mcs are marked by the receiver. The working oscillogram is displayed in fig. 5.25. When determining the sensitivity, it is necessary to average the voltage oscillations and to relate the mean value with that on the manometer before the perforation of the diaphragm.

When the excess pressure is above the atmospheric one by about 10 at and more, there may be an error due to disregard of pressure oscillations, but such error is not large. If the excess pressures equal several atmospheres, the values should be averaged more thoroughly.

Calibration method by means the shock wave. The essence of this method is in that the sensitivity of the receiver of pressure pulsations is found by the value of electric voltage caused by the shock wave at the outlet of the receiver. The amplitude of the wave is established by the measured velocity of its propagation. The velocity of the shock wave and the voltage on the receiver outlet are found by the oscillogram photographed from the screen of the oscillograph (Roi, Frolov, 1961).

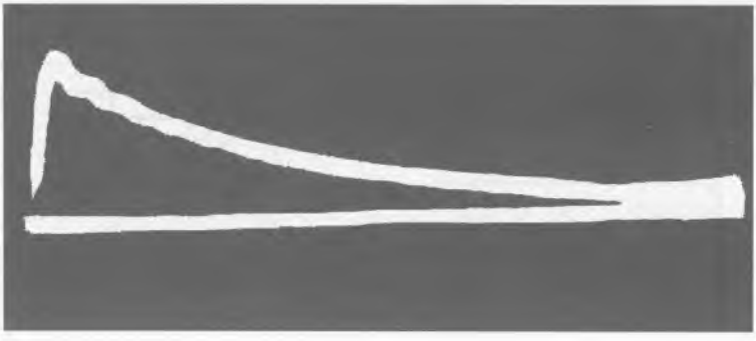

Fig. 5.25. The oscilloscope pattern. (Redrawn from Roy, Frolov, 1961).

Fig. 5.26 shows the block-scheme of the device to calibrate such a receiver. Like in the previous case, the method was designed for calibration of hydrophones but it can be successfully applied to calibrate receivers of pressure pulsations. The shock tube 1 (in which the shock wave is initiated) is 50 mm in diameter and its wall is 5 mm thick. It is composed of sections 500 and 1400 mm long. The sections are divided by a diaphragm 1 made of film. The diaphragm is clamped between flanges provided with packed rubber rings. From the bottle 3, compressed air is supplied to the short section of the tube at pressure of about 7 at before the perforation of the diaphragm. After the latter is perforated, the second section gets attacked by the shock wave of pressure. To prevent the receiver under calibration 4 from blows of fragments of the diaphragm, an insert is clamped between the flanges. It is shaped as a tube of 50 mm in diameter and 50 mm in length. The tube is tightened by a soldered brass grid 5 made of 0.5 mm wire with a mesh 5 x 5 mm. Soldering prevents the grid from breaking of wires after several perforations of the diaphragm.

To find the propagation velocity of the shock wave, there is a device measuring the time of its path over a certain known track. The sensors of the device are composed of detectors (6 and 7) installed in the wall of the second section of the tube. Detector 6 is 700 mm away from the diaphragm, which is sufficient for the formation of a shock wave. Detector 7 occurs at 500 mm from detector 6. When the shock wave reaches detector 6, the oscillograph switches in its sweep marking the time traces. When the shock wave reaches detector 7, the time traces get switched off. The velocity of the shock wave is found as a relation of the distance between the detectors and the time necessary to cover this distance. The receiver under calibration is installed either along

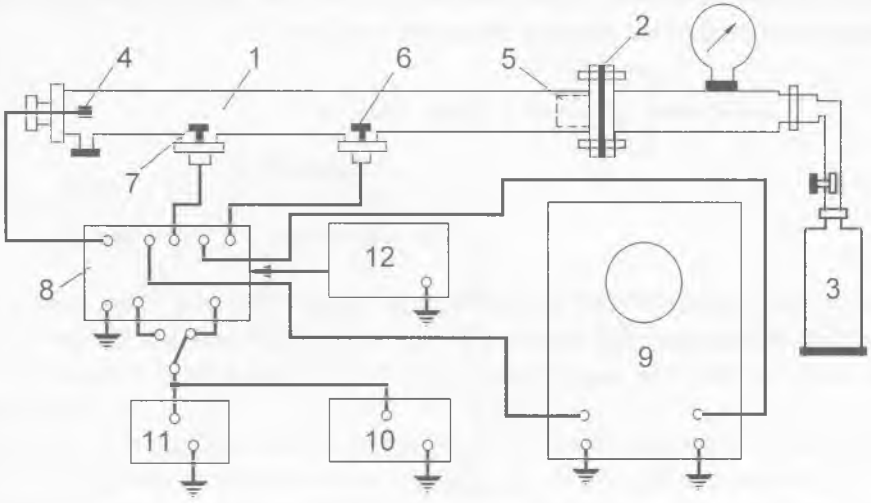

Fig. 5.26. Block-diagram of device. (Redrawn from Roy, Frolov, 1961).

the axis of the tube on its butt-end jam, or near the jam in the wall of the tube. It is possible to alter the position of the receiver so that to examine its sensitivity at different orientations in terms of the direction of the shock wave propagation.

The radiotechnical set-up of the device 8 should provide the following:

- the single-time triggering (start-up) of the oscillograph sweep 9 by a signal from the first detector, so that the reflected waves could not restart the sweep.
- the accuracy of the start-up, i.e. to initiate the starting pulses with a sufficiently steep front.
- sufficient accuracy to mark the moment when the shock wave arrives to the second detector.
- a sufficiently wide band of the transmitted frequencies, so that the signal from the receiver under calibration should not be distorted.
- the possibility to calibrate the channel amplifying the electric voltage gain of known value.

The block-scheme of the radiotechnical component is displayed in fig. 5.27 This component includes four main units. Unit I forms the starting pulse to trigger the sweep of the oscillograph from the voltage pulse of negative polarity coming from detector 6 (see fig. 5.26) onto inlet 1 of unit 1. The starting pulse from outlet 1 enters the inlet of the oscillograph sweepblock.

Unit II forms the time traces. To this end, inlet 5, with the closed switch B_1, receives the non-interrupted sinusoidal voltage from a special generator (10 in fig. 5.26) with the frequency of 50 kHz. It is controlled by the voltmeter 11 and is converted into a sequence of negative pulses, which serve as time traces. The latter leave outlet 2 and enter the inlet of the channel amplifier which vertically deflects the ray from the oscillograph.

Unit III forms the electric signal switching off the time traces at the moment when the shock wave reaches the detector connected with inlet 2.

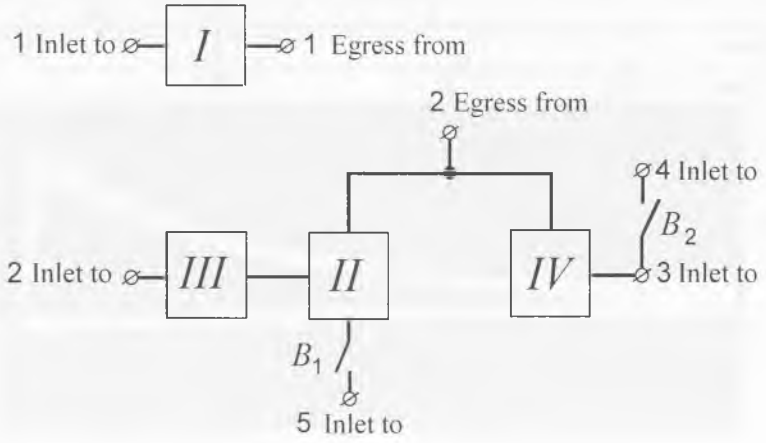

Fig. 5.27. Block-diagram of a radiotechnic scheme. (Redrawn from Roy, Frolov, 1961).

Unit IV serves to amplify the signal coming from the receiver under calibration which is connected with inlet 2. The amplified signal goes through inlet 2 to the inlet of the oscillograph. Inlet 4 serves for directing the calibrated electric voltage of known value and of 50 kHz in frequency. With that, the switch B_1 is disconnected and the switch B_2 is closed. The single-time start-up of the oscillograph to photograph the calibrated signal is effected by pressing a special button in unit I. The radiotechnical part of the scheme is fed from the voltage source 12.

The pressure wave, propagating in the second section of the tube, is transformed into a shock wave with a steep front and a flat-dipping pressure drop behind the front. The pressure is dropping slowly, according to the volume of the first section of the tube: the larger is the latter's volume, the slower is the pressure drop. The pressure immediately behind the front is related with the propagation velocity of the shock wave in the following way:

$$\frac{P_2}{P_1} = \frac{2\gamma M_1^2 - (\gamma - 1)}{\gamma + 1}, \tag{5.59}$$

where P_1 and P_2 are the pressure behind the shock wave front and before it respectively (P_1 equals the initial pressure in the second section), M_1 is the relation between the velocity of the shock wave and that of sound at given temperature, γ is the relation between the air heat capacities at constant pressure and constant volume.

The shock wave gets reflected from the jam at the end of the second section. The pressure behind the front of the reflected wave (P_3) is found from the relation:

$$\frac{P_3}{P_2} = \frac{2\gamma M_2^2 - (\gamma - 1)}{\gamma + 1}, \tag{5.60}$$

where

$$M_2^2 = \frac{2\gamma M_1^2 - (\gamma - 1)}{2 + (\gamma - 1) M_1^2}. \tag{5.61}$$

The value of P_2 may be accepted as equaling the pressure behind the front of the incident wave if the distance from the jam to the point of observation is not too large and the pressure behind the front of the incident wave will have no time to drop considerably.

The value γ in the formulas is supposed to be constant, equaling 1.4. This is valid of shock wave pressures within several atmospheres. With higher pressures, this value may change due to dissociation of gas caused by its heating at the wave front.

The above formulas make it possible to present in graphs (fig. 5.28 and 5.29) the following relations:

$$P_2 - P_1 = \varphi(M_1), \tag{5.62}$$

$$P_3 - P_1 = \varphi(M_1), \tag{5.63}$$

which connect the excess pressure behind the front of the incident and reflected waves in the tube section, where the shock wave is propagating with the wave propagation velocity. As a rule, the value P_1 is established as equaling the atmospheric pressure.

One thing should be born in mind: if behind the front of the reflected wave, at small distances from the jam, the velocity of gas particles is close to zero, then this velocity behind the front of the incident wave may be very high. The velocity of air particles behind the front of the incident wave may be found by using the formula

$$v = C_{sh} \frac{2(M_1^2 - 1)}{(\gamma + 1)M_1^2}. \tag{5.64}$$

For instance, if the propagation velocity of the shock wave C_{sh} equals 500 ms^{-1}, which corresponds to Mach number M_1 = 1.46, the value of v = 220 ms^{-1}. Therefore, while calibrating in incident waves, one should always remember that when the receiver is streamlined by an air current at high velocity, the pressure on the surface of the receiver sensor may considerably differ from that in the shock wave.

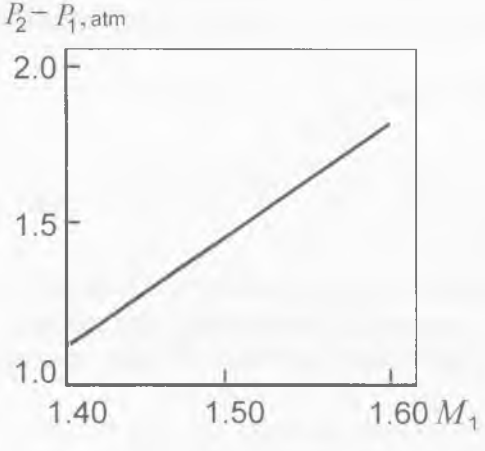

Fig. 5.28. Gauge air pressure back of the incident wave front. (Redrawn from Roy, Frolov, 1961).

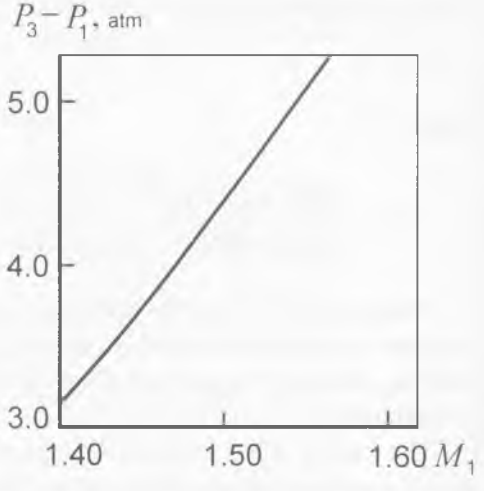

Fig. 5.29. Gauge air pressure back of the reflected wave front. (Redrawn from Roy, Frolov, 1961).

5.1.5. Velocity meters of streamlining

To measure the averaged velocity of the flow near the body of a freely swimming dolphin is a rather difficult process. One cannot employ Pitot tubes. The meter should be autonomous and the measurements should be effected automatically. Besides, the meter should be of low weight, of small dimensions and inert. It must also have a large dynamic range of values under measurement. Three types of velocity meters were successfully used to measure the velocities of streamlining over fishes and dolphins. These meters were as follows: impellers, a magnetic meter and that based upon the phenomenon of vortex stalls from the streamlined cylinder.

In case of biohydrodynamic studies, electrolytic impellers (Eguidis, Shakalo, 1971) and magnetic ones were used (Kaduk et al., 1971; Romanenko, Yanov, 1973). An electrolytic impeller is an electrolytic cell with its ohmic resistance changing in accordance with the rotation of its vanes. The necessary elements of such cell are two electrodes and one impeller submerged into liquid. The velocity of the latter is measured. The electrodes may be both immobile. In this case, the resistance of the cell alters, when the dielectric vanes of the impeller pass between the electrodes. One of the electrodes may be mobile (it is situated on the vane of the impeller). Then the resistance of the cell will alter due to the changes in the mutual location of the electrodes. The resistance of the liquid between the electrodes may be presented as follows:

$$R = \tilde{R} + A, \tag{5.65}$$

where A - const. and $\tilde{R}$ is the variable part conditioned by the changes in the distance between the electrodes. In fresh water, when the electrodes are connected to some constant voltage, one can see the relation

$$\tilde{R} >> A. \tag{5.66}$$

Then, the variable component of the voltage, developing on the electrodes due to the rotation of the impeller, can be easily registered.

In marine water, at some constant voltage between the electrodes, one can observe a reverse relation between the values $\tilde{R}$ and A. These values prove to be of the same order only when some variable voltage of acoustic frequency is applied between the electrodes. With this, the voltage between the electrodes happens to be amplitudially modulated with such frequency of modulation which is governed by the rotation frequency of the impeller. It is true, the depth of the modulation is very small (about 0.015) but, nevertheless, it may be quite conclusively specified by certain methods.

Fig. 5.30 shows the set-up principle of the magnetic impeller. The body 1 is made of some non-magnetic material (for example, duralumin) and contains impeller 2 and coil

3. The impeller has four vanes, two of them have permanent magnets which are glued-in (SN) as shown in fig. 5.30, *b*. Each vane is 10 mm long, 5 mm wide and 1 mm thick. The material of the vanes without magnets is stainless steel. That in the vanes with glued-in magnets is organic glass. The impeller axis is made flushed with the steel vanes and rotates inside bronze nests. The coil is glued-in tightly into the body. It contains about 200 loops of wire of 0.1 mm in diameter. The taps of the coil are connected with the meter by a screened cable 4.

The velocity meter works as follows. A stream of water runs onto the impeller in the way shown by arrows in fig. 5.30, *a*. A water stream impacts the sections of vanes, protruding from the impeller body, and induces their rotation. The poles of the constant magnets, moving in relation to the coil, initiate there an electromotive force of induction as short pulses of sufficient amplitude. These pulses are registered. The frequency of the pulses unambiguously depends upon the velocity of the on-running stream of water. Fig.5.31 shows the calibration dependence between the frequency of pulses and the velocity of the stream in such an impeller.

The working principle of a magnetic (electromagnetic) velocity meter is described in that part of this book which deals with meters of velocity pulsations.

The above meters of stream velocity have an essential drawback: they measure only one component of velocity (the longitudinal one). As a rule, the animal's movements are non-stationary, and the velocity vector during the animal's motion may slightly change its direction. It is particularly noticeable in the caudal part of the dolphin's body, which fluctuates especially strongly. In this part of the animal's body the longitudinal component of velocity may be quite considerable. In some cases, it may prove feasible to measure the full vector of velocity in the streamlining current. To measure such complete vector

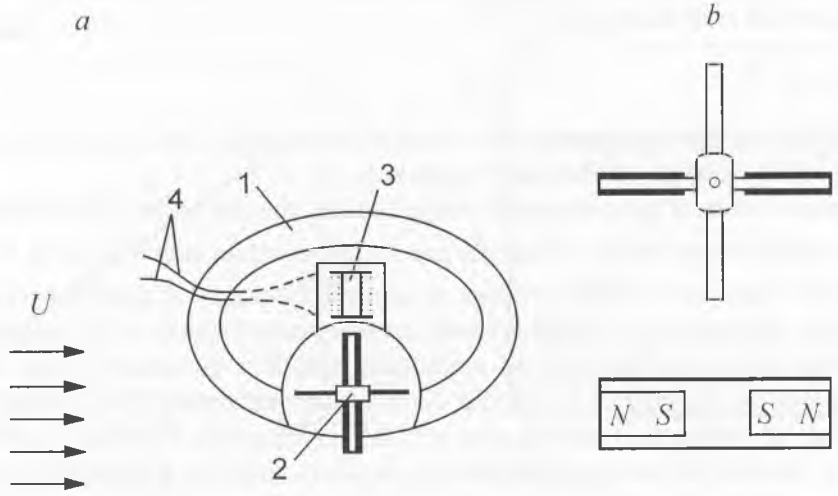

Fig. 5.30. Scheme of a set-up principle of the magnetic impeller. The designations are in the text.

of velocity is possible by using a meter based upon the phenomenon of the separation of a laminar flow during its transverse streamlining over a round cylinder, when a vortex track is formed (Katys, 1965). The frequency of such vortex separation can be found by the expression

$$f = Sh\frac{U}{d}, \tag{5.67}$$

where d is the diameter of the cylinder, U is the flow velocity, Sh is the Strouhal number which does not change much within the wide range of Reynolds numbers and equals 0.21. The relation (5.67) unambiguously binds the frequency of vortex separations and the velocity of the current. In this way, the assessment of flow velocity can be easily limited to measuring the frequency of vortex separations behind the streamlined cylinder. It was exactly such a meter which was designed and employed in biohydrodynamic studies (Romanenko, 1976).

Fig. 5.32 shows a velocity meter composed of a support 1 with an installed steel curved rod (diameter 1.5 mm) 2 and a receiver of pressure pulsations 3. The support is placed on the animal either on a special belt, or by means of the sucker, so that the receiver of pulsations could be in the vortex trace of the cylinder streamlined by the current. Inasmuch as the vortex trace behind the cylinder is sufficiently wide, the receiver

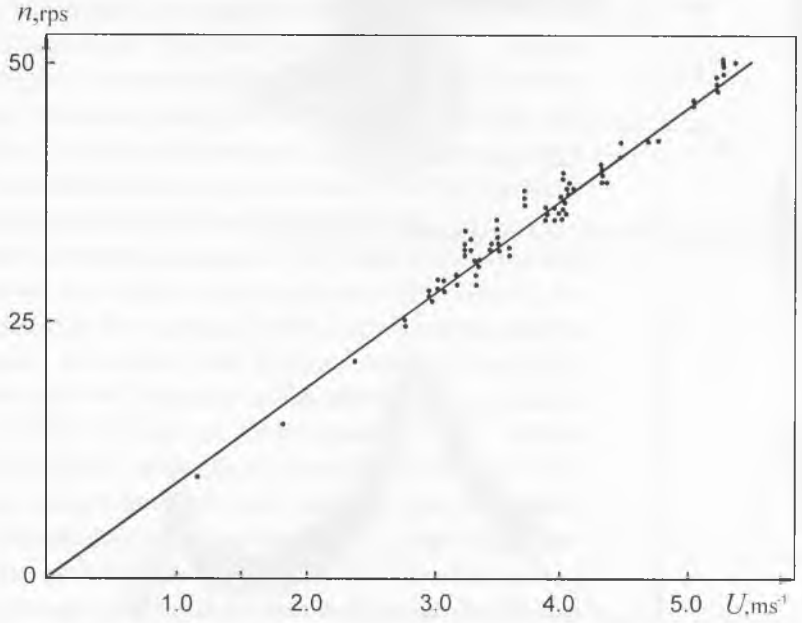

Fig. 5.31. Calibration dependence between the frequency of pulses and the velocity of the stream in such an impeller.

of pulsations will remain in it or near it even when the velocity vector considerably deviates from its longitudinal direction. And it is the complete vector of velocity that will govern the frequency of vortex separations. In this way, the position of the maximum spectrum of pressure pulsations, registered by the receiver of pulsations, will unambiguously determine the complete vector of velocity in the on-running current if the streamlined cylinder is perpendicular to the surface of the animal's body and occurs sufficiently close to it. When the streamlined cylinder, together with the receiver of pulsations, is rather far from the animal's body, there may be errors in measuring the complete vector of velocity due to the component of velocity perpendicular to the animal's body, because this component practically does not impact the pattern of streamlining over the cylinder.

Fig. 5.33 demonstrates an approximate spectrogram of pressure pulsations behind the streamlined cylinder. The spectrogram clearly reveals two maximums. The second maximum corresponds to the frequency f_2, which is twice larger than that of the first maximum f_1. The presence of two maximums can be attributed to the fact that vortexes get separated from the streamlined cylinder alternately from its right and left sides in

Fig. 5.32. Meter of a flow velocity. The designations are in the text.

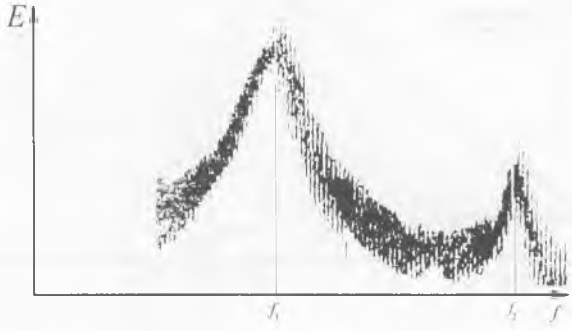

Fig. 5.33. Approximate spectrogram of pressure pulsations behind the streamlined cylinder.

turn. If the receiver of pressure pulsations were situated strictly in the middle of the vortex track, the first maximum in the spectrum would not exist. However, in practice, as a rule, the receiver of pulsations is slightly shifted to this or that side from the axis of the vortex track. For this reason, the receiver can better register those vortexes, which occure closer to it. As a result, there develops some subharmonics of Struhal frequency. When calculating the streamlining velocity, one should take the frequency of the second maximum of the spectrum.

This specific feature of the velocity meter limits, to some extent, its applicability. For instance, it cannot be used to measure velocities in currents when their direction is not known beforehand or can vary within 360^0. This drawback was eliminated in the design of a velocity meter displayed in fig. 5.34. This meter works on the same principle as the previous one. Its difference is in that both its streamlined cylinder and its meter of pressure pulsations are united in one element 1. The unit is a tube of piezoelectric ceramics. Its length is much greater than its diameter (for example, when the external diameter of the tube is 1.5 mm, its length may be 10 - 15 mm). The internal and external surfaces of the tube are metallized. The central cable 2 of the screened cable 3 passes through the internal channel of the tube. Thanks to the soldering 4, cable 3 is in an electric contact with the metallized internal surface of the tube. The screening braiding 5 of cable 3 is welded to the external metallized surface of the tube. The place, where the tube joins the screened cable, is hermetically sealed by an alloy 6 of wax and rosin. The same alloy hermetically seals the butt-end of the tube 7 with the soldering 4. The tap of the screened cable 3 is connected to a recorder of any kind (for instance, a tape-recorder with sufficiently wide bands).

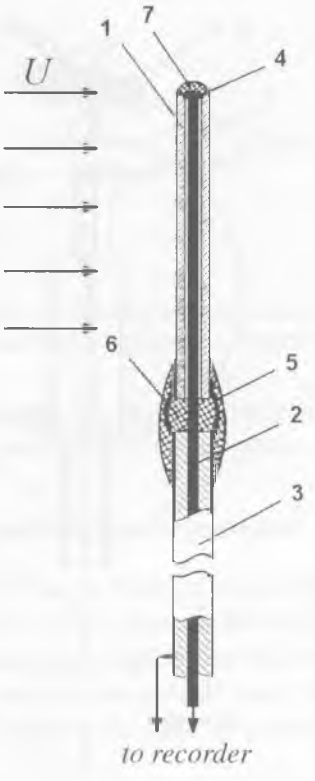

Fig. 5.34. Meter of a flow velocity. The designations are in the text.

The device works as follows. The meter is installed into the current in such a way that the tube should be perpendicular to the current. In this case, when the tube is streamlined, its surface will separate vortexes and their separation will be frequency determined by the relation (5.67). At the moment of their separation, the stalled vortexes affect the streamlined piezoelectric tube and, as a result, an electric potential will appear on its metallized surfaces (electrodes). The spectrum of this potential contains a clearly expressed maximum at the frequency corresponding to that of the vortex separation. Unlike the previous device, this one has no subharmonics. Besides, its work does not depend on the direction of the current.

It goes without saying that streamlining over animals can be also measured by the thermoanemometric method described above.

5.1.6. Measurement of shearing stressis

To measure shearing stresses in the boundary layer is, in general, a task of exceptional technical difficulty (Shlechting, 1974). The universally accepted method requires simultaneous application of two thermal anemometers with a complicated scheme of power supply and of information procession. In view of this, application of this method to freely swimming dolphins seems to be practically unrealistic. Nevertheless, it became possible to design a meter for registration of shearing stresses in the boundary layer of a freely swimming dolphin and for automatic recording of the obtained information. The scheme of this device is presented in fig.5.35. The sensor of the device is a platelet 1 fixed on a fine steel wire 0.25 mm thick 2. The platelet is 10 x 5 x 0.1 mm in size. The end of the wire, on which the platelet is fixed, protrudes to 1.5 cm from the protecting tube with oval cross section 3. The oval cross section of the tube is 0.3 x 0.5 cm. Inside this oval protecting tube there is another guiding tube 4 of circular cross section. The wire with the platelet passes through this circular tube. The internal diameter of the guiding tube is slightly larger than that of the wire with the platelet, which permits the wire to be freely rotating in the guiding tube. The end of the guiding tube, being inside the device body 5, is welded to the end of the flat spring 6, which is 0.08 mm thick (the safe razor blade). The other end of the spring is clamped in the holder 7. The wire with the platelet is a lever receiving the shearing stress from the side of the water current, and transmitting this stress as a bending force to the flat spring 6. On the latter, near the holder 7 there is a tensosensor (a sensing element of strain gauge) 8, which accepts the stress and responds to it. The taps of the tensosensor leave the device body and, by means of a screened cable 9, get connected to the measuring circuit and to the recording device (a small-scale autonomous tape recorder) fixed on the dorsal fin of the dolphin.

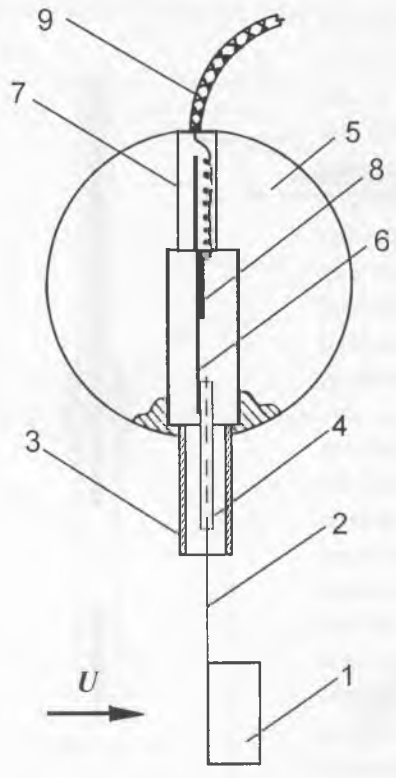

Fig. 5.35. Meter of the shearing stresses. The designations are in the text.

Fig. 5.36, *0* shows a picture of the meter of shearing stresses.

The meter works as follows. It is fixed on the dolphin's body by means of the sucker, as shown in fig. 5.36, *b*. The sensing platelet is located at 0.2 - 0.3 cm from the animal's body. Bearing in mind that the turbulent boundary layer on the dolphin within the area of the middle and behind it is 10 - 12 mm thick (Romanenko, 1976), the distance between the platelet and the body surface makes up about 0.2 - 0.3 of the boundary layer thickness. At this point of the boundary layer, the shearing stresses do not differ much from those on the streamlined surface (Shlihting, 1974). The shearing stresses, affecting the sensor in the onrunning stream of water, induce a certain strain deflecting the platelet towards the effect direction of the stream. This leads to the bending of the wire carrying the tensosensor and, accordingly, to changes in the latter's resistance which are registered by the measuring circuit and by the recorder.

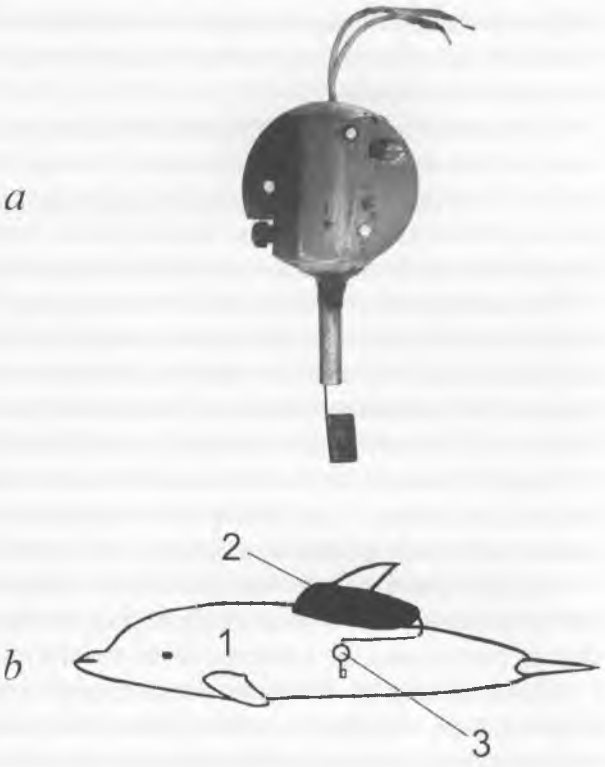

Fig. 5.36. Picture of a meter of the shearing stresses (*a*) and a fixing version of a meter on the dolphin's body (*b*): 1 – dolphin, 2 – recorder, 3 – meter.

5.1.7. The techniques used to study dolphin kinematics. Accelerometers

The research has been carried out in two ways: with cine filming and with accelerometers. Usually the cine filming is performed with a fixed camera. However during a single run, the time, when the animal is in the camera coverage, is insufficient for the tracing and studying of the motion of reference points at the animal body. In particular, it is difficult to measure phase velocity of the propulsive wave on several areas of the dolphin body with this method.

In the described experiments there was fulfilled the cine filming with a movable camera, which slid slowly and smoothly, tracing the animal. As a result, the animal was captured and held in the frame for a certain time. In this case we were able to trace the

dolphin movement during some periods of the body oscillation. Qualified diver performed the underwater cine filming through the meshy wall of sea cell, where the dolphin swam on the trainer orders.

The cine filming method has certain advantages. It is easy enough; it allows to get visual information on dolphin kinematics during free swimming. But this method also has sufficient limitations: the animal is held in the picture during the limited time period and it is difficult to decide if the dolphin moves uniformly or with acceleration. That is why the obtained information on dolphin kinematics has significant spread.

The accelerometer method, which we are going to describe, is much more accurate. It deals with diminutive accelerometers, which are fixed at the different points of dolphin body and make it possible to study the movement of these points during swimming. Signals of all accelerometers are simultaneously recorded on a single magnetic carrier. It allows us to study phase relations between these individual signals.

Another convenience of the accelerometer method is that it allows us to record information during a long time period; hence we can choose a certain interval of the record, which corresponds to a certain mode of the animal movement, and analyze it.

The diminutive recorder was fixed on the dolphin dorsal fin (Romanenko, Tchikalkin 1974; Romanenko 1976); thus we could study the kinematics of a free-swimming dolphin (taking into account the influence of the attached devices).

The oscillating accelerations, measured at the points, where the accelerometers were attached, were recorded. In order to obtain the values of biases of these points we must twice integrate these accelerations over the time. It is not difficult, and does not add any errors under the condition that the step of integration is sufficiently small.

The mechanism of accelerometer is shown in fig. 5.37. It is a thin steel plate 1. Its thickness is 0.08 mm. It is fixed by one end in the holder 2. On one end of the plate the strain sensor 3 is glued; a small lead 4 is fixed on the other end of the plate. This mechanical part of the accelerometer is contained in a glass ampoule 5, 1.4 cm in diameter and 7.5 in length. The inner chamber 6 of the ampoule is filled with oil (for example,

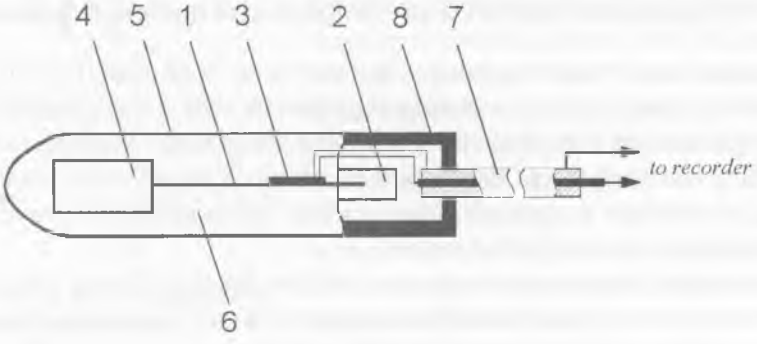

Fig. 5.37. Scheme of an accelerometer. The designations are in the text.

silicone oil) that prevents seawater infiltration and damps the oscillating system of the accelerometer. The strain sensor is connected to the measuring system on the dolphin dorsal fin with the cable 7. The measuring system records the small variations of active resistance of the strain sensor that arise during oscillatory movement of the accelerometer.

5.1.8. Dolphin swimming speed measuring methods

One can think that it is not a very complicated task to measure the dolphin swimming speed in capture. There are two the most commonly used methods: the method of cine filming (Pyatetsky,Kayan, 1975; Pyatetsky, Kayan, Kozlov, Semyonov, 1978; Romanenko, 1986a, Romanenko, 1995a) and the method of a diminutive impeller (Egidis, Shakalo, 1971, Romanenko, 1976a, Yanov, Romanenko, 1972). We also used the third method, based on the dependence of the vortex detachment frequency on the incoming flow velocity (Romanenko, 1976a). The structure and the mode of functioning of the flow speed meter of the second and the third types are described in section 5.1.5.

When the first method is used, they film a dolphin swimming along the straight trajectory. Then frame-by-frame analysis is fulfilled. We measure the biases of the clear-cut points on the animal body in the stationary coordinate system during the known time interval.

When the second method is used, the calibrated diminutive impeller is fixed at a certain point on the dolphin body. Its rotation under incoming water flow causes electric pulses, which are recorded. If we know the frequency of the generated pulses, we can estimate the speed of the dolphin movement. Strictly speaking, the value that we measure in this case is not the speed of the dolphin movement, but this is the speed of the incoming water flow in the point of the impeller location. If we neglect the difference between these values we can come to wrong conclusions. This remark is right for the measuring of the speed of movement with the third method. Errors are also possible if the cine filming method is used incorrectly. For example, the plot of periodic variation of progressive speed of the dolphin is adduced in the work of Pyatetsky, Kayan, (1975). This variation amounts to 17–20% of the speed value and the variation frequency is equal to double frequency of the animal body oscillation.

The work of Videler and Kamermans (1985) describes the periodic variation of the dolphin speed, which is measured with the method of cine filming. This variation amounts to 20% of the speed itself. But in this case the frequency of variation coincides with the frequency of the animal body oscillation. Here to obtain the animal speed the authors chose a reference point: the point of transition from the rear edge of the dorsal fin to the dorsal surface. There was found a significant variation of the animal speed during one period of the tail fin oscillation. This proves that the values of acceleration and deceleration of dolphin movement are rather big. In particular, we fulfilled some estimates based on the data from work of Videler, Kamermans (1985), and they show that the

acceleration amounts to 1.7 m s^{-2}. In order to move with this acceleration a dolphin whose mass is 232 kg needs the thrust force of at least 394.4 kg, but this value is almost five times more than the thrust actually generated by the dolphin. The authors of the mentioned above work came to the same conclusions and were bewildered. The results of the measuring of the progressive speed of the dolphin movement contained significant error of the method. That is why there is a considerable periodic variation of the measured dolphin swimming speed. The work of Pyatetsky, Kayan, (1975) has the same drawback.

Similar errors are caused by inefficient choice of the reference point, which is used for calculation of the animal progressive speed. Videler and Kamermans (1985) chose the reference point in the area of transition from the rear edge of the dorsal fin to the dolphin dorsal surface (fig. 5.38). In this case the shift of this point projected on the movement direction varies its value with the frequency of body oscillation. In the work of Pyatetsky, Kayan (1975) the reference point was located at the divergence of the tail fin (fig. 5.39). In this case the shift of this point projected on the movement direction will vary its value with the doubled frequency of body oscillation.

Fig. 5.38 shows the shift of the point *B* (the point of transition from the rear edge of the dorsal fin to the dolphin dorsal surface) during the active dolphin swimming. There are three phases of an oscillating cycle of the animal movement. During the first phase

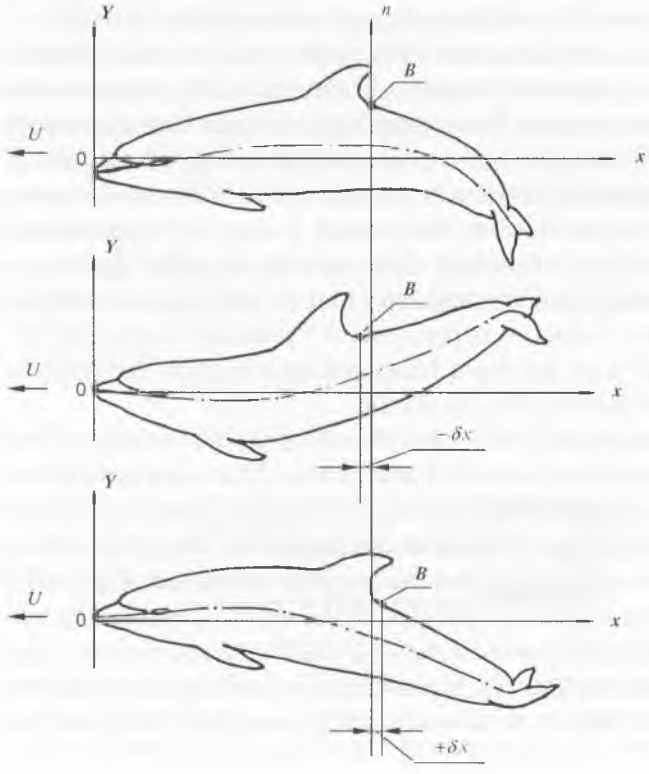

Fig. 5.38. A schematic representation of the shift of the point *B* during the active dolphin swimming.

the tangent to the medial line of the dolphin in the region of the point B is horizontal, during the second phase, it is sloping under positive angle, and during the third phase, it is sloping under a negative angle. Correspondingly, the point B shifted forward in the second phase (by value of $-\delta x$) and shifted backward in the third phase (by value of $+\delta x$) in relation to the vertical axis n, which passes through the point B in the first phase of the movement. When point B moves forward, its speed in a stationary coordinate system is greater than the average speed of the dolphin swimming, when point B moves backward its speed is less than the average speed of the dolphin swimming. The period of speed variation is equal to the one of the animal body oscillation. For the case adduced in fig. 5.39, the point B located near the dolphin tail fin twice for a period slips forward by the value of $-\delta x$ relatively the line n, which passed through this point at the moment when it was crossing x-axis. As a result, the speed variation has double frequency.

To support this statement we adduce the results of the experimental measurement of the dolphin progressive speed with the cine filming method. This experiment was accomplished on three dolphins (*Tursiops truncatus*). There were two female and one male dolphin. One of the females was of 2.08 m at length and of 180 kg, the other female was of 2.36 m at length and of 220 kg; the male was of 2.12 m at length and its mass was 200 kg. Kinematics of the dolphins was studied in a sea enclosure with the

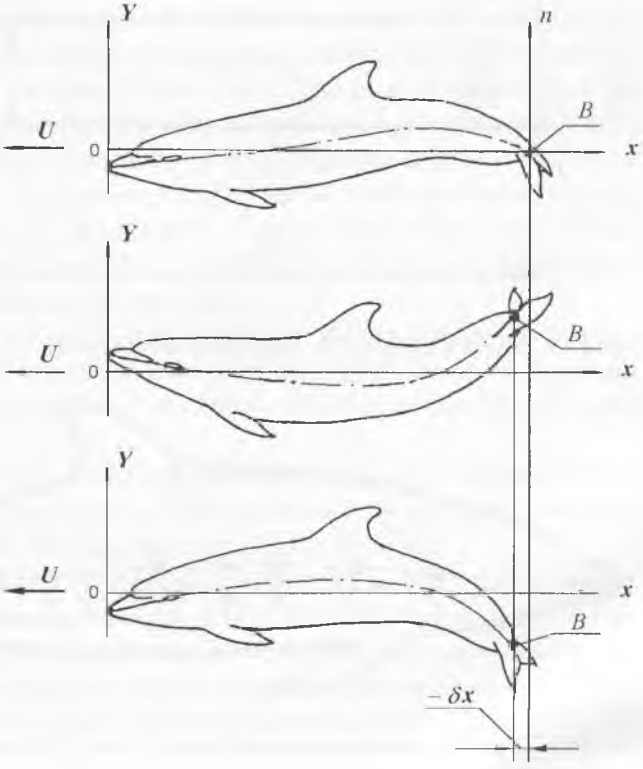

Fig. 5.39. A schematic representation of the shift of the point *B* during the active dolphin swimming.

cine filming method (figure 5.40). The sea enclosure belongs to the Utrish sea station of the RAS A. N. Severtsov Institute of Ecology and Evolution. The enclosure had two parts. The animals were kept in the first part, which was a 100 m^2 (10 x 10 m). It was formed by nylon netting with mesh size of 10 x 10 cm, which had a shape of a sack and was fixed within the frame of steel pipes. There was a platform in this part of the enclosure, marked as number 2. The other part of the enclosure is marked as number 3. It was a long passageway that linked the first part of the enclosure with the waterside. It was made of the same nylon netting. The passageway length was 70 m, its width was 6 m, and the depth was 3 m. There was a floating platform 4 at the waterside. During the experiment the dolphin was in the second part of the enclosure. The dolphin was taught to swim from one end of the passageway to the other. The dolphin was motivated by feeding at the both ends of the passageway. The operators, who fed the dolphin, were

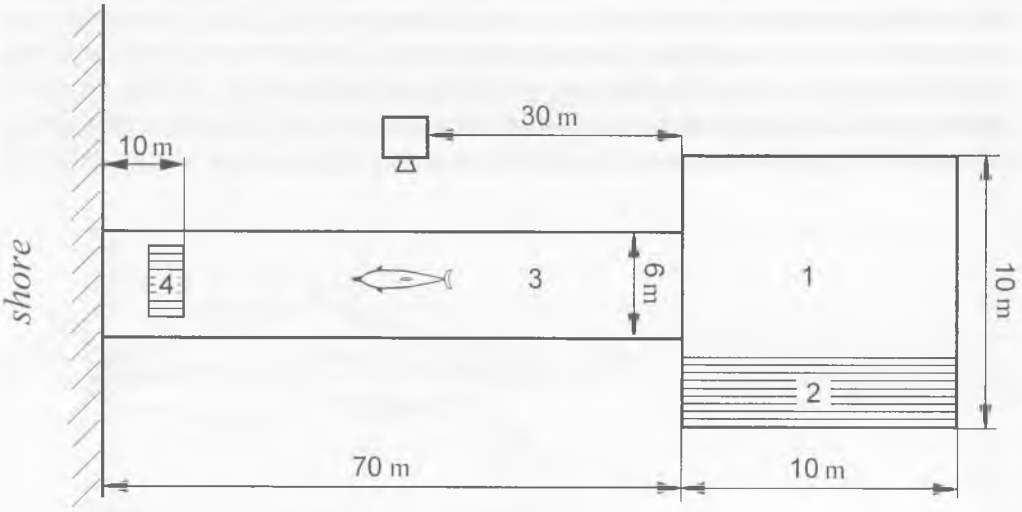

Fig. 5.40. The sea enclosure. The designations are in the text.

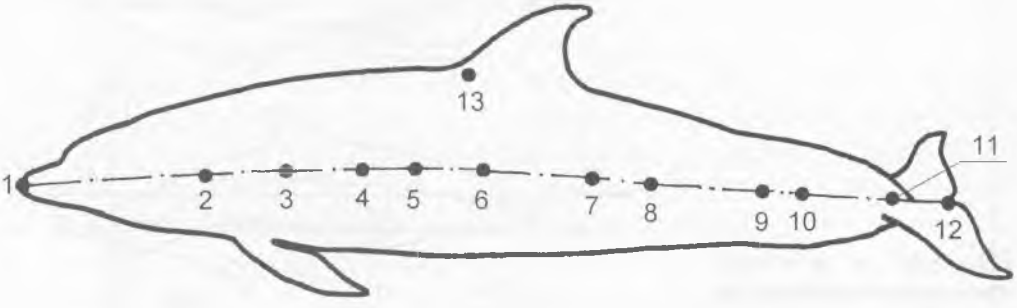

Fig. 5.41. The rubber vacuum caps on the dolphin's body. The designations are in the text.

located on the platforms 2 and 4. A camera-man-diver accomplished cine filming through the side-wall of the enclosure.

The main feature of the experiment was that among the points on the animal body it was possible to choose those, which defined conditions for optimal estimation of the dolphin progressive speed with the least possible error. In order the points were clear, they were marked with white rubber vacuum cups (fig. 5.41, points 2-11 and 13). The vacuum cups 2-11 were fixed on the animal flank along its median with a certain interval. Other points on the animal body that we used were point 1 (the end of rostrum) and 12 (divergence point of the tail fin). These points were clear on the film pictures without any marking.

Fig.5.42 shows the plots of speeds of movement for various points of the dolphin body during a period of oscillation. The averaged values in points 1-10 are adduced in the upper plot (*a*). The confidence interval contains two standard errors; the confidence probability is 95%. Clear periodic variation of the speed is marked for the points 9 – 13 (*b, c, d, e, f*). In this case the period of the speed variation in the points 9 – 12 is double period of the body oscillation. Variation of the speed at point 12 from its minimal value to the maximal one amounts to 28%. This agrees with the data from the work of Pyatetsky, Kayan (1975). The period of variation of speed of point 13 (fig. 5.42*f*) is equal to the dolphin body oscillation period. In this case the values of speed differ by 21%. This result agrees with the data from the work of Videler, Kamermans 1985, though the locations of the points being compared do not exactly coincide. But the character of shifts of the observed points is the same in both cases. The plots of variation of the longitudinal component of the speed for two points of the dolphin body are adduced in the fig. 2 from the work of Videler, Kamermans (1985). These points are the end of tail fin and the point of transition from the rear edge of dorsal fin to the dorsal surface, whose location is relatively close to the location of point 13 from fig. 5.42 *f* of this work. These plots well agree with ours (fig. 5.42 *e, f*). But Videler and Kamermans could not give satisfactory explanation for their data.

Variation of speed for points 1-8 are of irregular pattern. As a rule it does not exceed ±4% of the average speed. These points are located on the medial line in the front and middle parts of the dolphin body. They are less involved in the oscillatory movement then the others.

Variations of speed of the points 9-13 (from its minimal value to the maximal value) are more significant when the dolphin moves with acceleration. In particular, variation of the speed of the point 12 is ≈47% of the mean value. See fig. 5.43.

The absence of visible variations of speed for points 1-8 can be explained by the character of the amplitude function shown in fig. 5.44 (on the data from works of Yanov 1990c, Romanenko 1994a, b; Romanenko 1995a). We can see that the amplitudes of the dolphin body oscillation at these points are significantly less than the amplitudes in the tail area (points 9-12). That is why at these points the phenomena shown in fig. 5.38 and

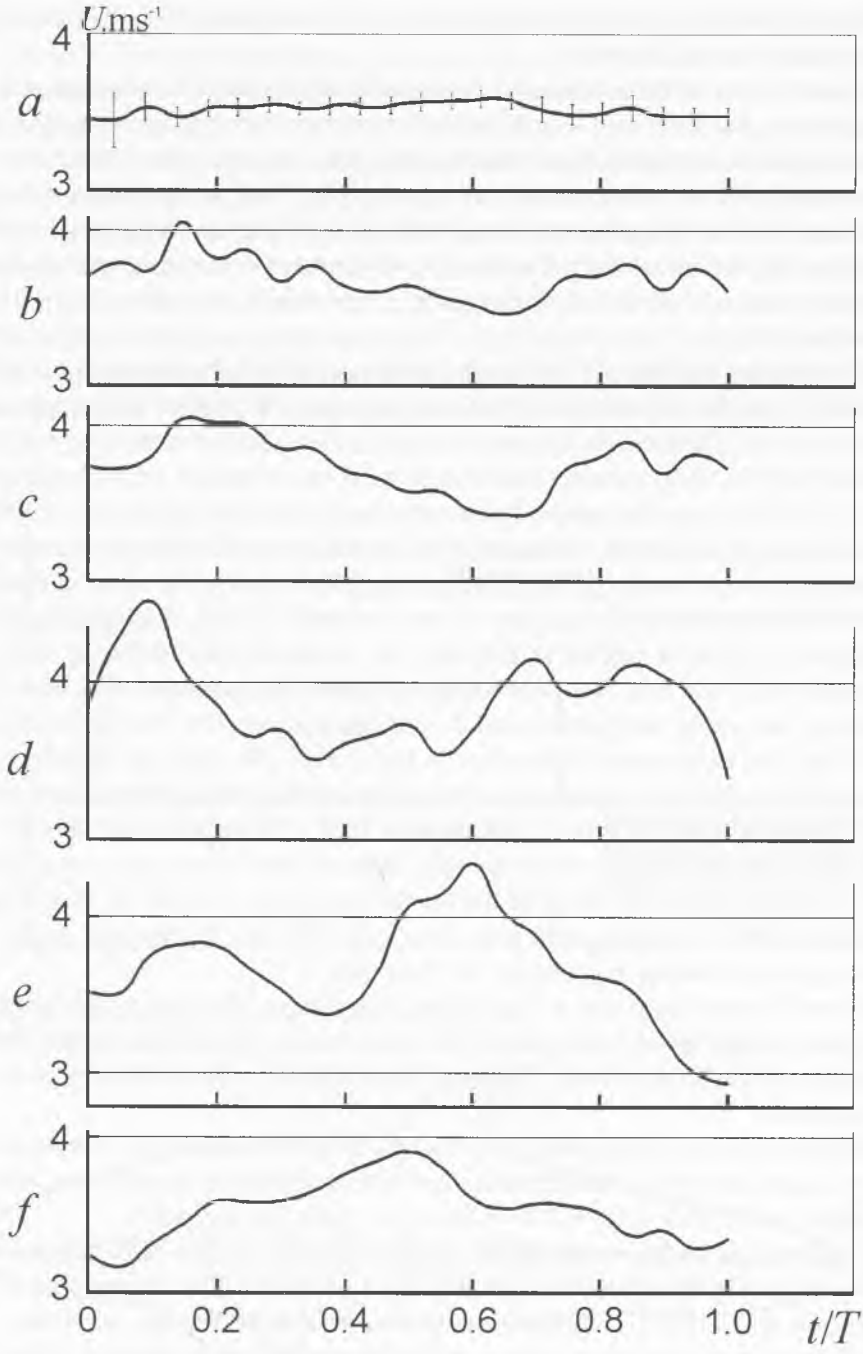

Fig. 5.42. The plots of speeds of movement for various points of the dolphins body during a period of oscillation. The designations are in the text.

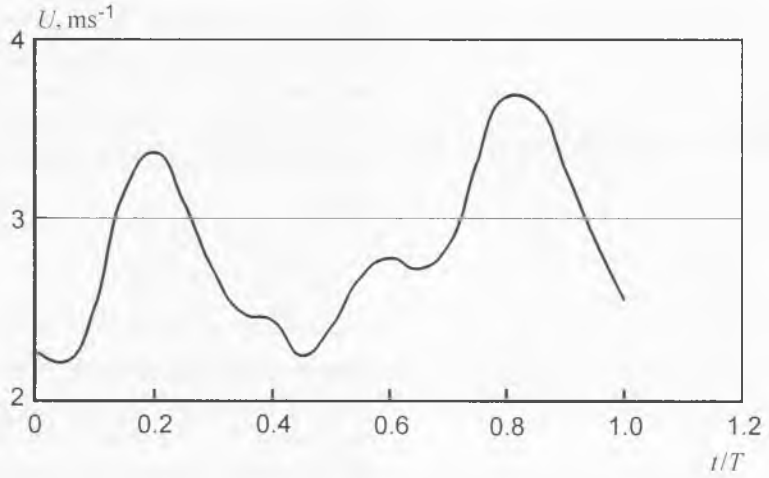

Fig. 5.43. The speed of the point 12 during a period of oscillation. The designations are in the text.

5.39 are less apparent. We can say that the points 3-5 are optimal for the measurement of the dolphin movement speed. These points are located on the median of the dolphin body in the region of the amplitude function minimum (fig. 5.44).

Let us estimate the pulsation component of the speed of dolphin swimming with a mathematical model. We assume that the dolphin moves under the effect of the pulsating force, which is graphically represented in fig. 5.45. Apparently, the frequency of the force pulsation is double frequency of the dolphin tail beating because the thrust is positive under either tail movement (up or down). The pulsating dolphin thrust F_T can be written as

$$F_T = F_0\left[1+\sin\left(2\omega t-\frac{\pi}{2}\right)\right]. \quad (5.68)$$

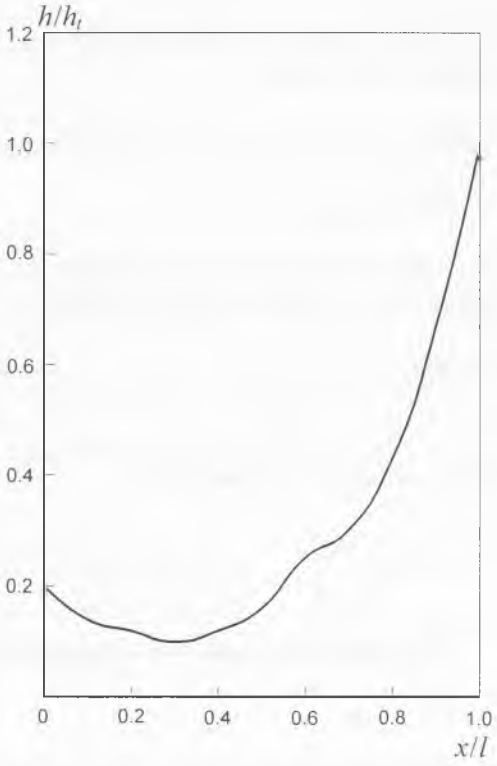

Fig. 5.44. The amplitude function of the dolphin. (Redrawn from Yanov, 1990).

$$u = -\frac{F_0}{m} \frac{\left(\frac{2AU_0}{m}\right)\cos 2\omega t + 2\omega \sin 2\omega t}{\left(\frac{2AU_0}{m}\right)^2 + (2\omega)^2} . \tag{5.82}$$

In order to evaluate the pulsation component of the speed by formula (5.82) we use the data from the work of Videler, Kamermans (1985) on *Tursiops truncatus*, which is adduced in table 5.2.

Firstly let us estimate the relation of terms of the numerator and denominator of the second fraction in the right part of expression (5.82):

$$\frac{2AU_0}{2m\omega} = \frac{C_D \rho S_b U_0}{2m\omega} = 0.0048 . \tag{5.83}$$

We assumed the value of the drag coefficient $C_D = 0.003$ (Romanenko, 1995 a). The estimation by (5.83) shows that the first terms of the numerator and denominator of the fraction in the right part of expression (5.82) are negligible in comparison with the second terms. Then formula (5.82) obtains its final appearance

$$u = -\frac{F_0}{m} \frac{\sin 2\omega t}{2\omega} . \tag{5.84}$$

In order to obtain the numerical estimates we need the relative amplitude of the pulsation component of the speed. We can obtain it if we divide both left and right parts of expression (5.84) by U_0 and use relation (5.75):

$$\left|\frac{u}{U_0}\right| = \frac{C_D \rho U_0 S_b}{4m\omega} . \tag{5.85}$$

The substitution of the data from table 5.2 into this formula yields

$$\left|\frac{u}{U_0}\right| = 0.0024 \quad (0.24\%). \tag{5.86}$$

U_0, ms^{-1}	S_b, m^2	m, kg	f, Hz
2.35	2.16	232	1.1

Table 5.2. Swimming parameters of *Tursiops truncatus*. (From Videler and Kamermans, 1985).

The final result proves that the pulsation component of the dolphin swimming speed is very small and it cannot be detected with traditional methods. Possibly this is the reason why there is no indication of the harmonic pulsation component of the dolphin swimming speed in the adduced above plot (fig. 5.4 *a*). We ought to consider that the existing irregularity (about ±4%) is caused by a measurement error.

Thus the pulsation components of the dolphin swimming speed, discovered by some researchers and amounting to 17-20% of the mean speed, are the results of a wrong choice of the reference point on the animal body. In order to exclude this error it is necessary to choose the reference point on the animal median in the forward part of its body, preferably at the distance of about 0.3 of the body length from the tip of its nose.

5.2. Methods and instruments for recording of biohydrodynamic information

Biohydrodynamic information can be recorded either with telemetry technique, or with autonomous instruments fastened directly on the animal's body.

Telemetry technique now has wide application above all for some technical sciences and for industry. For many decades telemetry has been used for oil industry, meteorology, space research etc.

In biology they started to use telemetry much later. At first it was applied to animal migration studies. The development of microelectronics allowed us to use telemetry technique to acquire some data related to physiological parameters of animals. There are two main telemetry methods: by means of wire communication between the object of the study and the research equipment, and by means of the wireless communication.

The first method is simpler and it is more frequently used in the laboratory studies. But often the usage of wire circuit that connects the object with the apparatus is not very convenient, especially if an object is a mobile one. For wireless communication they often use radio waves, or sometimes, acoustic waves, or on very rare occasions optical communication. The best technique is radio telemetry. It provides wide range of capabilities. In particular, the researcher can acquire data of observations directly in the course of experiment. Sure, this way is more complicated because some interferences and information distortion can arise in the radio channel and we must take some especial action to correct it. Here we adduce the opposite remark of the American scientist Holter who said at the biotelemetry symposium in New York in 1962: "Solving the problem of co-operation between a physicist and biologist I would like to appeal for using electronic equipment which corresponds the aims of the biological experiments being at the same time as simple as possible. Among the engineers there is a trend to go in for the splendid circuit decisions and to forget the destination of this equipment". And more: "I propose to use telemetry not for telemetry itself but only in those cases when it is the best technique." (Holter, 1965). We can hardly add anything to this.

Telemetry makes its first steps in the area of biohydrodynamics. There are only a few works that use the telemetry technique in a certain degree. There is no hazard of over-indulgence to telemetry. We rather need a wide advocacy of this method of studying.

The technique of recording of biohydrodynamics information with the autonomous devices fastened on the object of study has no precedent. This is quite a new method. Taking into account fast progress of technology we see that this method is very promising. Our experience in usage of diminutive autonomous recorder for the biohydrodynamic and bioacoustic information recording directly on the animal was very fruitful. We ought to remember that our experiments were fulfilled in 60-70s of the 20 century, when contemporary storage devices did not exist. Thus our instruments have now rather historical value. But the scientific materials, which were achieved with those devices, are still relevant. So we choose to give here the comprehensive description.

Before we come to the description of particular designs in this area, let us explicate the basic principles of the communication theory and information theory. Knowledge of these principles is useful for everyone who deals with measuring technology, communication, information recording and storage.

5.2.1. General concepts

We can define the concept of information as data that are acquired, communicated, stored and processed (We adduce here the general concepts of information theory as they were formulated in the book "Biological telemetry" , edited by academician V.V. Parin, 1971). Information has either statistical form, when it is stored (as records, images, etc.) or dynamical form, when it is transmitted (as physical, biological, chemical and other processes).

The quantitative measure of information or of information capacity of a storage or communication system was proposed in 1927. It is called binary unit or bit. If the cell where information is stored has n allowable states then two such cells have n^2 possible states, and m cells have n^m possible states. It means that there is an exponential dependence between the number of cells and the number of allowable states. According to this fact there was introduced the logarithmic measure of information capacity

$$C = \log N. \tag{5.87}$$

Here N is the number of possible states of the system. This measure meets the additiveness condition, i.e. the quantity of information that is stored in m identical cells is m times greater than the quantity of information that is stored in one such cell. Information capacity of the system that consists of m cells and has $N = n^m$ states is equal the capacity of one cell multiplied by the number of cells

$$C = \log n^m = m \log n. \quad (5.88)$$

If we use the binary logarithm then the information capacity of the system is the number of elementary cells, each has two possible states. The capacity of this simplest binary cell is "binary unit" or "bit".

Certain information capacity can be filled by various quantity of information depending on technique of information coding.

Information can be communicated from one point to another with a communication system, which consists of a transmitter and a receiver connected by a communication line. The communication line is either wires or a space where waves of light or sound or radio spread.

A set of data that must be transmitted to an acceptor is a message. A sender is a source of the message. In a biotelemetry system this is an alive organism which we study with applied sensors. The message is transformed into corresponding signal in the transmitter and transmitted with the line of communication to the receiver, where the reverse transformation of the signal into the message is performed.

Carrying capacity is one of the main characteristics of the communication system. This is a quantity of information that can be transmitted in this communication system in the unit of time with a certain accuracy of transmission. In reality, any message is always affected by interferences. Therefore a communication system must be capable to withstand interference effect. This feature of the communication system is called noise-immunity.

Several different messages can be transmitted simultaneously through a communication line. Each message is transmitted in a separate channel. The channel means here the set of technical devices that support the transmission of the message through the common communication line regardless of another messages transmitted simultaneously. Thus, if our communication system becomes a multichannel one, then its efficiency increases. However in this case the problem of separation of the different channel signals arises because all the signals are transmitted in a single communication line.

Some electric processes can not effectively spread along communication circuit. Only direct current and low frequency alternating current easily pass through a wire line. Only electromagnetic oscillation of high enough frequency easily passes through a radio channel. That is why to form a signal we need a carrier, which spreads most effectively in a particular communication line. For radio line this carrier is usually a sine-like electromagnetic oscillation, described with certain parameters such as amplitude, frequency and phase. If these parameters are constant, we cannot transmit any message. That is why we must vary one of the parameters according to the message, i.e. we must

modulate carrier. The carrier whose parameters are modulated is a signal. This signal is emitted into space by the antenna of transmitter and spreads to the antenna of the receiver. The amplitude modulation (AM), frequency modulation (FM) and phase modulation (PhM) are used in wireless communication.

We also can use a series of pulses of direct current as a carrier. In this case the parameters of the pulse series are the following: the amplitude, pulse-repetition frequency, pulse duration. Accordingly we have the pulse-amplitude modulation (PAM), pulse-phase modulation (PPhM), and pulse-duration modulation (PDM). There is also so-called pulse-code modulation (PCM). This modulation transfers different messages into corresponding pulse combinations, which are the codewords. We can also use the sequence of radio-frequency pulses as a carrier. Beside the modulations based on the pulse amplitude, pulse-repetition frequency and pulse duration we can modulate the carrier waveform itself. There are a great number of these complicated modulations. We designate them by two groups of letters: the first group designates the type of modulation of the auxiliary oscillation (subcarrier), the second group designate the type of modulation of the carrier by the subcarrier. For example, the frequency modulation of the subcarrier and the frequency modulation of the carrier is FM-FM, the amplitude modulation of the subcarrier and the frequency modulation of the carrier is AM-FM etc. In terms of system simplicity, required input power and reliability the FM-FM system is the best. But all systems with FM have one essential imperfection. The signals, whose level is lower than some threshold, are heavily distorted due to spurious AM modulation caused by the transmitter field interference.

Let us consider interrelation between the parameters of the signal and the parameters of the channel communicating this signal. One of the signal characteristics is its volume.

$$V_s = T_s F_s H_s. \tag{5.89}$$

Here T_s and F_s are correspondingly the duration and the bandwidth of the signal,

$$H_s = \log \frac{P_s}{P_n}, \tag{5.90}$$

P_s and P_n are the mean powers of the signal and of the noise.

Similarly we can characterize the communication channel.

$$V_c = T_c F_c H_c. \tag{5.91}$$

Evidently, the condition of the signal transmission is

$$V_c >> V_s. \tag{5.92}$$

and so we can vary the signal parameters, but if the volume of the signal remains the same, the signal and the channel will be still matching. For example we can increase the transmission time and by this decrease the bandwidth, and so on. For this purpose we can apply different coding methods.

Coding is transferring of the message from one form to another in order to solve a certain task. The coding is used in communication engineering to form rational and efficient conditions for the message transmission. The code is some law or system of rules, which determines message transferring from one form to another. A lot of different coding methods were developed and studied.

In practice important characteristic of the communication channel is the limit of throughput or capacity C, i.e. the quantity of information that can be transmitted with infinitely small error probability through the communication channel.

$$C = F_c \log\left(1 + \frac{P_s}{P_n}\right). \tag{5.93}$$

We can see from this formula that if the signal power and the channel bandwidth increase the extreme rate of throughput of the channel and the maximal speed of the message transmission also increases. If the channel has very high interference level ($P_n >> P_s$) then its capacity and its maximal speed of transmission are near zero. But such channel has some throughput although it is significantly decreased. We could use even this channel if we apply special methods of accumulation, correlation and coding. But formation of the channel, which has unlimited throughput is practically impossible, because there are various fallibilities in transmitting and receiving devices.

The characteristic feature of a multichannel system is a channeling device on its receiving end. In fact, the channeling is a signal extraction on the interference background. In this case the interference is the signal of the neighbor channel. The most accepted methods of channeling are time channeling and frequency channeling. Any signal has a limited frequency spectrum. Any receiver has to contain a frequency filter passing only the frequency spectrum of its signal. Such division is called frequency channeling.

In time channeling system the communication line alternately passes signals of different channels. This occurs due to a special commutator (switcher). The similar commutator at the receiving end, which works synchronously with the first one, separates signals of different channels. Under the condition of the multichannel transmission there is always a hazard of mutual impact of different channels. This phenomenon is called mutual interference.

In the case of frequency channeling signals of neighboring channels passing through a filter of a certain channel interfere with useful signal reception. To depress this interference, protective frequency bands are introduced between channels.

In case of time channeling the mutual interference is caused by the "inertia" of the communication line. Each communication line contains elements that can store electric energy. These are inductances and capacitances. Existence of these elements causes a distortion of the transmitted signal waveform as the energy that is stored in the line due to a certain channel signal is summed with the energy of neighboring channel signals. Now let us consider specific telemetry developments that were used in the biohydrodynamics researches.

5.2.2. Telemetry in biohydrodynamics

The progress of the microelectronics gave us the possibility to make the autonomous telemetry instruments that can be fastened on a dolphin or any other animal of similar size. The choice of the telemetry technique is defined by the kind of information, which we must transmit with this telemetry equipment, and by the conditions of the information transmission.

The equipment that we are going to describe here (Yanov, Romanenko, 1972) is assigned to transmit the information on the structure of dolphin boundary layer and the speed of the flow around the dolphin body. If the speed of the dolphin's movement is below 5 – 10 ms^{-1}, we can consider the information about the flow speed to be a narrowband process (50 – 100 Hz) and the information about the flow pulsation to be a wideband one (1 – 2 kHz). Besides, we need similar information at several points of the dolphin body surface.

When the dolphin is in a limited area of netting passageway, the conditions of the transmission from the dolphin let us choose the radio-current communication channel. This channel has a small range but there is no reverberation, which is typical for an acoustical communication channel.

We needed a short-range communication inside the netting passageway. But in the area there was relatively narrowband interference from the frequency close radio stations and radio beacons. This communication conditions made us choose the amplitude modulation of the carrier of the autonomous transmitter.

Taking into account the described features of the useful information and communication conditions we developed multichannel telemetry autonomous equipment that allowed logging of the following parameters:

1. The speed of the flow around the dolphin body at three different points simultaneously
2. The pressure pulsation (or the speed pulsation) at three different points simultaneously
3. The frequency of the dolphin body undulation
4. The frequency of the dolphin respiration

Alongside with these parameters three calibrating signals were transmitted. They allowed measuring of absolute value of pressure or speed pulsation, if the sensibility of pulsation receivers were known. The calibrating signals also let us monitor the communication channel (to check the equipment correctness and readiness).

There were three radio transmitters in the apparatus. The transmitters had the carrier frequencies 106.85, 148.75 and 161 kHz. The amplitudes of these carriers were modulated by a noise signal from the sensors of pressure pulsation or speed pulsation (in the band 20 – 1500 kHz) and by a signal of the amplitude calibrating with the frequency of 2 kHz. The depth of the carrier modulation by the calibrating signal was 6%.

To transmit the information on the speed of flow around the body and undulation frequency, each transmitter used two subcarriers. The first subcarrier was the calibrating signal (2 kHz), manipulated with amplitude pulses of the second subcarrier, which was a sequence of square waveform pulses. The rate of the pulse repetition carried the information on flow speed and on the dolphin body undulation frequency (2 – 3 Hz). The pulse-frequency modulation of the second subcarrier took place. The first subcarrier, which was modulated on amplitude by square wave pulses remained the calibrating signal, but it also can carry the low-frequency (to 100 Hz) information on the flow speed. This information was concentrated in the frequency range near the first subcarrier frequency (2 kHz) and did not overlap with the band of the noisy signal of the pressure or speed pulsation from 20 to 1500 Hz.

The power of the transmitter outputs on the resistance of 10 Ohm in the silence mode was 50 mW. The equipment could work in the continuous mode or in the waiting mode. Duration of the continuous work amounts to 1 – 1.5 hour, duration of the work in the waiting mode amounts to 50 – 100 hour. Control of the radio transmitters in the waiting mode was performed with the command radio line by means of a transmitter, which was a standard oscillator (G3-33), and a receiver, incorporated in the housing of the autonomous complex.

The frequency of the controlling radio signals of the command radio line was 185 kHz, the current consumption in the waiting mode amounts to 1.5 mA, in the continuous mode it amounts to 200 mA. The equipment was supplied from the autonomous power sources, which were the storage batteries (7D-0.1).

The volume of the apparatus with the power source was 400 cm^3, with the encapsulating housing it was 500 cm^3.

The weight of the apparatus without the power sources was 500 g, the weight of the apparatus with the power source was 700 g.

Reception of the signals was performed by industrial radio receivers "Volna-K". Each of them was tuned to one of the carriers. The bandwidth of the receiver (6 kHz) provided undistorted reception of the information.

Let us discuss how the telemetry communication circuit operates (fig. 5.46). If we need to observe the animal behavior for a long time, the transmitters of available

information in all three channels are usually off. Only the receiver of the command line is switched on. This receiver is a part of the autonomous apparatus. Its power consumption is very small. When we need to turn the transmitters on, we supply the pure sine signal of 185 kHz from the oscillator G3-33 to the radio current channel during 2 – 3 seconds. The receiver of the command line receives this signal and turns the transmitters on by closing their supply circuits during 20 – 25 second. During this time available information is transmitted to the shore on the three carrier frequencies (f_1, f_2, f_3). This information is received by the receivers (Volna-K) and then logged by multichannel recorder.

When we study the dolphin hydrodynamics within the limited water space, it is worth to use the apparatus in the continuous mode because the experiment duration is less than 1 hour. In this case the receiver of the command radio line is switched off, the transmitters are connected with the power supply source and continuously transmit the information, and the receivers continuously receive the information, which comes from the flow speed sensors and from the pressure or speed pulsation sensors.

The measuring system contains three pressure or speed pulsation piezoceramic sensors and three flow speed meters of the impeller type. The scheme of the multichannel measuring system, which is used to determine the dolphin hydrodynamic parameters, is shown in fig. 5.47.

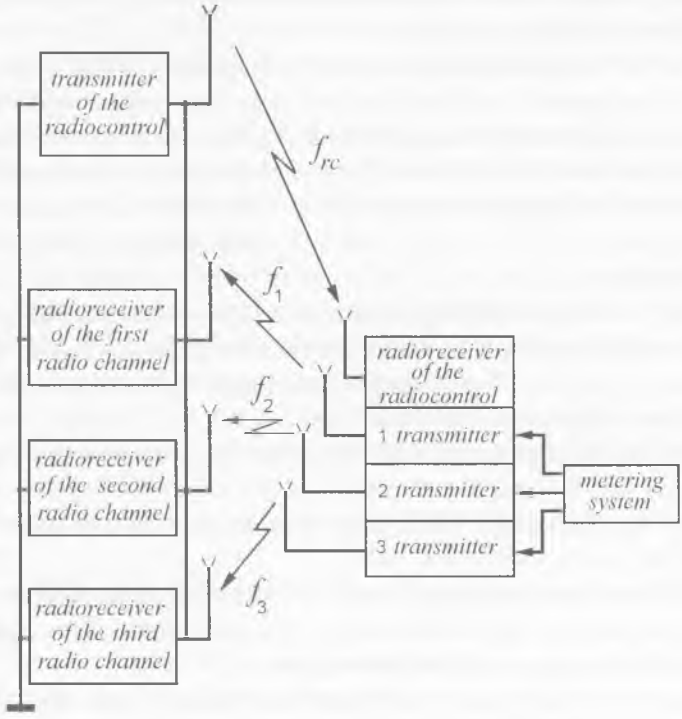

Fig. 5.46. The telemetry communication circuit. The designations are in the text.

The dolphin 1 is in the netting corridor 2 of 75-120 m length, of 3 m width and of 2-3 m depth. The sensor system and the autonomous apparatus are fastened on the dolphin. During the dolphin movement the radiating antennas of the three autonomous transmitters and the antenna of the command line receiver are drawn behind the autonomous complex as four thin wires 4 of 1.2 mm in diameter. These wires electrically touch water. For this purpose 20-30 mm at the end of each wire are stripped. The rest parts of the wires (from the transmitters to the bare ends) are insulated from water. The metal housing of the autonomous complex serves as the grounding pole of the radiated antennas. The lengths of the antennas vary from 1.5 m to 2.5 m in order to avoid contacts between the bare parts which can destroy the transmitters operation. The receiving antenna of the data channel receivers is made of wires, which are stretched along the perimeter of the corridor. At the same time, these wires form the radiating antenna of the command radio line. The ends of these wires are soldered to the metal plates 5, which electrically touch water. The grounding is formed by the metal plates 6, which are located at the opposite end of the corridor. They also are contacting water. Antenna is connected with three receivers 7-9 tuned to the corresponding carrier frequencies. And during the launching signal radiation (2 - 3 s) the transmitter of the command radio line 10 also gets engaged with the antenna. Relevant information from the transmitter outputs is recorded by the multichannel recorder 11.

Fig. 5.48 shows the functional arrangement of the telemetry complex, which contains three identical transmitters of relevant information and the receiver of the command radio line. Each transmitter consists of three functional circuits:

1. The circuit that forms the carrier, modulates it by available information and magnifies its power;

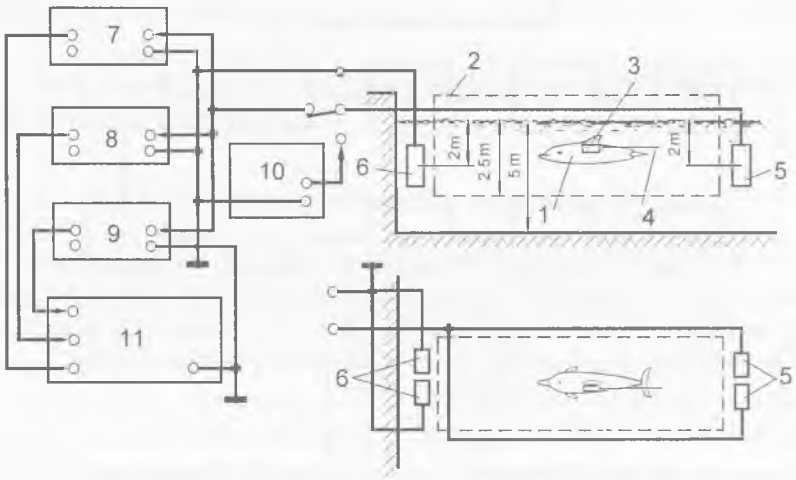

Fig. 5.47. The scheme of the multichannel measuring system. The designations are in the text.

2. The circuits of preamplifier, noise signal of pressure or speed pulsation delimiting and summation of this signal with the signal of the amplitude calibration;

3. The system of the streamline speed measurement, which uses additional pulse frequency – pulse amplitude modulation of the amplitude calibration signal.

The sine-like oscillation generated by the basic frequency generator 1 is supplied through the matching stage to the amplitude modulator 2, which modulates it by the low-frequency signal of available information (the total signal of pressure or speed pulsation and pulse frequency – pulse amplitude modulated signal of the amplitude calibration). The amplitude-modulated carrier from the modulator is supplied to the power amplifier 3 and is radiated into the sea water.

The noise signal of pressure or speed pulsation from the piezoelectric capacitive sensor 4 comes to input of the preamplifier 5, which has high input resistance (around hundreds of megOhm) and a low level of self-noise (several μV in the frequency band

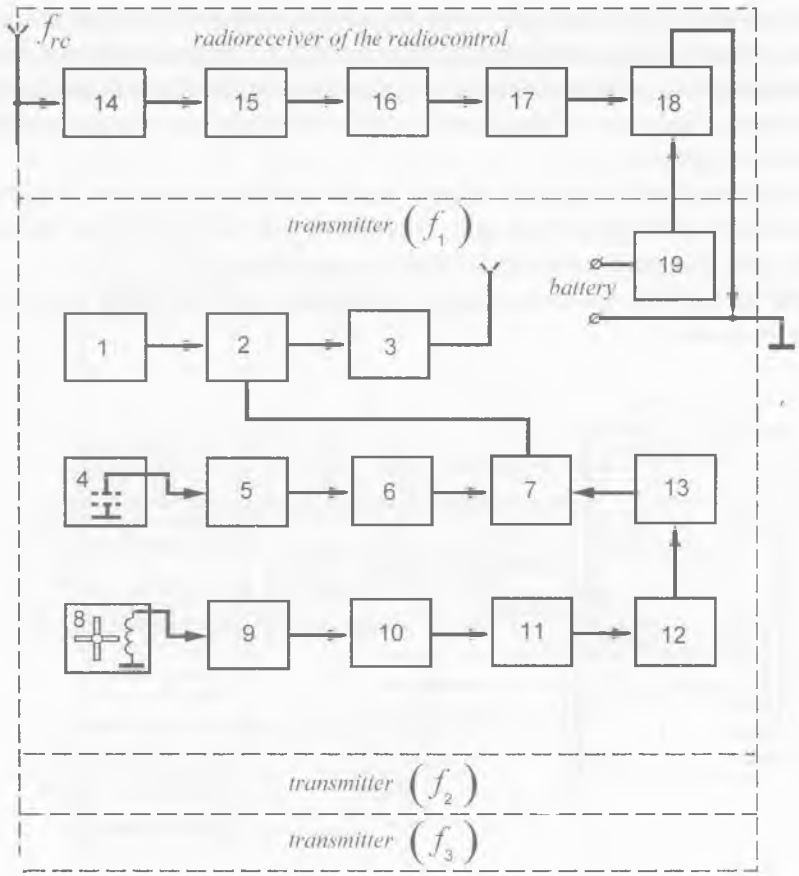

Fig. 5.48. The functional arrangement of the telemetry complex. The designations are in the text.

20 – 2000 Hz). The gained signal comes through the filter of low frequencies 6, whose cutoff frequency is 1500 Hz, and then it is supplied to the linear adder 7. There it is added to the pulse-frequency – pulse-amplitude modulated signal of amplitude calibration.

Incoming flow rotates impeller 8 during the dolphin movement. The constant ferrite magnet is mounted on one (or two) of the impeller vanes. When the impeller rotates it generates electric pulses in the coil. The pulse repetition frequency carries information on the speed of the incoming flow and on low frequency undulation of the dolphin body during its active movement. Impeller pulses are gained by the amplifier 9 and differentiated. Then they actuate pulses of the blocking generator, which are supplied to the transformer of the signal that carries information on the streamline speed. This transformer is the T- trigger 11. The trigger pulses of square waveform control the generator of the amplitude calibration signal by means of pulse-amplitude modulation of its signal. This generator is a symmetrical multivibrator 12. Then the modulated signal of amplitude calibration comes to the high frequency filter 13. This filter eliminates the zero-frequency component and the low-frequency part (below 50 – 100 Hz) of the spectrum of complicated signal, which is modulated by the pulsation of pressure or speed. Modulation of this signal is implemented by its pulse frequency – pulse amplitude control. Then the filtered signal is supplied to the summator 7.

The pure sine signal, whose frequency is 185 kHz, comes from receiving antenna to the resonance amplifier 14 and then to the amplitude-limiting amplifier 15 and diode detector 16. The constant voltage signal from the detector is supplied to the time-delay device 17 and then to the keyed circuit 18. When it opens, the plus of the feeding element (E) comes through the opened keyed circuit to the housing of the autonomous complex and the transmitters of the three channels of available information start their operation. The time interval of the transmitters operation is defined by the sine signal delay of the time-delay device after the sine tone signal of the command radio line is ended (after 20 – 25 s).

The autonomous complex is arranged as a modular structure of solid micromodules where each module is a functional unit.

5.2.3. Underwater magnetic recording devices

When biological objects as fish, cetaceans, and pinnipeds are studied in natural or close to natural conditions, one of the main methodical problems is to obtain any information on the vital functions in general and on their biohydrodynamical parameters in particular. The telemetry devices that give us solution of this problem are described in literature (Schakalo, 1972, Yanov, Romanenko, 1972). But every device has its own drawbacks. The communication cable limits the animal movements, and radio communication channel is bound up with the necessity of complex information coding and decoding. Besides, in this case the action range is heavily limited. Usually it is a magnetic tape recorder that

serves as a logging device. Therefore there is a question: if we can avoid information transmission through the communication channels and record the information from sensors directly on the magnetic recorder that is placed on the studied object.

We have developed three variants of a multichannel magnetic recorder that is fastened directly on the animal. These recorders are designed for underwater recording of available information in a sufficient frequency band directly from the sensors. Recording is performed with a standard writing heads either on several standard wire sound carriers or on a single sound carrier with frequency channeling.

We must note that the described works were done about 30 years ago. Because the original results on dolphin hydrodynamics were obtained at those years, we chose to give description of the applied recording devices. Now much more accomplished means for information recording is developed.

The first variant of the three-channel magnetic recorder was made as light and economical as possible. In this appliance the wire sound carrier transport mechanism is not hermetically closed. It is freely rinsed by water. Besides, it has no electric motor. It operates with a turbine driven by the incoming flow of water. This allows us to make a lightweight design. Each of the three cassettes that are loaded into the recorder had a capacity of about 1500 m of wire. The time of continuous recording is about 15 minutes. This recorder has a certain drawback. It operates only when the animal is moving. Therefore it can be used only to solve the problems concerning animal movement, and in particular, biohydrodynamical problems.

Fig. 5.49 shows the carrier transport mechanism. Here 1 is the turbine placed on the shaft of the three-section receiving cassette 2, 3 are three hermetic writing heads, 4 are three feed cassettes with the wire sound carrier, 5 are the braking consoles, 6 are the shielded conductors to supply bias current and available signal to the writing heads.

The mechanism operates the following way: the incoming flow of water is rotating the turbine 1 while the animal is moving. The turbine 1 is partly covered by a lid so that

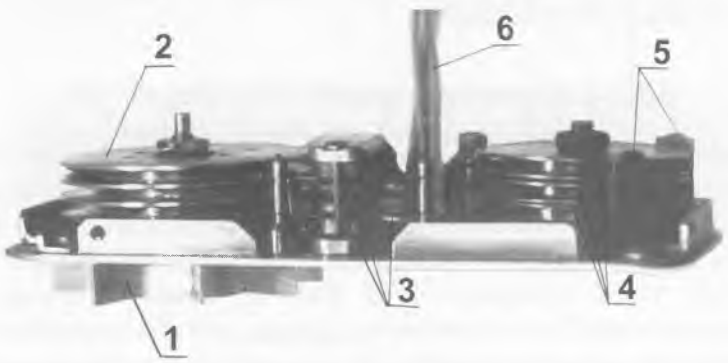

Fig. 5.49. The carrier transport mechanism. The designations are in the text.

the incoming flow impacts only the blades protruding from under the lid. The turbine rotates three-section take-up cassette 2 that reels the wire sound carriers up after they were drawn through the operating gap of the writing heads 3. At the same time the consoles 5 brake the feeding cassettes in order to obtain the required strain of the carrier.

In operation the mechanism is partly cloaked by the lid, which is not shown in the figure, to prevent it from mechanical damage. The lid is perforated and water penetrates freely into the mechanism. As the heads and sound carriers are made of corrosion resistant materials, short-time action of salt water does not deteriorate the record quality.

The term "three-channel recorder" is not quite correct in relation to the described appliance. We ought to call this device "triple recorder" because in one arrangement there are three recorders, which have a common system of carrier transport.

Fig. 5.50 shows the block diagram of the writing amplifiers. Available signals from the sensors are supplied to the inputs of the three identical voltage amplifiers 1, 5 and 9 and then to the inputs of summators 2, 6 and 9. The identical reference sine signals also come to these summators from the generator 13. There the available signals are summed with the reference signals and then totals are gained by power amplifiers 3, 7 and 11, whose outputs are connected with the writing heads 4, 8 and 12. The biasing of these heads is effected by direct current. All the circuits are feed by stable power source 14.

The purpose of the reference signal is synchronization of the available signal records on three independent sound carriers. The speed of carrier transportation varies depending on the speed of the incoming water stream and consequently on the animal swimming speed. The reference signal, whose frequency is known and invariable, gives the possibility to determine the recording speed with permissible accuracy during playback under the known transportation speed. The reference signal amounts to 2-3% of the maximal available signal.

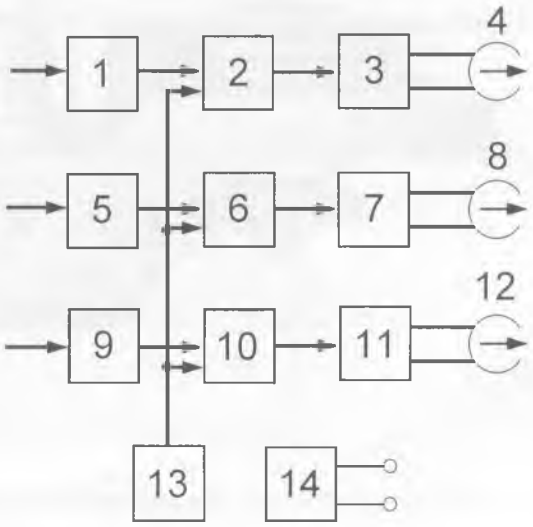

Fig. 5.50. The block diagram of the writing amplifiers. The designations are in the text.

The recorded frequency band depends on the speed of the carrier transportation. When the speed is 3 ms^{-1}, the recorded frequencies lie within the interval from 100 Hz to 120 kHz. The wide band of the working frequencies lets record both the pulsation of pressure or speed and the acoustical component of the streamline noise.

The reference signal frequency is 1230 Hz.

We have already mentioned that we tried to make this recorder as simple as possible. It cannot be controlled during its work. The speed of the carrier transportation is variable. The second variant of the recorder does not have such a drawback. It differs from the first one by the presence of an electromotor, which ensures relatively unchangeable speed of the carrier transportation and gives the possibility to work with a static animal. Besides, it has a radio remote control system. This lets record information at experimenter's will in required moments. Between the intervals of recoding the system stays in economical duty mode. It is ready to start work on the experimenter's radio command.

The kinematical scheme of the second recorder is the same as the scheme of the first one but instead of the turbine rotated by the incoming flow we use the electromotor DPM-25 with the friction gear, which matches the speeds of the electromotor and leading three-section cassette. The second variant of the recorder is shown in fig. 5.51.

The application of the electromotor lets us increase the speed of the carrier transportation to 3 – 4 ms^{-1}, ensure its stability and high quality of recording in the frequency band 100 Hz – 120 kHz. In this variant we use the same writing amplifiers as in the previous variant. The circuit of remote control, which switches on the power supply of the motor and writing amplifiers, is added to the electronic part of the recorder.

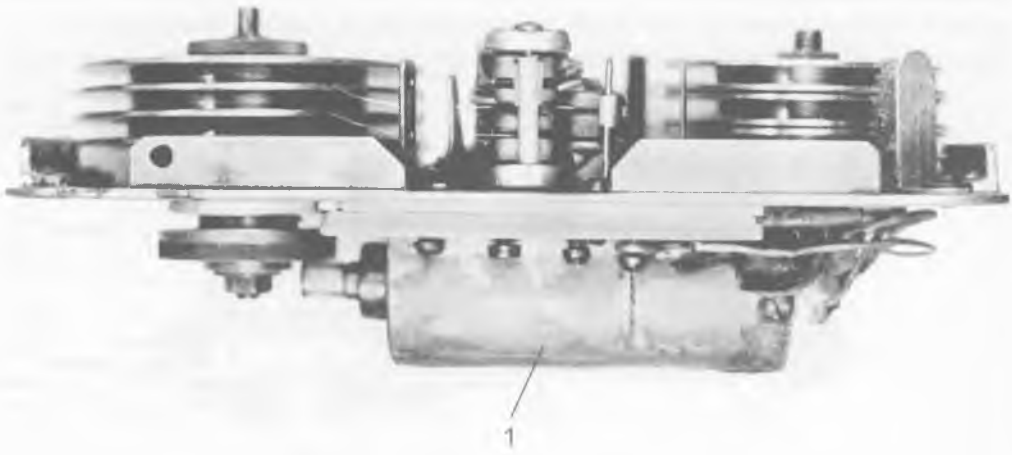

Fig. 5.51.The second variant of the recorder. 1 – the electromotor.

Also there is a time relay circuit, which sets the time interval of the recorder operating after it is turned on.

Fig. 5.52 shows the scheme of the experiment in case of the remote control of the recorder. The dolphin 2 or another animal is swimming in a basin 1. The recorder 3 with the remote control circuit whose input is connected to the receiving antenna 4 is fixed on the animal. There is a radiating antenna 5 in the water. This antenna consists of a metal plate electrically touching water and electrically grounded plate. The radiating antenna is connected to the generator 7 through the breaker :. At the required time the breaker closes the circuit and several volts of voltage of 150 kHz frequency come to the plate 5. Till this moment the recorder is in the waiting mode. Then the radio-current field is arisen in the water of the basin. Its nature is not quite clear, but it induces the voltage of the same frequency in the receiving antenna. The value of this voltage is quite enough for actuation of the power switching circuit of the recorder. If the distance between the radiating antenna and the receiving antenna is about several tens of meters then we can obtain reliable communication between the antennas.

Time interval of the operating mode is 8 s. While setup we can adjust this time in a wide range.

Recorded phonogram playback is performed with the advanced recorder MN-61. We applied the playback amplifier, which was specially developed for the purpose. There was low frequency and high frequency correction, which allowed reconstructing the recorded information without distortions.

We have already noted that we applied direct current for the biasing of carriers in order to simplify the circuit of the recorder. This narrows the dynamic range of the record to 30-35 dB. But the fact that we have three recorders operating simultaneously allows us to record signals under the dynamic range of about 100 dB. In order to obtain that we have to connect the only sensor of available signal to three recorded channels simultaneously and set the gain coefficients to triple covering of the dynamic range of

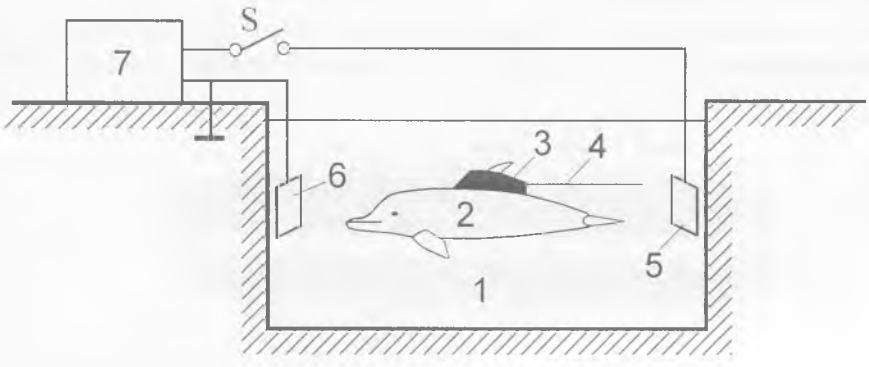

Fig. 5.52. The scheme of the experiment. The designations are in the text.

the only one recording channel. Then the weakest signals are recorded on the first sound carrier (and the stronger signals are distorted), the medium signals are recorded on the second sound carrier and the strongest signals are recorded on the third one. Signals of low and medium levels are recorded on the third sound carrier faintly.

The third variant of the recorder was designed as compact as it was possible. Unlike the previous variants the record amplifiers and the power sources were mounted in a single housing together with the carrier transport mechanism. This recorder can operate in two ways. The first way is the two-channel mode with the frequency band of available information recording from 20 Hz to 8 kHz. We used this mode especially for recording pressure and speed pulsation in the course biohydrodynamical research. The other way is the single channel mode with the frequency band of available information recording from 20 Hz to 120 kHz. We used this mode for recording pressure and speed pulsation along with the acoustic component. In the first mode the speed of transportation of the sound carrier is 1.5 m/s, in the second mode it is 3 m/s. In the first mode all the information that comes to both channels is recorded on the same sound carrier, which is a standard magnetic wire. It allows us to perform spatial correlation measurement.

Let us discuss in details the recorder operation in the first mode. The information that comes to the first channel is recorded directly on the sound carrier in the frequency band from 20 Hz to 8 kHz. The information that comes to the second channel modulates the frequency of a special multivibrator whose output is recorded on the sound carrier. This voltage is a carrier of information. Its frequency is 20 kHz and it can vary in the interval ±8 kHz as a result of modulation. Therefore, two-channel information recording is performed in common frequency band from 20 Hz to 28 kHz; within two subbands: 20 Hz – 8 kHz and 12 kHz - 28 kHz, which are isolated by 4 kHz interval.

The level of 20 kHz carrier makes 5-10% of maximal recording level. It causes the narrowing of the first channel dynamic range, which hardly reaches 25 dB. The second cannel dynamic range amounts to 35 dB. The carrier is at the same time the reference signal that gives the possibility to monitor the speed of recording and whether the recording units are in order.

There is a block diagram of writing amplifiers in fig. 5.53. The available signals from the pulsation sensors are supplied to the inputs of identical voltage amplifiers 1

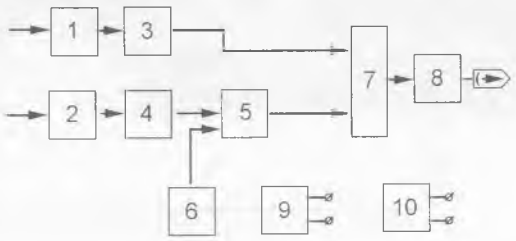

Fig. 5.53.The block diagram of the writing amplifiers. The designations are in the text.

and 2 and the to the inputs of filters 3 and 4 with cutoff frequency 8 kHz. The voltage from the filter 3 comes directly to summator and the voltage from the filter 4 comes to the frequency modulator 5, which performs modulation of the multivibrator 6 frequency. The output of the frequency modulator is supplied to the summator 7. The total voltage through the power amplifier 8 goes to the write head. Power supply of the channels is performed separately by the sources 9 and 1). The power amplifier feeding is performed from the first channel power source.

Playback is performed with the recorder MN-61 through special amplifiers. There is common playback amplifier in the first channel, whose frequency band is limited by 8 kHz. The second channel playback amplifier includes the band filter that extracts the band 12 - 28 kHz. The amplifier output is connected to a demodulator.

When the recorder operates in the second mode, available information comes to the first channel where the recording amplifier supports recording up to 120 kHz. The power source is disconnected from the second channel. It is inserted consequently with the electromotor power source to maintain the speed of carrier transportation up to 3 ms^{-1}. This recorder also has radio remote control system.

The weight of the recorder in the air is 900 g, its volume is 500 cm^3. The cassette capacity is 750 m of standard wire sound carrier (wire diameter is 50 mcm). In fig. 5.54 one can see the recorder without casing (*a*) and its configuration (*b*).

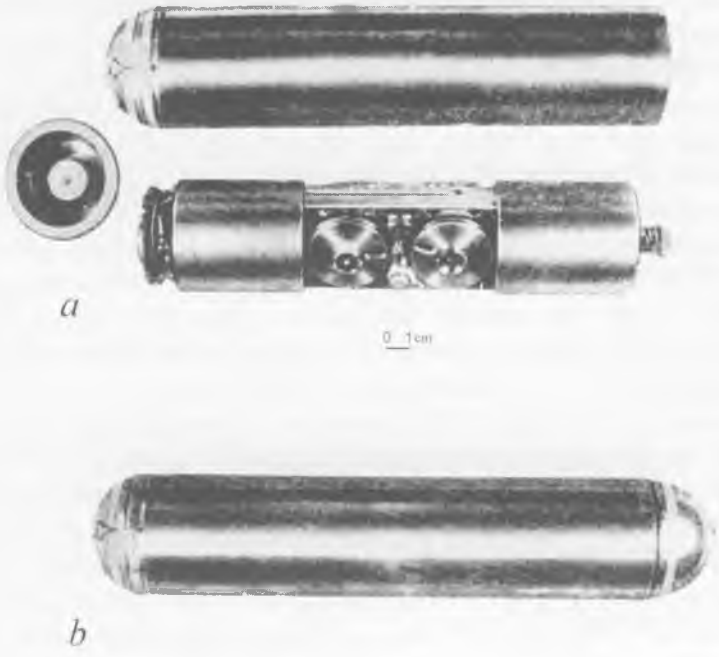

Fig. 5.54. The recorder without casing (*a*) and its configuration (*b*).

5.2.4. Fixing the equipment on a dolphin

The measuring equipment should be arranged so that it does not cause an appreciable perturbation of the incoming flow at the points of measuring. The attachment must be reliable enough to stand the pressure of the incoming flow which speed amounts to 5 – 8 ms^{-1}. Two main elements of the measuring system, which we have to fix on the dolphin, are the sensor and the logging device (or the radio transmitter). The sensor can be an accelerometer, a sensor of the flow speed, a measurer of pulsation of the flow pressure or speed, a tangential stress meter.

Possibility of subcutaneous encapsulation of the measuring equipment elements was discussed in literature (Agarkov, Vischnyakov 1975; Agarkov, Manger, Khadjinskiy, Khomenko, 1975; Agarkov, Khadjinskiy, Tchernyaev, 1972, 1977). In the work of Varitch, 1971 there is a description of how this method was applied in practice in the course of studying of alive sharks streamline.

Where it was necessary to fix the pulsation sensor they cut off the piece of shark skin the size of the sensor base (5x5 mm). They used a surgeon's needle and two wires coming out of the sensor to implant the sensor into the body. Fixing procedure duration was about 5 minutes. After these operations all the sharks were used for the experiments during 4 - 6 days. Control shark lived in the basin for 18 days. During this period it underwent three such operations and then they let it go.

It is difficult to obtain ideal transition from the skin to the sensor body. Hence, if we use this method there is a danger of perturbation of the incoming flow at the border of implantation. Besides, a dolphin lives in captivity for many years and it is used in experiments many times. So it is better not to use such a traumatic method and to fix the equipment some other way. Perhaps, that is the reason why this method is not used in biohydrodynamical experimental works on dolphins.

There were two ways to fix the logging equipment: to fix it with a special rubber belt, which tightly embraced the dolphin body in the middle, and with the clamp, which is put onto the dorsal fin and held by friction. Sometimes we added a vacuum cup to the clamp to make it safer. We could fix the sensors on the rubber belt or on the springy clamp along with the logging equipment. But more often the sensors were fixed at the points of measurements on the dolphin body with the sucker.

When we designed the belt we bore in mind that it must tightly adjoin to the dolphin body. One of the most apposite belt models is shown in figure 5.55. We successfully used this belt on dolphins. This belt is made of two layers of elastic rubber 1.5 mm thick. The layers are glued to each other. The cutting consists of two parts ("*a*" and "*b*"). The sizes are adduced in the figure. The length of AC span corresponds to the length of the related span of part "*b*". Part "*b*" has a complicated form. The length of the split for the dorsal fin has a principal significance. For a medium-sized animal this value is about 20 cm. The angle between the lines "*bc*" and "*a'b'*" is another important value.

This angle is close to 120°. Besides, the equations AB = *ab*, BC = *b'c'*, *cd* = *d*0 and *a'd'* = 0*d'* must be true. When we conglutinate the blank parts, lines *bc* and *a'b'* must be conjoined together and lines *ab* and *b'c'* must form a single line which length is equal to the length of AC. Then the cutting is glued along the lines *abb'c'* and AC. Two such layers are glued together; slots for the fin in the parts must coincide. Another slashes must not coincide in order to avoid decreasing of the belt reliability. There are instantly acting snaps on either ends of the belt. These snaps are analogous to those used in aircrafts. The belt is put on the dorsal fin; it envelops the body and is snapped on the dolphin side. Figures 5.56 and 5.57 show how the belt looks on the dolphin. We can also see how the equipment is arranged on the belt.

Figure 5.58 shows the springy clamp for the equipment fastening on the dolphin dorsal fin. The clamp consists of a flat spring 1. The two light-weight duralumin plates 2 with perforations 3 are glued at the spring ends. The thin sheets of foamed plastic (10 – 15 mm thickness) are glued at the inner side of the plates. The equipment components are glued at the outer side of the plates. The ends of the plates are converged together and adjusted for a tight fit on the fin. This clamp is efficiently held down the fin of the dolphin. It may be replenished by the belt or suckers. In figure 5.59 we can see the arrangement of the springy clamp with the equipment, which is set on the freely swimming dolphin. It is shown at the moment of respiration. The sensors of pressure pulsation or speed pulsation are mounted in a special holder, which is attached to the animal body. The structure of the holder is shown in figure 5.60. It consists of three parts: platform 1, plate 2 and console 3. The platform (5x40x70 mm) is mounted on the plate (1.5x75x105 mm) with the screw 4 and retainer 5. The console (57x17x3 mm) is mounted on the platform axis 6. The spring is winded on the axis to keep the console right-angled to the platform (figure 5.61). The console may be held pressed down to the platform with the springy retainer 7.

The plate 2 is to carry the holder platform. The plate itself is glued in between the belt layers. The purpose of the retainer 5 is to set the platform (and hence the pulsation sensor) under different

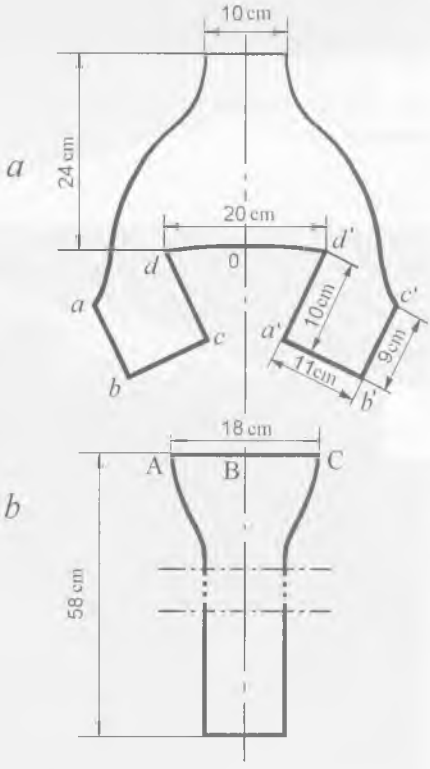

Fig. 5.55. The rubber belt construction. See text for details.

Fig. 5.56. The belt and the equipment are arranged on the dolphin. 1 – belt, 2 – equipment, 3 – pressure pulsation sensor.

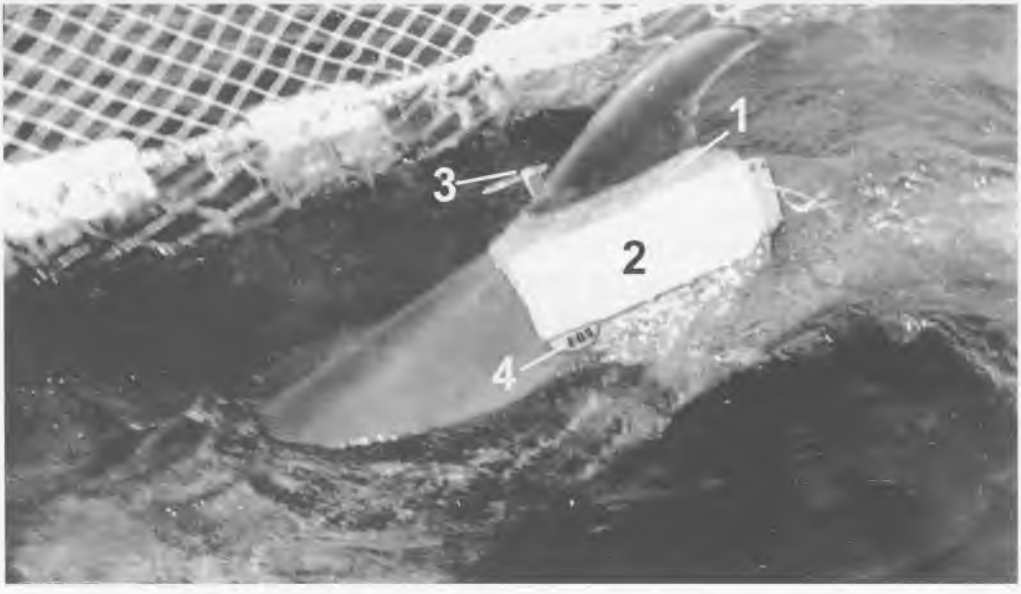

Fig. 5.57. The belt and the equipment are arranged on the dolphin. 1 – belt, 2 – equipment, 3 – pressure pulsation sensor, 4 – velocity meter.

angles relatively the incoming flow. Seven positions of the retainer let us vary a direction in the range of 21° by the step of 3°. The axis of the platform rotation is the screw 4.

The pressure pulsation sensor is fixed on the console as it is shown in figure 5.62. The shielded wire 2 goes from the sensor through the console channel. It is connected either with the radio transmitter or with the logging device. The pulsation sensor can be set with the console in two positions. The first position is close to the skin, at the distance about 2 – 3 mm. This position occurs when the console is pressed to the platform. When the console is in the position as it is shown in figure 5.61, the sensor of pulsation is located at the distance of about 50 mm from the skin. In figure 5.56 we can clearly see the holder with the pulsation sensor, fixed on the belt in the working position.

Fig. 5.58. The clamp. The designations are in the text.

Fig. 5.59. The arrangement of the springy clamp with the equipment, which is set on the freely swimming dolphin. 1 – dolphin, 2 – arrangement, 3 – pressure pulsation meter, 4 – velocity meter.

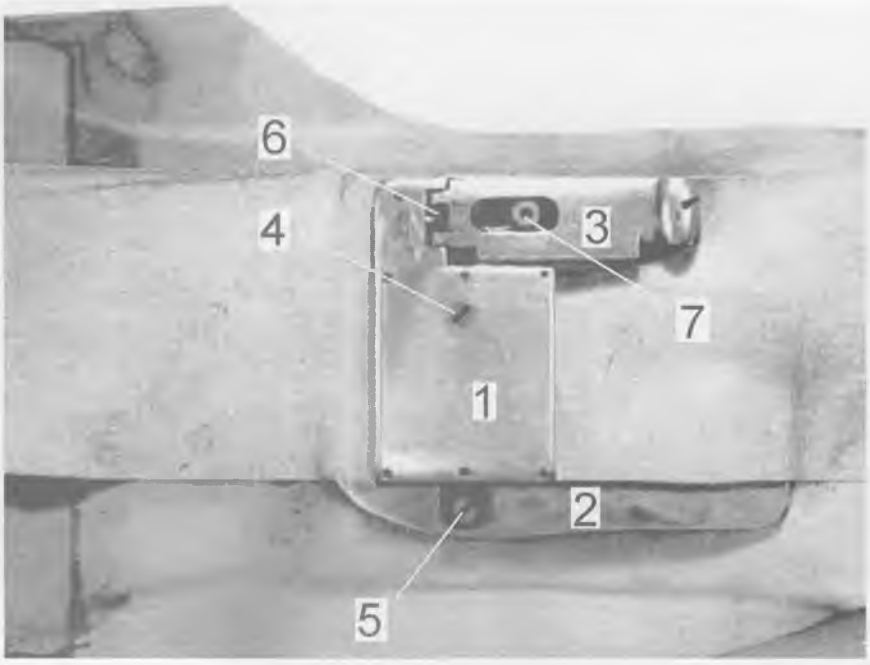

Fig. 5.60. The structure of the holder of pressure pulsation meter and velocity meter. The designations are in the text.

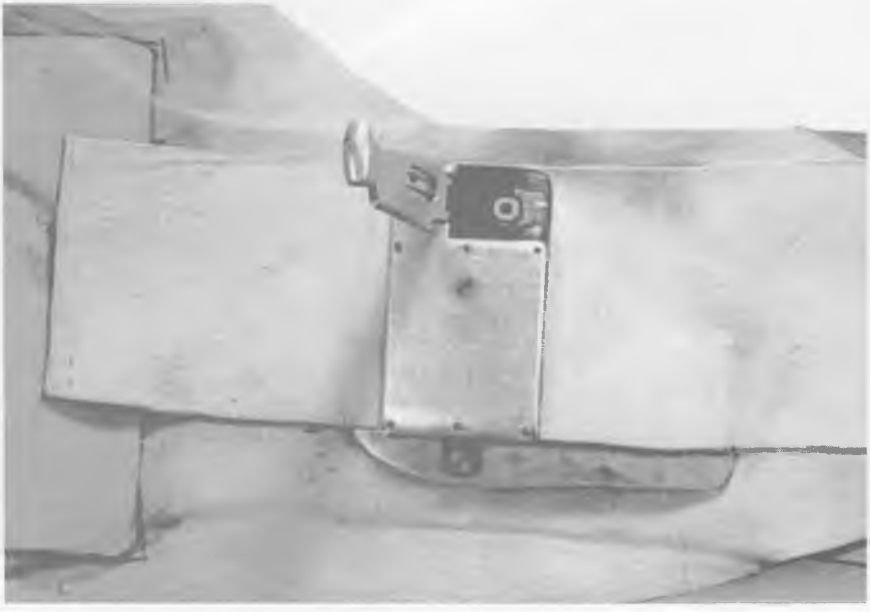

Fig. 5.61. The console is right-angled to the platform.

In order to fix the pulsation sensor with the vacuum cups we use another platform. It is shown in figure 5.63. There we can see the perforations for the suckers mounting. We can fix this platform with the suckers at any place of the dolphin body. All other components of this holder are the same as of the previous one. The suckers do not always surely hold the platform with the pulsation sensors at the required place. Sometimes they drift under the pressure of the incoming flow. We can get additive fixation on the dolphin body with the fast polymerizing glue. In this case the reliability grows significantly.

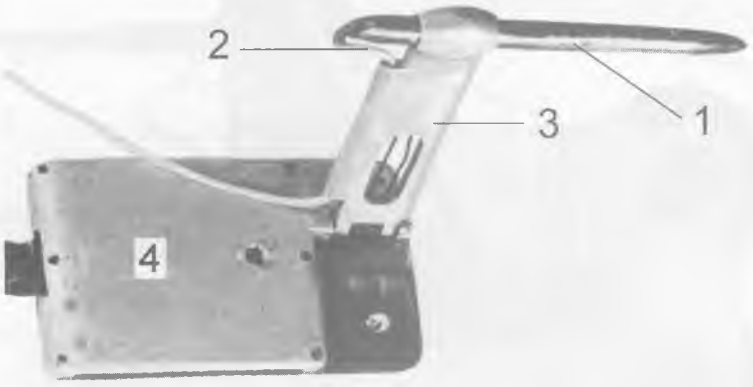

Fig. 5.62. The pressure pulsation sensor is fixed on the console. 1 – pressure pulsation meter, 2 – cable, 3 – console, 4 – platform.

Fig. 5.63. The platform is provided with the vacuum cups. 1 – platform, 2 – vacuum cups.

Another variant of the holder is a cartridge, which can contain up to 9 sensors of pressure or speed pulsation. It is shown in figure 5.64. The rest of the holder does not differ from the one described above.

In figure 5.59 we can see the platform with the suckers and the pressure pulsation sensors fixed on the dolphin. Figure 5.65 shows the frame with 8 sensors of speed pulsation. It is mounted on the rigid half-model, which is covered with the Baikal seal fur.

Another sensors of available information (flow speed meters, accelerometers, tangential stress meters etc.) can be mounted in any of the described ways.

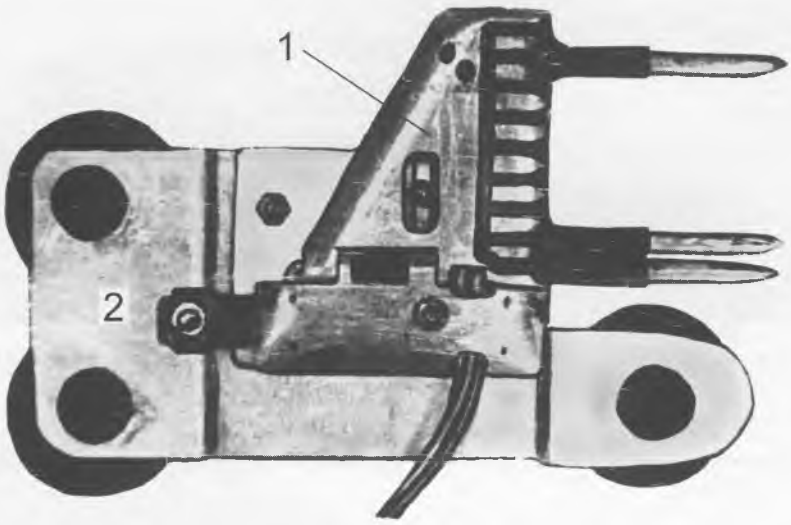

Fig. 5.64. The platform is provided with the vacuum cups. 1 - cartridge, which can contain up to 9 sensors of pressure or speed pulsation, 2 - platform.

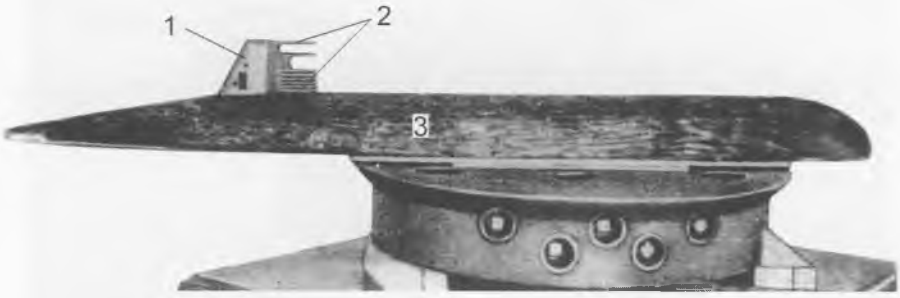

Fig. 5.65. The frame with 8 sensors of speed pulsation. 1 – cartridge, 2 – velocity meters, 3 - rigid half-model, which is covered with the Baikal seal fur.

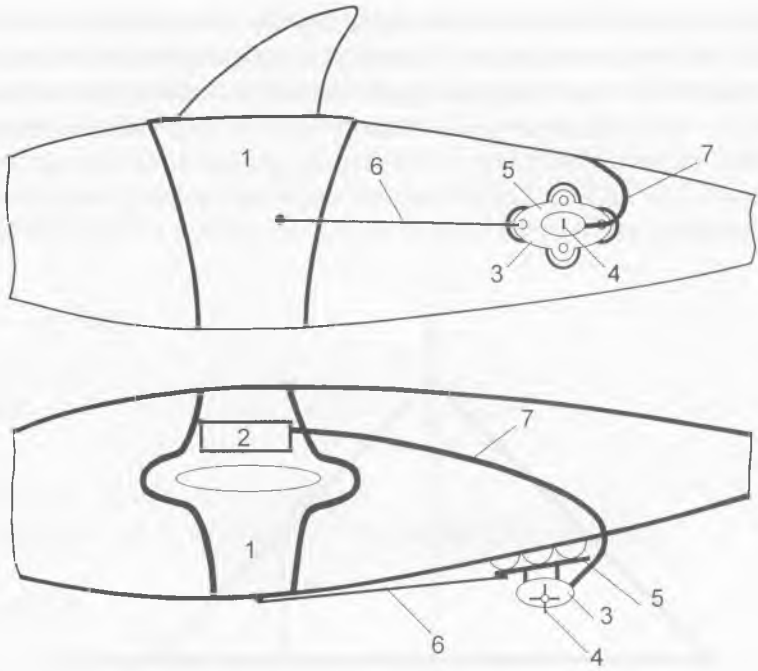

Fig. 5.66. Velocity meter is fixed with special rods, attaching the meter to the belt. 1 – belt, 2 – equipment, 3 – velocity meter, 4 – impeller, 5 – platform, 6 – rod, 7 – cable.

In figure 5.57 we can see the flow speed meter (impeller), which is glued to the apparatus on the incoming flow side.

If we measure the flow speed outside the boundary layer by a flow speed meter, which is mounted on the sucker, it is useful to fix it with special rods, attaching the meter to the belt. This mounting is especially effective when we measure the speed of the incoming flow behind the middle of the animal. This mounting is shown in figure 5.66.

5.2.5. Measuring of virtual mass for complex configuration bodies

Existing mathematical models of the fish and dolphin swimming give us the estimates of the hydrodynamical parameters of swimming on the base of the experimentally measured kinematical characteristics of the animals. But the equations that we use to calculate these estimates contain also the value of the added mass per body length unit. This value can be found easily and exactly with the formula (Logvinovitch, 1970a)

$$m^*(x) = \rho\pi R^2(x). \tag{5.94}$$

This R is the transversal half-size of the fish or dolphin body. At the tail fin edge it transforms into the half-span of the tail fin. The virtual mass of the fluke of dolphin and

fish with the half-moon fin cannot be calculated with this formula, because the inequality $dR/dx << 1$ is not true around the tail fin, and we cannot assume that the value of dR/dx is small. In dolphin *Tursiops truncatus* around the tail fin this derivative amounts to 1.5. But it is easy to obtain the equation for rough estimate of added mass of the dolphin tail fin and the half-moon tail fin of fish. Let us consider the tail fin as of an arrow-like wing shown in figure 5.67 or 5.68. Let us look at these wings in the Oz-axis direction. The value r is considered as the current size of the fin. Then $dR/dz \approx 0.35$. This value can be

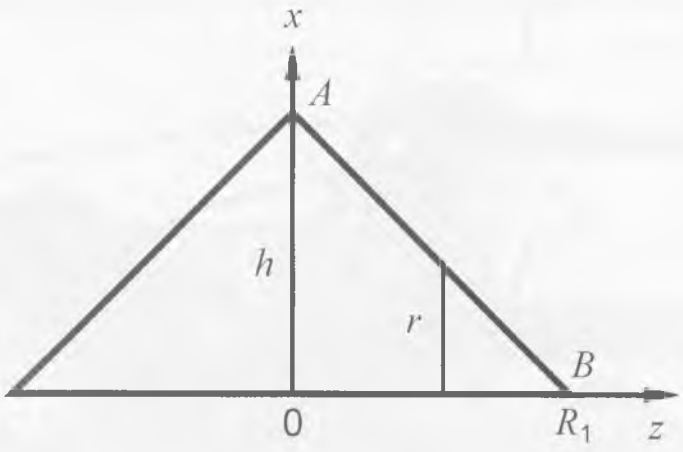

Fig. 5.67. Approximation of a dolphin fluke by the triangular wing (variant 1).. The designations are in the text.

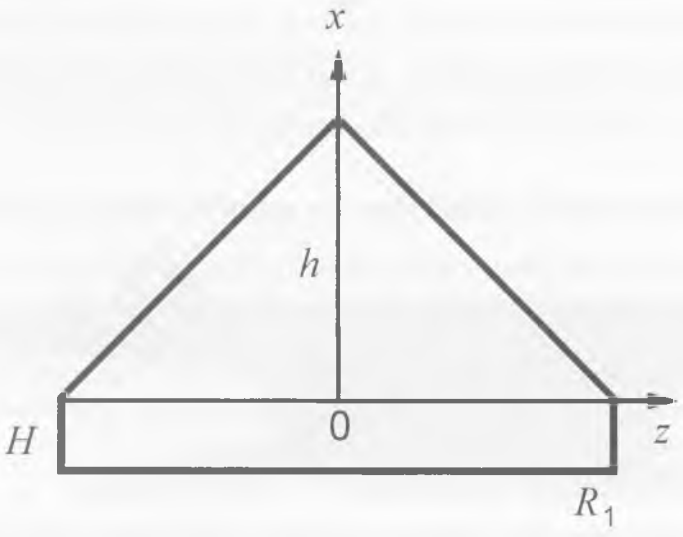

Fig. 5.68. Approximation of a dolphin fluke by the triangular wing (variant 2). The designations are in the text.

considered small. Hence, the method of the added mass calculation proposed by Logvinovitch (1970a) is applicable. This approach was proposed by S. G. Pushkov. We can represent the added mass of the plate shown in figure 5.67, which oscillates in the axis $0y$ direction, as

$$m_{pl}^{*} = 2\rho\pi \int_0^{R_1} \frac{r^2}{4} dz . \tag{5.95}$$

It is evidently that

$$r = \frac{h}{R_1}(R_1 - z). \tag{5.96}$$

Here h is the root chord; R_1 is the half span.

After substitution of (5.96) into (5.95) and integration we obtain

$$m_{pl}^{*} = \frac{\rho\pi h^2 R_1}{6}. \tag{5.97}$$

We have calculated the virtual mass taken as a whole. But the theoretical models use the value of the virtual mass per body length unit. So, let us divide this value by the effective longitudinal extent of the plate, which we represent as

$$a = \frac{S_t}{2R_1}. \tag{5.98}$$

Here S_t is the square of the plate (the tail fin).

Finally we get

$$m_t^{*} = \frac{\rho\pi h^2 R_1^2}{3S_t}. \tag{5.99}$$

As S_t is

$$S_t = \frac{4R_1^2}{\lambda}, \tag{5.100}$$

where λ is the aspect ratio, we can represent (5.99) as

$$m_t^* = \frac{\rho\pi h^2 \lambda}{12}. \tag{5.101}$$

If we replace the dolphin tail fin by the arrow-type wing shown in figure (5.68) then analogous calculation leads to another expression for the added mass of the tail fin per the length unit:

$$m_{xa}^* = \frac{\rho\pi R_1}{2H + h}\left(\frac{h^2}{3} + hH + H^2\right). \tag{5.102}$$

Here H is the height of the right-angled part of the wing.

These expressions give us rough estimates of the virtual mass of the fish and dolphin tail fins.

The most convenient base for finding the virtual mass of complex configuration bodies is the second Newton's law:

$$F = \left(m_b^* + m_{water}^*\right)a. \tag{5.103}$$

Here F is force, a is acceleration, m_b^* and m_{water}^* are the body mass and virtual mass of the ambient water correspondingly.

We must move the complex configuration body through the medium with known constant acceleration while the moving force is measured. If the body mass is known, we can easily calculate the added mass of the medium with formula (5.103).

The scheme of installation for this measurement is shown in figure 5.69. The body 2, whose added mass is measured, is hung in a reservoir 1 with a suspension strand 3. The body

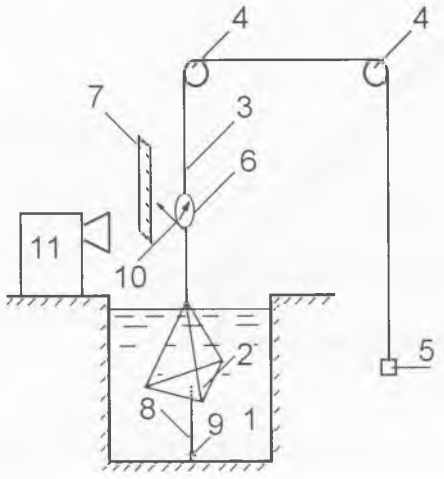

Fig. 5.69. The scheme for measurement of virtual mass. The designations are in the text.

may be, for example, a model of the tail fluke. The strand is passed through blocks 4. On the other end of the strand there is a load 5. A dynamometer 6, which continuously measures the tension, is included in the break of the strand. There is a ruler bar 7 alongside of the dynamometer. At initial moment the body is fixed with a strand 8, which is locked in a restrainer 9. The dynamometer pointer 10 shows the initial position of the dynamometer and the body. Also it shows the body position at any consecutive moment. The strand must be strong enough so that we could neglect its expansion. At the initial moment the system is in the state of equilibrium and the dynamometer shows the strand static tension. At a certain moment the body is turned loose and it begins to move sheer up in water. The movement of the dynamometer (and of the body) is logged with a cine camera 11. As the analysis of the cine film shows, the tension rather decreases at the starting moment of movement and then it stays constant and equal to the dynamical tension. When the speed increases, the hydrodynamic resistance distinctly increases too and the tension of the strand increases again. In order to estimate the constant acceleration and the moving force, we choose the cine frames, where the resistance is still negligible. The stability of the acceleration is tested by the relation of the successive lengths of intervals shown by the film.

$$\frac{S_n}{S_k} = \left(\frac{t_n}{t_k}\right)^2. \tag{5.104}$$

Here S_n and S_k are the lengths of intervals that are passed during the time intervals t_n and t_k.

Using this scheme, we made the installation and checked its efficiency by measuring of the added mass of a circular plate and comparing it with the value, which was calculated with the exact expression:

$$m = \frac{8}{3}\rho r^3, \tag{5.105}$$

r is radius of the plate and ρ is water density.

We have measured the added mass of the circular plate whose radius was 17 cm. This measured value practically coincided with the calculated value. The difference was less than 5%. The root-mean-square error was less than 4%. This means that the proposed measuring method and the developed installation does not contain any serious defects. It can be used in practice.

5.2.6. Increasing of dolphin swimming speed

One of the main difficulties of animal hydrodynamics studies is to make the animal carrying the equipment to swim at the highest possible speed. It is known (Kozlov, Nikishova, 1974) that the highest speed shown by the dolphin *Tureiops truncatus* in

captivity is only 8 – 9 ms^{-1}. The animal can only achieve this speed for short-term intervals and with no equipment attached to it. The speed of dolphin swimming with the apparatus is yet less. We don't use any fierce, painful methods of stimulation, as it is extremely undesirable, when you work with tame animals. In our work with tame dolphins we could employ only the methods based on conditional reflex formation and on individual features of animal behavior. The first experiments were accomplished with wild animals. They were placed into the netting corridor of about 80 m long, 2 m wide and 2.5 m deep. The dolphin was caught, we attached the equipment and let the animal loose. We hoped the dolphin would elaborate high speed because it was frightened. But its speed did not exceed 2 – 2.5 ms^{-1}. After this we decided to train the dolphin to swim on the sound signal from one end of the volier to the other. The signal was emitted in different ends of the volier and as the dolphin came to this place it was sustained by food. Eventually, the speed of the dolphin increased to 3 – 4 ms^{-1}.

In order to increase the speed of swimming we decided to use the competitive spirit. For this purpose we added another dolphin, which was also trained to swim on the sound signal. We hoped that they would race from one end of the volier to the other each of them trying to be the first. And so it was in the beginning. But very soon the dolphins set apart and took places at the different ends of the volier. The trainer could not make them swim simultaneously and they did not swim faster than 3 – 4 ms^{-1}. After this we decided to feed both dolphins at the same end of the volier. The dolphins were given only one fish, and it was eaten by the fastest one. But the dolphins very soon learned to define which of them was closer to the fish at the moment. This dolphin swam easily towards the fish and ate it. The other dolphin did not move. If the fish was placed at equal distances from both dolphins, they both went for it moving with a significant speed. This method proved the greatest efficiency. Thus we made the dolphins swim at the speed up to 5.5 ms^{-1} with the attached apparatus.

While we worked with the dolphins, we found another way to increase the dolphin speed by about 15 – 20%. In addition to the belt with the equipment we put on the dolphin head a vortex generator. The vortex generator is a rubber ring, 10 - 12 cm thick. It is placed in front of the chest fins. The dolphin is trained not to take it off until the trainer takes it off himself or commands the dolphin to do so. For about 15 – 20 min the dolphin swims with the apparatus and vortex generator and then the vortex generator is removed. Right after that the speed of dolphin swimming is higher than it was before the vortex generator was installed. It seems, the dolphin needs some time to get used to a new condition. The dolphin is accustomed to elaborate excess power in order to overcome the additional resistance. When the vortex generator is removed the dolphin for some period continues elaborating the excessive power from the habit. During the experiments on the dolphins we discovered an interesting feature of their behavior. Once in the middle of the experiment we ran out of fish and had to stop the experiment for 15 minutes until a new portion of fish was delivered. We did not pay attention to the

dolphin. Several minutes later the dolphin made a spurt and elaborated the speed, which was higher than during the measurement. We used this feature of dolphin behavior at the end of each experiment. Our apparatus worked continuously and at the end of each experiment we logged the information at the maximum speed till the apparatus would slip off.

But we ought to acknowledge that the achieved speeds of dolphin swimming with the equipment are still insufficient. We wished to achieve the speeds of 9 – 10 ms^{-1}. Perhaps, we could have obtained these speeds if we used the dolphin ability to jump high above the water surface. Perhaps, we should have searched methodical possibilities of increasing the swimming speed. We should have trained the dolphins to jump vigorously forward or upward in the direction of swimming. It seems it is efficient to train the dolphins to overcome obstacles protruding from the water surface. It goes without saying that the equipment mounted on the animal must be reliable enough to withstand this speed.

Brief conclusions

In this chapter we describe the tools and methods for researching of kinematics, hydrodynamics and fine structure of the boundary layer on dolphin. The most of these devices and methods are unique. Some of these instruments such as the magnetic wire recorder and radiotelemetry devices are now outdated. But in that time these instruments allowed to obtain unique results, and that is the reason why we pay so much attention to them.

CHAPTER 6. THE RESULTS OF THE EXPERIMENTAL RESEARCHES

We carried out the experimental studies on dolphin hydrodynamics since 1969 to 1986. They were performed in the sea volier at Utrish sea station of A.N. Severtsov Institute of Ecology and Evolution. The object of the researches was the *Tursiops truncatus* dolphin of the Black-Sea. The scheme of the volier and its layout is shown in figure 5.40 of the previous chapter. Some researches were fulfilled with autonomous equipment fixed on the animal. If a dolphin was well trained it swam up to the trainer on his command and gave the possibility to fix the equipment on it. If the dolphin was not well trained, we were reluctant to catch it and fix the equipment on it.

Then we used cine filming, a diver performed it through the sidewall of the volier.

6.1. Experimental studies of dolphins' kinematics

During dolphins' swimming, the thrust is created due to the bending oscillations of their body. The amplitude of such oscillations is growing from the head towards the tail, reaching its highest value in the area of the caudal fin. It is believed that in the dolphins' hydrodynamics and in the creation of the thrust, it is the oscillating movements of the caudal fin that determine the development of thrust. For this reason, most experimental studies concentrate on the dynamics of the dolphin flukes. With that, the scientists employ the well-known method of movie-taking. In the papers of Land and Daybell (1963), Kayan (1979) the authors describe their measurements of the attack angle, the inclination angle of flukes towards the direction of the dolphin's motion and towards the trajectory of the fluke movement. Many scholars (Pyatetsky, Kayan, 1972; Pyatetsky, Kayan, 1975; Kayan, Pyatetsky, 1977; Kozlov, 1983) measured the relative amplitude and the oscillation frequency in the dolphin flukes, as well as the velocity of the propulsive wave spreading along the body, as dependent upon the swimming regime of the animal.

However, some recent studies (Romanenko, 1981, 1986) revealed that not only the kinematics of flukes is important in estimating the hydrodynamics of dolphins but also the kinematics of the entire body of the animal. In particular, some kinematic peculiarities of the dolphin's body essentially determine the pattern of streamlining and the structure of the animal's boundary layer.

In his paper of 1981, Romanenko was the first to suggest that the phase velocity of the propulsive wave within the dolphin's body was not constant. He made an attempt to measure the kinematic parameters simultaneously in three points of the animal's body (the amplitude of oscillations and the phase velocity of the propulsive wave): in the area of the head, dorsal and caudal fins. The kinematics of dolphins was assessed by two methods: by movie-taking and by accelerometers. As a rule, movie-taking is effected by using a tightly fixed movie camera. However, in such case the time of the animal's exposure within the sight of the camera objective is insufficient for tracing it and for examining the movement of individual

parts of its body during one run. In particular, this method is difficult for measuring the phase velocity of the propulsive wave in individual parts of the animal's body.

The experiments we are describing employed the method of movie-taking by using a movable camera which was shifted slowly and smoothly during the movie-taking. As a result, the animal was caught in the frame exposure and then it was for some time followed and traced. Owing to this, we could watch the dolphin's movement during several periods of its body's oscillations. The movie-taking was performed by an expert diver who worked under water, observing the animal through the reticulated wall of the sea pen along which the dolphin was swimming by the command of its trainer.

The method of movie-taking has certain merits: it is sufficiently simple, permits to obtain visual information about the dolphin's kinematics in its free swimming (without any devices fixed on it). But this method has a number of shortcomings too: the animal remains within the sight of the movie camera only for a limited time during which it is hard to determine the regime of the animal's motion (whether this motion is uniform or accelerated). For this reason, the information obtained about the animal's kinematics proves to be considerably scattered.

The cine films were decoded in the following way. The cinema frames of a certain run of the dolphin were marked to show the position of three points of its body (for example, the tip of the nose, the tip of the dorsal fin and the fork of the caudal fin) in relation to the film frame boundaries. These marks were used for building a trajectory to demonstrate the transposition of the marked points of the body. Fig. 6.1, as an example,

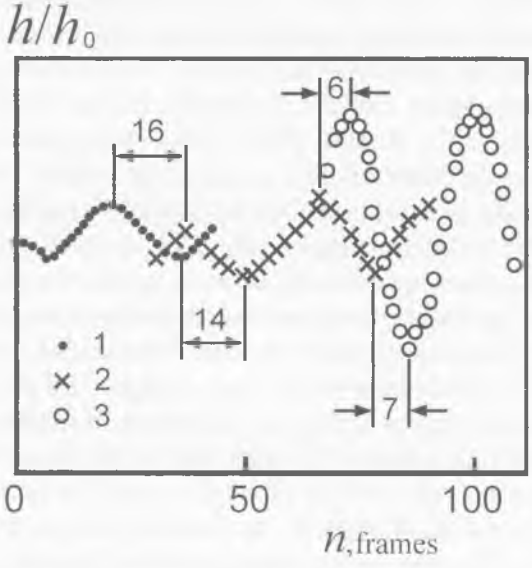

Fig. 6.1. Values of the selected points of the dolphin's body as displaced from a certain mean value in random: 1 - tip of the nose, 2 - tip of the dorsal fin, 3 - fork of the caudal fin.

displays the results of decoding of such a run of the dolphin. The horizontal axis presents the ordinal numbers of the film frames. This axis is equivalent to that of time. The vertical axis shows the values of the selected points of the dolphin's body as displaced from a certain mean value in random units (say, in mm) but necessarily within the same scale. The black circles demonstrate the position of the nose tip of the dolphin, the crosses - the tip of the dorsal fin, the light-coloured circles - the forks of the caudal fin. These traced trajectories helped to identify the amplitudes of oscillations in the marked points of the body, as well as the phase velocity of the propulsive wave. In this case the known length of the dolphin's body served as the scale.

The phase velocity of the propulsive wave was found in the following way. We measured the number of film frames (and, hence, the time interval) during which the minimum (or the maximum) of the trajectory of the nose tip shifted towards the fork of the caudal fin (in the case presented in this figure, there were 21 (or 22) frames). After that we calculated the mean value of the phase velocity of the propulsive wave as the relation between the length of the dolphin's body and the specified time interval. However, it is easy to see that the velocity of the propulsive wave is not constant within the limits of the animal's body. To notice it, it is sufficient to estimate in the same way the velocity of the propulsive wave separately for the section from the nose to the dorsal fin and for that from the dorsal fin to the fork of the caudal fin. The number of film frames (the time interval) during which the trajectory of the nose tip shifted towards the dorsal fin equalled 14 in this case. The number of film frames during which the trajectory of the dorsal fin tip shifted towards the tail fork equalled 7. With that, in the latter case it was possible to have 4 counts: two for the shifts of two minimums of the trajectory and two for the shift of two maximums (the latter yielded 16 and 6 film frames respectively). After that, we established the value proportional to the mean value of the phase velocity of the propulsive wave in the section from the nose to the dorsal fin as the relation between the distance from the nose and the dorsal fin (130 cm) and the mean arithmetic number of film frames during which their minimum and maximum shifted to this distance

$$kC_{1-2} = \frac{130\ cm}{15\ frames}. \tag{6.1}$$

Here, k is proportional coefficient.

The same very approach was used to find the mean value of the phase velocity in the section from the dorsal fin to the tail fork, but here the mean arithmetic value involved 6 and 7 film frames.

$$kC_{2-3} \approx \frac{90\ cm}{6.5\ frames}. \tag{6.2}$$

Taking into account that the linear and the time scales in both cases were the same, we shall get the genuine relation between the calculated mean values of the phase velocity

$$\frac{C_{2-3}}{C_{1-2}} = 1.59. \tag{6.3}$$

Indeed, it came out that the phase velocity of the propulsive wave was considerably increasing from the head to the tail of the animal. The same result was obtained upon the analysis of all films.

However, to be able to employ the established values of the phase velocity of the propulsive wave in further calculations, it is necessary to consider first the relations of the mean values and then to transit to boundary values, i.e. the ones revealing the phase velocity at the tail fork and on the nose of the dolphin respectively. In our suggestion about some linear dependence between the phase velocity and the co-ordinate we could do it by using some geometry.

Fig. 6.2 displays a scheme permitting such transition. Let us write down some obvious relations

$$C_{1-2} = \frac{C_1 + C_2}{2}, \tag{6.4}$$

$$C_{2-3} = \frac{C_2 + C_3}{2}, \tag{6.5}$$

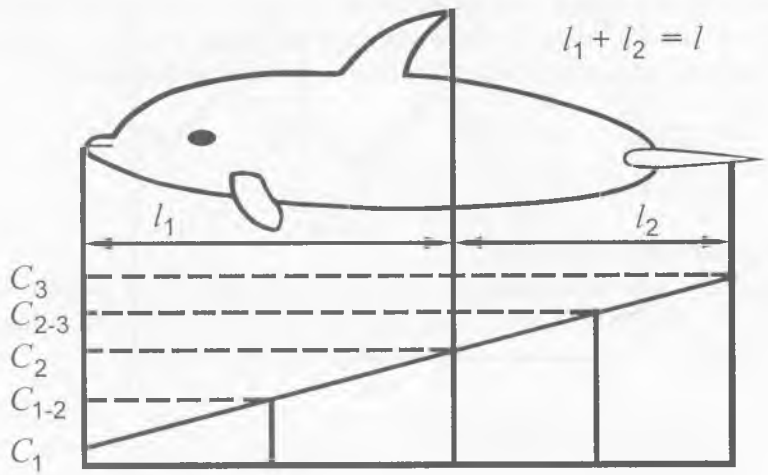

Fig. 6.2. Scheme permitting to transit from the mean values to boundary values. The designations are in the text.

$$C_2 = C_1(1 + b_0 l_1), \tag{6.6}$$

$$C_3 = C_1(1 + b_0 l). \tag{6.7}$$

Here, C_1, C_2 and C_3 are the phase velocity of the propulsive wave on the nose tip, dorsal fin and at the tail fork respectively.

Let us substitute (6.6) and (6.7) into (6.4) and (6.5):

$$C_{2-3} = \frac{C_1[2 + (l + l_1)b_0]}{2}, \tag{6.8}$$

$$C_{1-2} = \frac{C_1(2 + b_0 l_1)}{2}. \tag{6.9}$$

Now we shall relate C_{2-3} to C_{1-2}

$$\frac{C_{2-3}}{C_{1-2}} = \frac{[2 + (l + l_1)b_0]}{(2 + bl_1)}. \tag{6.10}$$

From formula (6.10) we shall define

$$b_0 = 2\frac{\left(\frac{C_{2-3}}{C_{1-2}} - 1\right)}{\left[l - l_1\left(\frac{C_{2-3}}{C_{1-2}} - 1\right)\right]}. \tag{6.11}$$

Substituting (6.11) into (6.7), we shall finally get

$$\frac{C_3}{C_1} = 1 + 2\frac{\left(\frac{C_{2-3}}{C_{1-2}} - 1\right)}{1 - \frac{l_1}{l}\left(\frac{C_{2-3}}{C_{1-2}} - 1\right)}. \tag{6.12}$$

Much more accurate is the method of accelerometers. Its essence is in the following. Miniature accelerometers are fixed in different points of the dolphin's body to examine

the pattern of their movement during the animal's swimming. In particular, Romanenko (1980) used such accelerometers in three points on the dolphin's body. Accelerometer 1 was situated on the melon, accelerometer 2 - in the anterior part of the dorsal fin at 1 m from the first one, accelerometer 3 - on the fluke at 1.1 m from the second one. In some cases, accelerometer 3 was fixed on the caudal stem of the animal near the fluke.

Signals from the accelerometers were recorded on the same magnetic carrier and in this way they proved to be rigidly related in their time phase which permitted to examine phase relationships between individual signals. Another advantage of this method is in the possibility of continuous recording of the information within a long time. It allows to chose for the analysis such section of the film record which corresponds to a quite certain regime of the animal's swimming.

During our measurements, the recording miniature tape recorder was fixed on the dorsal fin of the animal (Romanenko, Chikalkin, 1974; Romanenko, 1976). Thanks to this, we could study the animal's kinematics in its free swimming (with regards of the impacts of the devices fixed on it).

During the measurements, the accelerometers registered the acceleration oscillations in those points on the animal's body where they were fixed. To analyse the values of the displacement amplitudes, it is necessary to provide double integration of the data in terms of time. However, this operation is not difficult and does not imply additional errors, if the integration step is sufficiently small.

Fig. 6.3 shows a recorded fragment of signals from three accelerometers (the solid lines). The upper curve presents two periods of the oscillating acceleration of the anterior part of the forehead protrusion of the dolphin, the middle curve - that in the anterior part of the dorsal fin, the lower curve - of the caudal fin fork. The dots show the displacement amplitudes of the same points of the animal's body corresponding to these curves. The amplitudes were obtained by double integration of the acceleration curves (with regards of the sensitivity of the accelerometers). The numerical integration was effected by using a computer and the method of trapezes. The integration step was $0.02T_0$ where T_0 was the period of oscillation. In the same way as in the previous method, we measured the amplitudes of the dolphin's body oscillations in the points where the accelerometers were situated, and also the relation between the mean values of the phase velocity of the propulsive wave in two sections of the dolphin's body: from the forehead protrusion to the dorsal fin and from the latter to the tail. With that, we traced the transposition of the zero values of the phase in the displacement curves of the body points where the accelerometers were located. (The zero values of the phase in the points φ_1 and φ_2 in fig. 6.3). Like in the analysis of the film frames, in this case we also received sufficiently reliable data showing the phase velocity of the propulsive wave to increase from the animal's head to its tail.

The information obtained by means of accelerometers also permits to specify two more parameters of the dolphin's movement which are very important: the relation

between the mean value of the phase velocity of the propulsive wave and the velocity of the dolphin's movement $C_{1\text{-}3}/U$, as well as that between the phase velocity of the propulsive wave in the anteriormost point of the dolphin's body (near the nose) and the velocity of the motion of the dolphin itself C_1/U.

Indeed, by using the curves in fig. 6.3, we can measure the time for passing the zero level of the phase from the accelerometer on the nose to that on the tail. If we know the distance between these accelerometers, we can find the mean value of the phase velocity of the propulsive wave. Knowing the velocity of the dolphin's swimming, it is easy to calculate the relation between these values.

To assess the relation C_1/U, when we know the expression $C_{1\text{-}3}/U$, it is possible to get the respective calculation formula. It can be written as

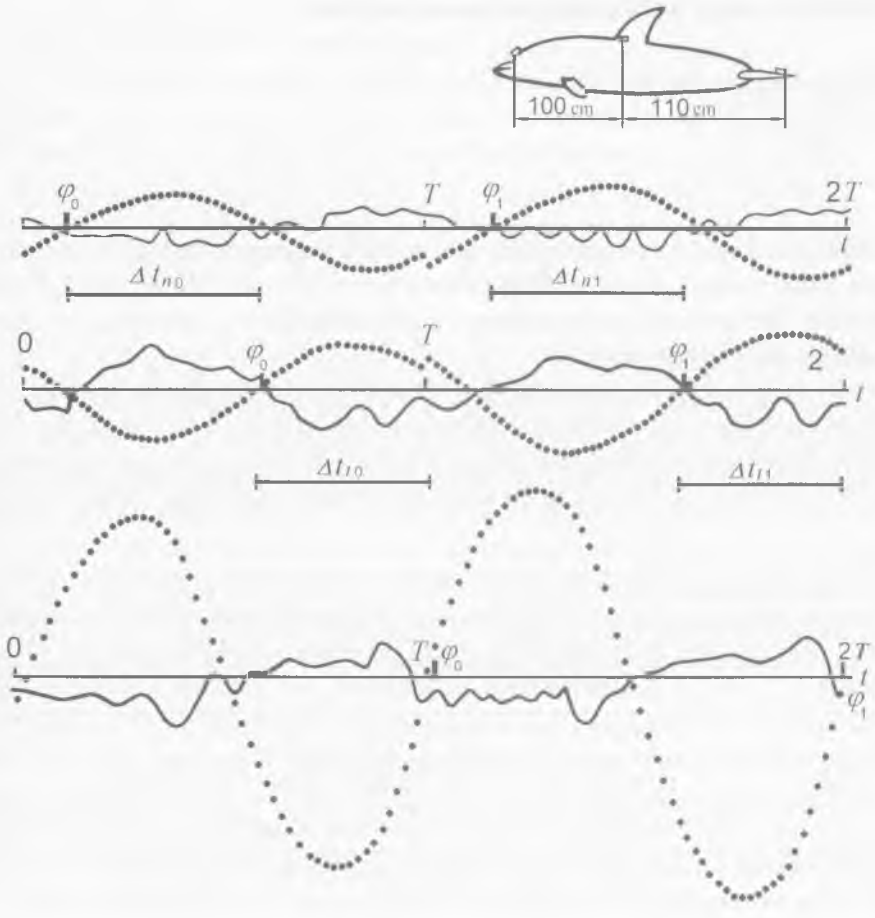

Fig. 6.3. Fragment of signals from three accelerometers (the solid lines). The designations are in the text.

$$C_{1-3} = \frac{C_1 + C_3}{2} = \frac{C_1\left(1 + \frac{C_3}{C_1}\right)}{2}. \tag{6.13}$$

Dividing the left and the right sides of expression (6.13) by the value of the dolphin's swimming velocity (U), we shall get

$$\frac{C_{1-3}}{U} = \frac{C_1\left(1 + \frac{C_3}{C_1}\right)}{2U}, \tag{6.14}$$

where from it is easy to obtain the expression we want:

$$\frac{C_1}{U} = \frac{2C_{1-3}}{U\left(1 + \frac{C_3}{C_1}\right)}. \tag{6.15}$$

Table 6.1 displays the averaged values of kinematic parameters derived by two methods on three experimental animals. Their bodies were 2.24 m, 2.18 m and 2.2 m long respectively. The errors of measurements cited in the table 6.1 correspond to one root-mean-square error of the result.

It is necessary to make a comment. One of the dolphin's body points, the trajectory of which was traced by means of the methods described here, was the fork of the animal's caudal fin. Generally speaking, the choice of this point was not very correct because the caudal fin is movable in relation to the stem. Its mobility may imply certain errors when

U, ms^{-1}	dU/dt, ms^{-2}	h_n/h_t	b_0, m^{-1}	γ	h_t/l	C_t/C_n	C_n/U	C_{av}/U	f, Hz
1.5	2.6	0.27	0.55	-	0.18	-	1.24	-	1.46
±0.07		±0.02	±0.02	-	±0.004	-	±0.08	-	-
2.2	0	0.11	0.07	3.5	0.112	1.15	1.05	1.13	1.10±0.11
±0.07		±0.02	±0.02	±0.9	±0.004	±0.04	±0.08	±0.01	-
4.3	0	0.21	0.23	4.2	0.112	1.50	0.97	1.31	2.22±0.11
±0.07		±0.02	±0.07	±0.9	±0.004	±0.04	±0.08	±0.02	-

Table 6.1. Kinematic parameters of a dolphin *Tursiops truncatus*. For explanations of variables, see text.

calculating the phase relationships of the oscillations of this point and of other points of the dolphin's body. To verify the possibility of such error, the third point of observations was chosen on the caudal stem near its joint with the caudal fin. After that its kinematics was traced and the obtained results were compared with the previous ones. It was found that the data did not diverge much, remaining within the limits of experimental errors.

The experiments discussed here were the first to yield such facts, which testified to the instability of the phase velocity of the propulsive wave spreading along the dolphin's body. The pattern of dependence between the velocity of the propulsive wave, in the first approximation, can be regarded as linear, because the measurements effected only in three points of the body do not permit to reveal a more complicated dependence which is quite possible, as can be seen from the data of the recent years (Yanov, 1990).

Up to the recent time, the velocity of the propulsive wave was thought to be constant within the limits of the fish or dolphin's body. We shall later demonstrate that the variable pattern of the phase velocity of the propulsive wave essentially influences the characteristics of streamlining over dolphins.

As to the amplitude function of the propulsive wave, the measured amplitudes of oscillations in the three points of the dolphin's body, namely h_1, h_2 and h_3, allow to approximate it by a monotonous function like the one below:

$$h(x,t)=h_3\left[\frac{h_1}{h_3}-1+\left(2-\frac{h_1}{h_3}\right)^{\left(\frac{x}{l}\right)^{\gamma}}\right]\sin[\omega t-k(x)x], \tag{6.16}$$

where γ=3.5 and 4.2 with the swimming velocity $U = 2.2$ ms^{-1} and 4.3 ms^{-1} respectively.

Nevertheless, as it is demonstrated in the paper of V. G.Yanov (1990), the amplitude function of the propulsive wave is of non-monotonous pattern and should be approximated by a more complicated function. The experimental studies described in the above paper were aimed at thorough and more detailed examination of kinematic characteristics of *Tursiops truncatus* by a cine method. The amplitude of the dolphin's body oscillations and the phase velocity of the propulsive wave were found in 12 points of the animal. To this end, white suction devices made of rubber were fixed on the dolphin's body (on its side along the median line) at approximately equal distances from one another. The dolphin was trained to swim in a long sea pen along a straightforward line (fig. 5.40 shows experimental scheme). The dolphin, swimming under water, was filmed through the lateral reticulated wall of the pen by a special cinema camera which could rotate horizontally while tracing the animal's movement. The cinema films so obtained were analysed by computers following a special programme, which precluded possible geometric errors. The results testify that the amplitude function of the propulsive wave on the dolphin's body is non-monotonous, having its minimum at $x/l = 0.3$ (fig. 5.44). The phase

velocity of the propulsive wave was not constant within the limits of the animal's body, as it was confirmed by the results of the study (Romanenko, 1980) described above. However, the detailed investigations of Yanov (1990) helped to establish that the function of the phase velocity of the propulsive wave is more complicated (fig. 6.4) than it was thought in the paper of Romanenko (1980). In particular, the function of the phase velocity has a number of minimums, which the author associates with the presence of zones of higher mobility of the animal's spine. The minimums of the function of the phase velocity coincide with such zones.

6.2. Dolphin fluke kinematics

For many years the researchers have been studying dolphin hydrodynamics (Gray's paradox) and swimming performance. One way to increase dolphin swimming performance is to optimize an operation of dolphin fluke. Much attention is paid to mathematical modelling of dolphin fluke (Lighthill, 1970; Wu, 1971; Chopra, 1976; Chopra, Kambe, 1977; Katz, Weihs, 1979; Lan, 1979; Ahmadi, Widnall, 1985). But dolphin fluke kinematics is scantily known experimentally. The available experimental data deserve further refinements.

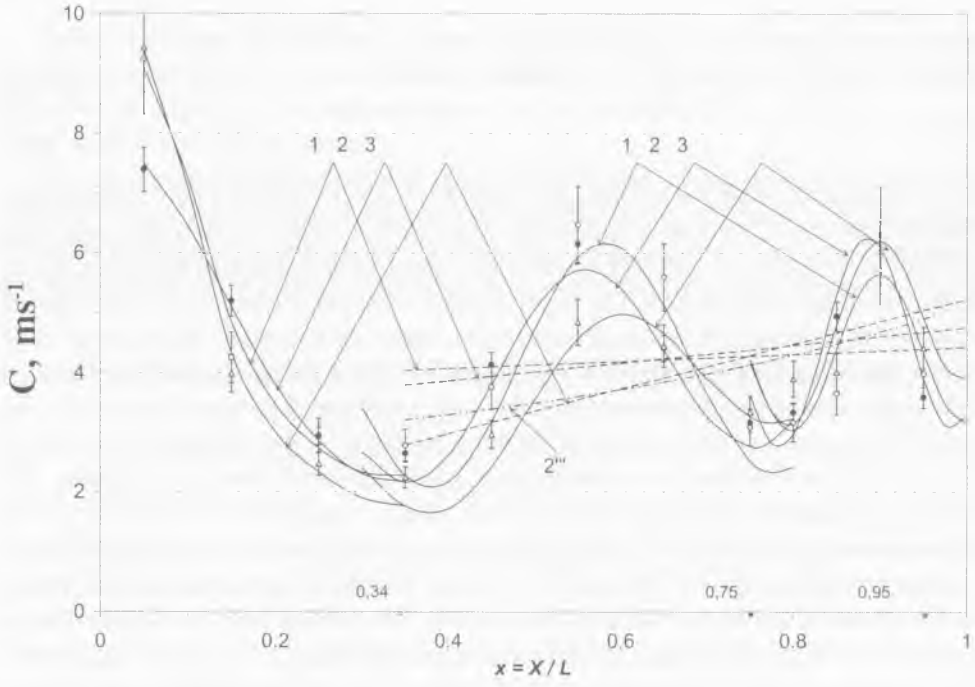

Fig. 6.4. Phase velocity of the propulsive wave. The designations are in the text. (Redrawn from Yanov, 1980).

6.2.1. Dolphins fluke deformation during the dolphin active swimming

The thing is that the few experimental papers published so far (Wu, 1971; Kayan, 1979; Fish, 1993) estimate the kinematic parameters of the dolphin's fluke as approximated by the flat rigid hydrodynamic wing. As an example, fig. 6.5 illustrates the data from paper (Fish, 1993). However, when analysed, the cinema films demonstrate that during the dolphin's active swimming its fluke gets considerably deformed, especially in the upper and lower positions. This is shown in fig. 6.6 displaying fluke in the lowermost position. Fluke is most markedly bent in the point where the caudal vertebra end. fig. 6.7

Fig. 6.5. Path and position of dolphin flukes throughout a stroke cycle. The tips of the flukes move along a sinusoidal path. Fluke position with respect to the path is shown as straight lines at intervals of 0.1 s. The inset shows the angle of attack was measured as the angle between the fluke axis and the tangent to the fluke pathway. (Redrawn with permission from Fish, 1993).

Fig. 6.6. Fluke in the lowermost position.

presents the shape of fluke in some middle position of its movement trajectory (between the upper and the lower extreme points). Fluke is seen to be shaped as an arc.

The above papers say absolutely nothing about the approximation method, which could clarify how the deformed fluke of the dolphin was replaced by the flat wing. This reason, most likely, explains why the literature data on the measured attack angle of the dolphin's fluke differ so much, which can be proved by the table 6.2.

Fig. 6.7. Fluke in the some middle position.

Species	ϑ, deg	α, deg	U, ms^{-1}	Source
Tursiops truncatus	30 - 40	4 - 6	2.3	Kayan, 1979
Same	23 - 27	2.8 - 4	2.35	Videler, Kamermans, 1985
Same		19.5	2.0	Fish, 1993
Same		12.0	6.0	Fish, 1993
Sotalia guianensis	6 - 32	6 - 13	2.4	Videler, Kamermans, 1985
Lagenorhynchus				
obliquidens	38		5.1	Yates, 1983
Same		16	5.1	Webb, 1975

Table 6.2. Measured inclination angle (ϑ) and attack angle (α) of the dolphin's fluke (From literature data).

The lack of experimental data on the position of the pitch-axe of the dolphin's fluke, likewise the widely scattered data on the attack angle, do not permit to sufficiently reliably estimate the efficiency of the work of fluke and of the thrust power, as assessed by the theoretical models known today.

We present the results of our experimental studies of the kinematics of fluke in *Tursiops truncatus*.

The experiments involved three male *Tursiops truncatus* of almost the same dimensions. Their body length was about 220 cm. The kinematics of their fluke was examined in a marine pin by the cinema method. The pin belonged to the Utrish marine station of the Severtsov Institute of Ecology and Evolution, the Russian Academy of Sciences. Fig.5.40 shows the location of the pin (for greater visuality, the scheme is not scaled).

The pin has two parts. One of them is square, 10 m x 10 m in size; it is for long-term keep of the experimental animal and is made of capron net meshed as 10 cm x 10 cm. The net is shaped as a sack and is fixed inside a framework of steel tubes. In detail the pin was described in chapter 5.

The animal under experiment was trained to swim up and down the corridor. To stimulate the dolphin, it was fed alternately in the first and in the second ends of the corridor. The filming was effected by a diving camera man through the side wall of the pin; the camera man worked with the camera and the 16 mm tape. Then we made the photocopies of the frames, scanned it and handled it with a computer. For example, figure 6.8 shows the photo of the tail fin, and its refined image is shown in figure 6.6.

Fig. 6.8. Photo of the dolphin fluke.

In order to evaluate the kinematical parameters of the fluke, we accomplished frame-by-frame analysis of a great number of photo images. Each image was replaced by the line, which repeats its curvature with the best fidelity. Figure 6.9 shows the image of the tail stem and the fluke, and figure 6.10 shows the same image with the applied line, which repeats the shape of the profile and curvature of the fluke.

Then the series of images were laid over so that the volier net elements (first of all, the knots) coincided. It is shown in figure 6.11. We assumed that the net remains immovable during the whole length of the analyzed fragment of the cine filming. Usually the duration of the fragment did not exceed 0.5 – 0.8 s. Then unnecessary elements were erased from the obtained pictures and we got frame-by-frame sequences of the fluke positions. The example of such sequence is shown in figure 6.12. The fin moved downward. The fragment duration was about 0.3 s. We can see that curvature of the fluke varies within a wide range. In frame 1 the fluke is almost plain. This moment corresponds to the fluke position right after the stowage at the upper part of its trajectory. The beginning of the stowage in the lower part is shown in frame 11. That is why the trajectory has a very complicated form.

6.2.2. Linear oscillation of dolphin fluke

The cine filming was performed by a moving camera, which was able to turn in the horizontal plane following the dolphin. We logged many fragments of the complete (or

Fig. 6.9. Photo of the dolphin fluke.

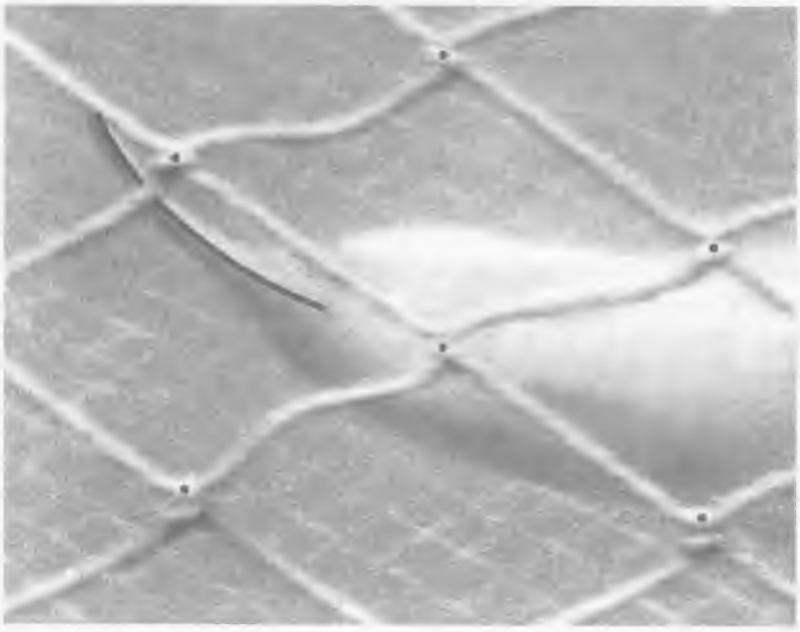

Fig. 6.10. Photo of the dolphin fluke.

Fig. 6.11. The series of fluke images (3 frames).

almost complete) cycle of the fluke oscillation. In these fragments we marked a point, which coincided with the rear end of the root chord, and defined its amplitude function. This point was selected for observation because the axis of the fluke rotation is very likely to pass through it. We will discuss it in detail in the next section.

Figure 6.13 shows experimentally defined values of the amplitude function and a harmonic function of the same amplitude for a comparison (the dotted line), The experimental points are fitted with the confidence intervals of a single standard error size. We can see that the amplitude function of the dolphin fluke oscillation is very close to the harmonic function.

The relative amplitude of the tail fin oscillation h_l/l is 0.112±0.004. Here h_l is the oscillation amplitude (m), l is the dolphin body length (m). The number of the fragments being analyzed is 22. We did not find any dependence of the relative amplitude on the speed of swimming in the range 2.2 ms^{-1} to 4.3 ms^{-1}.

6.2.3. Position determination of the pitch-axes of fluke

For further consideration it is feasible to present the main elements of fluke as it is done in fig. 6.14 (which shows the picture of the real dolphin's fluke). Comparing figs. 6.6 and 6.14, one can see that in the rotating points of fluke trajectory (the upper and the lower ones) the part from -c to +c practically remains rectilinear and it can be treated by Lighthill's law of motion (Lighthill, 1970) describing the motion of the oscillating two-dimensional rigid wing (fig. 6.15). It imitates the caudal semi-lunar fin of fishes. This can be expressed in the following form:

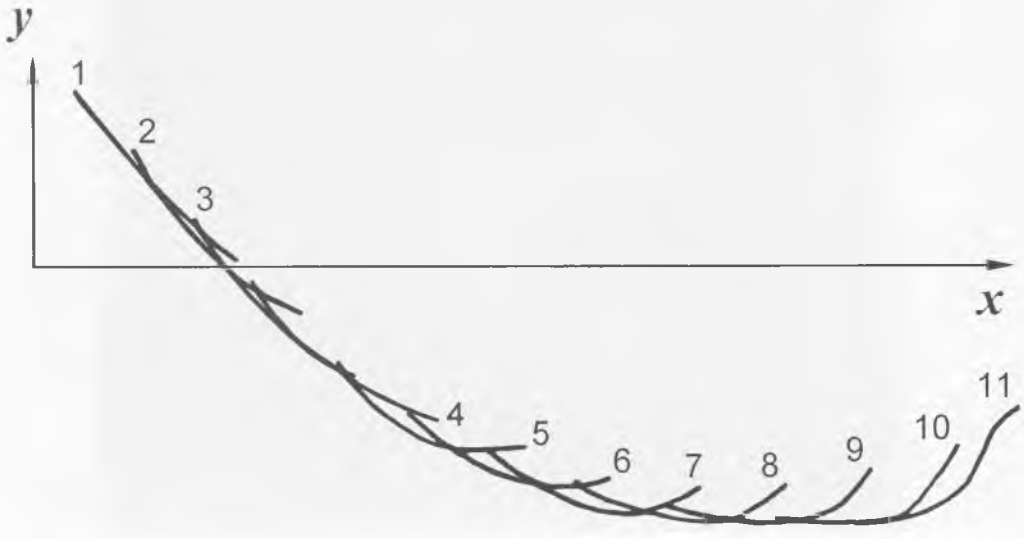

Fig. 6.12. The series of fluke images (11 frames).

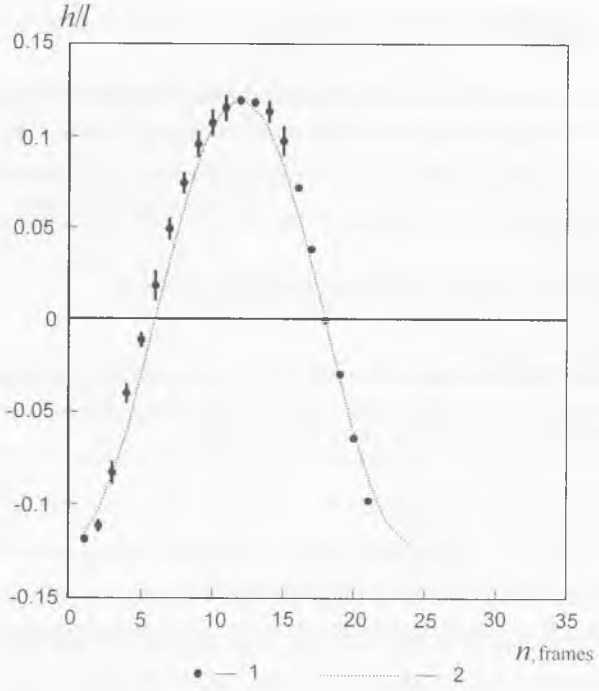

Fig. 6.13. Amplitude function of an oscillating fluke (1) and harmonic function (2).

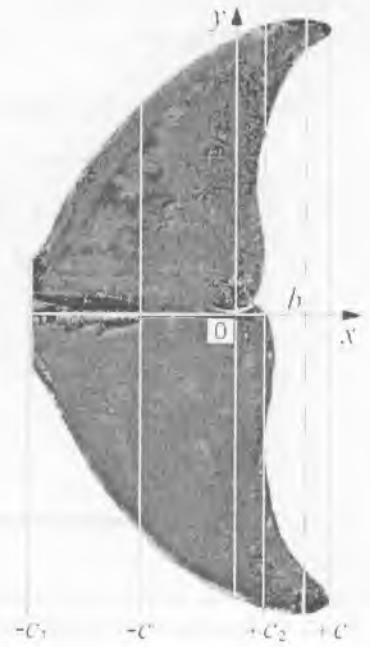

Fig. 6.14. Picture of the real dolphin's fluke. The designations are in the text.

$$y = [h - i\vartheta(x-b)]e^{i\omega t} \qquad (-c \le x \le +c), \tag{6.17}$$

where h and ϑ are the amplitudes of the heaving and pitching of fluke respectively, b is the distance from the beginning of co-ordinates to the pitch-axe, c is the semi-chord of the wing, $e^{i\omega t}$ is the time multiplier characterising the harmonic pattern of fluke motion. Further on we shall omit this multiplier because it does not affect the results under consideration.

The amplitude value of the oscillations looks as follows:

$$y = \sqrt{\left[h^2 + \vartheta^2(x-b)^2\right]} \tag{6.18}$$

or when normalised by the length of the semi-chord:

$$\frac{y}{c} = \sqrt{\left[\left(\frac{h}{c}\right)^2 + \vartheta^2\left(\frac{x}{c} - \frac{b}{c}\right)^2\right]}. \tag{6.19}$$

The amplitude of the shift in fluke with the co-ordinate (-c) in fig. 6.14 will be found by the expression

$$\frac{y^{(-c)}}{c} = \sqrt{\left[\left(\frac{h}{c}\right)^2 + \vartheta^2\left(-1 - \frac{b}{c}\right)^2\right]}. \tag{6.20}$$

Respectively, for the points with the co-ordinate (+c)

$$\frac{y^{(+c)}}{c} = \sqrt{\left[\left(\frac{h}{c}\right)^2 + \vartheta^2\left(1 - \frac{b}{c}\right)^2\right]}. \tag{6.21}$$

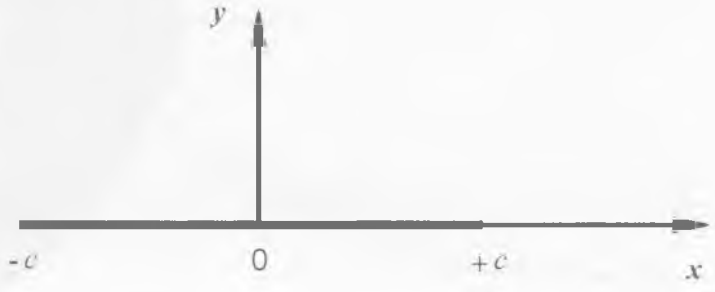

Fig. 6.15. Two-dimentional rigid wing.

The relation of amplitudes in the above points looks as follows:

$$\frac{y^{(-c)}}{y^{(+c)}} = \frac{\sqrt{\left[\left(\frac{h}{c}\right)^2 + \vartheta^2\left(-1-\frac{b}{c}\right)^2\right]}}{\sqrt{\left[\left(\frac{h}{c}\right)^2 + \vartheta^2\left(1-\frac{b}{c}\right)^2\right]}} . \qquad (6.22)$$

As it can be seen from the formula, the amplitudes of the shift in the points (-*c*) and (+*c*) of fluke are identical only in one case when *b*/*c* = 0. If *b*/*c* differs from 0, the relation between the amplitudes $y^{(-c)}/y^{(+c)}$ is determined by three values: *h*/*c*, ϑ and *b*/*c*. We are interested in the position of the pitch-axes, i.e. in the value *b*/*c*. The cinema films containing the results of the experiment permit assessing the relation between the amplitudes $y^{(-c)}/y^{(+c)}$, the amplitude of oscillations *h*/*c* and the maximum inclination angle of fluke towards the horizontal axe ϑ. We analysed a great number of films (over several scores) and found out that the relation between the amplitudes $y^{(-c)}/y^{(+c)}$ varies within 1 to 1.1, the relative oscillation amplitude of the fluke *h*/*c* = 3.5. It is more habitual to relate the oscillation amplitude of the fluke to its root chord (from $-c_1$ to $+c_2$, fig. 6.14). Presenting the root chord as c_0, we shall get $h/c_0 = 1.43$.

To find the angle ϑ, we shall present fluke of the dolphin in fig. 6.7 as an arc of respective curvature. fig. 6.16 *a* shows 4 arcs reflecting the position of fluke in four

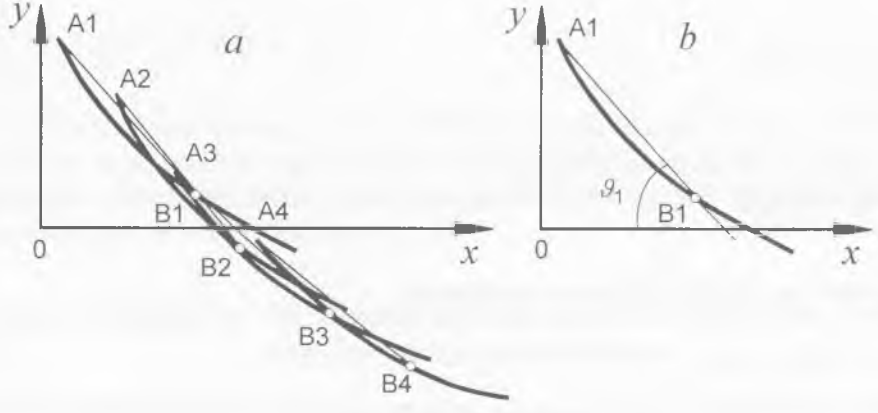

Fig. 6.16. Four arcs reflecting the position of fluke in four sequential frames of the film at the moments when fluke moved from its upper position to the lower one. The designations are in the text.

sequential frames of the film at the moments when fluke moved from its upper position to the lower one. The arcs have emphasised sections A1B1, A2B2, A3B3 and A4B4 which correspond to the part of fluke (from -c to +c) in fig. 6.14 (the letters B1 - B4 mark the points where the vertebra ends within fluke and are labelled as light dots). The inclination angles of the chords A1B1, A2B2, A3B3 and A4B4 in this actual case respectively equalled $\vartheta_1 = 48.5^\circ$, $\vartheta_2 = 51^\circ$, $\vartheta_3 = 42^\circ$ and $\vartheta_4 = 38^\circ$. (The upper arc and the measured angle are shown separately in figure 6.16*b*). They reflect the dynamics of the angle between the fluke sector from –c to +c and the horizontal axis during its the movement. We must differentiate these values from the slope angles of the whole fluke. We shall discuss how to measure these angles in the next section.

They reflect the dynamics in the changes of the inclination angle of fluke (to be more exact, of fluke section from -c to +c) during its motion. To assess the position of the pitch-axes in fluke we shall use the maximum value of its inclination angle averaged by the great number of the films (22) within the range of swimming velocities from 2.1 ms^{-1} to 3.3 ms^{-1}, which equals $\vartheta = 45.4^\circ \pm 1^\circ$. Substituting the measured values $y^{(-c)}/y^{(+c)}$, h/c and ϑ in formula (6.21), we shall see that $b/c = 0$ at $y^{(-c)}/y^{(+c)} = 1$ and $b/c = 1.024$ at $y^{(-c)}/y^{(+c)} = 1.1$.

Taking into account that fig. 6.14 displays the picture of the actual fluke of *Tursiops truncatus*, we shall write down some obvious relationships connecting the dimensions of its individual parts:

$$\frac{c_1 - c}{c_1 + c} = 0.35, \tag{6.23}$$

$$\frac{c_2 + c}{c_1 + c} = 0.41, \tag{6.24}$$

$$\frac{c - c_2}{c_1 + c} = 0.22, \tag{6.25}$$

from which we yield the following expressions:

$$c = 0.32(c_1 + c), \tag{6.26}$$

$$c_1 = 0.67(c_1 + c), \tag{6.27}$$

$$c_2 = 0.09(c_1 + c). \tag{6.28}$$

Let us introduce the following values: $b^0 = c_1 + b$, which is the distance between the pitch-axes and the anterior edge of fluke, and $c_0 = c_1 + c_2$ which is the root chord of fluke. Then the relative position of the pitch-axes may be written as follows:

$$\frac{b^0}{c_0} = \frac{(c_1 + b)}{c_1 + c_2}. \tag{6.29}$$

Dividing the numerator and the denominator in the right part into c, and using the relationships (6.26) - (6.28), we shall get

$$\frac{b^0}{c_0} = 0.88 + 0.42\left(\frac{b}{c}\right). \tag{6.30}$$

The relation between the amplitudes $y^{(-c)}/y^{(+c)}$ of the ends in fluke section from -c to +c during the dolphin's active swimming within the velocity range from 2.1 ms^{-1} to 3.3 ms^{-1} varies from 1 to 1.1, while the value b/c varies from 0 to 1.024. Taking this into account, we can employ formula (6.30) to calculate the relative position of the pitch-axes with the extreme values of b/c. We shall have the following:

$$\frac{b^0}{c_0} = 0.88 \quad \text{at} \quad b/c = 0, \tag{6.31}$$

$$\frac{b^0}{c_0} = 1.31 \quad \text{at} \quad b/c = 1.024. \tag{6.32}$$

The obtained results testify that the pitch-axes of the dolphin's fluke is situated near its posterior edge, which is in good agreement with Lighthill's suggestion (Lighthill, 1970). (There is an uncertainty in the works Romanenko, Pushkov, 1997. But this uncertainty did not influence the main final result).

6.2.4. Evaluation of the angles of inclination of the dolphin fluke and its trajectory to the horizontal axis

We need these values in order to calculate the attack angles of the dolphin fluke and to evaluate the hydrodynamic forces generated by the fluke. Keeping in mind the curvature

of the fluke, we developed some methods of estimation of the slope angles of the fluke itself and of its trajectory, which we are going to discuss first of all. The series of the three fluke positions is shown in figure 6.17. The points A1, A2, A3 show the position of the pitch-axis of the fluke. According to the results of the previous section, this position coincides with the rear edge of the fluke (more exactly, with the line $+c_2$ in figure 6.14). We measured the angles θ_1 and θ_2 between the lines A1A2, A2A3 and the horizontal coordinate axis. Then we calculated average values $\theta_{av}=(\theta_1+\theta_2)/2$, and assumed this value to be the angle (θ_T) between the tangent and the track of the fluke pitch-axis A2. In the same way we evaluated the angles between the tangents and the pitch-axes of the fluke in all the analyzed fragments of the cine filming. Strictly speaking, this averaged angle can differ from the real angle of the slope of the trajectory. But for the middle positions of the fluke (crossing of the horizontal axis) this angle of the trajectory slope is practically constant. That is why the averaging of the angles of two neighbor positions leads to negligible error. However, the error can be appreciable at the upper and lower turning points, where the curvature of the trajectory is close to the maximum.

The averaged function of the experimentally defined angles of the trajectory slope (θ_T) is shown in figure 6.18 (values). Averaging has been performed in the speed range from 2.2 to 4.3 ms^{-1}. For a comparison there is also a harmonic function (dashed line). Every experimental point is supplied by an interval (one standard error size). We can see that the function of the slope angle of the trajectory is sufficiently close to the harmonic function. However at some points the experimentally measured values certainly differ

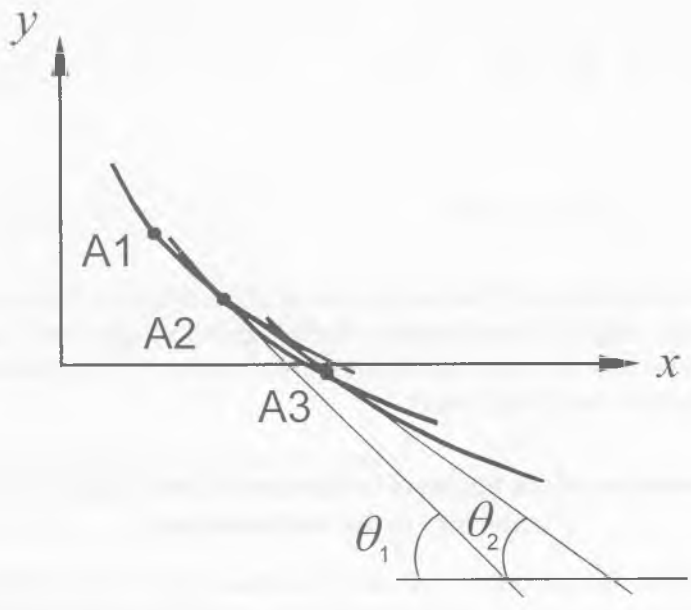

Fig. 6.17. The series of the three fluke positions.

from the harmonic function. This phenomenon takes place at the moments when the fluke motion changes its direction. One of those moments is demonstrated in figure 6.19. Switching occurs between the positions of the fluke marked by figures 2 and 3. As a result, the angle of its slope changes drastically.

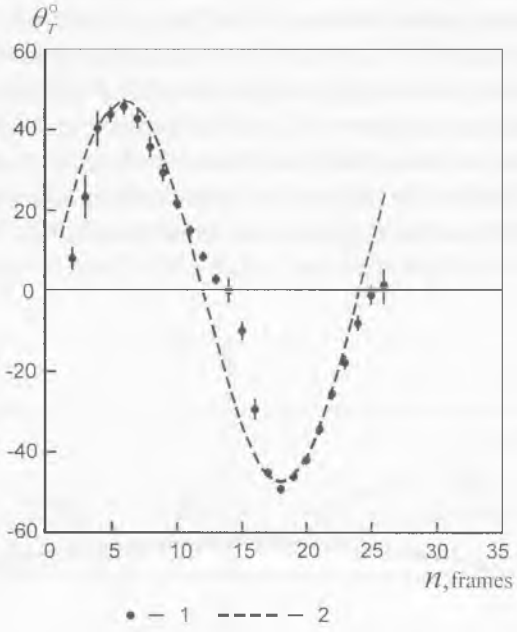

Fig. 6.18. The averaged function of the experimentally defined angles of the trajectory slope (1) and harmonic function (2).

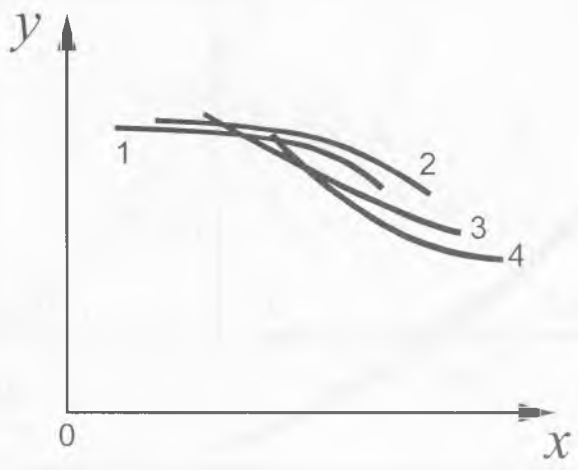

Fig. 6.19. Switching of the fluke positions (1 – 4).

In order to explain the method of the slope angle measuring, let us consider the wing which profile is a sort of an arc (figure 6.20). Here the direction of the zero angle of attack is marked by V^0_∞. For such a wing this direction coincides with the line, which comes through the points A and B (Loitsyanskiy, 1987). The vector of the flow speed V^1_∞ is shown in the same figure. Its direction to the arc forms the angle of attack α. We can suppose that the streamline of the arc-like fluke of a dolphin is approximately the same as of the arc in figure 6.20. Apparently we can assume that the slope of the fluke is the slope of the line of the zero attack angle. In figure 6.21*a* there are the same series of the fluke positions as in figure 6.17. Let us consider the fluke to be in its upper positions (figure 6.21*b*). As it was previously mentioned point A1 denotes the position of the pitch-axis; point B1 denotes the position of the leading edge of the fluke. The fluke here moves down. We draw the perpendicular from the middle of interval A1B1 to the crossing with the line that represents the profile of the fluke (to the point C1). We draw

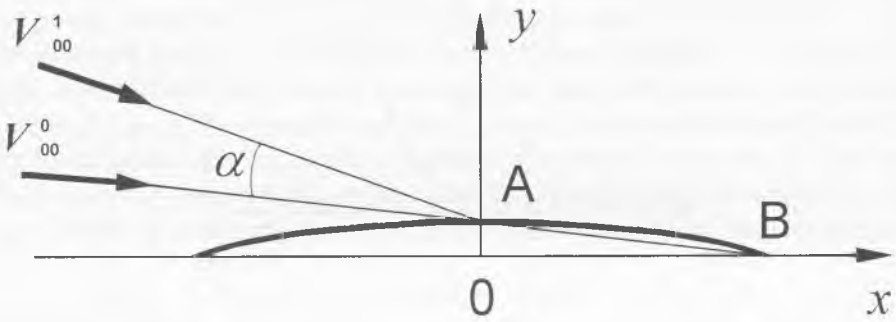

Fig. 6.20. The wing which profile is a sort of an arc.

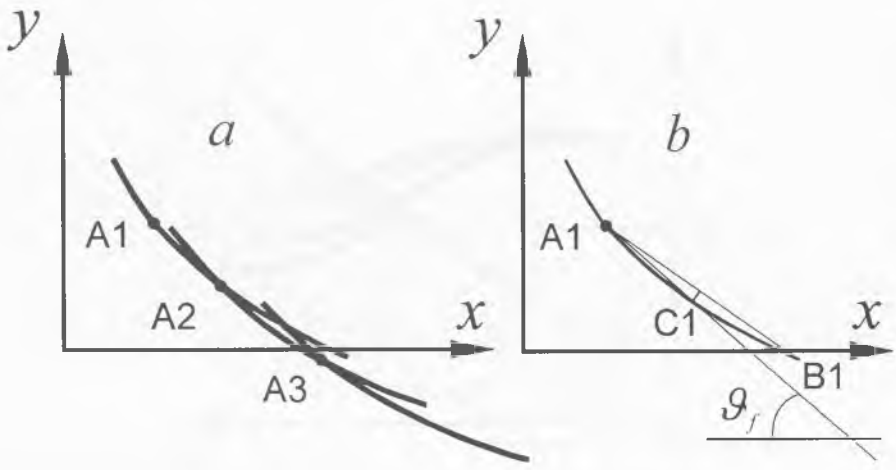

Fig. 6.21. The series of the three fluke positions (*a*) and measuring method of the fluke slope (*b*).

the line through points A1 and C1. We measure the slope angle of this line and consider it to be the slope angle of the fluke. We perform the similar measuring with the other fluke images.

The averaged function of the experimentally defined angles of the fluke slope is shown in figure 6.22. Averaging has been performed in the speed range from 2.2 to 4.3 ms^{-1}. For comparison there is also a harmonic function (dotted line). Every experimental point is supplied by an interval (one standard error size). We can see that the function of the fluke slope angle closer corresponds to the harmonic function than the function of the slope angle of the trajectory (see figure 6.18). However, at the moments when the fluke motion is turning back measured values certainly differ from the harmonic function. This difference is significantly less than it occurs in the plot of the function of the slope angle of the trajectory. The obtained values of the angle are perceptibly greater than those adduced in table 6.2.

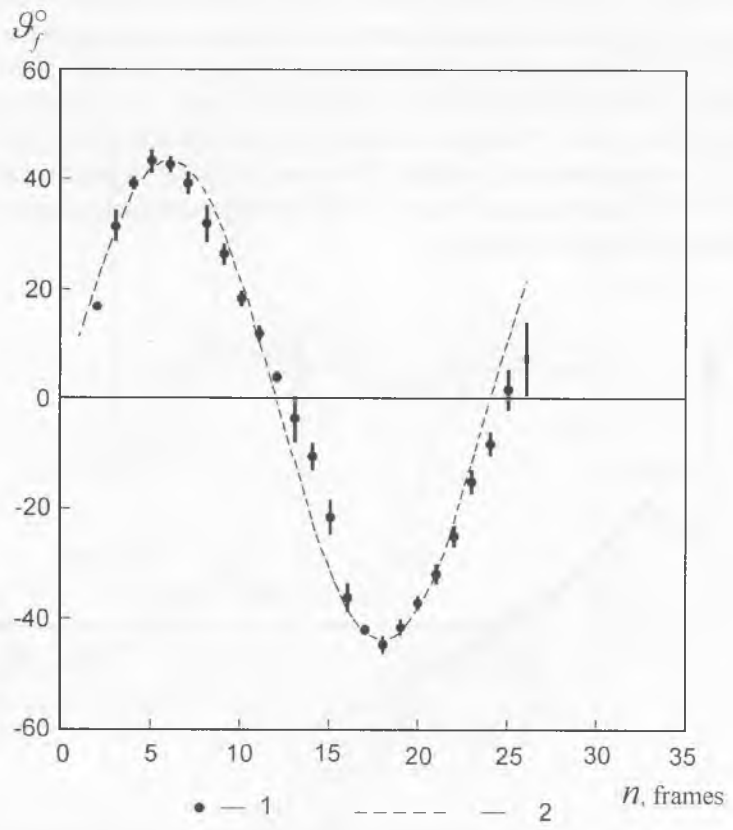

Fig. 6.22. The averaged function of the experimentally defined angles of the fluke slope (1) and harmonic function (2).

6.2.5. The determinations of the angle of attack of dolphin flukes

To determinate the angle of attack of dolphin fluke we'll approximate it as an "arc" (as before). Fig. 6.23*a* shows three arcs (as on fig. 6.17), according to dolphin flukes position in the consecutive frames. A1 – A3 designate the location of the fluke pitch-axes according to its space trajectory. According to previous part the location of the flukes pitch-axes can be taken as coinciding with the tips of the flukes (position $+c_2$ on fig. 6.14). The angle of attack is between the tangent to the fluke pathway and direction of the zeroth angle of attack (V_{00}^0 on fig. 6.20). The tangent to the fluke pathway on fig. 6.23*a* and *b* is designed as θ_{mean} for the fluke A2. The line of the zeroth angle of attack of the fluke with pitch-axes A2 passes through the points A2 and the end of a short length of *d* (fig. 6.23*b*. d is located at right angles to the middle of chord). The mean of 33 measurements of the angle of attack is equal to 3.3^0 on the interval of swimming speed 2.2 – 4.3 ms^{-1}. Fig. 6.24 shows function of the angle of attack of dolphin flukes throughout a stroke cycle (closed circles), amplitude function (crosses), the angle function of the tangent to the fluke pathway (rhombus) and the angle function of the fluke slope (closed squares). Broken and spot curves are harmonic functions. The error bars are the standard error of the mean. The angle of attack function has a complex view. The angle of attack varies in magnitude only slightly. However, it can reach the amount about 8^0 in a turning points of a fluke (top and lower). A relationship between an angle of attack and swimming velocity escaped detection.

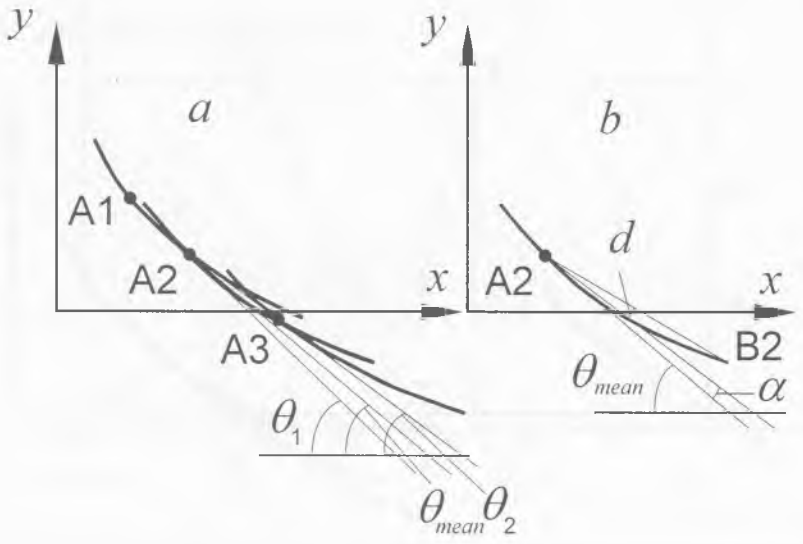

Fig. 6.23. The series of the three fluke positions (*a*) and measuring method of the fluke angle of attack (*b*)

A complex view of an angle of attack function is attributable to complex nature expression

$$\alpha = arctg\left(\frac{V_y}{U_0}\right) - \vartheta_{fl}, \tag{6.33}$$

where $V_y = h_t \omega \cos\omega t$, $\vartheta_{fl} = \vartheta_1 \cos\omega t$, h_{fl} and ϑ_1 - amplitude of heaving and pitching correspondingly, U_0 - swimming velocity, $\omega = 2\pi f$, f – a frequency of fluke oscillation. Fig. 6.25 shows an angle of attack function according to the expression (6.33). One can see that experimental function of an angle of attack is in the qualitative agreement with expression (6.33). The function of an angle of attack of a similar nature was measured previously (Kayan, 1979).

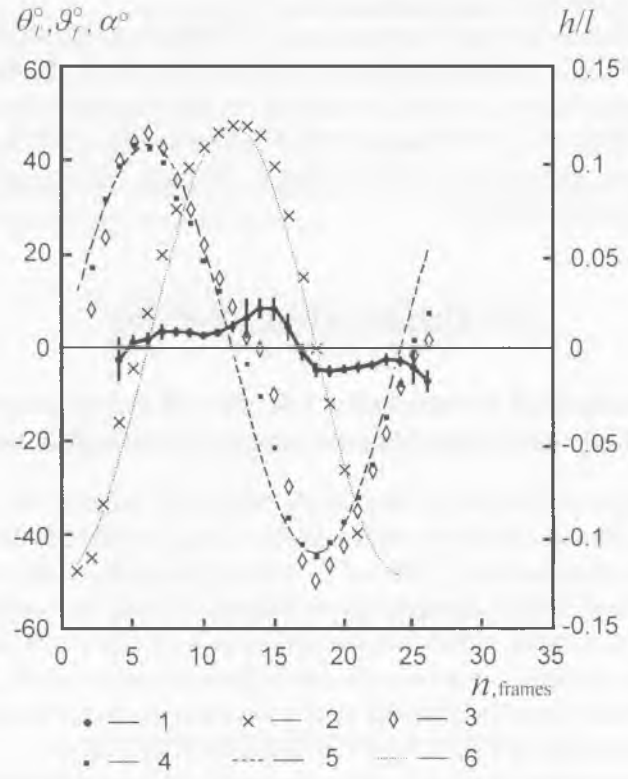

Fig. 6.24. The function of the angle of attack of dolphin flukes throughout a stroke cycle (closed circles - 1), amplitude function (crosses - 2), the angle function of the tangent to the fluke pathway (rhombus - 3) and the angle function of the fluke slope (closed squares - 4). 5 and 6 - harmonic functions.

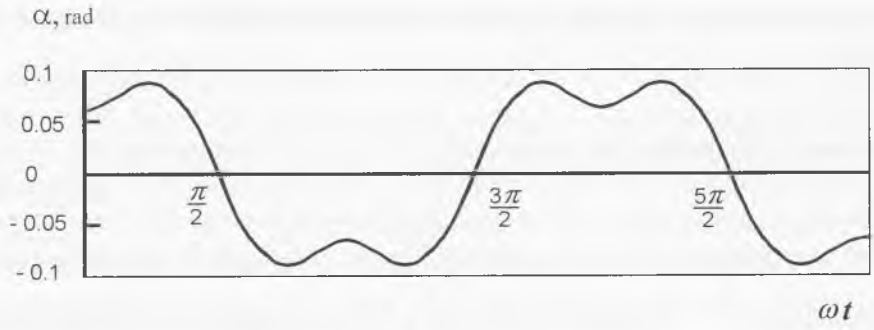

Fig. 6.25. Theoretical function of the fluke angle of attack.

The outlined way of looking at measurement of an angle of attack offers to explain its over-estimations in some works (Wu, 1971; Fish, 1993). If during the measurement of an angle of attack we use direction of chord A2B2 but no direction of the zeroth angle of attack (fig. 6.23*b*) the result will be equal 10^0.

The obtained results are clarify two aspects of dolphin's hydrodynamics: the location of the flukes pitch-axes and the value of its real angle of attack. To date these aspects were not clearly understood resulting in hampers the use of mathematical models (Parry, 1949; Lighthill, 1970; Wu, 1971; Chopra, 1976; Chopra, Kambe, 1977; Katz, Weihs, 1979; Lan, 1979; Videler, Kamermans, 10985; Ahmadi, Widnall, 1985) to estimate the thrust and efficiency of dolphin flukes.

6.3. Dolphin's body flow over

6.3.1. Measurements of stream-lining velocities of the water stream over the dolphin's body and of the dynamic pressure distribution on this body

The experimental verification of the Gray's hypothesis included the measurement of streamlining velocities on a freely swimming dolphin at three points of the lateral surface of its body. The points were situated at 1.2, 1.5 and 1.7 m from the animal's nose, while the dolphin's body was 2.24 m long. The measurements were effected by means of a couple of micro-vanes (Romanenko, 1976) with one of them permanently fixed at 1.2 m from the animal's nose (on a rubber belt). The second micro-vane was alternately fixed at the distance of 1.5 and 1.7 m from the nose (fig. 5.59 and 5.66). The information from the vanes was radio-channeled to the shore. A small-sized radio transmitter was fixed on the dorsal fin of the dolphin.

The results are presented in fig. 6.26. Along the vertical axis we show the relation between the streamlining velocities recorded in the third and the first points of the body (curve 1), and in the second and the first points (curve 2). Horizontally displayed are the values of acceleration

at which the dolphin was swimming. It is easy to note that when the dolphin was moving at a constant velocity or with a positive acceleration, the streamlining flow in the proximal part of its body was accelerated. The results were obtained at the mean velocity of the dolphin's swimming equalling 4 ± 0.5 ms^{-1}. By means of Bernoulli equation it is not difficult to use the streamlining velocities for finding the gradients of dynamic pressure. Fig. 6.27 demonstrates

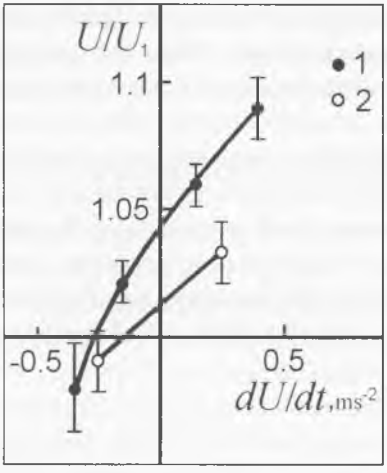

Fig. 6.26. Relation between the streamlining velocities recorded in the third and first points of the body (curve 1), and in the second and first points (curve 2).

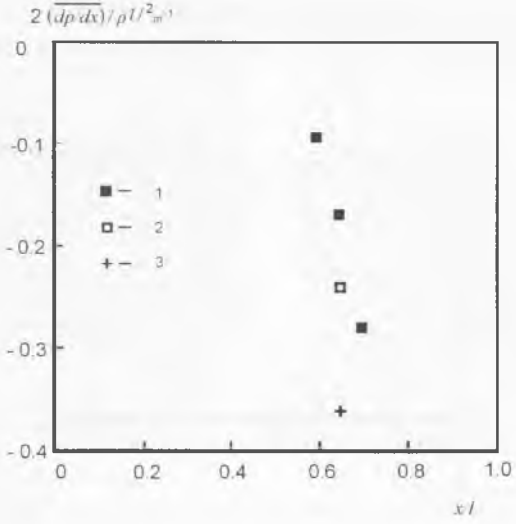

Fig. 6.27. Gradients of dynamic pressure when the dolphin moves at a constant velocity (1) and with an acceleration (2 - the acceleration is 0.14 ms^{-2}, 3 - the acceleration is 0.4 ms^{-2}).

the results of such scaling when the dolphin moves at a constant velocity 1 and with an acceleration (2 - the acceleration is 0.14 ms^{-2}, 3 - the acceleration is 0.4 ms^{-2}). Along the vertical axis there are values of the normalised gradient of pressure within the area under measurement.

Fig. 6.28 shows temporary dependence of dolphin velocity (solid curves) and dynamic pressure gradient on its body (broken lines) during one course. The breaks of a line coincide with the moments of expiration-inhaling. During an active motion of a dolphin the pressure gradient becomes negative. When the motion becomes weak and non-active the pressure gradient becomes positive. The last moment of the motion is exceptional when the decrease of motion velocity coincides with the pressure gradient decrease. At this moment the dolphin finished the motion and took a vertical position waving the tail. In this case the mechanism of negative gradient formation is caused by throwing aside the water by the tail fin and creating of a flow over along the body.

To estimate the impact of the dynamic pressure gradient upon the pattern of streamlining over the dolphin's body, it is demonstrative to consider the form-parameter of the profile of velocities (Schlichting, 1974). The latter looks as follows:

$$\overline{\Lambda} = -\frac{\delta^2}{\nu\rho U}\frac{\overline{dp}}{dx}. \qquad (6.34)$$

Here, ν is the kinematic viscosity of water, δ is the thickness of the boundary layer, ρ is the water density, U is the velocity of the on-running stream, p is the dynamic pressure, x is the co-ordinate.

The experimental values of the pressure gradient, presented in fig. 6.27, correspond to the values of the form-parameter of the profile of velocities cited in table 6.3.

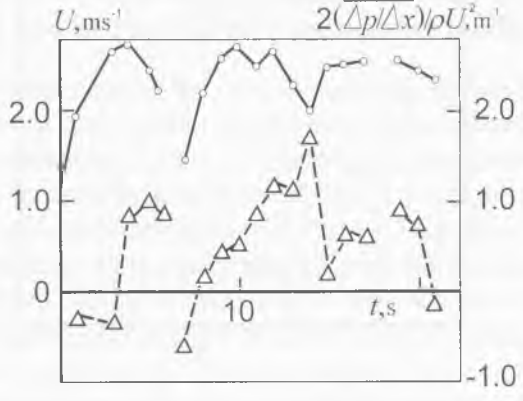

Fig. 6.28. Temporary dependence of dolphin velocity (solid curves) and dynamic pressure gradient on its body (broken lines) during one course.

It is known (Schlichting, 1974) that at positive values of the form-parameter the Reynolds number is increasing and the laminar streamlining is observed to stabilise. As seen from table 6.3, the values of the form-parameter corresponding to the experimentally found values of the dynamic pressure gradient prove to be quite sufficient to stabilise the laminar streamlining (or, which is the same, to increase the critical Reynolds number).

In one of the following parts we will show that in fact the Reynolds number transition of laminar boundary layer into turbulent one on a free swimming dolphin is much higher than on a flat plate and solid dolphin model. The dependence of the Reynolds number transition on dolphin motion acceleration was also found.

6.3.2. Flow over of an oscillating rubber wedge

In order to estimate the negative gradient of dynamic pressure along the oscillating plate we carried out an experiment. A rubber wedge was made (fig. 6.29). Three holes are made along the side surface of the wedge. They are connected with three liquid manometer. In the front part of the wedge a rode is fixed with the help of which the wedge can make transversal oscillations. The bending wave aroused in the front part of the wedge spread from its thick to the thin part with an amplitude increasing. The experiment was carried out in still water. In the case of no oscillations the liquid levels in all three manometers are the same (fig. 6.29*a*).

As soon as the front part of the wedge is oscillated and the bending wave spreads from its front part to the rear part the manometers show the pressure fall and the lowest pressure is shown by the manometer fixed closer to the wedge rear. The highest is shown by the manometer

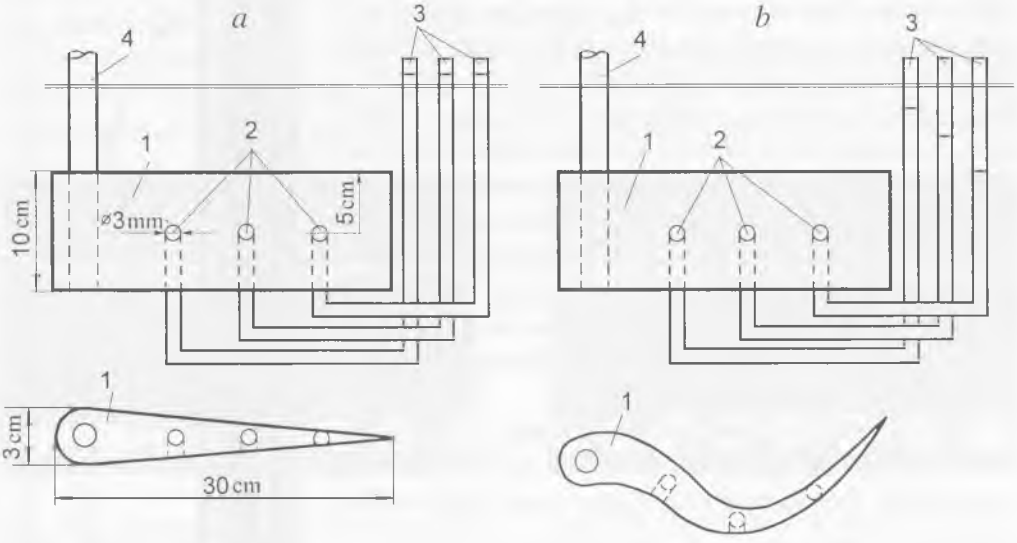

Fig. 6.29. Experimental scheme: *a* – the absence of oscillations, *b* – during the oscillations. 1 - rubber wedge, 2 – holes, 3 – manometers, 4 – rod.

x/l	a, ms^{-2}	$\frac{2}{\rho U^2}\frac{\overline{dp}}{dx}$, m^{-1}	$\overline{\Lambda}$
0.6	0	0.093	1.6
0.65	0	-0.168	3.0
0.65	0.14	-0.24	4.35
0.65	0.4	-0.36	6.5
0.71	0	-0.28	5.6

Table 6.3. Formparameter of the profile of velocities ($\overline{\Lambda}$) *vs.* an acceleration (a) and pressure gradient ($2dp / dx / \rho U^2$) along the dolphin's body (x/l).

fixed closer to the front part (fig. 6.29*b*). It is necessary to note that the manometers were constructed to register only the constant pressure component. An amount flow of water was formed along the wedge. The negative pressure gradient created at this moment equal about $10^{-5} - 10^{-4}$ atm per cm.

6.4. Pressure pulsations as measured in the boundary layer of the dolphin

It is common knowledge that the favorable (negative) gradient of dynamic pressure on the streamlined rigid body not only stabilises laminar streamlining but also favours turbulent streamlining by decreasing the degree of turbulence down to a complete reverse transition (Schlichting, 1974; Repik, 1971; Nazarchuk, Kovetskaya, Panchenko, 1974; Lander, 1964). Now, it remains to be verified if the favourable (negative) gradient of dynamic pressure can actually benefit the pattern of streamlining over the animal's body. In this connection, it is interesting to consider our own radio-telemetric measurements of the pressure pulsation level in the boundary layer on the body of a freely swimming dolphin within the area of its middle (at the distance of 1.2 m from the nose) (Romanenko, 1972, 1978, 1986; Romanenko, Yanov, 1973).

Fig. 6.30 reflects a short-time after-fish plunge of the dolphin. The entire process took about 2.5 s. (the time is presented horizontally). The lower part of the Figure shows a graph with the

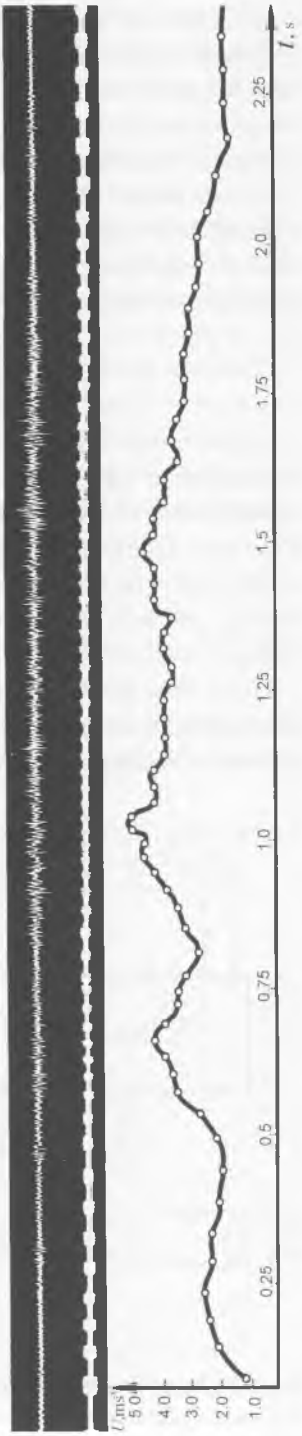

Fig. 6.30. Swimming velocity and pressure pulsations during the short-time after-fish plunge of the dolphin.

streamlining velocity of the dolphin's body nearly to dorsal fin at about 20 cm from the point where the pressure pulsations were measured (The explanation of flow over velocity changes coinciding with dolphin body frequency oscillation is given in 5.1.8. Ch. 5). In the first approximation, the streamlining velocity may equal 5 ms^{-1}. In the upper part of the Figure we display two oscillograms. The first one (in the bottom) presents some useful information as radiochanneled from the dolphin by means of radio-telemetric devices (Yanov, Romanenko, 1972) and then registered on a magnetic tape. This information involves a total of pressure pulsations (the noise pattern) and a sequence of radio-pulses. The frequency of their order is proportional to the streamlining velocity at the point of measurement. The second oscillogram shows the pressure pulsations as such (they are filtered from the pulses). The whole process of the dolphin's motion, reflected in this Figure, can be conventionally divided into three sections: that of acceleration (till the moment of 1.05 s), the one of motion with approximately constant velocity (from 1.05 s to 1.5 s) and the last one of slowed motion (by inertia) (from 1.5 to 2.45 s). Within the section of accelerated motion the streamlining velocity is changing from time to time. The noise of streamlining (the pressure pulsations), likewise the streamlining velocity, is non-stationary. The noise proves to be amplitude-modulated. The maximums of noise rather accurately coincide with those of streamlining velocity. The pattern of hydrodynamic noise, presented in the oscillogram, testifies to an almost turbulent regime of the dolphin's streamlining within the area of its middle when the animal moves at a constant velocity. The meaning of the word "almost" will be explained later when we shall consider the quantification of pressure pulsations. For the time being, we shall speak only about a very important thing. Let us compare the noise in the section of the dolphin's motion corresponding to the time intervals from 0.5 to 0.75 s and from 1.5 to 1.75 s. In these sections, the mean values of streamlining velocity are practically the same. But the level of noise in the second section (retarded or slowed motion) is considerably higher than in the first one (accelerated motion).

Figs. 6.31 and 6.32 provide larger-scaled fragments of the oscillograms of pressure pulsations in the motion sections mentioned above. The fragments permit a very important conclusion: the intensity of pressure pulsations in the boundary layer of the dolphin depends

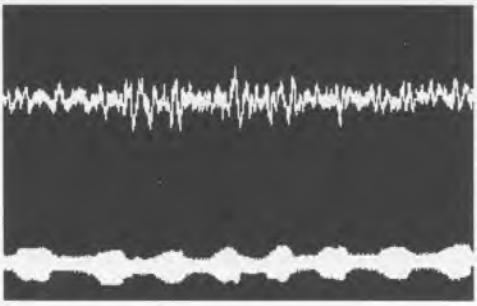

Fig. 6.31. Larger-scaled fragments of the oscillograms of pressure pulsations in the section of the dolphin's motion corresponding to the time intervals from 0.5 to 0.75 s.

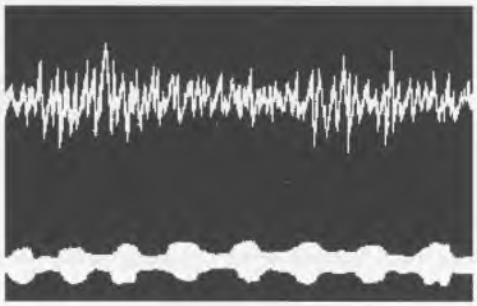

Fig. 6.32. Larger-scaled fragments of the oscillograms of pressure pulsations in the section of the dolphin's motion corresponding to the time intervals from 1.5 to 1.75 s.

upon the pattern of its motion. In the sections of the animal's active motion the level of pressure pulsations is obviously lower than in those of its passive motion (by inertia).

We shall begin our quantification of the obtained results with an estimation of the value of the so-called acoustic-hydrodynamic efficiency ratio (Petrovsky, 1966). The latter characterises the relation between the energy of turbulent pulsations and the kinetic energy of the velocity thrust (pressure head). This efficiency ratio looks as follows:

$$\eta = \frac{2\sqrt{\overline{p}^2}}{\rho U^2}, \tag{6.35}$$

where $\sqrt{\overline{p}^2}$ is the mean square value of turbulent pressure pulsations, ρ is the water density, U is the flow velocity. In some publications this efficiency ratio is called as the transformation coefficient since it characterises the share of the kinetic energy of the flow transforming into the energy of turbulent pulsations.

Now we shall estimate the value of this coefficient for three cases of the dolphin's motion: by inertia, weakly active with acceleration of about 0.4 - 0,6 ms^{-2}, and strongly active with acceleration of about 3.0 ms^{-2}.

The transformation coefficient in case of the inert motion of the dolphin proved to be $8.9.10^{-3} \pm 0.5.10^{-3}$. In case of the weakly active motion of the dolphin, this coefficient equalled $4.6.10^{-3} \pm 0.4.10^{-3}$. In case of the dolphin's strongly active motion the transformation coefficient was $3.9.10^{-3} \pm 0.4.10^{-3}$.

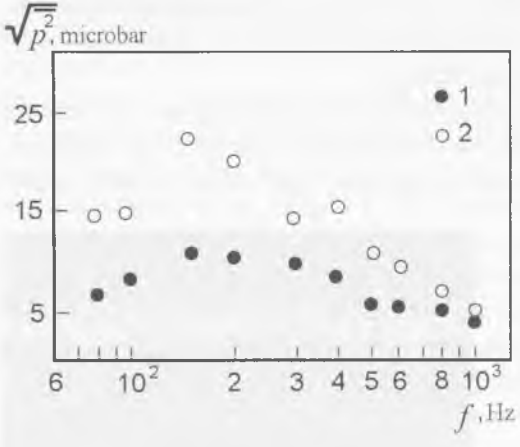

Fig. 6.33. Spectral density of mean square pressure pulsations on the lateral surface of the dolphin's body (at 1.2 m from the animal's nose) during the dolphin's free swimming in the regime of active motion with acceleration of about 3 ms^{-2} (1), and in inert motion (2) with the same swimming velocity (about 3.5 ms^{-1}).

The developed turbulent boundary layer is known to be characterised by the value approximately equalling 6.10^{-3}(Petrovsky, 1966). When the boundary layer is laminar, this value should be at least by six times smaller, i.e. $\eta < 1.10^{-3}$. It means that the above value of $\eta = 3.9.10^{-3}$, corresponding to the more accelerated motion of the dolphin, characterises the boundary layer of some intermediate structure between the turbulent and the laminar layers, or, as it was called previously, an "almost" turbulent one. Therefore, the absolute value of the coefficient η including the inevitable part of system errors is not important, as the

relation between $8.9.10^{-3} \pm 0.5.10^{-3}$ and $3.9.10^{-3} \pm 0.4.10^{-3}$. And their relation, being devoid of system errors, equals 2.3.

The level of pressure pulsations, which comprises the formula (6.35), is unambiguously associated with the shearing stresses on the streamlined body, because they determine the resistance to the body's movement under water. A decreased level of pressure pulsations in the dolphin's active motion, as compared with the level of the passive regime, testifies to the fact that the coefficient of friction resistance in the dolphin's active motion should be smaller than that in its passive motion. And it is this very fact that can explain Gray's paradox.

Fig. 6.33 shows our measurements of the spectral density of mean square pressure pulsations on the lateral surface of the dolphin's body (at 1.2 m from the animal's nose) during the dolphin's free swimming in the regime of active motion (with an acceleration of about 3 ms^{-2}) 1, and in inert motion 2 with the same swimming velocity (about 3.5 ms^{-1}). One can see that when the dolphin moves with a larger acceleration, the level of mean square pressure pulsations is almost twice lower than in case of the inert motion (at the point of measurement).

Fig. 6.34. shows the spectral density of $\sqrt{\overline{p^2}}$ at small active dolphin movement (acceleration is about 0.5 ms^{-2}) with turbulisator and different values of swimming velocity (1 – 4). A rubber ring 1.2 cm thick put on a dolphin body at front peduncles was used as a turbulisator. The measurements are made at the same point of the body as in the previous case. It is obvious that during the artificial turbulisation of the boundary layer and non-active dolphin swimming at a speed of 3.5 ms^{-1} the pulsation level at a measurement point is practically the same as it was in the previous case (fig. 6.33) during the inertial movement.

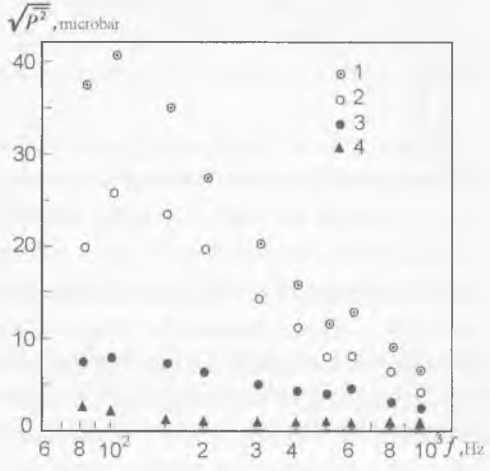

Fig. 6.34. The spectral density of $\sqrt{\overline{p^2}}$ at small active dolphin movement (acceleration is about 0.5 ms^{-2}) with turbulisator and different values of swimming velocity: 1 – 4 ms^{-1}, 2 – 3.5 ms^{-1}, 3 – 2.1 ms^{-1}, 4 – less than 0.8 ms^{-1}.

Fig. 6.35 shows analogous illustration for the case of non-active dolphin movement without turbulisator.

Some interesting results of measuring the velocity pulsations in the boundary layer are cited in the paper of L. F. Kozlov and V. M. Shakalo (1973). For their measurements they employed a thermo-anemometer fixed on the dolphin's side in

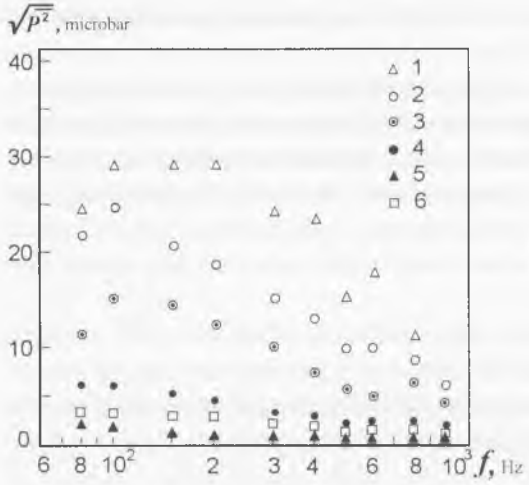

Fig. 6.35. The spectral density at small active dolphin movement (acceleration is about 0.5 ms^{-2}) without turbulisator and different values of swimming velocity: 1 – 5.3 ms^{-1}, 2 – 4.1 ms^{-1}, 3 – 3.6 ms^{-1}, 4 – 1.9 ms^{-1}, 5 – less than 0.8 ms^{-1}.

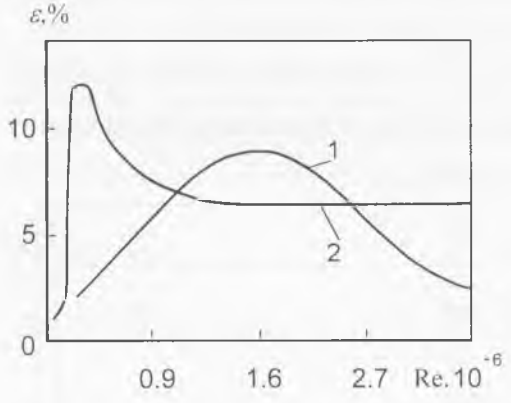

Fig. 6.36. Results of a measuring of the velocity pulsations in the boundary layer on a dolphin (1) and body of a revolution (2). (Based on data Kozlov, Shakalo, 1973 and Tsyganyuk, 1971).

front of its dorsal fin. The distance between the animal's nose and the point of measurement was 0.9 m. That between the thread of the thermo-anemometer and the skin surface of the dolphin was about 1 mm. The degree of free turbulence in the water area was 0.5%. Fig. 6.36 displays the experimental data 1. For comparison, the same Figure shows the data of A. M. Tsyganyuk (1971) who measured the degree of turbulence in the boundary layer of a tagged rigid body of rotation 2. The nose end of the body was shaped as a rotating ellipsoid with the axial ratio of 2 : 1. The body diameter was 22 cm. The distance between the nose of the body and the point of measurement equalled 1.2 m that from the body's surface to the point of measurement was 0.5 mm. The measurements were taken during the steady-speed movement of the body.

When analysing the experimental data of fig. 6.36, these authors conclude that the degree of turbulence in the boundary layer of the dolphin does not depend upon the regime of its motion. Logically, the degree of turbulence in the boundary layer should

depend upon the regime of motion and upon the non-stationary pattern of this motion. The same conclusion is made when we consider the above measurements of pressure pulsations within the dolphin's boundary layer.

The next conclusion made by the authors of the cited paper claims that the transition of the laminar flow into the turbulent one in the dolphin's boundary layer and on a rigid body begins approximately under the same Reynolds numbers. However, the transition area on the dolphin is considerably wider than that on the rigid body.

With $Re = 2.7.10^6$, the level of turbulence on the dolphin is found to be essentially lower, down to the level of the laminar flow, while on the rigid body this level is lowering quite inconsiderably. It is also noted that in some individual cases the high level of turbulence remains there even under large Reynolds numbers.

6.5. Measurement of the shearing stresses in the dolphin's boundary layer

The level of pressure pulsations is unambiguously associated with the shearing stresses on the streamlined body. These stresses determine the resistance to the body's movement under water. A decreased level of pressure pulsations observed in the active movement of the dolphin (movement with acceleration or at a constant velocity), as compared with the level of pressure pulsations in the inert movement of the animal (see fig. 6.33), testifies to the fact that the coefficient of friction resistance in the active movement of the dolphin should be smaller than that in its inert movement. And this very fact explains Gray's paradox.

This conclusion is so important that it cannot be accepted without doubts, despite its looking obvious in the light of the above investigations and their results. To confirm this conclusion, it is necessary to measure the shearing stresses within the boundary layer directly on the body of a freely swimming dolphin. Such measurements were taken by means of a specially designed meter of shearing stresses and an autonomous recording device fixed on the dolphin's dorsal fin.

Simultaneously with the information about the shearing stresses, the recorder takes that on the streamlining velocity, in the way described above. Thus it becomes possible to find the accordance between the streamlining velocity and the value of the shearing stresses.

The meter of shearing stresses was alternately placed in different points on the dolphin's right side at the following distances from the animal's nose: 0.4, 0.5, 0.67 and 0.78 of its length, as well as directly on the caudal fin of the animal (fig. 5.36). The sensor of the meter was situated at 3 mm from the body surface which comprised about 0.2 - 0.25 of the boundary layer width (thickness). According to Shlihting (1974), shearing stresses at such distance from the surface practically coincide with those on the very surface.

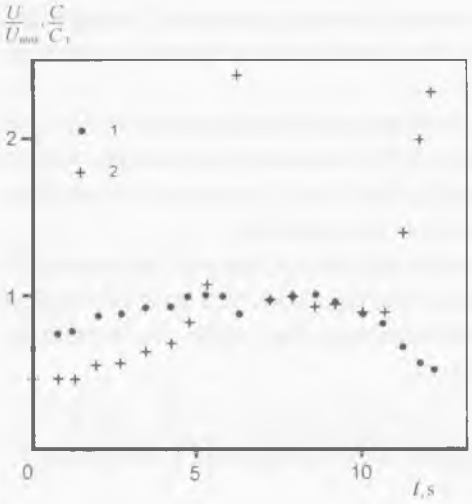

Fig. 6.37. Swimming velocity (1) and the local drag coefficient of (2) in relative units.

The most typical results for all points where the measurements were taken are presented in fig. 6.37. The horizontal axis shows the time in seconds from the onset of the animal's movement, the vertical axis presents the swimming velocity (the black dots) and the local drag coefficient (the crosses) in relative units.

One can clearly see the sections of the animal's movement with positive acceleration, at constant velocity and with delay. Within the time interval from 6.4 and 7.4 s the dolphin emerged to the surface for inhalation - expiration. Before the animal emerged, its swimming velocity was observed to be slightly lower which might be due to the end of thrust. One can see that in the section of the dolphin's accelerated movement the local coefficient of resistance is the smallest, while it was the largest when the dolphin moved with delay (by inertia). The difference between the smallest and the largest values is quite essential. It is noteworthy that in this case the local coefficient of resistance was the largest two times during the dolphin's movement: right before the expiration-inhalation and during the transition to the inert movement at the end of the run. In other cases when the dolphin emerged for inhalation-expiration the swimming velocity did not always decreased, and the local coefficient of resistance did not always increased, corresponding to the decrease in the velocity. However, such decrease-increase was always observed at the end of the dolphin's swimming.

When the meter of shearing stresses was situated in the points at $0.4l$ and $0.78l$ at the distance from the dolphin's nose the local coefficient of resistance in case of the dolphin's movement at constant velocity was found to be by 4.7 times smaller in the point of 0.781 than that in the point of $0.4l$. Here, l is the animal's body length. This fact will be explained somewhat later.

When the meter of shearing stresses was located directly on the fluke of the dolphin, we discovered that the pattern of streamlining was alternating and the values of the local

coefficient of resistance were extremely unstable. This fact is easy to explain by the non-stability of the pressure gradient values in the fluke at different stages of the animal's movement.

6.6. Transition of a laminar flow over of dolphin into a turbulent one

The phenomenon of the transition of a laminar flow into a turbulent one in the boundary layer of three dolphins was studied with the help of pressure pulsation meters and the shearing stress meters. They were fixed at the different points of the side surface of dolphin (at the right side). The pressure pulsation meters were fixed at 100 cm from dolphin's nose and the shearing stress meters – at 90, 120 and 150 cm.

Figs. 6.38 and 6.39 show a typical transition pattern at the distances 120 and 150 cm from dolphin's nose. Fig. 6.30 shows analogous pattern at the point at the distances 100 cm. In all cases transition is run at the instant of changing an accelerated dolphin's swimming by swimming with constant velocity (or with the slowing down).

All patterns are characterized by initial part where shearing stress (or pressure pulsation) approaches to the zero. The lines of shearing stress off the horizontal axes when the velocity of flow over is near to 4 – 4.5 ms^{-1}. The transition time is different (0.4 s – on the first pattern, on the second pattern the interval is much smaller and 0.8 s – on Fig. 6.30).

After transition shearing stresses don't remain constant even at a constant average velocity of dolphin. There are periodic changes of shearing stresses level due to the oscillations of dolphin body. These level oscillations correlate with flow over velocity oscillations. They are reflected in increasing and decreasing of impulse frequency of meter measuring the flow over velocity. These impulses are mapped on horizontal axis of mentioned above illustrations. There is one peculiarity common for the both illustrations (Fig. 6.38 and 6.39). Besides the stationary part (or quasi-stationary) of shearing stress there is also non-stationary part (pulsations). The existence of the non-stationary part

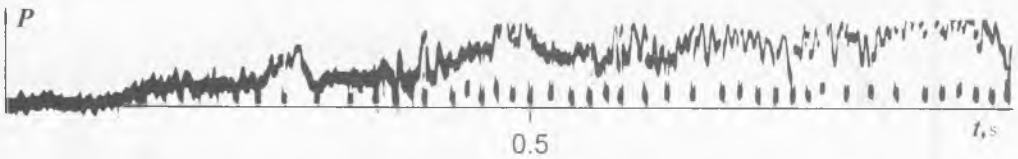

Fig. 6.38. The shearing stress in the boundary layer of dolphin at the distances 120 cm from dolphin's nose.

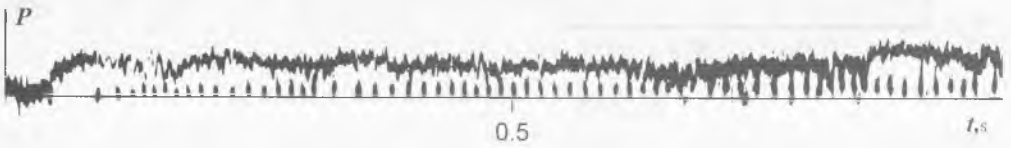

Fig. 6.39. The shearing stress in the boundary layer of dolphin at the distances 150 cm from dolphin's nose.

can be explained by the fact that sensor of shearing stress meter is rather small (5 x 10 mm) and that's why it can register single pulsations which scale is twice bigger than one half of a sensor.

There are some important differences:

1. Non-stationary part of the shearing stresses (fig. 6.38) is much bigger than in the fig. 6.39.
2. Non-stationary part of the shearing stresses (fig. 6.38) is more low frequent.
3. Stationary part of the shearing stresses (fig. 6.38) is about twice bigger.

The characteristic feature found in the mentioned above experiments is that the transition in different points of animal body takes place at the same velocity. It means that the transition starts not at the rear part of the dolphin's body as it usually happens on the solid bodies but at the medium part where the negative gradient of the dynamic pressure is the least.

There is one more peculiarity. The value of the local critical Reynolds number of transition depends on dolphin acceleration: the higher acceleration the higher critical Reynolds number of transition. At increasing of acceleration from 0.25 to 1.2 ms^{-2} critical Reynolds number of transition increases 1.9 times (fig. 6.40).

The mentioned above results allow us to make a conclusion that at the acceleration of about 1.5 – 2 ms^{-2} the critical Reynolds number of transition equals to $1.2.10^7$.

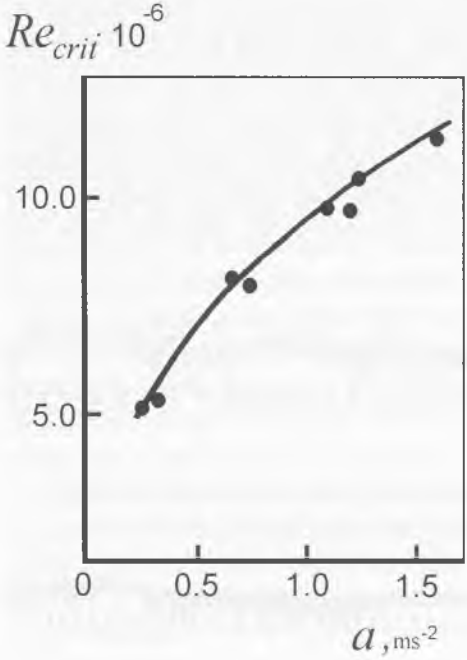

Fig. 6.40. The value of the local critical Reynolds number of transition *vs.* dolphin acceleration.

6.7. Correlation measurements in the dolphin's boundary layer

It is very interesting to consider correlation measurements in the boundary layer of the dolphin's body. Such measurements permit estimating the pattern of turbulence, the scales of turbulent pulsations, the degree of their coherence. Our method of multichannel measurements of pressure pulsations in the dolphin's boundary layer allowed us not only to effect an auto-correlation analysis but also a spatial-correlation one. It should be reminded that we measured the pressure pulsations simultaneously in three points of the transversal profile of the boundary layer when the pulsation receivers (sensors) were divided from one another by a minimum distance of about 6 mm (Romanenko, 1978). It was possible to alter the division distance from 6 to 48 mm. The measurements were taken when the dolphin moved with the velocity of up to 5 ms ^{1}.

Fig. 6.41 shows the auto-correlation function (within the frequency band of 80 - 850 Hz) of pressure pulsations in the dolphin's boundary layer at 1.2 m from its nose. The dolphin was weakly active and moved with the velocity of 4.5 ms^{-1}. The horizontal axis demonstrates the time of delay. The pattern of the function testifies to the wide band of pressure pulsations. Indeed, if the interval of time between the zeroes of the function is considered as the interval of correlation, it is found to equal $\tau_0 = 4.10^{-3}$ s. In our case, the width of the useful signal band, estimated as $1/\tau_0$, approximates 250 Hz, which is in good agreement with the data from fig. 6.33 – 6.35.

The auto-correlation function also permits to assess the convective velocity in the boundary layer (the velocity of vortex transfer) which is connected with the correlation interval τ_0 and with the radius of correlation d_0 by means of the relation

$$U_c = \frac{d_0}{\tau_0}. \tag{6.36}$$

In our case, we roughly considered the width of the boundary layer, estimated as 1 - 2 cm, as the radius of correlation. Then, with $d_0 = 1$ cm, we have $U_c = 2.6$ ms^{-1}, and with

Fig. 6.41. Auto-correlation function (within the frequency band of 80 - 850 Hz) of pressure pulsations in the dolphin's boundary layer at 1.2 m from its nose.

d_0 = 2 cm, the value of U_c = 5.2 ms^{-1}. This value fairly well agrees with the measured velocity of 4.5 ms^{-1}. However, we should bear in mind that the velocity of vortex transfer, which in the first approximation can be thought to coincide with that of the on-running flow, seems to be easier measured than the width of the boundary layer. Then it seems more feasible to employ the relation (6.36) for assessing the width of the boundary layer (or, to be more exact, of the radius of correlation) when the values of U_c and τ_0 are known. The calculations demonstrate that in our case d_0 = 1.8 cm. It goes without saying that such estimates are not very accurate. Nevertheless, if we want to find the trends of changes in the values under measurement when the animal's swimming regimes change, such estimates may prove to be extremely useful.

Fig. 6.42 shows our measurements of the transversal spatial correlation $R(0,0,\zeta)$ in case of the dolphin's inert motion.

The horizontal axis in this Figure demonstrates the mean frequencies of the 1/3 octave bands of the analysis. The vertical axis presents the value $R(0,0,\zeta)$ when the receivers of pressure pulsation were separated by the distance of 6 mm, and the dolphin's motion velocity equal to 3.2 ms^{-1} (circles). The same graph (triangles) displays the value of correlation when the dolphin had a turbulizer, shaped as a rubber ring 5 mm thick, which was fixed in the area of the animal's thoracic fins.

Fig. 6.43 presents the function of transversal correlation as depending upon the value of the division between the receivers of pressure pulsations. The analysis was effected within the 1/3 octave band of frequencies equalling 60 - 85 Hz.

Fig. 6.44 shows the transversal spatial correlation within the common frequency band as dependent upon the relation of the distance between the receivers and the width of the replaced boundary layer (the black circles). The same graph has a continuous line to

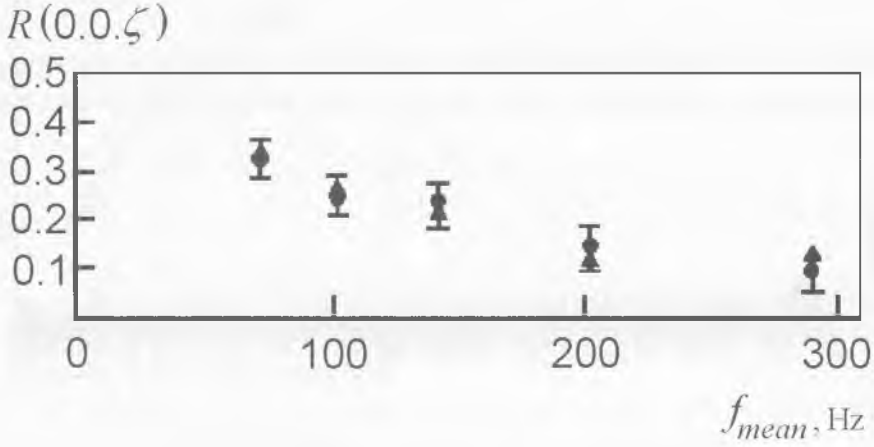

Fig. 6.42. Transversal spatial correlation $R(0,0,\zeta)$ in the boundary layer on a dolphin in case of the dolphin's inert motion.

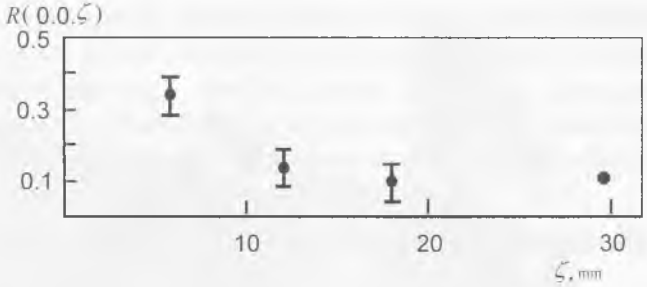

Fig. 6.43. Transversal correlation as depending upon the value of the division between the meters of the pressure pulsations.

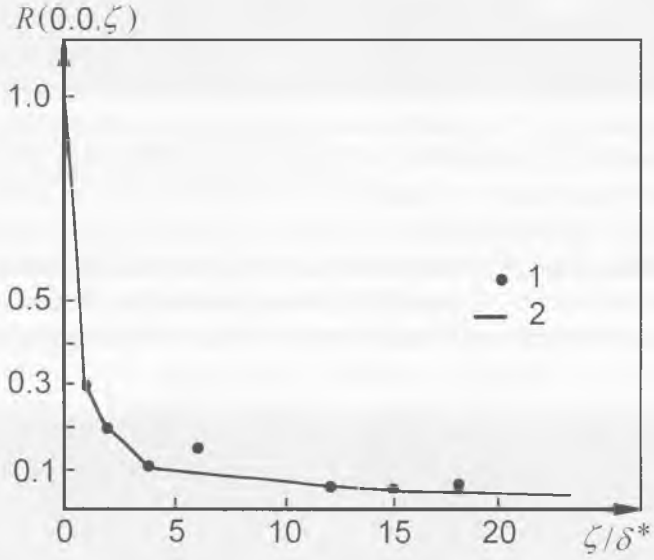

Fig. 6.44. Transversal spatial correlation within the common frequency band as depending upon the relation of the distance between the meters and the width of the replaced boundary layer on a dolphin (1) and a flat plate (2). (Based on data Willmarth, Wooldridge, 1962).

show the data of W. W. Willmarth and C. E. Woolbridge (1962) for the case of a turbulently streamlined flat platelet.

The displayed results once more confirm that the streamlining over a dolphin moving by inertia prove to be purely turbulent within the Reynolds numbers from 2.10^6 to $5.5.10^6$, which correspond to the point where the meters of pressure pulsations are situated.

As it was shown above, a considerable negative gradient of pressure is formed on the body of an actively swimming dolphin. This gradient causes essential changes in the fine

structure of the boundary layer: its level is declining and the spectrum of pressure pulsations gets altered. When the dolphin moves by inertia, the structure of the boundary layer on the animal's body is the same as that on the rigid body. These results permit to make a very important conclusion that the shearing stresses and the local resistance coefficient in different parts of the dolphin's body depend upon the regime of the animal's swimming.

6.8. The verification of the hypotheses for a dolphin's skin breathing

Among the hypotheses for explanation for the Gray's paradox there is a further hypotheses for possible role of a dolphin's skin breathing in total expenditure of energy (Tinyakov, Tchumakov, Sevastyanov, 1973). This hypotheses was verified by an experimental approach (Darholz, Romanenko, Sokolov, 1978). In experiments three dolphins (*Tursiops truncatus*) were used which were kept in the pool (12.5 x 6 x 1.2 m).

The intake of oxygen by the dolphin's skin was measured by vary in concentration of oxygen in the water which was held in a special chamber. The rubber cylindrical chamber (680 cm^3) was constructed with the metallic bottom. The chamber bottom had built-in two rubber tube to fill and empty. The chamber was cemented to the dolphin's skin. A concentration of oxygen in the water was measured by the Winkler method (Polyakov, 1950; Minkh, 1971). Early in the experiment water level in the pool was lowered to 20 – 25 cm for the purpose of the baring of a back skin and decrease of mobility. A chamber was fixed either on the back (dolphin N 1 and N2 - fig. 6.45) or on the dorsal fin (dolphin N 3 - fig. 6.46). The water level in the pool was raised to 35 – 40 cm. During the experiment the samples of the water were withdrawn from the chamber and from the vessel in which the water was contained to fill the

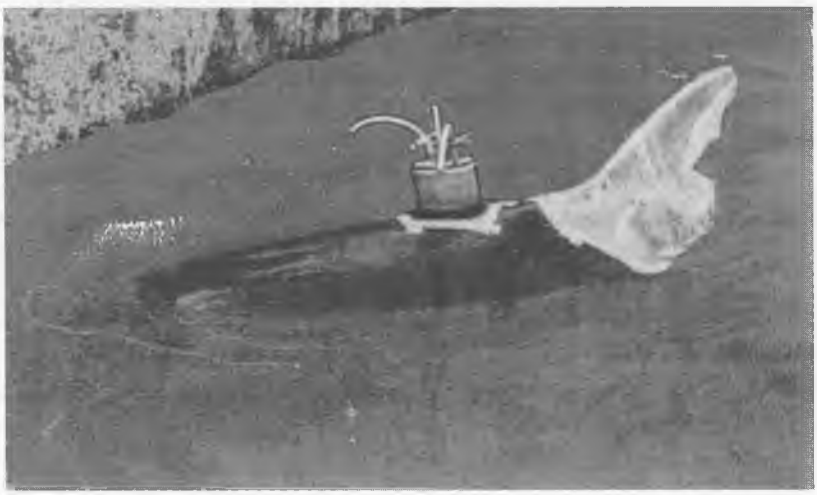

Fig. 6.45. A chamber position on the dolphin back.

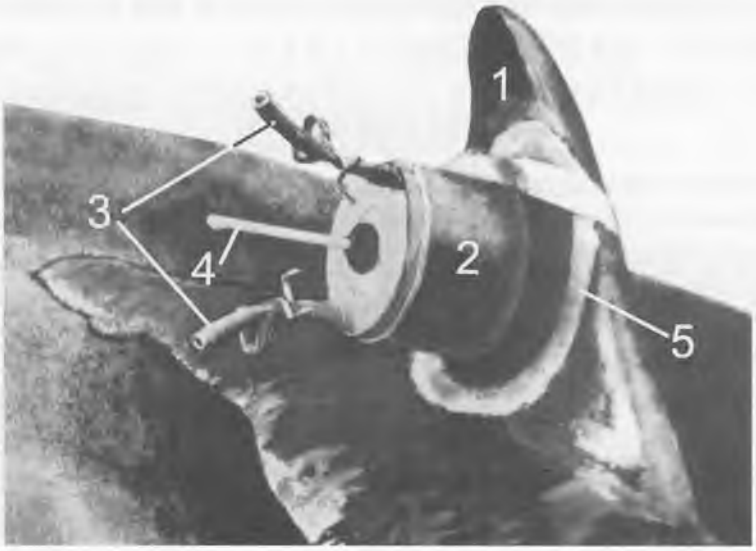

Fig. 6.46. A chamber position on the dolphin dorsal fin. 1 - dorsal fin, 2 - chamber, 3 - rubber tubes, 4 - thermometer, 5 - the junction of chamber and dolphin skin.

chamber. The difference in quantities of oxygen in the control and experimental samples was measured. Duration of the expositions was 15 – 20 min.

To estimate the metabolism level in the rest data of works were used (Karandeeva, Protasov, Semyonov, 1970; Karandeeva, Matisheva, Shapunov, 1971; Kolchinskaya, Karandeeva, Mischenko, Shapunov, Matisheva, Stepanov, 1971) about the intake of oxygen by one kilogram of the dolphins (at 21 - 23^{0}C).

Table 6.4 shows the results of experiments. Here l – the dolphin's length, S – the total body surface area, P – dolphin's mass, n – a number of the experiments, T^0C – temperature inside the chamber.

Dolphin number	l,m	S,m^2*	P,kg**	Standard metabolism 21-23^{0}C, ml O_2/h***	n	T^0C	% of standard metabolism
No. 1	2.45	2.1	165	42960	6	18.5	0.36
No. 2	1.9	1.25	80	21070	11	17.8	0.37
No. 2	1.9	1.25	80	21070	5	14.5	0.1
No. 3	2.15	1.6	150	39060	12	13.8	-0.04

* Calculated (Lang,1963)

** Culculated (Zenkevitch, 1952)

*** Calculated (Karandeeva at al., 1970, 1971; Kolchinskaya at al. 1971).

Table 6.4. The intake of oxygen by the dolphin skin.

One can see that the role of a dolphin's skin breathing in total expenditure of energy is negligible.

Brief conclusions

This chapter presents all the original experimental researches on dolphin kinematics and hydrodynamics. The most of the obtained results are pioneering and till now they have not been repeated. The main value of the obtained results is that they prove the existence of some adaptation mechanisms, which give the dolphin an opportunity to increase critical Reynolds number, decrease the hydrodynamic friction drag and have high efficiency propeller.

CHAPTER 7. EVALUATION OF DOLPHIN'S HYDRODINAMIC CHARACTERISTICS ON THE BASIS OF MEASURED KINEMATICAL PARAMETERS. THEORY AND EXPERIMENT

7.1. Estimate of theoretical distribution of the dynamic pressure on dolphin's body surface in comparison to experimental data

In ch. 3 we discussed mathematical models of the mechanism, which generates the dynamic pressure (and its gradient) on the body of active swimming fish and dolphin due to undulation of the animal body and due to fluke oscillation. Now, having the experimental data on the dolphin's kinematics (see ch. 6), let us numerically estimate the dynamic pressure gradient on dolphin's body and compare it with the experimental data.

7.1.1. The dynamic pressure caused by the body undulation

In chapter 3 we obtained expression (3.4) for the instantaneous value of the dynamic pressure gradient on the body of active swimming dolphin normalized on dynamic pressure. Here it is:

$$\frac{2}{\rho U^2}\frac{dp}{dx} = \frac{2}{U^2}\left\{ v_n \frac{dv_n}{dx}\left(1 - 4\sin^2\theta_0\right) + \frac{d}{dx}\left[\frac{\rho\cos\theta_0}{R}\frac{d\left(R^2 v_n\right)}{dt}\right]\right\}. \qquad (7.1)$$

Here U is the velocity of the dolphin movement. To measure its value is relatively easy. ρ is the density of water. Its value is known. $R(x)$ and θ_0, are the cylindrical coordinates, which define the point where the pressure gradient is estimated. These values are the parameters of the counting and they can be presented in every case. R is the radius of dolphin body. Table 7.1 contains the values of the dolphin body half-size along dorsal direction. These sizes we use as a body radius. The velocity of the transversal movements of the body v_n is the argument of this evaluation. It can be defined on the base of the known law of the body alteration. It was showed earlier (Yanov, 1997) that the expression

x, m	$R(x)$, m
0.8	0.2
1.0	0.19
1.2	0.17
1.4	0.155
1.6	0.14
1.8	0.125
2.0	0.1

Table 7.1. Values of the dolphin's body half-size along dorsal direction ($\theta_0 = 0$).

(7.2) is the best approximation for the experimentally measured amplitude function of the body oscillation ($U = 3.12$ ms^{-1})

$$h(x,t)=h_t\left[0.21-0.66\left(\frac{x}{l}\right)+1.1\left(\frac{x}{l}\right)^2+0.35\left(\frac{x}{l}\right)^8\right]\sin\left\{\omega t-\left(\frac{k_0}{b}\right)\ln[1+lb(x/l)]\right\}. \quad (7.2)$$

We assume that the phase velocity of the propulsive wave linearly increases along the dolphin body from its head to tail. This law is established experimentally as a first approximation in the work of Romanenko (1981) and it agrees with the averaged trend remarked by Yanov (1997). We use this law of body alteration for the evaluation of the dynamic pressure gradient, which forms on the dolphin's body while active swimming.

Fig. 7.1 shows the results of the calculation of the minimal 1 and maximal 2 values of dynamic pressure gradient on the lateral side of the dolphin's body ($\theta_0 = \pi/2$ and $\theta_0 = 3\pi/2$), which is normalized by the value of the dynamic pressure $\rho U^2/2$. These values of the gradient are reached twice on a period of oscillation. The calculation was performed under the values of cinematic swimming parameters cited in the bottom line of table 7.2 and under the constant swimming velocity of 4.3 ms^{-1}. We suggest that expression (7.2) is correct for this velocity. We can see that the maximal values are near zero, and minimal values are of significant negative values. The current instantaneous values of

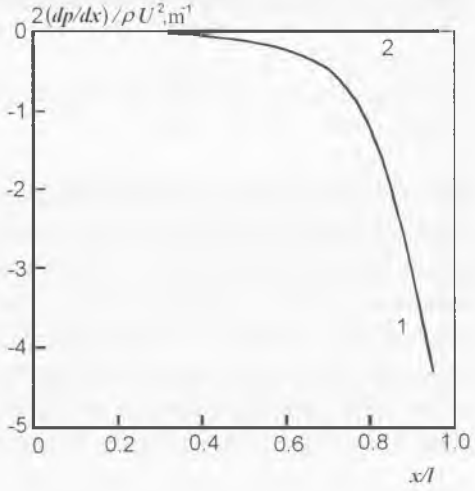

Fig. 7.1. Minimal (1) and maximal (2) values of dynamic pressure gradient on the lateral side of the dolphin's body ($\theta_0 = \pi/2$ and $\theta_0 = 3\pi/2$).

U, ms^{-1}	dU/dt, ms^{-2}	l, m	h_t/l	f, Hz	b_0, m^{-1}
1.5	2.6	2.24	0.18	1.46	0.55
4.3±0.07	0	2.24	0.112±0.004	2.22	0.23±0.07

Table 7.2. Kinematic parameters of a dolphin *Tursiops truncatus*. For explanations of variables, see text.

the pressure gradient on the undulating body of a swimming dolphin are restricted by these margins.

Fig. 7.2 shows analogous results of the calculation for the dorsal side of dolphin body ($\theta_0 = 0$). The same picture takes place on ventral side of dolphin body.

Data from fig. 7.1 and 7.2 do not take into account the shape of dolphin body characterized by a certain distribution of dynamic pressure and of its gradient. In the work of Alekseeva and others (1968) there was shown the computational technique which allows to calculate the pressure distribution on the bodies of revolution similar to dolphin's body and there were also shown the results of the calculations.

Fig. 7.3 shows the distribution of dynamic pressure gradient on the bodies of revolution similar to dolphin's body, normalized by the value of dynamic pressure $\rho U^2/2$. The body of revolution is considered to be in the water flow, whose velocity is equal to dolphin's velocity.

Fig. 7.4 shows the aggregate distribution of the dynamic pressure gradient on the lateral side of dolphin's body caused by the body shape and by oscillatory motion of the animal. It is true for the swimming modes, whose parameters are shown at the top and bottom lines of table 7.2. According to Yanov (Yanov, 1997) the first approximation of the amplitude function of accelerated motion is

$$\frac{h(x,t)}{h_t} = 0.27 - 0.58\frac{x}{l} + \left(\frac{x}{l}\right)^2 + 0.31\left(\frac{x}{l}\right)^8. \qquad (7.3)$$

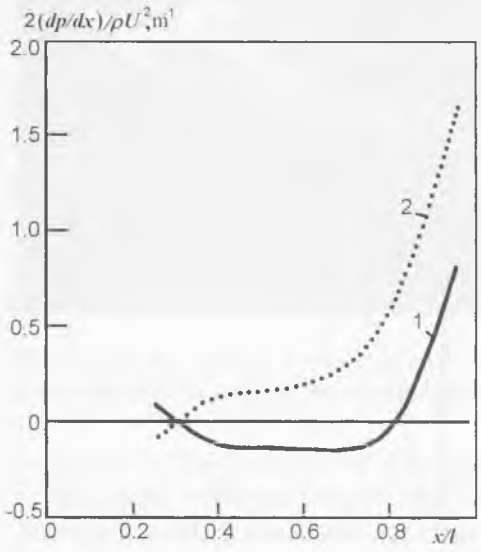

Fig. 7.2. Minimal (1) and maximal (2) values of dynamic pressure gradient on the dorsal side of the dolphin's body ($\theta_0 = 0$).

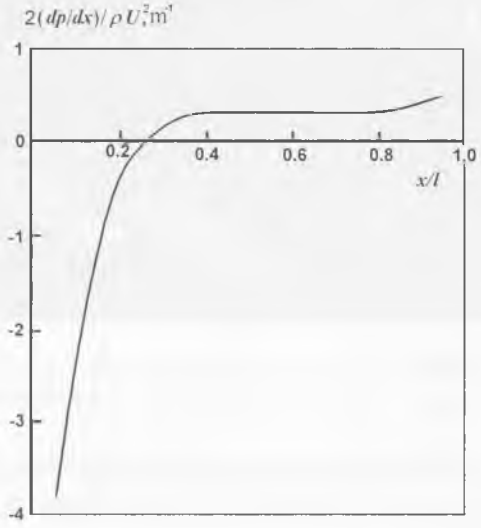

Fig. 7.3. Distribution of dynamic pressure gradient on the bodies of revolution similar to dolphin's body.

Analogous aggregate distribution of the dynamic pressure gradient on the dorsal side of dolphin's body is shown in fig. 7.5.

Let us compare the results of calculation and the above mentioned experimental data. To this effect let us overlay fig. 7.4 and 6.27 from chapter 6. The result is shown in fig. 7.6. We can see that the experimental data fairly correspond to the calculations. It is clear that the accelerated motion forms greater pressure gradient. The character of the calculated curves in fig. 7.6 leads to some important conclusions. The negative gradient of dynamic pressure reaches significant values at the head and at the tail of the animal body while at the middle part of the body it is comparatively small. It means that favorable influence of the negative gradient of pressure on the boundary layer must be notable mostly at the head and tail parts of the body. In this case the turbulization of boundary layer can start from the middle part of the body, where the pressure gradient is near zero. However in case of the flow around rigid bodies the turbulization arises on the rear part of the body. The situation, when the flow at the middle part is turbulent and the flow at the head and tail is laminar (or almost laminar), is possible. This can take place when the constant velocity swimming alters to greatly accelerated movement. There are some experimental facts, which prove the possibility of this situation.

1. The observations and sketches made by W. E. Evans and L. A. McKinley from a catamaran with an underwater cell. They saw the group of Pacific dolphins, swimming in phosphorescent water. These observations and sketches are described in the book of Wood (1979). Fig.7.7 shows these sketches. The light areas on the dolphin body correspond to turbulized boundary layer. We can see that turbulization covers the middle part of the

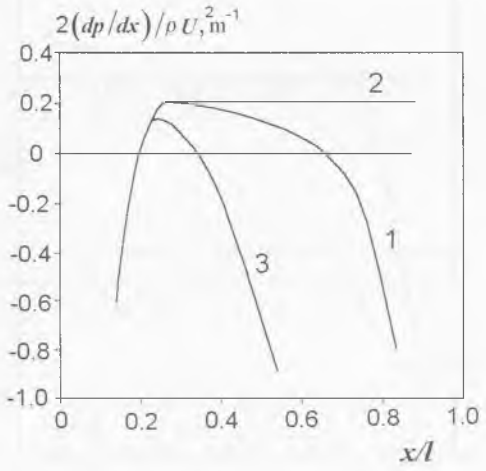

Fig. 7.4. Aggregate distribution of the dynamic pressure gradient on the lateral side of dolphin's body caused by the body shape and by oscillatory motion of the animal.

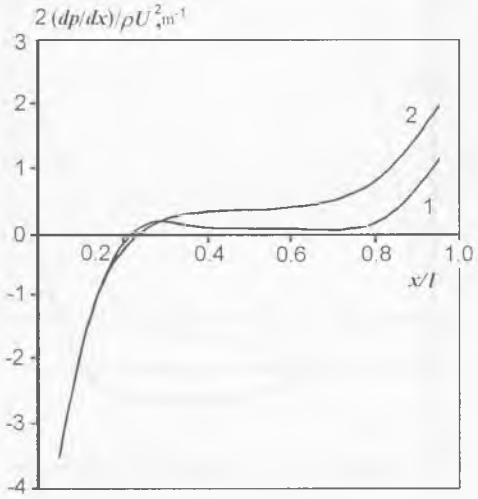

Fig. 7.5. Aggregate distribution of the dynamic pressure gradient on the dorsal side of dolphin's body.

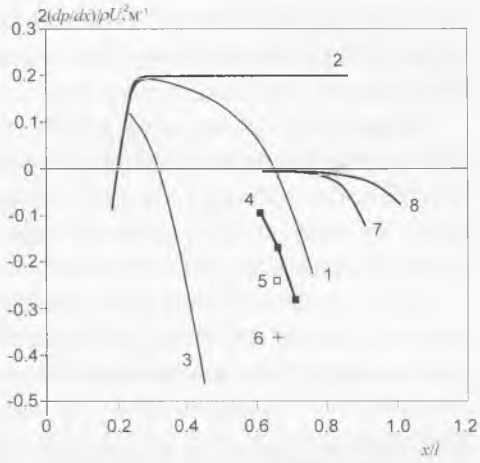

Fig. 7.6. Comparison of the results of calculation and the experimental data: 1 – 3 - the results of calculation, 4 – 6 experimental data. 7, 8 - dynamic pressure caused by the tail fin oscillation.

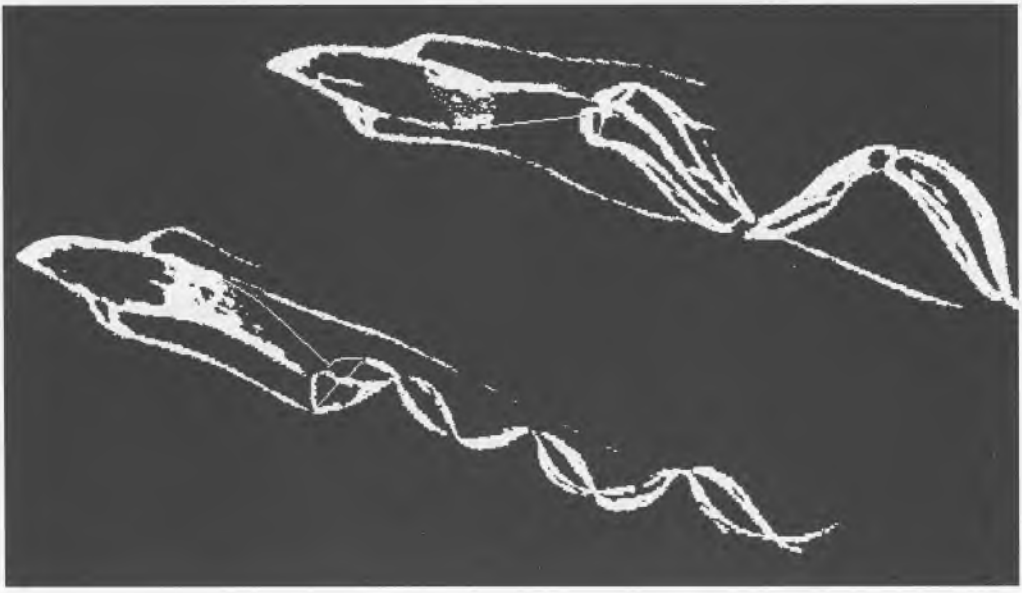

Fig. 7.7. Sketch made by W. E. Evans and L. A. McKinley from a catamaran with an underwater cell. It shows the group of Pacific dolphins, swimming in phosphorescent water. (Redrawn from Wood, 1979).

body, and on the fore part and tail stem we can see some dark areas, which correspond to laminar flow. We can see there that the upper and lower parts of the body are distinctly phosphorescent. It means that there are the narrow areas of turbulization on the ventral and dorsal sides of the animals. This fact also suits the above-cited calculations.

2. The results of shearing stresses measuring at the body points $0.4l$ and $0.78l$ (see ch. 6) show that the local resistance coefficient at the first point is 4.7 times greater than

the one at the second point. There can be only one explanation of this fact: the level of boundary layer turbulization at the second point is less than the one at the first point. It fits the above-cited results very well.

Earlier (in ch. 3) we adduced the experimental data on measuring of the dynamic pressure distribution on a fish body while active swimming (Dubois et al., 1974). These data prove that although in dolphin the negative gradient of pressure arises on the lateral side of the body, in fish it arises on dorsal side. It is caused by the difference between the planes of undulation, which is horizontal in fish and vertical in dolphin.

In ch. 3 we also discussed the possibility of the opposite transformation of a turbulent flow to a laminar one when the values of the negative gradient of dynamic pressure are great enough. This transformation is possible when the values of the form parameter $B=-(2\div3)\cdot10^{-6}$. Estimates show that opposite transformation is possible on the dolphin body interval $0.7 < x/l < 1$ while active swimming mode, which corresponds to the second line of table 7.2.

7.1.2. Dynamic pressure caused by the fluke oscillation

In 1936 James Gray, who was an English zoologist, hazarded a conjecture that high energy efficiency of cetacean swimming, and of dolphin swimming in particular, is determinated mainly by the stabilization of the laminar flow during active motion. He said that the existence of the negative gradient of dynamic pressure along the body of the animal, while it swims actively increases the Reynolds number of the transformation of a laminar flow into a turbulent one. This gradient is caused by the suction effect of the tail fin. The following studies of the hydrodynamic features of dolphin and fish motion (Romanenko, 1980a, 1981, 1986a, 1994) show that there are two reasons for the negative pressure gradients formation. In addition to the suction effect of the propulsive part, there is a redistribution of pressure caused by the undulating body movement when the amplitude and phase velocity of propulsive wave increase from head to tail fin. At the same time it isn't completely clear till now how the tail fin effects flow formation.

In ch. 3 we discussed the mathematical models of two possible mechanisms of the dynamic pressure gradient formation on dolphin body caused by the fluke oscillation. The first one is caused by the vortex wake following the fluke edge, and the second one is caused by the additive field of velocities, induced by the oscillating palm treated as a dipole (Pushkov, Romanenko, 2001).

We use the expressions from ch. 3 to obtain the numerical estimates with the kinematics parameters that were measured in the experiments on dolphin. The first mechanism gives us the expressions of induced velocity component along the horizontal axis. One of these expressions gives the value of the component at the moment when the wing , which is the tail fluke, passes through the axis $0X$, and the other gives the value at the moment when the bias from the axis $0X$ is maximal. The first expression looks like

$$V_{ix}=\frac{\Gamma l_0}{4\pi\left[(x\sin\varphi)^2+\frac{l_0^2}{4}\right]}\left(\frac{a+x\cos\varphi}{\sqrt{(x+a\cos\varphi)^2+h^2+\frac{l_0^2}{4}}}-\frac{x\cos\varphi}{\sqrt{x^2+\frac{l_0^2}{4}}}\right)\sin\varphi+$$

$$+\frac{\Gamma l_0}{4\pi\left[\left(x+\frac{UT}{2}\right)^2\sin^2\varphi+\frac{l_0^2}{4}\right]}\left[\frac{\left(x+\frac{UT}{2}\right)\cos\varphi}{\sqrt{\left(x+\frac{UT}{2}\right)^2+\frac{l_0^2}{4}}}-\frac{\left(x+\frac{UT}{2}\right)\cos\varphi-a}{\sqrt{\left(x+\frac{UT}{4}\right)^2+h^2+\frac{l_0^2}{4}}}\right]\sin\varphi+ \tag{7.4}$$

$$+\frac{\Gamma l_0 h}{2\pi\left[\left(x+\frac{UT}{4}\right)^2+h^2\right]\sqrt{\left(x+\frac{UT}{4}\right)^2+h^2+\frac{l_0^2}{4}}},$$

the second one looks like

$$V_{ix}=\frac{\Gamma l_0\sin\varphi}{4\pi\left[\left(x+\frac{UT}{4}\right)^2\sin^2\varphi+\frac{l_0^2}{4}\right]}\left[\frac{a+\left(x+\frac{UT}{4}\right)\cos\varphi}{\sqrt{\left(x+\frac{UT}{2}\right)^2+h^2+\frac{l_0^2}{4}}}-\frac{\left(x+\frac{UT}{4}\right)\cos\varphi-a}{\sqrt{x^2+h^2+\frac{l_0^2}{4}}}\right]+$$

$$+\frac{\Gamma l_0 h}{4\pi\left(x^2+h^2\right)\sqrt{x^2+h^2+\frac{l_0^2}{4}}}+\frac{\Gamma l_0 h}{4\pi\left[\left(x+\frac{UT}{2}\right)^2+h^2\right]\sqrt{\left(x+\frac{UT}{2}\right)^2+h^2+\frac{l_0^2}{4}}}, \tag{7.5}$$

These expressions of V_{ix} define the value of the dynamic pressure gradient $\partial p/\partial x$:

$$\frac{\partial p}{\partial x}\approx\rho U\frac{\partial V_{ix}}{\partial x}. \tag{7.6}$$

It is easy to obtain the expressions for the induced velocity gradients by means of differentiation of the expressions (7.4) and (7.5) with respect to x-coordinate. In the first case we get

$$\frac{\partial V_{iX}}{\partial x}=\frac{\Gamma l_0}{2\pi}\left\{-\frac{x\sin^3\varphi}{\left[(x\sin\varphi)^2+\frac{l_0^2}{4}\right]^2}\left(\frac{a+x\cos\varphi}{\sqrt{(x+a\cos\varphi)^2+h^2+\frac{l_0^2}{4}}}-\frac{x\cos\varphi}{\sqrt{x^2+\frac{l_0^2}{4}}}\right)+\right.$$

$$+\frac{\sin\varphi}{2\left[(x\sin\varphi)^2+\frac{l_0^2}{4}\right]}\left(\frac{\left(h^2+\frac{l_0^2}{4}-a^2\sin^2\varphi\right)\cos\varphi-ax\sin^2\varphi}{\left[(x+a\cos\varphi)^2+h^2+\frac{l_0^2}{4}\right]\sqrt{(x+a\cos\varphi)^2+h^2+\frac{l_0^2}{4}}}-\right.$$

$$\left.\left.-\frac{\frac{l_0^2}{4}\cos\varphi}{\left(x^2+\frac{l_0^2}{4}\right)\sqrt{x^2+\frac{l_0^2}{4}}}\right)-\right.$$

$$-\frac{\left(x+\frac{UT}{2}\right)\sin^3\varphi}{\left[\left(x+\frac{UT}{2}\right)^2\sin^2\varphi+\frac{l_0^2}{4}\right]^2}\left(\frac{\left(x+\frac{UT}{2}\right)\cos\varphi}{\sqrt{\left(x+\frac{UT}{2}\right)^2+\frac{l_0^2}{4}}}-\frac{\left(x+\frac{UT}{2}\right)\cos\varphi-a}{\sqrt{\left(x+\frac{UT}{4}\right)^2+h^2+\frac{l_0^2}{4}}}\right)+$$

$$+\frac{\sin\varphi}{2\left[\left(x+\frac{UT}{2}\right)^2\sin^2\varphi+\frac{l_0^2}{4}\right]}\left(\frac{\frac{l_0^2}{4}\cos\varphi}{\left[\left(x+\frac{UT}{2}\right)^2+\frac{l_0^2}{4}\right]\sqrt{\left(x+\frac{UT}{2}\right)^2+\frac{l_0^2}{4}}}-\right.$$

$$\left.-\frac{\left[h^2+\frac{l_0^2}{4}-\left(\frac{UT}{4}\right)^2-\frac{UTx}{4}\right]\cos\varphi+a\left(x+\frac{UT}{4}\right)}{\left[\left(x+\frac{UT}{4}\right)^2+h^2+\frac{l_0^2}{4}\right]\sqrt{\left(x+\frac{UT}{4}\right)^2+h^2+\frac{l_0^2}{4}}}\right)-$$

$$\left.-\frac{h\left(x+\frac{UT}{4}\right)}{\left[\left(x+\frac{UT}{4}\right)^2+h^2\right]\sqrt{\left(x+\frac{UT}{4}\right)^2+h^2+\frac{l_0^2}{4}}}\left(\frac{2}{\left(x+\frac{UT}{4}\right)^2+h^2}+\right.\right.$$

$$\left.\left.+\frac{1}{\left(x+\frac{UT}{4}\right)^2+h^2+\frac{l_0^2}{4}}\right)\right\} \qquad (7.7)$$

and in the second case we get

$$\frac{\partial V_{iX}}{\partial x}=\frac{\Gamma l_0}{2\pi}\left\{-\frac{\left(x+\frac{UT}{4}\right)\sin^3\varphi}{\left[\left(x+\frac{UT}{4}\right)^2\sin^2\varphi+\frac{l_0^2}{4}\right]^2}\left(\frac{a+\left(x+\frac{UT}{4}\right)\cos\varphi}{\sqrt{\left(x+\frac{UT}{2}\right)^2+h^2+\frac{l_0^2}{4}}}-\frac{\left(x+\frac{UT}{4}\right)\cos\varphi-a}{\sqrt{x^2+h^2+\frac{l_0^2}{4}}}\right)+\right.$$

$$+\frac{\sin\varphi}{2\left[\left(x+\frac{UT}{4}\right)^2\sin^2\varphi+\frac{l_0^2}{4}\right]}\left(\frac{\left(h^2+\frac{l_0^2}{4}\right)\cos\varphi+\left(\frac{UT}{4}\cos\varphi-a\right)\left(x+\frac{UT}{2}\right)}{\left[\left(x+\frac{UT}{2}\right)^2+h^2+\frac{l_0^2}{4}\right]\sqrt{\left(x+\frac{UT}{2}\right)^2+h^2+\frac{l_0^2}{4}}}-\right.$$

$$\left.-\frac{\left(h^2+\frac{l_0^2}{4}-\frac{UTx}{4}\right)\cos\varphi+ax}{\left(x^2+h^2+\frac{l_0^2}{4}\right)\sqrt{x^2+h^2+\frac{l_0^2}{4}}}\right)-$$

$$-\frac{hx}{2\left(x^2+h^2\right)\sqrt{x^2+h^2+\frac{l_0^2}{4}}}\left(\frac{2}{x^2+h^2}+\frac{1}{\left(x^2+h^2+\frac{l_0^2}{4}\right)}\right)-$$

$$\left.-\frac{h\left(x+\frac{UT}{2}\right)}{2\left[\left(x+\frac{UT}{2}\right)^2+h^2\right]\sqrt{\left(x+\frac{UT}{2}\right)^2+h^2+\frac{l_0^2}{4}}}\left(\frac{2}{\left(x+\frac{UT}{2}\right)^2+h^2}+\right.\right.$$

$$\left.\left.+\frac{1}{\left(x+\frac{UT}{2}\right)^2+h^2+\frac{l_0^2}{4}}\right)\right\} \tag{7.8}$$

Using the expressions (7.7) and (7.8) we can evaluate with formula (7.6) the dynamic pressure gradients, caused by vortex lines along dolphin body. The necessary kinematics and morphometric parameters of dolphin (*Tursiops truncatus*) fluke are cited in chapter 6 and in table 7.3. In table 7.4 there are given some values necessary to evaluate the pressure gradients which were calculated with corresponding expressions from chapter 3. Fig. 7.8 shows the values of the dynamic pressure gradients (1 and 2). These values are calculated with formula (7.6) and depend on the distance between the wing center and the position of observation point on the horizontal axis. We can see that the gradient

l, m	R, m	h_f/l	S_f, m^2	U, ms^{-1}	T, s	α, rad	C_v^{α}
2.24	0.5	0.12	0.063	4.3	0.45	0.058	3.17

Table 7.3. Kinematic and morphometric parameters of a dolphin *Tursiops truncatus*. For explanations of variables, see text.

Γ	l_0, m	a, m	φ, rad
0.088	0.39	0.55	0.51

Table 7.4. Additional parameters. For explanations of variables, see text.

values are of the same magnitude, but the first dependence is monotonic and the second dependence has an extremum. In both cases the part caused by the vortex wisp, which adjoin to the bearing line *AB* (see fig. 3.3 in ch. 3), obtain maximum (about 80%) at the point near the wing center. The farther point of observation from the wing center, the nearer parts caused by the all vortex wisps. They become of the same magnitude already at the distance of 1m from the wing center.

Now let us use the formulas, which we obtained on the base of the second mechanism model, handling the tail fin as an acoustic dipole (see ch. 3). There was obtained the formula for estimation of dynamic pressure gradient instantaneous value:

$$\frac{2}{\rho U^2}\frac{dp}{dr} = -\frac{6\alpha S_f^{1.5}}{r^4\pi^{1.5}}\sqrt{1+\frac{\omega^2 h_0^2}{U^2}\cos^2\omega t}\cos\theta_{fl}. \qquad (7.9)$$

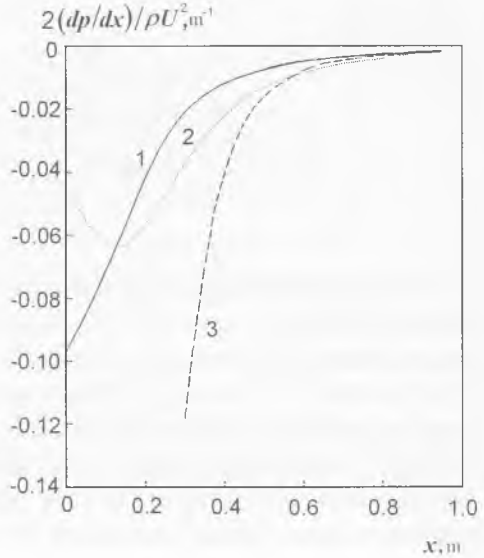

Fig. 7.8. Distribution of dynamic pressure gradient on a posterior part of the dolphin's body. The designations are in the text.

Let's evaluate the dynamic pressure gradient value, which arises along the horizontal axis due to dolphin's fluke. For this purpose let us use the kinematics and morphological parameters of the dolphin's fluke from table 7.3 and the data from ch. 6, from which we derive that the angle ϑ_1 between the fluke and the horizontal axis is near 45°. We shall estimate the maximal instantaneous negative value of the dynamic pressure gradient which corresponds to the moment when $\cos\omega t = 1$. In this case formula (7.9) is rather simplified.

$$\frac{2}{\rho U^2}\frac{dp}{dr} = \frac{3\alpha S_t^{1.5}}{r^4\pi^{1.5}}\sqrt{2\left(1+\frac{\omega^2 h_0^2}{U^2}\right)}. \qquad (7.10)$$

Swimming characteristics, which are used for calculations, are cited in table 7.3.

The dynamic pressure gradient instantaneous values 3, which are calculated according to formula (7.10), are shown in fig. 7.8. It is conspicuous that near the dolphin fluke the results of calculations, according to formulas (7.6) and (7.10) differ from each other. But in the distance of a few tens centimeters from the dolphin fluke the results of calculation practically coincide.

Let us compare the obtained estimates of dynamic pressure gradients along the dolphin body caused by the oscillating movement of the fluke with the estimates of the gradients caused by the body of dolphin and with the experimentally measured values, cited in the previous section of this chapter. Curves 7 and 8 of fig. 7.6 show the values of dynamic pressure gradients caused by the two mechanisms mentioned above. Curve 7, which corresponds to the fist of the considered mechanisms, shows results, obtained for the case when the dolphin fluke crosses the horizontal axis. The case of the maximal deviation of fluke from the horizontal axis is not shown in the figure because the estimates in both cases are of the same magnitude. We can see that the pressure gradients near the middle part of body and near tail stem caused by the tail movements are negligible with respect to the gradients caused by the dolphin body. The pressure gradient becomes observable only near fluke. Perhaps, the approach flow around the fluke is defined by the locally formed dynamic pressure gradient.

So, the Gray's hypothesis of the decisive influence of the sucking action of the fluke on features of the flow around dolphin body does not agree with the facts. This hypothesis seems to be true only with respect to the flow about the fluke.

7.2. Thrust, hydrodynamic drag and coefficient of efficiency

The hydrodynamics of dolphin has been an object of the scientists' attention for many years. The main point is whether dolphin has mechanisms to decrease the drag while swimming when Reynolds numbers (*Re*) are greater than the critical one. J. Gray assumed (1936) that there is such a mechanism, connected with the formation of the favorable (negative) dynamic pressure gradient on the dolphin body while active swimming. Several more hypotheses were proposed later: it was supposed that the dermal integument causes some damping action (Kramer, 1960; Babenko, 1972), and that dermal and ocular discharge decreases the drag (Uskova and others, 1975).

Also there are the researchers, who think that there are not any mechanisms of decreasing active swimming friction drag. They think that a dolphin has a sufficient power to maintain real swimming velocity. This conclusion was usually based on the estimates of thrust and drag coefficient with the wing theories (both stationary and non-stationary) and the measured kinematical parameters of animal swimming (Webb, 1975; Yates, 1983; Fish and Hui, 1991; Fish, 1993). Fig. 7.9 from the work of Fish, 1993, shows that the greater part of the obtained values of the drag estimates exceed greatly the

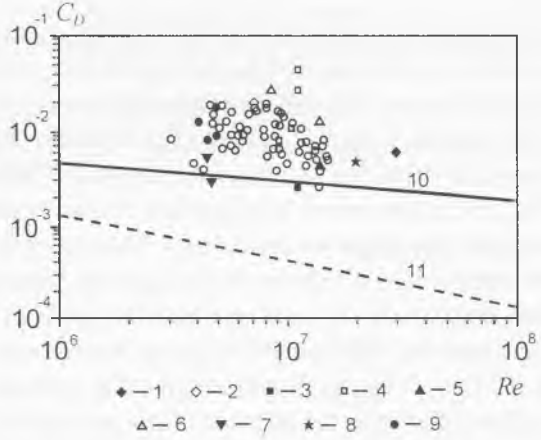

Fig. 7.9. Comparison of cetacean drag coefficients estimated from hydromechanical models based on kinematics and rigid bodies. Drag coefficients are plotted against Reynolds number, *Re*. Open circles represent depth-corrected drag coefficients for *Tursiops truncatus* from Fish (1993). Other symbols represent *Delphinus delphis* (1 and 2), *Lagenorhynchus obliquidens* (3 and 4), *Phocoena phocoena* (5), *Phocoenoides dalli* (6), *Sotalia fluviatilis* (7), *Stenella attenuata* (8) and *Tursiops truncatus* (9). Open symbols represent values of drag coefficient estimated using hydromechanical models based on swimming kinematics; filled symbols represent values obtained from gliding or towing experiments. Data are from Lang and Daybell (1963), Lang and Pryor (1966), Purves et al. (1975), Webb (1975), Aleyev (1977), Chopra and Kambe (1977), Yates (1983) and Videler and Kamermans (1983). The solid line (10) represents the minimum drag coefficient assuming turbulent boundary conditions; the broken line (11) is for minimum drag coefficient assuming laminar conditions. (Based on data by Fish, 1993, with permission).

values of drag of laminar flow 11, and even the values of drag of turbulent flow 10. However, we ought to note there are two reasons why this estimation can not be a foundation for the final conclusions. The first is that this estimation method is indirect, and the second is that this estimation method uses many roughly measured parameters. It means that the resultant error can be heavy and lead to unpredictable results. Further we will give an example of it. Only direct measuring of the boundary layer parameters (the level of velocity or pressure pulsation, tangential stresses, the distribution of hydrodynamic pressure along the body of dolphin) can be acceptable (see ch. 6). Only direct measures permit to estimate the hydrodynamic features of dolphin (such as the thrust and resistance coefficient) correctly. But even indirect estimation of the thrust generated by dolphin, implemented under the correct accounting of all assumptions, can lead to the conclusions, which are opposite to those in the cited works. To illustrate this, let us analyze the works of Webb, 1975; Yates, 1983 and Fish, 1993.

7.2.1. The thrust

Webb (1975) evaluated the thrust coefficient (C_T) of an active swimming dolphin on the base of the small amplitude stationary theory of wing (Parry, 1949) and of the two-dimensional non-stationary theory of wing (Lighthill, 1969, 1970). Fish (1993) and Yates (1983) evaluated the coefficients of thrust and drag on the base of the non-stationary three-dimensional theory of the half-moon wing (whose aspect ratio is equal to 8), which performs small oscillations (Chopra and Kambe, 1977). The estimates of the thrust power of the three dolphin species are shown in table 7.5. These estimates are cited in the work of Webb (1983). They are based on the stationary low-amplitude theory of wing (Parry, 1949).

We can see that calculated power of the three dolphin species, presented by the figures of the last column without brackets, exceed the theoretical values correspondingly 6.3, 9.4, and 16 times. The theoretical values of the thrust power are calculated with formula

Species	L	U	n	EU	S_B	$(EU)_T$	$EU/(EU)_T$
	(cm)	(cm/s)	(s^{-1})	(erg/s)	(cm^2)	(erg/s)	
Delphinus							
bairdi	170	430	1.8	$8.96(0.3).10^9$	11560	$1.42.10^9$	6.3(0.21)
Phocoenoides							
dalli	200	430	2.1	$18.0(1.1).10^9$	16000	$1.91.10^9$	9.4(0.57)
Lagenorhinchus							
obliqidens	204	554(518)	3.9(2.8)	$61.8(1.8).10^9$	16646	$3.96(3.0).10^9$	16(0.45)

Table 7.5. Calculations of swimming power output of three cetaceans from the quasi-static proposed by Parry (1949), and a comparison with theoretical frictional drag power (without brackets). (Based on data by Webb, 1975). For explanations of variables, see text.

$$EU = C_{fl}\frac{\rho S_B U^3}{2}. \tag{7.11}$$

Here U is the speed of dolphin swimming, S_B is the wet surface of the body, ρ is water density, C_{fl} is theoretical turbulent friction coefficient, E is thrust. Calculations of the thrust power were fulfilled with the thrust formula from the work of Parry, 1949, multiplied by the velocity U,

$$EU = 0.0175L^2U^3\left[\frac{0.38Ln}{U} - 0.047\right]. \tag{7.12}$$

As analysis shows, that the values of the coefficients of this expression are defined with significant errors. To demonstrate it, let us represent this formula in general terms, without evaluations of the coefficients.

$$EU = \frac{1}{2}\rho A_f U^3\left(C'_\alpha \alpha_1 \pi a \nu - \frac{1}{2}C'^2_\alpha \alpha_1^2 \frac{1}{\pi\Lambda} - C_{\omega p}\right). \tag{7.13}$$

All denotations, which we use here (with the exception of U) are from the work of Parry, 1949: $C'_\alpha = 2\pi\Lambda/(2+\Lambda)$, $\nu = ns/U$; $C_{\omega p}$=0.023; n is the frequency of body oscillation; $s = 0.13L$ – is the half-width of the fluke; Λ is aspect ratio, a is the fluke oscillation amplitude represented via the half-width of the fluke s, α_1 is the maximal value of attack angle, α is its current value.

Let us write the part of formula (7.12), which stands before the brackets, separately:

$$0.0175L^2U^3 = \rho A_f U^3/2. \tag{7.14}$$

Here $A_f = 0.034L^2$ is the summary two-sided wetted surface of the dolphin's fluke. However, the thrust is formed by only one side of the fluke. Therefore we have to use the half-value of A_f. This error made the result two times higher than it actually was. The incorrect evaluation of tail fluke square causes the wrong evaluation of its aspect ratio, which in its turn leads to the wrong value of coefficient C_α'

We can write initial expression for the first term of formula (7.12) inside the brackets as

$$\frac{0.38Ln}{U} = C'_\alpha \alpha_1 \pi a \nu. \tag{7.15}$$

Parry (1949), who had no experimental data, used an arbitrary chosen amplitude of the fluke oscillation as=0.221L and angle of attack $\alpha_1 = 10^\circ$. Now these cinematic parameters of dolphin are well studied experimentally and published (at least for the

Tursiops truncatus). So fluke oscillation amplitude can be represented as $h = (0.1 \pm 0.03)L$ (Fish, 1993). Here L is the length of the dolphin body. We can see that Parry used the amplitude, which was on average twofold larger than the real one. On the base of the experimental data (Romanenko 19860 and also ch. 6 of this book) we can suppose that the angle of attack of the dolphin fluke is 3.3° at most. So, having taken wrong values of the oscillation amplitude and angle of attack of the dolphin fluke, Parry overestimated the value of formula (7.12) sixfold.

Assuming that the wing is absolutely rigid we inevitably overestimate the value of the trust. In fact, the fluke of dolphin and especially its rear edge has some flexibility. The works by Katz and Weihs, 1979 and by Bose and Lien, 1989 showed that this flexibility decreased thrust by around 20%.

Two more adjustments. The tail stem of dolphin prevents formation of the suction force on some part of the leading edge of the fluke. The shape of a fluke differs from the rectangular form of the theoretical wing (Chopra and Kambe, 1977). These circumstances lead to the decrease of the thrust by 10% and 12% accordingly.

At all, Parry should not have used the uninvestigated kinematical parameters in the numerical coefficients to simplify the original formula of the wing theory. It will be more correct to use this formula in the most general appearance (7.13) without the numerical coefficients.

We have to note that the parameters of swimming speed and frequency of the tail oscillations in *Lagenorhynhus obliquidens* , which Yates used in his work (U = 5.18 ms^{-1}, n = 2.8 Hz) are taken from the work (Lang and Daybell, 1963) and differ from those cited in the work (Webb, 1975). We also used these values in our estimates (see table 7.5).

In addition to the parameters adduced in table 7.5, some adjusted parameters, needed for calculations on formula 7.13, are shown in table 7.6. Parameter C_α was estimated with formula $C_\alpha^{'} = \dfrac{2\pi}{\sqrt{\Lambda^2 + 4} + 2}$ (Kozlov, 1979), which is more exact than the one used by Parry (1949). Wing aspect ratio was estimated with $\Lambda = \dfrac{(2s)^2}{S_f}$. Here $s = 0.13L$ and $S_f = A/2 = 0.0178L^2$. Values of the form resistance coefficients C_p (this is Parry's C_{vp})

Species	Λ	$C_\alpha^{'}$	α, rad	*as/L*	C_p	$E_{correct}$, N	C_f
Delphinus bairdi	4	3.88	0.058	0.12	0.02	10.8	0.00066
Phocoenoides dalli	4.6	4.12	0.058	0.12	0.019	26.6	0.00146
Lagenorhynchus							
obliquidens	5.4	4.37	0.058	0.12	0.018	34.0	0.00131

Table 7.6. Some adjusted parameters and calculated thrust and frictional drag coefficient of three cetaceans. For explanations of variables, see text.

are taken from the work of Barstow (1939). The seventh column of this table shows the values of thrust, which had been calculated with formula (7.13) taking into account all adjustments. The results of calculations with this formula are adduced in brackets in the fifth column of table 7.5. In brackets in the last column there are relations between assessed and theoretical values of thrust. We can see that on accounting all the inaccuracies and assumptions, which had been made during derivation of the formula, the assessed values became notably less than the theoretical ones.

We must say some words about the original formula (7.13), which was used by Parry (1949) as a foundation. We have already noted before that it corresponds to the solution of low-amplitude stationary three-dimensioned theory of wing with presumption of harmonic function of attack angle. Comprehensive study of the fluke kinematics, described in ch. 6, shows that function of attack angle is not a harmonic function, unlike the angle between the fluke and horizontal axis which is harmonic. This fact lets us assume that the estimates with formula 7.13 can be incorrect. This means that the assessments from the fifth column of table 7.5, which take into account the main detected errors, are not completely reliable despite of all adjustments.

Webb (1975) also adduces estimate of the thrust coefficient on the base of two-dimensioned nonstationary theory of wing (Lighthill . 1969, 1970). His estimates are adduced in the second line of table 7.7. There are also some additional parameters of dolphin swimming, which are absent in table 7.5. The value of thrust coefficient is 1.5 and this is remarkable. This value is obtained from the plot, which is adduced in figure 9 in the work of Lighthill, 1969 by using calculated values of feathering parameter $\theta = 0.21$ and effective frequency $\sigma = 0.4$ (these values are shown in the second line of table 7.7). But we have to remember that in this plot the vertical axis relates to the thrust coefficient C_T, which is defined by the expression $C_T = \frac{\overline{P}}{\omega^2 h^2 a}$. Here $\overline{P}$ is the thrust, h is the amplitude of oscillation, a is the half-chord of the wing. Using some simple transformations we can come to the conventional expression for the thrust coefficient $\left(C_{T0} = \frac{2\overline{P}}{\rho S_B U^2} \right)$,

variant	A (cm)	α rad	θ	σ	C_T	S_t (cm^2)	EU $ergs^{-1}$	$\frac{EU}{(EU)_T}$	C_f
Data from Webb (1975)	60	0.28	0.21	0.40	1.5	466	$4.03.10^{10}$	10.2	
Data based on Lighthill (1969)	50	0.66	0.91	0.66	0.13	466	$0.32.10^{10}$	0.82	0.0019
Data based on Chopra, Kambe (1977)	50	0.66	0.91	0.66	0.08	466	$0.35.10^{10}$	0.87	0.0024

Table 7.7. Swimming parameters of *Lagenorhinchus obliquidens* (Based on data by Webb, 1975).

which is equal $C_{T0} = C_T\left(\frac{\omega^2 c^2}{U^2}\right)\left(\frac{h^2}{c^2}\right)$. Here $c=2a$ is the chord of the wing. If we take into account this circumstance, then the thrust coefficient is only 0.4 even with the above mentioned values of θ and σ. Also this value is highly overstated because the feathering parameter is defined incorrectly. To obtain this value, we have to use formula

$$\theta = \frac{U\alpha}{\omega h}, \tag{7.16}$$

which was proposed in the work by Lighthill, 1970. Here U is the speed of dolphin swimming, α is the angle between the fluke and horizontal axis, h is the amplitude of oscillation, $\omega = 2\pi f$, f is the frequency of tail oscillation. Chopra and Kambe elaborated this formula in their work of 1977 to the following appearance

$$\theta = \frac{Utg\alpha}{\omega h}. \tag{7.17}$$

Yates (1983) informs that there are no data on the angle between fluke and horizontal axis in the work of Lang and Daybell (1963) (We are sorry to say that this work is inaccessible to us). At the same time Webb (1975) calls this slope "the angle of attack" and adduces its value (0.28 rad). As we are interested in the slope of the fluke to horizontal axis (not in an attack angle) we assume after Yates (1983) that its value equals 0.66 rad. Then the feathering parameter $\theta = \frac{Utg\alpha}{\omega h}$ is 0.91, not 0.21 as it is stated in the work by Webb (1975).

There is another ambiguity in the work by Webb (1975) concerning calculation of effective frequency $\sigma = \frac{\omega c}{U}$. The value of the chord, which is necessary for evaluation of effective frequency, is not given in the works by Webb (1975) and Yates (1983). Consequently we took it from the work of Wu, (1971). There the chord is equal to 19 cm. Besides, we can see from table 7.6 that the twofold amplitude of tail oscillation is 60 cm (Webb, 1975), but Wu (1971) and Yates (1983), referring to the same work as Webb (Lang and Daybell, 1963), adduced the value 50 cm. In our works we also suppose it to be 50 cm.

If we bear in mind the above mentioned remarks on dolphin swimming speed and its body oscillation frequency, we will assume the value of effective frequency $\sigma = \frac{\omega c}{U}$

equal to 0.65 instead of 0.40 as it is assumed in the work of Webb, 1975. Here c is the chord of the fluke.

Using the obtained values of effective frequency (0.65) and feathering parameter (0.91), we define the thrust coefficient with plots in fig. 9 (from the work of Lighthill, 1969) and fig. 6 (from the work of Chopra and Kambe, 1977). In case of two-dimensional theory it is equal 0.13, and in case of three-dimensional theory 0.08. We can see that the thrust coefficient assessment from the work of Webb is overstated 12-19 times in comparison with these values. The relation between the assessment and theoretical thrust power, which is adduced in the last column of table 7.7, shows that the estimated power is less than the theoretical one.

Yates (1983) as well as Webb (1975) estimated the thrust coefficient of *Lagenorhinchus obliquidens* dolphin on the base of the data on kinematics from the work of Lang and Daybell (1963) using conclusions of non-stationary three-dimensional theory of wing (Chopra and Kambe, 1977). Initial data do not differ very much from those adduced in the last rows of tables 7.5 (in brackets) and 7.6. The main mistake of Yates (1983) is that he used the angle of the slope of the fluke to horizontal axis while evaluating the feathering parameter, but actually he had to use the tangent of this angle. Table 7.7 contains the correct value of feathering parameter. With this value of feathering parameter, the plot in fig. 6 of Chopra and Kambe, 1977 and the value of effective frequency from table 7.6 we can easily obtain the thrust coefficient. It is $C_T = 0.08$ but not 0.23 as it was stated by Yates, 1983. Thus Yates (1983) introduced a wrong estimate, which is three times higher than the thrust capability of a dolphin.

The work of Fish (1993) compares favorably with the above-considered works. It contains its own experimental data. But there is a serious error. Evaluating the feathering parameter, the author used the angle of attack of fluke instead of the tangent of the angle of fin slope to horizontal axis. Furthermore, the measured values of angle of attack adduced in this work are unlikely high. As a result, estimates in the work of Fish (1993) are overvalued about five times.

Adjusted data give us an opportunity for the following conclusions:

1. The values of dolphin thrust power, obtained with the consideration of all the above listed errors, sufficiently match the theoretical ones. In some cases they are much less than the theoretical ones.

2. All these results are very rough and relative, because they are based upon some low amplitude theoretical models, which are not quite correct. In particular, all theoretical models, which were considered until now, proceeded from an assumption that the angle of attack of the wing is harmonic. In dolphin it is wrong (see chapter 6) because in dolphin the angle of the fin slope is harmonic and the angle of attack is not. In addition, some assumptions, which are difficult or impossible to evaluate numerically, were not taken into account. These are the ambiguity of the pivot of dolphin fluke, the shortage of accurate data on the depth of dolphin swimming in the experiments, curvature of fluke,

presumable character and significant spread in values of some parameters (angles of attack and slope of fluke to horizontal axis).

3. There is no information on error values of kinematic parameter measurements. This circumstance does not allow us to assess the validity of obtained results.

We ought to note, that there are theoretical models (Ahmadi, 1980; Lan, 1979), which differ from those used in the considered works. These models lead to rather different results.

We will estimate the thrust and drag coefficient of dolphin using the theoretical model considered in section 1.3.6 of ch. 1 and our own experimental data adduced in ch. 6. This model views dolphin fluke as a rigid wing going through linear and angular oscillation of high amplitude. Let's estimate the thrust of a triangular wing. We will adduce here the main estimation formulas.

The general expression on time averaging thrust is

$$\overline{T_c} = \frac{k\rho S}{2}\left\{C_y^{\alpha}\overline{v_{nc}V_{yc}} + \left[-\frac{x}{b}\left(C_y^{\alpha} - \frac{2m^*}{\rho Sb}\right) - C_y^{\dot{\omega}_z}\right]b^2\overline{\dot{\omega}_z \sin\theta_c} - \frac{\pi}{2}\overline{v_{nc}^2\cos\vartheta} - C_p\overline{U_c^2\cos\vartheta}\right\}. \quad (7.18)$$

All involved expressions (averaged) in (7.18) are in the form

$$\overline{v_{nc}V_{yc}} \cong \overline{v_n V_y} + \frac{\vartheta_1^2\omega^2x^2}{2}\left[1 - \frac{\vartheta_1^2}{8}\left(1 - \frac{\vartheta_1^2}{24}\right)\right], \quad (7.19)$$

$$b^2\overline{\dot{\omega}_z \sin\theta_c} \cong b^2\overline{\dot{\omega}_z \sin\theta} \cong -\frac{\vartheta_1^2U_0^2}{2}(Sh_0)^2, \quad (7.20)$$

$$\overline{v_{nc}^2\cos\vartheta} \cong \overline{v_n^2\cos\vartheta} + \frac{\vartheta_1^2\omega^2x^2}{2}\left[1 - \frac{\vartheta_1^2}{8}\left(1 - \frac{\vartheta_1^2}{24}\right)\right], \quad (7.21)$$

$$\overline{U_c^2\cos\vartheta} \cong \overline{U_i^2\cos\vartheta} + \frac{\vartheta_1^2\omega^2x^2}{2}\left[1 - \frac{\vartheta_1^2}{8}\left(1 - \frac{19}{48}\vartheta_1^2\right)\right], \quad (7.22)$$

where the first terms at the right part of formula (7.19 –7.22) are:

$$\overline{v_n V_y} \cong U_0^2 \frac{1}{\lambda_p}\left(\begin{array}{l}\frac{1}{2}\left(\frac{1}{\lambda_p}-\vartheta_1\right)-\frac{3}{8}\frac{\vartheta_1^2}{2!}\left(\frac{1}{\lambda_p}-\frac{1}{3}\vartheta_1\right)+\\ +\frac{5}{16}\frac{\vartheta_1^4}{4!}\left(\frac{1}{\lambda_p}-\frac{1}{5}\vartheta_1\right)\end{array}\right), \tag{7.23}$$

$$\overline{v_n^2 \cos\vartheta} \cong \frac{1}{2}U_0^2\left[\begin{array}{l}\left(\frac{1}{\lambda_p}-\vartheta_1\right)^2-\frac{9}{8}\vartheta_1^2\left(\frac{1}{\lambda_p^2}-\frac{14}{9}\frac{\vartheta_1}{\lambda_p}+\frac{5}{9}\vartheta_1^2\right)+\\ +\frac{15}{32}\vartheta_1^4\left(\frac{1}{\lambda_p^2}-\frac{10}{9}\frac{\vartheta_1}{\lambda_p}+\frac{7}{27}\vartheta_1^2\right)\end{array}\right], \tag{7.24}$$

$$\overline{U_i^2 \cos\vartheta} \cong U_0^2\left(1+\frac{1}{2\lambda_p^2}-\frac{3\vartheta_1^2}{16\lambda_p^2}-\frac{\vartheta_1^2}{4}\right). \tag{7.25}$$

The virtual mass of the triangular wing (Romanenko, 1986 and ch. 5)

$$m^* = \frac{\rho\pi b^2 l}{6}. \tag{7.26}$$

In the shown above expressions:

$$\theta = arctg\frac{V_y}{U_0}, \tag{7.27}$$

$$\frac{1}{\lambda_p} = \frac{h_t\omega}{U_0}, \tag{7.28}$$

$$Sh_0 = \frac{\omega b}{U_0}, \tag{7.29}$$

$$U_i^2 = U_0^2 + \left(\frac{dh}{dt}\right)^2, \tag{7.30}$$

$$h = h_t \sin \omega t, \tag{7.31}$$

U_0 is velocity of dolphin moving. C_y^{α}, $C_y^{\dot{\alpha}}$, $C_y^{\omega_z}$ are coefficients of hydrodynamic derivatives which are determined by Strouhal number $Sh = \frac{h_t b}{U_i}$ (see table 1.8), ρ is the water density. $\omega = 2\pi f$, f is the frequency of body oscillation, S_t is the surface area of one side of the fluke, b is the root chord of the fluke, l is the body length, ϑ_1 and θ_1 are the amplitudes of angle of fluke slope and its trajectory to horizontal axis. The factor k is added in formula (7.18) as compared with original formula from ch. 1. This coefficient considers some differentiation between the mathematical model and the real fluke of dolphin. It reflects the fact that the tail fin stem decreases thrust by approximately 15%. Besides, unlike the rigid wing, the fluke is flexible and this fact also decreases the thrust 20% approximately. Taking into account all these qualifications we assume $k = 0.68$. Expressions (7.23) and (7.24) let us obtain the following expression. Although it is evident it is very important.

$$\frac{1}{\lambda_p} = tg\theta_1. \tag{7.32}$$

During the calculations we used by average value

$$\left(\frac{1}{\lambda_p}\right)_{av} = \frac{1}{2}\left(\frac{\omega h_t}{U_0} + tg\theta_1\right). \tag{7.33}$$

We can with great fidelity consider the values of ρ, S_t, b, C_p known or measurable. We will use the speed U_0 as a parameter.

Errors of estimates obtained with these formula depend on errors of measuring of the angles ϑ_1, θ_1. and other kinematics parameters (h_t, ω).

We will use the results of angle measurements, adduced in ch. 6. These results are represented as a plot in fig. 7.10. There are two groups of the experimental points. Through these groups there have been drawn two regression lines. One of them shows

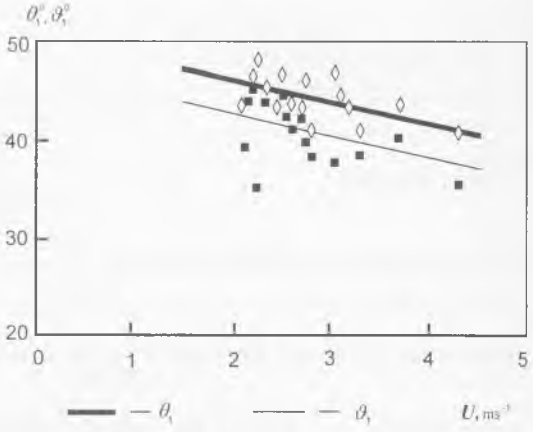

Fig. 7.10. Results of an experimental investigation into kinematics of the dolphin's fluke: the inclination of the fluke axis (ϑ_1) and the tangent of the fluke pathway (θ_1) to the horizontal.

the angle of fin slope, and the other shows the trajectory of its movement. The equation of trajectory slope angles line looks like

$$\theta_1 = (50.1 - 2.025U) \tag{7.34}$$

and the equation of the line of fin slope angles looks like

$$\vartheta_1 = (47 - 2.07U). \tag{7.35}$$

Considering that formula (7.34) and (7.35) were got during the experiments on dolphins, which average length of the body equal $l_{av} = 2.24$m, let's show them as a formula:

$$\theta_1 = 50.1 - 4.54\frac{U_0}{l}, \tag{7.36}$$

$$\vartheta_1 = 47 - 4.63\frac{U_0}{l}. \tag{7.37}$$

Using these equations we can easily calculate the values of the corresponding angles for a particular speed of swimming and also the values of attack angles. The results of calculations are represented in table 7.8 with one standard error.

U, ms^{-1}	ϑ_1, deg	θ_1, deg	α_1, deg
2.2	42.5 ± 0.7	45.6 ± 0.5	3.1 ± 1.2
4.3	38.1 ± 0.7	41.4 ± 0.5	3.3 ± 1.2

Table 7.8. Measured values of an inclination angle (ϑ_1), attack angle (α_1) of the dolphin's fluke and a trajectory slope angle (θ_1).

To calculate the trust with formula (7.18) – (7.29) it is necessary to know some kinematics and morphometric parameters of a dolphin. These parameters are shown in table 7.9. Water density is considered equal 1016 kgm^{-3} as it is in the Black Sea.

The second column of table 7.10 shows the obtained values of thrust.

Before analyzing these results, let us estimate the thrust on the base of the theoretical model from the work of Chopra and Kambe (1977). This model according to our opinion is the most advanced. The values of effective frequencies, which are necessary for estimating, are given in table 7.8. The sense of these values coincides with that of Strouhal number. The feathering parameter can be written (following Chopra (1976)) as

$$\Theta = \frac{tg\vartheta_1}{tg\theta_1}. \tag{7.38}$$

The results of calculation of the feathering parameter with formula (7.38) and the data from table 7.9 practically coincide, i.e. 0.9 and 0.89 for the swimming speeds 2.2 and 4.3 ms^{-1} correspondingly. If we know Strouhal numbers and the feathering parameters, we can graphically define thrust coefficients with plots in figure 6 from Chopra and Kambe (1977). But this procedure is sophisticated. We will gather all the data in the separate table, and trace the stages of the thrust coefficient evaluation step by step. The first column of table 7.11 shows the speeds to estimate. The second column shows the values of Strouhal numbers (effective frequencies), the third and the fourth show angles of slope of trajectory and fin. The fifth column shows values of feathering parameter. The sixth column contains the values of thrust coefficient, which are obtained from the plot B1 of fig. 6 of the mentioned work. Here the pivot is located at the distance 0.8 of the chord from the leading edge, the feathering parameter is 0.8 and efficient frequencies are adduced in the table. There is no line for the feathering parameter value of 0.9 in fig. 6. But there is an indication (Chopra, Kambe, 1977) that if feathering parameter equals

U, ms^{-1}	l, m	S_f, m^2	S_b, m^2	b, m	h/l,	f, Hz
2.2	2.24	0.063	2.226	0.19	0.112±0.004	1.1±0.11
4.3	2.24	0.063	2.226	0.19	0.112±0.004	2.22±0.11

Table 7.9. Kinematic, hydrodynamic and morphometric parameters of a dolphin. For explanations of variables, see text.

U,	T,	K	KT,	$K(T+2\sigma)$,	$K(T-2\sigma)$,	C_f	$C_f+2\sigma$	$C_f-2\sigma$
ms^{-1}	N		N	N	N			
2.2	9.0	1.1	9.9	27.3	0	0.00102	0.00363	0
4.3	57.0	1.25	71.3	143.1	0	0.00233	0.00515	0

Table 7.10. Estimation of the thrust and frictional drag coefficients for the dolphin. For explanations of variables, see text.

to 0.9 then thrust coefficient is twice less than the coefficient, which corresponds to parameter value of 0.8. The seventh column contains updated values of thrust coefficient for the feathering parameter values of 0.89 and 0.9. There is another important indication on dependence of the thrust on ratio of oscillation amplitude to chord of a wing in the mentioned work. The authors believe that thrust must be calculated with the formula

$$T = C_T \left(\frac{h_t}{c_0} \right)^2 \frac{\rho S_t U^2}{2} . \qquad (7.39)$$

However, it is shown in the work of Zaitsev and Fedotov (1986) that the dependence of thrust on the fin oscillation amplitude is not strictly quadratic. The exponent of relative amplitude in formula (7.33) has to be 1.33, when Strouhal number is 0.63, and 1.52 when Strouhal number is 0.7. The eighth column contains the values of thrust for the wing B1, which are given by formula (7.39) with accounting these exponents. The ninth column contains the values of thrust for the wing B2, where the pitch-axes location coincides with its rear edge. But we must consider the thrust, which was calculated like this, overstated, because the differences between the theoretical model and a dolphin fluke were not taken into account. These differences are: influence of the tail stem on suction force, flexibility of the fluke, the smaller aspect ratio of the fluke in comparison with the aspect ratio of the wing, the shape of the fluke, which is not rectangular.

If we take into account all these differences, we'll have to multiply the values of thrust from the eighth and ninth columns by factor 0.51. Updated values of thrust are adduced in the second and third columns of table 7.12.

U, ms^{-1}	Sh	θ_1, rad	ϑ_1, rad	$\Theta = \frac{tg\vartheta_1}{tg\theta_1}$	C_T at $\Theta = 0.8$	C_T at $\Theta = \frac{tg\vartheta_1}{tg\theta_1}$	T, N wing B1	T, N wing B2
2.2	0.7	45.6	42.5	0.9	0.17	0.085	22.3	25.4
4.3	0.63	41.4	38.1	0.89	0.14	0.077	72.3	86.4

Table 7.11. Estimation of the thrust on the base of the three – dimensional theory of wing (Based on data by Chopra and Kambe, 1977).

U, ms^{-1}	T, N		K	KT, N		C_f	
	wing B1	wing B2		wing B1	wing B2	wing B1	wing B2
2.2	11.4	12.9	1.1	12.5	14.2	0.00084	0.00115
4.3	36.9	44.1	1.25	46.1	55.1	0.00078	0.00122

Table 7.12. Estimation of the frictional drag coefficients on the base of the three – dimensional theory of wing (Based on data by Chopra and Kambe, 1977).

7.2.2. Distribution of thrust force and thrust along dolphin's body

When fish or dolphin actively swims, propulsive wave, which spreads along the animal body from its head to its tail, forms the thrust. In this case, as the theory of thin body concludes, conditions of the tail fin movements are the most essential for the thrust formation. However, this statement is correct only if there is no disruption of the vortex wake along the rest of the body. There are some experimental data and observations (Romanenko, 1986a), which show that the boundary layer on a dolphin body is turbulized to a great extent. Sometimes the vortex disruption from the dorsal fin, from the chest fins and from other parts of body behind the middle is observed (Wood, 1979). In this case conditions of the flow around the body vary and therefore the mechanism of the thrust formation varies too. The thrust can be produced not only by the tail fin, but also by the body movements. We need to keep in mind this circumstance while estimating of the fish and dolphin propulsive device efficiency.

Let us analyze two models of swimming: with and without the flow disruption.

The first theoretical models were developed by Lighthill (1960) and Logvinovitch (1970) in appliance to fish swimming, but they can also be applied to dolphin swimming. These works were analyzed in detail in chapter 1 of this book (also see fig. 1.18). That is why we adduce here only the final expression for the thrust:

$$\overline{T} = \frac{m(l)}{2}\left[\overline{\left(\frac{\partial h}{\partial t}\right)^2} - \overline{U^2\left(\frac{\partial h}{\partial x}\right)^2}\right]_{x=l}. \tag{7.40}$$

Analysis of this formula shows that in the discussed variant the thrust is formed by only the tail fin. The body does not bring any component to the whole thrust. The thrust value is defined by cinematic parameters of the tail fin (more accurately, of the edge of the tail fin) and does not depend on the law of deformation of animal body.

Now let us discuss the model of dolphin swimming with vortex wake separation on the range of dolphin body from its maximal section to minimal section in the tail region. Wu (1971) solved this problem. He obtained the following expression for the thrust:

$$\overline{T} = \frac{1}{2}m(l)\left[\overline{\left(\frac{\partial h}{\partial t}\right)^2} - \overline{U^2\left(\frac{\partial h}{\partial x}\right)^2}\right]_{x=l} -$$

$$-\frac{1}{2}\int_0^l\left[\overline{\left(\frac{\partial h}{\partial t}\right)^2} - \overline{U^2\left(\frac{\partial h}{\partial x}\right)^2}\right]\frac{\partial m(x)}{\partial x}dx = \overline{T}_1 + \overline{T}_2, \tag{7.41}$$

The first term coincides with the expression (7.40), obtained by Lighthill (1960), the second term is caused by the separation of the vortex wake at the body range $0 < x < l$ (see fig. 1.20).

If we compare expressions (7.40) and (7.41), we can see that there is an additional force defined by the second term of expression (7.41). The sign of this force depends on proportion of the terms of the expression under the integral.

We can obtain expression (7.41) straightly on the base of the "penetrated layer" conception, developed by Logvinovitch (1970). In this case the second term has simple physical interpretation since it is defined by the rate to shedding of pulses $Uv(x)dm(x)$ in the area behind the body middle: $0 < x < l$.

At present there are quite enough data on kinematics of the dolphin swimming (Romanenko, 1986a; Yanov, 1990, 1997, 1998, Fish 1993) to evaluate forces, which are formed by the tail fin and by the body alone (we can't say it about fish swimming researches). To do it, we write some calculating equations in differential form.

The equation for the distribution of the thrust force along the dolphin body in Lighthill – Logvinovitch variant is defined by

$$\overline{dT} = \overline{\left(\frac{\partial}{\partial t} + U\frac{\partial}{\partial x}\right)\left[m(x)\left(\frac{\partial h}{\partial t} + U\frac{\partial h}{\partial x}\right)\right]\frac{\partial h}{\partial x}dx} \quad \text{if } 0 < x < l. \tag{7.42}$$

Distribution of the suction force along the dolphin body (in Lighthill – Logvinovitch variant) is defined by

$$\overline{dT_S} = -\frac{1}{2}\overline{\left(\frac{\partial h}{\partial t} + U\frac{\partial h}{\partial x}\right)^2}\frac{\partial m}{\partial x}dx \qquad \text{if } 0 < x < l. \tag{7.43}$$

Distribution of the thrust force (in Wu variant) is defined by

$$\overline{dT_1} = \overline{\left(\frac{\partial}{\partial t} + U\frac{\partial}{\partial x}\right)\left[m(x)\left(\frac{\partial h}{\partial t} + U\frac{\partial h}{\partial x}\right)\right]\frac{\partial h}{\partial x}dx}, \qquad \text{if} \quad -l_n < x < 0, \tag{7.44}$$

$$\overline{dT_2} = \overline{\left[\left(\frac{\partial}{\partial t} + U\frac{\partial}{\partial x}\right)\left(\frac{\partial h}{\partial t} + U\frac{\partial h}{\partial x}\right)\right]m(x)\frac{\partial h}{\partial x}dx}, \qquad \text{if} \quad 0 < x < 1. \tag{7.45}$$

Distribution of the suction force (in Wu variant) is defined by

$$\overline{dT_S} = -\frac{1}{2}\overline{\left(\frac{\partial h}{\partial t} + U\frac{\partial h}{\partial x}\right)^2}\frac{\partial m}{\partial x}dx, \quad \text{if } -l_n < x < 0. \tag{7.46}$$

To make a comparison, it is useful to represent the second term of expression (7.41) in its differential form:

$$\overline{dT_2} = \left[\overline{\left(\frac{\partial h}{\partial t}\right)^2} - U^2\overline{\left(\frac{\partial h}{\partial x}\right)^2}\right]\frac{\partial m}{\partial x}dx, \quad \text{if} \quad 0 < x < 1. \tag{7.47}$$

In order to obtain numerical estimates we need the law of the dolphin body deformation. We can write the general expression:

$$h(x,t) = h_0(x)\sin[\omega t + \tau(x)]. \tag{7.48}$$

Expressions (7.42) – (7.48) involve cinematic parameters of dolphin swimming, which can be obtained only by experiment. These parameters are the amplitude function $h_0(x)$, the cyclic frequency of the body oscillation $\omega = 2\pi f$, phase function $\tau(x)$, U - speed of swimming, $m(x)$ – virtual mass per body length unit, $\partial m/\partial x$ – trend of the virtual mass along the body. The superscript "*" used by Logvinovitch in his works is omitted here and below. All these experimentally defined cinematic parameters of dolphin swimming are most fully represented in chapter 6 and also in work by (Romanenko, 1986a). There are some data in works (Kayan and Pyatetsky, 1977, Kozlov, 1983, Yanov, 1990, 1997, 1998; Fish, 1993). In particular, adequate empirical dependencies, which tie the frequency of the body oscillation to the speed of swimming, were adduced in the first three works. For our estimates we use dependence like that in the work of Kozlov (1983):

$$\omega = 2\pi\left(1.05\frac{U}{l} + 0.25\right). \tag{7.49}$$

The following empirical expression for the amplitude and phase functions were proposed in the work of Romanenko (1986a):

$$h_0(x) = h_t\left[K_n - 1 + (2 - K_n)\left(\frac{x}{l}\right)^n\right] \tag{7.50}$$

and

$$\tau(x) = -\frac{k_0 \ln(1 + b_0 x)}{b_0}. \qquad (7.51)$$

Here $k_0 = \omega/U$, $K_n = h_n/h_t$, h_n and h_t are the amplitudes of oscillations of the tip of the nose and the tail fin of dolphin correspondingly, b_0 is a parameter, which characterizes dependence of the phase velocity of the propulsive wave on coordinate, γ is the parameter that describes ascent of the amplitude function from animal head to its tail.

Numerical values of kinematic parameters are adduced in tables 7.13 and 7.14.

The values of $m(x)$ adduced in table 7.13 are calculated with the expression from the work of Logvinovitch (1970)

$$m(x) = \rho\pi R^2(x). \qquad (7.52)$$

Here $R(x)$ is the cross-cut size of the dolphin body in horizontal plane, which is well known. It is adduced in the same table 7.13.

x, m	$R(x)$, m	$m(x)$, kgm^{-1}	$\Delta m/\Delta x$, kgm^{-2}
0.1	0.02	1.27	102.0
0.2	0.08	20.4	250.7
0.3	0.127	51.4	301.0
0.4	0.159	80.6	253.5
0.5	0.179	102.1	209.0
0.6	0.196	122.4	152.5
0.7	0.204	132.6	44.5
0.8	0.203	131.3	-69.5
0.9	0.193	118.7	-140.0
1.0	0.180	103.3	-149.0
1.1	0.167	88.9	-148.5
1.2	0.152	73.6	-162.5
1.3	0.133	56.4	-164.5
1.4	0.113	40.7	-135.0
1.5	0.096	29.4	-104.0
1.6	0.079	19.9	-97.0
1.7	0.056	10.0	-76.5
1.8	0.038	4.6	-37.5
1.9	0.028	2.5	-10.5
2.0	0.028	2.5	0

Table 7.13. Distribution of a virtual mass and its first derivative along the dolphin's body.

U, ms^{-1}	K_n	b_0, m^{-1}	γ	h_t/l
4.3	0.21	0.23	4.2	0.112

Table 7.14. Kinematic parameters of a dolphin *Tursiops truncatus* (l = 2.24 m). For explanations of variables, see text.

Using expressions (7.50) and (7.51) we can easily write the final form of expressions (7.42) - (7.43) in the variant of Lighthill and Logvinovitch

$$\overline{dT} = \left[\begin{array}{l} 2\pi^2\left(1.05\frac{U}{l}+0.25\right)^2 \frac{\partial h_0}{\partial x} m(x) - \frac{U^2}{2}\frac{\partial h_0}{\partial x}\frac{\partial^2 h_0}{\partial x^2} m(x) - \frac{U^2}{2} h_0 \frac{\partial h_0}{\partial x}\left(\frac{\partial \tau}{\partial x}\right)^2 m(x) - \\ -\frac{U^2}{2} h_0^2 \frac{\partial \tau}{\partial x}\frac{\partial^2 \tau}{\partial x^2} m(x) - \pi U\left(1.05\frac{U}{l}+0.25\right) h_0^2 \frac{\partial \tau}{\partial x}\frac{\partial m}{\partial x} - \frac{U^2}{2}\left(\frac{\partial h_0}{\partial x}\right)^2 \frac{\partial m}{\partial x} - \\ -\frac{U^2}{2} h_0^2 \left(\frac{\partial \tau}{\partial x}\right)^2 \frac{\partial m}{\partial x} \end{array} \right] dx \qquad (7.53)$$

and

$$\overline{dT_S} = \left\{ \frac{1}{4}\left[2\pi\left(1.05\frac{U}{l}+0.25\right) h_0 + U h_0 \frac{\partial \tau}{\partial x}\right]^2 \frac{\partial m}{\partial x} + \frac{U^2}{4}\left(\frac{\partial h_0}{\partial x}\right)^2 \frac{\partial m}{\partial x} \right\} dx . \qquad (7.54)$$

In the variant of Wu formula (7.44) exactly coincides with formula (7.53) at the body range $-l_0 < x < 0$ (see fig. 1.20 from ch. 1). Formula (7.46) includes the first four terms of formula (7.53). It is correct within the bounds $0 < x < 1$. In the variant of Wu sucking force is defined by formula (7.54) within the bounds $-l_n < x < 0$.

Formula (7.47) can be represented as

$$\overline{dT2} = \left[-\pi^2\left(1.05\frac{U}{l}+0.25\right)^2 h_0^2 + \frac{U^2}{4}\left(\frac{\partial h_0}{\partial x}\right)^2 + \frac{U^2}{4} h_0^2 \left(\frac{\partial \tau}{\partial x}\right)^2 \right] \frac{\partial m}{\partial x} dx . \qquad (7.55)$$

This formula is correct under $0 < x < 1$. We have to make one more remark that till now we have analyzed only the forces, which are formed within the animal body excluding its tail fin.

We shall obtain numerical estimates for two modes of dolphin swimming with constant speed: with and without disruption of the vortex wake in body area $0 < x < 1$. Both of these modes are characterized by cinematic parameters, which are adduced in tables 7.13 and 7.14. To do this, we shall use the amplitude and phase functions, which are represented by expressions (7.50) and (7.51).

We have already estimated the value of thrust, which is formed by the tail fin of the dolphin. The results are adduced in tables 7.10 and 7.12. Let us use the data of the second column of table 7.10 for the speed value of 4.3 ms^{-1}.

The results of calculation in the case of flow around the dolphin without disruption of the vortex wake with formulas (7.44) and (7.45) are shown in fig. 7.11. Also the distribution of the consolidated value of the pulling force and suction force ($dT + dT_s = dT_b$) is shown there along with the integral distribution of this value (T_b). The value of thrust T_b formed by the tail fin has been calculated in accordance with the data of table 7.10. It is shown in fig. 7.11 for the point x = 2.24 m, which corresponds to the edge of the fin. The adduced results indicate that the component of the whole thrust produced by the body is negligible. It is less than 3% of the thrust formed by the tail fin. Nevertheless, we must keep in mind that this value of the thrust is nonzero, but it must be zero under disrupt-free flow conditions. This result was obtained by formal numerical integration (summation) of the distributed pulling and suction forces along the animal body. It is defined by the finite value of the virtual mass in the terminal point of the integration range and therefore, by the value of impulse, which gutters at the terminal point.

The results of calculations with formulas (7.44), (7.46) and (7.47) are shown in fig. 7.12. We can see that the additive thrust is formed when the vortices come off the flow at the narrowing part of the animal body. This thrust can amount to 25% of the total thrust formed by the tail fin of a dolphin. The estimate fulfilled for the case, when dolphin speed equals to 2.2 ms^{-1}, shows that the thrust formed by the animal body amounts to 10% of the tail fin thrust. We cannot neglect this additive thrust when we estimate dolphin propulsive capabilities, and especially when we estimate its resistance coefficient.

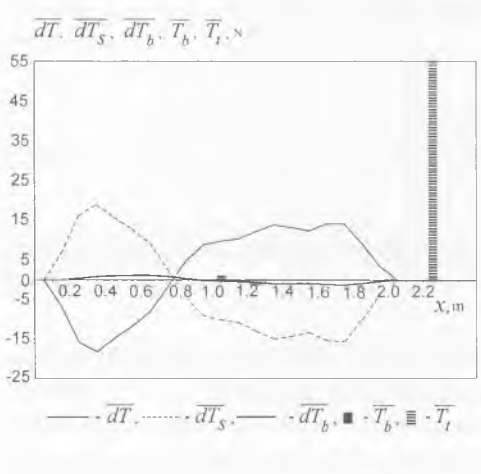

Fig. 7.11. Distribution of the pulling, suction force and the thrust along the active swimming dolphin in the case of flow around the dolphin without turbulization. The comments are in the text.

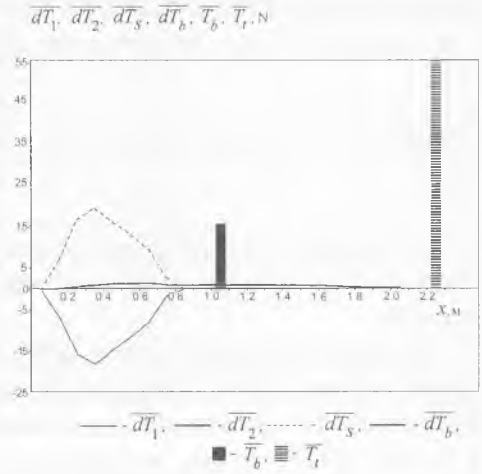

Fig. 7.12. Distribution of the pulling, suction force and the thrust along the active swimming dolphin in the case of the turbulent flow around the dolphin. The comments are in the text.

7.2.3. Drag and efficiency coefficient

Foremost we are interested in studying of friction drag, as this component of the drag as a whole can be altered by different mechanisms of the animal boundary layer control. So let us estimate the friction drag.

Generally speaking, the complete drag coefficient of the dolphin can be represented as the sum of its components:

$$C = C_1 + C_2 + C_3 + C_4 + C_5 + C_6. \tag{7.61}$$

Here the coefficients C_1, C_2, C_3, C_4, C_5, C_6, characterize the drag friction, shape, and the fluke profile, inductive drag of the fluke, drag of the dorsal fin profile and chest fins profile drag. It is known that the drag of the body shape is about 0.22 of the friction drag of a rigid dolphin-like body (Droblenkov, 1960; Semenov, 1969). Let us consider the combine profile of the dorsal and chest fins drag equal to the dolphin fluke profile drag. Taking this into account we can write the following evident expressions:

$$C_1 = C_f, \tag{7.62}$$

$$C_2 = 0.22 C_f, \tag{7.63}$$

$$C_3 = C_p \frac{S_t}{S_b}, \tag{7.64}$$

$$C_4 = C_i \frac{S_t}{S_b}, \tag{7.65}$$

$$C_5 = 0.5 C_p \frac{S_t}{S_b}, \tag{7.66}$$

$$C_6 = 0.5 C_p \frac{S_t}{S_b}. \tag{7.67}$$

Here, C_i is the inductive drag coefficient of the fluke. We do not take into account wave drag as we assume that the dolphin swims deeply enough. If we take into consideration expressions (7.62) - (7.66), we can represent formula (7.61) as

$$C = 1.22C_f + \left(2C_p + C_i\right)\frac{S_t}{S_b}. \tag{7.68}$$

From this relation we can obtain expression for the friction drag coefficient:

$$C_f = \frac{C}{1.22} - \left(2C_p + C_i\right)\frac{S_t}{1.22S_b}. \tag{7.69}$$

If the thrust is known, we can calculate the whole drag coefficient using formula

$$C = \frac{2T}{\rho S_b U_0^2}. \tag{7.70}$$

With this formula we can rewrite expression (7.69) as

$$C_f = \frac{2\overline{T}}{1.22\rho S_b U_0^2} - \left(2C_p + C_i\right)\frac{S_t}{1.22S_b}. \tag{7.71}$$

To evaluate the drag coefficient using the thrust value adduced in the second column of table 7.10 we can write formula (7.71) in the following way

$$C_f = \frac{2\overline{T}}{1.22\rho S_b U_0^2} - C_p\frac{S_t}{1.22S_b}. \tag{7.72}$$

There is no coefficient of inductive drag of fluke C_i in this formula and the numerical coefficient in the second term is changed from 2 to 1 because inductive and profile drag of the wing has been accounted in the model discussed in chapter 1. The estimates of friction drag coefficient, shown in the second column of table 7.10, are obtained with the help of this formula. When the speed value was 2.2 ms^{-1} we used corresponding value of the thrust from the second column of table 7.10, which was increased by 10% (shown in the fourth column), which corresponds to the results of preceding section (the coefficient K = 1.1 from the third column). In the same way, for the speed equaled 4.3 ms^{-1}, the thrust value is increased by 25% (the coefficient K = 1.25). In the eighth and the ninth columns there are drag coefficients, which differ from those of the seventh column by twin standard error $\pm 2\sigma$. We can see that the confidence interval two standard errors long, which ensures

confidence probability value of 95%, comprises the whole area of the drag coefficients from laminar to turbulent mode of the flow. Strictly speaking, it means that the fulfilled estimates of the thrust and drag are meaningless. They do not allow us to obtain the unambiguous conclusions about the dolphin's mechanisms of laminarization. They only permit to hope that such mechanisms do exist. Here we can once again remind that only the direct measurement of the boundary layer structure and dynamic pressure distribution on dolphin's body can give the unambiguous conclusions about the dolphin hydrodynamic capabilities. However we proceed with the estimation of dolphin thrust and drag coefficient using existing data.

To calculate the drag coefficient using the thrust values from the second and the third columns of table 7.12, we rewrite formula (7.71) as

$$C_f = \frac{2\overline{T}}{1.22\rho S_b U^2} - 2C_p \frac{S_t}{1.22 S_b} . \tag{7.73}$$

The values of the drag coefficients, which were calculated with formula (7.73) using the values of thrust from the fifth and sixth columns of table 7.12, are adduced in the seventh and eighth columns of table 7.12. As well as before, in formula (7.73) we used corresponding value of the thrust (the second column) increased by 10% for the speed of 2.2 ms^{-1} and increased by 25% (the third column) for the speed 4.3 ms^{-1}.

The results of calculations of the drag coefficients from tables 7.10 and 7.12 are shown in figure 7.13. In addition, the corrected values of the drag coefficients of the three dolphin species (*Delphinus bairdi, Phocoenoides dalli and Lagenorhinchus obliquidens*) are plotted in this figure. These coefficients are calculated with formula (7.72) using data from table 7.6. Also, the corrected values of the drag coefficients, which were calculated using the thrust values from the third and fourth lines of the eight column of table 7.7, are adduced there. In the case of the two-dimensional theory of Lighthill (1969) the drag coefficient was calculated with formula (7.73), where there was also taken into account inductive drag of the fluke C_i = 0.008 (Bairstow, 1939), because the theory of Lighthill neglects the power loss due to this component of drag.

$$C_f = \frac{2\overline{T}}{1.22\rho S_b U^2} - \left(2C_p + C_i\right) \frac{S_t}{1.22 S_b} . \tag{7.74}$$

In the case of the three-dimensional theory (Chopra, Kambe 1977) the drag coefficient was calculated with formula (7.73). We consider $\overline{T} = E$ from table 7.7 for the both formulas. As well as before, the values of thrust were increased by 25%, taking into account the thrust, formed by the undulating body of dolphin.

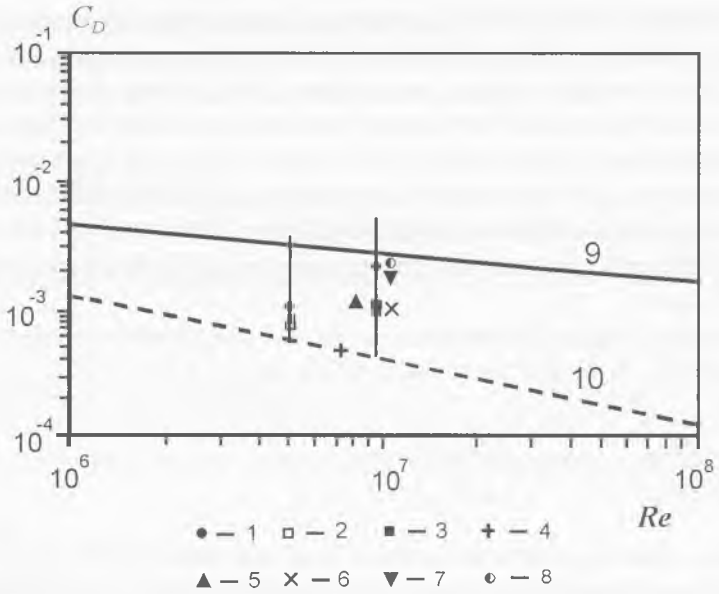

Fig. 7.13. Comparison of cetacean drag coefficients estimated from hydromechanical models based on kinematics. Drag coefficients are plotted against Reynolds number, *Re*. Symbols represent *Tursiops truncatus* (1 – values were calculated from formula 7.18); *Tursiops truncatus* (2 – values based on the three-dimensional theory of Chopra and Kambe, 1977, for the wing B1); 3 – same for the wing B2; *Delphinus bairdi*, *Phocoenoides dalli* and *Lagenorhynchus obliquidens* (4-6 – values were calculated from formula 7.13); *Lagenorhynchus obliquidens* (7 - values were calculated from two- dimensional theory of Lighthill, 1970); *Lagenorhynchus obliquidens* (8 - values were calculated from the three-dimensional theory of Chopra and Kambe, 1977); The solid line (9) represents the minimum drag coefficient assuming turbulent boundary conditions; the broken line (10) is for minimum drag coefficient assuming laminar conditions.

The results are adduced in tables 7.7, 7.10, 7.12 and in figure 7.13. These results indicate that there is a significant spread of estimates of the friction drag, while the average is twofold less than the value under the turbulent flow conditions.

We'd like to say some words about an efficiency of a dolphin propeller. The plots from the work of Chopra and Kambe, 1977 can give some information on this subject. We regret to note there is no plot for the case of $\Theta = 0.9$. Nevertheless, we can say that the efficiency is about 97%. As it was found in the work (Zaytsev, Fedotov, 1986), the efficiency is about 90%. However, the estimates in this work were made for the wing with attack angle of 10° and the angle of attack of the dolphin fluke is a third of it. It means that the efficiency is certainly more than 90%. Perhaps, it is enclosed in the range between 90% and 97%.

7.3. Ultimate speed of swimming

Using advanced conception of the dolphin hydrodynamics we can estimate the ultimate speed of its swimming under the known elaborated power and compare it with the experimentally measured speeds.

We shall rely on the known relation (Kozlov, 1983), which connects the power elaborated by the dolphin with the time of swimming and mass.

$$P(t) = 0.19 t^{-1/3} m^{2/3} \text{ kW}. \tag{7.75}$$

Estimates of the ultimate power elaborated by the dolphin were made on the base of analysis of dolphin's jumps. Under the condition that the dolphin length is 2 m and its mass is 80 kg, this estimate indicates that the ultimate power amounts to 3000 W (Kozlov, 1983). Consequently we assume that the dolphin with mass of 80 kg can't elaborate power greater than 3000 W during the first second of movement. We assume that during ulterior movement of dolphin its power is decreased with a rule $t^{-1/3}$ accordingly to expression (7.74). Also we shall assume that the thrust formed by the dolphin's tail fin is limited and amounts to its weight (at least, no less than the weight and perhaps greater than the weight):

$$T = mg. \tag{7.76}$$

This assumption is based on the dolphin ability "to stand on its tail" during some short time interval, when the thrust formed by the tail fin is quite equal to animal weight. We shall represent the whole thrust as the sum of the two components. One of these components is formed by the fluke and other is formed by the body and amounts to 25% of the fluke thrust (see the previous section).

The dolphin's movement from a quiescent state can be thought as consisting of a few stages. At the first of these stages, when the speed is near zero, the movement rises under the constant thrust. We can represent with sufficient accuracy the equation of dolphin movement as

$$k_1 m \frac{dU}{dt} = k_2 mg \tag{7.77}$$

with starting condition $U = 0$ when $t = 0$. We took into account the added mass of water in the coefficient $k_1 = 1.05$ (Pershin, 1988) and the thrust formed by the body in the coefficient $k_2 = 1.25$. The solution of the equation (7.77) gives us

$$U = \frac{k_2}{k_1} gt. \tag{7.78}$$

As the speed increases, drag under laminar flow and the drag of shape become sensible. At this stage we can write the equation of animal movement as

$$k_2 mg U = k_1 mU \frac{dU}{dt} + \left(C_{fl} + C_{pb}\right)\frac{\rho U^3 S_b}{2} \tag{7.79}$$

Here C_{fl} is the coefficient of friction drag under laminar flow conditions, C_{pb} is the drag coefficient of the shape of body, which include also the profile drag coefficient of a dorsal fin (see previous section).

$$C_{fl} = \frac{1.328}{\sqrt{\mathrm{Re}}},\ C_{pb} = 0.00103 \tag{7.80}$$

Here

$$\mathrm{Re} = \frac{Ul}{\nu} \tag{7.81}$$

ν is cinematic viscosity, l is length of animal body, ρ is water density, S_b is the wetted surface of animal body, which amounts to 1.56 m^2 for the dolphin having mass of 80 kg and length 2 m.

We do not consider the coefficient of the profile drag in formula (7.79) because power loss is already taken into account by the assumption, that the thrust is equal to the weight of the dolphin body. Indeed, when the dolphin stands on its tail, its tail fin works actively and a part of the thrust is spent on overpowering of the profile drag and the inductive drag of the fluke. The rest of the thrust generated by the tail fin supports the body in the upright position.

We obtain from expression (7.79)

$$\frac{dU}{dt} = \frac{k_2}{k_1} g - 0.0087U\sqrt{U} - 0.0096U^2 \tag{7.82}$$

When the dolphin attains a certain speed, its power reaches the limit amounted to 3000W. It happens at the speed U=3.06 ms^{-1}. We can find this value from the relation

$$T_{max} U = P_{max}, \tag{7.83}$$

where P_{max} = 3000W, $T_{max} = k_2 mg$.

During a second after this speed is attained, the dolphin movement is described by the equation

$$\frac{dU}{dt} = \frac{k_2}{k_1} g\left(\frac{3.06}{U}\right) - 0.0087U\sqrt{U} - 0.0096U^2. \tag{7.84}$$

We assume that the power elaborated by the dolphin during this first second of movement is constant, and the expression in brackets in the right part of (7.84) takes into account this assumption.

After the first second of the dolphin movement the power decreases as $t^{1/3}$. This fact can be accounted by the corresponding factor in the first term of the right part of (7.84). Therefore

$$\frac{dU}{dt} = \frac{k_2}{k_1} g\left(\frac{3.06}{Ut^{1/3}}\right) - 0.0087U\sqrt{U} - 0.0096U^2. \tag{7.85}$$

The equation for dolphin motion (7.85) is correct until the boundary layer becomes turbulent. Then the drag sharply increases. From this moment the growth of speed sharply decelerates. Grushanskaya and Korotkin (1973) especially studied the dolphin swimming at ultimate speed in captivity. They came to the conclusion that the dolphin attains the maximal speed during 2 sec after the beginning of the movement. Then the speed distinctly decreases. It is logical to suppose that this is the moment of the turbulization of the boundary layer. From this moment the drag coefficient of the dolphin is defined by the relation (Schlihting, 1974):

$$C_f = \frac{0.455}{(\lg \mathrm{Re})^{2.58}} - \frac{A}{\mathrm{Re}}, \tag{7.86}$$

where A=1700. Then the equation of dolphin motion after turbulization ($t > 2$s) looks like

$$\frac{dU}{dt} = \frac{k_2}{k_1} g\left(\frac{3.06}{Ut^{1/3}}\right) - K\left[\frac{4.046U^2}{(6.3 + \lg U)^{2.58}} - 0.0075U\right] - 0.0096U^2. \tag{7.87}$$

Here the coefficient K before the second term of the right part is less than 1. In this coefficient we take into account the fact that during active dolphin swimming after turbulization of the boundary layer the coefficient of the turbulent friction drag is less than the one of the rigid body of dolphin-like shape. It was shown above that this is explained by the big negative pressure gradient on the body of active swimming dolphin. It was proved by a direct measurement of tangential stresses in the boundary layer.

The calculated dependence of the speed of bottlenose dolphin movement on time is shown in fig. 7.14 (curves 1, 2, 3). This dependence is obtained by numerical integration

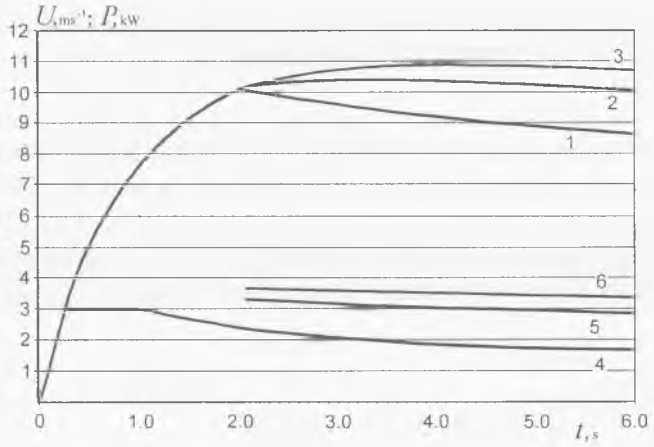

Fig. 7.14. The calculated dependence of the speed of *Tursiops truncatus* movement on time. The curves 1, 2 and 3 were obtained under $K = 1$, $1/2$ and $1/3$ correspondingly in the formula (7.75). Curves 5 and 6 show the values of power, which dolphin would develop in order to ensure increasing of speed corresponding to curves 2 and 3, if its streamline was the same as the streamline of a rigid dolphin-like body. Curve 4 shows alteration of power factually generated by the dolphin in the length of time.

of the movement equations (7.77), (7.82), (7.84) - (7.86) with Runge-Kutta method (Korn, Korn, 1973). The curves 1, 2 and 3 were obtained under $K = 1$, $1/2$ and $1/3$ correspondingly in the formula (7.87). In the same figure on curves 5 and 6 there were marked the values of power, which dolphin would develop in order to ensure increasing of speed corresponding to curves 2 and 3, if its streamline was the same as the streamline of a rigid dolphin-like body. Curve 4 shows a function of power factually generated by the dolphin in the length of time.

The known experimental data (Grushanskaya and Korotkin, 1973) show that the ultimate speed of swimming of the bottlenose dolphin in captivity is 11 ± 0.5 ms^{-1}. It well corresponds with the calculated values adduced in figure 7.14, where $K = 1/2$ and $1/3$.

Thus the dolphin ability to increase the critical Reynolds number and to decrease the level of turbulence in the boundary layer (and, consequently, the resistance coefficient) due to the big negative gradient of pressure gives it the possibility to spend its power economically. However it does not give the dolphin any 7 or 8-fold economy, as Gray supposed, but only a two-fold one or a bit more. This circumstance allows us to explain partially a long-range migration of cetaceans.

7.4. Body shape assessment for the dolphin and other cetaceans

The gradient of dynamic pressure, which is formed on the animal body during its active swimming, plays the main role in the support of flow without disruption. This conclusion is the result of analysis of the body shape. There are the three basic parameters, which affect the flow grain: relative elongation, which is the ratio of the body length to the diameter of the circle, whose square equals to the maximal square of the body cross-section (l/d_{max}), relative location of the maximal cross-section (l_1/l) and the angle α of exit of the body of revolution, which approximates the animal body best. The sketchy image of dolphin body with the corresponding designation is shown in fig. 7.15. Not all dolphin species and big whales have the body shape, which can be well approximated by a body of revolution. However, it is useful to adduce the table of comparative data on the shape of the body of different dolphin and whale species. We must only note that we have no accurate data on the maximal cross-section areas of cetacean. That is why we consider the maximal diameter as the maximal cross size of the body in horizontal plain. The dimensions of cetacean bodies, which we needed, were taken from the catalog (Leatherwood et al., 1972) on the base of the photos adduced there. Consolidated data are adduced in table 7.15

We can see that the relative elongations of all studied cetacean species range from 4 to 7.6. The relative locations of the maximal cross section range from 0.33 to 0.45. The angles of exit range from 7° to 15°. In order to estimate these values, we turn to the work Alekseeva et all (1968), where there is a calculation of parameters of laminar boundary layer of the various bodies of revolution with different shape parameters. We do not analyze the methods of calculation and adduce only the basic results. These results run as following:

1. The condition, under which the flow in the boundary layer is practically disruptless, is $\alpha \leq 6.5°$.

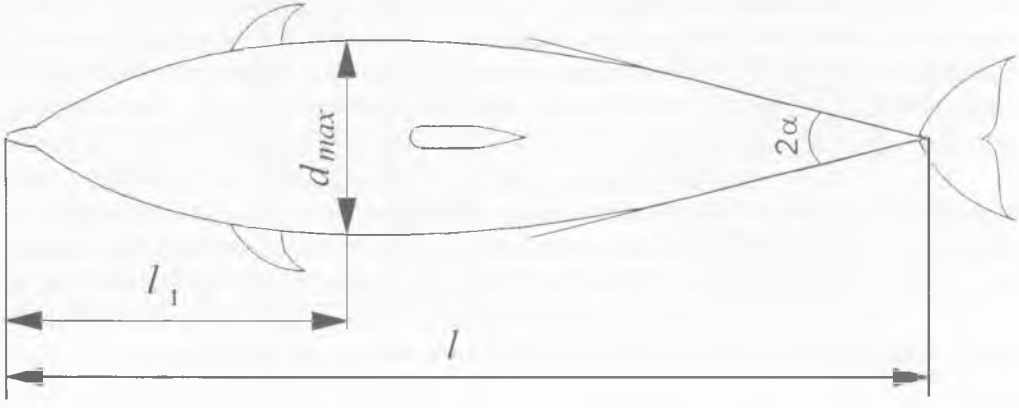

Fig. 7.15. The sketchy image of dolphin body with the corresponding designation.

2. If the flow is laminar and the order of Reynolds number is 10^8, then the body of revolution, whose elongation is about 9 and relative location of the maximal cross section equals to 0.21, has minimal drag.
3. If the flow is turbulent, then the body of revolution, whose elongation ranges from 5.5 to 7 and relative location of the maximal cross section is about 0.4, has minimal drag.

If we compare these data with the data from table 4, we shall come to the following conclusions:
1. The angles of exit of a cetacean body exceed the angle under which the laminar boundary layer disruption must be observed. This fact means that either the dolphin has a disruption of the boundary layer in case of the laminar flow or it has the possibility to prevent this disruption. We saw above that in process of active swimming the negative gradient of pressure is formed on the dolphin body, and this gradient can prevent the disruption of laminar boundary layer.
2. Cetacean body is not optimal for minimizing the drag under the laminar flow condition. The foremost it means that there is a possibility of disruption of the laminar boundary layer, mentioned above. However, as we have already seen, there is no such a danger for cetacean and, in particular, for the dolphin.
3. The shape of cetacean body approaches the optimal for minimizing the drag under the turbulent flow condition.

So, if we keep in mind the negative gradient of pressure on the dolphin body, we can think that the shape of its body is optimal for both laminar and turbulent flows. This is one of the most important adaptations in cetacean created by nature.

№	Species	l/d_{max}	l_1/l	α, deg
1	*Tursiops truncatus*	5.4	0.35	10
2	*Phocoena phocoena*	4.7	0.40	15
3	*Lagenorhynchus obliquidens*	6.9	0.36	8
4	*Stenella graffmani*	7.1	0.35	7
5	*Stenella longirostris*	7.6	0.34	7
6	*Delphinus delphis*	6.1	0.36	-
7	*Phocoenoides dalli*	4.6	0.33	13
8	*Lissodephis borealis*	7.5	0.36	7
9	*Eschrichtius robustus*	4.5	0.40	10
10	*Berardius bairdi*	6.0	0.39	-
11	*Pseudorca crassioleus*	6.9	0.38	-
12	*Physeter catodon*	5.1	0.45	-
13	*Kogia breviceps*	4.0	0.42	-

Table 7.15. Morphometric parameters of the cetaceans. For explanations of variables, see text.

7.5. Hydrodynamics of dolphin according to recent data

Let us consider the formation of the boundary layer on the dolphin body in its swimming from quiescent state according to the recent scientific data.

At the first moment the dolphin moves with a certain positive acceleration. If we assume that the maximal thrust is equal to the animal weight, than the maximal acceleration is seemingly about 10 ms^{-2}. The fact that the thrust can be equal to the animal weight is proved by the well-known cases of "standing on the tail". The movement under the acceleration results in the significant favorable (negative) gradient of dynamic pressure formed on the dolphin body. This gradient leads to a noticeable increase (3 or 4 times) in the critical Reynolds number. As the negative gradient obtains the least absolute value in the middle part of the dolphin body, the instability of the laminar flow arises first of all in this place. When Reynolds number comes to some critical value, which depends on the value of acceleration of the motion, then the laminar flow in the point with the relative coordinate of about $x/l = 0.4 \div 0.5$ becomes turbulent. After the turbulization of the boundary layer at the middle part of the dolphin body has happened, its further motion, as a rule, becomes practically uniform during a certain time interval. Sometimes this interval of the dolphin motion with a constant velocity is practically absent, and the dolphin goes to the inertial motion right after acceleration. Analysis of experimental data shows that the increase in the speed after the boundary layer turbulization does not exceed 10-20%. At the same time the higher starting acceleration is, the higher the maximal speed of dolphin swimming will be. The level of turbulization in the boundary layer on the body of a uniformly swimming dolphin is 2 – 3 times less than the level in the boundary layer on the rigid dolphin-like body or in the boundary layer on the body of the dolphin while its inertial motion. Naturally, in this case the coefficient of friction drag averaged over the wetted surface of the dolphin body is less than corresponding coefficient of the rigid body drag. When the uniform motion transforms into inertial motion then the significant positive gradient of dynamic pressure arises along the dolphin body behind its middle. At the same time the gradient of pressure in the middle area is slightly positive or close to zero. The gradient of pressure remains negative only at the head area. The level of turbulence in the boundary layer at the middle and after parts of the body increases and obtains the value, which corresponds to the turbulent flow around the rigid body. The drag coefficient also increases to the value, which corresponds to the rigid body.

If the inertial motion is replaced with the accelerated motion then the negative gradient of the pressure again arises on the dolphin body and causes decreasing of the level of turbulization of the boundary layer. If the value of gradient is big enough, then the inverse transition from the turbulent flow to laminar one becomes possible at the area behind the middle.

Brief conclusions

The most reliable and convincing estimates in this chapter are the estimates of the distribution of dynamic pressure and its gradients over the dolphin body. They prove the presence of the negative gradient of dynamic pressure on the body of the actively swimming dolphin and its significant value, which is sufficient for increasing of critical Reynolds number and sometimes for realization of the inverse transition from the turbulent flow to the laminar one.

The estimates of the thrust and friction drag coefficient based on the kinematical parameters are less convincing, although they prove that dolphins, possibly, have some mechanism of the boundary layer control. Thus these estimates well match the estimates of distribution of the dynamic pressure and its gradients on the dolphin body.

The estimates of the thrust, which is formed only by the dolphin body, have qualitative character. But these estimates are very significant because they are the first to show the capability of the dolphin (and whale) to live normally and accomplish their migration even with partly or completely lost tail fin. Besides, these estimates show that the dolphin thrust is not only the thrust of the tail fin, and we must take into account this circumstance, when we estimate the efficiency of the dolphin propeller.

The estimates of ultimate speed of dolphin swimming well match the experimental data and prove indirectly that the coefficient of dolphin friction drag is at least two times less than the turbulent one.

The estimate of the dolphin body shape proves that the shape is optimal for both laminar and turbulent flows.

CONCLUSION

In this book an attempt was made to present a state of fish and dolphin hydrodynamics and to attract attention of scientists to the most actual problems. These problems are: the elaboration of a direct methods of an investigation of a thin structure of a boundary layer, shearing stress, animals flow over and a pursuance of a necessary measurements. The resolution of these problems has been presented in this book to some extent. However, a large share of original results has not been replicated and verified by other investigators.

Data presented in this book attest that a favorable gradient of dynamic pressure is a controlling consideration of a boundary layer operating and a critical Reinolds increasing. This factor was premised by Gray (1936) and proved by the theoretical and experimental studies (Romanenko, 1972, 1976, 1986a; Romanenko, Yanov, 1973). It is not inconceivable that some other drag-reduction mechanisms exist: compliant dampening (Kramer, 1955; Babenko, 1971; Babenko, Kozlov, Perschin, 1972; Kozlov, 1983), secretions from the dolphin eye (Sokolov et al., 1969; Uskova, Raevsky, Momot, Uskov, 1975), and others. However, some elaborate experimental research is necessary for estimation of a contribution from each mechanism into total effect.

REFERENCES

Achkinadze, A. Sh. (1995). Utilization of the theory of perfect propulsor for evaluation of effeciency of propulsive arrangement of animals (in Russ.). *Tez. dokl. Mezhd.konfer. «Plavanie i polet v prirode i tehnike AQUAPROP'95» S-Peterburg, SPbGMTU.*

Agarkov, G. B., V. V. Babenko, Z. I. Ferents. (1973). On the skin and the skin musculature innervation in dolfin in connection with the hypothesis of fllow stabilization in boundary layer (in Russ.). In *Problemy bioniki.* Nauka, Moscow, 478-483.

Agarkov, G. B., Z. I. Ferents. (1967). On the intraorganic innervation of the skin musculature in Tursiops truncatus ponticus Barabasch (in Russ.). Communication 1. *Vestnik zoologii* 3

Agarkov, G. B., V. Ya. Lukhanin. (1970). On the question of locomotion musculature of caudal section in Delphinus delphis (in Russ.). *Bionika* **4**, 61-64.

Agarkov, G. B., A. P. Manger, V. G. Khadzhinskiy, B. G. Khomenko. (1975). On the peculiarities of implantation of alloplastic materilas in the skin of some Cetaceans (in Russ.). *Bionika* **9**: 134-137.

Agarkov, G. B., V. F. Sych. (1974). Morpho-functional analysis of epaxial musculature of locomotion complex in Phocoena phocoena (in Russ.). *Bionika* **8**: 122-127.

Agarkov, G. B., V. G. Khadzhinskiy. (1970). On the problem of constitution and innervation of skin in Black sea dolphins in connection with their defensive function (in Russ.). *Bionika* **4**: 64-69.

Agarkov, G. B., V. G. Khadzhinskiy, E. G. Chernyayev. (1972). Experimental studies of the possibility of implantation of telemetric apparatus in the body of aquatic mammals (in Russ.). *Materialy 4 Ukrainskoj respublikanskoj nauchnoj konferentsii. Biokibernetika. Bionika*, Kijev: 133-136.

Agarkov, G. B., V. G. Khadzhinskiy, E. G. Chernyayev. (1972). On the methods of implantation of telemetric apparatus in the skin of marine animals (in Russ.). *Bionika* **6**: 114-118.

Agarkov, G. B., V. G. Khadzhinskiy, E. G. Chernyayev. (1977). Short-term implantation of biotelemetric complex in the skin of dolphins (in Russ.). *Bionika* **11**: 94-98.

Agarkov, G. B., B. G. Khomenko, V. G. Khadzhinskiy. (1974). *Morphology of dolphins* (in Russ.). Naukova Dumka, Kiev. 169 pp.

Agarkov, G. B., B. G. Khomenko, A. P. Manger. (1979). *Functional morphology of Cetaceans* (in Russ.). Naukova dumka, Kiev. 224 pp.

Agarkov, G. B., A. A. Vishnyakov. (1975). On the implantation of mean and pulse pressure gauges in the skin of marine animals (in Russ.). *Bionika* **9**: 131-133.

Agarkov, G. B., A. A. Vronskiy, A. P. Nosar'. (1978). Hydrobionic investigations of aquatic animals locomotion in connection with problems of functional morphology (in Russ.). In *Bionika - 78,* Nauka, Moscow-Leningrad, 1: 71-74.

Ahmadi, A. R. (1980) An asymptotic unsteady lifting-line theory with energetics and optimum motion of thrust-producing lifting surfaces. *MIT, Department of Aeronautics and Astronautics Fluid Dynamics Research Laboratory Report* **80**.2.

Ahmadi, A., S. E. Widnall. (1985). Unsteady lifting-line theory as a singular-perturbation problem. *J. Fluid Mech.* **153**: 59-81.

Ahmadi, A., S. E. Widnall. (1986). Energetics and optimum motion of oscillating lifting surfaces of finite span. *J. Fluid Mech.* **162**: 261-282.

Akhutin, V. M., S. P. Balitskiy, A. S. Katrin, B. G. Kulikov, G. N. Pakhar'kov, V. N. Khropot. (1978). About evaluation of efficiency of swimming biomechanics with the condition of optimization of cost of energy (in Russ.). *Bionika* - 78, **1**, Moscow-Leningrad: 235-237.

Aleyev, Yu. G. (1963). *Functional basis of fish external integument* (in Russ.). Izdat. AN SSSR, Moscow. 247 pp.

Aleyev, Yu. G. (1964). On the means for drag reduction through the fish external integument (in Russ.). *Trudy Sevastop. Biol. stan. AN SSSR.* **15**: 288-291.

Aleyev, Yu. G. (1965a). On the investigations into the fish functional morphology (in Russ.). *Bionika*: 192-198.

Aleyev, Yu. G. (1965b). The body of dolphins as a carrying surface (in Russ.). *Zool. Zh.* **44**: 626-630.

Aleyev, Yu. G. (1966). Flotability and hydrodynamic function of the corps of nektone animals (in Rus.). *Zool. zhurn.* **45**: 575-584.

Aleyev Yu. G. (1969a). *Function and gross morphology in fish.* Transl. From Russian by M. Ravek. Washington: Smithsonian Inst. And Nat. Sci. Foundation, **IV**. 268 pp.

Aleyev, Yu. G. (1969b). Topography of locomotive function in necters (in Russ.), In *Funktsional'no-morfologicheskiye issledovaniya nektonnikh zhivotnikh* 16. Naukova dumka. Kijev: 3-12.

Aleyev, Yu. G. (1970a). On the means for hydrodynamic drag reduction of necters through the mobile surface irregularities (in Russ.). *Zool. Zhurn.* **49**:

Aleyev, Yu. G. (1970b). On the feature of hydrodynamic of Xiphioidae (in Russ.). *Zool. Zhurn.* **49**: 1676-1684.

Aleyev, Yu. G. (1972). Hydrodynamic quality of body shape of necters (in Russ.). *Zool. Zhurn.* **51**: 949-953.

Aleyev, Yu. G. (1976). Biohydrodynamics and ecology of life forms of pelagial. *Intern.Rev.ges.Hydrobiol* **61**: 137-147.

Aleyev, Yu. G. (1976). *Nekton* (in Russ.). Naukova dumka, Kijev: 391 pp.

Aleyev, Yu. G. (1977). *Nekton.* Hagua: Junk: 435 pp.

Aleyev, Yu. G. (1986). *Ecomorphology* (in Russ.).: Naukova dumka, Kijev. 424 pp.

Aleyev, Yu. G., B. V. Kurbatov. (1974). Hydrodsynamic resistance in live fishes and in some other necters in the inertial movement (in Russ.). *Voprosy ikhtiologii* **14**: 173-176.

Aleyev, Yu. G., I. V. Leonenko (1974). On the hydrodynamic meaning of the rostrum of swordfish (in Russ.). *Bionika* **8**: 21-23.

Aleyev, Yu. G., O. P. Ovcharov (1969a). On the development of processes of vortical shaping and property of the boundary layer during the moving of fish (in Russ.). *Zool. Zhurn.* **48**

Aleyev, Yu. G., O. P. Ovcharov (1969b). On the function of vortical shaping during fish locomotion and influence of dividing line between two medium on the flow over (in Russ.). *Zool. Zhurn.* **50**:

Alexander, R. Mc. N. (1965). The lift produced by the heterocercal tails of selachii. *J. Exptl. Biol.* **43**: 131-138.

Alexander, R. Mc. N. (1966). Physical aspects of swimbladder function. *Biol. Revs. Cambridge Physiol. Soc.* 1: 141-176.

Alexander, R. Mc. N. (1966). Lift produced by the heterocercal tail of *Acipenser. Nature* **210**: 1049-1050.

Alexander, R. Mc. N. (1967). *Functional design in fishes.* London. Hutchinson.

Alexander, R. Mc. N. (1969). *Animal mechanics.* Seattle. Univ. Wash. Press., 346 pp.

Alexander, R. Mc. N. *Biomechanics* (in Russ.). Moscow. Izdat. MIR. 1970. 339 pp.

Alekseeva, K. D. (1967). Influence of muscular functioning on energy metabolism (in Russ.). In *Obmen veschestv i biochimiya ryb.* Nauka. Moscow: 193 pp.

Alekseeva, K. D. (1972). Expenditure of energy for swimming of grey mullet (in Russ.). *Bionika* **6**: 7-12.

Alekseeva, K. D. (1973). On the measuring method for expenditure of energy for swimming of salt-water fish (in Russ.). In *Problemy bioniki.* Nauka. Moscow: 447-451.

Alekseeva, K. D., V. P. Gromov, A. F. Dmitrieva, B. P. Kolobov, B. G. Kuznetsov, B. N. Semyonov, N. N. Yanenko. (1968). *Calculation of characteristics of laminar boundary layer on the bodies of revolution* (in Russ.). Nauka, Novosibirsk. 220 pp.

Alekseeva, T. E., B. N. Semenov. (1971). To the defenition of hydrodynamic resistance of dolphin (in Russ.). *Zhurn. prikl. mekh. i tekhn. fis.* **2**: 160-164.

Algazin, V. A. (1976). To the calculation of aerodynamic characteristics of wing of finite span (in Russ.). *Dinamika sploshnoy sredy*, **26**: 23-37.

Algazin, V. A. (1980). Calculation of nonlinear aerodynamic characteristics of wing of finite span (in Russ.). *Zhurn. prikl. mekh. i tekhn. fis.* **4**: 87-96.

Algazin, V. A. (1982). The screen impact on aerodynamic characteristics of oscillating airfoil (in Russ.). *Zhurn. prikl. mekh. i tekhn. fis.* **4**: 13-21.

Algazin, V. A. (1984). Theoretical study of propulsive force in oscillating wing of finite span (in Russ.). *Bionika* **18**: 52-57.

Algazin, V. A., D. N. Gorelov. (1974). On the arbitrary movement of wing of finite span (in Russ.). In *Izv. Sib. otdel. Akadem. Nauk.SSSR. Ser. tekhnich. nauki,* **4**: 43-58.

Amfilokhiyev, V. B. (1969). Turbulent flows with elastic borders (in Russ.). *Bionika* 3: 46-53.

Amfilokhiyev, V. B. (1995). Experimental studies of the hydrodynamic properties of the flexible covers (in Russ.). *Tez. dokl. Mezhd.konfer. «Plavanie i polet v prirode i tehnike AQUAPROP'95» S-Peterburg, SPbGMTU.*

Amfilokhiyev, V. B., V. V. Droblenkov. Stability of laminar boundary layer on elastic plate in different boundary conditions (in Russ.). In *Soprotivlenije dvizheniju i morekhodnost' sudov l: Sudostrojenije*. 89 pp.

Anisimova, T. N. *Bionika. Bibliograficheskii ukazatel otechestvennoy i inostrannoy literatury* (in Russ.). 1958-1968. Nauka, Moscow. 168 pp.

Anokhin, Yu. S. (1965). Measurement and registration of moment values of pressure inside the liquid flow (in Russ.). *Meteorologija i gidrologija* **12**: 52-55.

Anokhin, Yu. S. (1965). Measurement of moment values of liquid flow rate electronic lamps with mechanical control (in Russ.). *Izmeritelnaja tekhnika* **8**: 11-12.

Antonov, A. N., E. N. Bondarev. (1968). Approxmative calculation method of turbulent boundary layer under conditions of positive pressure gradient (in Russ.). *Mekhanika zhidkosti i gaza* **1**:

Antoniuk, R. A. (1975). Experimental studies of the velocity profile inside the boundary layer on the partly moving surfase (in Russ.). *Gidromekhanika. Respublikanskii mezhwedomstwenniy sbornik*. Naukova dumka: 87-89.

Aphonin, A., V. Grebennikov., V. Kayan., A. Schiptsov. (1996). Electric drive of underwater robots hydrobionic propulsers (in Russ.). In 2 *International scientific and technical conference on unconventional electromechanical and electrotechnical systems*. Szczecin and Miedzyzdroje, Poland.

A. s. 413286 (SSSR) Damping cover (in Russ.). Babenko V. V., Kozlov L. F., Pershin S. V. - (1974). - Opublikovano v Bull. izobret.

A. s. 483538 (SSSR) Damping cover (in Russ.). Babenko V. V., Kozlov L. F., Korobov V. I. – (1975). - Opublikovano v Bull. izobret.

A. s. 597866 (SSSR) Regulated damping cover (in Russ.). Babenko V. V., Kozlov L. F., Korobov V. I. – (1975). - Opublikovano v Bull. izobret. - 1978. - **10**.

A. s. 607145 (SSSR) Liquid an gaz flow Speed gauge (in Russ.). E. V. Romanenko. – (1978). - Opublikovano v Bull. izobret.

A. s. 592671 B63H19/02 Ship wave propulsor (in Russ.). Yu. F. Sen'kin. - Published 04.09.79 Bull. Izobret. **6**.

A. s. 1516424 SSSR MKI B63N Method of regulation of propulsion in ship flapping propulsor (in Russ.). A. A. Afonin, A. M. Burdenko, V. N. Glushko et al. Otkrytiya. Izobretenya. – (1989). - **39**..25.

A. s. 1615051 SSSR, MKI B63H / Method of regulation of propulsion in flapping propulsor (in Russ.). V.N.Glushko, V.P.Kayan et al. Otkrytya. Izobretenya. – (1989). - **47**. - 28.

Atlas of marine mammals of the USSR (in Russ.). (1980). Pischevaya promyshlennost'. 183 p.

Au, D., D. Weihs. (1980). At high speed dolphins save energy by leaping. *Nature* **284**: 548-550.

Babenko, V. V. (1967). Methods of speed measurement in the boundary layer of viscous liquid (in Russ.). *Gidrodinamika bol'shikh skorostej* 3. Naukova dumka, Kiev.

Babenko, V. V. (1971a). Main characteristics of flexible covers and similarity criteria (in Russ.). *Bionika* **5**: 73-76.

Babenko, V. V. (1971b). Some mechanical characteristics of dolphins skin (in Russ.). *Bionika* **5**: 76-81.

Babenko, V. V. (1973a). Methods of definition of mechanical properties and the criteria for flexible covers construction choice (in Russ.). *Bionika* **7**: 71-79.

Babenko, V. V. (1973b). Experimental study of hydrodynamic stability of the streamline of simple membrane surfaces (in Russ.). *Gidromekhanika* **24**. Naukova dumka, Kiev.

Babenko, V. V. (1974). Experimental study of hydrodynamic stability of the streamline of complex membrane surfaces (in Russ.). *Bionika* **8**: 9-13.

Babenko, V. V. (1976). Experimental study of perturbance motion in laminar boundary layer with the streamline of damping surfaces (in Russ.). Bionika **10**: 40-46.

Babenko, V. V. (1978). Turbulence development in the streamlined elastic plate (in Russ.). *Bionika* **12**: 33-40.

Babenko, V. V. (1979). Study of the skin elasticity in live dolphins (in Russ.). *Bionika* **13**: 43-52.

Babenko, V. V. (1980a). On alternating mass of dolphins' skin (in Russ.). *Bionika* **14**: 57-64.

Babenko, V. V. (1980b). To the interaction of a flow with the elastic surface (in Russ.). In *Mechanics of turbulent flows*. Nauka, Moscow. 292-300.

Babenko, V. V. (1981). To the methods of experimental studies on hydrobionics (in Russ.). *Bionika* **15**: 88-98.

Babenko, V. V. (1983). Some peculiarities of the thermoregulation of outer covers of animals (in Russ.). *Bionika* **17**: 35-39.

Babenko, V. V. (1992). On interaction of hydrobionts with a flow (in Russ.). *Bionika* **25**: 1-11.

Babenko, V. V. (1995). Methods of control of the coherent vortex structure in the boundary layer of hydrobiont (in Russ.). *Tez. dokl. Mezhd.konfer. «Plavanie i polet v prirode i tehnike AQUAPROP'95» S-Peterburg, SPbGMTU.*

Babenko, V. V., N. A. Gnitetskij., L. F. Kozlov. (1969). Preliminary results of the investigation of elastic properties of live dolphins' skin (in Russ.). *Bionika* **3**: 12-19.

Babenko, V. V., N. A. Gnitetskij., L. F. Kozlov. (1970). Preliminary results of the investigation of temperature distribution on the surface of dolphin's body (in Russ.). *Bionika* **4**: 83-88.

Babenko, V. V., N. A. Gnitetskij, L. F. Kozlov. (1972). Hydrodynamic stand with little turbulence, apparatus and methods of carrying-off the investigations on laminar boundary layer stability (in Russ.). *Bionika* **6**: 84-90.

Babenko, V. V., L. F. Kozlov. (1972). Experimental study of hydrodynamic stability of the laminar boundary layer on elastically damping surface in water flow (in Russ.). *Bionika* **6**: 22-24.

Babenko, V. V., L. F. Kozlov. (1973a). Experimental study of the amplitude behaviour during perturbing motion in the laminar boundary layer (in Russ.). *Gidromekhanika* **23**. Naukova dumka, Kiev.

Babenko, V. V., L. F. Kozlov. (1973b). Experimental studies of hydrodynamic stability on rigid and elastic damping surfaces (in Russ.). *Izv. AN SSSR. Mekhanika Zhidkosti i gaza* **1**: 122-127.

Babenko, V. V., L. F. Kozlov., S. V. Pershin. (1972). On the alternate damping of dolphins' skin in different swimming speeds (in Russ.). *Bionika* **6**: 42-52.

Babenko, V. V., L. F. Kozlov., S. V. Pershin, A. G. Tomilin. (1982). Self-regulation of skin damping in Cetaceans during active swimming (in Russ.). *Bionika* **16**: 3-14.

Babenko, V. V., A. P. Koval'. (1982). Hydrodynamic functions of swordfish gill system. *Bionika* **16**: 11-15.

Babenko, V. V., A. P. Koval'. (1989). On hydrodynamic properties of the skin of aquatic animals (in Russ.). *Bionika* **23**: 38-42.

Babenko, V. V., O. D. Nikishova. (1976). Some hydrodynamic regularities of skin morphiligy in marine animals (in Russ.). *Bionika* **10**: 27-33.

Babenko, V. V., R. M. Surkina. (1969). Some hydrodynamic peculiarities of dolphins' swimming (in Russ.). *Bionika* **3**: 19-26.

Babenko, V. V., R. M. Surkina. (1971). Definition of parameters of oscillating skin masse in some marine animals (in Russ.). *Bionika* **5**: 94-98.

Babenko, V. V., G. A Voropajev, N. F. Yurchenko. (1980). To the problem of simulation of interaction of outer covers of aquatic animals with the boundary layer (in Russ.). *Gidromekhanika* **42**: 73-81.

Babenko, V. V., N. F. Yurchenko. (1980). . Experimental studies of the stability of Gortler on the rigid and elastic plates (in Russ.). *Gidromekhanika* **41**: 103-108.

Badry, Narayanan M. A., V. J. Ramjee. (1968). Reverse transition from tunrbulent to laminar boundary-layer in a highly accelerated flow. *J. Fluid Mech.* **31**:

Baier, R., M. Meenaghan, J. Wirth, H. Gucinski, S. Nakeeb. (1984). Porpoise and killer whale skin as natural examples of low drag. low adhesion biomaterial surfaces. *Trans. World Congr. Biomater., 2nd, Washington, D.C.,* 7: 190, San Antonio. Tcx: Soc. Biomater.

Bainbridge, R. (1958a). The locomotion of fish. *New Sci.* **4**: 476-478.

Bainbridge, R. (1958b). The speed of swimming of fish as related to size and to the frequency and amplitude of the tail beat. *J. Exp. Biol.* **35**: 109-133

Bainbridge, R. (1960). Speed and stamina in three fish. *J. Exp. Biol.* **37**: 129-153.

Bainbridge, R. (1961). Problems of fish locomotion. In: *Vertebrate Locomotion.- Symp. Zool. Soc. lond.* **5**: 13-32.

Bainbridge, R. (1962). Training, speed and stamina in truot. *J. Exp. Biol.* **39**: 537-555.

Bainbridge, R. (1963). Candal fin and body movements in the propulsion of somefish. *J. Exp. Biol.* **40**: 23—56.

Bainbridge, R., R. H. J. Brovun. (1958). An apparatus for the study of the locomotion of fish. *J. Exp. Biol.* **35**: 134-137.

Bandyopadhyay, P. R. (1988). Viscous drag reduction of a nose body. *AIAA Journ.* **27**: 274-282.

Bandyopadhyay, P. R (1989). Convex curvature concept of viscous drag reduction. In: *Viscous drag reduction in boundary layer*, ed. Dennis M. Bushnell, Jerry N Hefner. NASA Langley Research Center Hampton, Virginia. Progress in astronautics and aeronautics, 123, Editor-in Chief A. Richard Seebass, University of Colorado at Boulder, Boulder, Colorado. Publ. By the American Institut of Aeronautics and Astronautics, Washington: 285-324.

Bandyopadhyay, P. R., A. Ahmed. (1993). Turbulent boundary layers subjected to multiple, curvatures and pressure gradients. *J. Fluid Mech.* **246**: 503-527.

Bannasch, R. (1993). Drag minimisation on bodies of revolution in nature and engineering. In *Proc. Of International Airship-Conference*, Stuttgart: 79-87.

Bannasch, R. (1994a). Mechanismen der biologischen Formgebung - neue Ergebnisse der bionischen Forschung an Meerestieren. In *LUFTSCHIFF - KOLLOQUIUM II. Lighter Than Air Flight Systems.* Schlos Lubbenau / Spreewald.. Tagungsunterlagen – Proceedings: 1-6.

Bannasch, R. (1994b). Functional anatomy of the «flight» apparatus in penguins. In *Mechanics and physiology of animal swimming* (ed.: Linda Maddock, Quentin Bone and Jeremy M.V. Rayner), Cambridge University Press: 163-197.

Bannasch, R. (1997). Experimental investigations on the boundary layer developement in swimming penguins: mechanisms of drag reduction and turbulence control. In *Book of abstracts. 10 European drag reduction working meeting*. Berlin.

Bannasch, R., R. P. Wilson, B. Culik. (1994). Hydrodynamic aspects of design and attachment of a back-mounted device in penguins. *J. Exp. Biol.* **194**: 83-96.

Barger, I. A., W. A. Von Winkle. (1961). Evaluation of a boundary layer stabiliza
tion coating. *JASA* **33**: 836.

Barstow, L. (1939). *Applied Aerodynamics*. Longmans. Green and Co. London-New York-Toronto.

Barsukov, V. V. (1960). Swimming velocity in fish (in Russ.). *Priroda* **3**: 103-104.

Barsukov, V. V. (1969). For which purpose fish scales (in Russ.). *Priroda* **4**:

Beamish, F. W. (1970). Oxygen consumption of largemouth bass, *Micropterus salmoideus*, in relation to swimming speed and temperature. *Canad. J. Zool.* **48**: 1221-1228.

Bechert, D. W., Bartenwerfer, M., Hoppe. G.. Reif, W.-E. (1986). Drag reduction mechanisms derived from shark skin. Presented at 15th Congr. Int. Counc. Aeronaut. Sci.., London

Belen'kij, Ya. E., S. M. Kidun. (1968). Small economical gauge for simultaneous measurement of depth and speed (in Russ.). In *Avtomatizatsiya nauchnykh issledovanij morej i okeanov.- Report theses. Simposium*. Sevastopol.

Belinsky, V. G., B. P. Ivanishin., V. A. Kochin., V. V. Moroz. (1992). On the resistance coefficient in easily streamlined corps in acceleration-braking regimes (in Russ.). *Bionika* **25**: 46-50.

Belotserkovsky, S. M., B. K. Skripatch, V. G. Tabatchnikov. (1971). *Wing inside unsteady gas flow* (in Russ.). Nauka, Moscow: 767 pp.

Belyaev, V. V. (1969). Geometric characteristics of the body shape of the Black sea dolphins (in Russ.). In *Vopr. morsk. biologii*. Naukova dumka, Kiev. 12-14.

Belyaev, V. V., R. A. Grundfest. (1974). Wave propulsor as a propulsive system (in Russ.). In *Izv. Sev.-Kavk. nauchn. Tsentra vysshei shkoly. Estestvennyje nauki* **4**: 18-23.

Belyaev, V. V., G. V. Zuev. (1969). Hydrodynamic hypothesis for shaping fish school (in Russ.). *Voprosy ikhtiol.* **9**: 716-725.

Belyaev, V. V., G. V. Zuev. (1969). Hydrodynamics of school swimming (in Russ.). *Vses. konf. molodykh uchenykh Polyarn. Nauchno-issled. I proektnogo Instituta morskogo rybnogo khosaystva i okeanografii*. Murmansk: 54-69.

Belyaev, V. V., A. P. Koval'. (1972). On the question of hydrodynamic function of mucus of some bony fishes (in Russ.). *Bionika* **6**: 78-83.

Bendat, D., A. Pirsol. (1974). *Measurements and analysis for accidental processe* (in Russ.). MIR, Leningrad: 464 pp.

Biological telemetry (in Russ.). (1971). (Ed. V.V. Parin.) Medizina. Moscow: 264 pp.

Bilo, D., W. Nachtigall. (1980). A simple method to determine drag coefficients in aquatic animals. *J. Exp. Biol.* **87**: 357-359.

Blake, J. R. (1971). Infinite models for ciliary propulsion. *J. Fluid Mech.*, **49**: 209-222.

Blaxier, J. S. (1969). Swimming speeds of fish. *FAO fish. Repts.* **29**: 69-100.

Bolotin, A. F. (1984). On influence of character of shark flow over on propulsive quality of propulsor (in Russ.). *Bionika* **18**: 36-40.

Bone, Q. (1972). Buoyancy and hydrodynamic functions of inlegument in the castor oil fish. *Ruvettus pretiosus* (Pisces: Gempylidae). *Copeia* **1**: 78-87

Bone, Q. (1975). Muscular and energetic aspects of fish swimming. In *Swimming and Flying in Nature*, eds. Th. Wu, Ch. Brokaw, Cn. Bremer. Plenum Press, New York: 493-528.

Bonthron, R. J., A. A. Fejer. (1962). A hydrodynamic study of fish locomotion. In *Proc. 4th U.S. Nat. Congr. Appl. Mech.*, Berkeley, Califirnia: 1249-1255.

Bose, N., J. Lien (1989) Propulsion of a fin whale (*Balaenoptera physalus*): why the fin whale is a fast swimmer. *Proceedings of the Royal Society of London* **B 237**: 175-200.

Bose, N., J. Lien. (1990). Energy absorption from ocean waves: a free ride for Cetaseans. *Proc. R. Soc. Lond.* **B 240**: 591-605.

Bose, N., J. Lien, J. Ahia. (1990). Measurements of the bodies and flukes of several cetacean species. *Proc. R. Soc. Lond.* **B 242**: 163-173.

Breder, C. M. Jr. (1965). Vortices and fish schools. *Zoologica* (USA) **50**: 97-114.

Brett, J. R. (1963). The energy required for swimming by young sockeye salmon with a comparison of the drag force on a dead fish. *Trans. Roy. Soc. Canada*, ser. **4**.: 441-457.

Brett J. R. (1964). The respiratory metabolism and swimming performance of young sockeye Salmon. *J. Fish. Res. Board Canada* **5**: 5.

Brett, J. R. (1965a). The relation of size to rate of oxygen consumption and sustained swimming speed of sockeye salmon (*Oncorhynchus nerka*). *J. Fish. Res.*, Bd. Canada. **22**: 1491-1501.

Brett, J. R. (1965b). The swimming energetics of salmon. *Scient. Amer.* **213**: 80-85.

Brett, J. R. (1971). Energetic responses of salmon to temperature. A study of some thermal relathions in the physiology and freshwater ecology of sockeye salmon (*Oncorhynchus nerka*). *Amer. Zoologist* **11**: 99-113.

Brokaw, C. J. (1970). Bending moments in free-swimming flagella. *J. Exp. Bioi.* **53**: 445-464.

Brown, A. W. (1965). The dolphins: «Like an arrow they fly through the sea». *US Naval Inst. Proc.* **91**: 42.

Brown, A. W., A. S. Muir (1970). Analisis of ram ventilation of fish gills with appli
cation to skipjack tune (*Katsuwonus pelamis*). *J. Fish. Res. Bd. Canada.* **27**: 1637-1652.

Buguslavskaya, S. N., E. V. Romanenko. (1968). On the thermodynamic and wave correction in pistonphon method (in Russ.). *Tez. dokl. 6 Vses. akust. Konf.* Moscow.

Burdak, V. D. (1968a). On the function of fish ctenoid scale (in Russ.). *Zool. Zhurn.* **47**: 732-738.

Burdak, V. D. (1968b). On the function of fish ctenoid scale in condition of turbulent boundary layer (in Russ.). *Zool. Zhurn.* **48**: 1053-1055.

Burdak, V. D. (1969). Ontogenetic evolution of scale of grey mullet (Migil saliens) (in Russ.). *Zool. Zhurn.* **48**: 242-248.

Burdak, V. D. (1970). On the relationship between hydrodynamic functions of cycloid ctenoid scale of fish (in Russ.). *Zool. Zhurn.* **49**: 868-871.

Burdak, V. D. (1972). On the hydrodynamic function of cycloid scale of fish (in Russ.). *Zool. Zhurn.* **51,** 1086-1089.

Burdak, V. D. (1973a). On the hydrodynamic function of fish scale (in Russ.). In *4 Vses. konf. po bionike 6. Biomekhanika. Izd. AN SSSR*, Moscow: 31-34.

Burdak, V. D. (1973b). Scale types as stages of historical evolution of hydrodynamic function of fish scale (in Russ.). *Zool. Zhurn.* **52,** 1208-1213.

Burdak, V. D. (1979). *Functional morphology of fish scal* (in Russ.). Naukova dumka, Kiev: 163 pp.

Bukhanevitch, I. B. (1969). An novative data about fish swimming velocity (in Russ.). *Rybnoe khozyaistvo* **10**, 9-10.

Burlakov, V. D., Zh. Ya. Grushanskaja., V. E. Sokolov. (1977). Geometric properties of bodies ant theoretical drawings of two species of the Black sea dolphins in connection with their hydrodynamic characteristics (in Russ.). *Bull. Mosk. obschestva ispytatelej prirody. Otdel biologii* 82(2): 62-66.

Bushnell, D. M.. J. N. Hefner, R. L. Ash. (1977). Effects of compliant wall motion on turbulent boundary layers. *Phys. Fluids* **10,** 31-48

Bushnell, D. M., K. J. Moore (1991). Drag reduction in nature. *Annu. Rev. Fluid Mech.*, **23**, 65-79.

Chaykovskaya, A. V. (1974). On the aminoacid composition of mucus of some species of the Black Sea fish (in Russ.). *Bionika* **8**, 145-148.

Chaykovskaya, A. V., E. T. Uskova, S. I. Davidenko, N. M. Belova. (1983). On the question of fish mucus variation during transition mucus from cell to solution (in Russ.). *Gidrodinamicheskie voprosy bioniki.* Naukova dumka. Kiev.

Chepurnov, A. V. (1968a). Swimming velocity and some peculiarity of outer whales texture (in Russ.). *Issledovaniya po bionike.* Naukova dumka. Kiev.

Chepurnov, A. V. (1968b). Body shape of some Cetaceans in connection with their swimming velocity (in Russ.). *Mekhanizmy peredvizheniya i orientatsii zhivotnikh.* Naukova dumka. Kiev.

Chepurnov, A. V., V. V. Ovchinnikov. (1967). Swimming velocity of marine animals (in Russ.). *Priroda* **4**, 59-63.

Cherkai, A. V. (1995). Study of use of longitudinal riblets as method of drag reduction (in Russ.). In *Plavanie i polet v prirode i tekhnike AQUAPROP'95. Tez. dokl. Mezhd. Konf.* S.-Peterburg, SPbGMTU.

Cherny, G. G. (1973). Boundary layer on the plate with moving surface (in Russ.). *DAN SSSR* **213**, 802-803.

Chernyschev, O. B., V. A. Zaets. (1974a). Some peculiarity of skin texture of shark (in Russ.). *Bionika* **4**, 77-83.

Chernyschev, O. B., V. A. Zaets. (1974b). Dependence of keels variation of shark placoid scale on swimming velocity (in Russ.). *Bionika* **8**, 82-86.

Chernyschev, O. B., A. P. Koval'. (1974). Peculiarity of corset texture and scale corsets of scombroid fish (in Russ.). *Bionika* **8**, 86-88.

Chestnoy, V. N. (1961). Maximum velocities of fish swimming (in Russ.). *Rybnoe khozaistvo* **9**, 22-27.

Chopra, M. G. (1974). Hydromechanics of lunate-tail swimming propulsion. *J. Fluid Mech.* **64**, 375—391.

Chopra, M. G. (1975). Lunate-tail swimming propulsion. In *Swimming and fiving in nature,* ed. T. Wu, C.J.Brokaw, and C.Brennan. Plenum press, New York: 635-650.

Chopra, M. G. (1976). Large amplitude lunate-tail theory of fish locomotion. *J. Fluid Mech.* 74, 161—182.

Chopra, M. G., T. Kambe. (1977). Hydromechanics of lunate-tail swimming propulsion. Pt 2. *J. Fluid Mech.* **79**, 49—69.

Clinch, A. Y. (1966). Miniature transducer assembly for measuring the properties ofthe wall-pressure field in turbulent flows. *JASA* **40**, 254.

Coche, R. (1975). The swimming of slender fish-like bodies in waves. In: *Swimming and flighing in nature*. **2**, 673-686.

Coene, R. (1975). The swimming of slender fish-like bodies in waves. In *Swimming and flying in nature* 2, ed. T.Y.Wu, C.J.Brokaw, and C.Brennan. Plenum, New York:673-686.

Cone. C. D. Jr. (1962). The theory of induced lift and minimum induced drag of nonplanar lifting systems. *NASA TR-139*

Cox, R. G. (1970). The motion of long slender bodies in a viscous fluid. Part 1. General theory. *J. Fluid Mech.* **44,** 791-810.

Culik, B., R. P. Wilson, R. Bannasch. (1993). Flipper-bands on penguins: what is the cost of a life-long commitment? *Mar. Ecol. Prog.* **98**, 209-214.

Culik, B., R. Bannasch., R. P. Wilson. (1994). External devices on penguins: how important is shape? *Marine Biology.* **118**, 353-357.

Curren, K. (1992). Designs for swimming: morphometrics and swimming dynamics of several cetacean species. *M. Sc. Thesis, Memorial University of Newfoundland*, St. John's, Newfoundland.

Cutchen C. W. Mc. (1970). The trout tail fin: a self - cambering hydrofoil. *J. Biomech.* **3**, 271-281.

Dam, C. P. (1987). Efficiency characteristics of crescent-shaped wings and caudal fins. *Nature* **325,** 435-437.

Dargolts, V. G., E. V. Romanenko, V. E. Sokolov. (1978). Oxygen expenses in the skin of dolphins and the problem of skin respiration in Cetaceans (in Russ.). *Zool. Zh.* **57**, 768-775.

Dargolts, V. G., E. V. Romanenko, V. E. Sokolov, E. A. Yumatov., V. G. Janov. (1978). Telemetric measurments of blood pressure in dolphins (in Russ.). In *7 Vsesoyuznaya konferentsya po morskim mlekopitayuschim. Report Theses*. Simferopol.

Dargolts, V. G., E. V. Romanenko, E. A. Yumatov, V. G. Yanov. (1981). Methods of telemetric registration of dynamics of blood pressure and respiration in free-swimming dolphins (in Russ.). *Fiziol. Zh.* **67,** 1744-1748.

Debye, P. (1933). A method for the determination of the mass of electrolytic ions. *Chem. Phys.* **1** 13-16.

Dombrov, B. M., E. D. Sorokodum. (1978). On kinematics of curvatory of oscillating plate (in Russ.). *Bionika* **12**, 62-67.

Donohae, G. L., W. G. Tiederman, M. M. Reischman. (1972). Flow visualisation of the near-wall region in a drag-reduction channal flow. *J. Fluid Mech.* **56** 559-575.

Dovgij, S. A., V. P. Kajan. (1981). To the methods of definition of propulsive force from developed by the oscillating wing (in Russ.). *Bionika* **15** 55-59.

Dovgii, A. S., O. V. Kopeyka. (1995). Systems if oscillating wings (in Russ.). In *Plavanie i polet v prirode i tekhnike AQUAPROP'95. Tez. dokl. Mezhd. Konf.* S.-Peterburg, SPbGMTU.

Dovgii, A. S., A. V. Shekhovtsov. (1995). Best regimes of operation of wing propulsor (in Russ.). In *Plavanie i polet v prirode i tekhnike AQUAPROP'95. Tez. dokl. Mezhd. Konf.* S.-Peterburg, SPbGMTU.

Dovgii, A. S., A. V. Shekhovtsov. (1995). On the contribution of different forces dolphin's flukes – generated (in Russ.). In *Plavanie i polet v prirode i tekhnike AQUAPROP'95. Tez. dokl. Mezhd. Konf.* S.-Peterburg, SPbGMTU.

Dyumarg, P. (1970). Method of measurements of pressure pulsation in indignant liquid (in Russ.). *Prikladnaya mekhanika* **37**.

DuBois, A. B., G. A. Cavagna, R. S. Fox. (1974a). Pressure distribution on body surface of swimming fish. *J. Exp. Biol.* **60** 581-591.

DuBois, A. B., G. A. Cavagna, R. S. Fox. (1974b). The forces resisting locomotion in bluefish. In: *Swimming and flying in Nature*, Symp. Pap. Abstr. Pasadena, Calif.: 43.

DuBois, A. B., G. A. Cavagna, R. S. Fox. (1975). The forces resisting locomotion in bluefish. In: *Swimming and flying in Nature*, eds. Th. Wu, Ch. Brokaw, Cn. Bremer. Plenum Press, New York: 541-551.

Dubrovin, A. P., L. F. Kozlov. (1974). Use of photogrammetry in investigations of dolphins kinematics (in Russ.). *Gidrobiologicheskij zh.* **2** 124-126.

Dubrovin, A. P., L. F. Kozlov. (1975). Use of stereo photography for the study of dolphins kinematics (in Russ.). *Bionika* **9** 33-36.

Egidis, B. M. (1964). *Study of turbulence of water flow by dynamic methods* (in Russ.). Kand. Diss. Kiev.

Egidis, B. M., V. M. Shakalo. (1971). Use of electrolythic microrotator for the measurement of flow rate of sea water (in Russ.). *Bionika* **5** 128-131.

Ellis, H. D. (1970). Effects of shear treatment on drag-reducing polimer solutionsand fibre suspension. *Nature* **226**, 352-353.

Eskinasi, S. (1958). Turbulence measurement in electrically conducting Fluids. *The Phys. of Fluids* **1**.

Essapian, F. S. (1955). Speed-induced skin folds in the bottle-nosed porpoise *Tursiops truncatus. Breviora. Museum of Comparative Zoology*. Cambrage, Mass. **43** 1-4.

Faddeev, Yu. I., V. M. Zhurava. (1969). Equations of laminar boundary layer on deformed body of revolution (in Russ.) *Bionika* **3**, 40-46.

Faddeev, Yu. I., V. M. Zhurava, B. P. Kovalenko. (1969). Calculation of potential liquid flow induced by forward movement of deformed body of revolution (in Russ.) *Bionika* **3**, 34-40.

Fierstine, H. L., V. Walters. (1968). Studies in locomotion and anatomy of sifishes. *Mem. South. Calif. Acad. Sci.* **6**, 1-31.

Filimonov, V. Ya., V. V. Sitnikov. (1966). Method of measurement of flow regime and turbulent pulsations in boundary layer of water flow (in Russ.) *Avtorskoe svidetel'stvo na isobretenie* N 203334.

Filimonov, V. Ya., V. V. Sitnikov, V. A. Selyutin. (1966). Equipment for measuring of flow regime and turbulent pulsations in boundary layer of water flow (in Russ.) *Avtorskoe svidetel'stvo na isobretenie* N 206925.

Fish, F. E. (1992). Aquatic locomotion., In: *Mammalian energetics: Interdisciplinary views of metabolism and reproduction* (T. E. Tomasi and T. H. Horton, eds.). Cornell University Press, Ithaca: 34-63.

Fish, F. E. (1993a). Power output and propulsive efficiency of swimming bottlenose dolphins (*Tursiops truncatus). J. exp. Biol.* **185**, 179-193.

Fish, F. E. (1993b). Influence of hydrodynamic design and propulsive mode on mammalian swimming energetics. *Aust. J. Zool.* **42**, 79-101.

Fish, F. E. and C. A. Hui,. (1991). Dolphin swimming - a review. *Mamm. Rev.* **21**, 181 - 195.

Fish, F. E. and J. J. Rohr. (1999). Review of dolphin hydrodynamics and swimming performance. Technical report 1801. SSC San Diego.137 pp.

Foche, H. (1965). The cause for high swimming speeds of dolphins. *Z. Fluschaft* **13**, 54-61.

Fong, M. L., R. M. Yamada, W. A. Friedl. (1989). Post exercices skin temperature and heat flux of atlantic bottlenose dolphins (*Tursiops truncatus*). In *Abstracts of the eighth biennial conference on the biology of marine mammals, Sos. for marine mammalogy.* Pacific grove, Califirnia..

Friedl, W. A., R. M. Yamada, M. L. Fong, J. E. Haun. (1987).Physical conditioning of bottlenose dolphins for bioenergetic studies. In *Abstracts of the seventh biennial conference on the biology of marine mammals, Sos. for marine mammalogy.* Miami, Florida.

Friedl, W. A., J. E. Haun, M. L. Fong, R.M. Yamada. (1989). Aerobic exercise by bottlenose dolphins. In *Abstracts of the eighth biennial conference on the biology of marine mammals, Sos. for marine mammalogy.* Pacific grove, Califirnia.

Fry, F. E. G., J. S.Hart. (1948). Cruising speed of goldfish in relation to water temperature. J. *Fish. Res. Bd. Can.* **8**, 169-175.

Gadd, G. E. (1965). Turbulence damping and drag reduction produced byadditives in water. *Nature* **206**, 463-467.

Ganiev, R. F., L. E. Ukrainsky, A. I. Telalov, V. M. Mendelutsa. (1980). Experimental study of liquid flow in tubes with pliable walls (in Russ.). *Bionika* **14**, 46-50.

Gans, C. How snakes move. (1970). *Scientific American.* **222**, 82-150.

Gazley, C. (1975). Laminar boundary-layer development and transition of fish-shaped bodies of revolution. In *Swimming and flying in nature* 2, ed. T.Y.Wu, C.J.Brokaw, and C.Brennan. Plenum, New York: 651-652.

Geib, F. E. (1966). Measurements on the effect of transducer size on the resolution of boundary-layer pressure fluctuations. *Pr. 72 meet. ASA. JASA* **40**, 1247.

Gero, D. R, (1952a). Power and Efficiency of Large Salt Water Fish. *Aeron.Engineering Rev.*, **1**, 10-15.

Gero, D. R. (1952b). The hydrodynamic aspects of fish propulsion. *Amer.Novit.*, 1601.

Gilchrist, R. B., W. A. Strawderman. (1965). Experimental hydrophon-size cornfactor for boundary-layer pressure fluctuation. *JASA,* **38,** 298-302.

Glushko, V. N., V. P. Kayan. (1992). Experimental study of hydrodynamics of a rigid oscillating wing (in Russ.). *Bionika* **25**, 71-75.

Glushko, V. N., V. P. Kayan, L. F. Kozlov. (1984). Hydrodynamic characteristics of rectangular oscillating wing (in Russ.). *Bionika* **18**, 40-44.

Glushko, V. N., V. P. Kayan, L. F. Kozlov. (1986a). Influence of elastic fitting on hydrodynamic characteristics of a rigid swaying wing (in Russ.). In *Matematicheskye metody mekhaniki zhidkosti i gaza*. DGU, Dnepropetrovsk: 30-32.

Glushko, V. N., V. P. Kayan, L. F. Kozlov. (1986b). Study of hydrodynamics of oscillating wing with a rigid and passively-deformed profile (in Russ.). In *Matematicheskye metody mekhaniki zhidkosti i gaza*. DGU, Dnepropetrovsk: 21-29.

Glushko, V. N., V. P. Kayan, L. F. Kozlov. (1990). On the hydrodynamic efficiency of a flapping propulsor (in Russ.). In *Nelinejnye zadachi gidromechaniki i teorii uprugocti*. DGU, Dnepropetrovsk: 31-40.

Glushko, V. N., V. P. Kayan, V. A. Kochin. (1992). On the optimization of propulsive characteristics of a flapping propulsor (in Russ.). *Bionika* **25**, 75-80.

Glushko, V. N., A. I. Tsiganyuk, A. I. Velyavtsev. (1995). Influence of marine choppiness on the thrust generated by the propulsor of «waving wing» type (in Russ.). In *Plavanie i polet v prirode i tekhnike AQUAPROP'95. Tez. dokl. Mezhd. Konf. S.-Peterburg, SPbGMTU.*

Gmurman, V. E. (1963). *Introduction to the theory of probability and mathematical statistics* (in Russ.). Vyschaya schkola, Moscow: 240 pp.

Goforth, H. W., Jr. (1990). Ergometry (Exercise Testing) of the Bottlenose Dolphin. In *The Bottlenose Dolphin*. Academic Press, Inc.: 559-574.

Gogolev, V. A., A. P. Dubravin., L. F. Kozlov., N. K. Maslov., V. D. Sorokina. (1976). Application of cineregistration for investigating the parameters of swimming of aquatic animals in the horizontal plane (in Russ.). *Bionika* **10,** 75-80.

Goldsmith, W. (1970). Biomechanical activities of some American and European institutions. *J. Biomech.* 3: 125-129.

Golubev, V. V. (1957). Propulsive force of the flapping wing (in Russ.). In *Trudy po aerodinamike*. Gostekhizdat, Moscow. 399-576.

Goodman, W. L., F. G. Howard. (1985). Axisymmetric bluff-body drag reduction through geometrical modilications. *J. Aircr.* **22,** 516 22

Gordon, P. V., V. A. Ryzhov. (1995). Mathematical model of springing oscillating wing used as propulsor (in Russ.). In *Plavanie i polet v prirode i tekhnike AQUAPROP'95. Tez. dokl. Mezhd. Konf.* S.-Peterburg, SPbGMTU.

Gorelov, D. N. (1975). Theory of a wing in the non-stationary flow (in Russ.). *Novosibirsky Universitet*, Novosibirsk. 152 pp.

Gorelov, D. N. (1976). On the effectiveness of the flapping wing as a propulsor (in Russ.). *Bionika* **10,** 49-53.

Gorelov, D. N. (1980a). To finding of best law of wing oscillation used as propulsor (in Russ.). *Izv. Sibir. otdelen. AN SSSR. Ser. tekhn. nauki.* 3: 12-17.

Gorelov, D. N. (1980b.) Experimantal study of a flapping wing (in Russ.). *Bionika* **14**, 42-45.

Gorelov, D. N. (1991). Propulsive characteristics of a flapping wing with an elastically fixed eleron (in Russ.). *Bionika* **24**, 18-24.

Gorelov, D. N., R. L. Kulyaev. (1971). Nonlinear problem on unsteady flow over of thin wing by incompressible fluid (in Russ.). *Izv. AN SSSR. Mekhan. Zhidkosty i gasa* **6**, 38-49.

Gould, R. K., W. L. Nyborg. (1959). Imbedded thermistor for boundary layer measurements. *JASA*, **31**, 249-250.

Gray, J. (1933a). Studies in animal locomotion. III. The propulsive mechanism of the Whiting. *J. Exp. Biology* **10**, 391-400.

Gray, J. (1933b). Studies of Animal Locomotion. *J. Exp. Biol.*, **10**, 88-103.

Gray, J. (1936). Studies of Animal Locomotion. VI. The Propulsiv Powers of the Dolphin. *J. Exp. Biol.*, **13,** 192-199.

Gray, J. (1948). Aspects of the locomotion of whales. *Nature* **4084**, 199-200.

Gray, J. (1953). *How animals move*. Cambridge.

Gray, J. (1957). How fishes swim. *Scient. Amer.*, **197,** 48-54.

Gray, J. (1961). *Animal Locomotion*.. Weidenfeld and Nicolson, Lond.. W **1**. 479 pp.

Gray, J. (1968). *Animal Locomotion*. Acad. Press. London.

Gray, J., H. W. Lissman. (1964). The locomotion of nematodes. *J. Exp. Biol.*, **41**, 135-154.

Grebeshov, E. P., O. A. Sagojan. (1976). Hydrodynamic characteristics of the oscillating wing using as a carrying surface and a propulsor (in Russ.). *Trudy TsAGI* **1725,** 3-30.

Grebeshov, E. P., E. P. Shakarvene. (1995). Method of drag reduction of ships at the cost of an energy of marine choppiness (in Russ.). In *Plavanie i polet v prirode i tekhnike AQUAPROP'95. Tez. dokl. Mezhd. Konf.* S.-Peterburg, SPbGMTU.

Greenway, Ph. (1965). Body form and behavioural types in fish. *Experientia*, **21**, 489-498.

Grillner, S. (1974). On the generation of locomotion in the spinal dogfish. *Exp. Brain Res.* **20**, 459-470.

Grillner, S., S. Kashin. (1976). On the generation and performance of swimming : fish. In: *Neural control of.locomotion*, ed. R. I. Herman et al. N. Y.; L Plenum press, 181—201.

Grossman, L. M., E. A. Shay. (1949). Turbulent velocity measurements. *Mech. Engn* **71**.

Grossman, L. M., A. E. Charwat. (1952). The measurements of turbulent velocit fluctuations by the method of electromagnetic induction. *Rev. Sci. Instrum* **23**.

Gruntfest, R. A. (1980). Refined theory of flow over of periodically oscillating small aspect ratio body (in Russ.). *Bionika* **14**: 26-34.

Gruntfest, R. A. (1995). Active oscillations of springing plate in fluid flow (in Russ.). In *Plavanie i polet v prirode i tekhnike AQUAPROP'95. Tez. dokl. Mezhd. Konf.* S.-Peterburg, SPbGMTU.

Gruntfest, R. A., N. P. Derezina. (1981). Oscillation of an elastic fin in a liquid flow (in Russ.). *Bionika* **15**, 29-39.

Gruntfest, R. A., N. P. Deresina. (1985). Spatial problem on oscillation of flipper with variable rigidity in fluid flow (in Russ.). *Bionika* **19**, 68-73.

Grushanskaya, Zh. Ya., N. A. Kol'tsova, A. I. Korotkin, (1995). Gray's paradox and involving problems of definition of dolphin's velocity, drag and power (in Russ.). In *Plavanie i polet v prirode i tekhnike AQUAPROP'95. Tez. dokl. Mezhd. Konf.* S.-Peterburg, SPbGMTU.

Grushanskaja, Zh. Ya., A. I. Korotkin. (1973). Several problems of dolphin's hydrodynamics (in Russ.). In *4 Vsesoyuznaya konf. po bionike. Report theses.* **6**, Moscow: 37-41.

Grushanskaya, Zh. Ya., A. I. Korotkin. (1985). Something problems in biological hydro- and aerodynamics (in Russ.). *Itogy nauki i tekhniki. Ser. Komplexnye i spetsial'nye razdely mekhaniki 1. VINITI,* Moscow: 143-229.

Grushanskaja, Zh. Ya., A. I. Korotkin, V.A. Tyushkevich. (1976). Investigation of a streamline and of hydrodynamic characteristics in rigid models of dolphin's fins. *Trudy Leningradskogo obschestva estestvoispytatelej* **73**, 42-52.

Gukhman, A. A., A. F. Gandelsman, G. K. Katsnelson, B. A. Kader, L. N. Naurits, V. V. Usanov. (1968). On the influence of large negative pressure gradients on the structure of turbulent flow (in Russ.). *Teplo- i massoperenos* 1. Energia, Moscow.

Guzeev, A. S. (1995). Pilot exploitation of finit span monoflipper (in Russ.). In *Plavanie i polet v prirode i tekhnike AQUAPROP'95. Tez. dokl. Mezhd. Konf.* S.-Peterburg, SPbGMTU.

Haider, M., D. B. Lindsley. (1964). Microvibrations in man and dolphin Science 146: 36-48.

Hall, D. D., M. E. Armstrong. (1969). An apparatus for quantitativly recording locomotor activity in fishes. *Tex. J. Sci.* **20**, 237-242.

Harrison, J. H. (1961). Fish propulsion. *Society of Automotiv Engineers*: 307.

Haun, J. E., E. W. Hendricks. (1988). Dolphin hydrodynamics. Physics news in 1987 - fluid dynamics. *Physics today*, , S. 39

Haun, J. E., E. W. Hendricks, F. R. Borkat, R. W. Kataoka, D. A. Carder, N. K. Chun. Dolphin hydrodynamics. *Annual report FY 82. Technical report* 935. (1983). Naval Ocean System Center, San Diego, California, 92152. 82 p.

Herald, E. S., R. L. Brownell, F. L. Frye, E. J. Morris, W. E. Evans, A. B. Scott (1969). Blind river dolphin: first sides-swimming cetacean. *Science* **166**, 1408-1410.

Hermans, I. I. (1938). Charged Colloid Particles in an Ultrasonic Field. *Philos. Mag.,* **25**, 26.

Hertel, H. (1966). *Structure-Form-Movement*. Reinhold Publ. Corp. N. Y. 258 pp.

Hertel, H. (1969). Hydrodynamics of swimming and wave-riding dolphins. In *The Biology of Marine Mammals*, ed. H. T. Andersen. Acad Press. N. Y.— Lond.

Hintse, I. O. (1963). *Turbulence*. GIFML. Moskva.

Hoyt, J. W. (1975). Hydrodynamic drag reduction due to fish slimes. *In Swimming and flying in nature* 2, ed. T.Y.Wu, C.J.Brokaw, and C.Brennan. Plenum Press, New York: 653-672.

Hoyt, J. W., A. G. Fabula. (1966). The effect of additives on fluid friction, Washington, D. C. *Office Naval Research. Dept. Navy:* 947-957.

Holst, E., D. Kuchemann. (1942). Biological and aerodynamical problems of animal flight. *J. Roy.Aero. Soc.* **46**(374): 39-56.

Hess, F., J. J. Videler. (1984). Fast continuous swimming of saithe (*Pollachius virens*): a dynamic analysis of bending moments and muscle power. *J. Exp. Biol.* **109**: 229-251.

Hui, C. (1987). Power and speed of swimming dolphins. *J. of Mammalogy*. **68**, 126-132.

Hunter, A. N., T. B. Jones. (1962). The Debye Effect in Electrolytes and Colloids. *Proc. Phys. Soc.* **80**, 795-797

Hydrobionics in shipbuilding (in Russ.). (1970). TsNIITEIS, Leningrad: 271 pp.

Ibragimova, L. M. (1985). Non-stationary hydrodynamic characteristics of a fine elastic profile (in Russ.). In *Gidridinamika bol'shikh skorostei*. Cheboksary: 55-59.

Ilgamov, M. A., M. M. Suleymanova, V. M. Taldykin, V. L. Fedyaev. (1978). On one model of wave propulsor (in Russ.). *Far-East Sci.Acad.* **241**, 309-311.

Investigations in bionika. 1965. Naukova dumka, Kiev. 115 p.

Investigations in bionics for purposes of increasing of ship velocity (in Russ.). (1968). Nauchno-tekhnich. obzory. TsNIITEIS.

Iohannesseil, C. L., J. A. Harder. (1960). Sustained swimming speed of dolphins. *Science* **132**, 1550-1551.

Ivchenko, V. M. (1962). Possibility of increasing of propulsive characteristics of ship (in Russ.). *Trudy TsNII akademika Krilova* 185.

Ivlev, Yu. P. (1972a). Investigation of turbulent air flow characteristics in a channel with elastic walls (in Russ.). *Bionika* **6**, 39-41.

Ivlev, Yu. P. (1972b). Stand for investigation of turbulent flow near elastic walls (in Russ.). *Bionika* **6**, 90-91.

Jones, D. R. (1971). Theoretical analysis of factors which may limit the maxirnun oxygen uptake of fish: the oxygen cost of the cardiac and branchial pumps.-*J.Theor. Biol.*, **32**, 341-349.

Kaduk B. G., N. A. Veryovka. (1971). On some electric properties of turbine magnetic speed gauge (in Russ.). *Bionika* **5**, 125-128.

Kalitkin, N. N. (1978). *Numerical methods* (in Russ.). Nauka. Moscow. 512 pp.

Kalugin, V. N. (1970). Study of stabilizing influence of interface elasticity on viscous liquid flow (in Russ.). *Trudy seminara "Raspredelennoe upravlenie processami v*

sploshnykh sredakh", Institut kibernetiky AN USSR, sb. Tekhnicheskaya kibernetika 16, Kiev.

Kalugin, V. N., V. I. Merkulov. (1968). Possible mechanism of fish drag reduction (in Russ.). In *Mekhanika peredvizheniya i orientatsii zhivotnikh*. Naukova dumka, Kiev.

Kalugin, V. N., V. I. Merkulov, L. Yu. Ferdigalov. (1967). Viscous uncompressible liquid flow in a flat channel with a lower wall having a forme of running wave (in Russ.). *Trudy 1 respublikanskoy konferentsii po aerodinamike: teplomassoobmen.*

Kalugin, V. N., V. I. Merkulov, L. Yu. Ferdigalov (1967). Digital calculation of one flow of viscous uncompressible liquid in the region with moving border (in Russ.). *Izvestiya SOAN SSSR* **13**, 34-40.

Kalugin, V. N., V. I. Merkulov, L. Yu. Ferdigalov. (1969). Flow of viscous incompressible liquid in flat canal which has lower wall as propagating wave (in Russ.). *Trudy 1 Resp. Konfer. po aerodynamike i teplomassoobmenu*. Izd. KGU, Kiev.

Kalugin, V. N., V. I. Panchuk. (1970). Viscous uncompressible liquid flow along the running wave (digital experimants) (in Russ.). *Bionika* **4**, 104-110.

Kaluzhnaya, T. A., A. P. Koval'. (1983). Something regularity of distribution of secretory cells on the skin of bony fish (in Russ.). *Hidrodinamicheskie voprosy bioniki*. Naukova dumka, Kiev: 102-106.

Kambe, T. (1978). The dynamics of carangiform swimming motions. *J. Fluid Mech.*, **87**, 533—560.

Kanarsky, M. V. (1981). Experimental study of a dynamic elastic module of elastic plate (in Russ.). *Bionika* **15**, 98-101.

Kanarsky, M. V., V. V. Babenko, L. F. Kozlov. (1979). Experimantsl study of turbulent boundary layer on elastic surface (in Russ.). In *Stratifitsirovannye i turbulentnye techeniya.* Naukova dumka, Kiev: 59-67.

Karandeeva, O. G., S. K. Matisheva, V. M. Shapunov. (1971). Peculiarity of dolphin's breath (in Russ.). Morfologiya i ekologiya morskikh mlekopitayuschikh (delfiny). Nauka. Moscow. 136–146.

Karandeeva, O. G., V. A. Protasov, N. P. Semenov. (1968). Peculiarity of dolphin's breath as the aquatic animals and in connection with high swimming velocity (in Russ.). *Tez. i ref dokl. 5 nauchn. sovech. posvyaschen. pamyaty L. A. Orbely*. Leningrad.

Karandeeva, O. G., A. V. Protasov, N. P. Semyonov. (1970). On a physioogical foundation of the Gray's paradox (in Russ.). *Bionika* **4,** 36-43.

Karman, T., J. M. Burgers. (1934). General aerodynamic theory— perfect fluids. In *Aerodynamic theory*. B. Springer **2**, 304–310.

Karpouzian, G., G. Spedding, H. K. Cheng. (1990). Lunate-tail swimming propulsion. Part 2. Performance analysis. *J. Fluid Mech.* **210**, 329-351.

Kasanof, D. (1963). Porpoise paradox. *Sea Frontiers* **9**, 24-33.

Katys, G. P. (1965). *Systems of automatic control of velocity fields and flow* (in Russ.). Nauka, Moscow: 464 pp.

Katz, J., D. Weihs. (1978). Hydrodynamic propulsion by large amplitude oscillation of an airfoil with chordwise flexibility. *J. Fluid Mech.* **88**, 485 - 497.

Katz, J., D. Weihs. (1979). Large amplitude unsteady motion of a flexible slender propulsor. *J.Fluid Mech.* **90,** 713 - 723.

Kayan, V. P. (1974). On a resistance coeficient of dolfin (in Russ.). *Bionika* **8**, 31-35.

Kayan, V. P. (1979). On hydrodynamic properties of fin propulsor in dolfin (in Russ.). *Bionika* **13,** 9-15.

Kayan, V. P. (1983). Experimental study of a hydrodynamic thrust, created by the swaying wing (in Russ.). *Bionika.* **17**, 45-49.

Kayan, V. P. (1995). Technical equipment for increasing of propulsive characteristics propulsor of "waving wing" type (in Russ.). In *Plavanie i polet v prirode i tekhnike AQUAPROP'95. Tez. dokl. Mezhd. Konf.* S.-Peterburg, SPbGMTU.

Kayan, V. P., L. F. Kozlov, V. E. Pyatetsky. (1978). Kinematic characteristics of swimming in some aquatic animals (in Russ.). *Izvestiya Akademii NAuk SSSR. Mekhanika zhidkosti i gaza* **5**, 3-9.

Kayan, V. P., V. E. Pyatetsky. (1971). Biohydrodynamic plant of closed type for a study of hydrdynamics of marine animals swimming (in Russ.). *Bionika* **5**, 121-124

Kayan, V. P., V. E Pyatetsky. (1977). Kinematics of swimming in bottle-nosed dolfin depending on the acceleration regime (in Russ.). *Bionika* **11**, 36-41.

Kayan, V. P., V. E Pyatetsky. (1978). Hydrodynamic characteristics of bottle-nozed dolphin at different acceleration regimes (in Russ.). *Bionika* **2,** 48-55.

Kayan, V. P., A. I. Tsiganyuk. (1995). Elaboration, realizing and testing of propulsop as waving wing with electromagnetic driver (in Russ.). In *Plavanie i polet v prirode i tekhnike AQUAPROP'95. Tez. dokl. Mezhd. Konf.* S.-Peterburg, SPbGMTU.

Kermack, K. A. (1948). The propulsive povers of Blue and Fin whales. *J. Exp Biol.* **25,** 237-240.

Kelly, H. R. (1961). Fish propulsion hydrodynamics. In *Developments in mecha nics: Proc. 7th midwest, mech. conf.* Michigan State Univ. I, 442—450.

Kelly, H. R., A. W. Rentz, J. Siekmann. (1964). Experimental studies on the motion of a flexible hydrofoil. *J. Fluid Mech.* **19**, 30—48.

Kendall, J. M. (1970). The turbulent boundary layer over a wall with progressive surface waves. *J. Fluid Mech.* **41**

Khadzhinsky, V. G. (1972). Some morpho-and-functional peculiarities of dolphin's skin (in Russ.). *Bionika* **6**, 58-66.

Khadzhinsky, V. G. (1990). On the question of modelling principle of dolphin's skin (in Russ.). *Morskie mlekopitayuschie. Tez. dokl. 10 vses. sovech. Po izucheniyu, okhrane i ratsional'nomu ispol'zovaniyu morskikh mlekopitayuschikh* (in Russ.). Svetlogorsk – Moskva: 318-319.

Khatuntsev, V. N. (1984). On the problem of functionning of flapping wing type propulsor at regimes with high relative translational movement (in Russ.). *Bionika* **18,** 57-62.

Khatuntsev, V. N. (1985). Peculiarity of thrust forming by model of wing propulsor in sloping flow (in Russ.). *Bionika* **19**, 47-50.

Kheskestad. (1965). Measurements by thermoanemometer in plane turbulent flow (in Russ.). *Prikladnaya mekhanika* **32**, seriya E.

Khodorkovsky, Ya. S. (1981). Friction resistance in hydrobionts at non-stabilized motion regimes (in Russ.). *Bionika* **15,** 78-84.

Khoit, Dg. (1980). Drag reduction by fish mucus (in Russ.). In *Mekhanika. Biogidrodinamika plavaniya i poleta. Novoe v zarubezhnoy nauke. Red. A. Yu. Ischlinskiy, G. G. Cherniy, vip.* 23. MIR. Moskva: 128-145.

Kholter, N. (1965). Some remark on use of telemetry to biology (in Russ.). In *Biotelemetriya.* MIR. Moskva.

Kholyavchuk, S. D. (1995). Fin propulsor-rudder complex for excavatoe having a special –bog purpose (in Russ.). In *Plavanie i polet v prirode i tekhnike AQUAPROP'95. Tez. dokl. Mezhd. Konf.* S.-Peterburg, SPbGMTU.

Khomenko, B. G., V. G. Khadzhinsky. (1974). Morpho-functional foundations of the skin reception in dolphins (in Russ.). *Bionuka* **8**, 106-113.

Khotinskaya, V. D., O. L. Alekseev. (1969). Conductivity of mucus solution of some fresh-water fish (in Russ.). *Bionika* **3**, 101-104.

Khudson, D. (1967). *Statistics for physicists.* MIR. Moskva.

Kidun, S. M. Tachometrie gauge for speed measuring in water (in Russ.). *Bionika* **8**, 61-64.

Kidun, S. M. (1979). Study of the speed of oscillation spreading on dolfin's skin (in Russ.). *Bionika* **13**, 52-58.

Kiyanovskii, L. Z. (1964). Increasing of measuring limit for registration of flow velocity using electromechanical sensor with tensiometer (in Russ.). *Priborostroenie* **9**.

Klausewitz, W. (1964). Der Lokomotionsmodus der Flugelrochen (Myliobatoidei).— *Zool. Anz.* **173**, 111-120.

Kleinenberg, S. E., N. V. Kokshaysky. (1967). Contemporary problems of biological aero-and hydrodynamics (in Russ.). In *Voprosy bionuiki.* Nauka, Moscow.

Klyukin, I. I., A. E. Kolesnikov. (1968). *Acoustical measurements in shipbuilding* (in Russ.). Sudostroenie. Leningrad.

Klyaschtorin, L. B., A. A. Yarjombek. (1973). Hydrodynamic characteristics of fishes from the data on active swimming energetic (in Russ.). *Oceanologiya* **13**, 1104-1107.

Kobets, G. F. (1968). Influence of surface wettability on the marine animals drag (in Russ.). In *mekhanizmi peredvizheniya i orientatsii zhivotnikh.* Naukova dumka. Kiev.

Kobets, G. F. (1969). On the mechanism of influence of dissolved macromolecule on the turbulent friction (in Russ.). *Bionika* **3**, 72-80.

Kobets, G. F., V. S. Zav'yalova, M. L. Komarova. (1969).Influence of fish mucus on the turbulent friction (in Russ.). *Bionika* **3,** 80-84.

Kobets, G. F., M. L. Komarova. (1971). Influence of peculiarity of outer texture on the hydrodynamics of fast-swimming fish (in Russ.). *Bionika* **5**, 101-108.

Kokshaysky, N. V. (1967). On the Reynolds number range in biological objects (in Russ.). In *Voprosy bioniki*. Nauka, Moscow: 543-549.

Kokshaysky, N. V. (1973). Biological hydrodynamics (in Russ.). In *Itogi nauki i tekhniki. Bionika* **1**, 9-85.

Kokshaysky, N. V. (1974). *Essay on biological aero- and hydrodynamics*. Nauka, Moscow. 256 pp.

Kokshaysky, N. V. (1978). On the methods of investigation of aquatic mammal kinematics. In *New in study of Cetaceans and Pennipedia*. Hauka, Moscow: 52-81

Kolchin, S. P., V. M. Belkovich. (1973). Tactile sensitivity in common dolfin (in Russ.). *Zoolog. Zhurnal* **52**, 620-631.

Kolchinskaya, A. Z., O. G. Karandeeva, V. S. Mischenko, V. M. Shapunov, S. K. Matisheva, Yu. V. Stepanov. (1971). On the dolphin's breath (in Russ.). Bionika **5**, 19–28.

Kolobov, P., B. Kolobov, L. Maltzev, R. Bannasch. (1997). Numerical analysis of penguin hydrodynamics. In *Book of abstracts. 10 European drag reduction working meeting*. Berlin.

Komarova, M. L. (1969). On the chemical make-up of mucus of pike and burbot (in Russ.). *Bionika* **3**, 84-90..

Komarov, V. T. (1971). Speed of fish swimming (in Russ.). *Vestnik zoologii* **4**, 67-71.

Komarov, V. T. (1979). Experimental methods and devices to determine motion speeds of nectone animals (in Russ.). *Zool. Zhurn.* **49**, 923-927.

Kondratyeva, L. V., V. V. Skripachev. (1971). Stability of a laminar boundary layer on the plate undergoing the deformation (in Russ.). *Bionika* **5**, 43-45.

Korennaya, L. I. (1974). Evaluating calculation of fin propulsor (in Russ.). *Bionika* 8:.49-52.

Korennaya, L. I. (1976). Plant for the study of the flexible plate hydrodynamics (in Russ.). *Bionika* **10**, 85-88.

Korennaya, L. I. (1980). Mechanism of propulsion generation in a undulatory deformed plate (in Russ.).. In *Opit experimental'no-teoreticheskogo izucheniya aktual'nikh zadach gidridinamiki sudov vnutrennego plavaniya. Sudostroyenie* 317. Leningrad: 109-116.

Korennaya, L. I. (1981). Methods of calculation of undulatory propulsor (in Russ.). *Bionika* **15**, 59-63.

Korennaya, L. I. (1983). Mechanism of friction resistance development at undulatory deformations of a body (in Russ.). In *Hidrodinamicheskie problemy bionici.* - Naukova dumka, Kiev: 71-81.

Korennaya, L. I. (1987). Constituents of viscous resistance of an undulatory deforming body (in Russ.). *Bionika* **21**, 53-58.

Korobov, V. I. (1980). Experimental study of integral characteristics of a boundary layer in pliable plates (in Russ.). *Bionika* **14**, 53-57.

Korotkin, A. I. (1966). Stability of laminar boundary layer in uncomressive liquid on an elastic surface (in Russ.). *Mechanika zhidkosti i gaza* 3.

Korotkin, A. I. (1973). On mechanism of dolfin's motion at bow- and wind-waves (in Russ.). *Bionika* **7**. 27-31.

Korzhev, V. K., S. I. Sizov. (1995). On the question of study of hydrodynamic forces acting on oscillating wing in unsteady flow (in Russ.). In *Plavanie i polet v prirode i tekhnike AQUAPROP'95. Tez. dokl. Mezhd. Konf.* S.-Peterburg, SPbGMTU.

Kotyuk, A. F., E. I. Tsvetkov. (1970). *Spectral and correlative analysis of unsteady casual process (in Russ.).* Izdat. Komiteta standartov , mer i izmeritel'nikh priborov ghb Sovete Ministrov SSSR. Moscow.

Koval', A. P. (1972). Roughness and something peculiarity of skin texture of swordfish (in Russ.). *Bionika* **6**, 73-77.

Koval', A. P. (1974). On the question of functional importance of something sailfish skin peculiarity (in Russ.). *Bionika* **8**, 88-93.

Kovalevskaya, L. A. (1956). Swimming fish energetics. *Trudy morskogo gidrofizicheskogo instituta AN SSSR* **7**.

Kozlov, L. F. (1961). Hydrodynamic problems of biomekhanics (in Russ.). *Biomekhanika* **7**, Sofiya, 88-91.

Kozlov, L. F. (1961). Flow stabilization in boundary layer by distributed damping (in Russ.). *Sudpromgiz:* 77 pp.

Kozlov, L. F. (1969). Visualization of laminar part of boundary layer by means coloured flow (in Russ.). *Bionika* **3**, 109-111.

Kozlov, L. F. (1970). On the biological efficiency something salt-water fish (in Russ.). *Bionika* **4,** 44-46.

Kozlov, L. F. (1973). Influence of body form on dolphin's hydrodynamic drag (in Russ.). *Tezisy dokladov 4 Vsesoyuznoi. konferentsii po bionike* Nauka. Moscow.

Kozlov, L. F. (1974). Some studies on hydrodynamics of aquatic animals (in Russ.). In *Vsesoyuznij sjezd po bionike. Report Theses*: 60-67

Kozlov, L. F. (1976). Hydrodynamic problems of biomechanics (in Russ.). In *Vsesoyuznij sjezd po teoreticheskoj i prikladnoj mekhanike. Report Theses*, Naukova dumka, Kiev.

Kozlov, L. F. (1978). Quantitative bioenergetics analysis of mammals in different physical activitis (in Russ.). *Doklady Academii nauk Ukranian SSR* **12**, 1069-1072.

Kozlov, L. F. (1979). Hydrodynamics of aquatic animals having semi-lunar flukes (in Russ.). *Bionika* **15**, 3-9.

Kozlov, L. F. (1981). Bioenergetic method of evaluation of hydrodynamic resistance in Cetaceans (in Russ.). *Bionika* **15**, 3-16.

Kozlov, L. F. (1983a). *Theoretical biohydrodynamics.* Vischa shkola, Kiev. 238 pp.

Kozlov, L. F. (1983b). Evaluation of expenditure of energy of fast swimming fish (in Russ.). *Hidrodinamicheskie voprosy bioniki.* Naukova dumka. Kiev: 3-8.

Kozlov, L. F. (1985). Mathematical and biological models of aquatic animal swimming (in Russ.). *Bionika* **19**, 7-25.

Kozlov, L. F. (1986). The theory of swimming in hydrobionts using the scombroidal technique taking into account the head occillations (in Russ.). *Bionika* **20,** 3-8.

Kozlov, L. F., V. V. Babenko. (1978). *Experimental study of boundary layer* (in Russ.). Naukova dumka. Kiev: 184 pp.

Kozlov, L. F., V. V. Babenko, S. V. Pershin. (1978). On self-regulation of skin damping in active swimming in some Cetaceans (in Russ.). *Bionika*-**78** A 2: 55-58.

Kozlov, L. F., V. V. Babenko, V. V. Skripachev. (1973). Preliminary results of experimental study of influence of flexible covering on the stability of laminar boundary layer (in Russ.) *Tezisy dokladov 4 konferentsii po bionike i biokibernetike.* Naukova dumka. Kiev.

Kozlov, L. F., S. A. Dovgiy. (1981). Slipping of Cetaceans on ripple waves (in Russ.). *Bionika.***15**, 49-54.

Kozlov, L. F., G. A. Goryanaya, Yu. N. Korolev. (1985). Experience of bioenergetic study of the Black Sea dolphins (in Russ.). *Bionika* **19**, 25-38.

Kozlov, L. F., O. D. Nikishova. Selective character of the Gray paradox (in Russ.). In *5 Ukrainskaya nauchno-tekhnicheskaya konferentsiya po bionike. Report Theses.* Znanie. Kiev.

Kozlov, L. F., A.Ya. Oleynik. (1975). Some results of hydrobionic studies (in Russ.). *Bionika.* **9**, 3-11.

Kozlov, L. F., A. Ya. Oleynik. (1976). Hydrodynamics of aquatic animals, swimming using scombroidal technique (in Russ.). *Doklady Akademii nauk USSR* A 11: 1001-1004.

Kozlov, L. F., A. Ya. Oleynik. (1978). Theoretical study on hydrodynamics of aquatic animals, swimming using scombroidal technique (in Russ.). *Bionika* **12**, 3-12.

Kozlov, L. F., S. V. Pershin. (1983). Complex investigations on active regulation by dolphin skin of hydrodynamic resistance lowering (in Russ.). *Bionika* **17**, 3-12.

Kozlov, L. F., V. E. Pyatetskii. (1968). Influence of co-polimers and mucus on hydrodynamic drag of models and fish (in Russ.). In *Mekhanizmi peredvizheniya i orientatsii zhivotnikh.* Naukova dumka. Kiev: 22-28.

Kozlov, L. F., V. E. Pyatetsky, Yu. N. Savchenko. (1968). Towing power and possible swimming speeds in dolfins (in Russ.). In *Mekhanizmy peredvizhenija i orientatsii zhivotnykh.* Naukova dumka, Kiev: 39-48.

Kozlov, L. F., V. M. Shakalo. (1970). Telemetric devices for the registration of flow regimes in the boundary layer in motion in water element (in Russ.). *Bionika* **4**, 55-60.

Kozlov, L. F., V. M Shakalo. (1973). Certain results of the determination of pulsation of velocities in the boundary layer of dolphins (in Russ.). *Bionika* **7**, 50-52.

Kozlov, L. F., V. M. Shakalo. (1980). On the flow regime in quasi-stationary boundary layer of some Cetaceans (in Russ.). *Bionika* **14,** 74-81.

Kozlov, L. F., V. M. Shakalo, L. D. Buryanova, N. N. Vorobyov. (1974). On the influence of non-stationary on the flow regime in the boundary layer of the Black Sea bottle-nosed dolfin (in Russ.). *Bionika* **8**, 13-16.

Kramer, E. (1960). Zur Form und Funktion des lokomotionsapparates der Fische. *Z. Wiss. Zool.* **163**, 1-36.

Kramer, M. O. (1957). Boundary layer stabilization by distributed damping. *J. Aeron. Sci.* **24**.

Kramer, M. O. (1960a). The dolphin's secret. *New Sci.* **7**, 1118-1120.

Kramer, M. O. (1960b). Boundary layer stabilization by distributed damping. *J. Am. Soc. Naval Engrs.* **72,** 25-33.

Kramer, M. O. (1961). The dolphins' secret. *J. Am. Soc. Naval Engrs.* **73**, 103-107.

Kramer, M. O. (1962). Boundary layer stabilization by distributed damping. *Naval Eng. J.* **74**, 341-348.

Kramer, M.O. (1965). Hydrodynamics of the dolphin. In *Advances in hydroscience*, ed. Ven Te Chow. University of Illinois. Urbana. Illinois. Academic Press. N.Y. and Lond. **2**, 111-130.

Krasnov, N. F. (1971). *Aerodynamics.* Vyschaya schkola. Moscow: 630 pp.

Krolenko, S. I. (1995). Wing as propulsive and steering gear – hydroecologycal propulsor for ecologycal sensitive region (in Russ.). In *Plavanie i polet v prirode i tekhnike AQUAPROP'95. Tez. dokl. Mezhd. Konf.* S.-Peterburg, SPbGMTU.

Kruger, H. M., J. B. Saddler, G. A. Chapman, I. J. Tiasley, R. R. Lowry. (1968) Biopnergetics, exercise and fatty acids of fish. *Amer. Zoologist.* **8**, 119-129.

Kruglov, A. D. (1995). Practical hydrobionics in shipbuilding (in Russ.). In *Plavanie i polet v prirode i tekhnike AQUAPROP'95. Tez. dokl. Mezhd. Konf.* S.-Peterburg, SPbGMTU.

Kudryashov, A. F. (1969). On the swimming fish drag (in Russ.). In *Biologiya morya* 16. Naukova dumka. Kiev: 21-38.

Kudryashov, A.F. (1969). On the mechanics of fish and dolphin swiming (in Russ.). *Biologiya morya*. **16**. Naukova dumka, Kiev: 59-69.

Kudryashov, A. F., V. V. Barsukov. (1967a). On the hydrodynamic function of fish scale as analogue of surface formed by vortical flow. Report 1. Similarity of scale irregularities with irregularities on the surface formed by vortical flow (in Russ.). *Zool. Zhurnal* **46**, 393-403.

Kudryashov, A. F., V. V. Barsukov. (1967b). On the hydrodynamic model of fish scale covering as analogue of surface formed by vortical flow. Report 2. Hydrodynamic function of scale covering (in Russ.). *Zool. Zhurnal* **46**

Kurbatov, B. V. (1972). Methods of experimental determination of the total hydrodynamics drag of marine mammals (in Russ.). In *5 Vsesoyuznoye soveschanie po izucheniyu morskikh mlekopitayuschikh. Report Theses.* Makhachkala: 122-124..

Kurbatov, B. V. (1973a). Hydrodynamic drag of live necters (in Russ.). *Bionika* **6,** 72-77.

Kurbatov, B. V. (1973b). Hydrodynamic drag of live necters (in Russ.). In *4 Vsesoyuznaya konferentsiya po bionike. Report Theses.* Moscow.

Kutty, M. N. (1969). Oxygen consumption in the mullet Liza macrolepis with speciareference to swimming velocity. *Marine Biol.* **4**, 239-242.

Lan, C. E. (1979). The unsteady quasi-vortex-lattice method with applications to animal propulsion. *J.Fluid Mech.* **93**, 747-765.

Landahl, M. T. (1962). On the stability of a laminar incompressible boundary layei over a flexible surface. *J. Fluid Mech.* **13**, 609-632.

Landau, L. D., E. M. Lifshits. (1965). *Mechanics.* Nauka. Moscow:

Lander, B. E. (1964). Laminarization of turbulent boundary layer under the condition of very accelerated flow (in Russ.). *Prikladnaya mekhanika* **4**, 151-153.

Lang, T. G. (1963). Porpoise, whales and fish. Comparision of predicted and observe speeds. *Naval Eng. J.* **75**, 437-441.

Lang, T. G. (1966a). Hydrodynamic analisis of cetacean performance. In *Whales Dolphins and Porpoises,* ed. S. Norris.. Univ Calif. Press. Berkeley—Los Angeles

Lang, T. G. (1966b). Hydrodynamic analisis of dolphin fin profiles. *Nature* **209**, 1110-1111.

Lang, T. G. (1975). Speed, power, and drag measurements of dolphins and porpoises., In *Swimming and flying in nature* 2, ed. T. Y. Wu, C. J. Brokaw, and C. Brennan. Plenum, New York: 553-572.

Lang, T. G., D. A. Daybell. (1963). *Porpoise performance tests in a seawater tank.* NAVWEPS Rep. 8060—NOTS Techn. Report, N 3063. Naval Ordnance Test Station, China Lake, Calif.

Lang, T. G., K. Pryor. (1966). Hydrodynamic performance of porpoises (*Stenella attenuata). Science* **152**, 531-533.

Lang, T. G., K. S. Norris. (1966). Swimming speed of a Pacific bottinose porpoise.— *Science* **151**, 588-590.

Lavrentyev, M. A. (1973). Model of motion of fishes and grass-snakes (in Russ.). *Zhurn. Prikladnoi Mekhan. i tekhnich. Fiziki* **2,** 164-165

Lavrentyev, M. A., M. M. Lavrentyev. (1962). On one principle of propulsive force generation for motion (in Russ.). *Zhurn. Prikl. i tekhnich. fiziki* **4**, 3-9.

Lewis, R. W. (1970). Fish cutaneous mucus: a new source of skin surface lipids. *Lipidx* **5**, 947 49

Liebe, W. (1963). Der Schwanzschlag der Fische. *VDI-Zeitschr. Bd.* **105**, 1298-1302.

Lighthill, M. J. (1960). Note on the Swimming of Slender Fish. *J. Fluid Mech.* **9,** 305—317.

Lighthill, M. J. (1960). Mathematics and aeronautics. J. Roy. Aeronaut Soc vol. 64, N 595, p. 375—393.

Lighthill, M. J. (1969). Hvdromechanics of Aquatic Animal Propulsion. *Ann. Rev.Fluid Mech.* **4**, 413—446

Lighthill, M. J. (1970a). How do fishes swim? *Endeavour* **29**, 77—97.

Lighthill, M. J. (1970b.) Aquatic animal propulsion of high hydromechanical efficiency. *J. Fluid Mech.* **44**, 265—301.

Lighthill, M. J. (1971). Large-amplitude elongated-body theory of fish locomotion. *Proc Roy Soc. Lond.* Ser. B. **179**, 125—138.

Lighthill, M. J. (1975a). *Mathematical biofluiddynamics*. Soc. to industr. and appl. math. Philadelphia (Pa). 281 p.

Lighthill, M. J. (1975b). Aerodynamic aspects of animal flight. *In Swimming and Flying in Nature,* eds. Th. Wu, Ch. Brokaw, Cn. Bremer. Plenum Press, New York: 423-491.

Lighthill, M. J. (1977). Mathematical theories of fish swimming. In *Fisherie mathematics*, ed. J. H. Steele. L. Acad. press, N. Y.: 131—144.

Lighthill, M. J. (1977). Introduction to the scaling of aerial locomotion. In *Scale Effects in Animal Locomotion.* ed. T. J. Pedley, 365 404. London: Academic

Lipatov, N. V. (1990). Peculiarity of body axial deformation of active swimming dolphin (in Russ.). *Morskie mlekopitayushie. Tez. dokladov 10 Vsesoyuznogo soveschaniya po izucheniyu, okhrane i ratsional'nomu ispol'zovaniyu morskikh mlekopitayuchikh. Svetlogorsk Kaliningradskoi oblasty,* Moscow: 171-173.

Little, R. C., M. Wiegard. (1970). Drag reduction and structural turbulence in flowing poliox solutions. *J. App . Polym.* Sci **14**, 409-419.

Logvinovich, G. V. (1969). *Hydrodynamics of a flow with free boundaries*. Naukova dumka, Kiev: 210 pp.

Logvinovich, G. V. (1970a). Hydrodynamics of a flexible long fine body (in Russ.). *Uchenyje Zapiski Tsentralnogo gidrodinamicheskogk Instituta* **1,** 11-18.

Logvinovich, G. V. (1970b). Hydrodynamics of a long fine body (Evaluation of fish hydrodynamics) (in Russ.). *Bionika* **4**, 5-11.

Logvinovich, G. V. (1972). Hydrodynamics of fish swimming (in Russ.). In *13 Mezshdunarodniy kongress po teoreticheskoj i prikladnoj mekhaniki. Report Theses*. Moscow.

Logvinovich, G. V. (1973a). Hydrodynamics of fish swimming (in Russ.). *Bionika* **7**, 3-8.

Logvinovich, G.V. (1973b). Hydrodynamics of fish swimming (in Russ.). *Izvestiya Sibirskogo otdeleniya Akademii Nauk SSSR. ser. tekhn.* **8**, 3-8.

Loitsyanskii, L. G. *Gas and liquid mechanics*. M.: Nauka, (1987), 840 pp.

Lush, P. A. (1973). Errors in static pressure measurements by probes in a fluctuating flow. *J. Sound, and Vibrat.* **26**. 429-431.

Lyather, V. M. (1968). *Turbulation in hidraulic building* (in Russ.). Energiya. Moscow.

Madigosky, W. M., G. F. Lee, J. Haun, F. Borkat, R. Kataoka. (1986). Acoustic surface wave measurements on live bottlenose dolphins. *J. Acoust. Soc. Am.* **79**, 153-159.

Magnuson, J. I. (1965). Tank facilities for tuna behaviour studies. *Progress. Fish-Culturist* **27**, 230-233.

Magnuson, J. I. (1978). Locomotion by scombroid fishes: hydromechanics, morphology and behaviour. *Fish physiology*, eds. W.S. Hoar and D.J. Randall. Acad. press, Ney York. **7,** 240-315.

Mair, W. A. (1955). The distribution of pressure on an aerofoil in a stream with a spanwise velocity gradient. *Aeronaut. Q.* **6**, 1 12

Makarov, A. P. (1974). Some hydrodynamic characteristics of a deformed element (in Russ.). *Bionika* **8,** 19-20.

Maslov, N. K. (1970). On the manoeuvrability and controllability of dolphins (in Russ.). *Bionika* **4**, 46-50.

Matyukhin, V. A. (1973). *Bioenergetics and physiology of swimming in fishes*, Nauka, Siberian Branch, Novosibirsk. 154 pp.

Matyukhin, V. A., Yu. S. Alikin, A. Ya. Stolbov, V. I. Turetskii. (1973). Experimental study of fish efficiency (in Russ.). *Bionika* **7**, 31-37.

Matyukhin, V. A., D. V. Demin. (1969). Biohydrodynamic analysis of aquatic organism movements (in Russ.). *Referaty dokladov 4 konferentsii fiziologov Sredney Azii i Kazakhstana.* Novosibirsk: 68-70.

Matyukhin, V. A., V. I. Turetskii. (1972). Study of swimming fish drag. *Bionika* **6**, 3-6.

Matyukhin, V. A., V. V. Khaskin, A. Ya. Stolbov. (1970). Equipment for complex study of energetics and phisiology of fish swimming (in Russ.). *Voprosy ikhtiologyi* **10**, 925-928.

Masuda, H., C. Araga, T. Yoshino. (1975). *Coastal fishes of Southern Japan.* Tokai Univ. press, Tokyo.

McGuthen, C. W. (1970). The trout tail fin: A self-cambering hydrofoil. *J. Biomechanics* **3**, 271-281.

Merkulov, V. I. (1967). Flow of the viscous uncompressive liquid along running wave (in Russ.). *Izv. SOAN SSSR*, ser. Tekhn. **8**, 3-11.

Merkulov, V. I. (1972). The running wave on an alastic body moving in the ideal liquid (in Russ.). *Bionika* **4**, 95-104.

Merkulov, V. I. (1976). *Popular hydrodynamics* (in Russ.).Tekhnika. Kiev: 143 pp

Merkulov, V. I., V. D. Khotinskaya. (1969). Mechanism of drag reduction of something fish species (in Russ.). *Bionika* **3**, 96-101.

Merkulov, V. I., Yu. N. Savchenko. (1970). Experimental study of a liquid flow along the running wave (in Russ.). *Bionika* **4**, 116-120.

Merculov, V. I., L. I. Maltzev, R. Bannasch. (1997). Swordfish rostrum as a generator of vorticies, reducing hydrodynamical drag. In *Book of abstracts. 10 European drag reduction working meeting.* Berlin.

Metelitsin, V. A. (1995). Approxmative method for calculation wing with elastic fastening as propulsor and rudder (in Russ.). In *Plavanie i polet v prirode i tekhnike AQUAPROP'95. Tez. dokl. Mezhd. Konf.* S.-Peterburg, SPbGMTU.

Mirskyi, G. Ya. (1972). *Study of characteristics of casual process by apparatus* (in Russ.). Energiya. Moscow.

Monin, A. S., A. M. Yaglom. (1965). *Statistical hydromechanics* (in Russ.). Nauka. Moscow.

Moore, K. J. (1995). Observations of the flow around swimming dolphin using bioluminescenceþ. In *Plavanie i polet v prirode i tekhnike AQUAPROP'95. Tez. dokl. Mezhd. Konf.* S.-Peterburg, SPbGMTU.

Mukoseev, B. I. (1968). Flow over of oscillating surface by viscous incompressible liquid (in Russ.). *Nauchnye trudy dal'nevostochnogo vyschego inzhenerno-morskogo uchilisha* **5,** 89-91.

Mukoseev, B. I. (1971). Flow over of oscillating surface by viscous incompressible liquid (in Russ.). *Mekhanika zhidkosty i gasa* **4**, 60-65.

Mukoseev, B. I. (1972). *Some problems of flow over and movement of oscillating flexible surface* (in Russ.). Kand diss.

Myasnikov, L. L. (1937). *Acoustical measurements*. ONTI NKTP SSSR.

Muller, U. K. (1997). In the wake of the fish: a brief introduction to the hydrodynamics and kinematics of fish swimming. In *In the wake of the fish: on the hydrodynamic interactions between swimming fish and water, the effects of the ontogenetic stages and swimming kinematics.* Rijksuniversiteit, Groningen, 1-18.

Muller, U. K., J. J. Videler. (1997). Inertia as a «safe harbour»: do fish larvae increase length growth to escape viscous drag? In *In the wake of the fish: on the hydrodynamic interactions between swimming fish and water, the effects of the ontogenetic stages and swimming kinematics.* Rijksuniversiteit, Groningen: 21-31.

Muller, U. K., E. J. Stamhuis, J. J. Videler. (1997). Hydrodynamics of unsteady fish swimming and the effect of body size: comparind fish larvae and adults. In *In the wake of the fish: on the hydrodynamic interactions between swimming fish and water, the effects of the ontogenetic stages and swimming kinematics.* Rijksuniversiteit, Groningen: 33-59.

Muller, U. K., L. E. Bart. van den Heuvel, E. J. Stamhuis. J. J. Videler. (1997). Fish foot prints: morphology and energetics of the wake behind a continuously swimming mullet (*Chelon labrosus*). In *In the wake of the fish: on the hydrodynamic interactions between swimming fish and water, the effects of the ontogenetic stages and swimming kinematics.* Rijksuniversiteit, Groningen: 61-85.

Muller, U. K., E. J. Stamhuis. J. J. Videler. (1997). Wake formation and swimming kinematics in mullet (*Chelon labrosus*). In: *In the wake of the fish: on the hydrodynamic interactions between swimming fish and water, the effects of the ontogenetic stages and swimming kinematics.* Rijksuniversiteit, Groningen: 87-109.

Muller, U. K., J. H. Smit, E. J. Stamhuis, J. J. Videler. (1997). Wake generation in undulatiry fish swimming: swimming kinematics and flow fields of eel (*Anguilla anguilla*). In *In the wake of the fish: on the hydrodynamic interactions between*

swimming fish and water, the effects of the ontogenetic stages and swimming kinematics. Rijksuniversiteit, Groningen: 111-133.

Narasako, Y. (1973). Drag of fish. *J. Seibu. Zosenkai* **45**, 1-15.

Naotsuqu Jashiki, Hirchisa Morikawa, Hisashi Kato, Hirishi Yanagihara, Yutaka Wada. (1980). The study on a propulsion system by fin stroke. *Bull. Of Marine Engineering Society in Japan* **8**, 74-77.

Narkhov, A. S. (1937). The morphology of caudal musculature. *Delphinus delphis.* Tursiops tursio (in Russ.). *Zool. Zhurn.* **16**

Narkhov, A. S. (1939). On the motions of *Delphinus delphis* and *Tursiops tursio* during swimming (in Russ.). *Zool. Zhurn.* **18**, 326-330.

Nazarchuk, M. M., M. M. Kovetskaya, V. N. Panchenko. (1974). *Reverse turbulent - laminar transition* (in Russ.). Naukova dumka. Kiev: 96 pp.

Nechayeva, O. V., V. N. Plekhov, V. G. Khadzhinsky. (1973). Peculiarities of potential distribution on dolphins' skin (in Russ.). *Bionika* **7**, 79-83.

Nekrasov, A. I. (1947).*Theory of wing in unsteady flow* (in Russ.). Izdat. AN SSSR. Moscow: 258 pp.

Newman, J. N. (1973). The force on a slender fish-like body. *J. Fluid Mech.* **58**, 689—702.

Newman, J. N., T. Y.-T. Wu. (1973). A generalized slender-body theory for fish-like forms. *J. Fluid Mech.* **57**, 673—693.

Newman, J. N., T. Y.-T. Wu. (1975). Hydromechanical aspects of fish swimming.— In *Swimming and flying in nature*, ed. T. Wu, C.J.Brokaw, and C.Brennan. Plenum press, N. Y., pp. 615—634.

Niiler, P. P., H. J. White. (1969). Note on theswimming deceleration of a dolphin. *J. Fluid Mech.* **38**, 613-617.

Nikishova, O. D. (1973). On the problem of dolphins' swimming bioenergetics (in Russ.). *Bionika* **7**, 44-49.

Nikishova, O. D. (1983). Stability of a boundary layer on bodies of actively moving aquatic animals (in Russ.). *Bionika* **17**, 31-35.

Nikishova, O. D., V. V. Babenko. (1975). On streamline of elastic bodies (in Russ.). *Bionika* **9**, 55-60.

Norris, K. S., J. H. Prescott. (1973). Observations on pacific cetaceans of Californian and Mexican waters. *University of Califirnia Publications in Zoology.* Ed.: (Los Angeles), ed. W. H. Furgason, R. B. Cowles, T. L. Jahn. **63**, 291-402.

Novikov, A. K. (1971). *Correlative measurements in ship acoustics* (in Russ.). Leningrad: 256 pp.

Nosov, E. P. (1995). Technical realization of bionical principle of movement (in Russ.). In *Plavanie i polet v prirode i tekhnike AQUAPROP'95. Tez. dokl. Mezhd. Konf.* S.-Peterburg, SPbGMTU.

Nursall, J. R. (1958a). A method of analysis of the swimming of fish. *Copeia* **2**, 136-141.

Nursall, J. R. (1958b). The caudal fin as a hydrofoil. *Evolution* **12**(1).

Ol'shevskyi, V. V. (1973). *Statistical methods in hydrolocation* (in Russ.). Sudostroenie. Leningrad: 184 pp.

Osborne, M. F. M. (1961). The hydrodynamical performance of migratory salmon. *J. Exp. Biol.* **38**, 365-390.

Ostroumov, G. A., L. N. Seravin. (1974). To the question of swimming hydrodynamics of aquatic animals. 2. Moving in the water of small and large animals by caudal fins (in Russ.). *Vestnik Leningradskogo Universiteta* **21**,: 28-36.

Ostrovsky, V. O. (1974). Forced griping on the course of hydrobionts in agitated waters (in Russ.). *Bionika* **8**, 76-81.

Ostrovsky, V. O. (1975). On the translational function of flakes in hydrobionts (in Russ.). *Bionuka* **9**, 112-115.

Ovcharov, O. P. (1970). On the hydrodynamic function of fish gills during a passive respiration (in Russ.). *Zool. zhurnal* **49**(10):

Ovchinnikov, V. V. (1966a). Functions of fins (in Russ.). In *Ecologo-morfologicheskie issledovaniya nekotorykh zhivotnikh*. Naukova dumka. Kiev: 53-62.

Ovchinnikov, V. V. (1966b). Turbulization of boundary layer as a method of drag reduction of swimming fish (in Russ.). *Biofizika* **11** 186-188.

Ovchinnikov, V. V. (1966c). A morphological and functional characteristic of the rostrum of Ziphioidae. In *Ekomorfologicheskie issledovaniya nektonnykh zhivotnikh.* Naukova Dumka. Kiev: 42-52.

Ovchinnikov, V. V. (1967a). On the function of sailfish dorsal fin (in Russ.). *Voprosy ikhtiologii* **7**, 194-196.

Ovchinnikov, V. V. (1967b). On the hydrodynamic characteristics of swordfish (in Russ.). *Nauchnye doklady vischey shkoly. Biologicheskie nauki* **1**

Ovchinnikov, V. V. (1971). Swordfishes and billfishes in the Atlantic Ocean—ecology and functional morphology. *Rep.*, Atl. Sci. Res. Inst. Fish. Oceanogr.. Kaliningrad. USSR. Transl. from Russian by Isr. Program for Sci. Transl., Jerusalem.

Packard, A. (1972). Cephalopods and fish: the limits of convergence. *Biol. Rev.* **47**, 241-307.

Palmer, E., G. Weddell. (1964). The relationship between structure, innervation and function of the skin of the bottinose dolphin (Tursiops truncatus). *Proc. Zool. Soc. Lond.* **143**, 553-568.

Pao, S. K., J. Siekmann. (1964). Note on the Smith-Stone theory of fish propulsion. *Proc. Roy. Soc. London* **A 280**, 398—408.

Parry, D. A. (1949). The swimming of whales and a discussion of Gray's paradox. *J. Exp. Biol.* **26**, 24-34.

Patel, V. C., M. R. Head. (1968). Reversion of turbulent to laminar flow. *J. Fluid Mech.* **34**.

Perry, B., A. J. Acosta., T. Kicenink. (1961). Simulated wave riding dolphins. *Nature* **192**, 148-150.

Pershin, S. V. (1956). Hydrodynamic aspects of a study of aquatic animals motion as a principle of optimization of motion of immerged corps (in Russ.). *Bionika* Nauka. Moscow.

Pershin, S. V. (1965a). Functional dependence of the maximum specific power output in aquatic animals on the duration of the swimming period (in Russ.). *Trudy Visshey voennomorskoy shkoly* **60**, 63-73.

Pershin, S. V. (1965b). To the hydrodynamic characteristics of motion in some aquatic animals (in Russ.). *Issledovaniya po bionike*. Kiev: 5-15.

Pershin, S. V. (1965c). Hydrodynamic aspects of a study of water animals motion (in Russ.). *Bionika* Nauka. Moscow: 207-214.

Pershin, S. V. (1965d). Energetic methods of calculation of quasi-stationary motion of aquatic animals in application to the hydrodynamics of immerged corps (in Russ.). *Sbornik trudov* 60. Dzerzhinsky VVMIOLU. Leningrad: 49-61.

Pershin, S. V. (1966). BIological and hydrodynamic studies of hygh-speed aquatic animals in nature and oceanariums (in Russ.). In *Mekhanizmy peredvizheniya i orientatsii zhivotnykh.* Naukova dumka, Kiev.

Pershin, S. V. (1967a). Dolphin's jumps as contributor of information the pulsed energetics of fast swimming animals (in Russ.). *Voprosy bioniki*. Nauka. Moscow: 31-36.

Pershin, S. V. (1967b). Biohydrodynamic laws of aquatic animals swimming as basis of optimization in nature of underwater body moving (in Russ.). *Voprosy bioniki*. Nauka. Moscow: 555-560.

Pershin, S. V. (1969a). Hydrodynamic characteristics of Cetaceans and normalized swimming speed of dolphins' in natural conditions and in captivity (in Russ.). *Bionika* **3**, 3-5.

Pershin, S. V. (1969b). Optimization of hind fin propeller in nature on the example of Cetaceans (in Russ.). *Bionika* **3**, 26-34.

Pershin, S. V. (1970a). On the frequency characteristics of hydrobionts (in Russ.). *Bionika* **4,** 27-31.

Pershin, S. V. (1970b). On resonance regime of dolphins' swimming (in Russ.). *Bionika* **4**, 31-36.

Pershin, S. V. (1973a). Normalization of layered model of damping skin of dolphins (in Russ.). *Bionika* **7,** 66-71.

Pershin, S. V. (1973b). Hydrodynamic dependences in non-stationary harmonic motion of fishes and dolphins as submerged bodies with variable shape (in Russ.). *Problemy bioniki*. Nauka, Moscow: 464-474.

Pershin, S. V. (1974). Some results of hydrodynamic studies of propulsor (in Russ.). *Bionika*.**8,** 35-43.

Pershin, S. V. (1975). Hydrodynamic analysis of fins' profiles in dolphins and whales (in Russ.). *Bionika* **9,** 26-32.

Pershin, S. V. (1976). Self-tuning of the skin damping and lower of hydrodynamic drag in active swimming in Cetaceans. *Bionika* **10,** 33-40.

Pershin, S. V. (1978). The biohydrodynamic phenomenon of the swordfish as the maximum case of fast hydrobionts. *Bionika* 1978(12): 40 48

Pershin, S. V. (1979). Swimming and flight in nature (in Russ.). *Itogi nauki i tekhniki. Bionika. Biokibernetika. Bioinzheneriya* **4**, 137-153.

Pershin, S. V. (1981). Flapping wing as a paddled maschine for forced circulation of element (in Russ.). *Bionika* **15**, 64-71

Pershin, S. V. (1982). Regularities of structural organization of support-and-locomotion apparatus in Cetaceans (in Russ.). *DAN SSSR* **266**, 719-721.

Pershin, S. V. (1983). Hydrobionic regularities of outer shapes optimization of a propultion complex in Cetaceans (in Russ.). *Bionika* **17**, 13-24.

Pershin, S. V. (1985a). On the regulation of structural organization of the body and of the locomotion organs and organisms (in Russ.). *Bionika*. **19**, 56-57.

Pershin, S. V. (1985b). On the regulation of the structural body organization and locomotion organs in organisms (in Russ.). *Bionika* **19**, 56-57.

Pershin, S. V. (1988). *Fundamentals of hydrobionics*. Sudostroenie, Leningrad. 263 pp.

Pershin, S. V. (1991). Invariant structure and various morphotypes of the vertebral column in Cetaceans (in Russ.). *Bionika* **24**, 60-66.

Pershin, S. V. (1995). Invariant and symmetry of structure of good flow over bodies of hydrobionts and wings of aerobionts (in Russ.). In *Plavanie i polet v prirode i tekhnike AQUAPROP'95. Tez. dokl. Mezhd. Konf.* S.-Peterburg, SPbGMTU.

Pershin, S. V., L. F. Chernyshov, L. F. Kozlov, A. P. Koval', V. A. Zayets. (1976). Patterns in the integuments of fast-swimming fishes. *Bionika* **10**, 3 21

Pershin, S. V., E. P. Nosov, V. P. Isakov. (1973). Schematic model of hydroelastic effect in cetacean fins and technical using of this effect (in Russ.). *Bionika* – 1973. Tez. dokl. **6**, 93-99.

Pershin, S. V., G. N. Orlov. (1979). Monolast - a perspective undulatory propulsor for high-speed swimming by "dolphin" style (in Russ.). *Bionika* **13**, 24-35.

Pershin, S. V., A. S. Sokolov, A. G. Tomilin. (1969). Morpho-functional peculiarities of arteries and veins in connection with locomotion (in Russ.). *4 Vsesoyuznaya konferentsiya po izucheniyu morskikh mlekopitayschikh. Report Theses.* Kaliningrad: 42-44.

Pershin, S. V., A. S. Sokolov, A. G. Tomilin. (1970). On regulated by special vascular organs of the elasticity of dolphin's fins (in Russ.). *Doklady Akad.Nauk SSSR* **190**, 709-712.

Pershin, S. V., A. S. Sokolov, A. G. Tomilin. (1971). The phenomenon of self-regulation of fins' hydroelasticity in Cetaceans (in Russ.). Certifical for discovery SSSR 95. *Bulleten* N23.

Pershin, S. V., A. S. Sokolov, A. G. Tomilin. (1972). On morpho-functional peculiarities of flukes in some Cetaceans (in Russ.). *Doklady Akad.Nauk SSSR* **203**, 502-504.

Pershin, S. V., A. S. Sokolov, A. G. Tomilin. (1973). On the selfregulation elasticity cetecean fins (in Russ.). *Bionika – 1973. Tez. dokl.* **6,** 87-92

Pershin, S. V., A. S. Sokolov, A. G. Tomilin. (1974). Biomechanical foundations of a regulated hydroelastic effect in fins - wing-like carrying surfaces of Cetaceans (dolphins and whales) (in Russ.). In *Functional morphology of Mammals.* Nauka, Leningrad: 266-305.

Pershin, S. V., A. S. Sokolov, A. G. Tomilin. (1979). Regulated hydroelastic effect in the fins of the largest and fastest dolphin, the killer whale. *Bionika* 1979(**13**), 35 43

Pershin, S. V., Ya. F. Sharov, E. P. Nosov. (1973). Hydrobiont as adaptative fluctuation system (in Russ.). *Bionika* **7**, 18-25.

Petersen, C. G. J. (1925). The motion of whales during swimming. *Nature* **116**, 327-329.

Petrova, I. M. (1968). Studies in the field of bionics, carried out for the purpose to enhance the speed of ships *Tsentralnyj nauchno-issledovatel'skij institut informatsii i tekhniko-ekonom. Issledovanij.*Moscow. 58 pp.

Petrova, I. M. (1970). Hydrobionics in ship-building. *Tsentralnyj nauchno-issledovatel'skij institut informatsii i tekhniko-ekonom. issledovanij.* Leningrad 271 pp.

Petrovsky, V. S. (1966). *Hydrodynamic problems of turbulent noise* (in Russ.). Sudostroenie.

Picken, J., C. T. Crowe. (1974). Performance efficiency of swim fins. *Ocean Engng.* **2**, 251-258.

Pilleri, G. (1970). *Platanista gangetica*, a dolphin that swims ontis side. *Rev. Suisse zool.* **77**, 305-307.

Pinchuk, V. E., B. B. Sheremetov. (1995). Estimation of possibility of parametric resonance in dynamical system "underwater apparatus – steamy fin propulsor" (in Russ.). .). In *Plavanie i polet v prirode i tekhnike AQUAPROP'95. Tez. dokl. Mezhd. Konf.* S.-Peterburg, SPbGMTU.

Polischuk, S. V. (1983). Physical modelling of cetacean energetic characteristics (in Russ.). *Gidrodinamicheskie voprosy bioniki.* Naukova dumka. Kiev: 81-84.

Possio, C. (1940). *Aerotecnica* 20, 655—681

Povkh, I. L. (1964). *Technical hydromechanics.* Mashinostroenie. Moscow-Leningrad.

Povkh, I. L., A. B. Stupin, G. G. Boyarkina. (1979). Hydrodynamic resistance of aqueous solutions of polymers and surface-active substances in rough tubes. *Inzh.-Fiz. Zh.* **36**, 16-19

Prandtl, L. (1949). *Hydroaeromechanics* (in Russ.). IL. Moscow: 520 pp.

Prange, H. D., K. Schmidt-Nielsen. (1970). The metabolic cost of swiming in ducks. *J. Exp. Biol.* **53**, 763-777.

Protasov, V. R., A. G., Starosel'skaya. (1978). *Hydrodynammic peculiarity of fish* (in Russ.). Nauka. Moscow: 104 PP.

Purves, P. E. (1963). Locomotion in whales. *Nature* **197**, 334-337.

Purves, P. E., W. H. Dudok van Heel, A. Jonk. (1975). Locomotion in dolphins. Part 1: Hydrodynamic experiments on a model of the bottle-nosed dolphin, *Tursiops truncatus*, (Mont.). *Aquatic mammals* **3**, 4-31.

Pushkov, S. G. (1985). Some questions of hydrodynamics of thin flexible body (in Russ.). *Teoreticheskie i experimental'nye issledovaniya dvizheniya zhidkosty i gasa.* M.S.: 88-92.

Pushkov, S. G., E. V. Romanenko. (2000). Hydrodynamic forces acting on rigid wing executing great amplitude heaving and pitching oscillations (in Russ.). *Uspekhi sovremennoi biologii* **120**, N2, 496-504.

Pyatetsky, V. E. (1970a). Kinematic characteristics of swimming of some fast swimming salt-water fish (in Russ.). *Bionika* **4**, 11-20.

Pyatetsky, V. E. (1970b). Hydrodynamic characteristics of swimming of some fast swimming salt-water fish (in Russ.). *Bionika* **4,** 20-27.

Pyatetsky, V. E., V. P. Kayan. (1971). Kinematics and hydrodynamics of swimming of Black Sea flat needlefish (in Russ.). *Bionika* **5,** 5-11.

Pyatetsky, V. E., V. P. Kayan. (1972). On the swimming characteristics of lake trout (in Russ.). *Bionika* **6**, 13-18.

Pyatetsky, V. E., V. P. Kayan. (1976). Hydrodynamic characteristics of swimming of Tursiops truncatus (in Russ.). *Bionika* – 1976, **10,** 80-85.

Pyatetskiy, V. E., V. P. Kayan. (1972). Some kinematic characteristics of swimming of *Phocoena phocoena. Bionika* **6,** 18-21.

Pyatetskiy, V. E., V. P Kayan. (1975). On kinematics of bottle-nose dolphin swimming (in Russ.). *Bionika* **9**, 41-46.

Pyatetskiy, V. E., V. P Kayan. Study on kinematics of aquatic animals swimming (in Russ.). In *4 Vsesoyuznogo sjezda po teoretich. I prikladn. Mekhanike. Report Theses.* Naukova Dumka, Kiev.

Pyatetskiy, V. E., V. P. Kayan, L. F. Kozllov, N. P. Semyonov. (1978). Device for studying the kinematics of dolphins swimming (in Russ.*). Bionika* **12**, 55-58.

Pyatetskiy, V. E., V. P. Kayan, A. M. Kravchenko. (1973). Experimental plant, apparatus and methods for studying the hydrodynamics of swimming in aquatic animals (in Russ.). *Bionika* **7**, 91-102.

Pyatetsky, V. E., V. N. Khatuntsev. (1985). On the cetacean propulsor efficiency (in Russ.). *Bionika* **19**, 43-47.

Pyatetskiy, V. E., V. N. Khatuntsev, I. I. Sizov. (1984). Peculiarities of determining the efficiency of a model ofpropulsor of hydrobiont (oscillating wing type) (in Russ.). *Bionika* **9,** 87-91.

Pyatetsky, V. E., A. P. Makarenko, L. F. Kozlov. (1968). Biohydrodynamometer equipment for study of swimming kinematics and energy of fish (in Russ.). *DAN USSR* 2.

Pyatetsky, V. E., Yu. N. Savchenko. (1969). On the influence of mucus on fish drag (in Russ.). *Bionika* **3**, 90-96.

Pyatetskiy, V. E., Yu. N. Savchenko, A. P. Makarenkov. (1969). Cinebox (lunge) for subaquatic filmings from a moving ship (in Russ.). *Bioniks* **3**, 111-117.

Pyatetskiy, V. E., V. M. Shakalo. (1975). Flow regime in a boundary layer of dolphin's model (in Russ.). *Bionika* **9**, 46-50

Pyatetskiy, V. E., V. M. Shakalo, A. I. Tsyganyuk, I. I. Sizov. (1982). Study of regime a streamline in aquatic animals (in Russ.). *Bionika* **16**, 31-36.

Radakov, D. V. (1964). Fish swimming velocity (in Russ.). In *Skorosty dvizheniya i nekotorye osobennosty zreniya ryb.* Red. Radakov D. V., Protasov V. R. Spravochnik. Nauka, Moscow.

Raschi, W. G., J. A. Musick. (1986). Hydrodynamic aspects of shark scales. *NASA* CR-3963

Rayner, M. D., M. J. Keenan. (1967). Role of red and white muscles in the swimmingof the skipjack tuna. *Nature* **214,** 392-393.

Reece, J. W., I. P. Uldrick, J. Siekmann. (1964). Some recent development in sea ani mal locomotion hydrodynamics. *Theor. and Appl. Mech.* **2**, 337—349.

Rehman, Ph. D. (1961). *«Project Notty». A Study of sea animal propusion and acoustics.* U.S.Naval Ordnans Test Station, China.

Reif, W.-E., (1978). Protective and hydrodynamic function of the dermal skeleton of Elasmobranchs. *Neues Jahrb. Geol. Palaontol. Abh.* **157**, 133-141.

Reif, W.-E., (1982). Morphogenesis and function of the squamation in sharks. *Neues Jahrb. Geol. Palaontol. Abh.* **164**, 172-183.

Reif, W.-E., A. Dinkelacker. (1982). Hydrodynamics of the squamation in fast-swimming sharks. *Neues Jahrb. Geol. Palaontol. Abh.* **164**, 184 -187

Repik, E. U. (1970). Experimental study of structure of boundary layer turbulence in condition of longitudinal pressure gradient (in Russ.). *Trudy TsAGY* **1218**, 19-25.

Repik, E. U., V. K. Kuznetsov. (1976). Experimental study frictional drag coefficient in turbulent boundary layer in condition of longitudinal pressure gradient (in Russ.). *Inzhenerno-fizicheskiy zhurnal* **30**, 793-802.

Richardson, E. G. (1936). The physical aspects of fish locomotion. *J. Exp. Biol.* **13**, 63-74.

Rodionov, V. A. (1978). On organization, function and origin of skin musculature in Cetaceans (in Russ.). In *Morskie mlekopitayuschiye. Resultaty i metody issledovanij*, ed. V.E.Sokolov. Nauka, Moscow, 17-27.

Rodionov, V. A. (1997). Histochemical structure of muscle of Black Sea bottlenose dolphin (in Russ.). In *Chernomorskaya afalina.* Red. V. E. Sokolov, E. V. Romanenko, Nauka. Moscow: 297-325.

Rodionov, V. A. (1997). Structure and adaptive peculiarity of postcranial skeleton of the Black Sea bottlenose dolphin (in Russ.). In *Chernomorskaya afalina.* Red. V. E. Sokolov, E. V. Romanenko, Nauka. Moscow: 326-368.

Rodionov, V. A. (1997).Something anatomic peculiarity of muscle of Black Sea bottlenose dolphin (in Russ.). In *Chernomorskaya afalina*. Red. V. E. Sokolov, E. V. Romanenko, Nauka. Moscow: 368-420.

Rohr, J., E. Hendricks. (1995). Experimental observations of dolphin induced bioluminescence. *Review Meeting on bio-locomotion and rotational flow over compliant surfaces. Abstract Theses*. John Hopkins University, Homewood Campus, Baltimore, Maryland.

Rohr, J., E. Hendricks, L. Quigley, F. Fish, J. Gilpatrick, J. Scardina-Ludwig. (1998). Observations of dolphin swimming speed and Strouhal number. Technical report 1769. Space and Naval Warfare Systems Center. San Diego. 48 pp.

Rohr, J., J. Losee, G. Anderson. (1994). The response of bioluminescent organisms to fully developed pipe flow. *Technical Report 1360. Naval Command, Control and Ocean Surveillance Center. RDT&E Division*. San Diego, CA, 92152-5001.

Romanenko, A. F., G. A. Sergeev. (1968). Problems of practical analysis of casual processes (in Russ.). *Sovetskoe radio*. Moscow.

Romanenko, E. V. (1967). Ultrasound receivers and calibration methods (in Russ.). In *Istochniki moshnogo ul'trazvuka*. Red. L. D. Rozenberg, Nauka. Moscow: 327-378.

Romanenko, E. V. (1971a). Receiver of pressure pulsations (in Russ.). *Avtorskoe svidetel'stvo na izobretenie* N 320739.

Romanenko, E. V. (1971b). Receivers of pressure pulsations, designed for work with dolphins (in Russ.). *Trudy Akusticheskogo Instituta* **17**.

Romanenko, E. V. (1972). On hydrodynamics of fishes and dolphins (in Russ.). In *Morskoye priborostroenie. Naucho-tekhnich. Sbornik*. Ser. Akustica **1**, 154-161.

Romanenko, E. V. (1974a). *Physical foundations of bioacoustics* (in Russ.). Nauka, Moscow. 180 pp.

Romanenko, E. V. (1974b). A method of speed pulsation measurement in liquid flow (in Russ.). In *Morfologya, fiziologja i akustika morskikh mlekopitayuschikh*, ed. V.E.Sokolov. Nauka, Moscow, pp. 160-165.

Romanenko, E. V. (1976a). *Foundations of statistical biohydrodynamics* (in Russ.). Nauka, Moscow. 168 pp.

Romanenko, E. V. (1976b). Acoustics and hydrodynamics of some marine mammals (in Russ.). *Akusticheskij Zhurnal* **22,** 628-629

Romanenko, E. V. (1978). The problems of marine mammal acoustics and hydrodynamics (in Russ.). In *Novoe v izuchenii kitoobraznikh i lastonogikh*, ed. V.E.Sokolov. Nauka, Moscow: 35-51.

Romanenko, E. V. (1980a). Experimental studies of dolphins' kinematic (in Russ.). *Doklady Akademii Nauk SSSR* **253**, 741-743. (Translated in Engl. Doklady biological science. Proceedings of the Academy of sciences of the USSR, January, 1981. Consultants Bureau, New York: 387-388.)

Romanenko, E. V. (1980b). Some problems in the theory of swimming of fishes and dolphins (in Russ.). *DAN SSSR* **253**, 1082-1085. (Translated in Engl. Sov. Phys. Dokl. **25,** August 1980. American Institute of Physics.)

Romanenko, E. V. (1981). Distribution of dynamic pressure on the body of actively swimming dolphin (in Russ.). *DAN SSSR* **261**, 310-312. (Translated in Engl. Phys. Dokl. **26**, November 1981. American Institute of Physics.)

Romanenko, E. V. (1985). On the law of deformation of a body of swimming fish or dolphin (in Russ.). *Bionika* **19**

Romanenko, E. V. (1986a). The function of sound in the fish swimming (in Russ.). *Priroda* **11**, 28-29.

Romanenko, E. V. (1986b). *Theory of swimming of fishes and dolphins* (in Russ.). Nauka, Moscow. 148 pp.

Romanenko, E. V. (1994a). Hydrodynamics of dolphins (in Russ.). *Uspekhi sovremennoi biologii* **114**, 283-303.

Romanenko, E. V. (1994b). Swimming of dolphins (experiments and modelling) (in Engl.). *SEB Symposium. Biological Fluid Dynamic. Abstracts.* Leeds. England.

Romanenko, E. V. (1994c). The state of biohydrodynamic investigations in Russia (survey) (in Engl.). *SEB Symposium. Biological Fluid Dynamic. Abstracts.*Leeds. England.

Romanenko, E. V. (1995a). Assessment of thrust and drag coefficient in dolphin (in Russ.). *Uspekhi sovremennoi biologii* **115**. 50-57.

Romanenko, E. V. (1995b). Swimming of dolphins: experiment and modelling (in Engl.). In *Biological Fluid Dynamics*, eds. Ellington C.P. and Pedley T.J.). The Company of Biolodists Limited, Cambridge, 21-33.

Romanenko, E. V. (1995c). Drag coefficient in the dolphin and mechanisms of its reduction (experiment and theory) (in Engl.). In *Book abstracts. 9 European drag reduction meeting. Universita di Napoii Federico II, Dipartimento di progettazione aeronautica,* Ravello, Itali.

Romanenko, E. V. (1995d). Estimation of thrust and drag of dolphin (in Russ.). In *Plavanie i polet v prirode i tekhnike AQUAPROP'95. Tez. dokl. Mezhd. Konf.* S.-Peterburg, SPbGMTU.

Romanenko, E. V. (1997a). The measuring devices as microfabricated pressure sensores for investigation of dolphins' boundary layer (in Engl.). In *Book of abstracts. 10 European drag reduction working meeting.* Berlin.

Romanenko, E. V. (1997b). Hydrodynamics of the Black sea bottle-nose dolphin (in Russ.). In *Chernomorskaya afalina,* eds. V. E. Sokolov, E. V. Romanenko, Nauka, Moscow, 672 pp.

Romanenko, E. V. (2001). *Hydrodynamics of the fish and dolphins* (in Russ.). KMK. Moscow. 412 p.

Romanenko, E. V., S. G.Pushkov. (1997). On position of rotation axis and attack angle of dolphin's flukes (in Russ.). *Uspekhi sovremennoi biologii* **117**, 496-504.

Romanenko, E. V., V. E. Sokolov, V. P. Sukhov. (1980). Application of telemetry methods in studyes of mammals in USSR (in Russ.). In *Itogi mechenia mlekopitayuschikh*. Nauka, Moscow, 282-296.

Romanenko, E. V., V. A. Chikalkin. (1974). Tape-recorder for subaquatic records (in Russ.). In *Morfologiya, Fiziologiya i akustika morskikh mlekopitayuschikh,* ed. V. E. Sokolov. Nauka, Moscow,'165-173.

Romanenko, E. V., A. I. Shishmaryov, V. G. Yanov. (1971). Results of the experimental study on dolphins' hydrodynamics (in Russ.). In *7 Vsesoyusnaya akusticheskaja konf.* Report Theses. Moscow.

Romanenko, E. V., V. G. Yanov. (1973). Results of experiments in the study of doplhin's hydrodynamics (in Russ.). *Bionika* **7**, 52-56.

Romanenko, E. V., V. G. Yanov. (1978). Streamline speed measurement in marine animals (in Russ.). In *Marine mammals. Results and methods of investigations,* ed. V. E. Sokolov. Nauka, Moscow, 241-245.

Romanenka, E. V., V. G. Yanov. (1998). Pulsation component of velocity in dolphin's active swimming (in Russ.). Uspekhi sovremennoi biologii **118**, 340–347.

Rosen, M. W. (1961). Experiments with swimming fish and dolphins. *Paper Amer. Soc. Mech. Engrs.* WA-203: 1-11.

Rosen, M. W., N. E. Cornford. (1971). Fluid friction of fish slimes. *Nature* **234**, 49-51.

Roth, W. (1974). Eine Theorie uber die Schwimmbewegung von Fischen. *Acta Mechanica* **20,** 285-301.

Rotta, I. K. (1967). *Turbulent boundary layer in incompressible liquid* (in Russ.). Sudostroenie. Leningrad.

Rozhdestvenskyi, K. V., V. A. Ryzhov. (1995). Study survey MTU in mathematical modelling of technical systems with oscillating wings (in Russ.). In *Plavanie i polet v prirode i tekhnike AQUAPROP'95. Tez. dokl. Mezhd. Konf.* S.-Peterburg, SPbGMTU.

Roy, N. A., D. P. Frolov. (1961). Equipment for calibration of wide-band pressure receivers (in Russ.). *Peredovoy nauchno-tekhnicheskiy i proizvodstvenniy opit. Tema* 36. N P-61-7/2.

Rudenko, A. O. (1991). Approximate method for the calculation of hydrodynamic characteristics of oscillating wing (in Russ.). *Bionika* **24**: 37-40.

Rutgers, A. (1946). Supersonic Vibration Potentials and Centrifugation Potentials. *Nature* **157**, 74-76.

Rybakov, V. P., A. G. Nikolaenko, Yu. P. Staseev. (1965). Use of photography and shooting for study of hydrodynamic processes (in Russ.). In *Razvitie morskikh podvodnikh issledovanii*. Nauka. Moscow: 154-164.

Saburenkov, E. N., D. S. Pavlov. (1968). Fish velocity moving (in Russ.). In *Vsesoyuznaya konferentsiya po voprosu izucheniya povedeniya rib v svyazi s tekhnikoi promisla*. Murmansk: 179-184.

Saburenkov, E. N., Yu. N. Sbikin, D. S. Pavlov. (1967). On the fish velocity moving (in Russ.). In *Povedenie rib v zone gidrotekhnicheskikh sooruzhenii*. Nauka. Moscow.

Sainsbury, J. C. (1963). The porpoise myth? *Ship and Boot Builder*. **16**, 38-40.

Savchenko, Yu. N. (1970). *Experimental study of flapping wing hydromechanics* (in Russ.). Candidates Techn. Dissertation Referat.

Savchenko, Yu. N. (1971a). Some peculiarities of hydrodynamics in propulsor of "flapping wing" type (in Russ.). *Bionika* **5**, 11-19..

Savchenko, Yu. N. (1971b). On the utilization of a wake kinetic energy by flapping wing (in Russ.). *DAN Ukr. SSR* **1**, 78-80.

Savchenko, Yu. N. (1974). Analysis of flapping propulsor in the light of the vortex theory (in Russ.). *Bionika* **8**, 43-49.

Savchenko, Yu. N. (1975). Optimum kinematics of flapping propulsor and resonance regimes in animals' swimming (in Russ.). *Bionika* **9**, 106-112.

Savchenko, Yu. N. (1979). Hydrodynamic effects of the running wave (in Russ.). *Bionika* **13**, 19-24.

Savchenko, Yu. N., V. I. Merkulov. (1970). Experimental study of a liquid flow along the running wave (in Russ.). *Bionika* **4**, 116-120.

Savchenko, Yu. N., V. N. Neznamov. (1976). On the one unsteady regime of animalse moving (in Russ.). *Bionika* 1976, **10**, 53-58.

Savchenko, Yu. N., V. T. Savchenko. (1973). Evaluation of inertie forces in the calcilation of a propulsive force in a swimming flexible body (in Russ.). *Bionika* **7**, 25-27.

Savchenko, Yu. N., V. T. Savchenko. (1983). Bionical aspects of animals swimming (in Russ.). *Gidrodinamicheskie voprosi bioniki*. Naukova dumka. Kiev: 46-57.

Schleemer, H. H. (1966). Effects of pressure gradients on turbulent boundary-layerwall-pressure fluctuations. *JASA* **40**, 1254.

Schmidt, E. M. R.J. Cresci. (1970). Hot wire anemometry in low density flows. *AIAA* 589: 20.

Schlichting, H. (1962). *Initiation of turbulence* (in Russ.). IL. Moskva: 203 pp.

Schlichting, H (1969). *Theory of boundary layer* (in Russ.). Nauka. Moskva: 742 pp.

Schlichting, H. (1973). Grenzschicht-Theorie. Verlag G. Braun, Karlsruhe.

Schlichting, H (1974). *Theory of boundary layer* (in Russ.). Nauka. Moskva: 712 pp.

Scholander, P. F. (1959). Wave-riding dolphins: how do thay do it? *Science* **129**, 1085-1087.

Schwarz, L. (1940). Berechnung der Druckvertellung einer harmonics sich verfor-inenden tragflache in ebener Stromung. *Luftfahrt-Forschungsber.* **17**, N 11/12.

Sedov, L. I. (1980). *Plane problems of hydrodynamics and aerodynamics* (in Russ.). Nauka. Moscow: 448 pp.

Semyonov, B. N. (1969). On the existence of hydrodynamic phenomena of the bottle-nosed dolphin (in Russ.). *Bionika* **3,** 54-61.

Semyonov, B. N. (1971). On the interaction between the elastic boundary and the viscous sublayer of a turbulent boundary layer (in Russ.). *Zh. Prikladnoy Mekhaniki i Tekhnich. Fiziki* **3**, 58-62.

Semyonov, B. N., T. E. Alekseeva. (1970). On the question of existence of dolphin's hydrodynamic phenomenon (in Russ.). *Biokibernetika. Bionika*. Kiev.

Semyonov, B. N., V. V. Babenko, V. P. Kayan. (1974). Experimental study of some peculiaritites of dolphins' swimming hydrodynamic (in Russ.). *Bionika* **8**, 23-31.

Sen'kin, Yu. F. (1995). Experience of making and test of ships with wave propulsor (in Russ.) In *Plavanie i polet v prirode i tekhnike AQUAPROP'95. Tez. dokl. Mezhd. Konf.* S.-Peterburg, SPbGMTU.

Sen'kin, Yu. F., M. N. Nikolayev. (1989). On one possible mechanism of speed enhancing in swimming of dolphins in conditions of agitated sea (in Russ.). *Bionika* **23**, 68-73.

Shakalo, V. M. (1969). On the problem of flow regime measurement in liquid by elelctrothermic methods (in Russ.). *Bionika* **3**, 104-108.

Shakalo, V. M. (1972). One method of mean square value of speed pulsations measurement in the non-stationary turbulent flow (in Russ.). *Bionika* **6,** 105-110.

Shakalo, V. M. (1980). Cable telemetric apparatus for speed pulsation measurement in a boundary layer of marine animals with wire thermoanemometer (in Russ.). *Bionika* **14**, 67-74.

Shakalo, V. M., L. D. Buryanova. (1973). Aparatus investigations on speeds in boundary layer of dolphin according to the swimming regime (in Russ.). In *4 Vsesojuznaja konf. po bionike. Report Theses.* Moscow.

Shebalov, A. N. (1969). Some problems of non-stationary influence on the "mechanism" of drag formation (in Russ.). *Bionika* **3**, 61-66.

Shekhovtsov, A. V. (1995). On the question of optimum regimes of dolphin's fin (in Russ.). *Bionika* **28**.

Shekhovtsov, A. V. (1999). Nonlinear mathematical model of the operation of a dolphin's fin (in Russ.). *Prikladnaya mekhanika* 1(73), 2. 71-88.

Sher, E. N. (1970). On the mechanisms of movement of grass-snake and fish (in Russ.). In *Nekotorye problemy matematiki i mekhaniki.* AN SSSR, Sibirskoe otdelenie, Novosibirsk: 267-276.

Sher, E. N. (1974). On the unsteady movement of autonomic system with waving wing (in Russ.). In *Dinamika sploshnoy sredy* 17. Nauka. Novosibirsk: 89-98.

Shigemitsu, I. (1957). Experimental studies on laiminar sub-layer in turbulent boundary-layer in valving separation. *J. Phys. Soc. Japan* 2, 2.

Shmalgauzen, I. I. (1916). On the functional role of fish fins (in Russ.). *Russkii Zool. zhurnal* **1,** 185-214.

Shpet, N. G. (1975). Peculiarities of body and flukes shape in whales (in Russ.). *Bionika* **9,** 36-41.

Shuleykin, V. V. (1934). Outer and inner fish dynamics (in Russ.). *Izvestiya AN SSSR, otdeleniya matematiki i estestvennykh nauk* **8,** 1151-1156.

Shuleykin, V. V. (1958). How the pilot-fish has the same velocity as shark? (in Russ.). *Doklady AN SSSR* **119**(5).

Shuleykin, V. V. (1963). Energetics of marine animals (in Russ.). *DAN SSSR* **163**, 754-757.

Shuleykin, V. V. (1966). Energetics and speeds of migrations in fishes, dolphins and whales (in Russ.). *Trudy VNII morskovo i rybnovo khoz. i okeanografii* **60**, 27-39.

Shuleykin, V. V. (1968). *Physics of the sea*. Nauka, Moscow: 1083.

Shuleykin, V. V., V. S. Lukyanov, I. I. Stas'. (1937). Hydrodynamic efficiency of fish and dolphin (in Russ.). *Izvestiya AN SSSR*: 581-591.

Siddon, T. E., Kh. S. Ribner. (1965). Foil sensor for measurement of transverse turbulent pulsations (in Russ.). *Raketnaya tekhnika i kosmonavtika* **9**.

Siekmann, J, (1962). Theoretical studies of sea animal locomotion, part 1. *Ingeneur-Archiv,* **31**, 214—227.

Siekinann, J. (1963). Theoretical studies of sea animal locomotion, part 2. *Ingenieur-Arch.*, **32**, 40—53.

Siekmann, (1963). On a pulsation jet from the end of a tube, with application to thepropulsion of certain aquatic animals. *J. Fluid Mech.* **15**, 399-418.

Silberberg, G. G. (1966). Sea animal-locomotion and fish-propulsion studies. In *Whales, Dolphins and Porpoises*, ed. K. S. Norris. Berkeley, Los Angeles, Univ. Calif. Press. 477-481.

Skripachev, V. V. (1972). Stability of laminar boundary layer on deformed membrane leaning on the layer of inviscous and incompressible liquid (in Russ.) *Gidromekhanika* **20**, 7-12.

Skudrzyk, E. J. (1971). *The foundations of acoustics. Basic mathematics and basic acoustics.* V.2. Springer-Verlag. Wien New York.

Skudrzyk, E. J., G. P. Haddle. (1960). Effect of the size of the sound receiver on the received noise level for boundary layer flow noise. *JASA* **32,** 921.

Slavchev, S. G. 1968. Stability of laminar boundary layer of incompressible liquid on elastic surface (in Russ.). *Vestnik Leningradskogo Universiteta* **2**, 113-117.

Slijper, E. J. (1961). Locomotion and locomotory organs in whiles and dolphins (Cetacea). In *Vertebrate Locomotion. Symp. Zool. Soc. Lond.* **5**, 77-94.

Slijper, E. J. (1962). *Whales*. Transi. from. Walvissen. London, Hutchinson.

Smith, E. H. (1965). Some experiments of the oxygen consumption of goldfish (*Carassing auratus* L) in relation to swimming speed. *Canad. J. Zool.* **43**, 623-633.

Smith, E. J., D. E. Stone. (1961). Perfect fluid forces in fish propulsion: The solution of the problem in an elliptic cylinder co-ordinate system. *Proc. Roy. Soc. London* **A 261**, 316—328.

Smyrnov, A. N., N. A. Smyrnov. (1970). Principles and main stages of hydrobionic studies (in Russ.). *Morskoy sbornik* **1**, 80-85.

Snegov, A. A. (1995). Models of power boat having the waving propulsor (in Russ.). In *Plavanie i polet v prirode i tekhnike AQUAPROP'95. Tez. dokl. Mezhd. Konf.* S.-Peterburg, SPbGMTU.

Sokolov, A. S., T. L. Yurchinskaya, S. V. Pershin. (1982). Pecualirity of distribution and structure complex blood vessels regulating of flexibility of dolphin's dorsal fin (in Russ.). *Trudy zoologicheskogo instituta* AN SSSR. **115**. Leningrad: 85-91.

Sokolov, V. E. (1953). *Skin structure of marine mammals* (in Russ.). Cand. Biol. Sci. Diss. thesis. Moscow.

Sokolov, V. E. (1955). Skin structure of some Cetaceans (in Russ.). Bull. MOIP. Otdel. Biologii **60**, 45-60.

Sokolov, V. E. (1959). Adaptations of the skin in marine mammal fauna of the USSR to some conditions of aquatic life. *Proc. XV Internat. Congr. Zool.*: 277-280.

Sokolov, V. E. (1960a). Structural peculiarity of skin in Mysticeti, enhancing the skin elasticity (in Russ.). *Zool. Zhurn.* **33**, 307-308.

Sokolov, V. E. (1960b). Some similarities and dissimilarities in the structure of the skin among the members of the suborder Odontoceti and Mystacoceti. *Nature* 185(4715):

Sokolov, V. E. (1961). Structure and causes of skin excrescence development in japanese whales (in Russ.). *Zool. Zhurn* **40**

Sokolov, V. E. (1962a). Skin structure in some Cetaceans. - Soobschenije 2 (in Russ.). *Nauchn. Doklady Vysshey shkoly. Biol. Nauki* **3**, 47-53.

Sokolov, V. E. (1962b). Adaptations of the mammalian skin to the aquatic mode of life. *Nature.* **195**, 464.

Sokolov, V. E. (1965a). Epidermis structure in three Cetaceans species (in Russ.). *Morskye mlekopitayuschie*. Nauka, Moscow.

Sokolov, V. E. (1965b). Adaptive peculiarities of the skin in aquatic mammals. *Morskye mlekopitayuschije*. Nauka, Moscow. 272 p.

Sokolov, V. E. (1971). Skin structure in some Cetaceans. - Soobschenije 3 In *Morfologiya i ekologiya morskikh mlekopitayuschikh*, ed. V.E.Sokolov. Nauka, Moscow.

Sokolov, V. E. (1973). *Skin of mammals*. Nauka, Moscow. 487 pp.

Sokolov, V. E. (1997). Survey of study on the Black Sea bottlenose dolphin (in Russ.). In *Chernomorskaya afalina. Red. V. E. Sokolov, E. V. Romanenko,* Nauka. Moscow: 9-19.

Sokolov, V. E., V. V. Babenko, L. F. Kozlov, S. V. Pershin, A. G. Tomilin, O. B. Chernyshov. (1983). The properties of the skin of Cetaceans of actively regulate the hydrodynamic resistance to swimming (in Russ.). Sertificate N 265 to Doscovery SSSR. Applic. NOT-8405 as to 21.02.73, published 07.05.83, Bull. N17.

Sokolov, V. E., O. M. Bocharova-Messner, T. P. Evgenyeva, E. I. Naumova. (1979). *Adaptive properties of epitelium and its derivatives: Atlas of macrophotographies, taken with electronic scanning microscope* (in Russ.). Nauka, Moscow. 180 p.

Sokolov, V. E., V. D. Burlakov, Zh. Ya. Grushanskaya. (1972). Theoretical drawing of the Black sea bottle-nosed dolphin (in Russ.). *Bull. Moskovskogo Obsch. Ispytat. Prirody* **77**, 45-53.

Sokolov, V. E., I. G. Bulina, V. A. Rodionov. (1969). Interaction of dolphin epidermis with flow boundary layer. *Nature*. **222**, 267-268.

Sokolov, V. E., I. G. Bulina, V. A. Rodionov. (1973). Study of mechanism of interaction between the skin epidermis of dolphins and the flow boundary layer (in Russ.). *Problemy bioniki.* Nauka, Moscow, 475-478.

Sokolov, V. E., M. M. Kalashnikova. (1971). The ultrastructure of epidermal cells in *Phocaena phocaena*. In *Investigations of Cetacea*, ed. G. Pilleri. **3**, 194-199.

Sokolov, V. E., M. M. Kalashnikova, V. A. Rodionov. (1971). Micro-and ultra-structure of skin of *Phocoena phocoena* (in Russ.). In *Morfologiya i ekologiya morskikh mlekopitayuschikh,* ed. V.E.Sokolov. Nauka, Moscow.

Sokolov V. E., T. V. Kuznetsov. (1966). Direction of dermal ridges at the skin of dolphins in connection with the peculiarities of water flow along the body (in Russ.). *Bull. Moskovsk. Obschestva ispytat. Prirody. Otdel biologii. Report Theses.* Nauka, Vladivostok. 18.

Sokolov, V. E., G. V. Kuznetsov, V. A. Rodionov. (1968). Direction of dermal ridges at the skin of dolphins in connection with the peculiarities of water flow along the body (in Russ.). *Bull. Obschestva ispytat.Prirody. Otdel Biologii* **73**, 123-126.

Sokolov, V. E., N. V. Kokshajskiy, V. A. Rodionov. (1971). Experience of the transportation and the investigation of dolphin swimming in the hydrochannel (in Russ.). *Bull. Obschestva ispytat. Prirody. Otdel Biologii* **76**, 37-46.

Sokolov, V. E., L. N. Skurat (1997). Skin morphology of the Black Sea bottlenose dolphin (in Russ.). In *Chernomorskaya afalina.* Red. V. E. Sokolov, E. V. Romanenko, Nauka. Moscow: 9-19.

Sokolov, V. E., L. V. Stepanova. (1997). Ultra-structural organization of epidermis of the Black Sea bottlenose dolphin (in Russ.). In *Chernomorskaya afalina.* Red. V. E. Sokolov, E. V. Romanenko, Nauka. Moscow: 9-19.

Sokolov, V. E., L. V. Stepanova, N. D. Bodyak. (1997). Skin gland of the Black Sea bottlenose dolphin (in Russ.). In *Chernomorskaya afalina.* Red. V. E. Sokolov, E. V. Romanenko, Nauka. Moscow: 9-19.

Sorokodum, E. D. (1995). On the perspective of introduction of study result of aerohydrodynamics of oscillating wings (in Russ.). In *Plavanie i polet v prirode i tekhnike AQUAPROP'95. Tez. dokl. Mezhd. Konf.* S.-Peterburg, SPbGMTU.

Sparenberg, J. A. (1995). On the partial optimization of lifting surface system; linear theory. In *Plavanie i polet v prirode i tekhnike AQUAPROP'95. Tez. dokl. Mezhd. Konf.* S.-Peterburg, SPbGMTU.

Spillman. J. J. (1978). The use of wing tip sails to reduce vortex drae. *Aeronaut. J.* **82**, 387-395

Stas', I. I. (1939). Registration of dolphin's movements in sea (in Russ.). *DAN SSSR* **24**, 534—537.

Stas', I. I. (1939). Once more on the registration of dolphin's movements (in Russ.). *DAN SSSR* **25**

Steve Leatherwood, W., E. Evans, Dale. W. Rice. (1972). *The whales, dolphins porpoises of the eastern North Pacific: A guide to their identificatiol: the water*. Nat. Ocean, and Atmos. Administration Property,. 34.

Struminsky, V. V., Yu. B. Lebedev, V. M. Fomichev. (1986). Influence of temperature gradient along the surface on the extent of the laminar boundary layer (in Russ.). *DAN SSSR* **289**, 813-816.

Surkina, R. M. (1968). Structure of the connective-tissue frame of dolphins' skin (in Russ.). In *Mekhanismy peredvizhenija i orientatsii zhivotnikh*. Naukova dumka, Kiev: 78-92.

Surkina, R. M. (1971a). On the structure and location of thew skin musculature in dolphins (in Russ.). *Bionika* **5**, 81-87.

Surkina, R. M. (1971b). Location of dermal ridges on the body of *Delphinus delphis* (in Russ.). *Bionika* **5**, 88-94

Surkina, R. M., E. T. Uskova, L. N. Momot. (1972). On some peculiarities of epidermis and on the composition surface secretions composition of dolphins skin (in Russ.). *Bionika* **6**, 52-57.

Swanson, W. M. (1965). Some observations of fish propulsion: qualitative boundary layer considerations. In *Developments in Mechanics* **2**.

Taggart, R. (1963). A look at the future in marine propulsion. *Naval Engrs. J.* **75**, 375-384.

Taneda, S., Y. Tomonari (1974). An Experiment on the flow around a waving plat. *J. Phys. Soc. Jap.* **36**, 1683-1689.

Taylor, G. (1952). Analysis of the swimming of long and narrow animals. *Proc Roy. Soc. Lond. Ser.* A 214(1117): 158-183.

Teslo, A. P., V. E. Filipchuk. (1974). Influence of compliant surface on the turbulent flow characteristics (in Russ.). *Gidromekhanika* **29**, 45-50.

The Black Sea bottlenose dolphin. (1997). Eds. V. E. Sokolov, E. V. Romanenko. Nauka. Moskva. 672 pp.

The Bottlenose Dolphin. Eds. Stephen Leatherwood, Randall R. Reeves. (1990). Academic Press, Inc. Harcourt Brace Jovanovich, Pablishers. San Diego, New York, Berkeley, Boston, London, Sydney, Tokyo, Toronto. 654 p.

Theodorsen, T. (1935). *General theory of aerodynamic stability and the mechanism of flatter*. NACA Rep. 496 p.

Timoshenko, S., S. Woinowsky-Krieger. (1959). *Theory of plates and shells*. McGRAW-HILL BOOK COMPANY, INC. Ney York, Toronto, London. 636 p.

Tinyakov, G. G., V. P. Chumakov, B. A. Sevastyanov. (1973). Some problems in the skin macrostructure of Cetacean (in Russ.). *Zool.Zhurn.* **52**, 399-407.

Toles, G. E. (1970). The extraordinary world of the dolphin. *Animals* **13**, 308-311.
Tomilin, A. G. (1940). Some problems of Cetacean ecology (in Russ.). *Bull. Mosk. obsch-va ispytateley prirody. Otdel Biologii* **49**, 18-24.
Tomilin, A. G. (1947a). Thermoregulation and geographical races of Cetaceans (in Russ.). *Doklady Akademii Nauk SSSR* **56**, 469-472.
Tomilin, A. G. (1947b). To the biology and physiology of *Delphinus delphis* (in Russ.). *DAN SSSR* **56**, 221-223.
Tomilin, A. G. (1961). Somthing modern problems of cetacean biology study (in Russ.). *Trudy soveshaniy ikhtiologicheskoy komissii Akademii nauk SSSR* **12**, 40-49.
Tomilin, A. G. (1962). On the adaptations of Cetaceans to swift swimming and on the possibility of these adaptations in ship construction (in Russ.). *Bull. Mosk. obsch-va ispytateley prirody. Otdel Biologii* **67,** 10-18.
Tomilin, A. G. (1963a). "Intellectuals" of sea deep. Secrets of dolphin's and wale's behaviour (in Russ.). *Priroda.* July: 70-77.
Tomilin, A. G. (1963b). Bionics and Cetaceans (in Russ.). *Priroda.* October **10**, 101-103.
Tomilin, A. G. (1969). *Dolphins at the service of man* (in Russ.). Nauka, Moscow. 96 pp.
Tomilin, A. G. (1975). Cetaceans. *Zveri SSSR i prilegayischikh stran. Izd. AN SSSR*, Moscow. 756 pp.
Tomilin, A. G. (1979). The change of the skin colour in bottle-nosed dolphins under the influence of the dynamic load in the process of swimming (in Russ.). *Trudy Vsesoyuaznogo selskokhozaystvennogo Instituta zaochnogo obuchenya* **159**, 44-47.
Toms, B. A. (1948). Some observations on the Flow of linear polimer solutions through straight tubes at large Reynolds numbers. *Proceedings 1-st International Congress on Theology,* Schreveningen, Netherlands **2**, 135-141.
Trurston, S., R. D. Jones. (1965). Experimental model studies of non-Newtonian soluble coatings for drag reduction. *J. Aircraft* **2**, 122-126.
Tsyganyuk, A. I. (1971). Kand. diss. Institut gidromekhaniki A. N. USSR. Kiiv.
Tuck, E. O. (1968). A note on a swimming problem. *J. Fluid Mech.* **31**, 305-308.
Tuck, E. O. (1975). Effect of span-wise variation in amplitude on the thrust-generating performance of a flapping wing. In *Swim and Flight in Nature.* **2**, 953-973.
Tucker, V. A. (1970). Energetic cost of locomotion in animals. *Comp.Biochem. physiol.* **34**, 841-846.
Uldrick, S. P. (1968). On the propulsion efficiency of swimming flexible hydrofoils of finite thickness. *J. Fluid Mech.* **32**, 29—53.
Uldrick, J. P., J. Siekmann. (1964). On the swimming of a flexible plate of arbitrary finite thickness. *J. Fluid Mech.* **20**, 1—33.
Uskova, E. T., A. V. Chaykovskaya, D. A. Ustimovitch, S. I. Davidenko. (1970). On the chemical composition of skin mucous material of some fish species of the Black Sea (in Russ.). *Gidrobiologicheskii zhurnal* **4**.

Uskova, E. T., S. I. Davidenko. (1974). Thickness of mucous covering of some salt-water species fish and content of mucus in this covering (in Russ.). *Bionika* **8**, 141-145.

Uskova, E. T., L. N. Momot. (1975). Hydrodynamic efficiency of surface dolphin's secretion (in Russ.). In *Morskie mlekopitayuschie*. 2. Naukova dumka. Kiev: 136-139.

Uskova, E. T., L. N. Momot, V. A. Krisal'ny. (1974). On the effectiveness of skin secretion in some marine mammals and on the lowering of hydrodynamic resistance (in Russ.). *Bionika* **8**, 148-151.

Uskova, E. T., L. N. Momot, R. M. Surkina. et al. (1975). Investigation of the chemical nature of eye's secretion of *Tursiops truncatus* (in Russ.). *Zh. Evoluts.biokhimii i fiziolgii* **11**, 371-375.

Uskova, E. T., V. S. Rayevskiy, L. N. Momot, I. A. Uskov. (1975). Comparative study of the hydrodynamic effectiveness of polyoxyethilene solutions and of skin secretions of marine mammals (in Russ.). *Bionika* **9**, 90-92.

Uskov, I. A., V. S. Rayevskiy, V. V. Dubrovskaya, V. Ya. Filimonov, E. T. Uskova. (1973). Reology and hydrodynamics of polimer solution. Characteristic viscosity and drag reduction in transition region and by condition of turbulence (in Russ.) *Bionika* **7**, 87-91.

Uskova, E. T., A. N. Shmyryov, V. S. Rayevskiy, L. N. Bogdanova, L. N. Momot, V. V. Belyayev, I. A. Uskov. (1983). On the nature and the hydrodynamic activity of eye's secretion in dolphins (in Russ.). *Bionika* **17**, 72-75.

Uskova, E. T., V. M. Zhartovsky. (1971). On the influence of some biopolymers on laminar and turbulent regimes of liquid flow (in Russ.). In *Fiziko-khimitscheskaya mekhanika i liofil'noct' dispersnykh sistem. 3. IKKhKhV*. Kiev.

Varitch, Yu. N. (1969). Information system for description of flow over of live necters (in Russ.). In *Voprosy morskoi biologii. Tez. dokl. 2 Vses. symp. molodykh uchenykh*. Sevastopol.

Varitch, Yu. N. (1970a). Analysis of flow over of Black Sea dogfish (in Russ.). In *Biokibernetika - bionika. Tez. dokl. 4 Ukrain. Respubl. Nauchn konfer. po bionike*, Naukova dumka, Kiev.

Varitch, Yu. N. (1970b). *Study in unsteady flow over of some fish* (in Russ.). Kand. Diss. Kiev.

Varitch, Yu. N. (1971a). Flow over dependence of physiological state of swimming fish (in Russ.). *Doklady AN USSR* **5**.

Varitch, Yu. N. (1971b). Analysis of flow over of live dogfish (Squalus acanthias) by means of information system (in Russ.). *Zool. Zhurn.* **50**, 126-129.

Vasil'ev, A. S., A. F. Il'ichev, G. N. Mikheev. (1985). Something aspects of fish hydrodynamic drag and models (in Russ.). *Bionika* **19**,50-56.

Videler, J. J. (1981). Swimming movements, body structure and propulsion in cod (*Gadus morhua*)., In *Vertebrate locomotion*, ed. M.H.Day. Zool. Soc. Lond., Academic press: 1-27

Videler, J. J. (1993). *Fish swimming*. Chapman and Hall. Lond. Glasgow. New York. Tokio. Melbourne. Madras. 260 pp.

Videler, J. J., F. Hess. (1984). Fast continuous swimming of two pelagic predators, saithe (*Pollachius virens*) and mackerel (*Scomber scombrus*): a kinematic analysis. *J. Exp. Biol.* **109**, 209-228.

Videler, J. J. (1985). Fish swimming movements: a study of one element of behaviour. *Neth. J. Zool.* **35,** 170-185.

Videler, J. J., P. Kamermans. (1985). Differences.between upstroke and downstroke in swimming dolphins. *J.Exptl.Biol.***119**, 265 - 274.

Vishnyakov, A. A., L. F. Kozlov, V. M. Shakalo. (1979). Some results of spectral analysis of pulsations in the boundary layer in Cetaceans (in Russ.). *Bionika* **13**, 58-62.

Voitkunsky, Ya. I., Yu. I. Faddeev. (1976). Some problems of technical hydrobionics (in Russ.). *Bionika* **10**, 21-27.

Voropaev, G. A., V. V. Babenko. (1978). Turbulent boundary layer on elastic surface (in Russ.). *Hydromechanics* **38**, 71-77.

Voropaev, G. A., E. A. Svirsky. (1980). On boundary conditons for turbulent flow on viscous-elastic border (in Russ.). *Bionika* **16**, 47-53.

Vijgcn, P. M. H. W., C. P. van Dam, B. J. Holmes. (1989). Sheared wing-lip aerodynamics: wind tunnel and computational investigation. *J. Aircr.* **26**, 207 13

Vijgen, P. M. H. W., C. P. van Dam, B. J. Holmes, F. G. Howard. (1990). Wind tunnel investigations of wings with serrat-ed sharp trailing edges. *Proc. Conf. Low-Ri'vnoklx-Numhcr Acroi/vii., Notre Dume. lnd.* Berlin: Sprinaer-Verlag.

Walsh, M. J., A. M. Lindemann. (1984). Opti-mization and application ofribicts for turbulent drag reduction. *AIAA Pap. No. 84-0347*

Walters, V. (1962). Body form and swimming performance on the scombroid fishes. *Amer. Zoologist* **2**, 143-149.

Walters, V. (1966). The «Problematic» hydrodynamic performance of Gero's Great Barraccuda. *Nature* **212.**

Walters, V., H. L. Fierstine. (1964). Measurements of swimming speeds of Yellowfin Tuna and Wahoo. *Nature* **202**, 208-209.

Watts, E. H. (1961). The relationship of fish locomotion to the design of ships. In *Vertebrate Locomotion. Simpos. Zool. Soc. London.* **5**, 37-41.

Webb, P. W. (l971a). The swimming energetics of trout. 1. Thrust and power outputat cruising speeds. *J. Exp. BioL* **55**, 489-520.

Webb, P. W. (1971b). The swimming energetics of trout. 2. Oxygen consumption andswimming efficiency. *J. Exp. Biol.* **55,** 521-540.

Webb, P. W. (1975). Hydrodynamics and energetics of fish propulsion. *Bull. Fish. Res. Bd Can.* **190**, 1-159.

Webb, P. W. (1978). Hydrodynamics: nonscombroid fish. In *Fish physiology*. Acad. press. **7**, 189—237.

Weihs. D. (1973a). Hydromechanics of fish schooling. *Nature* **241**, 290 91

Weihs. D. (1973b). Mechanically efficient swimming techniques For fish with negative buoyancy. J. *Mar. Res.* **31,** 194-209

Weihs, D. (1974). Energetic advantages of burst swimming of fish. *J. Theor. Biol.* **48**, 215-229.

Weihs, D. (1975). Some hydrodynamical aspects of fish schooling.. In *Swimming and flying in nature* 2, ed. T. Y. Wu, C. J. Brokaw, and C. Brennan. Plenum, New York: 703-718.

Weinmann, A. (1959). Phenomenological theory of ultrasonic vibration potentials inliquids and electrolytes. *Proc. Phys. Soc.* 73 part. 3. N 471: 345-353.

Weinmann, A. (1960). Theory of ultrasonic vibration potentials in pure liquids. *Proc.Phys. Soc.* **75**.

Willmarth, W. W. (1956). Wall pressure fluctuations in a turbulent boundary layer. *JASA* **28**, 1048.

Willmarth W. W., C. E. Wooldridge. (1962). Measurements of the fluctuating pressure at the wall beneath a thick turbulent boundary layer. *J. Fluid Mech.* **14**.

Wood, Forrest G. (1973). *Marine mammals and man.* Washington - New York. **6**.

Woodcock, A. H. (1948). The swimming of dolphins. *Nature* **161**, 602.

Wu, T. Y—T. (1961). Swimming of a waving plate. *J. Fluid Mech.* **10**, 321—344.

Wu, T. Y.-T. (1964). Accelerated swimming of a waving plate. In *IV Symp. on naval hydrodynamics.* Wash.: 457—473.

Wu, T. Y.—T. (1964). Hidromechanics of swimming propulsions. *J. Fluid Mech.* **16**, 2.

Wu, T. Y.-T. (1971a). Hydromechanics of swimming propulsion. Pt 1. Swimming of a two-dimensional flexible plate at variable forward speeds in an inviscid fluid. *J. Fluid Mech.* **46**, 337—355.

Wu, T. Y.-T. (1971b). Hydromechanics of swimming propulsion. Pt 2. Some optimumshape problems. *J. Fluid Mech.* **46**, 521—544.

Wu, T. Y.-T. (1971c). Hydromechanics of swimming propulsion. Pt 3. Swimmings and optimum movements of slender fish with side fins. *J. Fluid Mech.* **46**, 545—568.

Wu, T. Y. (1972). Extraction of flow energy by a wing oscillating in waves. *J. Ship Res.* **14**, 66-78.

Wu, T. Y. (1977). Introduction to the scaling of aquatic animal locomotion. Ed. T. J. Pedley.. *Academic Press, London.*: 203-232

Wu, T. Y.-T., A. T. Chwang. (1975). Extraction of flow energy by fish and birds in a wavy stream. In *Swimming and flying in nature*, ed. T. Wu, C. J. Brokaw, and C. Brennan. Plenum Press, New York:687-702.

Wu, T. Y., A. T. Chwang, P. K. C Wang. (1973). Optimization problems in hydrofoil propulsion. In *Optimization and Stability problems in continuum mechanics*. Ed. P.K.C. Wang. Lecture Notes in Physics, Springer-Verlag, **21**, 38-62.

Yablokov, A.V., V. M. Belkovich, V. I. Borisov. (1972). *Whales and dolphins* (in Russ.). Nauka, Moscow. 472 pp.

Yakimov, Yu. L. (1995). Wave propulsors of ship (in Russ.). In *Plavanie i polet v prirode i tekhnike AQUAPROP'95. Tez. dokl. Mezhd. Konf.* S.-Peterburg, SPbGMTU.

Yakovenko, V. V. (1953). On the distribution of pressure along the profile waving harmonically in flow (in Russ.). *Trudy Leningradskogo politekhnicheskogo instituta* **5**, 153-167.

Yanov, V. G. (1990). Kinematics of dolphins. New results of experimental studies (in Russ.). *DAN SSSR* **315,** 49-52.

Yanov, V. G. (1990a). On the correlation of skeleton-muscle structure and kinematics of the Black Sea bottlenose dolphin (in Russ.). *Morskie mlekopitayuschie. Tez. dokl. 10 vses. sovech. Po izucheniyu, okhrane i ratsional'nomu ispol'zovaniyu morskikh mlekopitayuschikh* (in Russ.). Svetlogorsk – Moskva: 339-340.

Yanov, V. G. (1990b). On the deformation law of body of active swimming bottlenose dolphin (in Russ.). *Morskie mlekopitayuschie. Tez. dokl. 10 vses. sovech. Po izucheniyu, okhrane i ratsional'nomu ispol'zovaniyu morskikh mlekopitayuschikh* (in Russ.). Svetlogorsk – Moskva: 340-341.

Yanov, V. G. (1991). Systemic-and-functional organization of the kinematics of swimming in dolphins (in Russ.). *DAN SSSR* **317**, 1089-1093.

Yanov, V. G. (1995a). Complex analysis of dolphin's kinematics (in Russ.). In *Plavanie i polet v prirode i tekhnike AQUAPROP'95. Tez. dokl. Mezhd. Konf.* S.-Peterburg, SPbGMTU.

Yanov, V. G. (1995b). *Complex analysis of kinematics of bottlenose dolphin active swimming (Tursiops truncatus)* (in Russ.). Kand. diss.

Yanov, V. G. (1997). Experimental investigating kinematics of three actively swimming modes in the Black sea bottlenose dolphin (*Tursiops truncatus*). (in Russ.). Uspekhi sovremennoi biologii **117**, 704–725.

Yanov, V. G. (1998). Kinematic parameters of bending oscillations in *Tursiops truncatus* body during active rectilinear swimming (in Russ). Uspekhi sovremennoi biologii **118**, 86–100.

Yanov, V. G. (2000). Structural and functional interrelation between swimming kinematics and specific features of dolphin's locomotory apparatus (in Russ.). Uspekhi sovremennoi biologii **120**, 88–102.

Yanov, V. G. (2001). Kinematic model of active swimming in dolphin and systemic and functional principles of the organization its locomotor skeleton-muscular structures (in Russ.). Uspekhi sovremennoi biologii **121**, 405–414.

Yanov, V. G. (2001). Effect of additional loading on the kinematics and hydrodynamics of dolphin (in Russ.). Biofizika sloznikh sistem **46**, 563–572.

Yanov, V. G., E. V. Romanenko. (1972). Radiotelemetric system for measurement of hydrodynamic parameters of dolphins in conditions of a limited aquatory (in Russ.). *Bionika* **6**, 92-99.

Yasui, W. Y. (1981). Morphometrics, hydrodynamics and energetics of locomotion for a small cetacean, *Phocoena phocoena* (L.). *M.Sc. thesis*, University of Guelph, Ontario.

Yates, G. T. (1983). Hydrodynamics of body and caudal fin propulsion. In *Fish Biomechanics,* ed. P. W. Webb and D. Weihs.. New York: Praeger: 177 - 213.

Yuen, H. S. H. 1970. Behavior of skipjack tuna, Katsuwonus pelamis, as determined by tracking with ultrasonic devices. *J. Fish. Res. Bd. Canada*, **27**, 2071-2079.

Yeager, E., J. Booker, F. Hovorka. (1959). Ultrasonic vibration potentials in Non — ionic liquids. *Proc. Phis. Soc.* **73**. 690-691.

Yurchenko, N. F., V. V. Babenko. (1979). On the stabilization of longitudinal wortexes by the skin of dolphins (in Russ.). *Biofizika* - 1979 **24** 72-78.

Yurchenko, N. F., V. V. Babenko. (1979). On the stabilization of longitudinal vortex by dolphin's skin (in Russ.). *Biofizika* **25**, 299-304.

Yurchenko, N. F., V. V. Babenko. (1983). On the modelling of hydrodynamic functions of outer covers of aquatic animals (in Russ.). *Gidrodinamicheskie voprosy bioniki.* Naukova dumka. Kiev: 37-46.

Yurokin, A. I. (1988). Consideration of damping properties of sreamlined surfaces in studying of hydrodynamic stability (in Russ.). *Bionika* **22**, 23-28.

Zaets, V. A. (1972). On the question of variable roughness of shark skin (in Russ.). *Bionika* **6**, 67-73.

Zaets, V. A. (1973). Distribution of placoid scale of shark skin (in Russ.). *Bionika* 7, 83-87.

Zaets, V. A. (1974). Interaction of superficial muscle layers with shark skin (in Russ.). *Bionika* **8,** 93-100.

Zaets, V. A. (1980). Analysis of something component of provision complex for fast swimming of shark (in Russ.). *Bionika* **14**

Zaytsev, A. A. (1976). Carrying surface at amply-dimensional deformations (in Russ.). In *Aeromekhanika i gazovaya dinamika*. Nauka. Moscow: 42-56.

Zaytsev, A. A., V. V. Tyurev. (1980). Calculation of flow over of carrying surface at arbitrary deformations (in Russ.). *Izv. AN SSSR, Mekhan. zhidkosty i gasa* **4**, 72-79.

Zaytsev, A. A., L. V. Sharina. (1983). Aerodynamic calculation of normal beating flight (in Russ.). *Izv. AN SSSR, Mekhan. zhidkosty i gasa* **4**, 71-78.

Zaytsev, A. A., A. A. Fedotov. (1986). Flow over of thin finite span wing by perfect incompressible liquid when oscillating amplitude of wing is large (in Russ.). *Mekhan. zhidkosty i gasa* **5,** 75-82.

Zhurava, V. M., Yu. M. Faddeev. (1971). Boundary layer equations for transformed contour (in Russ.). *Bionika* **5**, 46-52.

Zhurava, V. M., Yu. M. Faddeev. (1973). On the question of influence of unsteadiness of gidrobionts forvard movement on friction drag (in Russ.). *Bionika* **7**, 56-59.

Zhurava, V. M., Yu. M. Faddeev. (1974). On the influence of body surface deformation on the boundary layer characteristics (in Russ.). *Bionika* **8**, 17-19.

Zhurava, V. M., Yu. M. Faddeev. (1977). Results of calculation of unsteady laminar boundary layer on the deformed ellipsoid of revolution (in Russ.). *Bionika* **11**, 44-50.

Zinkevich, L. A. (1944). Essay on the evolution of locomotion apparatus in animals (in Russ.). *Zhurnal obschey biologii* **5**

Zolotov, S. S., Ya. S. Khodorkovskii. (1973). Friction drag peculiarities of like-swordfish form of body (in Russ.). *Bionika* **7**, 14-18.

Zuev, G. V., A. V. Kudryashov. (1968). On the manoeuvrability of aquatic animalse (in Russ.). *Voprosy ikhtiologii* **8**. 1057-1062.

This is a monographic, fully original treatment devoted to fish and dolphin swimming mechanics, with an up-to-date review of the modern concepts of and approaches to biohydrodynamics. The opinion is supported and advanced that at least the dolphins show certain mechanisms to control the boundary layer and to decrease the hydrodynamic friction resistance (Gray's paradox). The treatise is destined for students and specialists in biology, hydrodynamics and hydromechanics.

Professor Evgeny V. Romanenko, DSc, Deputy of the A. N. Severtzov Institute of Ecology and Evolution, Russian Academy of Sciences, Moscow. Since 1960, one of Russia's leading research fellows in the field of biohydrodynamics, with special emphasis on the locomotion of such active and successful swimmers as fish and dolphins. His first monongraph, of 1976, entitled "Foundations of statistic biohydrodynamics" (Moscow) focused on the study of the fine structure of the boundary layer in free-living fish and dolphins. The next monograph, of 1986, entitled "Theory of fish and dolphin swimming" (Moscow), concentrated on a mathematical simulation of the mechanisms controlling the formation of a favourable gradient of the dynamic pressure on undulating fish and dolphin bodies. Finally, his recent monograph, of 2001, entitled "Hydrodynamics of fishes and dolphins" (Moscow), represents a Russian prototype of the present book, with several new theoretical and experimental results in body and fluke kinematics proposed.

Russian Academic Monographs, No 2 ISBN 954-642-150-2